

POLITECNICO DI MILANO

School of Civil, Environmental and Land Management Engineering

Master of Science in Civil Engineering, Structures



**UNIVERSITY
OF MIAMI**



FRP Anchors for External Reinforcement of Concrete Structural Elements

Advisor: Prof. Carlo POGGI

Co-Advisor: Prof. Antonio NANNI

Master's Thesis by:

Marco ROSSINI

817293

Academic Year 2015 – 2016

*To my Family,
Deeply Grateful*

*“Nothing is as sweet as his Home and Family,
though one has in strange and distant lands
the most opulent mansion”*

*“Nulla è tanto dolce quanto la propria Patria e Famiglia,
per quanto uno abbia in terre strane e lontane
la magione più opulenta”*

Homer?

“Vijiti katika kifungu ni madhubuti”

“Sticks in a bundle are unbreakable”

“I Bastoni in un Fascio sono Infrangibili”

Kenyan Proverb

1	ABSTRACT.....	19
2	INTRODUZIONE.....	21
3	COMPOSITES MATERIALS: AN OVERVIEW	23
3.1	Historical Background	23
3.1.1.1	<i>Classical Building Applications.....</i>	23
3.1.1.2	<i>Lighter and Stronger: The War Industry</i>	24
3.1.1.3	<i>A Durable Solution for Civil Engineering</i>	24
3.2	Fiber Reinforced Polymers: Material Overview.....	26
3.2.1	The Fibers	26
3.2.1.1	<i>Glass Fibers (GFRP)</i>	26
3.2.1.2	<i>Aramid Fibers (AFRP)</i>	27
3.2.1.3	<i>Carbon Fibers (CFRP).....</i>	28
3.2.2	The Resins	29
3.2.2.1	<i>Thermosetting polymers</i>	29
3.2.2.2	<i>Thermoplastic polymers.....</i>	31
3.2.3	The Industry, Chemistry and Production Process	32
3.2.3.1	<i>Carbon Fibers</i>	32
3.2.3.2	<i>Epoxy Resin</i>	33
3.3	FRP Laminates for Rehabilitation Purposes.....	35
3.3.1	Mechanical Behavior.....	36
3.3.2	Elastic Response	38
3.3.3	Failure Criteria.....	41
3.3.3.1	<i>Maximum Strength Criterion</i>	41
3.3.3.2	<i>Tsai-Hill Failure Criterion.....</i>	43
3.3.3.3	<i>Tsai-Wu Failure Criterion</i>	44
3.3.3.4	<i>Summing Up</i>	46
3.3.4	Lamina Orientation.....	46
3.3.4.1	<i>Hooke’s Law for an Angle Lamina.....</i>	47

3.3.4.2	<i>Failure Criteria for an Angle Lamina</i>	48
3.3.5	Mechanical Characterization	48
3.3.5.1	<i>Micromechanics</i>	48
3.3.5.2	<i>Direct Testing</i>	49
3.3.6	Structural Applications and Design Criteria Overview	50
3.3.6.1	<i>Design Philosophy & Regulations</i>	51
3.3.6.2	<i>Flexural Strengthening</i>	53
3.3.6.3	<i>Shear and Torsion Strengthening</i>	54
3.3.6.4	<i>Columns Confinement</i>	55
3.3.6.5	<i>Other Applications</i>	55
3.4	The Debonding Problem	56
3.4.1	Debonding Failure Modes in Flexural Applications	57
3.4.1.1	<i>End Debonding</i>	59
3.4.1.2	<i>Debonding by Flexural Cracks – Intermediate Debonding</i>	60
3.4.1.3	<i>Debonding by Shear Cracks</i>	60
3.4.1.4	<i>Debonding by Irregularities and Roughness of the Concrete Surface</i>	61
3.4.2	Bond Mechanism & Development Length	61
3.4.2.1	<i>Bond-Slip Law, Specific Fracture Energy, Bond Strength</i>	62
3.4.2.2	<i>Maximum Shear Force, Optimal Development Length</i>	64
3.4.2.3	<i>Bond Length Design</i>	67
3.4.3	Debonding Modeling in Flexural Applications	70
3.4.3.1	<i>End Debonding</i>	70
3.4.3.2	<i>Intermediate Debonding</i>	72
3.5	Anchoring Systems for FRP Laminates	74
3.5.1	Categorization Based on the Resisted Force	74
3.5.2	Categorization Based on Debonding Type	75
3.5.3	Categorization Based on Strengthening Application	75
3.5.3.1	<i>Anchoring Solution for Flexural Strengthening</i>	75
3.5.3.2	<i>Anchoring Solutions for Shear Strengthening</i>	76
3.5.3.3	<i>Anchoring Solutions for Column Confinement & Joint Strengthening</i>	77
3.5.3.4	<i>Other Applications</i>	77

3.5.4	Categorization Based on Mechanical Function.....	78
3.5.4.1	<i>Type I – Bond Improvement: Pull-Out Critical.....</i>	78
3.5.4.2	<i>Type II – Bond Improvement: Shear Critical.....</i>	78
3.5.4.3	<i>Type III – Equilibrium Critical.....</i>	79
3.5.4.4	<i>Type IV – Ductility Critical.....</i>	80
3.5.5	Categorization Based on Construction Typology.....	81
3.5.5.1	<i>Transverse Wrapping.....</i>	81
3.5.5.2	<i>Anchor Spikes.....</i>	82
3.5.5.3	<i>Metallic Anchors.....</i>	85
3.5.5.4	<i>Concrete Embedment.....</i>	87
3.5.5.5	<i>Surface Preparation.....</i>	88
3.5.6	Anchor Testing.....	90
3.5.6.1	<i>Pull-Out Test.....</i>	91
3.5.6.2	<i>Direct Shear Test.....</i>	92
3.5.6.3	<i>Bending Tests.....</i>	94
3.5.7	Research Direction.....	94
3.5.7.1	<i>The Need for a Unified Approach.....</i>	94
3.5.7.2	<i>Available Guidelines.....</i>	95
4	ANCHORING SPIKES: STATE OF THE ART REVIEW.....	97
4.1	Manufacturing & Installation.....	97
4.1.1.1	<i>Fiber Rolls / Fiber Bundles.....</i>	97
4.1.1.2	<i>Pre-Cured / Wet Dowel.....</i>	97
4.1.1.3	<i>One-Step / Two-Step Fan-Sheet Impregnation.....</i>	98
4.1.1.4	<i>Sheet Drilling / Undrilled Application.....</i>	98
4.1.1.5	<i>Wet / Dry Applications.....</i>	98
4.2	Characterization.....	100
4.2.1	Fundamental Parameters.....	100
4.2.1.1	<i>Material Properties.....</i>	100
4.2.1.2	<i>Dowel Geometry.....</i>	101
4.2.1.3	<i>Fan Geometry.....</i>	102

4.2.1.4	<i>Global Geometry</i>	105
4.2.1.5	<i>Position</i>	107
4.2.1.6	<i>Configuration</i>	107
4.2.1.7	<i>Quality</i>	108
4.2.1.8	<i>Surrounding</i>	108
4.2.2	Pull-out Characterization	108
4.2.2.1	<i>Collapse Mechanisms</i>	108
4.2.2.2	<i>Ozbakkaloglu & Saatcioglu (2009)</i>	109
4.2.2.3	<i>Kim & Smith (2010)</i>	111
4.2.3	Shear Characterization	114
4.2.3.1	<i>Collapse Mechanism</i>	114
4.2.3.2	<i>Kobayashi et al. (2001)</i>	116
4.2.3.3	<i>Eshwar et al. (2008)</i>	118
4.2.3.4	<i>Orton et al. (2008)</i>	119
4.2.3.5	<i>Zhang & Smith (2013)</i>	120
4.2.3.6	<i>Brena & McGuirk (2013)</i>	124
4.2.3.7	<i>Berneschi (2015)</i>	126
4.2.3.8	<i>Sun et al. (2016)</i>	127
4.3	Strengthening Applications	129
4.3.1	Flexural Strengthening	129
4.3.1.1	<i>Lam & Teng (2001)</i>	129
4.3.1.2	<i>Piyong et al. (2003)</i>	130
4.3.1.3	<i>Eshwar et al. (2005)</i>	130
4.3.1.4	<i>Smith et al. (2011)</i>	131
4.3.1.5	<i>Smith et al. (2013)</i>	134
4.3.1.6	<i>Nardone et al. (2011)</i>	137
4.3.2	Shear Strengthening	137
4.3.3	Column & Joint Strengthening	137
5	EXPERIMENTAL PROGRAM	139
5.1	Material Characterization	139

5.1.1	Concrete	139
5.1.1.1	<i>Compressive Strength – ASTM C39.....</i>	139
5.1.1.2	<i>Derived Properties – ACI 318</i>	141
5.1.1.3	<i>Derived Properties – EC2.....</i>	141
5.1.1.4	<i>Design Properties.....</i>	143
5.1.2	Steel.....	144
5.1.2.1	<i>Tensile Strength – ASTM A370.....</i>	144
5.1.2.2	<i>Design Properties.....</i>	145
5.1.3	CFRP Sheet	148
5.1.3.1	<i>Dry Fibers</i>	148
5.1.3.2	<i>Epoxy.....</i>	148
5.1.3.3	<i>Impregnated Sheet</i>	149
5.1.3.4	<i>Bond Strength</i>	150
5.1.3.5	<i>Design Properties.....</i>	151
5.1.4	CFRP Anchor Spikes	152
5.1.4.1	<i>Dry Fiber & Epoxy.....</i>	152
5.1.4.2	<i>Pull-Out Characterization</i>	152
5.1.4.3	<i>Shear Characterization</i>	154
5.1.4.4	<i>Design Properties.....</i>	156
5.2	Specimens Preparation.....	160
5.2.1	Concrete Specimens.....	160
5.2.1.1	<i>Rebars Instrumentation</i>	160
5.2.1.2	<i>Molds Set-Up</i>	161
5.2.1.3	<i>Casting.....</i>	161
5.2.1.4	<i>Demolding.....</i>	161
5.2.1.5	<i>Sandblasting</i>	163
5.2.2	FRP Application	164
5.2.2.1	<i>Sheet Application</i>	164
5.2.2.2	<i>Drilling & Hole Preparation.....</i>	166
5.2.2.3	<i>Anchors Installation.....</i>	167
5.2.2.4	<i>Strain Gages Application.....</i>	170

5.3	Experimental Matrix	171
5.3.1	Unreinforced Sample.....	171
5.3.1.1	<i>Materials.....</i>	171
5.3.1.2	<i>Geometry</i>	172
5.3.2	Anchored Series	173
5.3.2.1	<i>Control Sample.....</i>	173
5.3.2.2	<i>Matching Series</i>	174
5.3.2.3	<i>Position Series.....</i>	175
5.3.2.4	<i>Number of Anchor Series</i>	176
5.3.2.5	<i>Sandwich Effectiveness Series.....</i>	177
5.3.3	Experimental Set-Up.....	178
5.3.3.1	<i>Load Application</i>	178
5.3.3.2	<i>Boundary Conditions.....</i>	179
5.3.3.3	<i>Deflection Measurement</i>	179
5.3.3.4	<i>Strain Measurement</i>	180
5.3.4	Final Matrix	182
5.3.4.1	<i>Geometry and Configurations.....</i>	182
5.3.4.2	<i>Load Cycles.....</i>	185
5.4	Preliminary Design	186
5.4.1	Conventions.....	186
5.4.2	Design Assumptions & Sectional Properties	186
5.4.2.1	<i>Stage I – Uncracked Elastic Section</i>	188
5.4.2.2	<i>Stage II – Cracked Elastic Section.....</i>	189
5.4.2.3	<i>Stage III – Cracked Inelastic Section.....</i>	190
5.4.3	Sectional Analysis	192
5.4.3.1	<i>Elastic Approach</i>	192
5.4.3.2	<i>Equilibrium Approach</i>	192
5.4.4	Structural Analysis.....	195
5.4.4.1	<i>Equilibrium – Point Load.....</i>	195
5.4.4.2	<i>Equilibrium – Self-Weight</i>	196
5.4.4.3	<i>Deflection – Euler-Bernoulli Beam Theory</i>	196
5.4.4.4	<i>Deflection – Timoshenko Beam Theory</i>	197

5.4.4.5	<i>Deflection – Strain-Based Approach</i>	197
5.4.4.6	<i>Deflection – Results Discussion</i>	199
5.4.5	Equivalent Ultimate Strain Approach	202
5.4.5.1	<i>End Debonding</i>	202
5.4.5.2	<i>Intermediate Debonding</i>	204
5.4.5.3	<i>Anchors’ Failure</i>	205
5.4.6	Balanced Section	208
5.4.6.1	<i>Internal Reinforcement Balance</i>	209
5.4.6.2	<i>External Reinforcement Balance</i>	210
5.4.7	Load Phases	211
5.4.7.1	<i>Cracking</i>	211
5.4.7.2	<i>Yielding</i>	212
5.4.7.3	<i>Intermediate Debonding</i>	212
5.4.7.4	<i>Anchors’ Failure</i>	213
5.4.7.5	<i>Sheet Rupture</i>	213
5.4.7.6	<i>Concrete Collapse</i>	214
5.4.7.7	<i>Steel Rupture</i>	214
5.4.7.8	<i>Results</i>	214
5.4.8	End Debonding Evaluation	217
5.4.8.1	<i>Optimal Development Length</i>	217
5.4.8.2	<i>Provided Development Length</i>	218
5.4.8.3	<i>End Debonding Check</i>	220
5.4.9	Shear Strength Evaluation	222
5.4.9.1	<i>Shear Strength – EC2</i>	222
5.4.9.2	<i>Shear Strength – ACI318</i>	223
5.4.9.3	<i>Shear Strength Check</i>	224
5.5	Data Analysis	225
5.5.1	Experimental Sectional Properties	225
5.5.1.1	<i>Neutral Axis Location</i>	225
5.5.1.2	<i>Flexural Stiffness</i>	225
5.5.2	Experimental Equivalent Ultimate Strain	226
5.5.2.1	<i>Backward Sectional Equilibrium</i>	226

5.5.2.2	<i>Solving the Non-Linear Implicit System</i>	227
5.5.3	Effectiveness and Efficiency Parameters	228
5.5.3.1	<i>Shear Effectiveness</i>	228
5.5.3.2	<i>Flexural Effectiveness</i>	229
5.5.3.3	<i>Flexural Efficiency</i>	230
5.5.4	Ductility Parameters	231
5.5.4.1	<i>Steel Strain Prospective</i>	231
5.5.4.2	<i>Deflection at Failure Prospective</i>	232
6	TEST RESULTS	233
6.1	Specimen Response	233
6.1.1	Unreinforced Sample	233
6.1.2	Control Sample	237
6.1.3	Matching Series	242
6.1.3.1	60x2	242
6.1.3.2	90x2	249
6.1.4	Position Series	255
6.1.4.1	90x2 L/4	255
6.1.4.2	90x2 L/3	262
6.1.5	Number of Anchors Series	269
6.1.5.1	90x3	269
6.1.6	Sandwich Effectiveness Series	275
6.1.6.1	Sx2-1	275
6.1.6.2	Sx2-2	283
6.2	Longitudinal Strain Shapes	288
6.2.1.1	C-CFRP.....	288
6.2.1.2	60x2	289
6.2.1.3	90x2	290
6.2.1.4	90x2 L/4	291
6.2.1.5	90x2 L/3	293
6.2.1.6	90x3	294

6.2.1.7	Sx2 – 1	296
6.2.1.8	Sx2 – 2	297
6.3	Results Recap	299
6.3.1.1	<i>Matching and Behavior</i>	299
6.3.1.2	<i>Effectiveness, Efficiency & Ductility Ratios</i>	303
6.4	Results Discussion	307
6.4.1	Behavior	307
6.4.1.1	<i>Slabs' behavior.....</i>	307
6.4.1.2	<i>Serviceability & Ultimate Limit States.....</i>	309
6.4.1.3	<i>Anchors' Failure</i>	309
6.4.1.4	<i>Strain Shapes over the Sheet's Width</i>	311
6.4.1.5	<i>Strain Shapes Over the Sheet's Length</i>	313
6.4.2	Design	314
6.4.2.1	<i>ULS Design</i>	314
6.4.2.2	<i>SLS Design</i>	315
6.4.3	Joint Characterization	316
6.4.3.1	<i>Strength Based Characterization</i>	316
6.4.3.2	<i>Strain Based Characterization</i>	317
6.4.4	Matching	318
6.4.4.1	<i>Load</i>	318
6.4.4.2	<i>Deflection.....</i>	319
6.4.4.3	<i>Stiffness.....</i>	319
6.4.4.4	<i>Strains</i>	320
6.4.5	Effectiveness.....	323
6.4.5.1	<i>At Increasing Joint's Strength</i>	323
6.4.5.2	<i>At Varying Anchors' Location.....</i>	325
6.4.5.3	<i>At Varying Anchor's Number</i>	331
6.4.5.4	<i>Sandwich Effectiveness.....</i>	332
6.4.5.5	<i>Defective installation</i>	334
6.4.5.6	<i>An Efficient Inspection Method.....</i>	336

7	CONCLUSIONS	339
8	APPENDICES	343
8.1	Appendix A: Units Conversion Table	343
8.2	Appendix B: Shear Tests on Sandwich Configurations	345
8.2.1.1	60x2 S – 1	345
8.2.1.2	90x2 S – 1	347
8.2.1.3	90x2 S – 2	349
8.3	Appendix C: PhD Project Proposal	351
8.4	Appendix D: Flexural Test Procedure	357
8.5	Appendix E: Hecht Bridge	371
8.6	Appendix F: Slabs’ Geometry	383
8.7	Appendix G: Strain Gages Locations.....	393
9	LIST OF FIGURES	405
10	REFERENCES.....	415

1 Abstract

Research into composite for external reinforcement and rehabilitation purposes has been going on for many years up to now; the confidence in implementing such solutions has increased and reliable design procedures are now available (CNR DT-200) (ACI 440). The main issue, pointed out thorough these years of research and field implementation, is premature failure due to debonding. The issue is particularly evident in flexure and severely undermine the efficiency and ductility of external reinforcement applications.

A proposed solution to counter debonding consists in mechanically anchoring the fiber sheet to the concrete substrate. A wide variety of anchoring devices has been proposed, but the most common solution, along with U-wrapping, is represented by anchoring spikes. These devices' effectiveness has been widely proved, both in research and field applications, though a quantitative approach is still in its early stages of development.

In order to develop a quantitative approach to anchors' design, firstly is required a reliable characterization for the single anchor's strength and a reliable model to describe a multiple anchors joint's behavior. Such a topic will be first approached from the compilatory point of view: organizing the already produced material and proposing a uniform, sound approach to the characterization issue.

Assessed the lack of reliable shear-characterizing models, a mixed experimental-analytical approach is developed, proposing an ultimate-load-derived *equivalent ultimate strain* as global characterizing parameter for the joint's shear strength.

Once a reliable joint characterization is available, in order to predict the strength increment provided by the chosen joint, a proper design algorithm is required. Such an algorithm can vice-versa be applied to compute the joint's strength, required to provide the system with the desired flexural strength enhancement.

A classical sectional analysis at ULS is proved to be effective, assuming the *joint-collapse equivalent ultimate strain*, instead of the CNR-defined intermediate debonding strain, as the FRP sheet's failure threshold. In developing such a characterization and design algorithm it was fundamental to evolve a clear understanding of the anchored system's overall behavior and specifically of the joints' role, deeply discussed in this dissertation.

Other issues were investigated as well: the anchors' spacing effect on the joint's coupled behavior, the effectiveness of a so-called sandwich configuration, the strain shapes over sheet's width and length, the consequences of an ill-installed solution. A cheap and easily-to-perform inspection method was developed and briefly discussed as well.

2 Introduzione

La ricerca nel campo dei compositi per rinforzo esterno, a scopi di riabilitazione, ha una lunga storia alle spalle; la fiducia in queste soluzioni è aumentata con il passare del tempo e affidabili codici di progettazione sono ora a disposizione dell'ingegnere (CNR DT-200) (ACI 440). Il problema principale, evidenziato nel corso di questi anni di ricerca e impiego sul campo, è il collasso prematuro dovuto a delaminazione del composito; particolarmente evidente nelle applicazioni a flessione e determinante nel limitare l'efficienza e la duttilità delle soluzioni di rinforzo esterno.

Una delle soluzioni proposte per ovviare al problema è rappresentata dall'ancoraggio meccanico della lamina di rinforzo al substrato di calcestruzzo. Un'ampia varietà di dispositivi di ancoraggio è stata proposta, ma tra i più comuni, insieme alla pratica dell'U-wrapping, vi sono certamente i cosiddetti fiocchi. L'efficacia di questa soluzione è stata ampiamente provata, sia a livello di ricerca che di applicazione sul campo, ma un approccio quantitativo è ancora nei primi stadi di sviluppo.

Al fine di sviluppare un approccio quantitativo, si richiede, per prima cosa, un affidabile metodo di caratterizzazione della resistenza a taglio del singolo ancoraggio, così come un modello che consenta di descrivere un giunto multi-ancoraggio. L'argomento verrà trattato inizialmente con approccio compilativo: organizzando il materiale già prodotto e proponendo un approccio ragionato e uniforme al problema della caratterizzazione.

Assodata la mancanza di affidabili modelli di caratterizzazione a taglio, si è provveduto a sviluppare un approccio misto sperimentale-analitico: proponendo una deformazione equivalente a collasso, derivata da valori di carico, come parametro caratterizzante la resistenza a taglio del giunto.

Una volta definito un affidabile approccio alla caratterizzazione, è richiesto lo sviluppo di un adeguato algoritmo di progettazione, al fine di predire l'incremento di resistenza fornito al sistema dal giunto selezionato. Lo stesso algoritmo può essere viceversa applicato al calcolo della capacità, richiesta all'ancoraggio, per incrementare la resistenza del sistema del valore desiderato.

Una classica soluzione a livello di analisi sezionale allo stato limite ultimo si è rivelata efficace, imponendo la deformazione equivalente di collasso del giunto come limite di collasso per la lamina di rinforzo esterno, in alternativa alla deformazione da delaminazione intermedia, calcolata secondo CNR DT-200.

Lo sviluppo di un efficace algoritmo di caratterizzazione e progetto non può prescindere da una piena comprensione del comportamento a collasso del sistema e del ruolo del giunto nell'economia globale, questione ampiamente discussa nella presente relazione. In aggiunta, altri argomenti sono stati analizzati: l'effetto della spaziatura tra gli ancoraggi nel determinare un comportamento accoppiato del giunto, l'efficacia della cosiddetta configurazione a sandwich (o patch, toppa), l'andamento delle deformazioni sulla larghezza della lamina e sullo sviluppo longitudinale, oltre alle conseguenze di una installazione mal eseguita. Infine, è stato sviluppato e brevemente discusso un metodo di ispezione tramite fotocamera termica, economico e facilmente applicabile.

3 Composites Materials: An Overview

A general overview of the composite world will be briefly discussed, touching all the basic topics needed to wittingly approach the main topic of this dissertation. An in-depth overview of anchor spikes will be later provided.

3.1 Historical Background

The broad idea of composites material has developed through the history of mankind since the very beginning: from the first caveman who realized how to combine the versatility of a workable piece of wood, with the durability and hardness of a sharpened flint stone, to the 50% fiber composites made 787 Dreamliner, a long way has passed and many were the steps in between.

3.1.1.1 Classical Building Applications

The use of straw and mud bricks by ancient Egyptians (4000 BC) and Israelites is well documented (Iyer and Sen, 1991) (Kaw, 2005) and conceptually very close to the modern idea of fiber-reinforced materials, characterized by a tensile resistant fiber enhancing the mechanical properties of a homogenizing matrix (e.g. dispersed fiber reinforced concrete, fiber reinforced polymers).

Two out of the three main building materials used nowadays are classifiable as composites and have been used by mankind for centuries:

- Concrete, as a mixture of cement, water and aggregates, was known to the Nabataeans (Arabia, 300 BC) (Gibson, 2002) and Ancient Romans (200 BC) (Vitruvius, 25 BC).
- Plywood, i.e. pieces of wood resin-glued at different angles, has been first used by Egyptians since 1500 BC (Kaw, 2005).

Steel, on the contrary, cannot be considered a composite, being an alloy, i.e. a solid solution in which the constituent materials can no longer be spotted and no longer maintain their original properties. Nonetheless, the idea of introducing steel resisting components inside a concrete element (1853 AD, Francois Coignet, France) gave birth to

the most widespread building material used nowadays: reinforced concrete, a combination of concrete (already a composite) and steel rebar.

3.1.1.2 Lighter and Stronger: The War Industry

The weapon industry has always been one of the main promotor for technological advances thorough the history of mankind. The need of a strong and light weapon, easily handle while horse-riding, leded the nomads of the Asiatic steppes to early develop the so-called Composite Bow: a combination of wood, bone and animal glue, wrapped with birch bark, that resulted in an extremely powerful, efficient and accurate weapon (Halpin & Halpin, 1992).

The weapon derived from the northern Asian laminated bows and dates back to around 2000 BC (Insulander, 2002) (Karpowicz, 2015) but its effectiveness was largely proved lately, during the 13th century, when Gengis Khan led its army of horse-mounted archers to conquer the largest empire the world has ever known.

The same request for strong and light materials characterized the aircraft industry (Nanni, 1999) since the II World War, when the first practical implementations of the newly invented Glass Fiber Reinforced Polymers (1935 AD, Owes Corning, USA) took place (Berneschi, 2015).

Since then many applications were developed in the defensive, automotive and aerospace industry; during the 70s, better plastic resins and new fibers were developed (aramid, boron and carbon) and since than the composite industry has been constantly growing (Kaw, 2005).

3.1.1.3 A Durable Solution for Civil Engineering

What was originally developed for military purposes to be light and strong, proved to be an ideal solution for durability-critical applications in civil engineering. Fiber Reinforced Polymers generally have worst mechanical properties compared to steel, but have the major advantage of being unrusting, meaning that a FRP structure, at least a carbon fiber one, has the potential of lasting virtually forever (Nanni, 1999). The mechanical and durability properties of FRP will be further discussed in the following.

During the last decades of the 20th century, reinforced concrete, once believed to be everlasting, showed all its durability limits related to rebar rusting and degradation. Steel structures as well require continuous inspections and interventions in order to maintain

their structural efficiency and expected strength. From this prospective, the adoption of a non-rusting material seems the ideal solution to the problem.

Even though some examples exist (Hollaway, 2009), a whole fiber structure is generally an unfeasible solution either from the mechanical and economical point of view. To overcome the problem, FRP applications in Civil Engineering has generally seen the material coupled with standard structural solutions, like concrete, timber, steel and masonry (Smith, 2010) (Nanni, 1999).

Namely, concrete appears to be the ideal coupling solution and two main applications are currently wide spreading:

- Internal Reinforcement: FRP rebar are currently used as reinforcing solution for newly built reinforced concrete structures (Nanni 1999, 2000). These structures have the potential to be almost everlasting – with service lives comparable to the great structures of the classical age – as none of the involved materials undergo severe time-related degradation processes. The internal application of FRP is not yet fully normed in the US and Europe, but the research has already showed the effectiveness of these solutions and a full implementation of the technology in standard buildings is getting closer and closer (Nanni 1999, 2000) (Nanni et al. 2014).
- External Reinforcement: internal applications are clearly inapplicable to structures already built and undergoing serious degradation, in this case the application of externally bond fibers is a well settled and reliable solution (Nanni 1999, 2000) although yet not fully exploited in terms of efficiency, mainly due to the debonding problem that will be fully discussed in the following. In this field, reliable design references are already available (CNR-DT 200 R1/2013) (ACI 440.2R-08) (ACI 440.7R-10) and the rehabilitation industry proves more confident in implementing these kind of solutions, made available as standardized systems (Nanni, 1999).

Along with the research proceeding in the field of FRP, new rehabilitation solutions have been proposed, namely FRCM (Fiber Reinforced Cementitious Matrix) that addresses the FRP flammability and conductivity problem at the cost of reduced mechanical properties, and SRG (Steel Reinforced Grout) that addresses the brittleness of the previous solutions, but reintroduce a metallic material with related rusting problems.

As the non-rusting property of polymers was never the most critical property in frequently inspected and maintained aerospace application, the need of super-light material has never been a critical issue in the civil engineering field. The implementation

of FRP in these so different fields is a clear example of the ability of modern engineering to adapt efficient solutions to new coming challenges.

3.2 Fiber Reinforced Polymers: Material Overview

A composite is a structural material that consists of two or more combined constituents that are combined at a macroscopic level and are not soluble in each other.

(Kaw, 2005)

The purpose of a composite material is to take the most from the combined materials minimizing their weakness. Even combined, the materials are clearly distinguishable and maintain their peculiar properties; this is the core difference between a composite and an alloy, in which the original materials combine to form a solid solution, meaning a new homogeneous material.

In the particular case of FRP, two are the components: a fiber-made *reinforcing phase* that gives the composite its mechanical properties of strength and stiffness, and a polymeric *matrix* – or resin – that gives continuity to the material, protect the fibers from damages, ensures fibers to stay aligned and, most important, allows stress distribution over adjacent fibers limiting the issue of localized failures (Nanni, 1999) (Kaw, 2005).

3.2.1 The Fibers

Different types of fibers are commercially available, ranging over different prices, mechanical and durability properties. Hereafter are analyzed ranking from the least to the best mechanically performing.

3.2.1.1 Glass Fibers (GFRP)

The first kind of fiber to be produced, usually manufactured from silica sand, glass is the cheapest and mechanically least performing solution, it is also the most widespread. It shows durability issues in application exposed to hot/wet cycles and highly alkaline environments (Nanni, 1999), it has poor fatigue performances and high sensitivity to

abrasion. Among the advantages, it provides good electrical isolation and thermal insulation (Nanni et al. 2014).

Being concrete a highly alkaline material, the occurrence of alkali-silica reaction in GFRP reinforced concrete can be a serious problem actually object of investigation, even though the existing applications are not showing degradation problems.

Glass fibers also show creep phenomena when subjected to constantly applied load, hence they are particularly suited for seismic upgrade applications, where the seismic load only engage the structure for a limited amount of time (Nanni, 1999).

Glass fibers are available in different grades, depending on the required properties, hereafter ranked from the least to the best mechanically performing: alkali-resistant (AR-Glass), Electrical (E-Glass), high-strength (S-Glass) (Nanni et al. 2014).

Basalt Fibers (BFRP)

Basalts fibers are slightly stronger and stiffer than standard E-glass (Nanni et al. 2014) (Fiore et al. 2015). They are manufactured from volcanic basalt rock, available all around the world and the manufacturing technique is less energy-consuming compared to E-glass (Nanni et al. 2014).

As glass fibers they maintain their properties of good thermal and electrical insulation, to these, a high heat stability and resistance to chemically active environment should be added. An additional property that may determine the basalt success in the future market is its high bio-solubility over medium-long terms, as bio-solubility is believed to guide future market demand (Nanni et al. 2014).

Research is currently ongoing to investigate and promote a full implementation of basalt fibers composite in the construction field (UM Structures & Material lab, Report Number IR-5.10_NRR_AC454/932). The chance to engineer the material properties modifying its chemical composition is a particularly interesting possibility (Nanni et al. 2014).

3.2.1.2 Aramid Fibers (AFRP)

Aramid is an aromatic polyamide organic fiber (Nanni et al. 2014), it is not widely used in civil engineering, even though its application in FRCM is spreading. Its most common commercial form is Kevlar, produced in three varieties: 29, 49 and 149.

It has mechanical properties in between Glass and Carbon, with the addition of an excellent impact resistance – hence why it is commonly applied to manufacturing of bulletproof vests (Nanni, 1999) – along with a low density, that grants it to be the best mechanically performing fiber per unit weight (Berneschi, 2015).

It is also a good thermal and electrical insulator, resistant to organic solvents, fuels and lubricant. Among the side effects a high UV sensitivity as well as poor durability performances in humid environment and when exposed to high temperatures. To give a clear idea, it is well known that bulletproof vests expire after in a couple of years.

3.2.1.3 Carbon Fibers (CFRP)

Carbon fiber is generally the best choice either for its superior mechanical properties, good performances under fatigue and permanent loads (no creep phenomena) and high resistance to most environmental conditions, either acid and alkaline (Nanni, 1999).

The better performances come for a high price: roughly a standard CFRP performs 3 times better than a GFRP counterparts, but also costs 10 times more (Nanni et al. 2014).

Apart for the high price, the main negative aspect is a low coefficient of thermal expansion that becomes eventually negative in the composite material (Ashraf et al. 2012). This can cause compatibility issues in case the structure is subjected to sensitive thermal gradients. Also the electrical conductivity can cause problem such as galvanic corrosion in steel-coupled solutions and the impact resistance is relatively low.

Carbon fibers are classified basing on the production technique, namely on the fiber precursor from which they are manufactured, that defines their mechanical properties. In the following the different typologies are ranked from the least stiff to the stiffest (Nanni et al. 2014).

- Rayon fibers precursors are used to produce Low Modulus carbon fibers.
- Polyacrylonitrile (PAN) precursors fiber are characterized by High Modulus and strength and are the most widespread in civil engineering applications.
- Pitch based fibers show an even higher modulus, but a lower strength. They are particularly suited for stiffness critical aerospace application.

Carbon fibers can have any kind of reinforcing application in civil engineering, but their cost makes them unfeasible solutions for standard reinforcement. They are preferred in application for which their superior stiffness is actually needed, as per pre-tensioned

application (Spadea, Rossini & Nanni, 2016) or external reinforcement purposes, as will be fully discussed in the following.

Table 2.1 Typical properties of glass, carbon, organic, boron, SiC, and ceramic fibers

Fiber	Modulus [Gpa]	Tensile Strength (*) [GPa]	Compression Strength [GPa]	Elongation [%]	Density [gr/cc]	Longitudinal Thermal Expansion [$10^{-6}/^{\circ}\text{C}$]	Transverse Thermal Expansion [$10^{-6}/^{\circ}\text{C}$]	Poisson Ratio	Thermal Conduct [W/m $^{\circ}\text{C}$]	Maximum Operating Temperature [$^{\circ}\text{C}$]	Resistivity [micro ohm-m]
E-Glass	72.345	3.45	–	4.4	2.5–2.59	5.04–5.4	–	0.22	1.05	550	–
S-Glass	85	4.8	–	5.3	2.46–2.49	1.6–2.9	–	0.22	1.05	650	–
C-Glass	69	3.31	–	4.8	2.56	6.3	–	–	1.05	600	–
D-Glass	55	2.5	–	4.7	2.14	3.06	–	–	–	477	–
Carbon											
T300	230	3.53	–	1.5	1.75	–0.6	7–12	0.2	3.06	–	18
M50	490	2.45	–	0.5	1.91	–	–	–	54.43	–	8
AS2	227	2.756	–	1.3	1.8	–	–	–	8.1–9.3	–	15–18
AS4-D	241	4.134	–	1.6	1.77	–0.9	–	–	8.1–9.3	–	15–18
IM6	275.6	5.133	–	1.73	1.74	–	–	–	8.1–9.3	–	15–18
HMS4	317	2.343	–	0.8	1.8	–	–	–	64–70	–	9–10
UHM	441	3.445	–	0.8	1.85	–	–	–	6.5	–	120
P55	379	1.9	–	0.5	2	–1.3	–	–	120	–	8.5
P100	758	2.41	–	0.32	2.16	–1.45	–	–	520	–	2.5
Kevlar 29	62	3.792	–	–	1.44	–	–	–	–	–	–
Kevlar 49	131	3.62	0.72	2.8	1.45	–2	59	0.35	0.04	160 (#)	–
Kevlar 149	179	3.62	0.69	1.9	1.47	–	–	–	–	–	–
Technora H	70	3	0.6	4.4	1.39	–6	59	0.35	–	160 (#)	–
Boron	400	2.7–3.7	6.9	0.79	2.57	4.5	0.2	0.2	38	315 (#)	–
SCS-6	427	2.4–4	–	0.6	3	4–4.8	–	0.2	10	–	–
Nextel 720	260	2.1	–	–	3.4	6	–	–	–	1200 (#)	–

Note: Typical data from product literature and other sources, some values estimated for broad class of materials. The designer is responsible for obtaining actual values. (*) See Table 2.2. (#) Long term temperature.

3.2.2 The Resins

Basing on their thermal behaviors, two different typologies of polymeric matrices can be defined: thermosetting and thermoplastic, with the former best suited for construction applications.

3.2.2.1 Thermosetting polymers

Are typically liquid at ambient temperature or low-melting point solid, they are cured thorough the introduction of a catalyst, using heat or with a combination of the two (Nanni et al. 2014). An increment in temperature cause the material to polymerize turning into a solid, the reaction is exothermic and once polymerized a thermosetting material cannot be returned to its original condition, posing a serious problem in terms of recycling (Berneschi, 2015).

The easiness to handle an ambient-temperature liquid material makes thermosetting resins the ideal solution for fiber impregnation (Nanni, 1999). The recycling issue is easily addressed considering that an FRP solution in civil engineering won't require to be disposed for decades at least, conforming to the philosophy that an "everlasting" solution can be as ecological as an easy disposable one and way cheaper in terms on energy consumption.

Thermosetting polymers are usually stronger than thermoplastic ones, thanks to a three dimensional network of bonds (Berneschi, 2015), thanks to their thermal hardening property they are better suited for high temperature application, but they are also flammable, so the temperature has always to be kept below a 70°C (160°F) limit (Nanni, 1999).

Among the properties of thermosetting resins can be numbered a good resistance to corrosive agents and solvents, good fatigue resistance, perfectly elastic properties, good adhesion with the fiber substrate and a clean finishing (Berneschi, 2015). Along with the flammability also a high sensitivity to UV has to be accounted for, requiring external applications to be properly sheltered (Nanni, 1999).

Three are the most commonly used typologies of thermosetting resins, ranging over different mechanical properties, prices and chemical properties:

- *Epoxies* are the best performing from the durability point of view (heat, humidity, acid, corrosive and caustic environments) and proved to be well performing from the mechanical point of view; they also show superior electrical insulation properties and good adhesion to the fiber substrate. They come with little shrinkage during curing and ease of processing. Epoxies are also versatile materials that can be mixed and blended with various additives and different resins in order to improve required properties or reduce the overall cost. Compatibility is guaranteed with glass, basalt, aramid and carbon fibers even though the high cost of the material makes epoxy solutions mainly applied to mechanically high performance, environmental resisting solution, such as external reinforcement applications. Along with the high cost, a slow curing is the main disadvantage of this kind of resins (Nanni et al. 2014).
- *polyesters* come with a lot of positive properties and can be chemically engineered in order to meet a wide range of requirements: mechanical properties, electrical properties, dimension stability during curing, heat insulation, UV resistance, fire retardancy, superior finishing. Styrene is added to

the polymer resin in order to enhance the viscosity of the uncured material. Among the advantages also a fast curing period and relatively low cost. The use of polyesters in the FRP industry is however discouraged because of a relatively low chemical resistance, compared to epoxies and vinyl esters (Nanni et al. 2014).

- *vinyl esters* show some of the advantages of epoxies, such as chemical resistance, along with viscosity and fast curing typical of polyesters. Vinyl esters doesn't reach mechanical properties of top-of-the-notch epoxies and polyesters, but guaranteed strength well aligned with average epoxies. The superior alkali resistance and good adhesion to glass fibers makes vinyl esters the first choice in GFRP manufacturing (Nanni et al. 2014).

3.2.2.2 Thermoplastic polymers

Are typically solid at ambient temperature and turns to viscous liquid as the temperature increase, undergoing an endothermic reaction.

The need to heat the resin before impregnation makes thermoplastic solutions difficult to apply in the FPR industry. Thermoplastic polymers are usually formed into shape and used to create a variety of products: PET for water bottles, Polypropylene for packaging containers, polycarbonate for safety goggles, PBT for toys, Vinyl for windows' frame and PVC for pipes (Berneschi, 2015).

Table 2.5 Typical properties of thermoplastic matrices

Thermoplastics	Tensile Modulus [GPa]	Tensile Strength [MPa]	Tensile Elong. [%]	Poisson Ratio	Thermal Expansion [$10^{-4}/^{\circ}\text{C}$]	Tg [$^{\circ}\text{C}$]	Tm [$^{\circ}\text{C}$]	Process Temp. [$^{\circ}\text{C}$]	Heat Deflection Temperature [$^{\circ}\text{C}$]	Fracture Toughness G _{IC} [KJ/m ²]	Density [gr/cc]
PEEK	3.24	100(*)	50	0.4	47	143	343	400	160	4.03	1.32
PPS	3.3	82.7	5	0.37	49	90	290	343	135	–	1.36
PSUL	2.48	70.3(*)	75	0.37	56	190	–	300	174	2.45	1.24
PEI	3	105(*)	60	0.37	56	217	–	343	200	2.8	1.27
PAI	2.756	89.57	30	0.37	36	243	–	300	274	3.5	1.4
K-III	3.76	102	14	0.365	–	250	–	–	–	1.9	1.31
LARC-TPI	3.72	119.2	5	0.36	35	264	325	343	–	1(**)	1.37

Note: Typical data from product literature and other sources; some values estimated for broad class of materials. The designer is responsible for obtaining actual values. (*) Yield point. (**) Extrapolated value.

3.2.3 The Industry, Chemistry and Production Process

Limiting to the two materials composing the structural system on which this research focuses, their physics, chemistry and production process will be discussed, along with an industrial historic background. This section largely refers to Berneschi (2015), Nanni (1999), Nanni et al. (2014).

3.2.3.1 Carbon Fibers

Carbon fiber is a material composed by fibers about 5-10 μm in diameter. The carbon atoms are bonded together in crystals that are aligned to the major axis of the fiber. This provides the carbon fiber a high resistance per unit volume. The atomic structure of carbon fiber is similar to that of graphite; it consists in sheets of carbon atoms arranged in a regular hexagonal pattern. Thousands of fibers are then bundle together and woven to create a fabric.

The first one that was able to develop carbon fibers was Thomas Edison in 1879, who used an all-carbon fiber filament to create the first incandescent light bulb. He generated carbon fiber by carbonizing cotton threads or bamboo slivers at high temperature in a controlled atmosphere. The result was a material able to conduct electricity. The process used by Edison is still followed today and it is called pyrolysis.

At the end of the 1950' Rayon became the first precursor used to create modern fibers, obtaining high tensile strength carbon fibers. Ultimately, Rayon was replaced by more effective materials such as polyacrylonitrile (PAN) and pitch. Carbon fibers became commercially available just at the end of the 1960', representing a breakthrough in really high performance, low-density material production.

As discussed PAN based fibers are the most suited to civil engineering applications. There are typically five steps in the manufacturing of carbon fiber PAN-based.

1. The first phase is the so-called spinning, in which the polyacrylonite is mixed with other ingredients and spun into fiber, which are washed and stretched. This operation allows a better chain orientation and, consequently, better mechanical properties.
2. The second step is the stabilization of the fibers. Before the fibers are carbonized, they need to be chemically altered to convert their linear atomic bonding to a more thermally stable ladder bonding. This operation is done by heating the

fibers in air to 200-300°C for 30-120 min; the fibers pick up oxygen molecules from the air and rearrange their atomic pattern. During this operation the fibers change color from white to yellow to brown and finally to black.

3. After the fibers are stabilized, they are heated to a temperature of about 1000-3000°C for several minutes in an inert atmosphere. The lack of oxygen prevents the fibers from burning in the very high temperature. This operation is called carbonization; the precursor fibers are transformed into carbon fibers and the impurities are eliminated.
4. After carbonizing, the fibers have a surface that does not allow a good bonding with epoxy resins and other matrix materials. To provide better bonding properties, fibers' surface is slightly treated by oxygenation. The addition of oxygen atoms gives to the surface better chemical and mechanical properties; the treatment critically enhances the interlaminar properties at the fiber-epoxy interface.
5. The last step is the so-called called sizing; in this phase the fibers are coated to protect them from damages during winding or weaving. The coating materials are chosen to be compatible with the adhesive used to form the composite material

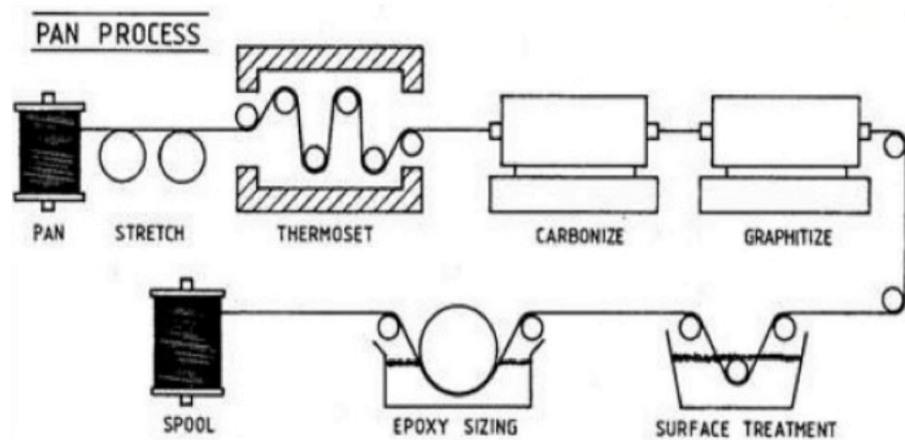


FIGURE 1 – CARBON FIBERS PRODUCTION PROCESS (BERNESCHI, 2015)

3.2.3.2 Epoxy Resin

Epoxy resins are the most commonly used thermoset plastic in polymer matrix composites. This polymer was synthesized for the first time in the early 1900' but it was commercialized in the late 1930'. The primary industrial application of epoxy resin was

in the coating, due to its high resistance to chemicals, durability and toughness. Later epoxy started to be used to encapsulate electrical and electronic component, due to its resistance and durability at high temperature and high electrical resistance.

Nowadays, epoxies are used to create tools, in spite of metal and wood. The main applications though see epoxy used as a two phase adhesive for the most various purposes, from home applications to industrial ones, due to the material properties scalability. In the construction field epoxy is largely used as a structural adhesive, linking metal, wood, FRP in place of rivets, bolts and welds.

Epoxy resins must be cross-linked in order to develop required characteristics. This cross-linking process is achieved by chemically reacting the resin with itself, through catalytic homopolymerisation, or with a wide range of co-reactants including polyfunctional amines, acids, phenols, alcohols and thiols. These co-reactants are often referred to as hardeners or curatives, and the crosslinking reaction is commonly referred to as curing. Epoxy resin does not give off reaction products during the curing period and so it has low cure shrinkage and no volatiles release that can lead to voids.

Different types of Epoxy resins can be created just using different types of materials as curing agents. For example, the chemistry can be adjusted to perfect the molecular weight or viscosity as required by the end use, the curing rate can be modified from very fast (second) to slow (hours) or one can obtain the final desired properties from soft, flexible compositions to hard, tough materials. Nowadays two-part epoxies adhesives for home, shop or hobby are available in stores and present a wide range of properties, depending on the final use.

Chemically speaking, epoxy resins are defined as low molecular weight pre-polymers or higher molecular weight polymers, characterized by the presence of at least two epoxide groups - sometimes referred to as a glycidyl or oxirane group - at the ends of a long chain-like molecular structure, similar to vinyl ester. The reactive groups of molecules in the epoxy resin formulations are the terminal epoxide groups and the hydroxyl groups. It is important to underline the fact that the absence of the ester groups makes epoxy resins a really good waterproof material.

The presence of two aromatic rings at the center of the epoxy molecule is critical in providing epoxy its ability to absorb either mechanical and thermal stresses, hence providing toughness, stiffness and heat resistance properties to the material.

Focusing on the curing process, the different between epoxies and polyester resins is that epoxies are generally cured by adding a hardener, often an amine, rather than a

catalyst. This meaning that either epoxy and hardening agent are involved in a new chemical reaction, different from homopolymerization.

Amines are organic groups containing a nitrogen atom linked to two hydrogen atoms (-NH₂). During curing, the active hydrogen of the amine is what reacts with the epoxide groups. The structure of the amine-containing organic compound and the number and type of amine groups in the compound is what determine the rate of cross-linking. This phase is fundamental for the epoxy to develop its mechanical properties: the two epoxy groups bind to the amine forming a complex three-dimensional molecular structure.

The involved molecules react at a fixed ratio, it is critical to define and respect the mix ratio in order to have a complete reaction. If reagents are not balanced, unreacted epoxy or hardener will remain inside the matrix, affecting the final material's properties. Every epoxy producing company have to provide the exact mixing ratio for each product, by weight and/or by volume.

The three most common type of epoxy resins are *cycloaliphatic resin*, *epoxidized oil* and *glycidated resin*, with the last one most largely used in commercial applications.

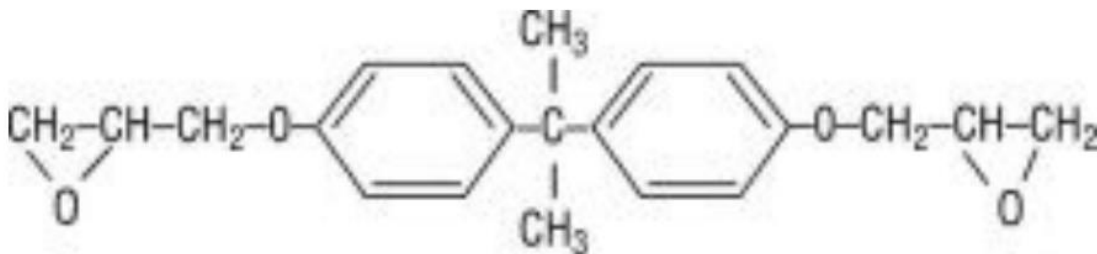


FIGURE 2 – EPOXY'S MOLECULAR STRUCTURE (BERNESCHI, 2015)

3.3 FRP Laminates for Rehabilitation Purposes

FRP shapes and manufacturing depends on the final application, in the civil field they are most commonly found as laminates for external application and rebar for internal reinforcement.

An FRP laminate typically consists of several million of thread-like fibers, embedded in a resin matrix. The most common solutions in civil engineering are mono-directional laminates, fiber-reinforced only in the principal direction; also bi-directional laminates

can be found and even balanced solutions in which the two main directions are evenly reinforced in order to guarantee the same level of strength and stiffness.

FRP laminates are applied to the external surface of existing structures, similar to steel plate bonding, FRP laminate bonding involves adhering a thin, flexible fiber sheet to the concrete surface with a thermoset resin. This technique, known as *manual lay-up*, may be used to increase the shear and flexural capacity of beams and slabs and to increase confinement in columns. This solution does not add significant dead load to the structure, and may be installed in a relatively short period of time (Nanni, 2000).

Carbon fibers FRP are the standard and most applied solution in the repairing and retrofitting industry, thanks to their durability performance and their stiffness. It must be noticed that additional reinforcement on an already existing structure can be engaged only if the structure experience additional deflection: the stiffer the applied material, the higher the engagement at equal displacement.

Matrix-wise speaking, epoxy is the preferred solution for rehabilitation application, thanks to its good mechanical properties and superior durability in a wide range of environments (Nanni, 1999).

3.3.1 Mechanical Behavior

FRP laminates are anisotropic, linear elastic until failure and characterized by a high tensile strength in the direction of the reinforcing fibers.

(Nanni, 1999)

The properties of the overall material depend on the layout of the carbon fiber and the proportion of fibers with respect to the polymeric matrix. It is fundamental to always remember that the mechanical properties – namely strength and stiffness – of the pure fiber are generally way higher than the mechanical properties of the composite material, while the matrix has ultimate strains higher than the composite itself (CNR, 2013).

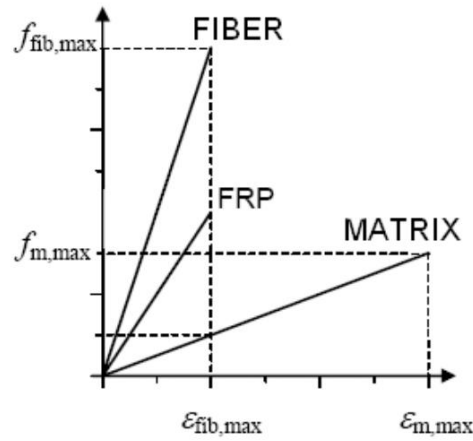


FIGURE 3 – FIBERS, EPOXY & COMPOSITE’S PROPERTIES COMPARISON (CNR, 2013)

Table 2-1 – Comparison between mechanical properties of a pre-cured laminate and fibers.

Pre-cured systems	Modulus of elasticity [GPa]		Ultimate strength [MPa]		Ultimate strain [%]	
	FRP E_f	Fiber E_{fib}	FRP f_f	Fiber f_{fib}	FRP ϵ_{fu}	Fiber $\epsilon_{fib,u}$
CFRP (low modulus)	160	210-230	2800	3500-4800	1.6	1.4-2.0
CFRP (high modulus)	300	350-500	1500	2500-3100	0.5	0.4-0.9

Table 1.1 Typical properties of unidirectional composites

Property	E-Glass/ Epoxy	S-Glass/ Epoxy	E-Glass/ Isophthalic Polyester	Kevlar 49/ Epoxy	Carbon/ Epoxy AS4/3501-6	Carbon/ Epoxy T800/3900-2	Carbon/ Epoxy IM7/8551-7	Carbon/ PEEK AS4/APC2	Carbon/ Polyimide AS4/ AvimidK-III
Density [g/cc]	2.076	1.993	1.85	1.380	1.58	–	–	1.6	–
Longitudinal Modulus E_1 [GPa]	45	55	37.9	75.8	142	155.8	151	138	110
Transverse Modulus E_2 [GPa]	12	16	11.3	5.5	10.3	8.89	9.0	10.2	8.3
Inplane Shear Modulus G_{12} [GPa]	5.5	7.6	3.3	2.07	7.2	5.14	5.6	5.7	–
Poisson's Ratio ν_{12}	0.19	0.28	0.3	0.34	0.27	0.3	0.3	0.3	–
Longitudinal Tensile Strength F_{1t} [MPa]	1020	1620	903	1380.0	1830	2698	–	2070	–
Transverse Tensile Strength F_{2t} [MPa]	40	40	40	34.5	57	–	–	86	37
Inplane Shear Strength F_6 [MPa]	60	60	40	44.1	71	–	–	186	63
Longitudinal Compressive Strength F_{1c} [MPa]	620	690	357	586.0	1096	1691	–	1360	1000
Transverse Compressive Strength F_{2c} [MPa]	140	140	68	138.0	228	–	–	–	–
Intralaminar Shear Strength (F_4 or F_5) [MPa]	60	80	76	48.69	–	–	–	150	–
Longitudinal Tensile Strain ϵ_{1t} [%]	2.3	2.9	2.4	1.8	1.29	1.68	1.64	1.45	–
Longitudinal CTE α_1 [$10^{-6}/^\circ\text{C}$]	3.7	3.5	6.5	–2.0	–0.9	–	–	0.5	–
Transverse CTE α_2 [$10^{-6}/^\circ\text{C}$]	30	32	22	60	27	–	–	30	–
Longitudinal moisture expansion β_1	0	0	0	0.01	0	0.0095	–	–	–
Transverse moisture expansion β_2	0.2	0.2	0.2	0.2	0.2	0.321	–	–	–
Fiber Volume Fraction V_f [%]	60	60	50	60	60	–	57.3	61	–
Void Content V_v [%]	–	–	2.0	–	–	–	0.1	–	0.5
Fiber Misalignment Ω [deg]	–	–	3.53	–	–	–	–	–	–

The presence of the polymeric matrix is fundamental in order to redistribute the load among adjacent fibers:

- *Unimpregnated Fibers.* If a single fiber breaks, the load is equally redistributed among the remaining fibers in the bundle. This behavior is commonly referred to as *Equal Load Sharing* (Phoenix and Taylor 1973).
- *Impregnated Fibers.* If a single fiber breaks, the load distribution is restrained by the matrix: the overload is carried by the fibers nearest to the broken fiber, then the stress is redirected back to the broken fiber by plain shear interaction with the matrix at the interface (Harlow and Phoenix 1978). This behavior critically reduces the brittleness of the system, allowing broken fibers to still contribute to the overall strength and stiffness until large scale ruptures occur.

In other words, the presence of the matrix allows adjacent fibers to interact in shear. The main consequence reflects in the ability of a polymeric material to redistribute localized stress peaks among less loaded fibers, preventing localized failure in the system.

As a result, a dry fiber bundle, theoretically way stronger, usually experiences earlier failures with respect to an impregnated counterpart, because of the occurrence of localized stress concentration that the material is unable to distribute among the rest of the fibers.

3.3.2 Elastic Response

- I. *Elastic Material up to failure.* This hypothesis is rigorously fulfilled and the stress-strain relation is fully defined by the Hook's Law.
- II. *Homogeneous Material.* Fiber reinforced polymers are heterogeneous by definition, as largely discussed. The heterogeneity, however, can be neglected looking at the material behavior from a macromechanical point of view.
- III. *Transversally Isotropic Material.* *The material's anisotropy cannot be neglected, but some degree of symmetry exists, being the material isotropic in the plane normal to the fiber direction.*
- IV. *Asymmetric Material: Only Working in Tension.* The material's response is not symmetric, with higher stiffness and ultimate strength in tension, rather than in compression. The asymmetry characterization can be avoided, assuming laminates working only in tension. The assumption is in line with guidelines

provisions (CNR, 2013) (ACI, 2008) to avoid applications where laminates are to carry compression.

This section largely refers to CNR – APPENDIX C (2013) and Kaw (2005). The homogeneity assumption allows to write a single elastic matrix for the whole system, without the need of separately characterize the components and add compatibility boundary conditions at the materials' interface. The isotropy assumption allows to reduce the number of independent constant required to fully characterize the 3D system (in tension) from 21 to 5, namely:

- E_1 Elastic Modulus in the fibers direction
- E_2 Elastic Modulus in the transversal plane
- ν_{12} Poisson Ratio linking longitudinal and transversal stains
- ν_{23} Poisson Ratio in the transversal plane
- G_{12} Shear Modulus

The elastic matrix of such a material is hereinafter reported:

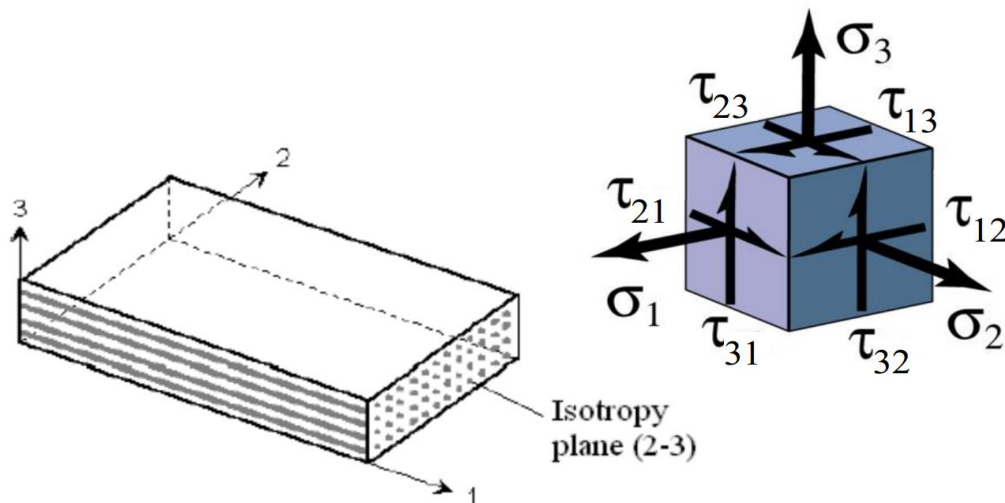


FIGURE 4 – STRESSES' CONVENTION (CNR, 2013)

$$\begin{bmatrix} \varepsilon_1 \\ \varepsilon_2 \\ \varepsilon_3 \\ \gamma_{12} \\ \gamma_{13} \\ \gamma_{23} \end{bmatrix} = \begin{bmatrix} \frac{1}{E_1} & -\frac{\nu_{12}}{E_1} & -\frac{\nu_{12}}{E_1} & 0 & 0 & 0 \\ -\frac{\nu_{12}}{E_1} & \frac{1}{E_2} & -\frac{\nu_{23}}{E_2} & 0 & 0 & 0 \\ -\frac{\nu_{12}}{E_1} & -\frac{\nu_{23}}{E_2} & \frac{1}{E_2} & 0 & 0 & 0 \\ 0 & 0 & 0 & \frac{1}{G_{12}} & 0 & 0 \\ 0 & 0 & 0 & 0 & \frac{1}{G_{12}} & 0 \\ 0 & 0 & 0 & 0 & 0 & \frac{2(1+\nu_{23})}{E_2} \end{bmatrix} \begin{bmatrix} \sigma_1 \\ \sigma_2 \\ \sigma_3 \\ \tau_{12} \\ \tau_{13} \\ \tau_{23} \end{bmatrix}$$

A complete 3D description is required for general shaped FRP, for example to fully describe the mechanical response of the FRP anchors spikes fully discussed in the following. A 2D description is generally sufficient to fully define the response of a laminate, given the additional hypothesis of plane stress state.

- V. *Plane Stress State.* If there are no loads transversally acting on the plate, the normal and tangential stresses on the upper and lower faces (σ_3 , τ_{13} , τ_{23}) are rigorously zero. If the plate is thin, these stresses can be assumed constant on the thickness and equal to zero everywhere.

This reduces to 4 the material's constant and reduces the matrix's dimensions to 3x3.

$$\begin{bmatrix} \varepsilon_1 \\ \varepsilon_2 \\ \gamma_{12} \end{bmatrix} = \begin{bmatrix} \frac{1}{E_1} & -\frac{\nu_{12}}{E_1} & 0 \\ -\frac{\nu_{12}}{E_1} & \frac{1}{E_2} & 0 \\ 0 & 0 & \frac{1}{G_{12}} \end{bmatrix} \begin{bmatrix} \sigma_1 \\ \sigma_2 \\ \tau_{12} \end{bmatrix}$$

$$\begin{bmatrix} \sigma_1 \\ \sigma_2 \\ \tau_{12} \end{bmatrix} = \begin{bmatrix} \frac{E_1}{1 - \nu_{12}^2} & \frac{\nu_{12} E_1}{1 - \nu_{12}^2} & 0 \\ \frac{\nu_{12} E_1}{1 - \nu_{12}^2} & \frac{E_2}{1 - \nu_{12}^2} & 0 \\ 0 & 0 & G_{12} \end{bmatrix} \begin{bmatrix} \varepsilon_1 \\ \varepsilon_2 \\ \gamma_{12} \end{bmatrix}$$

It is worth considering that, from a flexural designing point of view, an FRP plate can be modelled as a unidirectional element, exactly as a standard rebar, neglecting the response in the transversal plane. Following this approach, only the elastic modulus in the fiber's direction is required to fully characterize the system:

$$\sigma_1 = E_1 \varepsilon_1$$

Finally, it is worth noticing that the elastic response and parameters characterizing a lamina depends on the loading angle with respect to the direction of the fibers. In civil engineering application with fiber diagonally or transversally loaded are however uncommon, refer to Kaw (2005) for a complete characterization of the issue.

3.3.3 Failure Criteria

Different failure criteria have been proposed, from simple maximum stress and strain decoupled formulation, to more complex and accurate ones deduced from Von Mises and Beltrami classical formulations for isotropic materials. This section largely refers to Jones (1998), Kaw (2005) and CNR – APPENDIX C (2013).

3.3.3.1 Maximum Strength Criterion

Assuming a fully decoupled behavior, the laminate failure happens when one of the stresses inside the material exceeds its maximum allowable value, measured through a pure tension, shear or compression load test.

The maximum strength criterion, along with its close relative, the Maximum Strain Criteria, allows to characterize the different material behavior in tension and compression, but doesn't consider the interaction between stresses of different nature. As a consequence, the results provided are close to the experimental ones only in decoupled situations.

The formulation of the maximum strength criteria, clearly points out how the ultimate strength of a composite laminate could be described basing on a minimum of 5 constant parameters, namely the material's strength in each direction of loading.

One more parameter is needed in case of transversally isotropic 3D composites to account for in plane shear strength. More refined criteria may require a higher number of parameters.

$$-\sigma_{1u}^c < \sigma_1 < \sigma_{1u}^t$$

$$-\sigma_{2u}^c < \sigma_2 < \sigma_{2u}^t$$

$$-\sigma_{2u}^c < \sigma_3 < \sigma_{2u}^t$$

$$|\tau_{12}| < \tau_{12u}$$

$$|\tau_{13}| < \tau_{12u}$$

$$|\tau_{23}| < \tau_{23u}$$

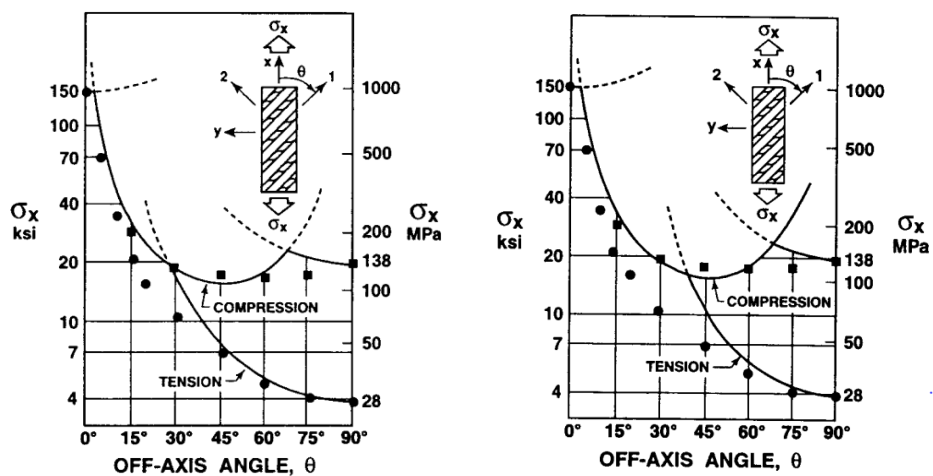


FIGURE 5 - MAXIMUM STRENGTH (A) & STRAIN (B) CRITERIA AT VARYING LAMINA ORIENTATION (JONES, 1998)

3.3.3.2 Tsai-Hill Failure Criterion

Hill adapted the classical Von Mises criterion to anisotropic material, while Tsai specialized it to the case of a unidirectional lamina (Kaw, 2005). Being the criterion based on the distortion energy as failure trigger, it does not account for isotropic failures. Also, the criterion does not allow to differentiate the strength in tension from the one in compression, limiting the applicability to tension-only situation. The interaction between stresses of different nature is well accounted for and the results are well in agreement with the experimental ones in the covered situations. The criterion has the following general quadratic expression for anisotropic 3D materials.

$$G_1(\sigma_2 - \sigma_3)^2 + G_2(\sigma_3 - \sigma_1)^2 + G_3(\sigma_1 - \sigma_2)^2 + 2G_4\tau_{23}^2 + 2G_5\tau_{13}^2 + 2G_6\tau_{12}^2 < 1$$

Reducing to a 2D laminate situation:

$$G_1\sigma_2^2 + G_2\sigma_1^2 + G_3(\sigma_1 - \sigma_2)^2 + 2G_6\tau_{12}^2 < 1$$

The G parameters can be related to the material's strength parameters writing down the collapse criterion in particular collapse situations, as follows:

$$G_1 = \frac{1}{2} \left(\frac{2}{[\sigma_{2u}^t]^2} - \frac{1}{[\sigma_{1u}^t]^2} \right)$$

$$G_2 = \frac{1}{2} \left(\frac{1}{[\sigma_{1u}^t]^2} \right)$$

$$G_3 = \frac{1}{2} \left(\frac{1}{[\sigma_{1u}^t]^2} \right)$$

$$G_6 = \frac{1}{2} \left(\frac{1}{[\tau_{12u}]^2} \right)$$

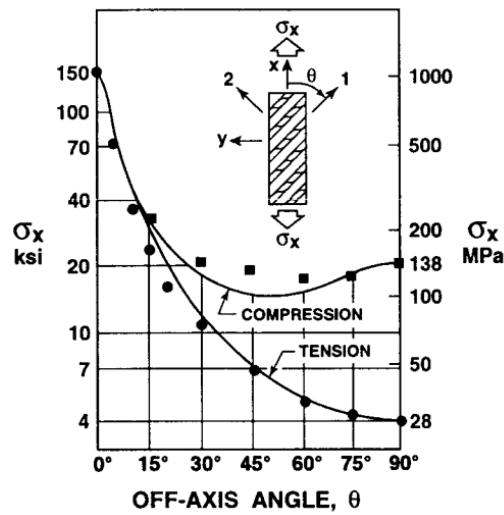


FIGURE 6 - TSAI-HILL CRITERION AT VARYING LAMINA ORIENTATION (JONES, 1998)

3.3.3.3 Tsai-Wu Failure Criterion

Approaching the problem from a wide prospective, Tsai and Wu postulated that a failure surface in the six-dimensional stress space can be defined using the tensor form (Jones, 1998):

$$\underline{H}^T \underline{\sigma} + \underline{\sigma}^T \underline{H} \underline{\sigma} = 1$$

The criterion is based on the total strain energy failure theory of Beltrami (Kaw, 2005), applied to a 2D lamina in plane stress condition it assume the simpler form:

$$H_1\sigma_1 + H_2\sigma_2 + H_6\tau_{23} + H_{11}\sigma_1^2 + H_{22}\sigma_2^2 + H_{66}\tau_{12}^2 + 2H_{12}\sigma_1\sigma_2 < 1$$

The criterion grants the best data fit, modeling very well the stress coupling effect; it also accounts for the different behavior in tension and compression, thanks to its higher number of independent parameters. Finally, its tensor form allows for an easy handling from the computational point of view.

Most of the H parameters can be defined similarly as per Tsai-III as follows:

$$H_1 = \frac{1}{\sigma_{1u}^t} - \frac{1}{\sigma_{1u}^c}$$

$$H_2 = \frac{1}{\sigma_{2u}^t} - \frac{1}{\sigma_{2u}^c}$$

$$H_6 = 0$$

$$H_{11} = \frac{1}{\sigma_{1u}^t \sigma_{1u}^c}$$

$$H_{22} = \frac{1}{\sigma_{2u}^t \sigma_{2u}^c}$$

$$H_{66} = \frac{1}{[\tau_{12u}]^2}$$

While the H_{12} terms requires a difficult-to-perform biaxial test in which the failure biaxial tension σ_{12u} is applied to both principal directions:

$$H_{12} = \frac{2}{\sigma_{12u}^2} - \frac{H_1 + H_2}{\sigma_{12u}} - \frac{1}{2} (H_{11} + H_{22} + H_{66})$$

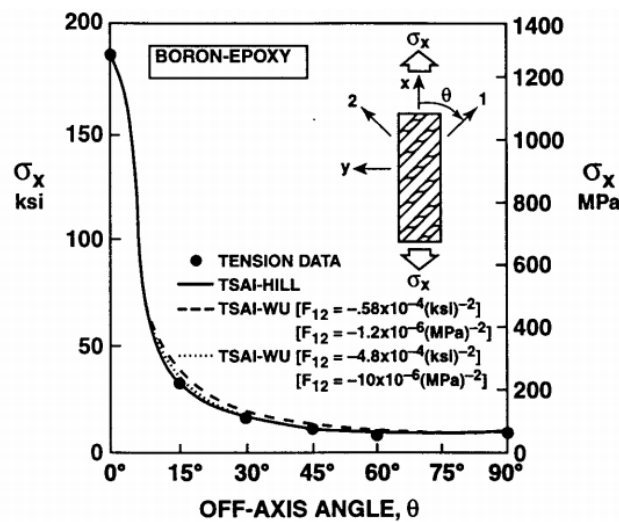


FIGURE 7 - TSAI-WU CRITERION AT VARYING LAMINA ORIENTATION (JONES, 1998)

3.3.3.4 Summing Up

As discussed, the simple Maximum Stress and Strain Criteria guarantee a good agreement only in decoupled situation, i.e. laminates loaded at low or high angle with respect to the fiber direction ($\theta < 15^\circ$, $\theta > 45^\circ$) (Kaw, 2005).

Tsai-III criterion offers good data matching without the need of performing a complex biaxial test to set up the model. Tsai-Wu represent the best option from the accuracy, wide applicability and easy handling point of view, but it is not really needed to implement such a model in tension-only applications.

An intermediate solution, proposed by Narayanaswami & Adelman (1977) is to apply the easy-handling Tsai-Wu criterion assuming H_{12} simply equal to zero, or using an empirical formulation derived from different criterion (Jones, 1998).

It is worth noticing that from the bending design point of view, only the strength of the lamina in its main direction is required, recalling a mono-dimensional rebar-like model; hence the collapse criteria applied to a bending application can be reduced to, using the common notation in civil engineering.

$$\sigma < f_{fu}$$

3.3.4 Lamina Orientation

The loading direction not always coincide with the fibers' one. For the sake of nomenclature, the fiber-related reference system is generally defined as *local*, being specific to each lamina of a hypothetic multilayer bundle; while the loading reference system is referred to as *global*, being the same for all the laminates in the bundle.

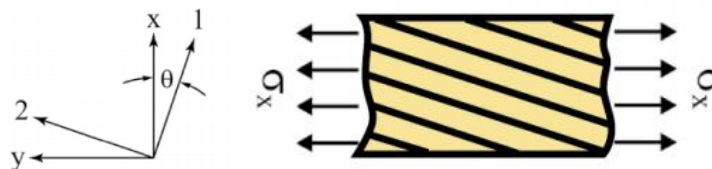


FIGURE 8 - CONVENTIONS FOR LAMINA ORIENTATION

3.3.4.1 Hooke's Law for an Angle Lamina

Focusing on a bi-dimensional lamina, transformation matrix can be easily introduced into the elastic stress-strain relation as follows:

$$\begin{bmatrix} \sigma_1 \\ \sigma_2 \\ \tau_{12} \end{bmatrix} = \underline{\underline{T}} \begin{bmatrix} \sigma_x \\ \sigma_y \\ \tau_{xy} \end{bmatrix}$$

$$\begin{bmatrix} \varepsilon_1 \\ \varepsilon_2 \\ \gamma_{12} \end{bmatrix} = \underline{\underline{R}} \underline{\underline{T}} \underline{\underline{R}}^{-1} \begin{bmatrix} \varepsilon_x \\ \varepsilon_y \\ \gamma_{xy} \end{bmatrix}$$

being T the transformation matrix and R the so-called Reuter matrix (Reuter, 1971) accounting for the difference between engineering and mathematical shear strain ($\gamma_{12} = 2\varepsilon_{12}$).

$$\underline{\underline{T}} = \begin{bmatrix} c^2 & s^2 & 2sc \\ s^2 & c^2 & -2sc \\ -sc & sc & c^2 - s^2 \end{bmatrix}$$

$$\underline{\underline{R}} = \begin{bmatrix} 1 & 0 & 0 \\ 0 & 1 & 0 \\ 0 & 0 & 2 \end{bmatrix}$$

Introducing the previous relations in the standard stress-strain relation, the stiffness matrix in x, y coordinates can be defined.

$$\begin{bmatrix} \sigma_x \\ \sigma_y \\ \tau_{xy} \end{bmatrix} = \underline{\underline{T}}^{-1} \underline{\underline{K}} \underline{\underline{R}} \underline{\underline{T}} \underline{\underline{R}}^{-1} \begin{bmatrix} \varepsilon_x \\ \varepsilon_y \\ \gamma_{xy} \end{bmatrix}$$

$$\underline{\underline{\sigma}}_{xy} = \underline{\underline{K}}_{xy} \underline{\underline{\varepsilon}}_{xy}$$

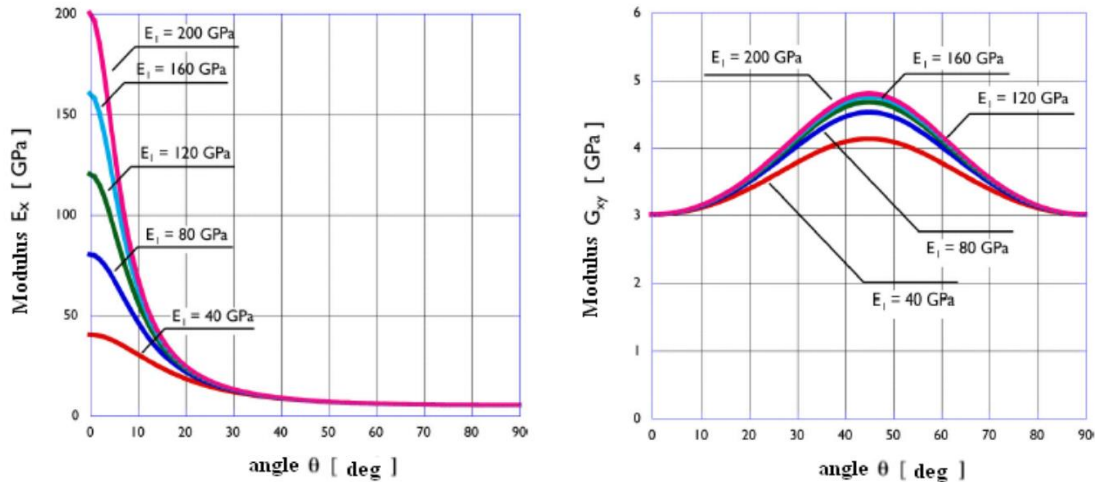


FIGURE 9 - MECHANICAL PROPERTIES AT VARYING LAMINA ORIENTATION (CNR, 2013)

3.3.4.2 Failure Criteria for an Angle Lamina

Two are the alternatives: to define the strength parameters for the lamina at varying θ (CNR, 2013) or to always check the material strength in terms of local stresses and strains (Kaw, 2005). The second one is way more feasible from the point of view of experimental results required to characterize a lamina. To compute the local stresses and strains given the global ones refer to the equation reported in the previous paragraph.

It is worth underlining that angled laminas are not commonly used for bending reinforcement in civil engineering applications.

3.3.5 Mechanical Characterization

3.3.5.1 Micromechanics

Knowing the mechanical properties of the single components and knowing the fiber to overall volume ratio, it is possible to apply a simple micromechanical approach, known as the *Rule of Mixtures* (CNR, 2013), to the characterization of a mono-directional laminate.

The approach is reliable in terms of stiffness characterization, either for Young Modulus in the main direction and Poisson's Ratio. The Young modulus in the secondary direction can be assumed equal to the one of the matrix only, not having fibers in the secondary direction.

$$E_1 = \frac{V_{fib}}{V_{tot}} E_{fib} + \left(1 - \frac{V_{fib}}{V_{tot}}\right) E_{mat}$$

$$\nu_{12} = \frac{V_{fib}}{V_{tot}} \nu_{fib} + \left(1 - \frac{V_{fib}}{V_{tot}}\right) \nu_{mat}$$

$$E_2 = E_{mat}$$

The approach is way less reliable in characterizing the laminate strength.

$$f_{fu} \approx \frac{V_{fib}}{V_{tot}} f_{fib} + \left(1 - \frac{V_{fib}}{V_{tot}}\right) f_{mat}$$

The solution can be applied anyway as a first approximation of the expected material properties, basing on the tested characteristic of each components or on the properties guaranteed by the manufacturer.

3.3.5.2 Direct Testing

A direct laminate test is the preferred approach to characterize the system properties. It is worth noticing that a single tensile test is theoretically enough to fully characterize a mono-directional laminate for civil engineering application. As discussed, the only elastic parameter really required is the Tensile Young Modulus and the only strength parameter of interest. A fully elastic characterization is possible anyway, measuring also the transversal displacement.

- E_1 can be computed knowing applied load and measured displacement
- ν_{12} can be computed measuring also the transversal displacement
- E_2 is known, knowing the matrix characterization

f_{fu} is measurable loading the specimen up to rupture

A standard procedure has been developed in the last years to analyze the in-plane tensile characteristic polymer matrix composite material reinforced by high-modulus fibers, namely the ASTM D3039-14. It consists in a tensile test performed on a thin flat strip of material having a constant rectangular cross section. This strip is gripped at the two ends by a mechanical testing machine and monotonically loaded in tension (Berneschi, 2015). The ultimate strength can be calculated from the maximum load carried before failure and the tensile modulus of elasticity, Poisson's ratio and transition strain can be calculated using strain transducers (Berneschi, 2015). As usual for ASTM procedures, a strong emphasis is posed in characterizing the failure modes of the tested specimens and requirements on the coefficient of variation are set (ASTM, 2014).

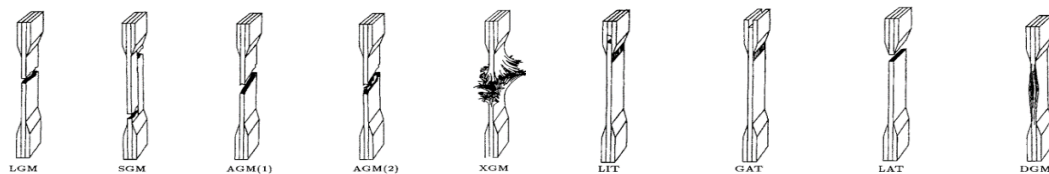


FIGURE 10 - FAILURE MODES FOR A LAMINA TENSILE TEST (ASTM, 2014)

TABLE 5 Averages of the Coefficients of Variation

Parameter	Average of S_f/X , %	Average of S_E/X , %
Strength	5.11	6.00
Modulus	2.22	3.22
Failure strain	5.94	7.32

3.3.6 Structural Applications and Design Criteria Overview

Unidirectional composites sheets are widely applied in civil engineering, offering a light, efficient and easy-to-apply solution to externally reinforce deficient structures (Nanni, 2000). The reasons behind a structural enhancement can be various: rehabilitation of a damaged structure, change of use, seismic upgrading are the most common scenarios

(Nanni, 2004), with performance improvement commonly required for already existing critical structures to comply with updated norms (Nanni, 2000).

The additional reinforcement will contribute either to the ultimate resistance of the structure and to the service performances in terms of deflections, fatigue and additional cracking prevention (Nanni, 2004), but it is worth underlining that the additional stiffness, coming from the reinforcement, will be engaged only by the additional load with respect to the ones determining the deflected shape at the time of application (CNR, 2013).

These consideration, along with the well-known low compression efficiency of FRP laminates, point out the need of well pondering whether an external solution is effective and feasible for each particular situation the designer has to deal with (ACI, 2008).

3.3.6.1 Design Philosophy & Regulations

Design principles applied to FRP solutions are generally based on the limit-states design principles, the nowadays leading design approach either in Europe and the US (ACI, 2008) (CNR, 2013).

The main difference between the American and European approaches can be found in the definition of the safety factors, with a partial approach characterizing the European regulations and a global approach characterizing the American counterpart. It is however worth noticing that, along with a global safety factor applied to the overall resistance, even the ACI provisions accounts for partial safety factors to describe the particular behavior expected from each composite material in terms of long-term behavior and reaction to an aggressive environment (ACI, 2008) and to account for the lower level of confidence in composite materials understanding and characterization, with respect to standard construction materials (Nanni, 2004).

Exposure conditions	Fiber type	Environmental reduction factor C_E	Exposure conditions	Type of fiber/resin	η_a
Interior exposure	Carbon	0.95	Internal	Glass/Epoxy	0.75
	Glass	0.75		Aramid/Epoxy	0.85
	Aramid	0.85		Carbon/Epoxy	0.95
Exterior exposure (bridges, piers, and unenclosed parking garages)	Carbon	0.85	External	Glass/Epoxy	0.65
	Glass	0.65		Aramid/Epoxy	0.75
	Aramid	0.75		Carbon/Epoxy	0.85
Aggressive environment (chemical plants and wastewater treatment plants)	Carbon	0.85	Aggressive environment	Glass/Epoxy	0.50
	Glass	0.50		Aramid/Epoxy	0.70
	Aramid	0.70		Carbon/Epoxy	0.85

FIGURE 11 – EXPOSURE & LONG TERM COEFFICIENTS FROM ACI (A) & CNR (B)

As a general approach, regulations tend to keep design procedures the more similar as possible to standard R/C ones, pointing out the peculiar differences related to applying an externally bonded system instead of standard rebars, as well as the obvious differences in the material behavior with respect to steel.

As discussed, FRP laminates are not effective solution for enhancing the compressive strength of a member, with the exception of confining solution, and thus laminates are assumed not to carry compressive stresses in civil applications (ACI, 2008) (CNR, 2013).

The norms tend to stress the brittle nature of the collapses a FRP reinforced structure can undergo: not only the FRP is a brittle material itself, but the most common collapse mechanism, i.e. debonding of the laminate from the concrete surface, happening at strains way lower than the ultimate one and further discussed in the following, is an instantaneous, potentially catastrophic, kind of failure.

The Italian counterpart in particular, referring to a well settled traditional design philosophy, requires the strengthening intervention to be designed in order to remove any kind of brittle collapse mechanism from the existing structure, of course without introducing new ones (CNR, 2013). This situation can be achieved designing the reinforcement to fail after the internal steel reinforcement has already yielded.

The norms stress also the external nature of the reinforcement and the safety issues that comes along: sensibility to scratches, vandalism, impacts, fire. In order to guarantee an acceptable safety level, it is required that the unreinforced structure is able to carry by itself a decent amount of the maximum expected load, without collapsing. According to ACI (2008) this level is set to the sum of 110% the dead load, plus 75% of the accidental:

$$(\phi R_n)_{existing} \geq (1.1 S_{DL} + 0.75 S_{LL})_{new}$$

Also, the un-factored strength at high temperatures – i.e. during a fire event – is required to be higher than the un-factored service load for the reinforced structure:

$$R_{n\theta} \geq S_{DL} + S_{LL}$$

CNR provisions, instead, requires the external solution to not increase the structural capacity more than 50% of that of the unstrengthen member and to provide the design

strength for *the required period of time* in case of fire (CNR, 2013). Additional considerations are added to account for members potentially exposed to vandalism and it is worth citing that FRP fire performances are undergoing further researches (Nanni, 2004).

Finally, it is worth pointing out the different definition of ductility adopted by the norms: while the ACI relies on a more standard approach, requiring the internal steel rebars to achieve a certain strain before failure (1.3%) in order to achieve an acceptable level of ductility, the CNR provisions focus on the actual failure mechanism, requiring a ductile one, but defining debonding as a brittle mechanism regardless of the achieved strain level.

3.3.6.2 *Flexural Strengthening*

Related Papers: Meier (1987), Rostasy (1987), Meier et al. (1992), Nanni (1997), Nanni (2000), Nanni et al. (2001), Bonacci & Maalej (2000), Schiebel et al. (2001), Schiebel et al. (2002), Parretti et al. (2003), Casadei et al. (2003), Nanni & Lopez (2004), Mohammadi (2009), Turco (2014) and many others.

Bending reinforcement of deficient beams, slabs or even bridge girders using FRP laminates is a well settled practice, validated either in terms of effectiveness and feasibility (Nanni, 2004). The solution is conceptually very simple, relying on mono-directional sheets applied on the tensioned side of the element, with fibers longitudinally oriented with respect to the beam's principal direction.

The design criteria for bending reinforcement are well settled (Nanni, 2004) and allows to design an externally reinforced section relying on the standard sectional model, simply accounting for the externally bonded FRP laminates as additional rebars, relying on the usual assumption of perfect bond up to failure (ACI, 2008) (CNR, 2013).

Particular care should be taken in foreseeing the actual failure mode of the system: a bonded laminate will always undergo debonding way before reaching its ultimate strength and the design ultimate strain should be kept adequately low to account for the issue (Nanni, 2004). The issue is strictly related to the focus of this dissertation and will be fully discussed in the following.



FIGURE 12 - FRP FLEXURAL APPLICATIONS (NANNI, 2000)

3.3.6.3 Shear and Torsion Strengthening

Related Papers: Triantafillou (1998), Khalifa et al. (1999), Khalifa & Nanni (2000), Chen & Teng (2003), Monti & Liotta (2006), Barros et al. (2007), Lu et al. (2008), Chen et al. (2010), Dong et al. (2012), Pellegrino & Vasic (2012), Godat et al. (2013), Belarbi & Acun (2013), Tetta et al. (2015), Jung et al. (2015), Kyusan et al. (2015) Ferreira et al. (2016).

It is well accepted and normed that the standard Morsch-like solutions, applied to shear strengthening design for internal reinforcement, can be also applied to external reinforcing intervention, at least in the form of U-wrap, complete wrapping of the section and 2-sides wrap (ACI, 2008) (CNR, 2013). In this applications the fibers are oriented transversally with respect to the principal bending direction or with a certain angle influencing the strengthening effectiveness (ACI, 2008) (CNR, 2013). Similar considerations are valid for torsional strengthening design (CNR, 2013).

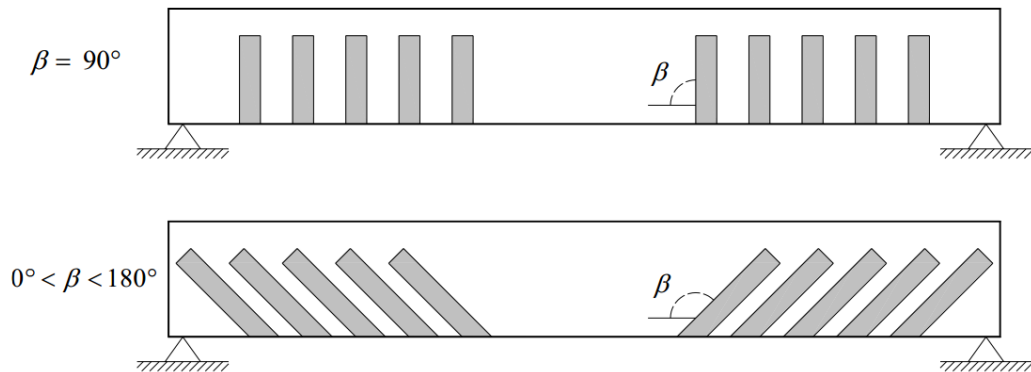


FIGURE 13 - SHEAR STRENGTHENING CONFIGURATIONS (CNR, 2013)

3.3.6.4 Columns Confinement

Related Papers: Fardis & Khalili (1981), Katsumata et al. (1987), Nanni & Bradford (1995), Toutanji (1999), Demers & Neale (1999), Pessiki et al. (2001) Teng et al. (2002), De Lorenzis & Tepfers (2003), Harries & Carrey (2003), Lam & Teng (2003), Carey & Harries (2005), Matthys et al. (2005), Rocca et al. (2006), and many others.

The effectiveness of FRP jackets in enhancing the compressive strength and ductility of compressed columns has been widely discussed (Nanni & Bradford, 1995) (Toutanji, 1999) and normed, providing formulas similar to the traditional solutions for steel-spiral confined concrete columns (ACI, 2008) (CNR, 2014). In order to provide confinement according to these standard formulations the fibers must be oriented transversally with respect to the principal compression direction and any contribution of longitudinally oriented fibers should be neglected, as already pointed out (ACI, 2008).

Similar formulations are available for columns subjected to combined compression and bending (Nosho, 1996) (Saadatmanes et al. 1996) (Chaallal and Shahawy, 2000) (Bousias et al. 2004) (Elnabelsy & Saatcioglu, 2004) (Harajli & Rteil, 2004) (Sause et al. 2004) (Memon & Sheikh, 2005).



FIGURE 14 - CONFINEMENT APPLICATIONS (NANNI, 1999)

3.3.6.5 Other Applications

Related Papers: Nanni (2000), Hollaway (2009)

Many other applications have been researched and implemented on the field: tanks and chimneys wrapping, beam-column joints reinforcement, prestressed application (either

standard FRP on prestressed elements and prestressed FRP on standard or prestressed elements) and seismic reinforcement solutions.

In the field of seismic design, the application of capacity design criteria to the FRP strengthening design is promoted, requiring the joints to stay in the elastic domain even under seismic load, while the flexural ductile failure of beams and slabs is preferred (Nanni, 2004).



FIGURE 15 - CHIMNEY & WALL REINFORCEMENT WITH FRP (NANNI, 2000)

3.4 The Debonding Problem

The bond mechanism is the most critical aspect for FRP structural systems applied in the field of civil engineering, being responsible for stress transfer from the already existing R/C structure to the newly applied additional reinforcement. Debonding is a not-yet addressed problem either from the point of view of efficiency and safety:

- I. From the *Efficiency* point of view, debonding enforce collapse at stress/strain levels way lower than the laminate ultimate strain.
- II. From the *Safety* point of view, debonding is a brittle failure happening at low stress-strain levels, without previous warning signals.

Many solutions have been proposed to account for the problem of debonding, from surface preparation (Mostofinejad & Mahmoudabadi, 2010) to the most various kind of

mechanical anchoring device (Kalfat et al. 2011). Up to now, the only normed solution force designers to limit the strains in the laminate to levels way lower than the ultimate one, thus guaranteeing a safe, though inefficient design.

In order to evaluate the effectiveness of alternative solutions, namely anchoring devices, it is fundamental to deeply understand the various debonding mechanisms and their mechanical modeling. Many theoretical formulations have been proposed to describe the bond behavior of a FRP-concrete interface: (FIB 2001, CNR 2004, ACI committee 440.2R 2008, Chen & Teng 2001, De Lorenzis et al. 3001, Smith & Teng 2002, Brosens & Van Gement 1999, Taljsten 1997, Bilotta et al. 2011, CNR 2014) these formulations are mostly similar, the differences are in how empirical coefficients and safety factors are defined (Nicolais & Borzacchiello, 2012).

The formulation proposed in CNR – APPENDIX D (2014) combines relative simplicity and a good experimental matching and will be furtherly discussed and applied to the purposes of this research. A comparison with ACI 440.2R (2008) will also be provided.

3.4.1 Debonding Failure Modes in Flexural Applications

An externally applied FRP sheet can undergo different debonding mechanism, all related to the same basic mechanical principles, but requiring different modeling approaches. Focusing on flexural strengthening allows to clearly differentiate the occurring cases, a similar classification can be applied to other kind of strengthening applications.

Debonding mechanisms can be classified depending on where they occur along the beam/FRP sheet and depending on which is the failing element in the concrete-adhesive-FRP system (ACI, 2008) (CNR, 2013) (ASTM, 2013):

- Debonding inside the concrete (Cohesive Failure)
- Debonding between adhesive & concrete (Adhesive Failure)
- Debonding inside the adhesive (Cohesive Failure)
- Debonding between multiple laminate sheets, wet lay-up (Cohesive Failure)
- Debonding between multiple laminate sheets, pre-cured (Adhesive Failure)

An adhesive failure or a FRP cohesive failure are unlikely to occur if the installation is well performed, the same can be said for adhesive failure involving pre-cured solutions (CNR, 2013). The most likely debonding is a superficial cohesive one in the concrete, hence a

strong dependence from the concrete strength properties can be found in most of the proposed literature models, including CNR and ACI.

Deep concrete debonding and cover peeling are also possible in presence of high tensile stresses, usually at the laminate ends in shear critical application (ACI, 2008). These situations are typically characterized by a low incidence in real life (CNR, 2013).

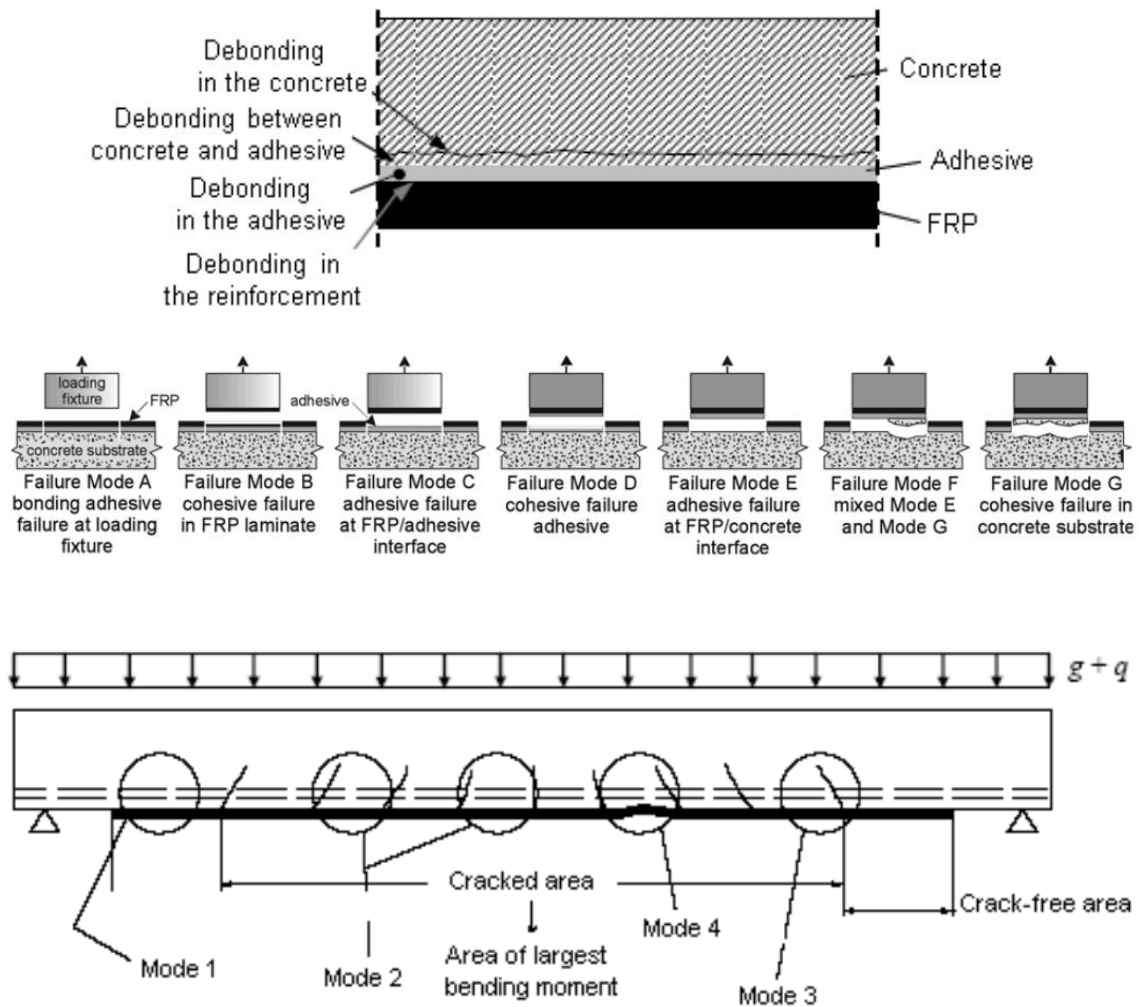


FIGURE 16 - DEBONDING DEFINITIONS ACCORDING TO CNR (A, c) & ASTM (B)

3.4.1.1 End Debonding

In bended members, the end portions of the FRP system are subjected to high interfacial shear and normal stresses for a length of approximately 100-200 mm (4-8 in) (CNR, 2013).

Normal stresses namely arise because of the severe stiffness of the FRP sheet, that refuses to bend along with the concrete element. These stresses tend to reduce the tangential component, reducing the bond effectiveness and actively pulling the FRP laminate away from the concrete surface (CNR, 2013).

This debonding mechanism happens in zones of low stresses for the beam and usually is not critical in defining the ultimate strength of well-designed strengthening solutions, while its understanding is fundamental in order to define the proper development length for the FRP laminate, further discussed later on.

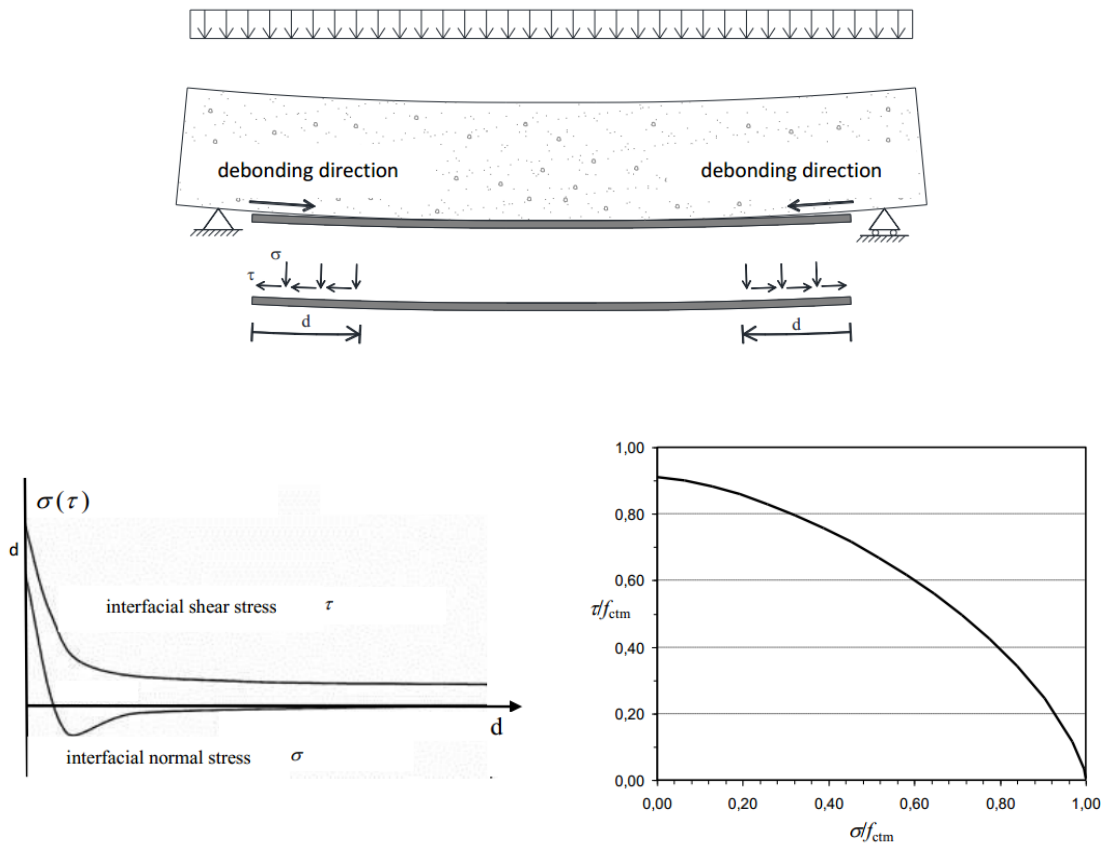


FIGURE 17 - DEBONDING & STRESSES AT SHEET'S ENDS (CNR, 2013)

3.4.1.2 Debonding by Flexural Cracks – Intermediate Debonding

Flexural cracking introduces discontinuity at the FRP-concrete interface, the consequent tangential stresses concentration promotes debonding starting from the central portion of the bended element and propagating towards the ends (ACI, 2008) (CNR, 2013). This mechanism can be triggered by vertical pure-bending or diagonal shear-bending cracks, as long as the bending stresses are the predominant component.

The mechanism occurs in the portion of maximum stresses for the beam and is generally the critical one in defining the ultimate strength of real applications. Also in this case the FRP stiffness plays an important role: the stiffer the laminate, the more severe the stresses concentration and the more likely is the debonding mechanism to happen.

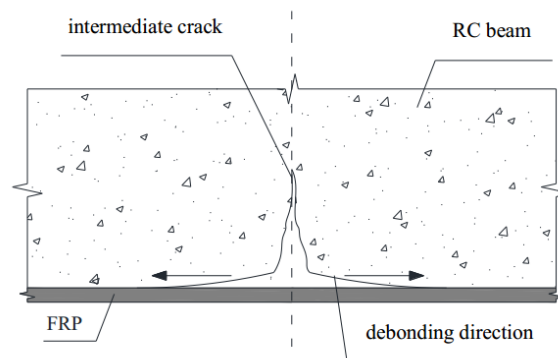


FIGURE 18 - INTERMEDIATE DEBONDING (CNR, 2013)

3.4.1.3 Debonding by Shear Cracks

When shear is the predominant component, a non-negligible vertical displacement between the crack's edges can be noticed, it is also worth noticing that in an element working in shear the most critical crack tends to be 45° inclined and develop close to the supports. Such displacement increases the pull-out normal stresses usually occurring at the laminate's ends, promoting a debonding mechanism traveling from the ends towards the beam's midspan. As in mode 1, the higher the FRP stiffness, the higher the normal stresses and the most likely the mechanism to occur.

Whether such a mechanism is common in shear-critical 4-point-bending lab tests, its occurrence in real application is rare and limited to low transversally reinforced concrete elements strengthened with high stiffness FRP laminates (CNR, 2013). As a consequence,

the mechanism is not modeled, while additional shear-related prescriptions are provided by CNR and ACI when dealing with standard end debonding.

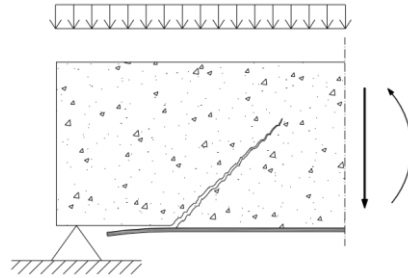


FIGURE 19 - SHEAR-CRACKS DEBONDING (CNR, 2013)

3.4.1.4 Debonding by Irregularities and Roughness of the Concrete Surface

Localized debonding due to surface irregularities of the concrete substrate may propagate and cause full debonding of the FRP system. This failure mode can be avoided if the concrete surface is treated in such a way to avoid excessive roughness (CNR, 2013).

3.4.2 Bond Mechanism & Development Length

The natural way to characterize the bonding properties of an FRP laminate is referring to a shear-bond test situation. A huge amount of this kind of test has been performed up to now (CNR, 2013) and has allowed to fully characterize the phenomenon in terms of bond-slip law, maximum transferrable strength and optimum bond length.

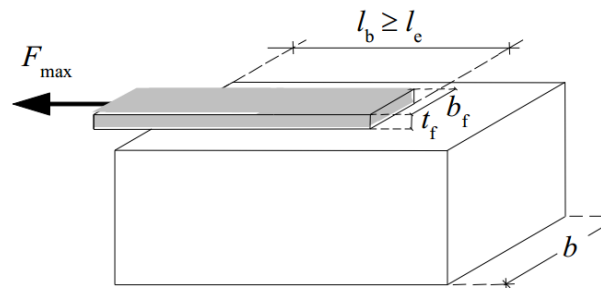


FIGURE 20 - SHEAR-BOND-TEST SCHEME (CNR, 2013)

3.4.2.1 Bond-Slip Law, Specific Fracture Energy, Bond Strength

The tested specimens generally show an almost linear behavior until the maximum bond stress is reached (Nicolais & Borzachiello, 2012), followed by a softening phase. For design purposes, a bi-linear model can be adopted (CNR, 2013).

It is worth underlining the deep differences in the bond-slip mechanism characterizing an externally applied laminate and an internal rebar. In the latter case, the concrete-provided confinement promote an elasto-plastic behavior, while the bi-linear mechanism is basically brittle (in load control). These difference has critical consequences in the definition of the optimal bond length for an externally bonded laminate, later discussed.

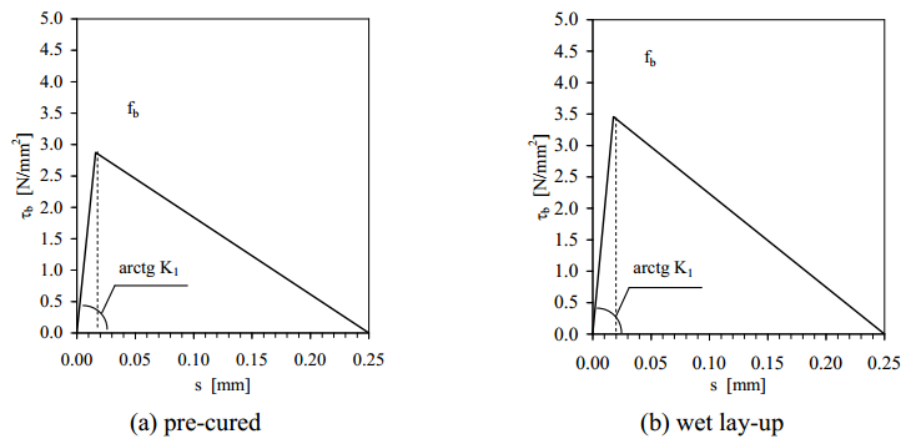


FIGURE 21 - SLIP LAWS (CNR, 2013)

The raising branch characterizes the bond behavior at serviceability and its stiffness is strictly related to the stiffness of the adhesive layer and concrete substrate modeled as springs in series:

$$\tau_b = K_1 s$$

$$K_1 = \frac{c_1}{\frac{t_a}{G_a} + \frac{t_c}{G_c}}$$

G_a	Adhesive Shear Modulus
G_c	Concrete Shear Modulus
t_a	Adhesive Nominal Thickness
t_c	Concrete Effective Depth (20 - 30 mm) (1 in)
c_1	0.5 – 0.7

The ULS is reached at the diagram peak. Following a simplified approach, three are the parameters characterizing the behavior at ULS from a global prospective: the *Fully Debonded Slip* (s_u), the *Bond Strength* (f_b) and the *Specific Fracture Energy* (Γ_F) defined as the area underlying the bond-slip diagram.

Assuming negligible the area underlying the raising branch, a stiff-softening model can be adopted (CNR, 2013) and the specific fracture energy can be simply computed as:

$$\Gamma_F = \frac{1}{2} f_b s_u$$

According to CNR, the *Fully Debonded Slip* can be assumed constant,

$$s_u = 0.25 \text{ mm} \quad (0.1 \text{ in})$$

While *Specific Fracture Energy* is picked as the representative parameter for the collapse mechanism; assuming debonding always happening inside the concrete substrate, only the concrete properties will affect its value:

$$\Gamma_F = \frac{k_b k_G}{FC} \sqrt{f_{cm} f_{ctm}}$$

f_{cm}

Average Compressive Strength

$$f_{ctm} = \begin{cases} 0.3 f_{ck}^{2/3} & f_{ck} < 50 \text{ MPa} \\ 2.12 \ln \left[1 + \frac{f_{cm}}{10} \right] & f_{ck} > 50 \text{ MPa} \end{cases} \quad \text{Concrete Average Tensile Strength}$$

$$f_{ck} = f_{cm} - 8 \quad \text{Characteristic Compressive Strength}$$

$$k_b = \sqrt{\frac{2 - b_f/b}{1 + b_f/b}} \geq 1 \quad \text{for } \frac{b_f}{b} \geq 0.25 \quad \text{Geometrical Corrective Factor}$$

$$k_G = \begin{cases} 0.077 \text{ mm} & \text{average} \\ 0.037 \text{ mm} & 5\% \text{ fractile} \end{cases} \quad \text{Exp. Corrective Factor (wet lay-up)}$$

$$FC \quad \text{Confidence Factor}$$

Using the proper k_G either the average value or the characteristic value of Γ_F can be computed. Introducing a FC higher than 1, the design value can be defined. Knowing the fully debonded slip and the specific fracture energy, the *Bond Strength* can be easily computed as:

$$f_b = \frac{2 \Gamma_F}{s_u}$$

3.4.2.2 Maximum Shear Force, Optimal Development Length

As mentioned, a critical difference exists in the definition of the optimal bond length for an externally applied laminate rather than an internal rebar.

The elasto-plastic mechanism allows the maximum bond strength to be transmitted at increasing slipping along all the bonded length, meaning that an increment in the bonding length always reflect in an increment of the total bonding force.

This is no longer valid in the case of a softening constitutive model: there will be one point in the bonding zone where the transmitted shear stress equals the bond strength, while all the other points will show lower lever of stress, being either on the linear branch or on the softening one.

This means the transmitted tangential stress will reach a zero level at a certain point over the bonded length, either before and after the maximum level; as a consequence, increasing the bonding length after these points will not have any effect on the maximum transmittable bonding force that will have a fixed maximum value.

Once computed the maximum bond force, the minimum bond length required to transmit that force can be evaluated, knowing that furtherly increasing its value will not guarantee any improvement in the bonding performances.

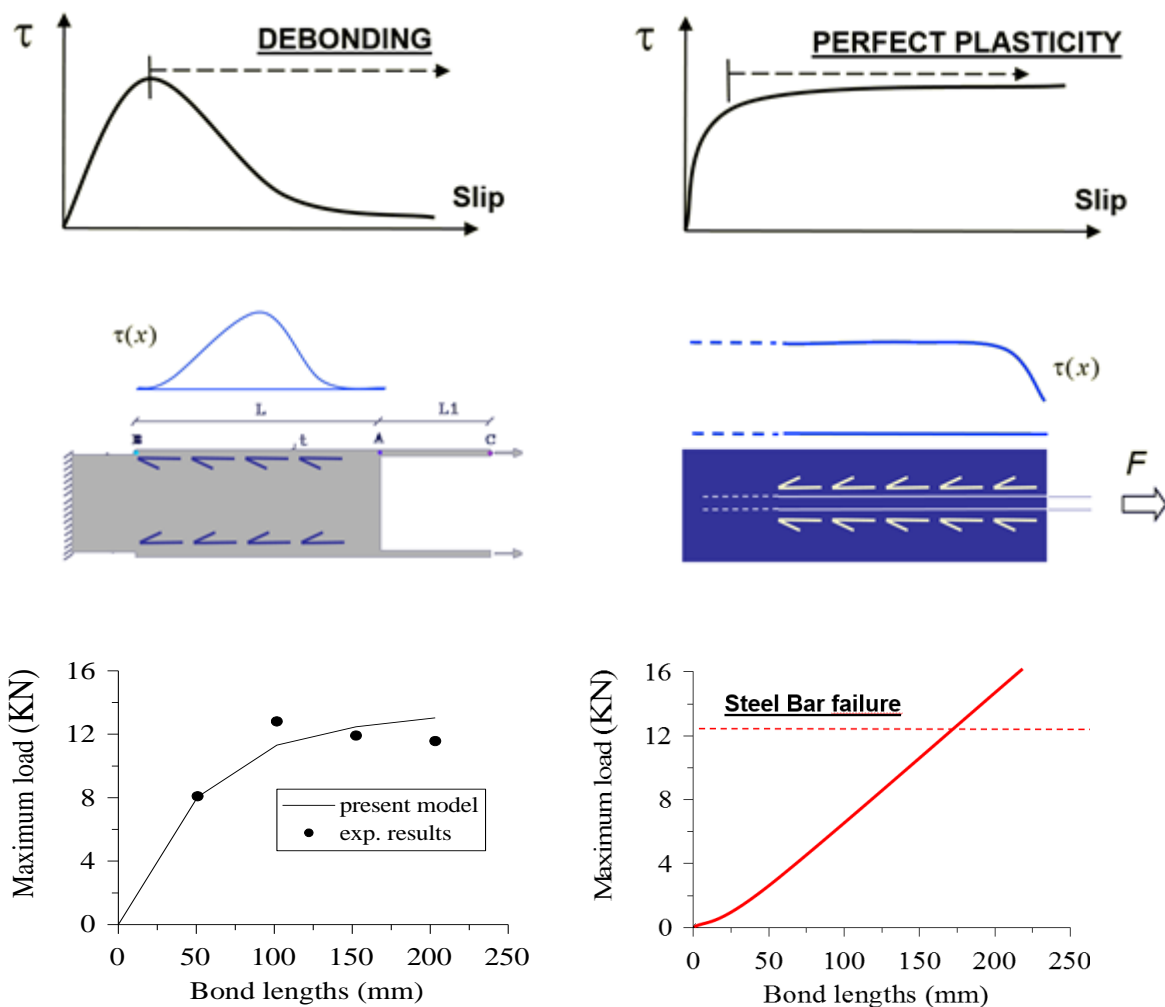


FIGURE 22 – EXTERNAL VS INTERNAL BONDING (SAVOIA, 2015)

Knowing the shear stress distribution over the FRP laminate when debonding occurs, the maximum force allowed in the FRP in a shear-bond test situation can be computed. Assuming the concrete element stiffer than the FRP external reinforcement, the following solution can generally be applied (CNR, 2013):

$$F_{max} = b_f \int_0^{\infty} \tau_b(x) dx = b_f \sqrt{2 E_f t_f \Gamma_f}$$

b_f FRP laminate nominal width

t_f FRP laminate nominal thickness

Knowing the maximum allowed force and the bond strength as previously defined, the Optimal Bond Length can be computed as follows, according to CNR (2013). The relation accounts for the non-uniform stress distribution over the length, the corrective factor should not be interpreted as a safety factor.

$$\begin{aligned} l_{ed} &= \frac{\pi}{2 \gamma_{Rd}} \frac{F_{max}}{f_{bd} b_f} \\ &= \frac{\pi}{\gamma_{Rd} f_{bd}} \sqrt{\frac{E_f t_f \Gamma_{Fd}}{2}} \\ &= \frac{\pi s_u}{2 \gamma_{Rd}} \sqrt{\frac{FC}{2 k_b k_G} \frac{E_f t_f}{\sqrt{f_{cm} f_{ctm}}}} \leq 200 \text{ mm} \end{aligned}$$

Developing explicitly all the terms and numerical coefficients a direct comparison with the ACI based formulation is possible (CNR, 2013) (ACI, 2008):

$$l_{ed} = 1.15 \sqrt{\frac{FC}{k_b} \frac{E_f t_f}{\sqrt{f_{cm} f_{ctm}}}} \quad \text{CNR, SI units}$$

$$l_{df} = 1 \sqrt{\frac{E_f t_f}{\sqrt{f'_c}}} \quad \text{ACI, SI units}$$

$$= 0.057 \sqrt{\frac{E_f t_f}{\sqrt{f'_c}}} \quad \text{ACI, US customary units}$$

- γ_{Rd} Corrective Factor (1.25)
- t_f FRP laminate nominal thickness
- f'_c specified concrete compressive strength

Both the formulations accounts for a direct dependency from the laminate stiffness and an inverse dependency from the concrete strength. The CNR formulation seems more detailed accounting for geometry related effects (k_b) and explicitly requiring the designer to account for the confidence level he has (FC) in applying this formulation to the particular situation, depending on the quality of the available data and on the adherence to the formulation hypothesis.

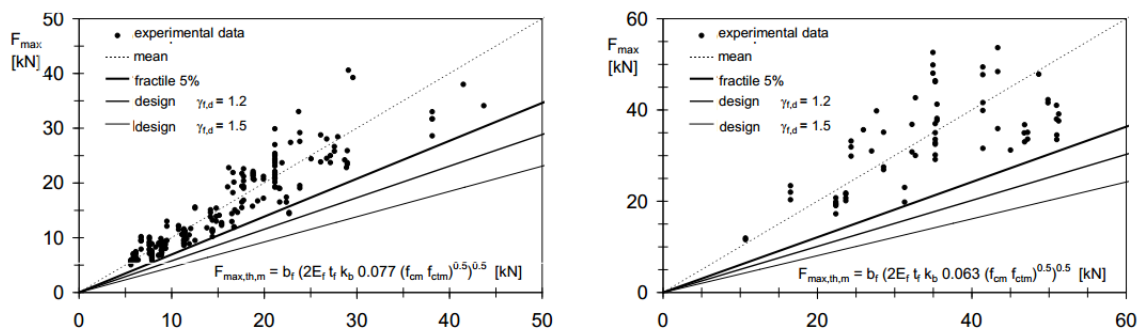


FIGURE 23 - EXPERIMENTAL CALIBRATION & MATCHING (A) WET LAY-UP (B) PRE-CURED FRP (CNR,2013)

3.4.2.3 Bond Length Design

According to CNR, in a simply supported situation, the bonded length is defined as the distance from the end of the FRP laminate and the first crack on the concrete tensioned

side. It is clear that the concrete cracked area enlarges at increasing load, hence the bonded length should be designed in order to be larger or equal to the optimum value at ULS, condition corresponding to the maximum sustainable load.

Knowing the ultimate sustainable load, the ultimate moment diagram can be drawn and the first cracked section can be located, as the one where the moment coming from the applied load equals the concrete section's cracking moment. In the simple case of three point bending the cracked section can simply be located as:

$$a^* = \frac{2 M_{crack}}{P_u}$$

In order to account for the moment presence on the supports, the diagram should be translated according to EC2 of the length:

$$a_1 = 0.9 d \frac{\cot(\theta) - \cot(\alpha)}{2}$$

d effective depth of the concrete member

θ concrete strut inclination

α transverse reinforcement inclination

The quantity is defined according to a Morsch-like theory, in absence of transversal reinforcement, a_1 can simply be assumed equal to:

$$a_1 = d$$

Hence the first cracked section in a 3-point-bended slab will be located in:

$$a^* = \frac{2 M_{crack}}{P_u} - d$$

Knowing the distance a , from the laminate's end to the slab's support, the bonded length can simply be computed as:

$$l_b = a^* - a = \frac{2 M_{crack}}{P_u} - d - a$$

The length a is the only term on which the designer can play, being all the materials' and concrete section's properties already defined for the existing structure. If possible it should be defined in order to guarantee a bonded length equal or higher than the optimal development length previously computed. If the optimal solution is not possible, a reduced resistance to end debonding should be accounted for.

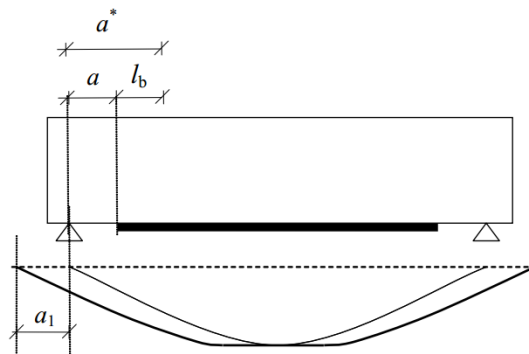


FIGURE 24 - BENDING MOMENT DIAGRAM SHIFTING (CNR, 2013)

It is important to underline that, according to CNR, in presence of negative moment at the supports, the FRP sheet located in the compressed region should be neglected and the length a^* should be taken stranding from the point of inflection of the translated moment diagram (CNR-DT 200R1-2013, 4.2.2.5 (5)). The provision is provided to account for possible fiber buckling in the compressed region.

This points out a fundamental difference with CNR: the American norm prefers bonding length to be placed in the compressed zone, adopting an internal-reinforcement-line approach and neglecting the risk of buckling happening on the compressed fibers (ACI 440.2R-08 13.1).

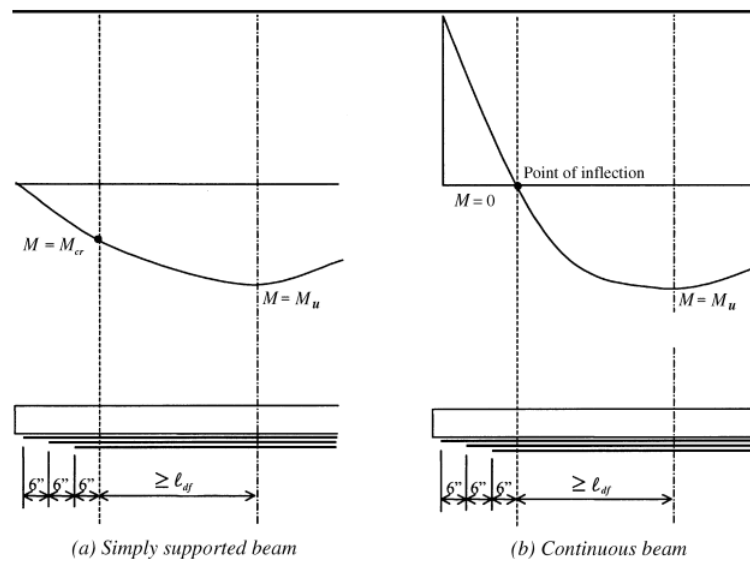


FIGURE 25 - GRAPHICAL REPRESENTATION OF THE PROVISIONS ON BONDING LENGTH (ACI, 2008)

3.4.3 Debonding Modeling in Flexural Applications

CNR provides good-matching models either for End and Intermediate debonding, shear debonding is not treated and no further discussion is required as none of the application treated in this dissertation will be shear critical.

It is anyway interesting to point out that shear critical applications are the only case in which available guidelines talk about anchors, even though only in the form of transversal wrapping. The item will be shortly discussed in the following.

3.4.3.1 End Debonding

According to CNR, the strain at the end of the FRP plate should be kept lower than a properly defined end debonding ultimate strain, defined as:

$$\varepsilon_{fdd} = \frac{1}{\gamma_{fd}} \sqrt{\frac{2 \Gamma_{Fd}}{E_f t_f}}$$

$$\varepsilon_{fdd} = \frac{1}{\gamma_{fd}} \sqrt{\frac{2}{E_f t_f} \frac{k_b k_G}{FC} \sqrt{f_{cm} f_{ctm}}}$$

γ_{fd} safety factor (1)

According to either its definitions, an increment in the Specific Fracture Energy correspond to an increment in the bond strength, clearly reflecting in an increment of the sustainable strain before debonding occurs. The negative effect of an increment in laminate's stiffness ($E_f t_f$) has already been discussed and is accounted for in the proposed formula. If the provided bond length is less than the optimal one, the ultimate strain should be reduced as follows:

$$\varepsilon_{fdd,red} = \varepsilon_{fdd} \frac{l_b}{l_{ed}} \left(2 - \frac{l_b}{l_{ed}}\right)$$

l_b provided bond length

l_{ed} optimal design bond length

Once computed the ultimate debonding strain, it should be checked not on the midspan, but in the FRP laminate end section. Namely, accounting for the moment diagram translation, the section to be checked is located in:

$$x_{fdd} = a + a_1$$

In the simple case of a slab subjected to three-point bending, the moment occurring in this section can simply be computed as:

$$M_{fdd} = \frac{P_u (a + d)}{2}$$

As discussed, this mechanism occurs in zones of low bending moment and is rarely the controlling one. The CNR based approach is more aimed to verify this mechanism is not controlling, once having designed the structure for another ultimate limit state.

ACI doesn't even provide design formulas, assuming that, once the optimal bond length is provided, the mechanism won't control the system failure. Additional provisions are given for multi-ply solutions and more complex situation rather than simply supported elements, but the general philosophy doesn't change much. Additional shear-related provisions are given as well to account for shear cracks' negative effect.

3.4.3.2 Intermediate Debonding

As per end debonding, the CNR norm provides a similar formula for an equivalent intermediate-debonding ultimate strain, to be simply checked in midspan, where the mechanism actually occurs.

$$\varepsilon_{fdd,2} = \frac{k_q}{\gamma_{fd}} \sqrt{\frac{2 \Gamma_{Fd,2}}{E_f t_f}}$$

$$\varepsilon_{fdd,2} = \frac{k_q}{\gamma_{fd}} \sqrt{\frac{2}{E_f t_f} \frac{k_b k_{G,2}}{FC} \sqrt{f_{cm} f_{ctm}}} \geq \varepsilon_{sy} - \varepsilon_0$$

ε_{syd}	Design yielding strain for the internal reinforcement
ε_0	Initial strain when the external reinforcement is applied
k_q	Load Factor (1 for concentrated loads, 1.25 for distributed loads)
$\Gamma_{Fd,2}$	Modified Specific Fracture Energy (defined basing on $k_{G,2}$)

$$k_{G,2} = \begin{cases} 0.32 \text{ mm} & \text{average} \\ 0.10 \text{ mm} & \text{5\% fractile} \end{cases} \quad \text{Exp. Corrective Factor (both wet \& dry)}$$

The formula accounts for the positive consequences of an increased bond strength, as well as for the negative influence of an increased FRP stiffness. The results are experimentally tared via k_{G2} but the same conceptual structure applied to end debonding is maintained. The positive influence of a distributed loading is accounted for. Finally, midspan debonding is assumed to start anyway after steel yielding.

Explicating the numerical terms allows for a direct comparison with the ACI proposed formulation. A concentrate load is considered:

$$\varepsilon_{fd,2} = 0.447 \sqrt{\frac{k_b \sqrt{f_{cm} f_{ctm}}}{FC E_f t_f}} \quad \text{CNR, SI units}$$

$$\varepsilon_{fd} = 0.41 \sqrt{\frac{f'_c}{E_f t_f}} \quad \text{ACI, SI units}$$

$$0.083 \sqrt{\frac{f'_c}{E_f t_f}} \quad \text{ACI, US customary units}$$

Also in this case the formulas show a similar dependency on the same parameters, even if the dependency on concrete properties is to the 4th root in the CNR formulation and to the 2nd in the ACI one. A geometry dependency and an internal confidence factor are accounted for in the CNR formula that appears to be better detailed.

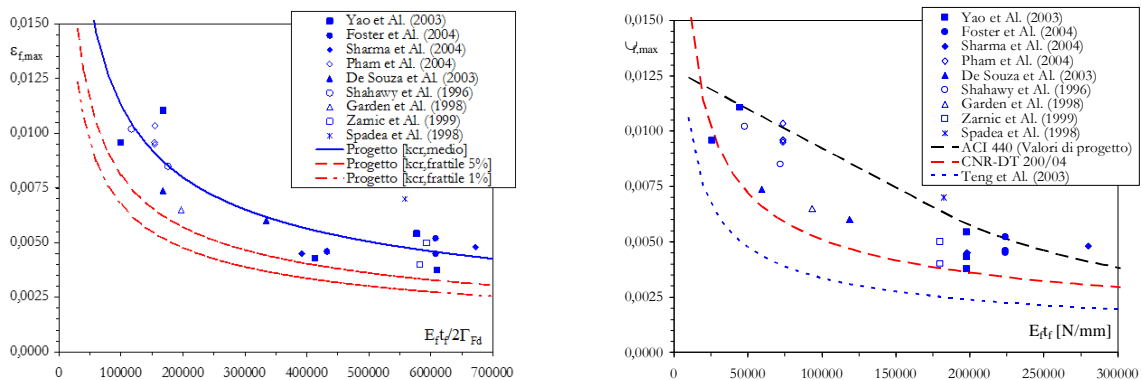


FIGURE 26 - INTERMEDIATE DEBONDING FORMULATIONS MATCHING (SAVOIA, 2015)

3.5 Anchoring Systems for FRP Laminates

Limiting the strains in the FRP to non debonding-critical level is clearly a suboptimal solution and doesn't deal with the ductility problem. It also comes with a mechanical paradox that makes it unfeasible once overcome a certain limit: in order to limit the strains in the laminate a stiffer solution is required, but either increasing the number and thickness of plies (t_f) or choosing a stiffer material (E_f) means reducing the debonding limit strain, being the term ($E_f t_f$) at the denominator in the discussed models.

An alternative promising solution consists in mechanically anchor the laminate sheet to the concrete substrate. The solution has proved to be feasible and to significantly improve the efficiency of the FRP system (Kalfat et al. 2011) and in some case to guarantee a ductile failure for the reinforced element (Grelle & Sneed, 2013).

A huge variety of different anchoring solutions has been proposed (kalfat et al. 2011) and tested using a variety of different set-ups (Grelle & Sneed) resulting in a huge amount of non-homogenized data, all showing the effectiveness of the anchoring solution in increasing the FRP bond strength (Galal & Mofidi, 2010) but with little help in quantifying the effects and providing generally applicable results and rational design criteria (Kalfat et al. 2011).

From the qualitative point of view anchors can be categorized depending on the kind of strengthening they are intended for (Kalfat et al. 2011) on their mechanical role in the structural system (Grelle & Sneed, 2013) or simply by construction typology. A qualitative overview of the various anchoring system proposed and tested up to now will be provided in the following, the issues related to testing will be discussed as well.

3.5.1 Categorization Based on the Resisted Force

A first simple characterization based on the direction of the applied force the anchor is resisting can be defined. A generic anchor can either resist *Normal Tension* or *Transversal Shear Force*. It has to be noticed that in most applications an anchor resists either tension and shear forces and the two mechanism are sometimes difficult to differentiate, in other cases, like anchor spikes in flexural applications, the two mechanism are well differentiated and requires different characterization approaches, a predominant one can be spotted as well.

3.5.2 Categorization Based on Debonding Type

It is critical to point out that, depending on the nature of the chosen anchoring solution and on the position along the bended element, the anchoring system can either work against *Intermediate Debonding* or *End Debonding*. As discussed, the two phenomena are mechanically different, hence requiring different solutions.

Even if the same kind of anchors can both work against end and intermediate debonding, it will behave differently in the two different situations. Clear examples are anchoring spikes at the end of flexural-strengthening FRP sheets, that can work either against end or intermediate debonding relying on two different stress transfer mechanisms: they are mainly engaged in pull-out against end-debonding, while they are engaged in shear when they provide critical equilibrium stress transfer after intermediate debonding.

Also talking about anchoring in shear, debonding can start from the very end of the laminate, propagating downward, or be triggered by shear cracks in intermediate locations.

3.5.3 Categorization Based on Strengthening Application

3.5.3.1 Anchoring Solution for Flexural Strengthening

Related Papers: Lam & Teng (2001), Piyong et al. (2003), Eshwar et al. (2005), Orton (2007), Orton et al. (2008), Eshwar et al. (2009), Micelli et al. (2010), Smith et al. (2011), Nardone et al. (2011), Baggio (2013), Smith et al. (2013), Smith & Teng (2003), Al-Amery et al.-Mahaidi (2006), Pham et al.-Mahaidi (2006), Yalim et al. (2008), Garden & Hollaway (1998), Spadea et al. (1998), Jensen et al. (1999), Duthin & Starnes (2001), Wu & Huang (2008).

The list is particularly focused on anchors spike, due to the purpose of this dissertation, but a huge variety of anchoring solutions has been tried in flexural applications with different mechanical roles: anchoring spikes and transversal wrapping are among the most common, either located at the very ends of the FRP sheet or all over its length.

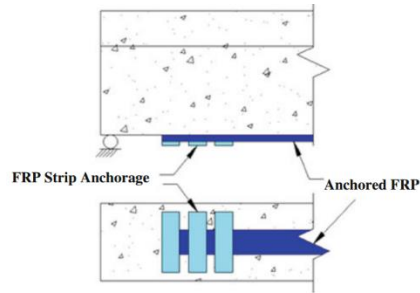
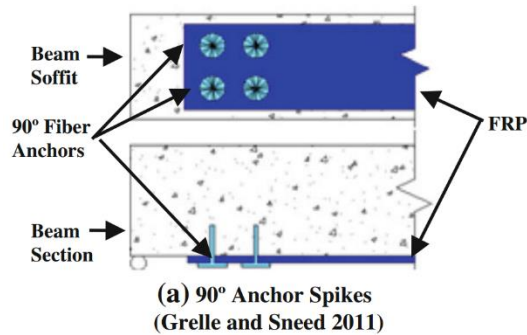


FIGURE 27 - ANCHORING SOLUTIONS FOR FLEXURAL STRENGTHENING (GRELLE & SNEED, 2013)

3.5.3.2 Anchoring Solutions for Shear Strengthening

Related papers: Baggio (2013), Kim et al. (2012), Kim et al. (2014), Kim et al. (2015), Hoult & Lees (2009), Deifalla & Ghobaran (2010), Micelli et al. (2002), Tanarlan et al. (2008), Lee et al.-Mahadi (2008), Kalfat et al.-Mahaidi (2011), Al-Mahaidi & Kalfat (2011).

U-wrapping is the standard solution for shear reinforcement using FRP. A whole variety of different devices has been proposed to anchor the wrapped laminates to the upper part of the section, improving the system performances once shear cracks show up.

It is interesting to notice that the U-wraps, usually applied as shear reinforcement to bended elements, act like anchoring devices for the FRP laminates applied as flexural reinforcement, making an efficient synergy, optimized by introducing a proper anchoring solution to keep the U-Wraps in place.

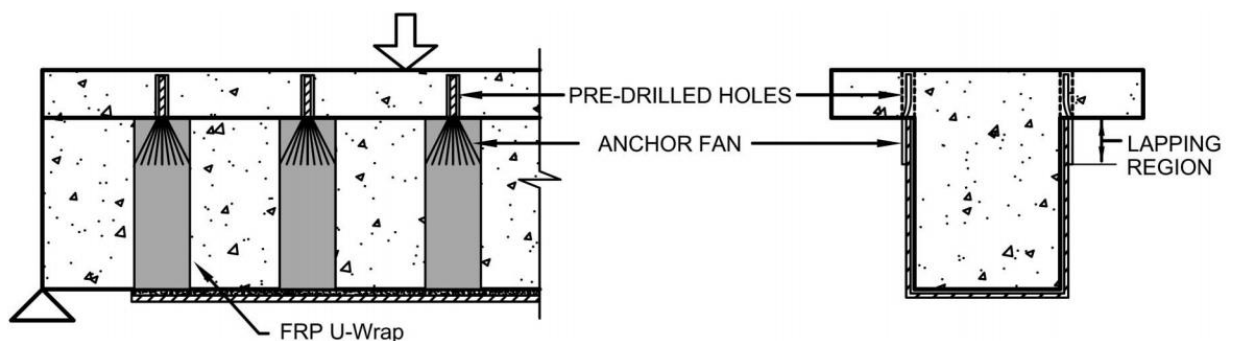


FIGURE 28 - ANCHORING SOLUTIONS FOR SHEAR STRENGTHENING (KALFAT ET AL. 2011)

3.5.3.3 Anchoring Solutions for Column Confinement & Joint Strengthening

Related Papers: Karantzakis et al. (2005), Sami et al. (2010), Kim et al. (2011), Grelle (2011), Ceroni et al. (2007), Li & Chua (2008).

Fully wrapping is the standard confinement solution for columns requiring additional strength or ductility, but it is not feasible in presence of continuous columns/wall solutions, here the need of anchoring devices jump into the equation. Anchors have also been successfully used to enhance the performances of beam-column joints.

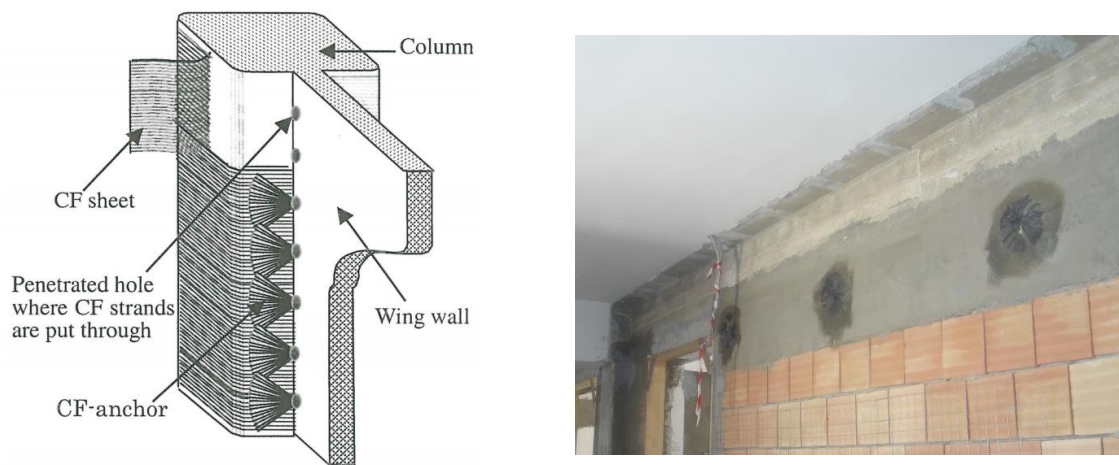


FIGURE 29 - ANCHORING SOLUTIONS FOR COLUMNS CONFINEMENT & WALLS STRENGTHENING (KOBAYASHI, 2001) (PROTA, 2015)

3.5.3.4 Other Applications

The effectiveness of anchorage systems has been proven in a variety of additional situation, ranging from storage tanks and shells, arches, walls (Kalfat et al. 2011), to prestressed elements (Piyong et al. 2003).

It must also be noticed that this works' focus is on concrete applications, while all these applications are applicable to masonry as well (Caggesi et al. 2013) (Fagone et al. 2014) and even to timber or steel structures (Smith, 2010).

3.5.4 Categorization Based on Mechanical Function

These characterization was proposed by Grelle & Sneed (2013), here the addition of ductility critical applications is proposed along with a new nomenclature. It is worth underlining how the same anchor, in the same application, can play more than one role at the same time.

3.5.4.1 Type I – Bond Improvement: Pull-Out Critical

Limit State: SLS

These anchors enhance the FRP bonding performances by resisting the normal stresses concentration at the ends of the laminates and after a shear crack. The goal is to prevent crack opening in the longitudinal direction and retard debonding itself. Anchoring Spikes are the ideal choice against end debonding, either for flexural and shear applications, U-wrapping is a guaranteed solution for anchoring flexural-strengthening sheets. It is well clear how improving the bonding strength and retarding debonding, the serviceability performances of the reinforced structure are improved.

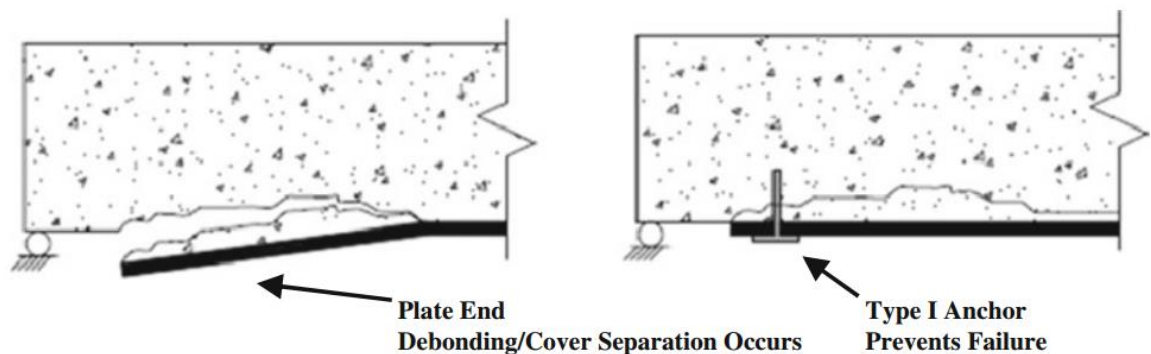


FIGURE 30 - EXAMPLE OF TYPE I ANCHORAGE DEVICE (GRELLE & SNEED, 2013)

3.5.4.2 Type II – Bond Improvement: Shear Critical

Limit State: SLS

These anchors enhance the FRP bonding performances by contributing in shear stress transmission from the laminate to the concrete substrate. The goal is to prevent crack

opening in the transversal direction and retard debonding itself. The usual solution is to enlarge the contact area via transversal sheet or wrapping, also anchoring spikes contribute to shear transfer even though through a different stress-transfer mechanism; concrete embedding and mechanical fastening is a feasible solution as well.

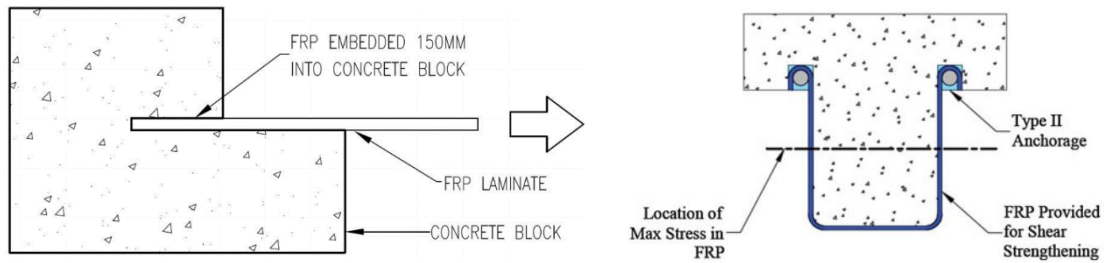


**FIGURE 31 - EXAMPLE OF TYPE II ANCHORING DEVICES
(KALFAT ET AL. 2011) (GRELLE & SNEED, 2013)**

3.5.4.3 Type III – Equilibrium Critical

Limit State: ULS

The previous categories refer to bond improving situations, where a bonding length exist, even if eventually insufficient, and a standard bond mechanism is in place. There exist applications where the stress transfer from concrete to FRP cannot take place at all without the presence of properly located anchors, for example in a cantilever projecting from a column, where the critical section is located right on the beam column interface. An anchoring system providing equilibrium-critical stress transfer has clearly a fundamental role up to structure's failure, eventually triggering the failure itself.

End-located anchoring spikes, providing ultimate strength to the bended element after intermediate debonding, can be included in this category. The issue will be widely discussed in the experimental part of this dissertation; a similar behavior was already noticed by Piyong et al. (2003).

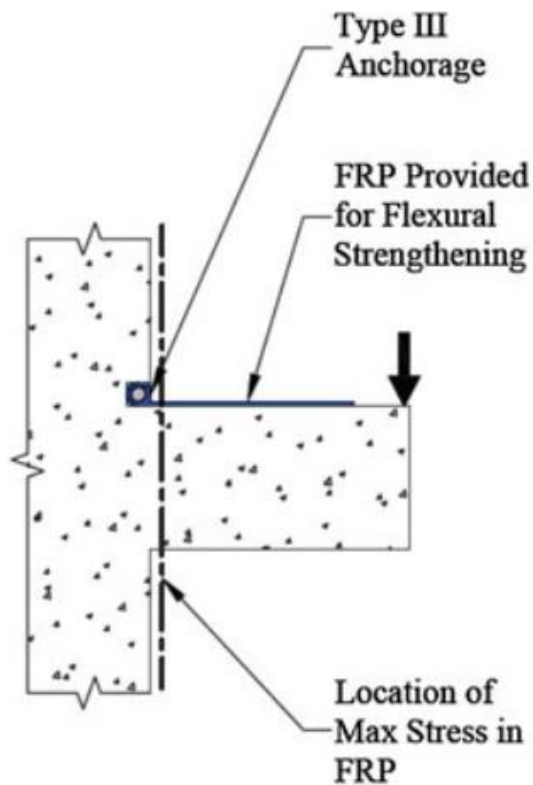


FIGURE 32 - EXAMPLE OF TYPE III ANCHORING DEVICES (GRELLÉ & SNEED, 2013)

3.5.4.4 Type IV – Ductility Critical

Limit State: ULS

The presence of anchoring devices can largely increase the deflection a bended element can undergo before FRP brittle failure. If the internal steel reinforcement is yielded once the FRP fails, the overall collapse mechanism can be eventually interpreted as ductile and the more strength the FRP can provide, the more ductility for the overall system. This approach is the one adopted by ACI-440.2R (2008), imposing a minimum strain to be achieved in the steel rebars before collapse, in order to guarantee an acceptable degree of ductility.

Moreover, a series of anchoring device, failing in series at ULS, can actually provide a pseudo-ductile plateau before the ultimate strain is reached. An approach of this type is more in line with CNR (2013) provisions that, focusing on the actual failure mechanism, define debonding as a brittle failure regardless of the strain level achieved.

Talking about columns the topic is much simpler: it is well known how confinement enhances the ductility of a bended-compressed element and the possible application of anchors in confining wall-columns solutions has already been discussed.

A structure's ductility is a concept strictly related to the nature of the element failure; clearly, a ductility improvement can be spotted only at the ultimate state.

3.5.5 Categorization Based on Construction Typology

3.5.5.1 *Transverse Wrapping*

Sub-Categories: Transversal U-Wraps, Diagonal U-Wraps, Prestressed U-Wraps, In-Plane-Wrapping

Resisted Force: Normal Tension, Shear Force.

Strengthening Applications: Flexural.

Debonding Type: Intermediate & End.

Mechanical Function: I, II, III, IV

As already noted, U-wraps represent the standard solution for external shear reinforcement in retrofitted beams; when coupled with a longitudinal sheet, they act as anchoring system for the flexural reinforcement (CNR, 2013).

Depending on their position along the bended element they can either act against intermediate or end debonding, either resisting normal and tangential stresses (Kalfat et al. 2011) (Type I, II).

When located at the very end of the laminate, they can as well provide a stress transfer mechanism critical for the equilibrium of the system: prolonging the structure's life after intermediate debonding and shifting the collapse mechanism to a slipping action of the longitudinal sheet under the end wraps (Smith & Teng, 2003) (Type III).

Finally, the enhances in ductility provided by this kind of anchors have been widely proven has well, from the increased-deflection-at-collapse point of view (Smith & Teng, 2003) (Buyle-Bodin, 2004) (Type IV).

Summing up, the effectiveness of this category has been widely proved, as well as its efficiency, given by the anchoring/shear reinforcement synergy. The knowledge level is

enough that some limited prescription can be found in the current guidelines, allowing designers to confidently apply the anchoring solution eventually without testing (ACI, 2008) (CNR, 2013).

What seems to be the ideal anchoring solution in flexural applications comes with limits though, first of all not every geometry allows U-wrapping and, even when feasible, it has been proved how the anchoring efficiency decreases as the section enlarges (Smith & Teng, 2002) (Smith & Teng, 2003). A proposed solution when U-Wrapping is not feasible is simple transversal wrapping in the sheet plane, but even this solution is not wide applicable because of geometry limit and not necessarily solve the efficiency problem.

Finally, different variants have been proposed to standard U-wrapping, with varying success, ranging from diagonal applications, bi-directional fiber sheets and even prestressed solutions (Pham et al.-Mahaidi, 2006).

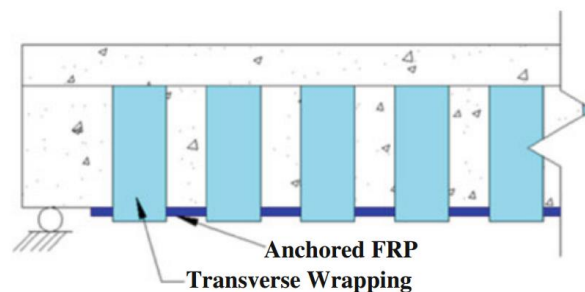


FIGURE 33 - TRANSVERSE WRAPPING (GRELLE & SNEED, 2013)

3.5.5.2 Anchor Spikes

Sub-Categories: Steel Spikes, FRP Hand-made Spikes, FRP Factory-Made Spikes.

Resisted Force: Normal Tension (Pull-Out), Shear Force.

Strengthening Applications: Flexural, Shear, Confinement, Joints, Walls.

Debonding Type: Intermediate & End.

Mechanical Function: I, II, III, IV

Anchor spikes comes with a wide applicability to nearly every situation where an anchoring system is required. They also come with a wide variety of names, all meaning the same: anchor spikes, fiber anchors, fiber bolts, FRP dowel, FRP spikes, FRP anchors (Kalfat et al. 2011) (Grelle & Sneed, 2013).

Made from a rolled fiber sheet or a bundle of loose fibers, once impregnated, one end – the so called *Dowel* – is inserted in a pre-drilled hole, while the fiber on the other end are opened in a *Fan* shape and epoxied over the FRP sheet. Metallic solutions exist as well, though not preferred because of corrosion sensibility and compatibility issues when coupled with FRP (Berneschi, 2015).

Even if studies have been conducted on spikes hole located outside from the FRP covered area (Kalfat et al.-Mahaidi, 2015) the chance to directly drill through the laminate simply address all the geometrical problems related to transversal wrapping.

Considering their bolt-like appearance, anchoring spikes seems mechanically intended to counter normal tension common in end-debonding-like failure modes (Grelle & Sneed, 2013) (Type I) but it has been proved how this system can efficiently counter shear stresses as well (Type II) providing an overall enhancement in bonding performances (Kalfat et al. 2011). A lot of research is currently undergoing in order to define the shear stresses related performance of anchor spikes through debonding-like bond-slip diagrams (Kim & Smith, 2009) (Smith, 2010) (Zhang et al. 2011).

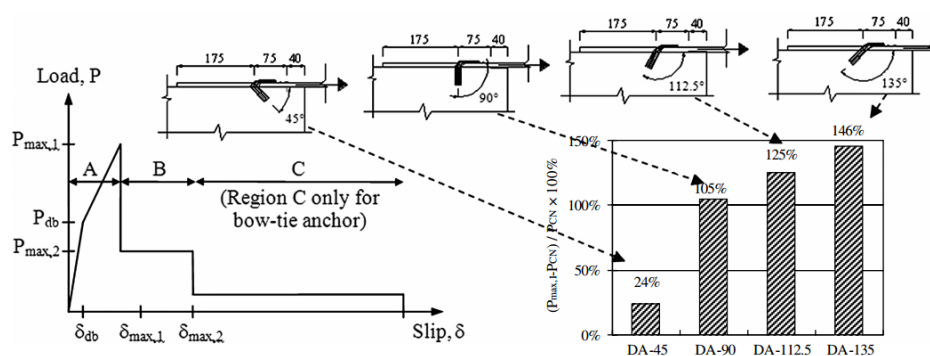


FIGURE 34 - ANCHORING SPIKE'S TYPICAL SLIP LAW (KALFAT ET AL. 2011)



FIGURE 35 - EXAMPLES OF ANCHORING SPIKES (SMITH, 2009)

In Particular situations, like anchoring shear-strengthening sheets on a T-shaped beam, anchors' dowel can even be drilled in the upper section's flange (Kalfat et al. 2011), inside the column in case of joint strengthening or inside the coupled wall, in case of column

confinement (Kobayashi et al. 2001). These particular applications will see a dowel working in pull-out, coupled to a shear-working fan.

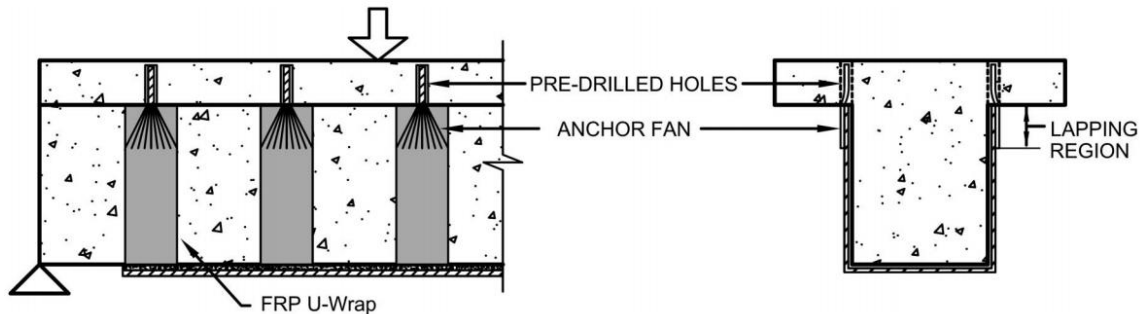


FIGURE 36 - ANCHORING SPIKES IN A PULL-OUT CRITICAL APPLICATION (KALFAT ET AL. 2011)

The confidence level in the research provided results is not yet enough to allow a standardization process toward design and characterization of this anchoring solution. Even the effectiveness in enhancing strength and ductility is still discussed (Micelli et al. 2010) (Type IV) though the results are encouraging and the research presented in the following aims to help answering some fundamental questions.

The capacity of these anchors to provide fundamental load transfer mechanism (Type III) has been already proved, for example in the case of cantilever beams' flexural strengthening (Lam & Teng, 2001). In the following it will be discussed how a similar mechanism can take place even in a bended simply supported element, where end anchors can provide the fundamental stress-transfer mechanism required for the FRP sheet to give strength to the bended element, after intermediate debonding occurs.

Research efforts are currently undergoing in order to characterize the behavior in terms of typical collapse mechanism and characterizing parameters:

- Ozbakkaloglu & Saatcioglu (2009) have widely discussed the pullout failure mode and its dependency on the embedment length, Kim & Smith (2007) (2009a) (2009b) (2010) have deeply discussed the issue as well coming developing a comprehensive characterization model.
- Zhang & Smith (2010) (2011) (2012) (2013) & Zhang (2013) have tested a huge amount of specimens in shear, discussing the influence of dowel angle, dry or wet application, fiber amount, fan configuration, different materials, different sheet stiffness and geometry. The quality of the work is beyond any doubt, though it focuses on a couple of particular kinds of failure: anchor shear rupture and FRP sheet rupture.

- Kobayashi (Kobayashi et al. 2001) was one of the first to investigate the anchor spikes efficiency, developing interesting results regarding the fan opening influence and experiencing different kind of failures (slipping, anchor rupture, sheet rupture) at varying test set-up.
- Zhang, Smith & Kim (2011) concluded that the anchors manufacturing is not effective on their performances, while Ozbakkaloglu & Saatcioglu (2009) pointed out the issues related to a poor hole cleaning and anchor installation in pull-out situations.
- Brena & McGuirk (2013) studied the anchors performance when arranged in series and/or parallel configurations, they pointed out as well how, in order for a unidirectional sheet to be fully engaged, all its width has to be covered by the anchor's fan. The relation between anchors spacing and sheet engagement was also discussed by Orton (Orton et al. 2008).
- Sun & Jirsa (2016) and Orton (2007) also identified the cross sectional area of the anchor, compared to the cross sectional area of the anchored sheet, as an influential parameter.

Studies also have been undergoing regarding the effectiveness of anchors spike in bending applications (Smith et al. 2011) (Smith et al. 2013) even though the experienced failure modes, when FRP sheet ultimate strength is not reached (pull-out, anchor shear failure) seems related to a certain under-dimensioning of the anchoring solution and not very well representative of a real case scenario.

Finally, it is worth noticing as analytical and numerical models have been developed as well, regarding either pull-out and shear characterization: Kim & Smith (2010), Zhang & Dai (2014), Kalfat et al.-Mahadi (2015), Sun & Ghannoum (2016).

3.5.5.3 *Metallic Anchors*

Sub-Categories: Bolted Plates, Bolted Angles, CHS, Mechanical Fasteners.

Resisted Force: Normal Tension, Shear Force.

Strengthening Applications: Flexural, Shear.

Debonding Type: Intermediate & End Debonding.

Mechanical Function: I, II, III, IV

Metallic anchorages were the earliest form of FRP end anchorage devices investigated (Kalfat et al. 2011).

End debonding either in shear and flexural strengthening can be countered applying bolted plates at the sheets' very end (Kalfat, 2008) (Deifalla & Ghobarah, 2010) (Grelle & Sneed, 2013) for shear applications on T-shaped sections, bolted angles have also been tested (Aridome et al. 1998) and even Cylindrical Hollow Sections (CHS) (Grelle & Sneed, 2013). Disposing the fasteners all over the element length, intermediate debonding as well can be countered, either enhancing performances with respect to normal and shear stresses (Type I, II) (Spadea et al. 1998) (Wu & Huang, 2008).

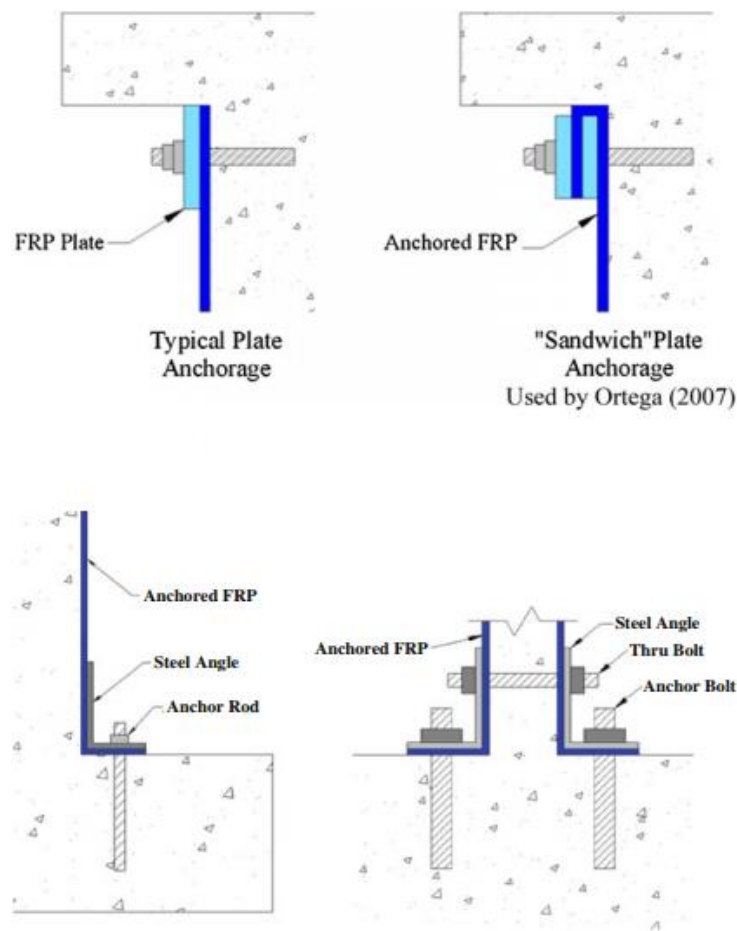


FIGURE 37 - METALLIC ANCHORS EXAMPLES (GRELLE & SNEED, 2013)

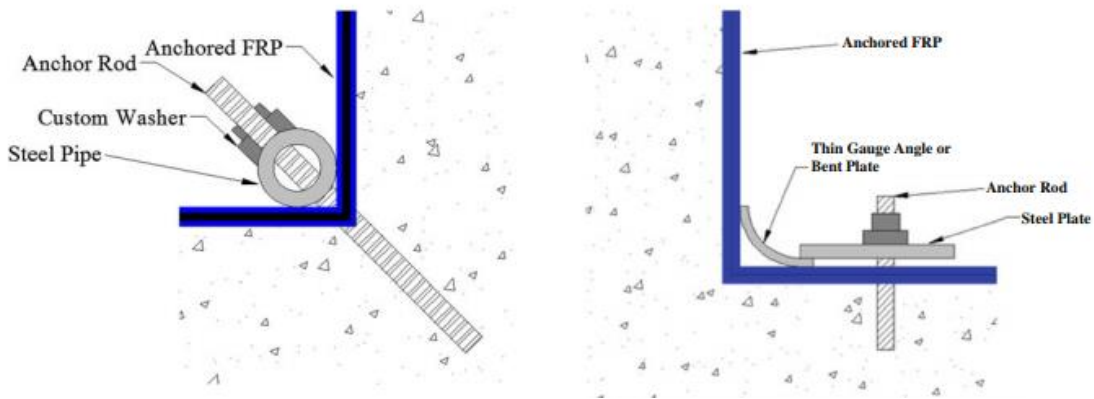


FIGURE 38 - METALLIC ANCHORS EXAMPLES (GRELLE & SNEED, 2013)

The anchoring systems contribution to strength & ductility (Type IV) has also been largely proved by the cited researchers (Kalfat et al. 2011). Equilibrium critical solutions exist as well, a peculiar one was proposed by Galal & Mofidi (2009) with and externally unbonded FRP sheet collaborating with the bended element through ductile steel fasteners (Type III, IV).

It is worth noticing that an interesting analytical model has been proposed by Nardone et al. (2011) describing the behavior of a bended element reinforced with an FRP sheet mechanically fastened over its all length.

3.5.5.4 Concrete Embedment

Sub-Categories: Pure Embedment, Rebar Wrapping.

Resisted Force: Normal Tension, Shear Force.

Strengthening Applications: Flexural, Shear, Joints.

Debonding Type: End Debonding.

Mechanical Function: I, II, III, IV

Pure embedment is a feasible solution to “create” bonding length when free space is not available, even if it can actually be applied to improve performances against end debonding either against shear and normal stresses (Type I, II) and to improve the ductility of the system allowing higher deflections (Type IV), the most suitable application is to provide equilibrium critical transfer stress-transfer mechanisms for examples in

cantilever-column joints (Type III). Examples of teste applications can be find in Kalfat et al. (2011) and in the related literature.

The main problem with this kind of anchoring system is the request of a deep cut into the concrete with all the related dangers. An alternative solution has been proposed to limit the depth: a larger cut has to be performed, large enough to suit a FRP rebar around which the FRP sheet will be wrapped; the all system will then be embedded in the hole, later filled with epoxy (Grelle & Sneed, 2013).

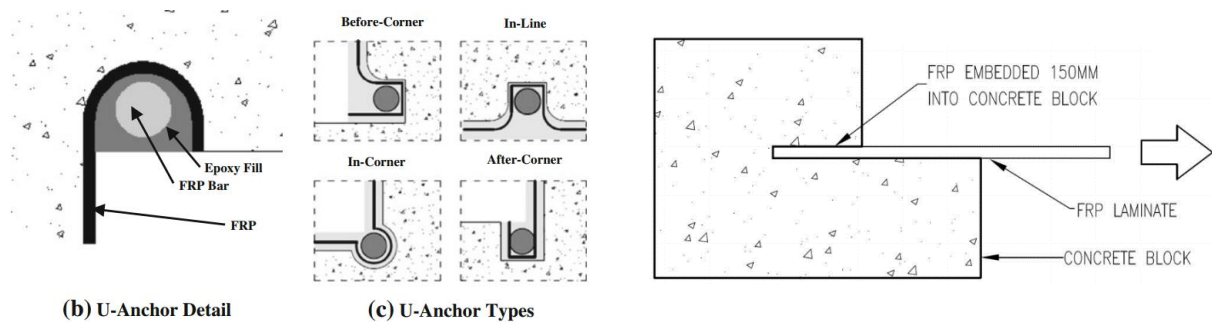


FIGURE 39 – CONCRETE EMBEDMENT (GRELLE & SNEED, 2013) (KALFAT ET AL. 2011)

3.5.5.5 Surface Preparation

Sub-Categories: Superficial, Surface Cutting.

Resisted Force: Normal Tension, Shear Force.

Strengthening Applications: Flexural, Shear.

Debonding Type: End & Intermediate Debonding.

Mechanical Function: I, II, IV

While it is clearly understood that surface preparation plays a fundamental role in defining FRP bonding performances (type I,II) and improving strength and ductility performances for the whole element (type IV), few are the studies focused on the matter (Kalfat et al. 2011).

Mostofinejad & Mahmoudabadi (2010) proposed an effective method for superficial surface preparation, while Al-Mahaidi & Sentry (2009) and Kalfat et al.-Mahaidi (2011) proposed a more radical solution, consisting in cutting a longitudinal strip of concrete, embedding a rebar in it and filling the hole with epoxy, over which the FRP strip will be

applied. The idea is that the FRP will bond effectively to the epoxy surface that will transfer shear stresses to the wider carved surface. The solution is somehow a Hybrid between standard FRP reinforcement and NSM, an alternative external strengthening method widely discussed by Nanni (2009) (2000) (2004).

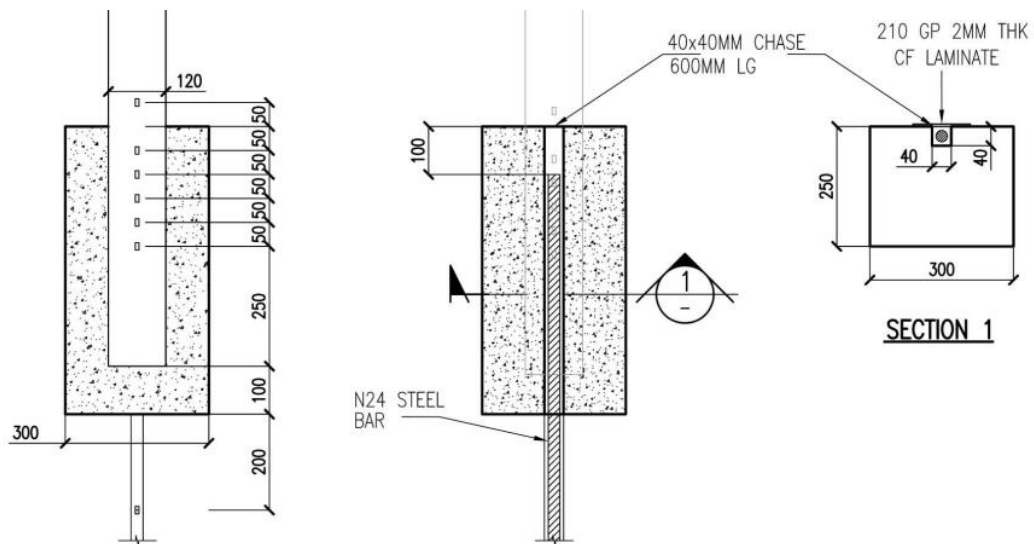


FIGURE 40 - SURFACE PREPARATION WITH EMBEDDED REBAR (KALFAT ET AL. 2011)



FIGURE 41 - NEAR SURFACE MOUNTED RODS (NSM) (NANNI, 2000)

3.5.6 Anchor Testing

Two different approaches to FRP anchors testing can be spotted (Grelle & Sneed, 2013):

- I. *Simplified Single Anchor Testing* allows to characterize the anchoring system behavior and its dependency on the basic geometric and material parameters involved.
- II. *Full Strengthened System Testing* is fundamental to validate the effectiveness of an anchoring solution in real-life applications.

Different goals are related to each kind of testing: with *Single Anchor Testing* the goal is developing characterization formulas, allowing to define the single anchor's strength in shear & pullout; with *Full System Testing* The goal is developing reliable design algorithms, allowing to design the strengthening system, knowing the single anchor characterization. A clear schematized approach to achieve a full characterization for a new anchoring system is proposed by Grelle & Sneed (2013).

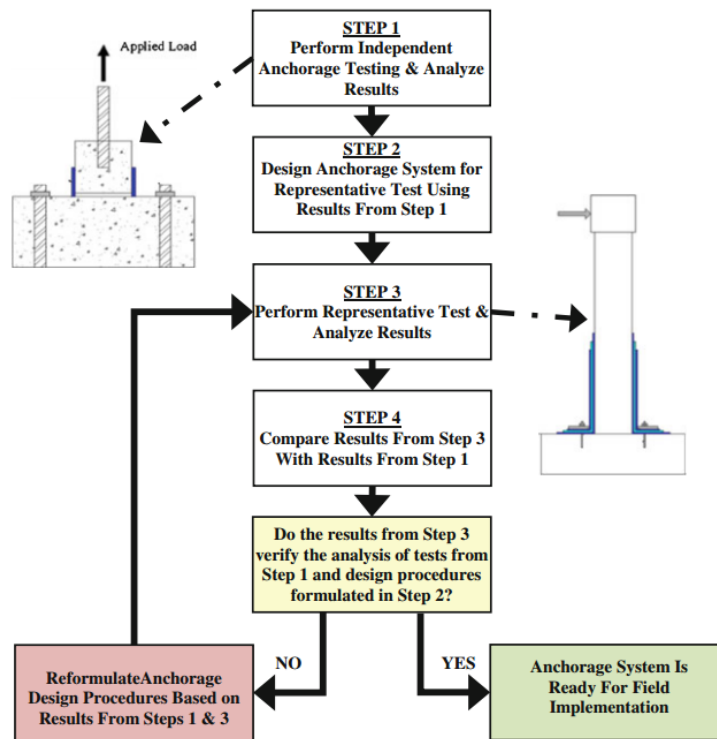


FIGURE 42 - ANCHORING SYSTEM DESIGN & VALIDATION (GRELE & SNEED, 2013)

Full scale modeling is strictly application-related, while some common approaches can be spotted in the field of single anchor testing. It is worth noticing that, in order to fully characterize the anchors' effectiveness in terms of ductility, a full system approach is always required, while some information in terms of ultimate strain increment can be spotted from every kind of simplified test.

3.5.6.1 Pull-Out Test

Resisted Force: Normal Tension.

Mechanical Function: I, III

It is the simplest and most basic form of anchor testing (Grelle & Sneed, 2013), the ability to transfer tensile load from the concrete to the anchoring system and vice-versa is evaluated, characterizing the anchors effectiveness against normal stresses (Type I) and in equilibrium critical tensile applications (Type III) (Grelle & Sneed, 2013).

The limits of the testing method are mostly related to the absence of concrete-anchor shear transfer (Grelle & Sneed, 2013) that limit the representativeness of the testing method to few real-life applications. Among the advantages also the possibility to directly measure the pull-out ultimate strength and the load-slip curve without the need to refer to conversion formulas.



FIGURE 43 - PULL-OUT SETUP (OZBAKKALOGLU & SAATCIOGLU, 2009)

3.5.6.2 Direct Shear Test

Resisted Force: Shear Force.

Mechanical Function: I, II

The chance to include FRP bonded length allows to better characterize the anchor's behavior in a real system, this, along with the nature of the applied load, makes this kind of tests the closest to most of the real-life applications for anchoring systems.

The method best fits type II characterization, slightly combined with type I behavior: the normal stresses concentration at the end of FRP laminates is well known, even though is largely increased in flexural application, because of beams' curvature, rather than pure shear ones. In absence of bonding length, the method is also suitable to characterize equilibrium-critical shear applications (Type III). Different set-ups have been proposed and applied with various fortunes:

- I. *Single Shear Tests* (e.g. Kalfat et al.-Mahaidi, 2010) are the most basic setup in this category (Grelle & Sneed, 2013), the main advantage it's the conceptual simplicity, while providing a solution to keep the block fixed during load application can provide some challenges, as well as applying a uniform non-eccentric load to the specimen.
- II. *Double Shear Tests* (e.g. Ceroni et al. 2007) automatically accounts for centered load application due to their symmetric set up, while the concrete block fixity problem still remains.
- III. *Double-Block Shear Tests* (e.g. Eshwar et al. 2008) provide also a solution to fix concrete blocks, used as contrast for load application. The issue is the long preparation required.
- IV. *Double Wrapped Shear Tests* (e.g. Berneschi, 2015) provide a symmetric auto-fixing experimental set-up, requiring an acceptable preparation effort. The feasibility of the double-wrapped set-up and its effectiveness in characterizing spike-anchors behavior will be discussed in the following.

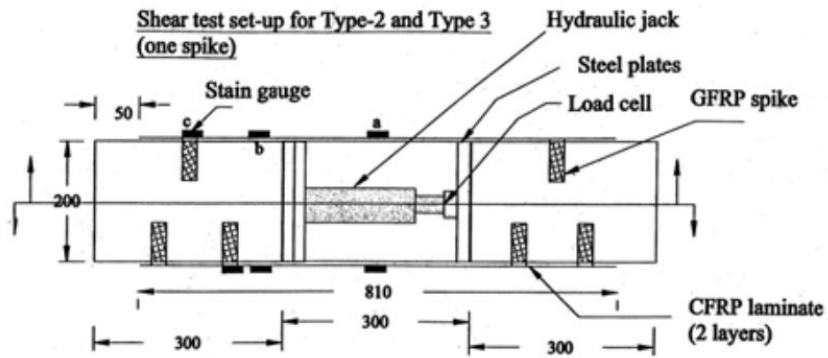
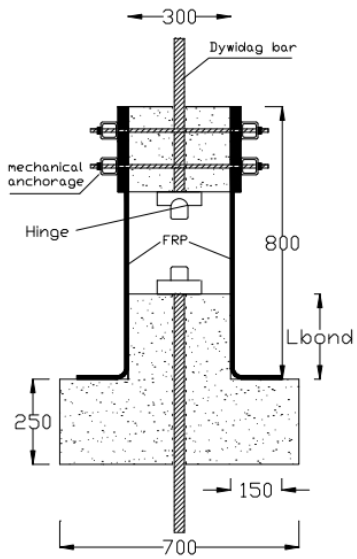


FIGURE 44 – SINGLE SHEAR TEST (KALFAT ET AL.-MAHAIDI, 2010), DOUBLE SHEAR TESTS (CERONI ET AL. 2007), DOUBLE BLOCKS SHEAR TEST (ESHWAR ET AL. 2008), DOUBLE WRAPPED SHEAR TEST (BERNESCHI, 2015)

3.5.6.3 Bending Tests

Resisted Force: Shear & Normal Forces

Mechanical Function: I, II, III

Small-scale bending tests provide a simply fixable set-up for anchors characterization in combined shear-bending (Type I, II) and even equilibrium critical application (Type III).

The stresses combination is probably the closest one to a real-scale bended system, achievable through a small-scale test (Grelle & Sneed, 2013). The main issue is recovering characterizing data from the applied transversal load measure.

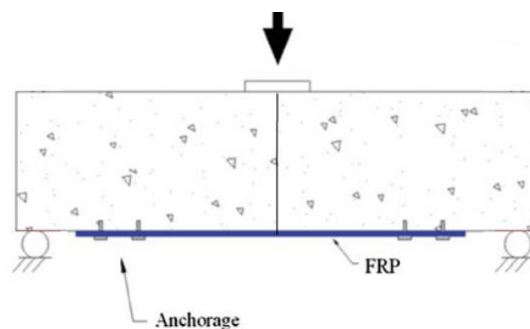


FIGURE 45 - BENDIN TEST (ADAPTED FROM GRELE & SNEED, 2013)

3.5.7 Research Direction

3.5.7.1 The Need for a Unified Approach

It is critical to underline how a unified approach is lacking and the quite significant amount of data available is not easily interpretable. A certain confusion in the data handling can be noticed, well characterized by the widespread practice of averaging ultimate loads over different collapse mechanism, making thus impossible to define the parameters characterizing each collapse mechanism. A certain lack of potentially critical information can also be spotted, ranging from ambiguous definition of the tested geometries, to missing elastic properties of the involved material, epoxies over all, to failure to present strain data (Kalfat et al. 2011).

These tendencies mark a general confusion in approaching anchors' characterization from a rational point of view. Spotting how a failure-mechanism oriented approach is

missing. Also confusion still exists towards understanding anchors mechanical behavior, identifying critical parameters involved and defining research priorities.

Questionable choices in anchors' design and configuration can be noticed, with a huge amount of data referring to under-dimensioned spikes, all failing in shear, and in general the tendency to test little scale application (Kalfat et al. 2011).

A certain tendency in presenting concrete-crushing related data can also be spotted (Kalfat et al. 2011): while it is important to know that such a failure mode can happen, the related results can hardly be applied to characterizing the anchor's behavior.

In general, the need for a uniform approach toward assembling a big anchor-related data-base has been underlined by many (Grelle & Sneed, 2013) and some efforts are already undergoing (Kalfat et al. 2011) (Grelle & Sneed, 2013). Much more needs to be done though.

3.5.7.2 Available Guidelines

The lack of reliable data reflects in the lack of guidelines focused on anchor design. The general requirement, either from ACI (2008) and CNR (2013), is to fully characterize the applied anchoring solution, that should be *heavily scrutinized through representative physical testing* (ACI, 2008) otherwise *no enhances in strength and ductility should be accounted for* (CNR, 2013).

It is worth noticing that requiring an experimental characterization of the implemented solution doesn't provide a complete solution to the problem, not even from a temporary prospective: a standardized testing approach is not available yet, leading to the already discussed confusing situation.

The only anchor variant somehow normed is the U-wrap solution, mainly due to its widespread shear-strengthening application:

- CNR allows to neglect normal stresses in SLS debonding check when end anchoring is provided via U-wraps, not requiring for testing to validate this particular behavior (CNR-DT 200 R1/2013 4.1.5(6)).
- ACI requires U-wrapping to avoid shear-induced end-debonding/peeling for shear values higher than $\frac{2}{3}$ of the concrete shear strength (ACI 440.2R-08 13.1.2). The cross-sectional area of the applied transverse anchoring system should be computed according to Reed et al. (2005).

4 Anchoring Spikes: State of the Art Review

As mentioned, anchor spikes are suitable to a wide range of application in the rehabilitation field. Referring to the general framework previously defined, an in-depth view of the topic will be here presented, focused on discussing what already has been published and eventually reinterpreting the results from a global prospective.

4.1 Manufacturing & Installation

A wide variety of procedures can be implemented while manufacturing and installing anchoring spikes with various consequences on the system performances. It is worth noticing how Zhang & Smith (2011) have pointed out the secondary effect of anchors' manufacturing and installation properties on shear performances. On the contrary Ozbakkaloglu & Saatcioglu (2009) underlined the significant influence of a bad installation on Pull-Out performances.

In general, a comprehensive comparative study is not available yet and more investigation is required in order to define the influence of each manufacturing and installation parameter. Refer to Zhang & Smith (2013) and referred paper for partial results and investigation into wet/dry applications.

4.1.1.1 Fiber Rolls / Fiber Bundles

The vast majority of tested anchors, including the ones tested by Ozbakkaloglu & Saatcioglu (2009), Kim & Smith (2010), Zhang & Smith (2013), Brena & McGuirk (2013) are hand-made anchors, manufactured from fiber rolls of varying width.

Factory made examples, provided as loose fibers bundles, are the one tested by Berneschi (2015) and discussed as well in the present dissertation.

4.1.1.2 Pre-Cured / Wet Dowel

The anchors' dowel can either be pre-impregnated and pre-cured (e.g. Ahang & Smith, 2011) or impregnated on site and inserted wet in the hole (Berneshi, 2015). While the

first one makes it easier to insert the dowel, the latter guarantee better adherence and bonding performances, allowing the uncured dowel to expand inside the hole.

Considering the results from Ozbakkaloglu & Saatcioglu (2009) an optimal installation should always be preferred in pull-out critical applications, a wet installation should hence be preferred. In shear critical installation the influence of the dowel condition is less critical, however a two-steps impregnation for dowel and fan may lead to stress concentrations and a suboptimal impregnation of the dowel's shear critical section.

4.1.1.3 One-Step / Two-Step Fan-Sheet Impregnation

Whether to wait for sheet curing before proceeding to impregnation (Berneschi, 2015) or do the application in one step (Zhang & Smith, 2011) is another variable. It should be noticed that waiting for curing allows an easy sheet drilling, while a one-step application is more suited for non-drilled applications. It is reasonable to expect better slipping performances for a one-step application, but whether this parameter might be critical or not, it still to be defined.

4.1.1.4 Sheet Drilling / Undrilled Application

Drilling in the middle of the cured sheet is an easy way to make room for spike application (Berneschi, 2015), an alternative is opening the sheet fibers and insert the spike in-between (Zhang & Smith, 2011). The latter solution is easily performable for small size dowels, becoming complex at increasing diameters.

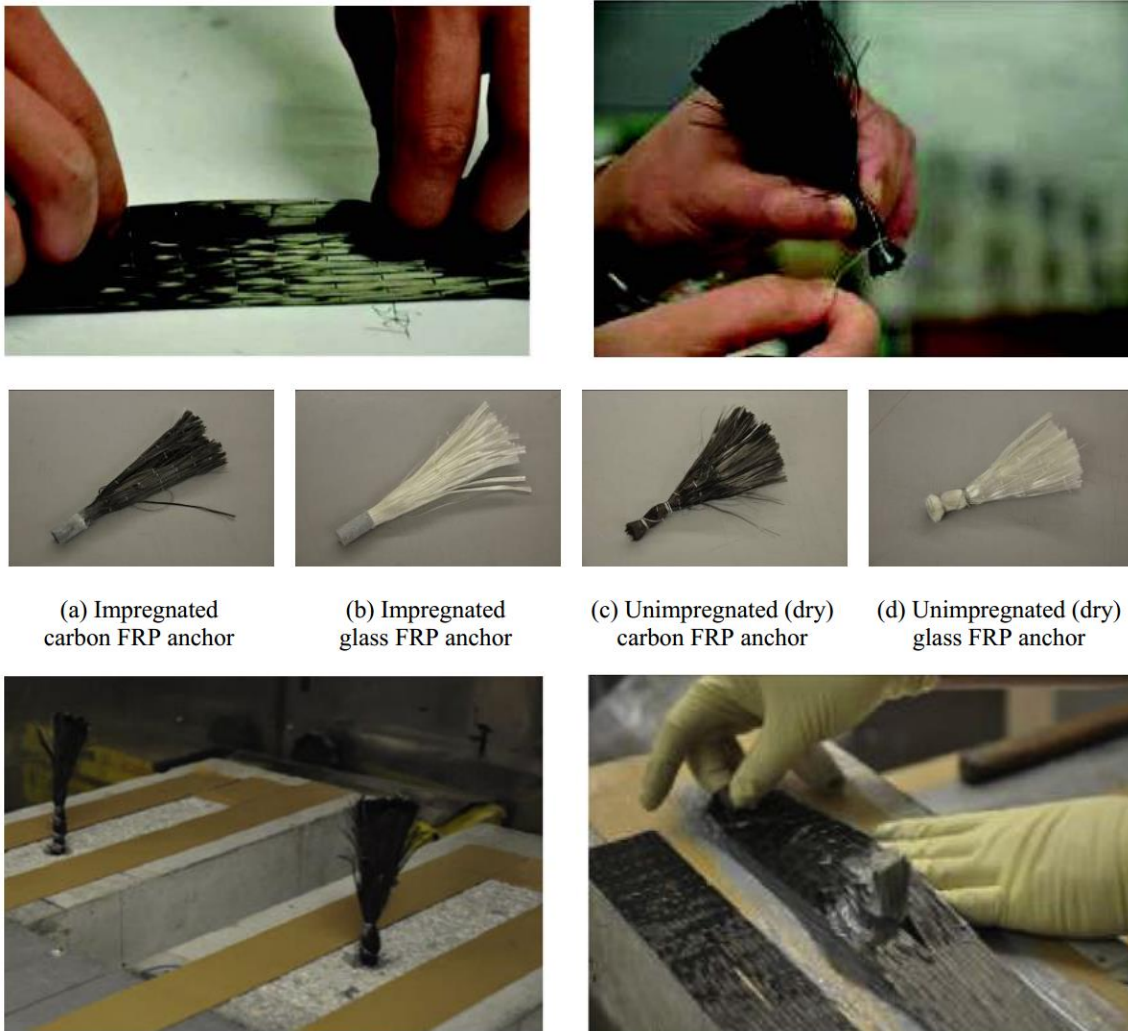
It is important to notice that drilling a hole prevent the mono-directional fibers behind the hole itself to contribute to the strength of the system; this might be influential in application in series, even though opening the sheet's fibers also implies varying the stress distribution around the dowel, enforcing stresses concentrations.

4.1.1.5 Wet / Dry Applications

The radical idea of non-impregnate the whole anchor or impregnate all but the portion between dowel and fan was suggested by Zhang & Smith (2013 and related papers).

The reasons behind such a solution, apart from the scientific curiosity, doesn't seem to justify such an application in real applications: while an uncured dowel may be simpler to apply and still reasonably able to provide the required strength, as long as its critical

section is impregnated; a non-impregnated critical section would be extremely sensible to stresses concentration and a non-impregnated fan would reasonably show worse shear-transfer capacity with no reasonable advantages in terms of installation.



(a) Impregnated carbon FRP anchor

(b) Impregnated glass FRP anchor

(c) Unimpregnated (dry) carbon FRP anchor

(d) Unimpregnated (dry) glass FRP anchor

FIGURE 46 - ANCHORING SPIKES MANUFACTURING & INSTALLATION (SMITH, 2009) (ZHANG ET AL. 2011)

4.2 Characterization

As discussed, anchors characterization, either from the experimental and analytical point of view, is object of current research and still an open problem. The results already achieved will be presented and discussed, trying an interpretation from a global, consistent prospective.

4.2.1 Fundamental Parameters

According to the up-to-date researches, a large number of parameters can play a role in defining the behavior of an anchor spikes, the influence of each parameter will be later discussed according to the most up-to-date research results.

The characterizing parameters can be subdivided in *Material Properties*, *Dowel Geometry Parameters*, *Fan Geometry Parameters*, *Global Geometry Parameters*, *Position Parameters*, *Configuration Parameters* and *Quality Parameters*. Also characterization of the surrounding environment can play an important role in defining the joint properties and should hence be accounted for.

4.2.1.1 *Material Properties*

$E_{f,dry,anch}$	Dry Fibers Elastic Modulus
$\nu_{f,dry,anch}$	Dry Fibers Poisson's Ratio
$f_{fu,dry,anch}$	Dry Fibers Ultimate Strength
$\varepsilon_{fu,dry,anch}$	Dry Fibers Elongation
$E_{a,anchor}$	Adhesive Elastic Modulus
$\nu_{a,anchor}$	Adhesive Poisson's Ratio
$f_{au,anchor}$	Adhesive Ultimate Strength
$\varepsilon_{fu,anchor}$	Adhesive Elongation

$E_{f,anchor}$	Impregnated Fibers Elastic Modulus
$\nu_{f,anchor}$	Impregnated Fibers Poisson's Ratio
$f_{fu,anchor}$	Impregnated Fibers Ultimate Strength
$\varepsilon_{fu,anchor}$	Impregnated Fibers Elongation
$V_{f,dry,anchor}$	Dry Fibers Volume
$V_{a,anchor}$	Adhesive Volume
$\rho_{f,dry,anchor}$	Dry Fibers Density
$\rho_{a,anchor}$	Adhesive Density

Whether a laminate-like characterization for the dry and impregnated fibers provides realistic results for the particular geometrical shape of anchor spikes is still to be assessed due to the lack of complete characterization models for the spikes themselves. Test results on impregnated laminates are generally provided as characterization data in technical reports for commercial products and in literature, for example by Zhang & Smith (2011a, 2011b) and Zhang et al. (2011). For the sake of consistency, the same approach will be applied hereinafter.

Some researchers pointed out the amount of dry fibers as a significant parameter in defining the anchor's behavior (e.g. Zhang & Smith, 2011a). Whether this parameter is actually significant on its own, or its effect in defining materials' behavior is already included in the definition of impregnated material properties – according to a laminate-like approach – is still to be assessed.

4.2.1.2 Dowel Geometry

h_{dowel}	Nominal Dowel Length / Hole Depth
d_{dowel}	Nominal Dowel Diameter / Hole Diameter
β_{dowel}	Dowel Angle
r_{ch}	Chamfer Radius

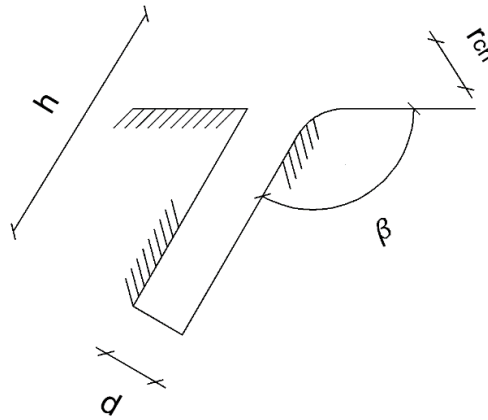


FIGURE 47 - DOWEL GEOMETRY

Notice that some researchers differentiate the dowel diameter from the hole diameter (Niemitz et al. 2010) (Zhang & Smith, 2011). In the present research they will always have the same value and, at least for what concern the application procedure here performed, they can always be assumed equal, the same can be said also for hole depth and dowel length. Generally speaking, assuming hole's geometry as nominal dowel geometry seems a simplified feasible approach.

4.2.1.3 Fan Geometry

α_{fan}	Fan Opening
R_{fan}	Fan Radius
w_{fan}	Fan Width
A_{fan}	Fan Area
t_{fan}	Fan Thickness

Notice that the fan geometry, showed in the picture below, is rarely an actual circular one. The fan radius definition is chosen in order to define the total anchor length as:

$$l_{anchor} = h_{dowel} + R_{fan}$$

Once fixed the hole diameter, only two parameters need to be assigned to define the fan configuration, being width, opening and radius linked. The fan area is a fundamental parameter to characterize the sheet-anchor shear-stress transfer and should be properly computed. A simplified approach consists in assuming a circular slice shape, centered in the hole center, the result is on the safe side but it is too conservative even from a design prospective. A more accurate approach considers the actual geometry of the fan – sketched below – assuming fibers starting to spread with the assigned angle from the transversal diameter’s edges and a parabolic shape for the fan.

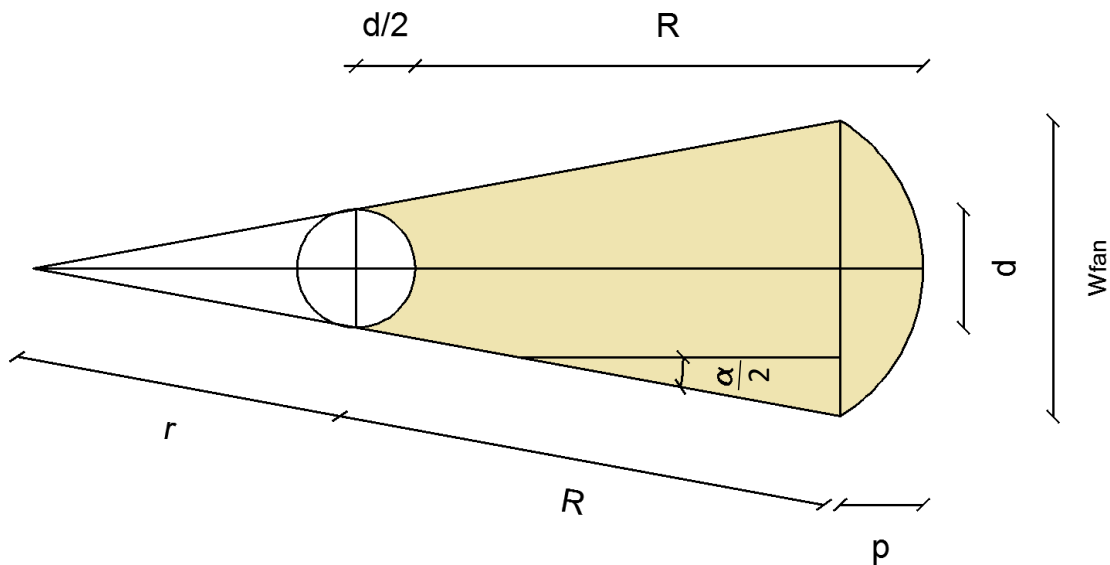


FIGURE 48 - FAN GEOMETRY

Refer to the following formulas for a complete geometrical fan description, assuming hole diameter, fan radius and opening assigned:

$$w_{fan} = d + 2R \sin(\alpha/2)$$

$$p = R + \frac{d}{2} - R \cos(\alpha/2)$$

$$r = \frac{d}{w_{fan} - d} R$$

$$A_{fan} = \frac{(r + R)w_{fan}}{2} \cos(\alpha/2) - \frac{rd}{2} \cos(\alpha/2) - \frac{\pi d^2}{8} + \frac{2}{3} p w_{fan}$$

In case the anchor width is larger than the sheet width, the difference should be accounted for adding additional terms:

$$A_{fan,mod} = A_{fan} - p \left[\frac{w_{sheet}^3 - w_{fan}^3}{3 w_{fan}^2} + w_{fan} - w_{sheet} \right] - \frac{(w_{fan} - w_{sheet})^2}{4} \cot(\alpha)$$

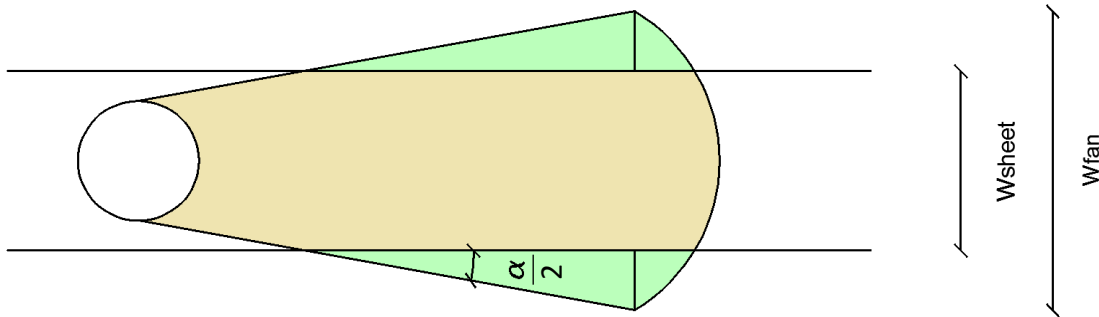


FIGURE 49 - FAN LARGER THAN THE FRP SHEET

In the table below different configurations are considered, ranging from the tested ones to a quite unusual example. The results provided by the proposed formula are reasonably accurate and always on the safe side when compared to the numerical result provided by a CAD software.

α	d	R	w_{fan}	w_{sheet}	A_{circle}	$A_{proposed}$	A_{cad}	Δ_{circle}	$\Delta_{proposed}$
[°]	[in]	[in]	[in]	[in]	[in ²]	[in ²]	[in ²]	[%]	[%]
60	1	3	4.00	6	4.71	8.51	8.60	-45.22%	-1.11%
90	1	3	5.24	6	7.07	11.05	11.30	-37.47%	-2.27%
90	1	4	6.66	6	12.57	17.64	17.97	-30.09%	-1.86%
20	2	8.33	4.89	3	12.10	24.57	25.44	-52.43%	-3.43%

It is worth noticing that the proposed formula provides good results for the anchors tested in the present work, for different applications (typically 180 ° and 360° ones) a circular formula might be closer to the actual value, remembering to measure the total radius starting from the hole's center:

$$R_{tot} = \frac{d}{2} + R$$

Finally, it has to be noticed how fan's thickness can play a critical parameter in defining anchor's stiffness and should hence be accounted for. It has to be noticed the fan thickness is a hard to measure quantity and variable from a maximum, close to the dowel, to a minimum at the fan's very end. Global geometry considerations can provide an easy way to define fan thickness, or account for its effect on anchor's stiffness.

4.2.1.4 Global Geometry

l_{anchor}	Total Length
CSR	Cross-Sectional Ratio

Some researchers (Sun, 2014) (Sun et al. 2016) provide a so called anchor material ratio (AMR) instead of the simple measure of fan's thickness, identifying the cross-sectional anchor/sheet area ratio as the critical parameter. Here the notation cross-sectional ratio (CSR) is preferred to avoid confusion with the fiber/adhesive ratio defining the strength of the composite.

$$CSR = \frac{t_{fan}W_{fan}}{t_{sheet}W_{sheet}}$$

Considering that the amount of fibers embedded in the concrete is the same as the amount of fibers spread in the fan, and assuming the drilled hole is not over-dimensioned for that amount of fiber, it is true that:

$$A_{cross, fan} = A_{cross, dowel} = A_{anchor}$$

$$A_{cross, fan} = f_{fan} w_{fan}$$

$$A_{cross, dowel} = \frac{\pi d_{dow}^2}{4}$$

Hence an easier way to define the CRS can be provided and CRS becomes a global parameter, characterizing both fan and dowel:

$$CRS = \frac{A_{anchor}}{A_{sheet}}$$

Knowing the dowel cross section, a nominal fan thickness on the largest fan section can be defined as:

$$t_{fan} = \frac{A_{anchor}}{w_{fan}} = \frac{\pi d_{dow}^2}{4 w_{fan}}$$

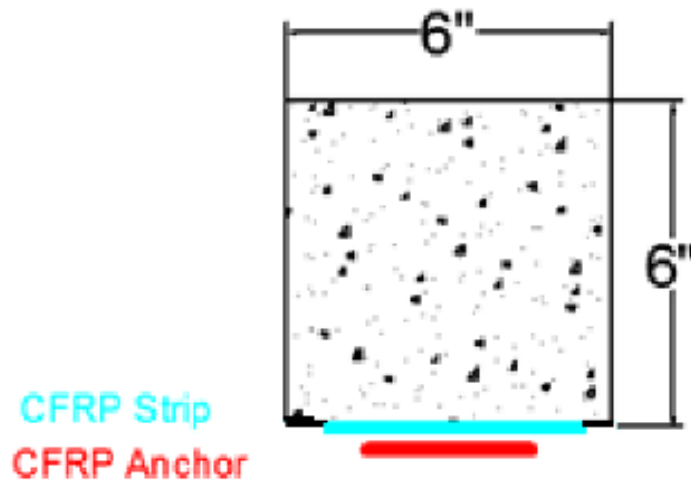


FIGURE 50 - CSR GRAPHIC REPRESENTATION (SUN, 2014)

4.2.1.5 Position

l_{end}	Distance from sheet's end / to hole's center
l_{side}	Distance from sheet's side / to hole's center
$l_{midspan}$	Distance from midspan / to hole's center

Notice that the distance from the end can be critical in defining how the anchor is engaging the normal and shear stresses concentrations close to the ends, while, in flexural applications at least, distance from midspan is critical in defining whether the anchor is in a cracking critical zone or not. The two quantities are obviously linked.

4.2.1.6 Configuration

n	Number of anchors
n_L	Number of lines in series / Longitudinally
n_P	Number of anchors in parallel per line / Transversally
s_L	Spacing between lines in series / Longitudinally
s_P	Spacing between anchors in parallel / Transversally

A wider range of qualitative considerations can be included in this category, for example whether particular solutions are implemented: sandwich configurations, coupling with different kind of anchors, anchors' fan inclined with respect to the main direction, anchors not drilled into the FRP sheet.

Good examples of these non-conventional solution are provided by Kalfat et al.-Mahaidi (2015) as well as Sun & Ghannoum (2015). Sandwich solution is discussed by Berneschi (2015) and will be treated in the following.

4.2.1.7 Quality

It has been proved that the quality of the *installation* can play a major role in defining the anchors' strength (Ozbakkaloglu & Saatcioglu, 2009). The influence of *manufacturing*, including whether to impregnate or not the anchor's dowel and fan, has been discussed as well and is believed to play a minor role (Zhang & Smith, 2011). Orton et al. (2008) pointed out that surface preparation may not be critical in presence of adequate anchorage, substrate bonding has though been showed to improve anchors performances and allow transversal stress redistribution (Sun et al. 2016).

4.2.1.8 Surrounding

Surrounding's properties involve material properties of concrete, FRP sheet and its constituents, as well as their geometry. Also the FRP bonding properties should be accounted for, either experimentally or analytically, as well as the adhesive properties that determine fan-sheet adhesion, for which analytical models are not available yet.

4.2.2 Pull-out Characterization

The pull-out behavior of FRP anchors is conceptually well known, thanks to the good understanding of pull-out behavior of steel anchors, achieved through a wide experimental campaign at the end of the past century. For more detail on steel anchors characterization please refer to Cook (1993).

Moving from steel to FRP pull-out required re-calibrating the already-available models, the effort has been carried on by Ozbakkaloglu & Saatcioglu (2009) and Kim & Smith (2010), a full analytical characterization for ground anchors was also provided by Zheng & Dai (2014).

4.2.2.1 Collapse Mechanisms

It is worth noticing that a collapse-mechanism focused approach is generally implemented and characterizing parameters for each mechanism have been identified (Ozbakkaloglu & Saatcioglu, 2009) (Kim & Smith, 2010). Four collapse mechanisms have

been identified, three pure and a combined one, along with a concrete specimen splitting, non-representative of real-case scenarios:

- I. Concrete Cone Failure
- II. Bond Failure
- III. Combined Concrete/Bond Failure
- IV. FRP Tensile Rupture



a) Concrete cone failure b) Combined cone/bond failure c) Anchor rupture

FIGURE 51 - PULL-OUT FAILURE MODES (OZBAKKALOGU & SAATCIOGLU, 2009)

4.2.2.2 Ozbakkaloglu & Saatcioglu (2009)

Test Method: Pull-Out.

Manufacturing: Hand-Made.

Collapse Mechanism: I, II, III, IV

Parameters: h_{dowel} , d_{dowel} , β_{dowel} , f_{ct} , A_{anchor} , f_{fu} , $f_{b,pull}$

The proposed model completely describes the pull-out strength of an FRP anchor spike, however the model is calibrated over a limited amount of data and, because of its formulation, is hardly applicable to design or experimental prediction.

The notation used here is modified for the sake of clarity and consistency, the model is intended to be used with SI units.

$$N_u = \min(N_c, N_b, N_{cb}, N_f)$$

The concrete cone failure is computed basing on an adapted ACI 349-85 formula, where h_c is the height of the concrete cone, difficult to predict in a design scenario. The concrete-cone strength increases at increasing cone height (h_c) and anchor diameter; the concrete tensile strength has a positive effect as well.

$$N_c = \pi h_c^2 \left(1 + \frac{d_{dowel}}{h_c} \right) f_{ct}$$

A physically meaningful formulation is proposed for the pure bond failure, based on the assumption of uniform bond stress distribution over the dowel length, but a formulation for the bond strength is not provided and a regression formula is proposed instead. In both formulations the pure-bond strength increases at increasing bonded length (h_b) and hole diameter, the first formulation explicitly accounts for the pull-out bond strength.

$$N_b = \pi d_h h_b f_{b,pull}$$

$$N_b = \alpha d_h^{0.66} h_b^{0.83}$$

The combined cone-bond strength is simply defined as the sum of the two contributions, each computed referring to the proper cone and bonded height:

$$N_{cb} = N_c + N_b$$

Finally, the tensile rupture strength is simply assumed proportional to the impregnated fiber strength and the dowel area:

$$N_f = A_{anchor} f_{fu,anchor}$$

As discussed, the anchor area can be defined in different ways: the authors suggest to refer to the cross sectional area of the fiber sheet, rolled up to manually realize the anchor's dowel.

The authors also showed that the anchor's pull-out strength decreases at increasing dowel angle, the result was related either to pure debonding failures and fiber rupture ones. An analytical model to account for the effect was not provided.

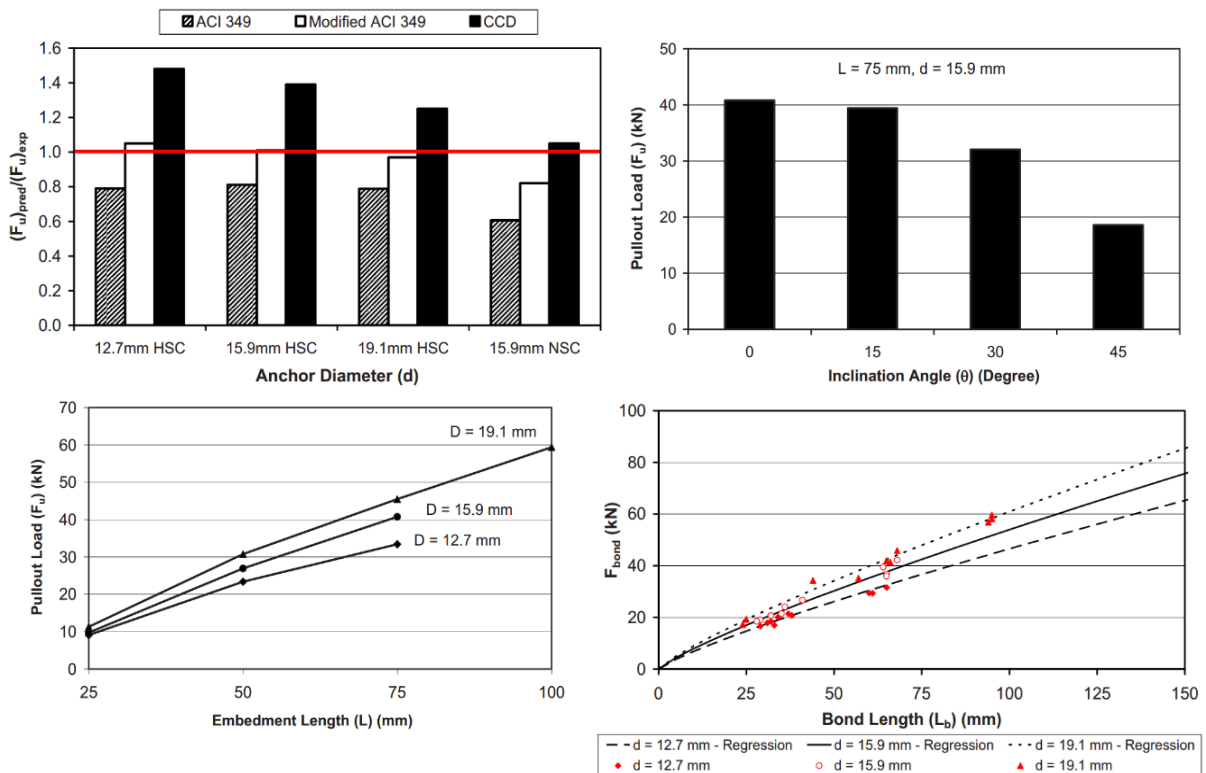


FIGURE 52 - RESULTS FROM OZBAKKALOGLU & SAATCIOGLU (2009)

4.2.2.3 Kim & Smith (2010)

Test Method: Pull-Out.

Manufacturing: Hand-Made.

Collapse Mechanism: I, III, IV

Parameters: h_{dowel} , d_{dowel} , β_{dowel} , f'_c , A_{anchor} , f_{fu} , $f_{b,pull}$

After an overview of the pull-out model proposed up to the time of writing, the authors propose either a comprehensive analytical model and a design variant. The notation used here is modified for the sake of clarity and consistency, the model is intended to be used with SI units.

It is worth notice that the pure debonding failure is not considered representative of real situation and hence neglected. The applicability problem of Ozbakkaloglu & Saatcioglu (2009) is also solved avoiding to differentiate between cone height and bond height, having all collapse strength (I, III) proportional to the whole dowel height.

$$N_u = \min(N_c, N_b, N_f)$$

The concrete-cone strength increases at increasing dowel depth and concrete strength, the cone height is not explicitly accounted for, and the hole diameter plays no role:

$$N_c = \alpha_c h_d^{1.5} \sqrt{f'_c}$$

$$N_c = 9.68 h_d^{1.5} \sqrt{f'_c}$$

A formulation similar to the one Ozbakkaloglu & Saatcioglu (2009) proposed for the pure bond failure is proposed for the combined failure, a safe-side constant design value is proposed for the bond strength, variable with concrete strength.

$$N_b = \pi d_h h_d f_{b,pull}$$

$$N_b = \begin{cases} 4.62 d_h h_d f_{b,pull} & f'_c < 20 \text{ MPa (2.9 Kips)} \\ 9.07 d_h h_d f_{b,pull} & f'_c > 20 \text{ MPa (2.9 Kips)} \end{cases}$$

Finally, the tensile rupture strength is simply assumed proportional to the impregnated fiber strength and the dowel area, computing the dowel area exactly as Ozbakkaloglu & Saatcioglu (2009). Only a corrective coefficient is added:

$$N_f = \alpha_f A_{anchor} f_{fu,anchor}$$

$$N_f = 0.59 A_{anchor} f_{fu,anchor}$$

The authors advise that a larger amount of data is required to properly calibrate the model and make it adequately reliable for design applications.

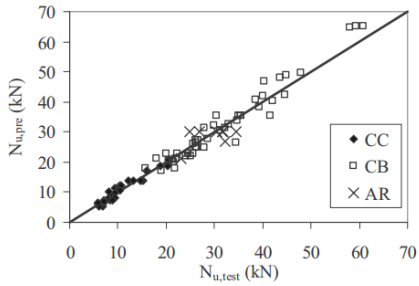


Fig. 3. Predicted versus test results (best-fit model)

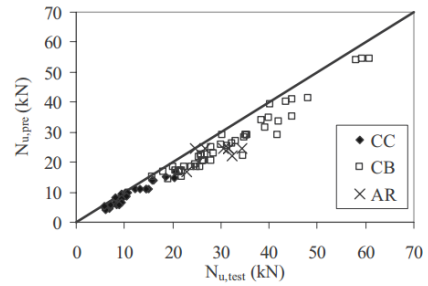
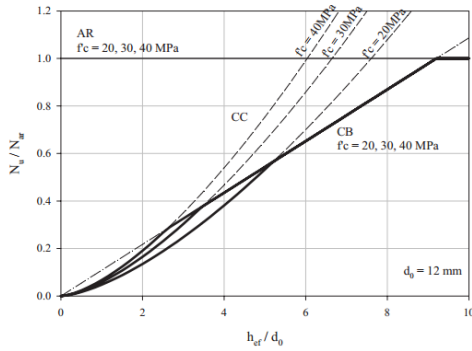
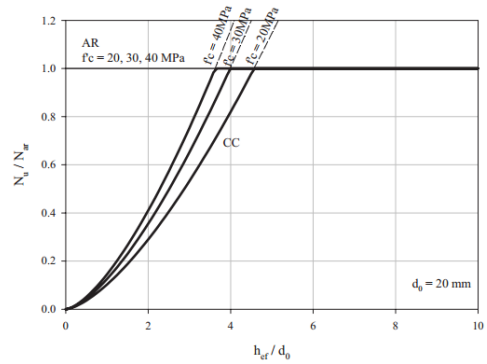


Fig. 4. Predicted versus test results (design model)



(a) Small anchor hole diameter ($d_0 = 12$ mm)



(b) Large anchor hole diameter ($d_0 = 20$ mm)

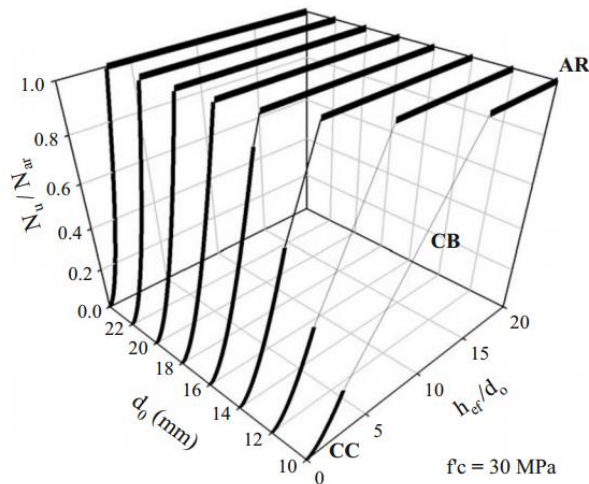


Fig. 5. Parametric study (design model)

FIGURE 53 – RESULTS FROM KIM & SMITH (2010)

4.2.3 Shear Characterization

The Shear behavior of an anchoring spikes is no similar to any available model, a whole new approach is required and, even if test have been performed for many years up to now, no comprehensive and reliable formulas are available.

It has to be noticed that, while pull-out is a pure tensile load condition, shear engaged anchors are always subjected to a certain amount of tensile stresses, due to normal stresses concentration at the end of a bonded lamina. This coupled behavior concur in making shear characterization a way more complex task, when compared to pull-out.

While pull-out characterization only relies on pure pull-out tests, shear characterization can either rely on shear tests or bending ones. While shear tests are closer to a pure shear situation, bending tests better model the shear-tension coupled load that anchors experiences in real applications, at least flexural strengthening ones. It has to be noticed that even particular tensile and pull-out tests configurations have been applied to anchor's shear characterization (Kobayashi et al. 2001) (Berneschi, 2015).

4.2.3.1 Collapse Mechanism

The early stage status of the research toward anchor's shear characterization can be spotted in the lack of a collapse-mechanism oriented approach: the importance of reporting the different experienced failure modes is clear to every involved researcher, the need to differentiate how each parameter affect different failure modes is generally not recognized. This tendency is well characterized by the widespread practice of averaging ultimate loads over different collapse mechanism.

It is important to notice as every anchor collapse start with the laminate debonding from the concrete substrate: when the debonding reaches the anchor it comes engaged and will lately fail once its ultimate capacity is reached. It can be generally assumed that an anchor failing as soon as debonding occurs is ill dimensioned, not providing a higher strength with respect to standard laminate bonding strength. This circumstance is not generally recognized and a certain number of contemporary failures can be found reported as meaningful results (e.g. Zhang & Smith, 2013).

Hereinafter the possible collapse mechanism a FRP anchor spike can undergo are listed and represented: (I) Laminate Tensile Rupture (II) Fan-Laminate Slipping (III) Dowel Shear Rupture (IV) Dowel Pull Out (V) Laminate Splitting (VI) Concrete Crushing.



FIGURE 54 - LAMINATE TENSILE RUPTURE & FAN-LAMINATE SLIPPING (NIEMITZ ET AL. 2010)



FIGURE 55 - DOWEL SHEAR RUPTURE & DOWEL PULL-OUT (BRENA & MCGUIRK, 2013) (SMITH ET AL. 2011)



FIGURE 56 - LAMINATE SPLITTING & CONCRETE CRUSHING (ZHANG & SMITH, 2011B) (BERNESCHI, 2015)

4.2.3.2 Kobayashi et al. (2001)

Test Method: Tensile.

Manufacturing: ?

Collapse Mechanism: I, II, III

Parameters: R_{fan} , α_{fan} , A_{fan} , CSR , n_p , s_p , *Side Drilled Configuration*

Kobayashi's paper is one of the first dealing with the issue of spike's characterization, the proposed testing method was a peculiar tensile set up with different collapse mechanisms induced by varying the bonding configuration. Namely notice that the slipping failure was experienced because of a steel lamina interposition between anchor fan and fiber sheet, and related eccentric load application.

The influence of a varying fan was analyzed and an increasing strength at contemporary decreasing fan opening and increasing fan area was noticed, for all the three experienced collapse mechanism. The authors related the variation only to fan opening, proposing a formula to compute the tensile strength ratio sheet's fibers can develop at varying angle of engagement. The notation was uniformed to what used in this dissertation:

$$r_{\alpha_{fan}}(\theta) = 1 - \frac{\theta}{\alpha_{fan}/2}$$

The formula has to be applied locally, to each infinitesimal portion of the FRP sheet, an integration over the fan angle can theoretically provide a global result. Considering the linear dependency on the fan opening though, the average value can be easily computed:

$$r_{\alpha_{fan}} = 1 - \frac{\alpha_{fan}/4}{\alpha_{fan}/2} = 50\%$$

The proposed formulation implies strength independency from the fan opening angle, as a consequence, at fixed width, the only parameter influencing the single anchor's strength is the fan radius.

It is however to be noticed that no matching analysis was developed by the authors, that only proposed the formula as a conceptual tool for understanding the system behavior,

as a consequence more studies into fan opening influence needs to be carried out to validate the opening uninfluenced and fixed 50% value. Even accepting the proposed model, the width influence was not discussed as well, leaving unclear whether the radius itself or the fan area is the ruling parameter in defining anchors' strength.

The anchor/sheet fiber ratio was discussed as well, suggesting that increasing the amount of fiber in the anchor, with respect to the amount of fiber in the laminate, increases the performances with respect to anchor rupture. The issue can be interpreted from the pure fiber amount prospective, as well as from the dowel area or cross-sectional-ratio one. No quantitative formulations are provided. It has to be noticed that, due to the particular experimental set-up, the experienced dowel rupture was in pure tension. A side drilled coupled configuration was tested as well and the influence of anchors' spacing and overlapping area was discussed with no quantitative conclusions.

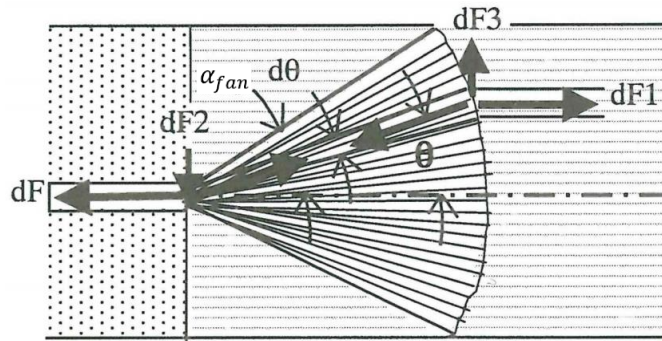


FIGURE 57 - GRAPHIC REPRESENTATION FOR KOBAYASHI'S LAW (ADAPTED FROM KOBAYASHI ET AL. 2001)

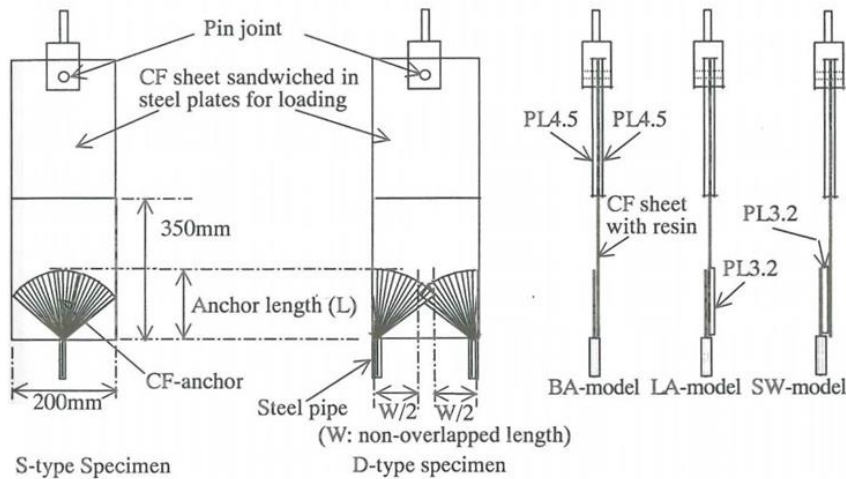


FIGURE 58 - KOBAYASHI'S CONFIGURATIONS (KOBAYASHI ET AL. 2001)

4.2.3.3 Eshwar et al. (2008)

Test Method: Shear.

Manufacturing: Fiber Bundle.

Collapse Mechanism: II, III

Parameters: h_{dowel} , n_s , n_p , s_s , s_p

Some design assumption and minimum design values are provided. Most interesting is the conclusion that dowel's depth is uninfluential on anchor's shear strength, as long as 2 inches (50 mm) are provided, for a 0.4 inches (10 mm) diameter dowel. Hence a minimum of 2 in embedded length and a minimum 0.4 in diameter is suggested.

A minimum fan radius of 4 in (200 mm) is suggested as well, along with a minimum longitudinal spacing of 6 in (150 mm), increasable up to 12 in (300 mm). One anchor series is assumed enough for an 8 in wide FRP sheet, while for wider sheets an additional line is required. Also area-related minimum and maximum requirements are proposed: a minimum of two anchors for 144 in² (900 cm²), and a maximum of three for 108 in² (225 cm²).

This second set of requirements is generally in line with what other researchers suggest, though not have been directly investigated. Interesting are the area related requirements, with the maximum one suggesting the effectiveness of the anchoring solution is related to the covered area as main parameter. Further research should be oriented in this direction.

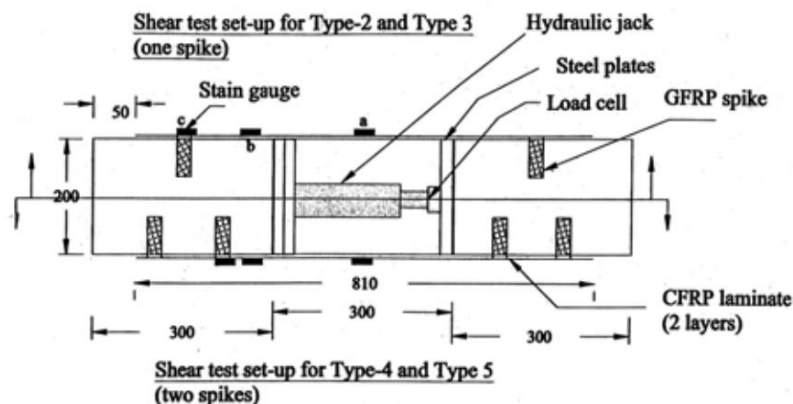


FIGURE 59 - SET-UP FROM ESHWAR ET AL. (2008)

4.2.3.4 Orton et al. (2008)

Test Method: Bending.

Manufacturing: Fiber Roll.

Collapse Mechanism: ?

Parameters: h_{dowel} , r_{ch} , d_{dowel} , n_s , n_p , s_s , s_p , CSR , *surface preparation*

A peculiar set of bending tests on sloped specimens is carried out, some design minimum requirements and characterization considerations are extrapolated, generally in line with results from other researchers.

The effectiveness of a rounded hole edge is confirmed, as well as the possibility to use solution in series. The improved effectiveness of smaller, well distributed anchors over the width is suggested. A minimum is imposed on the cross sectional area of each line of anchors – or better on the cross sectional ratio – required to be at least two times the area of the anchored sheet in order to withstand applied shear force. This is consistent with findings from Kobayashi et al. (2001) among the others.

A minimum is imposed also on the dowel depth, set to 5-6 in (13-15 cm). The value seems unnecessary higher than what suggested by Eshwar et al. (2008).

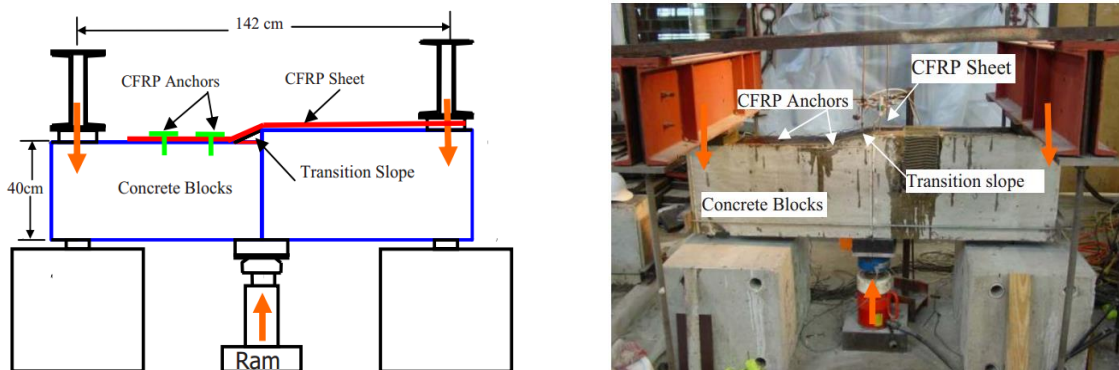


FIGURE 60 - SET-UP FROM NORTON ET AL. (2008)

4.2.3.5 Zhang & Smith (2013)

Test Method: Shear.

Manufacturing: Fiber Roll.

Collapse Mechanism: I, II, III, IV, V

Parameters: α_{fan} , β_{dowel} , $V_{f,anchor}$, l_{end} , n_s , s_s , w_{sheet} , E_{sheet} , t_{sheet} , f_c , Anchors' Material & Manufacturing, Revers & Bow-Tie Configurations, Wet & Dry.

The paper sums up the results coming from a large experimental campaign performed at the University of Hong Kong and exposed in Zhang & Smith (2010), Zhang & Smith (2011a) Zhang & Smith (2011b) Zhang et al. (2011) Zhang (2013). The influence of a large amount of parameters have been investigated and a regression model has been proposed accounting for the most influencing ones, it is again worth noticing that the proposed model doesn't follows a collapse-mechanism approach and is derived from data related to different collapse mechanisms, with a large predominance of dowel shear ruptures and pull-outs (III & IV). The notation has been uniformed to what used in this dissertation.

$$S = k_s S_{bond}$$

$$k_s = 1.59 (k_{l_{end}} - 1)(k_{\beta} - 1)(k_{w_s} - 1)$$

S_{bond}	Joint Shear Strength without anchor
$k_{l_{end}}$	Distance from End Coefficient
k_{β}	Dowel Angle Coefficient
k_{w_s}	Sheet Width Coefficient
l_{ed}	Effective Bonding Length

According to the proposed model, the anchor's strength improves at increasing bonded length behind the anchor itself, this may be related to a higher bond contribution to the overall strength of the joint. The increment stops once reached a certain bonded length, consistently with the localized nature of shear bond transferred at the laminate's end,

already mentioned when discussing the bonding problem. The effective bond length here referred is defined in Chen & Teng (2001).

$$k_{l_{end}} = \begin{cases} 0.7 \frac{l_{end}}{l_{ed}} + 1 & 0.22 < \frac{l_{end}}{l_{ed}} < 1.76 \\ 2.23 & \frac{l_{end}}{l_{ed}} > 1.76 \end{cases}$$

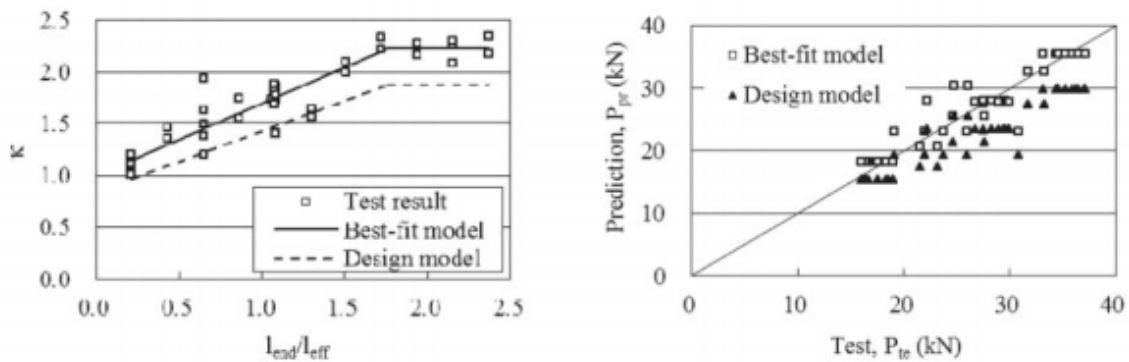


FIGURE 61 – SHEAR STRENGTH DISTANCE FROM END DEPENDENCY (ZHANG & SMITH, 2013)

it is worth noticing that this end-distance related tendency seems not consistent with other researches, also from the same authors, (Brena & McGuirk, 2013) (Smith et al. 2011) stating the ineffectiveness of anchors placed too far from the sheet end and generally suggesting an increasing effectiveness moving the anchor toward the sheet end. A solution to the discrepancy might be assuming *Zhang Effect* valid as long as the anchor lies within the effective bond length, with a *Brena Effect* happening afterward. Further research is required to solve this characterization issue.

Ozbakkaloglu & Saatcioglu (2009) showed the negative influence of increasing dowel angles on tensile strength, while Zhang & Smith (2013) pointed out the positive influence on shear strength. It is reasonable to assume that an obliquous anchor dowel allows for smoother stress transfers and is clearly critical in defining the anchor's strength in rupture and pull-out critical applications, as the ones mainly referred in Zhang & Smith's work. Dowel's anchor influence in different collapse mechanisms has not been investigated, but seems reasonable to assume a lower incidence in fan-slip mechanisms or sheet rupture ones.

$$k_{\beta} = 2.34 \frac{\beta_{dowel}}{180} + 0.67 \quad 45^{\circ} < \beta_{dowel} < 157.5^{\circ}$$

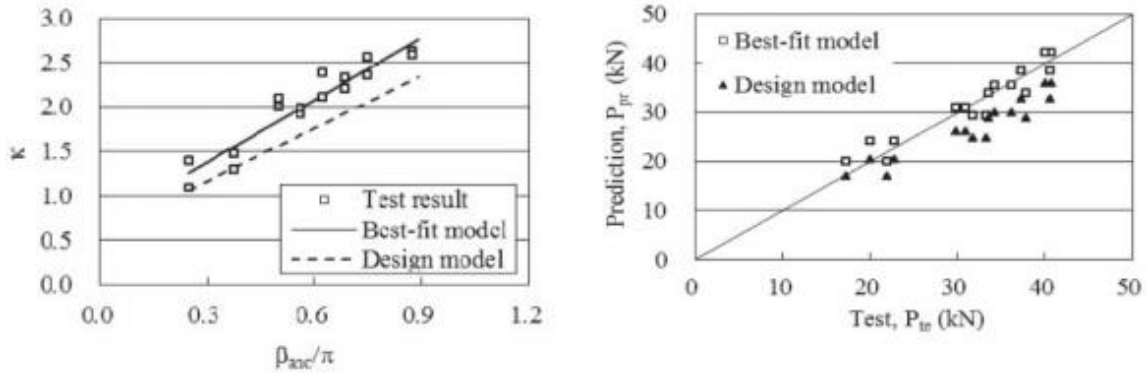


FIGURE 62 - SHEAR STRENGTH DOWEL ANGLE DEPENDENCY (ZHANG & SMITH, 2013)

Sheet width is proposed as a critical parameter, though it seems reasonable to assume the parameter itself not to be that important, rather taking the fan width to sheet width ratio as the critical one, as other authors proposed (Brena & McGuirk, 2013). The proposed model is here reported and it can be noticed anyway a reduction of the joint efficiency strength at increasing sheet width and constant fan width, hence at reducing fan/sheet width ratio.

$$k_w = 1.02 \left(\frac{w_{sheet}}{200} \right)^{-0.39} \quad 50 \text{ mm (2 in)} < w_{sheet} < 150 \text{ mm (6 in)}$$

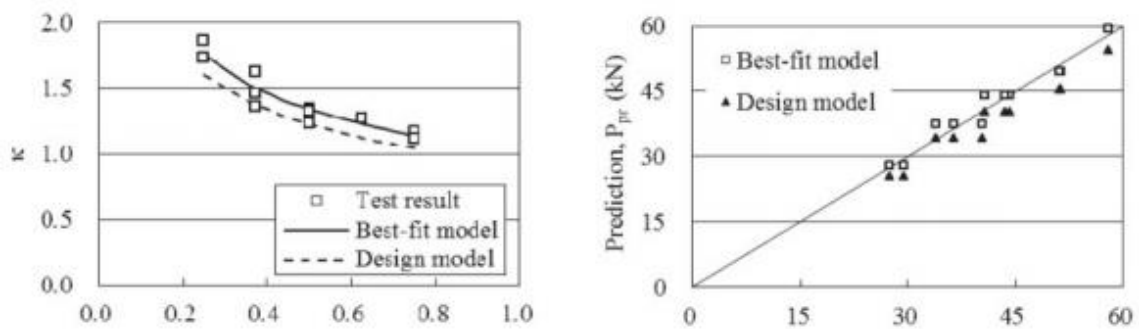


FIGURE 63 - SHEAR STRENGTH SHEET WIDTH DEPENDENCY (ZHANG & SMITH, 2013)

The limits of the proposed models have already been discussed, along with those, it can be spotted the lack of any studies regarding varying anchor's fan. While the investigation into uncommon parameters is surely interesting, considering the early stages of the overall research, focusing on intuitively more significant parameters might have been a better choice.

Referring to the unanchored joint strength as baseline parameter seems also a questionable choice, being load-condition related (shear, bending, etc.) and ubiquitous to define, if not through direct experimentation, due to the lack of a widely accepted model for bond strength.

A preferable choice might have been defining the anchor strength as a function of the sheets ultimate strength: easy to define and function of simple and well known material properties. Also conceptually, having a load ratio capped at one would be clearer.

It must also be noticed how a large amount of the presented results is related to anchors failing as soon as debonding occurs, hence not providing an increment in joint's strength. It was still pointed out how such a behavior seems reasonably related to a ill dimensioned solution and should not be considered representative of the standard anchors' behavior.

Finally, the referred paper from Zhang, Smith et al. widely presents a bond-slip law approach. Such an approach to joint characterization seems reasonable for bond-critical collapse mechanisms, such as fan-sheet slipping, while, for shear rupture mechanisms a simpler dowel's shear strength characterization seems a more reasonable approach, at least from the point of view of defining a characterization formula. The issue related to a bond-slip characterization was pointed out as well by Sun & Ghannoum (2015).

For pull-out critical situations, extending the pure pull-out model proposed by Kim & Smith (2010) to shear situations might have been an interesting approach.

The same model proposed for a single anchor strength has been extended to multiple anchors in series, assuming their contribution can simply be summed up without considering multiple anchors interaction. The assumption is in contradiction with other authors conclusions (Brena & McGuirk, 2013) and the matching of the multiple anchors model is actually sensibly worse than the single anchor one, with visibly more dispersed results.

$$S = k_{series} S_{bond}$$

$$k_{series} = \sum_1^{n_s} (k_s - 1) + 1$$

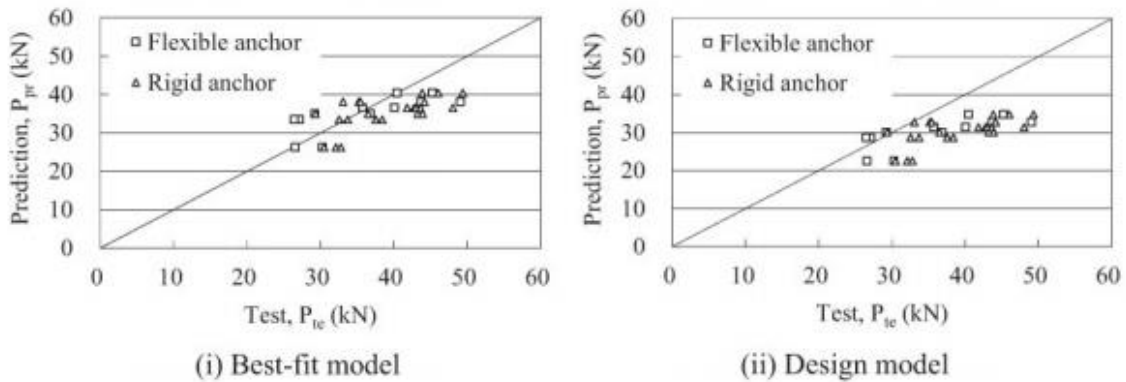


FIGURE 64 - MULTIPLE ANCHORS MATCHING

4.2.3.6 Brena & McGuirk (2013)

Test Method: Shear.

Manufacturing: Fiber Roll.

Collapse Mechanism: I, II, III, IV

Parameters: R_{fan} , A_{fan} , l_{end} , n_s , s_s , n_p , s_p , d_h , t_{sheet} , Bonded/Unbonded Configurations

The paper sums up the results coming from Niemitz et al. (2010) and McGuirk & Brena (2012) in order to develop a numerical model for anchors' characterization. The numerical model itself is not of major interest for the present dissertation, but the behavioral trend spotted by the authors in these papers will be discussed. It is worth noticing that the authors point out the need for a wider database in order to develop a better tailored characterization model.

All the tested configurations show a 360° fan and varying diameter. Different patterns have been tested, at varying number of anchors in series and parallel and varying longitudinal and transversal spacing.

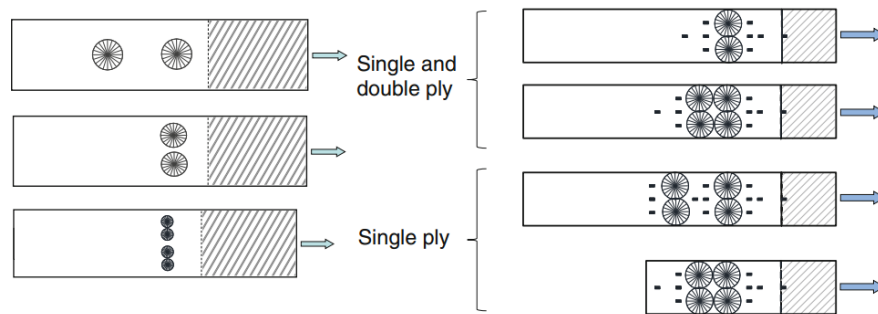


FIGURE 65 - TESTED CONFIGURATIONS FROM BRENA & MCGUIRK (2013)

One most interesting aspect is how the authors clearly point out the presence of different mechanism defining the strength of the anchored system and suggest that different parameters differently influence the various mechanisms.

The need to design the anchor's dowel in shear, identifying the diameter as the ruling parameter is clearly discussed, as well as the need to separately characterize the interlinear sheet- fan strength. The sheet thickness is identified as a ruling parameter in defining the load carried by the joint: clearly a thicker sheet can carry a higher load before rupture and transfer that load to the joint.

The influence of the fan radius is discussed, pointing out how a higher radius implies a higher shear force transferred to the dowel and hence carried by the anchor. It is however showed that the efficiency of the anchor decreases at increasing diameter, meaning that disposing smaller anchors in parallel is a more efficient solution rather than relying on larger, wide spaced anchors. The need to fully cover the sheets width in order to fully engage the sheet itself is clearly pointed out.

Most interesting are the results related to series configurations with a significantly longitudinal spacing dependent behavior: close spaced anchors behave like a combined system, failing together and concurring to enhance the strength of the joint; wide spaced anchors tend to behaves independently, failing one after the other and enhancing the ductility of the system without coupled effects on the system's strength.

The authors also point out that anchors not only need to be close together in order to work in series, but also must be placed in the so called *stress-transfer-zone* – meaning what is commonly defined bond length – in order to be effective.

Whether the effectiveness zone should be strictly limited in the boundaries of the bonded length will be lately further discussed, but an increased anchors' effectiveness

at reduced distance from the plate end seems consistent with results from other authors (Smith et al. 2011) and the research here presents. Finally, the positive contribution of the bonded substrate on transversal stress redistribution is discussed as well.

4.2.3.7 Berneschi (2015)

Test Method: Shear, Reverse Pull-Out.

Manufacturing: Fiber Bundle.

Collapse Mechanism: II, IV

Parameters: α_{fan} , A_{fan} , w_{fan} , r_{ch} , Sandwich Configuration

Berneschi directly tested in shear two different fan configuration at varying opening, width and area: an increased strength at increasing area, width and opening is reported. The contemporary variation of every fan parameter, apart from the radius, makes impossible to spot the influence of each parameter.

Accepting Kobayashi's conclusion (Kobayashi et al. 2001), an increased fan opening should have no effect on anchor's strength or eventually a negative effect, hence the positive contribution should come from area and width increment, in line with Brena's conclusions (Brena & McGuirk, 2015).

Most of the specimen failed in fan-sheet slipping, with a few failing because of concrete crushing. Such a failure mode has not been noticed in other studies and further investigation should be performed in order to understand it. Namely, it is unclear whether the tested specimens were able to provide residual strength after the concrete failure, maybe a higher one; in this case the concrete crushing would configure simply as a deeper debonding mechanism and the anchor's strength was not fully developed yet. The chance for such a mechanism to occur is anyway critical to point out.

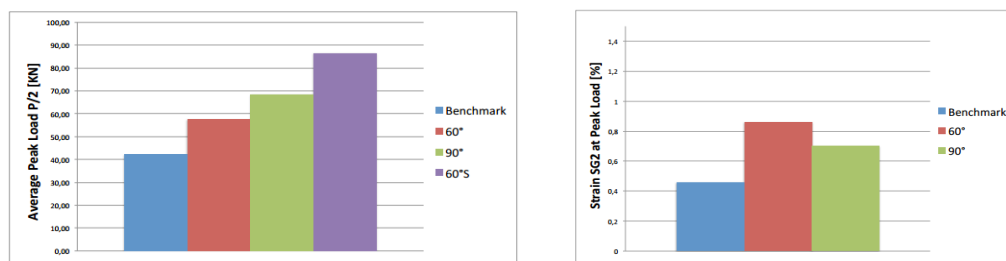


FIGURE 66 - RESULTS FROM BERNESCHI (2015)

4.2.3.8 Sun et al. (2016)

Test Method: Bending.

Manufacturing: ?

Collapse Mechanism: I, III

Parameters: α_{fan} , R_{fan} , A_{fan} , CSR , w_{sheet} , f_c , *Bonded/Unbonded, Patch/Sandwich*

The paper presents the results coming from a series of bending test on FRP-anchored reinforced beams. All the applications were characterized by the presence of FRP patches between the sheet and the anchor's fans and over the fan; the effectiveness of such a solution is not quantified or actually investigated.

The authors recognized the need to differentiate the results according to a collapse mechanism-oriented approach, but only FRP sheet tensile rupture (I) and dowel shear rupture are covered (III). Also only a few parameters are discussed and no analytical models are presented. Generally, the data presented seems quite scattered and their interpretation should account for their dispersion.

The results show that variations of fan radius and opening angle have very little effect on the joint strength when sheet rupture is ruling. The results make sense considering that, if a fan configuration is already able to carry the sheet rupture load, increasing the interfacial strength won't have any effect on the different ruling collapse mechanism.

The absence of any trend is anyway in contrast with Kobayashi et al. (2001) and is probably due to data scatteredness: varying the same parameters, in the same way, Kobayashi showed how increasing the fan area the anchor performances increase, regardless of the experienced collapse mechanism, probably because a more uniform stress distribution is enforced. The chance that the transversal redistribution in presence of a concrete substrate – absent in Kobayashi's tests – makes negligible the further homogenizing effect coming from a larger fan is also to be considered. The positive effect of concrete bonding on joint performances is discussed as well in Sun's paper.

The width of the FRP sheet has been studied as well, showing how a larger sheet is more prone to premature rupture failures due to stress concentrations. The concrete strength was also shown to play a positive role in enhancing the joint strength when collapse is determined by anchor shear rupture. Finally, the CNR (addressed as AMR in the paper) is discussed, but no clear trend can be spotted and generally it seems like the ratio merges together the influences of different parameters that seems clearer to analyze on their own, namely sheet width and thickness and fan width.

In a previous paper Sun also pointed out the little influence of the material elastic properties, mentioning epoxy and fiber elastic modulus (Sun & Ghannoum, 2015). The conclusion make sense considering the joint behavior at its ultimate limit state.

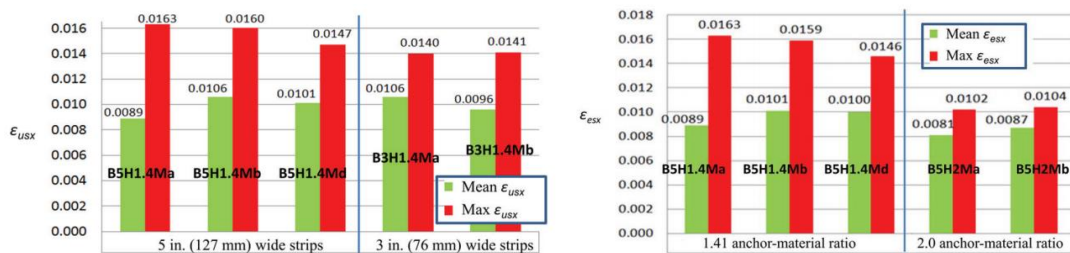
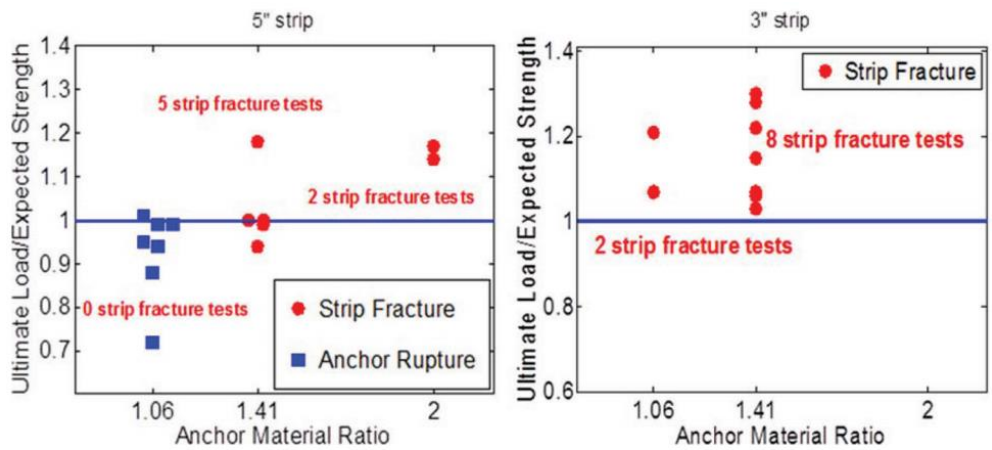
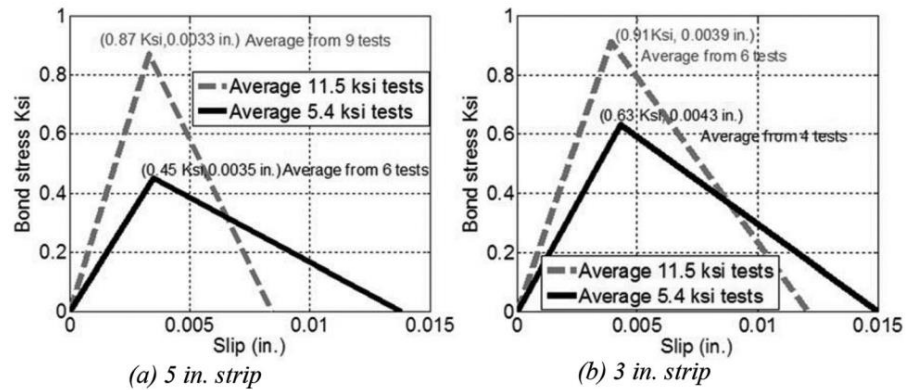


Fig. 13—Comparison of mean and maximum strains at 98% ultimate load (ϵ_{usx}) for different strip widths (BA; SW = 5 in. [127 mm]; $f'_c = 11.5$ ksi [79 MPa]; AMR = 1.41.)

Fig. 15—Comparison of mean and maximum strains at 95% expected load at failure (ϵ_{esx}) for different anchor-material ratio (BA; SW = 5 in. [127 mm]; $f'_c = 11.5$ ksi [79 MPa]; FA = 45 degrees).

FIGURE 67 - RESULTS FROM SUN ET AL. (2016)

4.3 Strengthening Applications

4.3.1 Flexural Strengthening

A certain number of flexural applications have already been tested, proving the effectiveness of the solution, but generally failing in providing comprehensive characterization formulas or reliable design algorithms. A review of the most interesting findings for the purpose of this dissertation results is here provided.

4.3.1.1 Lam & Teng (2001)

Resisted Force: Shear

Debonding Type: Intermediate?

Mechanical Function: II, III

One of the earliest studies about anchor spikes in bending application show FRP sheets laterally applied on cantilever elements. The FRP is secured to the column portion via steel bolts and to the cantilever through FRP anchor spikes.

The results show the effectiveness of FRP in retarding debonding (II) and later providing a fundamental stress transfer mechanism, after debonding (III). The anchors' mainly resist shear stresses, also considering the side application.

Interesting is the validation of a standard sectional model as a ULS design tool for FRP flexurally strengthened bended elements in presence of FRP anchoring spikes.

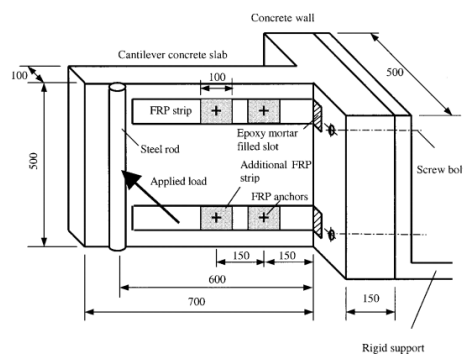


FIGURE 68 - SET-UP FROM LAM & TENG (2001)

4.3.1.2 Piyong et al. (2003)

Resisted Force: Shear

Debonding Type: Intermediate

Mechanical Function: III

This early study on slabs show similarities with the experiments discussed in this dissertation: a concrete element is reinforced with a FRP sheet, anchored with end spikes in order to keep the sheet itself in place once intermediate debonding occurs, hence providing an equilibrium/critical shear transfer mechanism (Type III).

Peculiar is the pre-stress applied to the FRP sheets that makes the test not directly comparable to what discussed in this dissertation. The results show anyway the effectiveness of the end-anchoring solution to postpone the structure's collapse.

It is worth noticing that the same end anchors also help avoiding end debonding, acting as type I, tension resisting elements. This role can very well be assumed as secondary, not usually being end-debonding the critical collapse mechanism in flexural applications, once a proper bonded length is provided (CNR, 2014) (ACI, 2008).

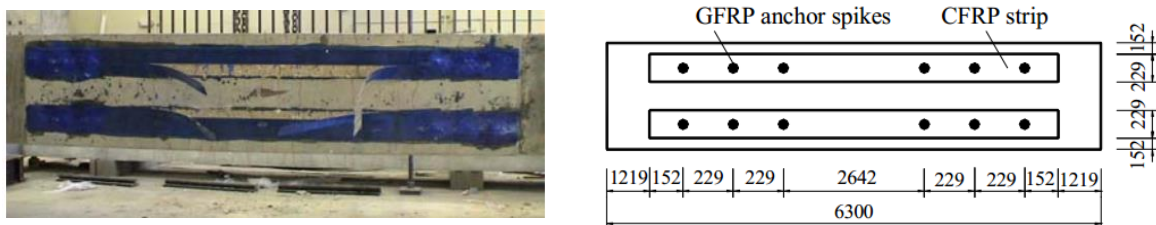


FIGURE 69 - TESTED CONFIGURATION & FAILURE MODE FROM PIYONG ET AL. (2003)

4.3.1.3 Eshwar et al. (2005)

Resisted Force: Tension

Debonding Type: Intermediate

Mechanical Function: I

In this case, the influence of an artificially imposed soffit curvature at the bottom of the bended element on FRP bonding performance is discussed. It is shown how anchors, distributed over the element length, effectively help in countering tensile stresses arising

from imposed curvature and postponing intermediate debonding (Type I, Tensile Resistant). The end anchors also play the secondary role of countering end-debonding tensile stresses (Type I, Tensile Resistant as well).

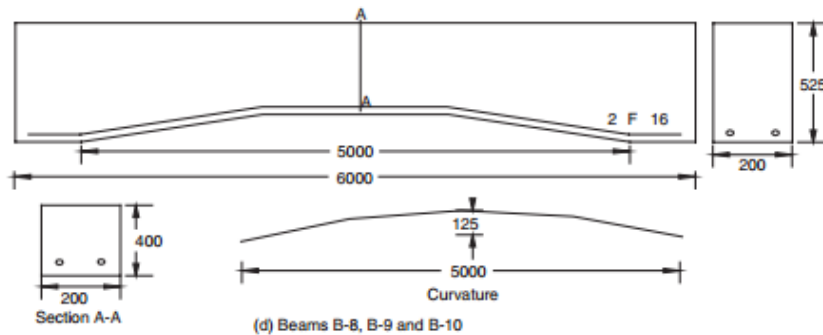


Figure 8. Peeling in beam 8 (preured laminate)



Figure 9. Beam 9 after failure (wet layup laminate)

FIGURE 70 - TESTED CONFIGURATION & FAILURE MODE FROM ESHWAR ET AL. (2005)

4.3.1.4 Smith et al. (2011)

Resisted Force: Shear

Debonding Type: Intermediate

Mechanical Function: III, IV

In this case a direct parallel with the research presented in this dissertation can be spotted: concrete slabs are flexurally strengthened using FRP sheets anchored with spikes, arranged in different patterns. Also notice that the ductility issue is directly discussed.

All the tested specimens showed a collapse mechanism triggered by the sheet's intermediate delamination, followed by the end anchors engagement and their collapse determining the slab's ultimate state.

First of all, the need to properly dimension the end anchors can be spotted: if the anchoring solution is unable to resist a shear force higher than the debonding one, no strength enhancement can be spotted. This is the case of specimen S6 where only a limited ductility enhancement can be spotted. Specimen S5, on the contrary, shows a properly dimensioned intervention and an enhanced system's strength.

A second important conclusion is the ineffectiveness of intermediate anchors in enhancing the system's strength: respectively compare specimen S3 to S5 and eventually S4 to S6. The result is consistent with the idea of distant anchors non collaborating in series and increased anchor effectiveness getting closer to the sheet's end, both suggested by Brena & McGuirk (2013). It is however worth-noticing that the same authors proposed a different behavior in a later paper, suggesting an increased effectiveness at increasing distance from end.

Finally, specimens S7 and S8 suggest that smaller, better distributed anchors, show better performances when compared to bigger ones. The result was suggested by Brena & McGuirk (2013) for parallel patterns and seems valid also for series configuration. Smaller anchors mean smaller radius and better shear transfer performances from the fan to the dowel, as noticed by Brena & McGuirk themselves.

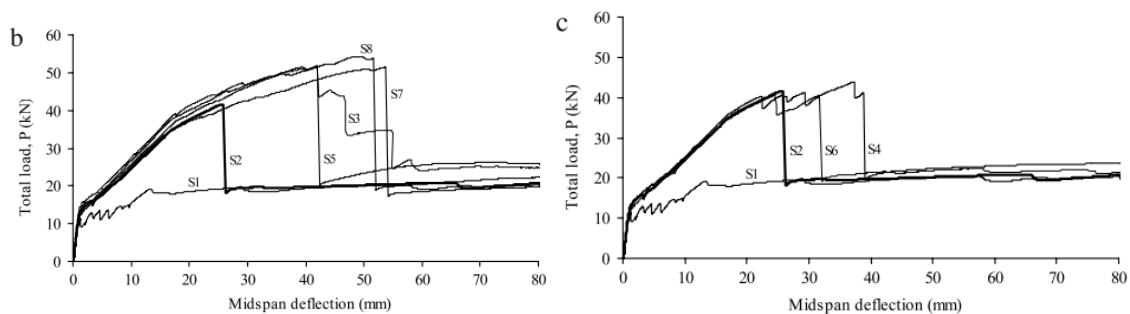


FIGURE 71 - LOAD/DEFLECTION RESPONSE OF TESTED SLABS (B) ANCHORED SLABS WITH INCREASING STRENGTH & DEFLECTION (C) ANCHORING SLAB WITH PREDOMINANTLY INCREASING DEFLECTION (SMITH ET AL. 2011)

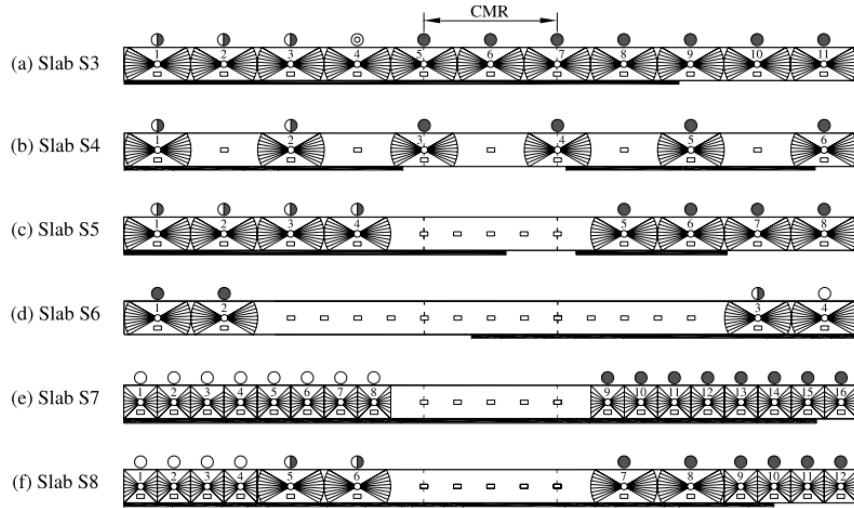


Fig. 9. FRP plate and FRP anchor conditions post-plate debonding. (— debonding crack; ◀▶ Type 1 FRP anchor; ▶◀ Type 2 FRP anchor; --- load point; CMR = constant moment region; ○ completely ruptured anchor; ◐ partially ruptured anchor; ● pulled-out anchor; ● undamaged anchor).

FIGURE 72 - TESTED CONFIGURATIONS FROM SMITH ET AL. (2011)

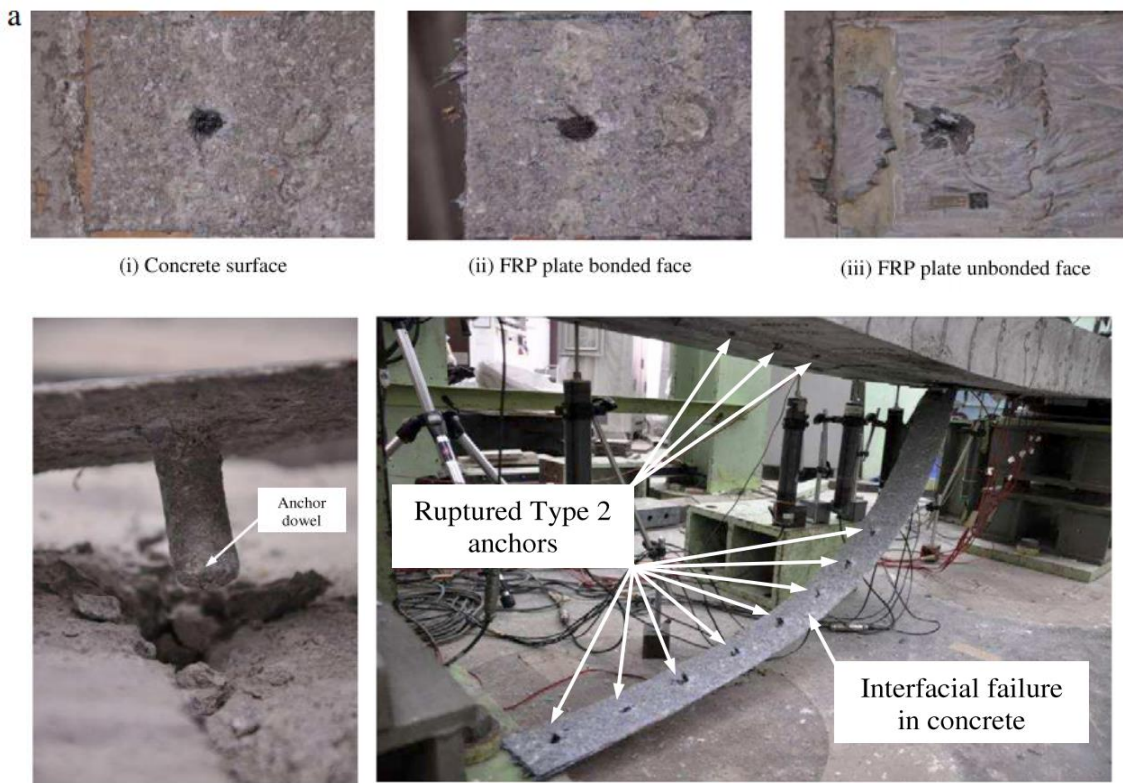


FIGURE 73- FAILURE MODES FROM SMITH ET AL. (2011)

4.3.1.5 Smith et al. (2013)

Resisted Force: Shear

Debonding Type: Intermediate

Mechanical Function: III, IV

The same set-up as in Smith et al. (2011) is used, results from the previous paper are confirmed and new conclusions can be inferred. Notice that the ductility issue is explicitly discussed.;

A consistent increment in strength at increasing anchored end area can be spotted, respectively compare: S2.5 & S2.3, S2.8 & S2.9. Also notice that S2.8 was under-dimensioned, not showing any strength increment when compared to the unanchored reference specimen. Also the dowel angle positive effected modelled in Zhang & Smith (2013) is here confirmed (S2.4, S2.5, S2.6).

The ineffectiveness of intermediate angle can be noticed comparing S2.9 & S2.10. Even a reduced ductility can be spotted as the intermediate anchor is introduced. On the opposite side, the improved effectiveness of smaller, distributed anchors is confirmed by slab S2.7, when compared to S2.3 or S2.5.

Finally, as already suggested in Smith et al. (2011), the Idea that bigger anchors in front of smaller distributed ones represent the optimal solution for end application, at least from the ductility point of view, seems confirmed comparing S2.9 to S2.7 and others.

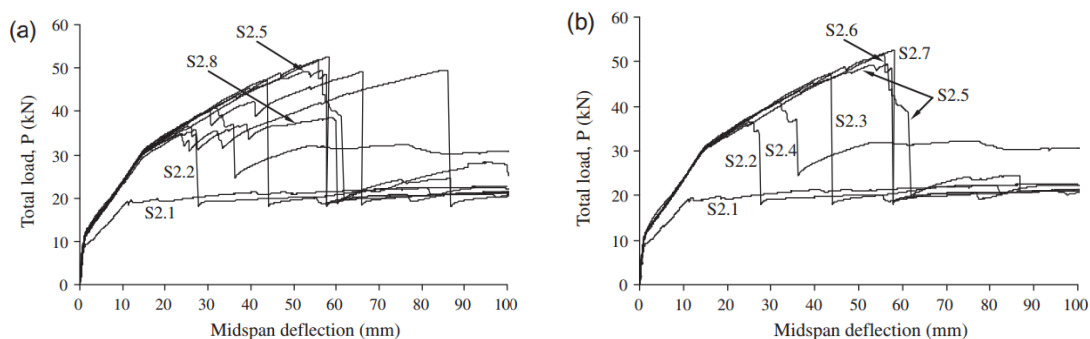


FIGURE 74 - LOAD/DEFLECTION RESPONSE OF TESTED SLABS (B) ANCHORED SLABS WITH SIMILAR STIFFNESS (C) ANCHORED SLABS WITH REDUCED STIFFNESS (SMITH ET AL. 2013)

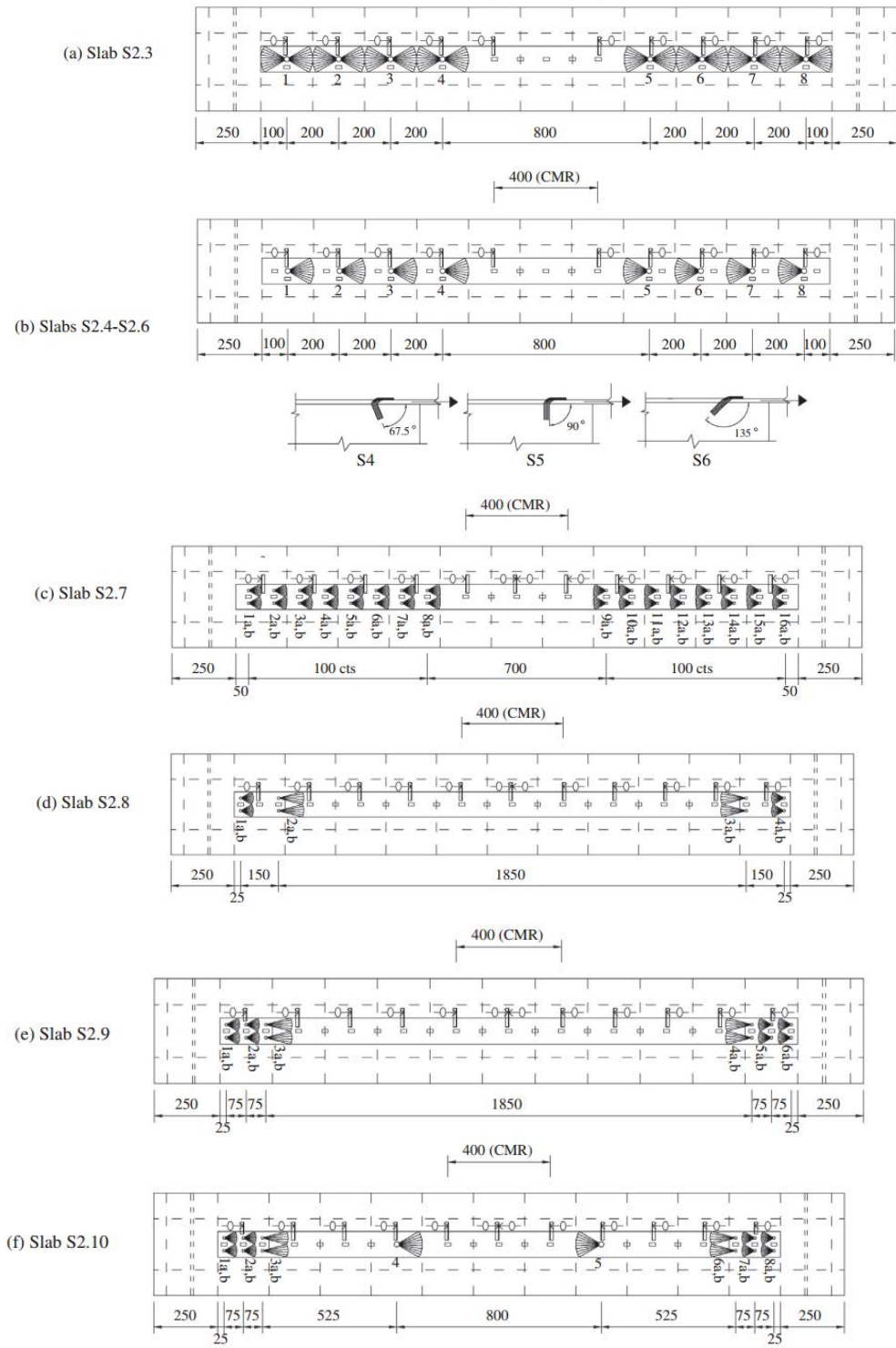


FIGURE 75 - TESTED CONFIGURATIONS FROM SMITH ET AL. (2013)

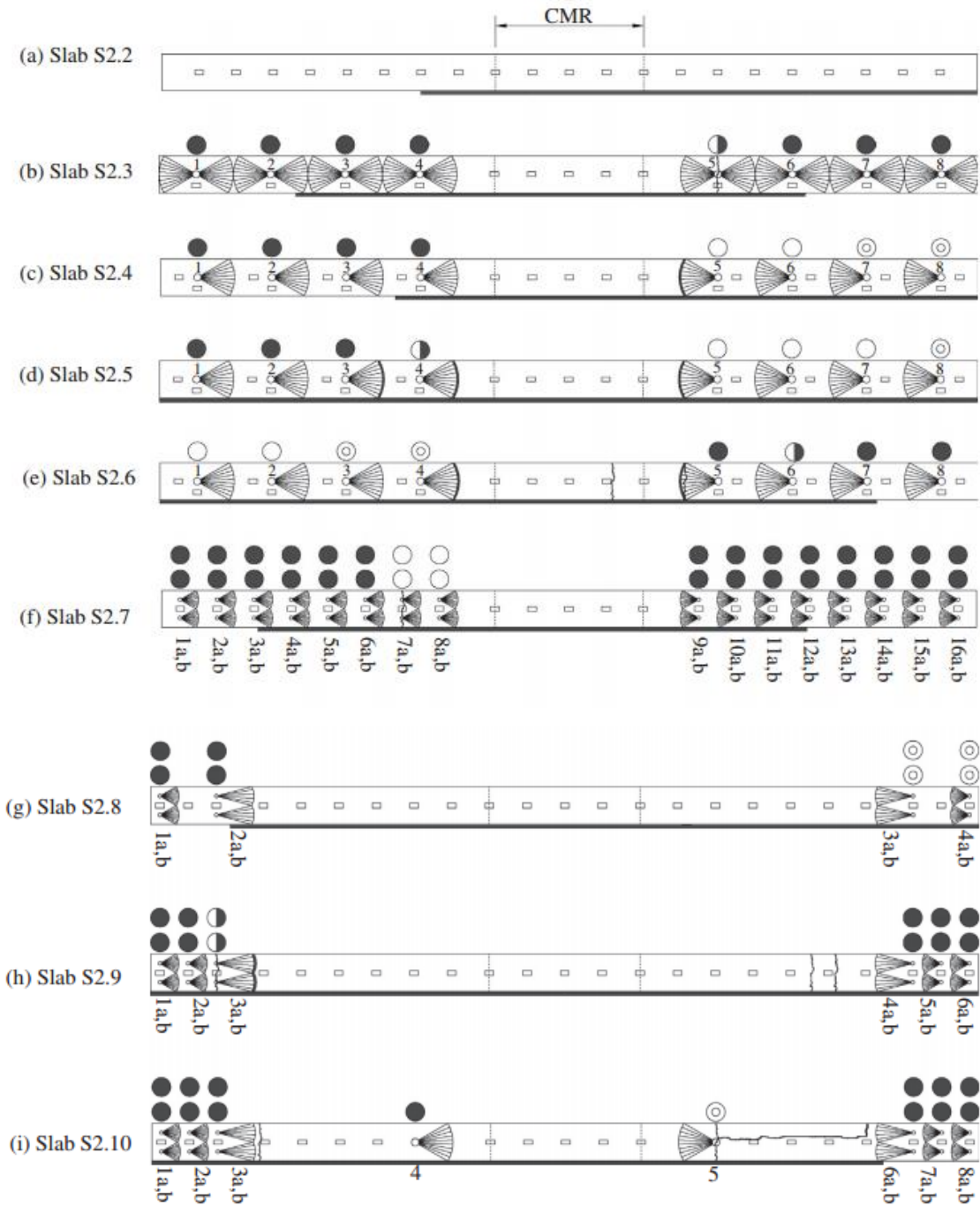


FIGURE 76 - FAILURE MODES FROM SMITH ET AL. (2013)

WHITE DOT – FAILED ANCHOR

BLACK DOT – NON-DAMAGED ANCHOR

4.3.1.6 Nardone et al. (2011)

The paper presents a complete model, characterizing mechanically fastened FRP reinforced beams at ULS and SLS, properly defining load/deflection curves, strain diagrams, curvatures and predicting failure modes and ultimate loads.

The anchors here treated are not the spike object of the present research, furthermore a database wide enough to validate such a model for spikes application is still lacking. Reference to the paper is made in order to point out what should be the ultimate goal of a research still at its early stages.

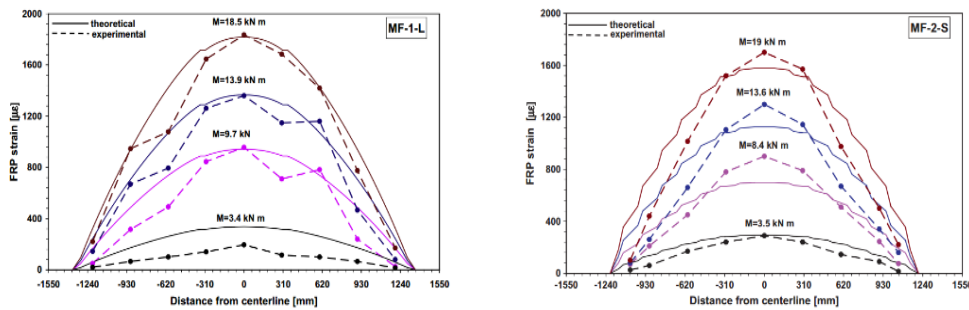


FIGURE 77 - MATCHING EXAMPLES (NARDONE ET AL. 2011)

4.3.2 Shear Strengthening

A comprehensive shear strengthening review is beyond the purposes of this dissertation. For more information, please refer to the section dedicated to anchors in general or to specific researches such: Baggio (2013), Kim et al. (2014), Kim et al. (2015).

4.3.3 Column & Joint Strengthening

It is interesting how one of the first spikes related paper treat the non-so-common column-confinement application (Kobayashi et al. 2001). As said for shear, the reader is referred to specific literature: Karantzakis et al. (2005), Ceroni et al. (2007), Li & Chua (2008), Sami et al. (2010), Kim et al. (2011), Grelle (2011).

5 Experimental Program

5.1 Material Characterization

All the materials involved in the present research are here fully characterized, a discussion on the reasons behind each material choice is left to the following, while discussing the experimental matrix.

5.1.1 Concrete

5.1.1.1 Compressive Strength – ASTM C39

The concrete compressive strength (f'_c or f_{cm}) has been measured performing compressive tests on concrete cylinders. A total of 15 cylinders has been realized using standardized plastic molds in accordance with ASTM C31 (2014). Flat surfaces were provided on the ends of the cylinders by following the *Standard Practice for Capping* (ASTM C617, 2015).

The cylinders were subdivided in groups of 5 and tested at 7, 14 and 28 days in compliance with ASTM C39 (2014). The compressive strength is assumed to remain constant after 28 days, the 28-days-average will hence be the value used for design and matching purposes.



FIGURE 78 - EXAMPLES OF TESTED CONCRETE CYLINDERS

7 Day - December 1, 2015						
Specimen ID	d	A	P _{max}	f'c	f'c	Failure Mode
	[in]	[in ²]	[lbf]	[psi]	[MPa]	
C1	4	12.57	103,320	8,222	55.91	3
C2	4	12.57	102,050	8,121	55.22	3
C3	4	12.57	97,550	7,763	52.79	3
C4	4	12.57	103,360	8,225	55.93	3
C5	4	12.57	98,840	7,865	53.48	3
<i>Average</i>	4	12.57	101,024	8,039	54.67	
<i>S_n</i>	0	0	2675	213	1.45	
<i>CV(%)</i>	0%	0%	3%	3%	3%	

14 Day - December 9, 2015						
Specimen ID	d	A	P _{max}	f'c	f'c	Failure Mode
	[in]	[in ²]	[lbf]	[psi]	[MPa]	
C6	4	12.57	98,200	7,815	53.14	3
C7	4	12.57	86,420	6,877	46.76	3
C8	4	12.57	115,960	9,228	62.75	3
C9	4	12.57	112,840	8,980	61.06	3
C10	4	12.57	107,800	8,578	58.33	3
<i>Average</i>	4	12.57	104,244	8,295	56.41	
<i>S_n</i>	0	0	12021	957	6.50	
<i>CV(%)</i>	0%	0%	12%	12%	12%	

28 Day - December 19, 2015						
Specimen ID	d	A	P _{max}	f'c	f'c	Failure Mode
	[in]	[in ²]	[lbf]	[psi]	[MPa]	
C1	4	12.57	123,800	9,852	66.99	3
C2	4	12.57	128,320	10,211	69.44	3
C3	4	12.57	126,440	10,062	68.42	3
C4	4	12.57	131,220	10,442	71.01	3
C5	4	12.57	127,820	10,172	69.17	3
<i>Average</i>	4	12.57	127,520	10,148	69.00	
<i>S_n</i>	0	0	2712	216	1.47	
<i>CV(%)</i>	0%	0%	2%	2%	2%	

5.1.1.2 Derived Properties – ACI 318

In the following a full concrete characterization according to ACI 318-14 (2014) is provided. Standard weight (145 pcf, 2300 kg/m³) is assumed for the concrete.

$$f_r = 0.0075 \sqrt{f'_c} \quad \text{Rupture Modulus (ksi)}$$

$$E_c = 57 \sqrt{f'_c} \quad \text{Elastic Modulus (ksi)}$$

$$\varepsilon_{cu} = 3 \quad \text{Ultimate Strain (‰)}$$

$$\beta_1 = \begin{cases} 0.85 & 2.5 \leq f'_c \leq 4 \text{ kips} \\ 0.85 - 0.05(f'_c - 4) & 4 < f'_c < 8 \text{ kips} \\ 0.65 & f'_c \geq 8 \text{ kips} \end{cases} \quad \text{Stress-Block Height Coeff.}$$

$$\eta = 0.85 \quad \text{Stress-Block Width Coeff.}$$

5.1.1.3 Derived Properties – EC2

In the following a full concrete characterization according to UNI EN 1992-1-1 (2008) is provided. The concrete stress-strain diagram will be modeled as a rectangular stress block, according to EC2 3.1.7(3). It is worth noticing that the particularly high strength of the concrete should be accounted for, applying the proper formulas. Notice also that EC2 formulas are meant for SI units.

$$f_{ck} = f_{cm} + 8 \quad \text{Char. Comp Strength (MPa)}$$

$$f_{ctm} = \begin{cases} 0.3 f_{ck}^{2/3} & f_{ck} < 50 \text{ MPa} \\ 2.12 \ln \left[1 + \frac{f_{cm}}{10} \right] & f_{ck} > 50 \text{ MPa} \end{cases} \quad \text{Av. Tensile Strength (MPa)}$$

$$E_{cm} = 22 \left[\frac{f_{cm}}{10} \right]^{0.3} * 1000 \quad \text{Av. Elastic Modulus (MPa)}$$

$$\varepsilon_{c2} = \begin{cases} 2 & f_{ck} < 50 \text{ MPa} \\ 2 + 0.085 [f_{ck} - 50]^{0.53} & f_{ck} > 50 \text{ MPa} \end{cases} \quad \text{Strain at Max. Stress (\%)}$$

$$\varepsilon_{c2u} = \begin{cases} 3.5 & f_{ck} < 50 \text{ MPa} \\ 2.6 + 35 \left[\frac{90-f_{ck}}{100} \right]^4 & f_{ck} > 50 \text{ MPa} \end{cases} \quad \text{Ultimate Strain (\%)}$$

$$\lambda = \begin{cases} 0.8 & f_{ck} < 50 \text{ MPa} \\ 0.8 - \frac{f_{ck}-50}{400} & f_{ck} > 50 \text{ MPa} \end{cases} \quad \text{Stress-Block Height Coeff.}$$

$$\eta = \begin{cases} 1 & f_{ck} < 50 \text{ MPa} \\ 1 - \frac{f_{ck}-50}{200} & f_{ck} > 50 \text{ MPa} \end{cases} \quad \text{Stress-Block Width Coeff.}$$

In order to account for the non-complete development of the parabola-rectangle in certain collapse mechanisms, the stress-block height and centroid location will be corrected applying the following coefficients:

$$\alpha_v = \begin{cases} \frac{\varepsilon_c(6-\varepsilon_c)}{8} / \frac{(3*\varepsilon_{cu}-2)}{3\varepsilon_{cu}} & \varepsilon_c \leq \varepsilon_{c2} \\ \frac{(3*\varepsilon_c-2)}{3*\varepsilon_c} / \frac{(3*\varepsilon_{cu}-2)}{3\varepsilon_{cu}} & \varepsilon_c > \varepsilon_{c2} \end{cases} \quad \text{Height Correction}$$

$$K_A = \begin{cases} \frac{8-\varepsilon_c}{4(6-\varepsilon_c)} / \frac{\varepsilon_{cu}(3\varepsilon_{cu}-4)+2}{2\varepsilon_{cu}(3\varepsilon_{cu}-2)} & \varepsilon_c \leq \varepsilon_{c2} \\ \frac{8-\varepsilon_c}{4(6-\varepsilon_c)} / \frac{\varepsilon_{cu}(3\varepsilon_{cu}-4)+2}{2\varepsilon_{cu}(3\varepsilon_{cu}-2)} & \varepsilon_c > \varepsilon_{c2} \end{cases} \quad \text{Application-Point Correction}$$

5.1.1.4 Design Properties

In the following, the numerical value for the discussed properties are summed up. Please notice that a conservative approach is not required in designing an experiment, hence the average values will be assumed as design ones, seeking for a good matching between analytical and measured experimental results.

The European norm allows a more detailed concrete characterization, the EC2 design data will hence be preferred in the following, as well as the EC2 notation. The ACI characterization will be referred to for comparison purposes and will be used in ACI debonding formulas for the sake of consistency.

Concrete Design Properties						
	US			SI		
	EC2	ACI		EC2	ACI	
f_{ck}	9	-	[Ksi]	62	-	[kN]
f_{cm}	10	10	[Ksi]	70	70	[kN]
f_{ctm}	0.64	0.76	[Ksi]	4.41	5.21	[kN]
E_{cm}	5,720	5,720	[Ksi]	39,436	39,436	[kN]
ν	0.2	-	[/]	0.2	-	[/]
G	2,383	-	[Ksi]	16,432	-	[kN]
ϵ_{crack}	0.11	0.13	[‰]	0.11	0.13	[‰]
ϵ_{c2}	2.32	-	[‰]	2.32	-	[‰]
ϵ_{cu2}	2.82	3.00	[‰]	2.82	3.00	[‰]
λ	0.77	0.85	[/]	0.77	0.85	[/]
η	0.94	0.85	[/]	0.94	0.85	[/]
$\lambda\eta$	0.72	0.72	[/]	0.72	0.72	[/]
ρ_c	150	145	[pcf]	2400	2,323	[kg/m ³]

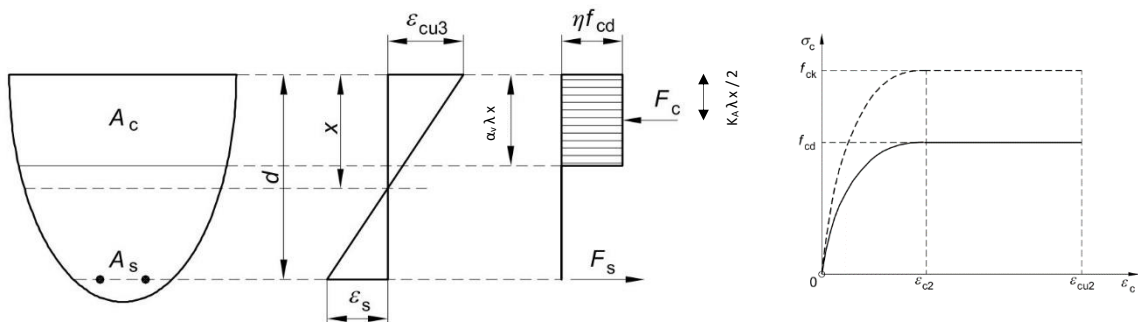


FIGURE 79 - CONCRETE CONSTITUTIVE LAW (EC2, 2008)

5.1.2 Steel

5.1.2.1 Tensile Strength – ASTM A370

Ten rebar specimens were tested in tension, in compliance with ASTM A370. The yield strength was measured as the load corresponding to a 0.2% permanent deformation, referring to the experimentally measured stiffness to draw the offset line.

All the specimens showed a consistent elasto-plastic behavior and yielding starting at around 70 kips; though, due to extensometer malfunctions, the elastic branch was properly measured only for 6 specimens, the other samples are hence disregarded.

Steel Measured Properties				
Specimen ID	Es		fy	
	[ksi]	[MPa]	[ksi]	[MPa]
S1	27,963	190,149	72	489
S3	27,862	189,462	76	518
S4	29,827	202,825	70	479
S8	28,611	194,553	77	521
S9	27,491	186,938	73	499
S10	27,976	190,235	74	504
<i>Average</i>	28,288	192,786	74	501.20
<i>S_n</i>	918.73	6247.34	2.67	18.18
<i>CV(%)</i>	3.25%	3.24%	3.63%	3.63%

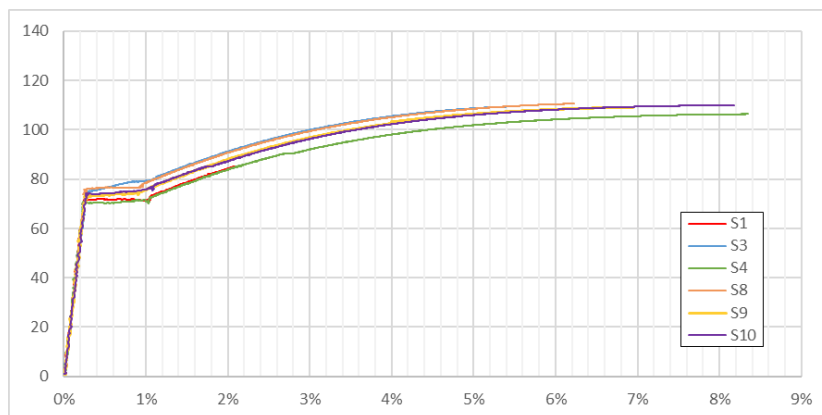


FIGURE 80 - STEEL STRESS [MPa]/STRAIN [%] DIAGRAMS FROM MATERIAL CHARACTERIZATION

5.1.2.2 Design Properties

An elastic-perfectly plastic constitutive law is assumed for steel, in compliance either with EC2 (2008) and ACI 318 (2014). The experimental average values will be assumed as design values, both for elastic modulus and tensile strength.

Regarding the ultimate strain, no limits are suggested by both the norms and no experimental data are available, having removed the extensometer before failure, willing to avoid damages. A very conservative design value of 1% was historically assumed by Italian designers, while all the experimented specimen failed way over 10%, from a qualitative evaluation; such a value will be assumed as design one, also considering the well-known steel's perfectly plastic plateau and the expected low influence of such a value on the overall behavior of the system.

It is worth noticing that the steel tensile failure will never represent the critical failure mode for the slabs, neither theoretically, nor experimentally, hence such a choice won't have major consequences.

Steel Design Properties				
	US		SI	
f_y	74	[Ksi]	501	[MPa]
ϵ_y	0.26	[%]	0.26	[%]
$\epsilon_{su,d}$	8	[%]	8	[%]
E_s	28,288	[Ksi]	192,786	[MPa]
n_s	4.95	[/]	4.95	[/]
\emptyset	0.375	[in]	9.5	[mm]
ID	#3	[/]	$\emptyset 10$	[/]



FIGURE 81 - STEEL & FRP LAMINATE TENSILE CHARACTERIZATION

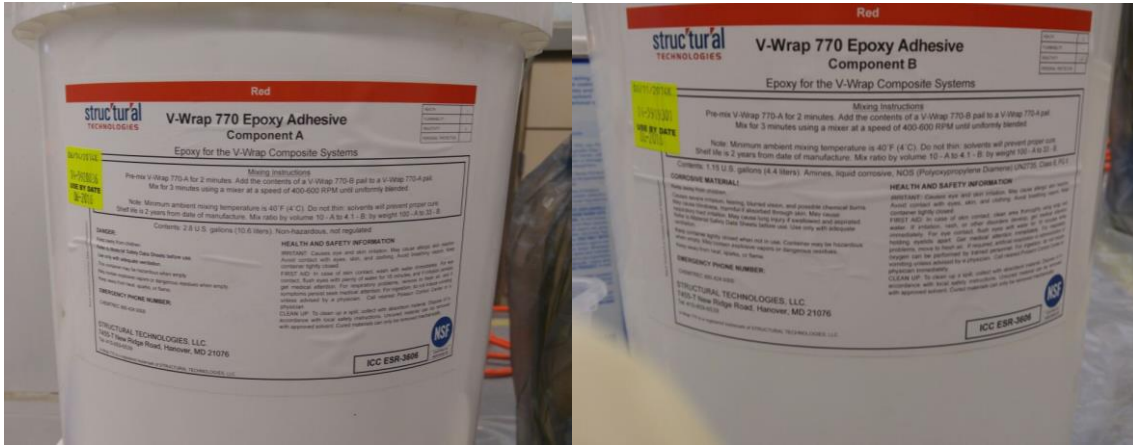


FIGURE 82 - LAMINATE SAMPLES PREPARATION

5.1.3 CFRP Sheet

5.1.3.1 Dry Fibers

Dry fiber characterization according to the manufacturer will be provided for the sake of completeness.

Storage Conditions:	Store dry at 40°F – 90°F (4°C – 32°C)
Color:	Black
Primary Fiber Direction:	0° (unidirectional)
Weight per Square Yard:	22 oz (750 g/m ²)
Shelf life:	10 years
Density:	0.065 lbs/in ³ (1.8 g/cm ³)

Fiber Properties (Dry)

Tensile Strength:	700,000 psi (4.82 GPa)
Tensile Modulus:	40 x 10 ⁶ psi (27.6 GPa)
Elongation:	1.7%

5.1.3.2 Epoxy

The same applies to epoxy characterization, performed according to ASTM D638 and ASTM D790.

Tensile Strength (ASTM D638):	10,500 psi (72.4 MPa)
Tensile Modulus (ASTM D638):	461,000 psi (3,180 MPa)
Flexural Strength (ASTM D790):	17,900 psi (123.4 MPa)
Flexural Modulus (ASTM D790):	452,000 psi (3,120 MPa)
Elongation at Break (ASTM D638):	5.0%
Tg (ASTM D4065):	180°F (82°C)
Density:	
Mixed Product	9.17 lbs/gal (1.11 kg/L)
Part A	9.7 lbs/gal (1.16 kg/L)
Part B	7.9 lbs/gal (0.95 kg/L)
VOC Content: (ASTM D-2369):	0% VOC

5.1.3.3 Impregnated Sheet

The CFRP impregnated sheet characterization was performed in the Structures and Material Laboratories at the University of Miami in compliance with ASTM D3039 (2008). Test details and a full material characterization can be found in the Certified Test Report Number R-5.10_STe_ESR-3606.5 (Revision 5, March 2015).

Specimen ID	A_{exp}		A_{nom}		p^{max}		F^{tu}_{exp}		F^{tu}_{nom}		E^{chord}		ϵ_u %	Mode of failure*
	mm ²	in ²	mm ²	in ²	kN	lbs	MPa	ksi	MPa	ksi	GPa	Msi		
STe_C277_TNS_CC_00_001	22.528	0.035	26.503	0.041	37.64	8458	1670.1	242.22	1419.6	205.89	79.12	11.48	1.79	XGM
STe_C277_TNS_CC_00_002	23.806	0.037	26.452	0.041	34.35	7720	1442.5	209.21	1298.2	188.29	72.71	10.55	1.78	XGM
STe_C277_TNS_CC_00_003	22.747	0.035	26.761	0.041	34.37	7724	1510.4	219.07	1283.9	186.21	74.64	10.83	1.72	XGM
STe_C277_TNS_CC_00_004	23.805	0.037	25.058	0.039	35.17	7903	1476.8	214.19	1402.9	203.48	79.94	11.60	1.75	SGM
STe_C277_TNS_CC_00_005	22.155	0.034	26.064	0.040	32.22	7241	1453.8	210.86	1235.8	179.23	72.09	10.46	1.71	XGM
STe_C277_TNS_CC_00_006	27.097	0.042	25.806	0.040	35.05	7877	1293.1	187.55	1357.8	196.93	74.36	10.79	1.83	SGM
STe_C277_TNS_CC_00_007	23.388	0.036	25.987	0.040	33.50	7529	1431.9	207.69	1288.7	186.92	81.19	11.78	1.59	XGM
STe_C277_TNS_CC_00_008	24.295	0.038	25.574	0.040	33.53	7534	1379.4	200.06	1310.4	190.06	72.02	10.45	1.82	SGM
STe_C277_TNS_CC_00_009	21.077	0.033	25.548	0.040	33.16	7452	1572.7	228.10	1297.5	188.18	71.81	10.42	1.81	XGM
STe_C277_TNS_CC_00_010	21.017	0.033	26.271	0.041	35.59	7997	1692.6	245.49	1354.1	196.39	69.68	10.11	1.94	SGM
STe_C277_TNS_CC_00_011	21.892	0.034	25.755	0.040	37.07	8331	1692.8	245.52	1438.9	208.69	76.91	11.16	1.87	SGM
STe_C277_TNS_CC_00_012	24.614	0.038	25.910	0.040	37.45	8415	1520.7	220.57	1444.7	209.54	75.12	10.90	1.92	SGM
STe_C277_TNS_CC_00_013	23.919	0.037	25.858	0.040	35.67	8015	1490.6	216.19	1378.8	199.98	79.74	11.57	1.73	XGM
STe_C277_TNS_CC_00_014	22.694	0.035	25.935	0.040	34.27	7700	1509.3	218.91	1320.6	191.54	72.09	10.46	1.83	XGM
STe_C277_TNS_CC_00_015	23.752	0.037	25.677	0.040	31.48	7074	1324.8	192.15	1225.5	177.74	72.57	10.53	1.69	XGM
STe_C277_TNS_CC_00_016	24.516	0.038	25.806	0.040	36.72	8251	1497.1	217.13	1422.2	206.28	72.36	10.50	1.96	XGM
STe_C277_TNS_CC_00_017	22.016	0.034	25.161	0.039	33.95	7630	1541.6	223.59	1348.9	195.64	73.54	10.67	1.83	SGM
STe_C277_TNS_CC_00_018	23.756	0.037	25.006	0.039	34.18	7682	1438.4	208.63	1366.5	198.19	75.05	10.89	1.82	SGM
STe_C277_TNS_CC_00_019	23.295	0.036	25.884	0.040	32.67	7341	1401.8	203.31	1261.6	182.98	73.81	10.71	1.71	XGM
STe_C277_TNS_CC_00_020	24.614	0.038	25.910	0.040	34.49	7750	1400.6	203.13	1330.5	192.98	73.05	10.60	1.82	XGM
AVERAGE	23.349	0.036	25.846	0.040	34.63	7781	1487.0	215.68	1339.4	194.26	74.59	10.82	1.80	
ST.DEV.	1.414	0.002	0.453	0.001	1.70	382	86.3	12.51	65.4	9.49	3.19	0.46	0.09	
C.O.V. (%)	6.1	6.1	1.8	1.8	4.9	4.9	5.8	5.8	4.9	4.9	4.3	4.3	5.1	

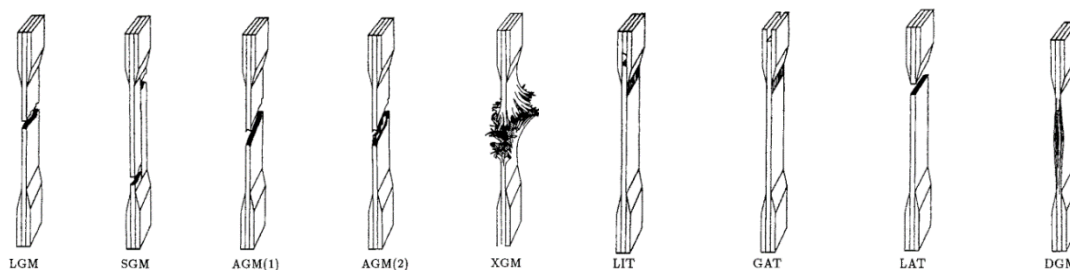


FIGURE 83 - FAILURE MODES FROM ASTM D3039 (2008)

5.1.3.4 Bond Strength

The CFRP sheet normal bond strength was characterized in compliance with ASTM D7234 (2012) while small scale bending tests were performed to characterize the shear bond strength. The average values coming from each source are here provided, for test details please refer to the already cited: Certified Test Report Number R-5.10_Ste_ESR-3606.5 (Revision 5, March 2015).

The shear bond strength, computed according to the already discussed CNR (2014) formulas is also provided, it can be spotted how referring to the 5% percentile value the difference with respect to the experimental one is not significant, while the average bond strength according to CNR formula is way higher than the measured one.

Shear Bond Strength (f_{bd})		
	US	SI
	[Kips]	[MPa]
Flexural Test	0.65	4.51
CNR (5%)	0.79	5.45
CNR (Average)	1.65	11.35

Normal Bond Strength (τ_{bd})		
ASTM D7234	0.61	4.22

5.1.3.5 Design Properties

Also for the FRP sheet the average measured properties are assumed as design ones. The material was always kept in laboratory condition and only few months passed between application and testing, also the applied FRP sheet was not engaged until testing, hence no exposure, aging or creep coefficient needs to be applied; also considering the very good environmental performance of carbon material and low tendency to creep deformation.

FRP Design Properties				
	US		SI	
$f_{fu,dry}$	700	[Ksi]	4,826	[MPa]
$E_{f,dry}$	40,000	[Ksi]	275,792	[MPa]
$\epsilon_{fu,dry}$	1.7	[%]	1.7	[%]
f_{au}	10.5	[Ksi]	72.4	[MPa]
E_a	461	[Ksi]	3,179	[MPa]
ϵ_{au}	5.0	[%]	5.0	[%]
f_{fu}	194	[Ksi]	1,338	[MPa]
E_f	10,820	[Ksi]	74,602	[MPa]
n_f	1.89	[/]	1.89	[/]
ϵ_{fu}	1.79	[%]	1.79	[%]
t_f	0.04	[in]	1.02	[mm]
f_{bd}	0.79	[Ksi]	5.45	[MPa]
l_{bd}	3.74	[in]	95	[mm]
$\epsilon_{fdd,1}$	0.42%	[%]	0.42%	[%]
$\epsilon_{fdd,2}$	0.70%	[%]	0.70%	[%]

5.1.4 CFRP Anchor Spikes

The discussed lack of certified characterization formulas force to rely on a fully experimental characterization. Such a task was carried out by Berneschi (2015), pointing out testing issues and providing valuable characterization results as well. Berneschi's dissertation is referred for further details, the results are reported hereinafter, along with their critical discussion.

5.1.4.1 Dry Fiber & Epoxy

The same epoxy and fibers as per the FRP sheet were used to form the spikes. The fibers were provided in a dowel, though, considering the absence of a specific standard testing method, the same characterization applied to the sheet is here referred.

5.1.4.2 Pull-Out Characterization

Five sample were tested in tension, all characterized by a 4 in (100 mm) bonded length inside a 5 ksi (36 MPa) concrete square block. Different failure modes were spotted: a premature dowel tensile rupture due to sub-optimal impregnation (A), a combined cone-bond failure (B) and a non-representative concrete block splitting (C).

Specimen ID	Embedded length	Peak load	Slippage at Peak	Failure mode	Comments
	[mm]	[kN]	[mm]		
T1_001	101,6	24,0	0,143	A	Premature failure
T1_002	101,6	33,5	0,150	B	
T1_003	101,6	39,6	0,160	C	
T1_004	101,6	34,7	0,142	C	
T1_005	101,6	35,9	0,073	C	
Average		33,5	0,134		
Standard deviation		5,8	0,035		
C.O.V (%)		17,3	26,1		

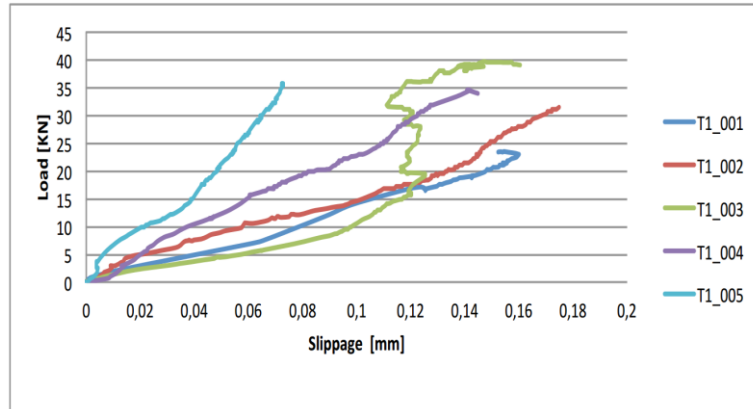


FIGURE 84 - LOAD/SLIP DIAGRAM FROM PULL-OUT CHARACTERIZATION (BERNESCHI, 2015)

The data are hardly applicable to a comprehensive characterization because of the testing issues encountered: failure A cannot be assumed representative of a well installed sample, while failures C are related to the particular test set-up and generally non-representative of a real-case scenario.

Considering the only meaningful failure mode encountered, a 33.5 kN (7.5 kips) pull-out strength can be assumed, keeping in mind the high uncertainties related to this value. The assumption seems anyway on the safe side, considering all the tested samples failing in (premature) splitting at a higher strength than the B sample. The value also coincides, by pure chance, with the overall average.

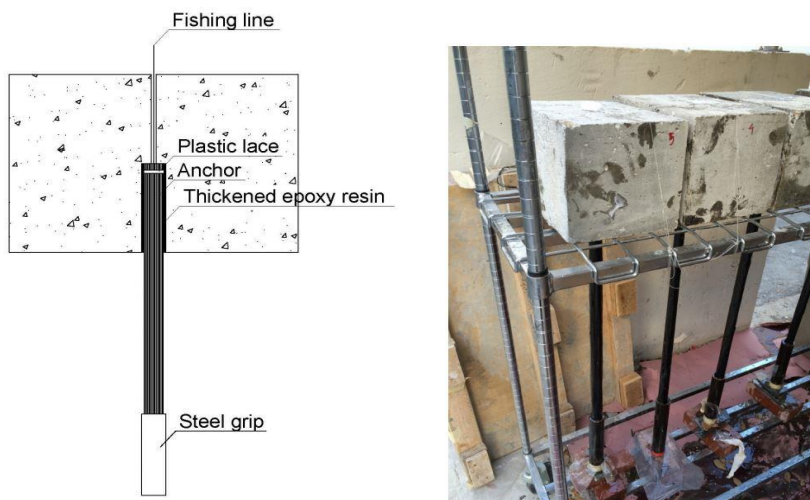


FIGURE 85 - PULL-OUT SPECIMENS (BERNESCHI, 2015)

5.1.4.3 Shear Characterization

Two different fan configurations were tested, named 60° and 90°, contemporary varying opening, width and area, but keeping constant the fan radius and dowel geometry. A sandwich configuration was tested as well, meaning a mono-directional longitudinal patch was placed on top of a standard 60° configuration. Three reference unanchored specimens were also tested.

Different failure modes were experienced, both mode B and mode C can be considered as slipping modes, as defined before, while mode D is a concrete crushing mode. No information is provided regarding the sandwich failure mode.

Assuming the concrete crushing mode strictly related to the properties of the concrete used by Berneschi (2015) and non-representative of the general anchor behavior, only the slipping modes will be applied to shear strength characterization. The assumption will be a-posteriori confirmed by the experienced failure modes in slab applications. Further discussion will be provided for sandwich's characterization.

Specimen		Anchor				Chamfer	Hole	
Type	n°	Fan Opening Angle [Deg]	Fan Radius [mm]	Dowel Diameter [mm]	Dowel Length [mm]	Radius [mm]	Diameter [mm]	Length [mm]
T3_0	3	-	-	-	-	-	-	-
T3_60	3	60°	76,2	19	101,6	6,35	25,4	101,6
T3_90	3	90°	76,2	19	101,6	6,35	25,4	101,6
T3_60s	1	60° + cover	76,2	19	101,6	6,35	25,4	101,6

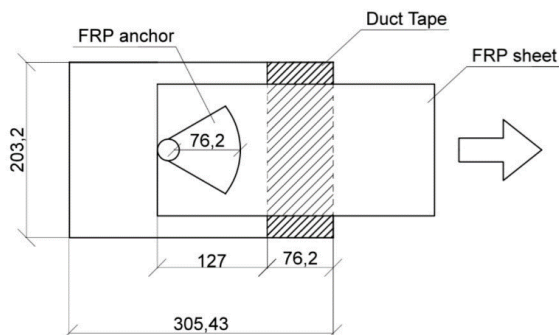


FIGURE 86 - SHEAR CHARACTERIZATION SET-UP (BERNESCHI, 2015)

Specimen ID	Fan Opening [Deg]	Peak Load P [kN]	P/2 [kN]	Average Increase in peak load [%]	Nominal Stress [MPa]	Corresponding Strain at Peak Load						Failure mode
						SG1 [%]	SG2 [%]	SG3 [%]	SG4 [%]	SG5 [%]	SG6 [%]	
T3_0_001	0	73,02	36,51	0,00	235,79	-	-	-	-	-	-	A
T3_0_002		91,12	45,56		294,25	0,41	0,40	-	-	-	0,01	A
T3_0_003		89,27	44,64		288,28	0,56	0,48	-	-	-	0,03	A
Average		84,47	42,24		272,77	0,49	0,44				0,02	
Standard deviation		9,96	4,98		32,17	0,11	0,05				0,02	
C.O.V (%)		11,79	11,79		11,79	21,79	12,00				95,36	
T3_60_001	60	114,06	57,03	36,86	371,24	-	-	-	-	-	-	B
T3_60_002		117,16	58,58		384,35	0,51	0,92	-	-	0,06	-	B
T_60_003		110,2	55,1		355,85	0,87	0,86	0,12	0,05	-	-	B
Average		115,61	57,80		377,80	0,74	0,86					
Standard deviation		2,19	1,10		9,27							
C.O.V (%)		1,89	1,89		2,45							
T3_90_001	90	137,00	68,50	57,18	449,45	-	-	-	-	-	-	C
T3_90_002		132,84	66,42		435,81	0,60	0,78	-	-	0,05	-	D
T3_90_003		128,47	64,23		421,45	0,69	0,63	0,12	0,07	-	-	D
Average		132,77	66,38		435,57	0,65	0,70					
Standard deviation		4,27	2,13		14,00							
C.O.V (%)		3,22	3,22		3,22							
T3_60S_001	60s	173,24	86,62	105,09	-	0,30	0,10	-	-	0,00	-	-



FIGURE 87 - SLIPPING FAILURE MODES (BERNESCHI, 2015)

5.1.4.4 *Design Properties*

A full anchor characterization in terms of material properties, geometry and strength is provided hereinafter. The wider possible selection of characterizing parameters will be provided in the following, following the conceptual structure earlier provided. Only in a couple of cases, namely the materials Poisson's ratios, the effort required for defining the parameter is considered too onerous, with respect to the importance of the parameter itself in defining the system's behavior.

Notice that the 90° fan configuration tested in this research will slightly differ from the ones characterized by Berneschi (2015), mainly as a consequence of the choice of increasing the fan radius in order to cover all the FRP width consistently with most researchers' suggestions (Kobayashi et al. 2001) (Brena & Mc Guirk, 2013). The difference is assumed of limited influence on the anchors behavior and neglected in characterizing the strength of the configurations here discussed.

Regarding the 60° configuration, no variations with respect to Berneschi's one were implemented, in order to have a direct comparison, in case the negligibility assumption would have proved wrong. The sandwich configuration tested on slabs is a 90° instead of a 60° as per Berneschi, having chosen a fully covering 90° configuration as the elected one for this testing phase.

Notes:

- a. The composite properties are measured on 0.04 in thick sheets.
- b. The nominal thickness is computed as discussed earlier, defining CSR.
- c. The distance from midspan is referred to the standard matching configurations.

Anchors Characterization [US]

	60°	90° (B)	90° (R)	S (B)	S (R)
$N_{pull-out}$ [kip]	7.53	7.53	7.53	7.53	7.53
S_{shear} [kip]	12.99	15.40	15.40	19.47	19.47
$E_{f,dry}$ [ksi]	40,000	40,000	40,000	40,000	40,000
$\nu_{f,dry}$ [/]	-	-	-	-	-
$\epsilon_{fu,dry}$ [%]	1.7	1.7	1.7	1.7	1.7
$f_{fu,dry}$ [ksi]	700	700	700	700	700
E_a [ksi]	461	461	461	461	461
ν_a [/]	-	-	-	-	-
ϵ_{au} [%]	5.0	5.0	5.0	5.0	5.0
f_{au} [ksi]	10.5	10.5	10.5	10.5	10.5
E_f [ksi]	10,820	10,820	10,820	10,820	10,820
ν_f [/]	-	-	-	-	-
ϵ_{fu} [%]	1.8	1.8	1.8	1.8	1.8
f_{fu} [ksi]	194	194	194	194	194
$m_{f,dry}$ [lb]	0.10	0.10	0.11	0.10	0.11
m_a [lb]	0.21	0.21	0.21	0.21	0.21
$V_{f,dry}$ [in ³]	1.54	1.54	1.69	1.54	1.69
V_a [in ³]	5.25	5.25	5.25	5.25	5.25
$\rho_{f,dry}$ [lbs/in ³]	0.065	0.065	0.065	0.065	0.065
ρ_a [lbs/in ³]	0.040	0.040	0.040	0.040	0.040
h_{dowel} [in]	4	4	4	4	4
d_{dowel} [in]	1	1	1	1	1
β_{dowel} [°]	90	90	90	90	90
r_{ch} [in]	0.25	0.25	0.25	0.25	0.25
A_{dowel} [in ²]	0.79	0.79	0.79	0.79	0.79
α_{fan} [°]	60	90	90	60	90
R_{fan} [in]	3	3	4	3	4
w_{fan} [in]	4.00	5.24	6.66	4.00	6.66
A_{fan} [in ²]	8.51	11.05	17.64	8.51	17.64
t_{fan} [in]	0.20	0.15	0.12	0.20	0.12
l_{anchor} [in]	7	7	8	7	8
CSR [/]	3.27	3.27	3.27	3.27	3.27
l_{end} [in]	3	3	3	3	3
l_{side} [in]	7	7	7	7	7
$l_{midspan}$ [in]	19\32	-	19\32	-	19\32
n [/]	1	1	2	1	2
n_L [/]	1	1	2	1	2
n_P [/]	1	1	1	1	1
s_L [/]	-	-	6	-	6
s_R [/]	-	-	-	-	-
$w_{concrete}$ [in]	14	14	14	14	14
w_{sheet} [in]	6	6	6	6	6
t_{sheet} [in]	0.04	0.04	0.04	0.04	0.04
A_{sheet} [in ²]	0.24	0.24	0.24	0.24	0.24
Material [/]	Carbon	Carbon	Carbon	Carbon	Carbon
Bonded [/]	Bonded	Bonded	Bonded	Bonded	Bonded
Wet / Dry [/]	Wet	Wet	Wet	Wet	Wet

a

b

c

Anchors Characterization [SI]

		60°	90° (B)	90° (R)	S (B)	S (R)
$N_{\text{pull-out}}$	[kN]	33.50	33.50	33.50	33.50	33.50
S_{shear}	[kN]	57.80	68.50	68.50	86.62	86.62
$E_{f,\text{dry}}$	[MPa]	275,790	275,790	275,790	275,790	275,790
$\nu_{f,\text{dry}}$	[/]	-	-	-	-	-
$\epsilon_{fu,\text{dry}}$	[%]	1.7	1.7	1.7	1.7	1.7
$f_{fu,\text{dry}}$	[MPa]	4,826	4,826	4,826	4,826	4,826
E_a	[MPa]	3,178	3,178	3,178	3,178	3,178
ν_a	[/]	-	-	-	-	-
ϵ_{au}	[%]	5.0	5.0	5.0	5.0	5.0
f_{au}	[MPa]	72	72	72	72	72
E_f	[MPa]	74,601	74,601	74,601	74,601	74,601
ν_f	[/]	-	-	-	-	-
ϵ_{fu}	[%]	1.8	1.8	1.8	1.8	1.8
f_{fu}	[MPa]	1,338	1,338	1,338	1,338	1,338
$m_{f,\text{dry}}$	[kg]	0.045	0.045	0.050	0.045	0.050
m_a	[kg]	0.095	0.095	0.095	0.095	0.095
$V_{f,\text{dry}}$	[mm ³]	0.25	0.25	0.28	0.25	0.28
V_a	[mm ³]	0.86	0.86	0.86	0.86	0.86
$\rho_{f,\text{dry}}$	[kg/mm ³]	0.18	0.18	0.18	0.18	0.18
ρ_a	[kg/mm ³]	0.11	0.11	0.11	0.11	0.11
h_{dowel}	[mm]	102	102	102	102	102
d_{dowel}	[mm]	25	25	25	25	25
β_{dowel}	[°]	90	90	90	90	90
r_{ch}	[mm]	6	6	6	6	6
A_{dowel}	[mm ²]	507	507	507	507	507
α_{fan}	[°]	60	90	90	60	90
R_{fan}	[mm]	76	76	102	76	102
w_{fan}	[mm]	101.60	133.16	169.08	101.60	169.08
A_{fan}	[mm ²]	5489	7127	11382	5489	11382
t_{fan}	[mm]	4.99	3.81	3.00	4.99	3.00
l_{anchor}	[mm]	178	178	203	178	203
CSR	[/]	3.27	3.27	3.27	3.27	3.27
l_{end}	[mm]	76	76	76	76	76
l_{side}	[mm]	178	178	178	178	178
l_{midspan}	[mm]	482\812	-	482\812	-	482\812
n	[/]	1	1	2	1	2
n_L	[/]	1	1	2	1	2
n_P	[/]	1	1	1	1	1
s_L	[/]	-	-	6	-	6
s_R	[/]	-	-	-	-	-
w_{concrete}	[mm]	356	356	356	356	356
w_{sheet}	[mm]	152	152	152	152	152
t_{sheet}	[mm]	1	1	1	1	1
A_{sheet}	[mm ²]	155	155	155	155	155
Material	[/]	Carbon	Carbon	Carbon	Carbon	Carbon
Bonded	[/]	Bonded	Bonded	Bonded	Bonded	Bonded
Wet / Dry	[/]	Wet	Wet	Wet	Wet	Wet

a

b

c

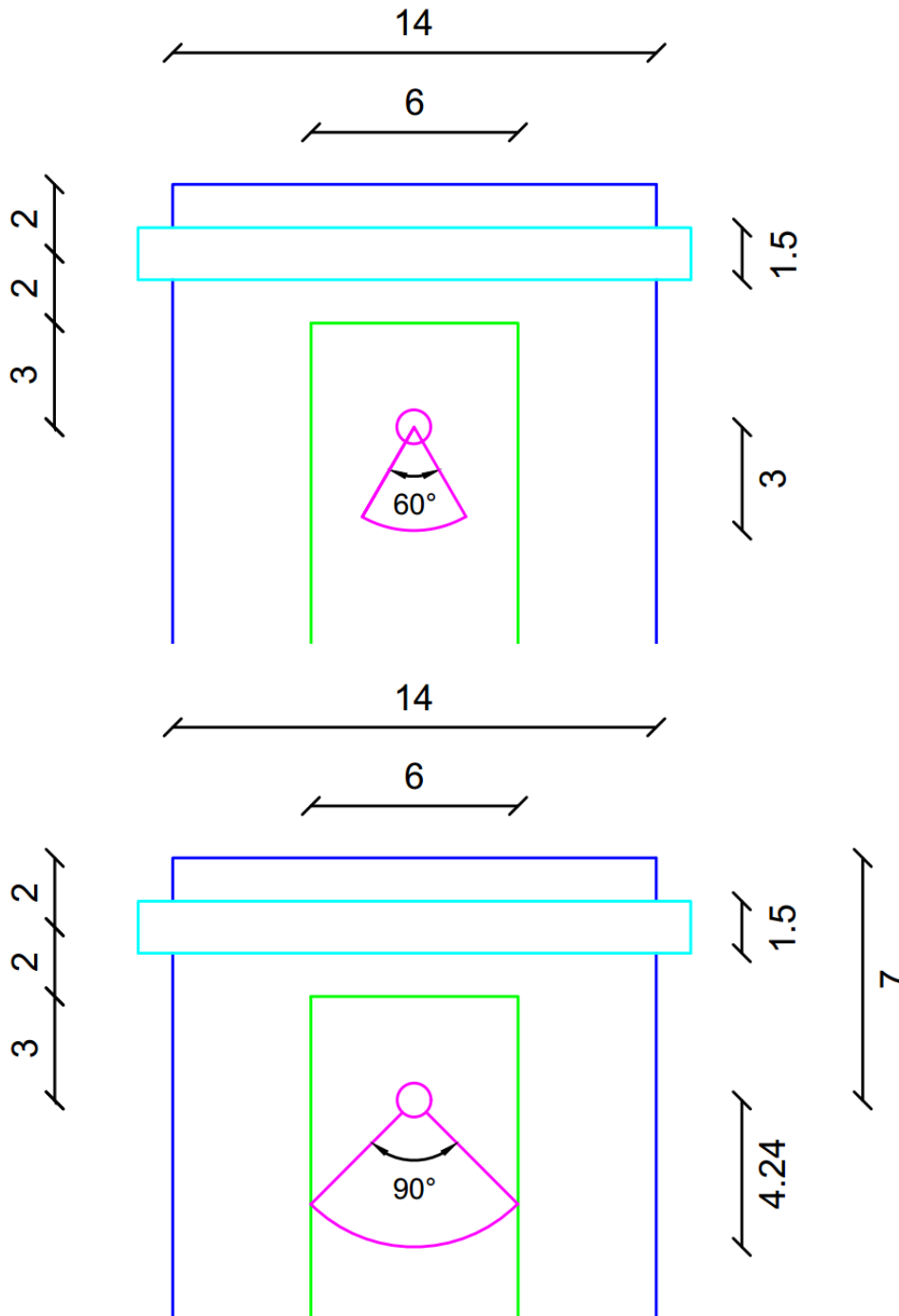


FIGURE 88 - APPLIED CONFIGURATIONS (A) 60° (B) 90°-R, THE SANDWICH ONE IS SIMPLY A 90° CONFIGURATION WITH A PATCH APPLIED ON TOP, REFER TO SLAB'S GEOMETRY FOR DETAILS. ALL THE DIMENSIONS ARE IN INCHES (1 IN = 25.4 MM).

5.2 Specimens Preparation

All the specimen preparation, instrumentation and experimental work was carried out by the author autonomously, apart from molds construction and concrete casting, for which the aid of the UM Structures and Technology lab's team is acknowledged with gratitude. Sandblasting was also performed by a professional operator.

5.2.1 Concrete Specimens

5.2.1.1 Rebars Instrumentation

The slabs were reinforced with two #3 rebars, for each slab two steel strain gages were applied, in some cases on the two sides of the same rebar, generally one on each rebar.

In order for the gage to properly stick to the steel, the rebar itself was sandpapered using a dremel, the strain gage was stuck to the smoothed surface with superglue and covered with an insulating fluid solution. Everything was then electric-taped.

Once the rebars are placed into the molds, it is critical to wire the gages' lines outside the mold and properly secure the loose wires and protect them from concrete pouring.



FIGURE 89 - REBAR INSTRUMENTATION

5.2.1.2 *Molds Set-Up*

Once all the rebars were all instrumented, they were linked two by two thorough proper spacers and placed in the already prepared wooden molds. A Voltmeter was used in order to verify all the applied strain gages were still working after installation, before sending the molds for concrete pouring. Before rebar positioning, a demolding agent was also sprayed on the wood surface, in order to favor concrete-mold separation after curing.



FIGURE 90 - MOLDS SET-UP

5.2.1.3 *Casting*

Casting was performed in a concrete factory: all the molds were brought to the facility and the finite product was brought back to the lab after 7 days for final curing. Right after casting, the specimens were covered with plastic sheets in order to avoid any loss of moisture.

5.2.1.4 *Demolding*

Demolding was manually performed in the laboratory, right after specimen were brought back from the factory. They were stored in open air waiting for sandblasting.

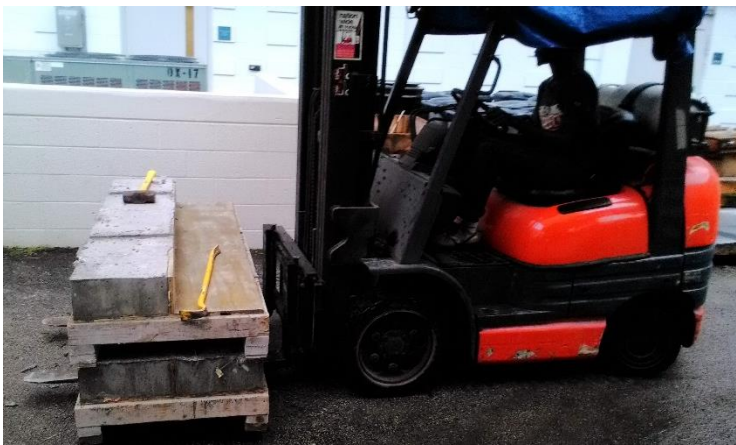


FIGURE 91 - CASTING & DEMOLDING

5.2.1.5 Sandblasting

It is widely accepted that the surface roughness influences bond capacity. The specimens' needs to be treated in order to increase the bond performances once the FRP sheet is applied to the concrete (Sarbescu et al. 2013).

Although most of the design guidelines include qualitative recommendations on the surface preparation, these recommendations are rather vague. A common requirement is that, before the installation of the FRP sheet, the superficial plain cement paste should be removed (Berneschi, 2015). On the other hand, high impact preparation, such as hammering, may potentially weaken the surface and high levels of roughness are reported to adversely affect the bonding performances by inducing micro cracks (Sarbescu, Guadagnini and Pilakoutas; 2013).

Preparation recommended by manufacturers guidelines are usually achieved by grinding or sand blasting in order to remove the plane cement surface and exposure of a relative plane surface of aggregates. Sandblasting was performed in compliance to Berneschi's (2015) recommendation, in order to stay the closer possible to the condition in which anchor's shear characterization was performed. The operation was performed by a professional during the curing period.



FIGURE 92 - SANDBLASTING PERFORMED BY A PROFESSIONAL

5.2.2 FRP Application

5.2.2.1 Sheet Application

Before applying the FRP sheet the slabs were moved in a temperature/humidity controlled environment and the concrete surface was properly dried and cleaned using compressed air, in order to have a good concrete-FRP bonding.

The fiber roll was cut in 68x70 in (150x1750 mm) sheets, then the two epoxies component were mixed with a 100 A to 33 B weight ratio (100 A to 41 B by volume); a primer was also prepared mixing a 100 epoxy to 75 fume silica by volume. The two epoxy components should be mixed for at least 3 minutes or until a uniform consistency is achieved, the same applies to the primer (also called thickened epoxy or putty).

On a covered clean table the fiber sheets are impregnated, pouring the mixed epoxy on top of them and then pressing the composite into the pores using a spatula and a roller.

Once the fibers are fully impregnated, the primer is applied on the concrete surface in order to fill all the gaps, another layer of standard epoxy is applied over the primer and then the fiber sheet. One last epoxy layer is poured on the fiber sheet, then the sheet is rolled and the exceeding epoxy is removed using a spatula.

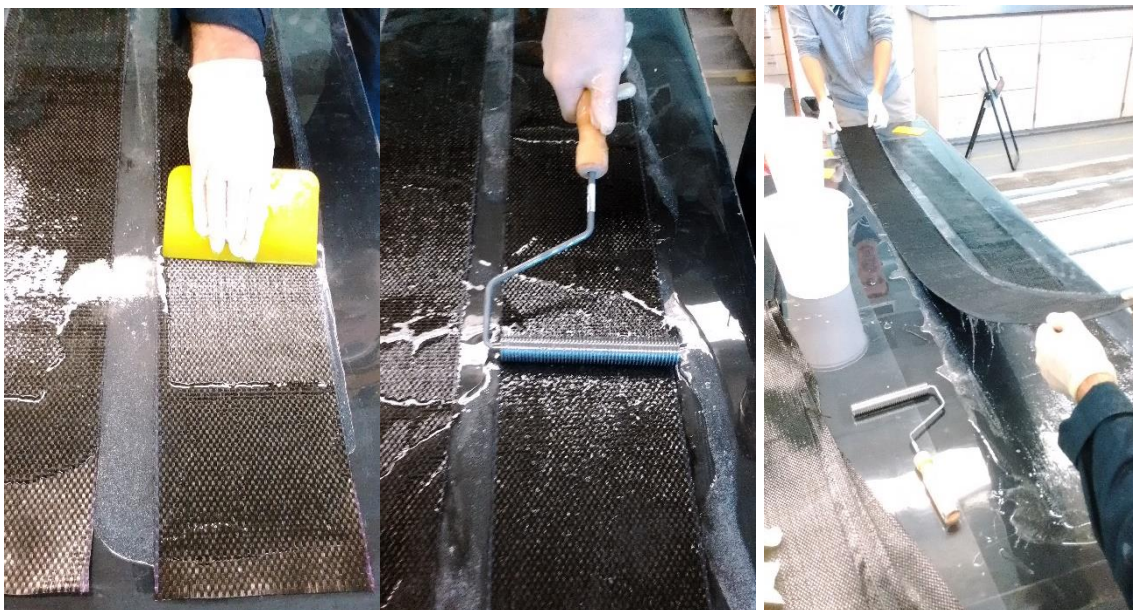


FIGURE 93 - CARBON FIBERS IMPREGNATION



FIGURE 94 - FRP APPLICATION

5.2.2.2 Drilling & Hole Preparation

After three days, the FRP sheets have cured and the epoxy is fully polymerized; at this point it is possible to directly drill through the sheet and the concrete beneath, for a depth of 4 inches (100 mm). A Hilti hammer is used to perform the operation, the hole is then cleaned with compressed air and a brush: the presence of dust or debris can undermine the dowel's bonding to the surrounding concrete.

The hole's edge should also be chamfered in order to prevent stresses concentration and actual fibers' cutting. The chosen chamfer radius is $\frac{1}{4}$ in (6 mm) in agreement with the choices made while performing anchors' shear characterization. To provide the required chamfer radius proper drill bits were used.



FIGURE 95 - HOLE DRILLING & CHAMFER RADIUS

5.2.2.3 Anchors Installation

The anchors came as dry fiber bundles to be cut at the desired length, in the present case 8 inches (200mm) for the 90° configurations and 7 inches (175 mm) for the 60° configurations. The Cut fibers should be held together using fishing line, a string or an elastic band to be placed at one anchor's end.

Once the dry anchors are ready, the epoxy is mixed and the anchors themselves impregnated. It is evident how the anchor's fan and the dowel's body should be properly impregnated, in order to do so, the anchor is held on the bounded side, while epoxy is pressed among the fibers on the other end.

The bounded end that will become the dowel's bottom should be not impregnated, being extremely difficult to insert a fully impregnated dowel; the solution is acceptable, being applied to a not-engaged portion of the dowel in a non-pullout-critical application.



FIGURE 96 - ANCHORS CUTTING & IMPREGNATION

Once the anchor is properly impregnated, the hole is prepared applying thickened epoxy on the internal surface and filling 1/3 of its depth with standard epoxy. To the sheet's surface, a layer of thickened and a layer of standard epoxy are applied as well.

The non-impregnated end is inserted in the hole down to the bottom, the impregnated fan is opened to the desired angle. Drawing the fan configuration before proceeding to anchor's installation makes the task way easier. Once the fan is properly opened, a last layer of epoxy is applied, making sure the hole is completely filled; leave some times for air bubbles inside the hole to spontaneously be pushed out by the epoxy's weight and add epoxy as needed. If a sandwich is required, after impregnation, apply it on top of the fan, making sure all the spaces in-between are properly filled with thickened epoxy.



FIGURE 97 - ANCHORS INSTALLATION

It was possible to extract one of the anchors from a tested slab, along with a portion of FRP sheet. These pictures give clear idea of what we are talking about.



FIGURE 98 - CURED ANCHOR EXTRACTED FROM A COLLAPSED SLAB

5.2.2.4 Strain Gages Application

Strain gages can be directly applied to the cured fiber sheet; the exceeding epoxy can eventually be brushed away using sand paper. Proper care should be taken in aligning the gages along the fiber direction and in properly sticking them to the substrate. Considering the huge amount of gages, a careful labeling is required as well.

Considering that the slabs are going to be flipped and positioned on the testing frame using a Forklift, the strain gages' wires should be properly wired in order to avoid interferences during moving and positioning.



FIGURE 99 - STRAIN GAGES APPLICATION ON FRP SHEETS

5.3 Experimental Matrix

As a general design consideration, it is important to underline how this research is focused on characterizing the behavior of anchoring spikes in flexural reinforcement applications, not on evaluating the global behavior of a real – full-scale – system in presence of anchors.

This means that, while the likelihood of the tested concrete elements and reinforcement configuration is always guaranteed, some peculiar choices were made, particularly in terms of concrete strength and amount of rebars, in order to maximize the influence of the anchoring solutions on the overall behavior of the system.

The experimental effort is focused on nine bending tests on slabs, all CFRP-externally-reinforced, apart from an unreinforced sample, and characterized by different anchors configurations. The choices made in terms of materials, elements' geometry, experimental set-up and instrumentation will be here discussed.

5.3.1 Unreinforced Sample

The most important design choices are probably the ones affecting the unreinforced sample's strength, representing the plain R/C element we want to provide with additional reinforcement, named C-C for *Control-Concrete*. An ill-designed reference will make way harder to extrapolate meaningful conclusion from the collected results.

5.3.1.1 Materials

It is important to underline how a particularly strong concrete (10 kip, C60/65) was prescribed, in order to avoid shear failures; while the choice of a stronger steel (S70, B450) was mainly dictated by material availability and doesn't really make a difference with respect to standard S60 generally used in the US.

Only two #3 ($\emptyset 10$) rebars are used as internal reinforcement, in order to be sure the element is under-reinforced: as well known, external reinforcement on over-reinforced elements is, if not ineffective, surely largely inefficient, considering that the internal reinforcement's strength is already non-entirely exploited at failure. The particularly

small amount of rebars is chosen in order to maximize the strength increment provided by the external reinforcement, allowing easier results interpretation.

5.3.1.2 Geometry

The element's geometry is basically fixed because of the limits imposed by the available testing frame: the total length of the concrete element is fixed at 78 in (1.98 m) while the supports are located in order to provide a 74 in (1.88 m) free span.

The will to maximize the free span comes from the consideration that a non-slender element tends to deviate from the behavior predicted by the standard beam theory. The effect is surely negligible on real-scale applications, but can be significant on the small span tested, mainly considering the presence of anchors along the span itself.

The minimal bond length provided to the rebars passing the external supports (2 in, 50 mm) is justified by the assumption that no severe cracks will develop away from the midspan, thanks to the particularly high concrete strength, hence no slipping-induced collapses should happen. Rebars' bonding is also promoted by the particularly little diameter chosen. The results will actually show that slipping did not happen at all, even at very high deflections, after load drop.

Regarding the section, the width is fixed at 14 in (356 mm) for the sake of consistency with anchors' shear characterization (Berneschi, 2015), while a 6 in (152 mm) height was chosen in order to have a reasonable dimensional ratio and enough room for drilling the dowels' holes.

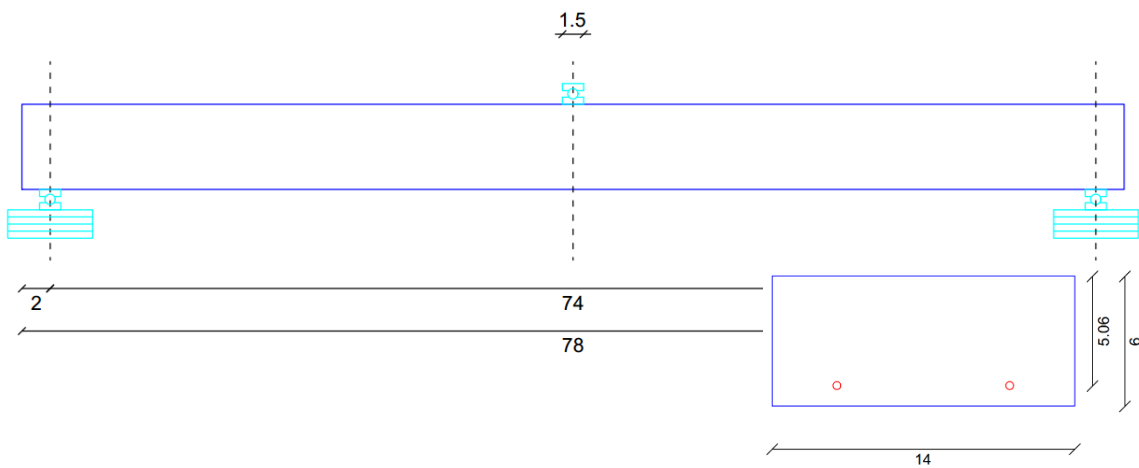


FIGURE 100 - UNREINFORCED SAMPLE (C-C). ALL THE DIMENSIONS ARE IN INCHES (1 IN = 25.4 MM).

5.3.2 Anchored Series

5.3.2.1 Control Sample

Specimen: C-FRP

A 70 in (1,78 m) long, 6 in (152 mm) wide, 0.04 in (1 mm) deep, CFRP sheet is applied to the bottom of all the 8 externally reinforced samples. The chosen width is consistent with the characterization specimens (Berneschi, 2015), while 2 in (50 mm) from the physical supports, central lines are provided, in order to avoid interferences, hence the sheet length.

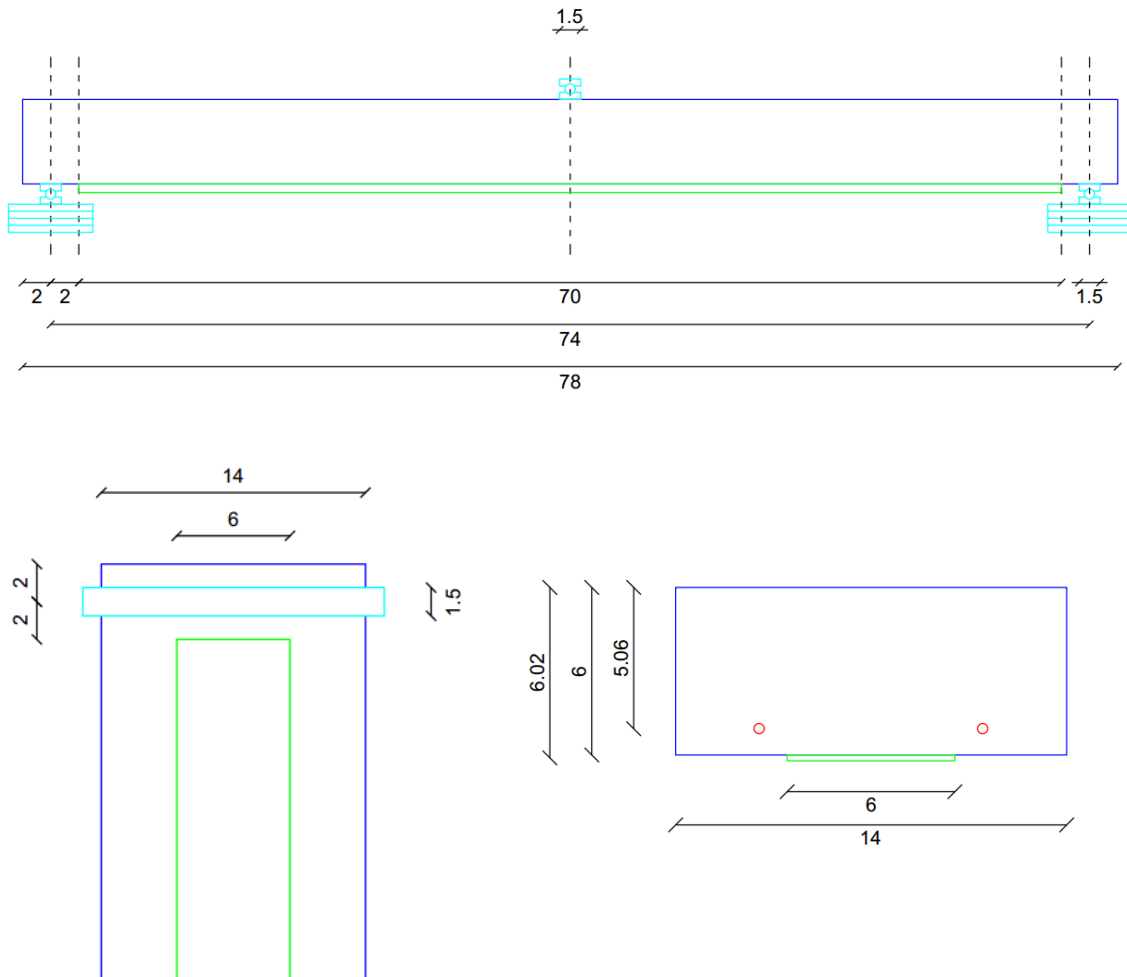


FIGURE 101 - FRP CONTROL SAMPLE (C-FRP). ALL THE DIMENSIONS ARE IN INCHES (1 IN = 25.4 MM).

5.3.2.2 Matching Series

Specimens: 60x2, 90x2

The principal purpose of the dissertation is to develop a ULS design algorithm for flexural anchors application. In order to do so, the two characterized spikes variant are applied to two different externally reinforced slabs and tested. This allows for an experimental-theoretical matching and a validation of the proposed algorithm.

The series also allows to certify the double shear test as a valid characterization test for flexural applications. Comparing the results with the one coming from unreinforced and control specimen, allows to quantify the strength increment as well.

Noticing that a single anchor was not able to withstand the tensile resultant, engaging the FRP sheet at occurring intermediate debonding, forced to apply a 2-anchor-series solution, designed assuming full coupling, as suggested by many authors (Zhang & Smith, 2013) (Brena & McGuirk, 2013).

Apart from the need to double the number of anchors per end, the same position and configuration as per Berneschi's characterization were applied: the dowels are drilled in the middle of the FRP sheet, leaving 3 in (75 mm) from sheet's end and 6 in (150 mm) from center to center, so that each anchor is working on an area of about 6x6 inches as in shear characterization specimens.

It is worth noticing that the dowels' distance is of the same order of magnitude of the bond length (2.92 to 3.74 in, depending on the applied formulas and chosen data) and the first anchor is located inside the bond transfer zone, as suggested by Brena & McGuirk (2013).

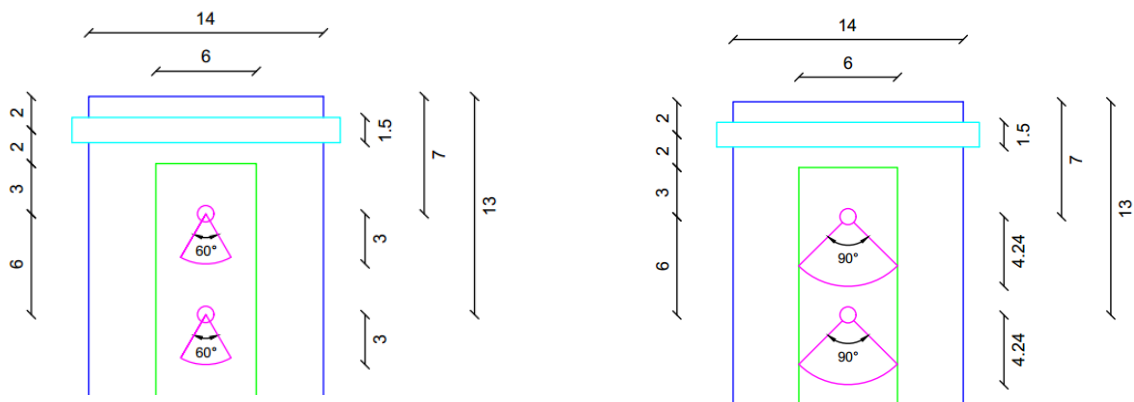


FIGURE 102 - 60x2 & 90x2 CONFIGURATIONS. ALL THE DIMENSIONS ARE IN INCHES (1 IN = 25.4 MM).

5.3.2.3 Position Series

Specimens: 90x2, 90x2 L/4, 90x2 L/3

Addressed the matching issue, the effect of varying anchors' spacing was investigated, namely moving the internal anchor toward the slab's midspan. As discussed, the standard solution is based on a spacing of 6 in (150 mm), two more solutions were tested, with an anchor placed at about 1/4 (13 in, 330 mm spacing) and 1/3 (19 in, 480 mm spacing) of the free span.

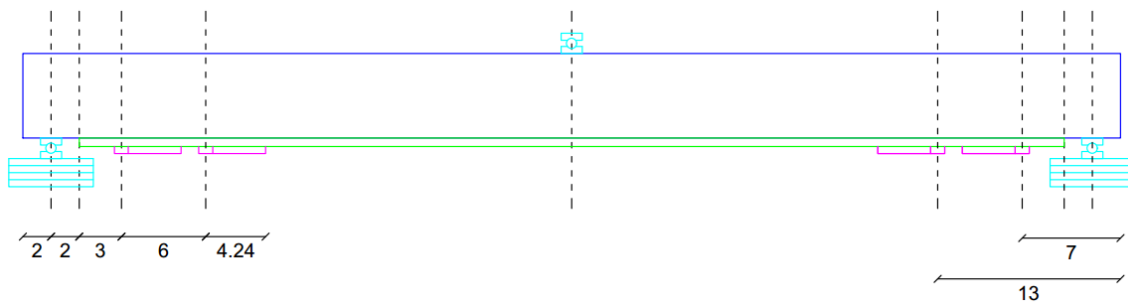


FIGURE 103 - 90x2

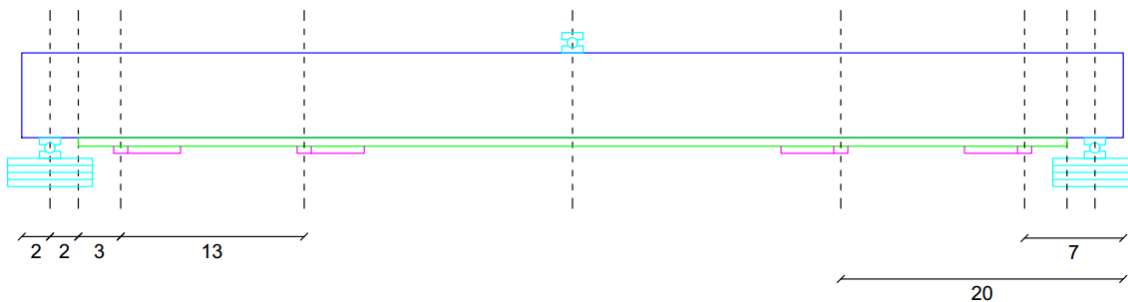


FIGURE 104 - 90x2 L/4

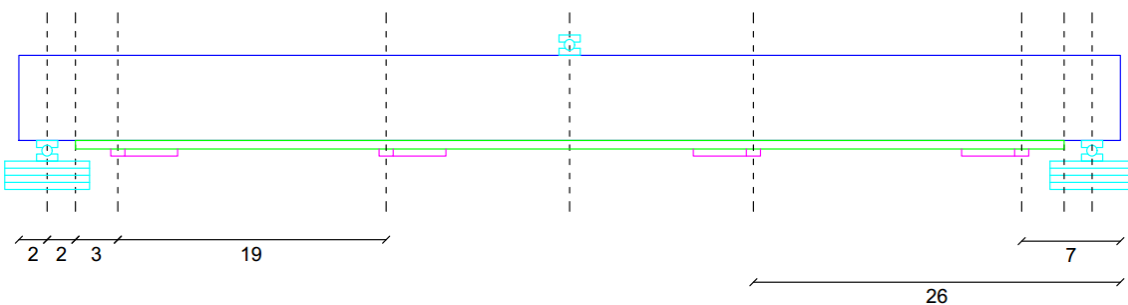


FIGURE 105 - 90x2 L/3. ALL THE DIMENSIONS ARE IN INCHES (1 IN = 25.4 MM).

5.3.2.4 Number of Anchor Series

Specimens: 90x2, 90x2 L/3, 90x3

As it will be fully discussed, the position series showed a reduced efficiency at increasing spacing. To address the problem, an additional anchor was positioned in an intermediate location hoping to recouple the behavior of the L/3 configuration; the 90x3 configuration hence showed 9 & 10 in (225 & 250mm) spaced anchors.

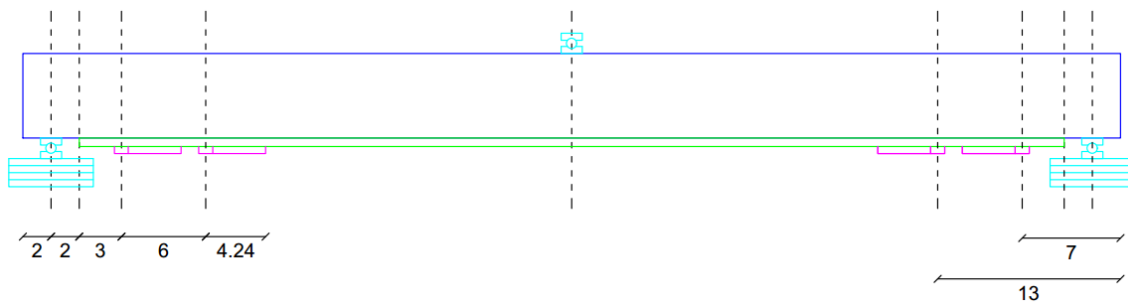


FIGURE 106 - 90x2

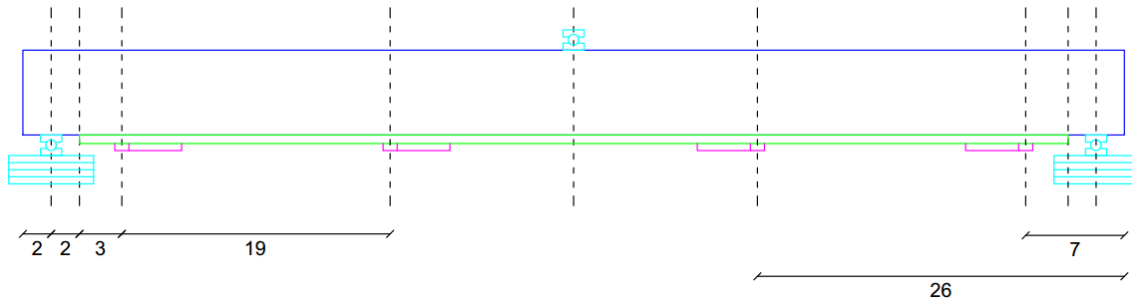


FIGURE 107 - 90x2 L/3

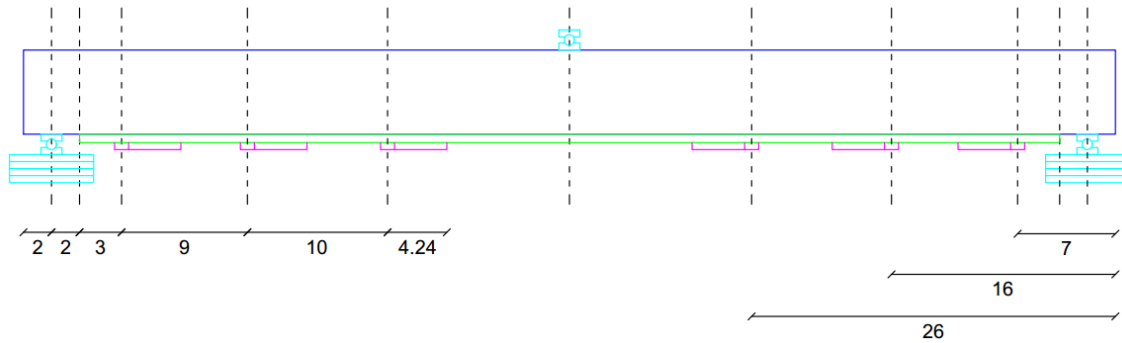


FIGURE 108 - 90x3. ALL THE DIMENSIONS ARE IN INCHES (1 IN = 25.4 MM).

5.3.2.5 Sandwich Effectiveness Series

Specimens: 90x2, Sx2-1, Sx2-2

The sandwich configuration was originally included in the matching series, but peculiar results coming from Sx2-1 lead to conduct an additional test and some specific considerations justify the discussion in a different series.

The Sx2-2 sample present anchors spaced 9" (225 mm) instead of the standard 6" (150mm), this is because the rebar's spacer moved during casting and prevented drilling in the standard location. Such a slight difference is believed not to affect in a significant way the strength of the joint, as it will be proved afterwards. The specimen allows also for further discussion regarding the position's effect.

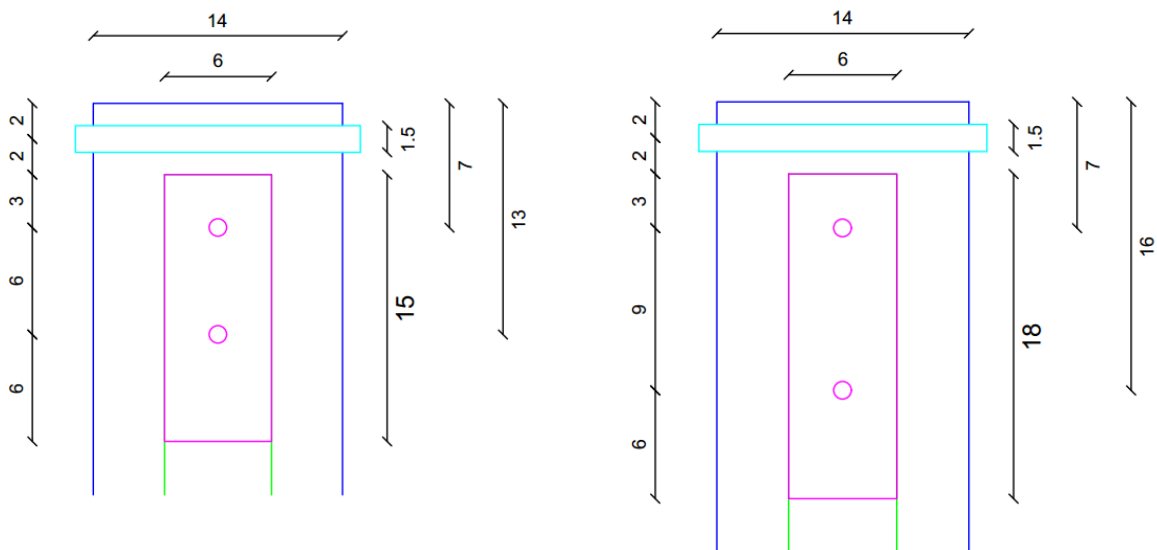


FIGURE 109 - Sx2-1 & Sx2-2 CONFIGURATIONS. ALL THE DIMENSIONS ARE IN INCHES (1 IN = 25.4 MM).

5.3.3 Experimental Set-Up

5.3.3.1 Load Application

The load is applied according to a three point bending configuration, through a 55-kip MTS hydraulic actuator mounted on a testing frame. While a 4-point bending configuration is surely preferable, guaranteeing a pure bending behavior in the central portion of the span, the limited span of the tested elements, constrained by the geometry of the frame itself, force to opt for the three-point solution.

Applying concentrated load close to the supports in a 4-point shape would cause the element to move from a bending-prevalent behavior to a shear-controlled one. Preventing the effectiveness of the standard beam theory and making the tests not representative of a flexural reinforcement application.

The load was applied in displacement control, with a load application rate varying from 0.00125 to 0.0025 in/s depending on the load goal for the particular cycle. The variation in the load application rate is believed to have no effect on the system's behavior, being anyway small enough to guarantee a quasi-static application. Even larger values are used after load drops, while trying to reach steel's failure, actually never reached because of the testing machine's limit on applicable deflection (about 5 in, 125 mm).

Load cycles were performed trying to catch each phase of the system failure (intermediate debonding, first ancho failure, second anchor failure, final collapse) and the related stiffness. The difficulty to program displacement controlled cycles forced to manually stop the machine once the desired load was reached, reprogram for unloading, load again and so on.

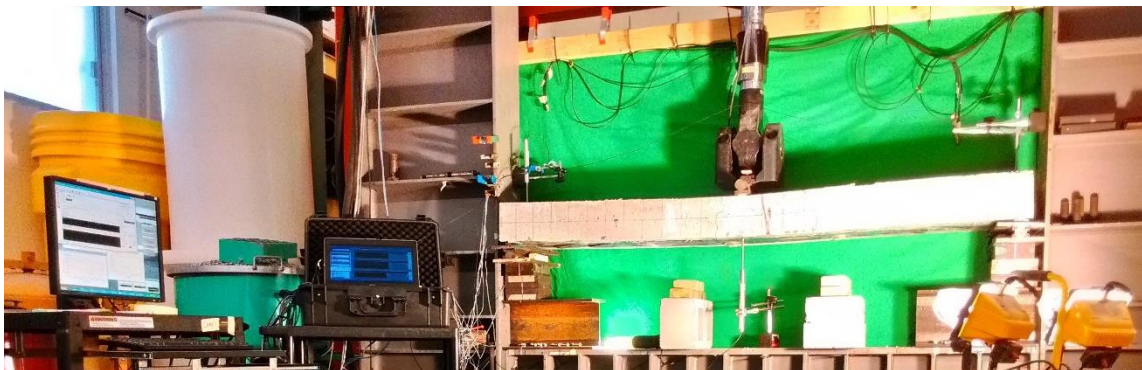


FIGURE 110 – FROM RIGHT TO LEFT: TESTING FRAME, DAQ & CONTROL SYSTEM

5.3.3.2 Boundary Conditions

The slabs are simply supported; the physical restraint is provided by two cylindrical hinges. Providing a roller at one end would have been preferable in order to avoid the confinement effect coming from the normal stresses, raising because of constrained sliding. The lack of available devices prevented this solution, however, on such a limited span, the prevented sliding and the related confinement effect is believed to be negligible.

5.3.3.3 Deflection Measurement

Three LVDT are applied to deflection measurement: a 10 in (250 mm) one in midspan and two 4 in (100 mm) ones on the supports. A midspan deflection measurement backup is also provided by the actuator itself. The consistency of the two measures has always been checked.

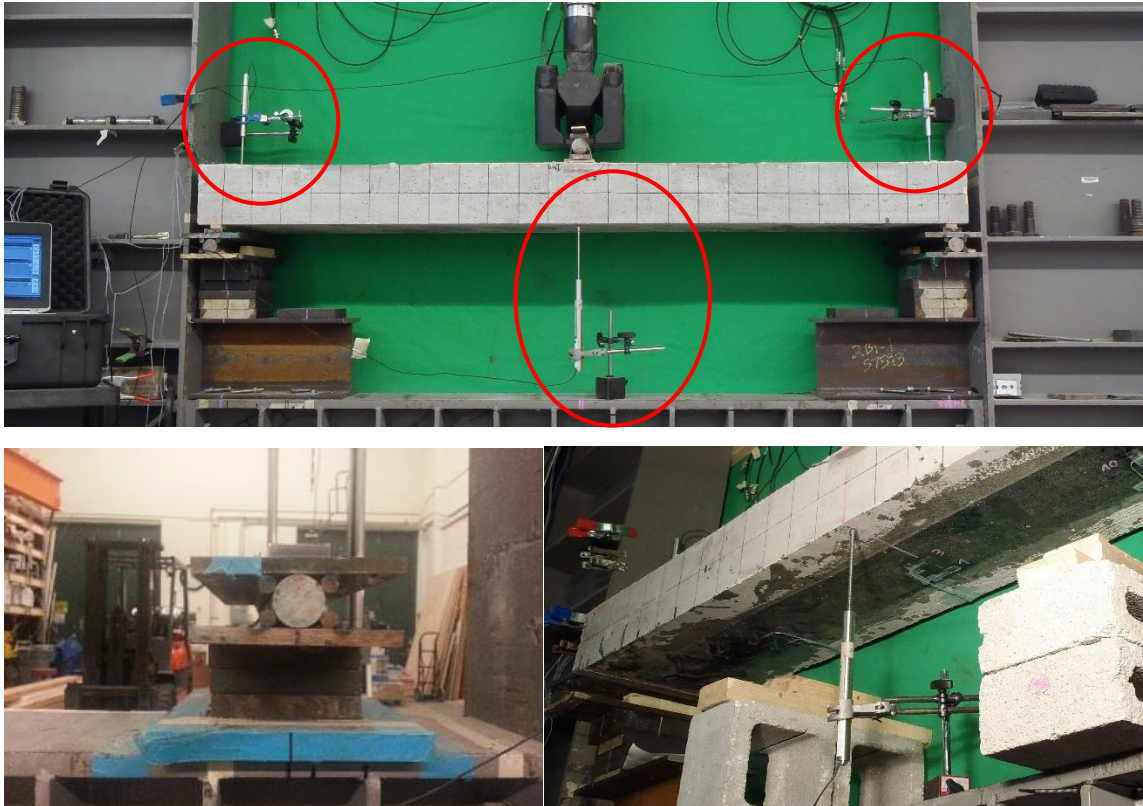


FIGURE 111 - LVDTs & CYLINDRICAL HINGE DETAIL

5.3.3.4 Strain Measurement

2.3 in (60 mm) strain gages are applied for concrete strain measurement, while 0.23 (6 mm) solutions are preferred for internal rebars and FRP sheet.

Concrete gages are applied on the slabs sides, about 0.75 in (19 mm) from section's top, in order to avoid the roughness of the extrados; they are directly applied to the concrete surface, after a little sand-papering. Steel gages are directly applied on rebars, after preparing the surface, and isolated in order to preserve them during casting operations. FRP gages are simply applied on the impregnated sheet, three should be applied on each critical section in order to read the strain shape over the width.

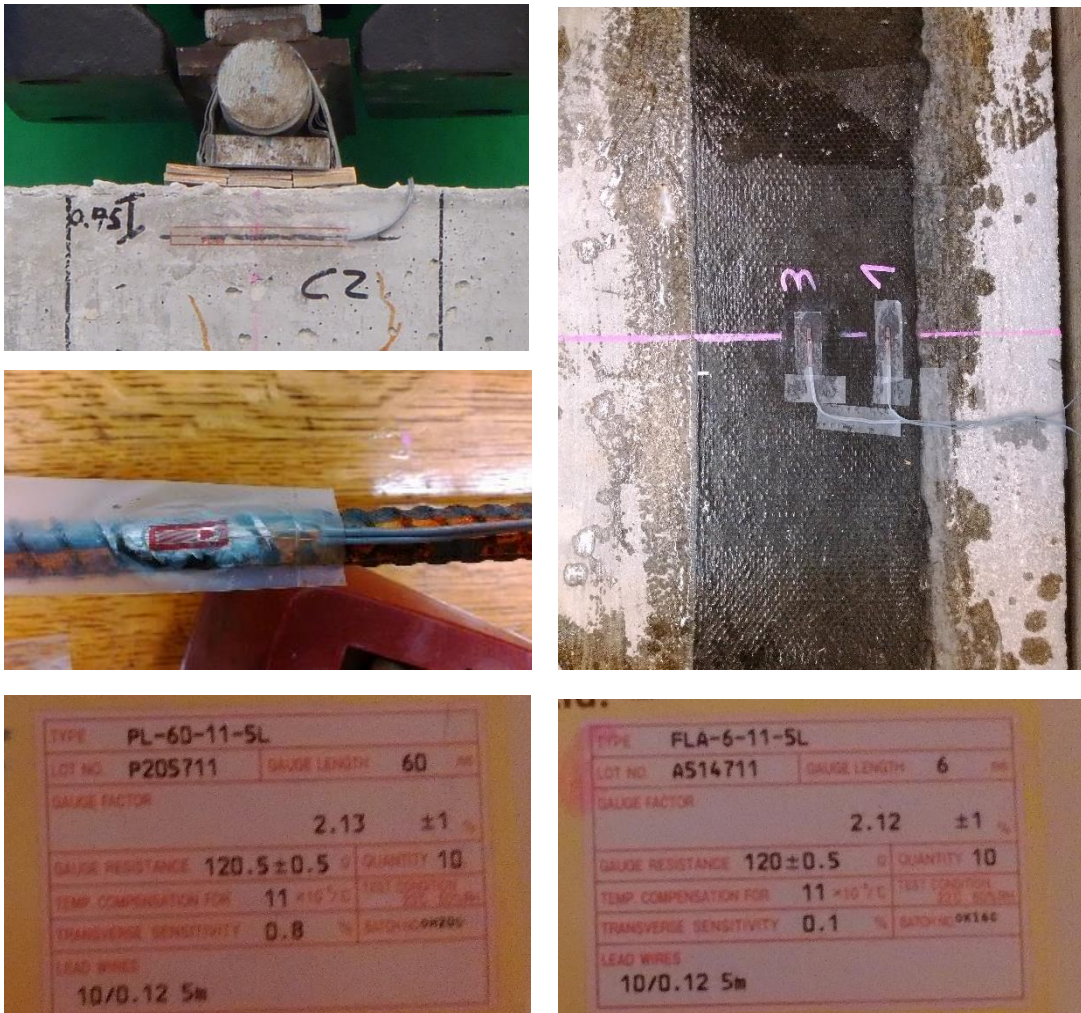


FIGURE 112 - CONCRETE, STEEL & FRP STRAIN GAGES

For a complete strain reading, a large number of gages would be required, namely: 2 concrete gages, 2 steel gages, 3 FRP gages on each critical section, meaning in front of each anchor and at midspan. In the worst case scenario (90x3) this means 25 gages in total. Having only 7 strain channels available for acquisition, alternative solutions were adopted in order to limit the number of required instruments.

In order to avoid instrumenting the non-failing side of the slab, on some samples, one end was over-anchored, guaranteeing the failing side to be known a-priori. Moving the applied load from midspan would have also been a solution, however unfeasible because of the testing frame configuration and limited dimensions.

Once validated the strain consistency over the section and an almost linear behavior, the concrete and steel strains were disregarded, in order to make room for a detailed FRP strain characterization. Detailed SG mapping is provided in appendix for each tested sample, a general scheme is here reported.

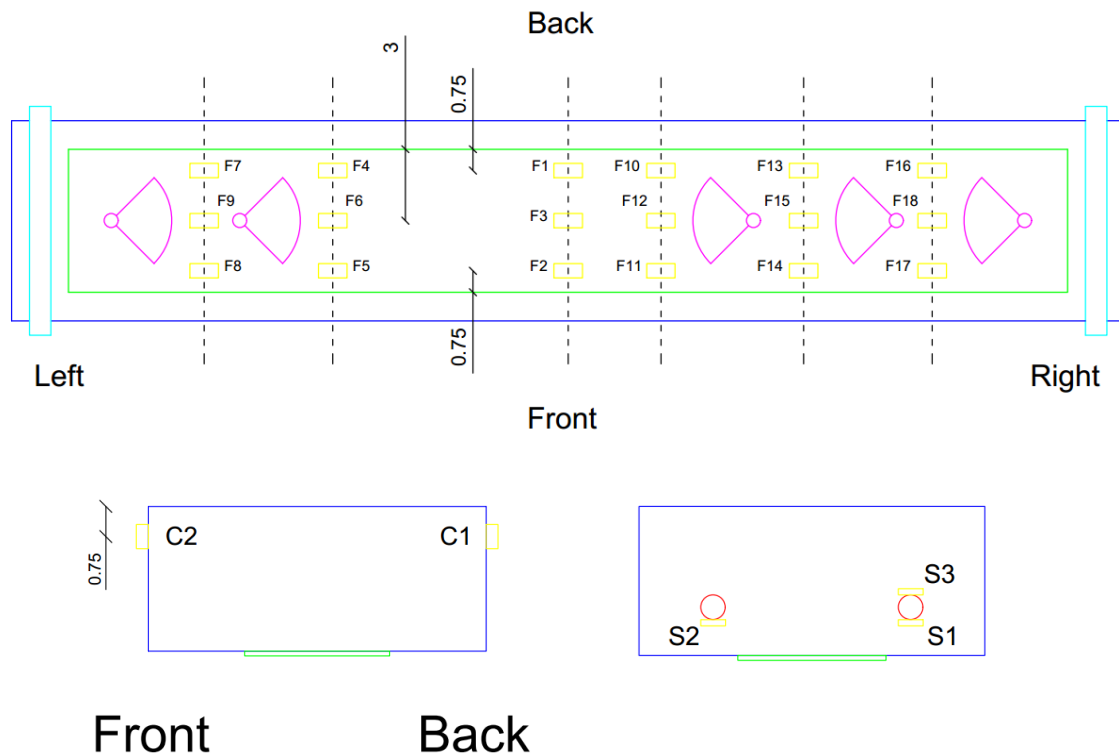


FIGURE 113 - STRAIN GAGES GENERAL POSITIONS. ALL THE DIMENSIONS ARE IN INCHES (1 IN = 25.4 MM).

5.3.4 Final Matrix

5.3.4.1 Geometry and Configurations

The fundamental information and geometry data for each tested slab are summed up. Please refer to anchor spikes' characterization for single anchor's configuration detail. The nomenclature, if ambiguous, is hereinafter clarified, also refer to the pictures.

a	FRP sheet's ends distance from supports
a'	End anchors' distance from sheet's ends
l_{FRP}	FRP sheet's length
$l_{anchored}$	FRP anchored length, i.e. distance between end anchors
#	Rebar Number, US identification
a_s	Single rebar's area
c	Concrete Cover
s	Rebar horizontal spacing
<i>Configuration</i>	Please refer to single anchor's characterization for more details
<i>Position i</i>	Distance of the I anchor from sheet's end.

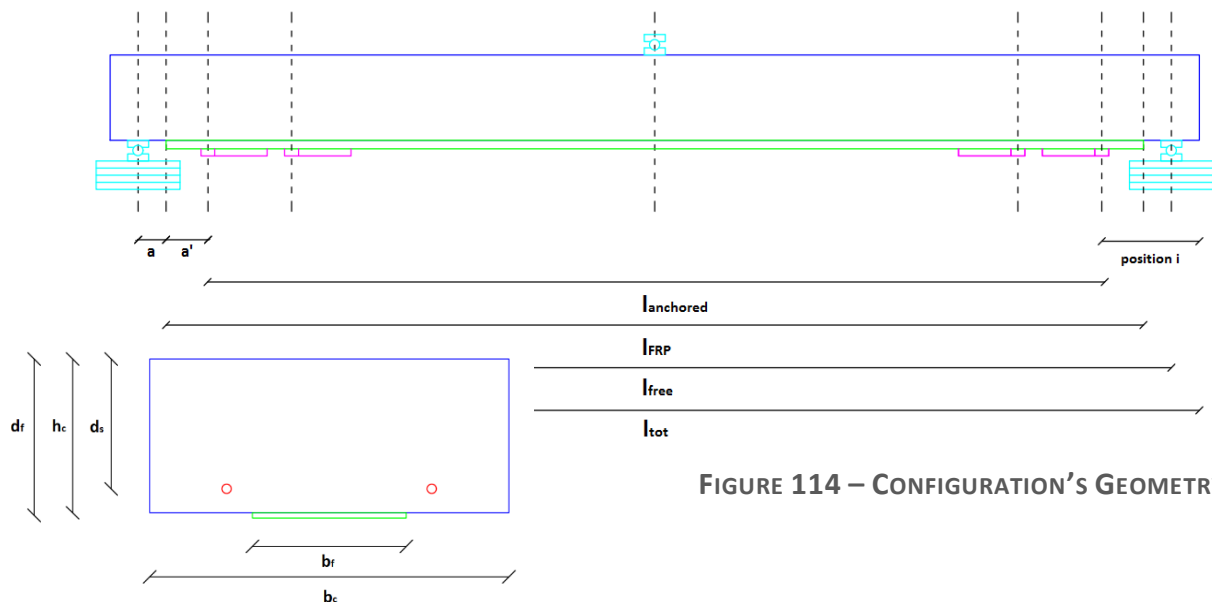


FIGURE 114 – CONFIGURATION'S GEOMETRY

Experimental Matrix [US]

		C-C	C-FRP	60x2	90x2	90x2 L/4	90x2 L/3	90x3	Sx2-1	Sx2-2
L_{tot}	[in]	78	78	78	78	78	78	78	78	78
L_{free}	[in]	74	74	74	74	74	74	74	74	74
a	[in]	-	2	2	2	2	2	2	2	2
a'	[in]	-	-	3	3	3	3	3	3	3
l_{FRP}	[in]	-	70	70	70	70	70	70	70	70
$l_{anchored}$	[in]	-	-	64	64	64	64	64	64	64
b_c	[in]	14	14	14	14	14	14	14	14	14
h_c	[in]	6	6	6	6	6	6	6	6	6
A_c	[in ²]	84.0	84.0	84.0	84.0	84.0	84.0	84.0	84.0	84.0
J_c	[in ⁴]	252	252	252	252	252	252	252	252	252
#	[/]	3	3	3	3	3	3	3	3	3
n° rebars	[/]	2	2	2	2	2	2	2	2	2
\emptyset	[in]	0.375	0.375	0.375	0.375	0.375	0.375	0.375	0.375	0.375
a_s	[in ²]	0.11	0.11	0.11	0.11	0.11	0.11	0.11	0.11	0.11
c	[in]	0.750	0.750	0.750	0.750	0.750	0.750	0.750	0.750	0.750
s	[in]	12.125	12.125	12.125	12.125	12.125	12.125	12.125	12.125	12.125
d_s	[in]	5.06	5.06	5.06	5.06	5.06	5.06	5.06	5.06	5.06
A_s	[in ²]	0.22	0.22	0.22	0.22	0.22	0.22	0.22	0.22	0.22
n° plies	[/]	-	1	1	1	1	1	1	1	1
b_f	[in]	-	6	6	6	6	6	6	6	6
t_f	[in]	-	0.04	0.04	0.04	0.04	0.04	0.04	0.04	0.04
d_f	[in]	-	6	6	6	6	6	6	6	6
A_f	[in ²]	-	0.24	0.24	0.24	0.24	0.24	0.24	0.24	0.24
Configuration	[/]	-	-	60	90	90	90	90	S	S
n°	[/]	-	-	2	2	2	2	3	2	2
Position 1	[/]	-	-	3	3	3	3	3	3	3
Position 2	[/]	-	-	9	9	16	22	12	9	12
Position 3	[/]	-	-	-	-	-	-	22	-	-

Experimental Matrix [SI]

		C-C	C-FRP	60x2	90x2	90x2 L/4	90x2 L/3	90x3	Sx2-1	Sx2-2
L_{tot}	[mm]	1,981	1,981	1,981	1,981	1,981	1,981	1,981	1,981	1,981
L_{free}	[mm]	1,880	1,880	1,880	1,880	1,880	1,880	1,880	1,880	1,880
a	[mm]	-	51	51	51	51	51	51	51	51
a'	[mm]	-	-	76	76	76	76	76	76	76
l_{FRP}	[mm]	-	1,778	1,778	1,778	1,778	1,778	1,778	1,778	1,778
$l_{anchored}$	[mm]	-	-	1,626	1,626	1,626	1,626	1,626	1,626	1,626
b_c	[mm]	356	356	356	356	356	356	356	356	356
h_c	[mm]	152	152	152	152	152	152	152	152	152
A_c	[mm ²]	54,193	54,193	54,193	54,193	54,193	54,193	54,193	54,193	54,193
J_c	[mm ⁴]	1.05E+08								
#	[/]	3	3	3	3	3	3	3	3	3
n° rebars	[/]	2	2	2	2	2	2	2	2	2
\emptyset	[mm]	9.5	9.5	9.5	9.5	9.5	9.5	9.5	9.5	9.5
a_s	[mm ²]	71	71.26	71.26	71.26	71.26	71.26	71.26	71.26	71.26
c	[mm]	19	19	19	19	19	19	19	19	19
s	[mm]	308	308	308	308	308	308	308	308	308
d_s	[mm]	129	129	129	129	129	129	129	129	129
A_s	[mm ²]	143	143	143	143	143	143	143	143	143
n° plies	[/]	-	1	1	1	1	1	1	1	1
b_f	[mm]	-	152	152	152	152	152	152	152	152
t_f	[mm]	-	1	1	1	1	1	1	1	1
d_f	[mm]	-	153	153	153	153	153	153	153	153
A_f	[mm ²]	-	155	155	155	155	155	155	155	155
Configuration	[/]	-	-	60	90	90	90	90	S	S
n°	[/]	-	-	2	2	2	2	3	2	2
Position 1	[/]	-	-	3	3	3	3	3	3	3
Position 2	[/]	-	-	9	9	16	22	12	9	12
Position 3	[/]	-	-	-	-	-	-	22	-	-

5.3.4.2 Load Cycles

The load cycles, here reported for the sake of completeness, are defined according to the calculations and considerations reported in the following paragraph.

The load levels here reported should be considered as indicative and subject to variation, as a function of the actual slabs' behavior. Also the load levels won't be perfectly matched, because of the need to manually control and stop the system, being basically impossible to program ULS cycles in deflection control.

Load Levels		
	US	SI
	[kip]	[kN]
Elastic	1.5	6.67
Cracking	4	17.8
Yielding	7	31.1
Debonding	11	48.9
Failure	14	62.3
Post-Failure	4.5	20.0

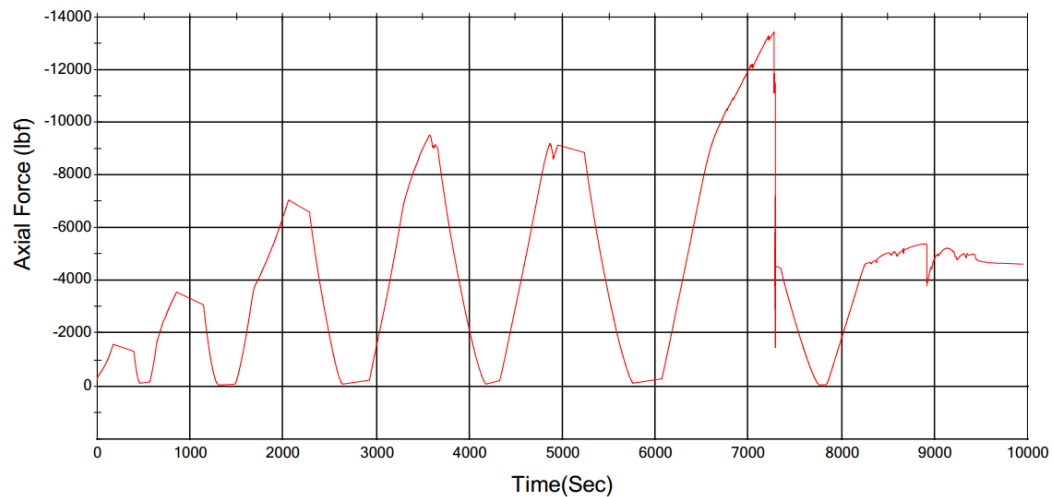


FIGURE 115 - 90x2 SAMPLE'S LOAD CYCLES FROM MTS.
1 LBF = 4.448 N

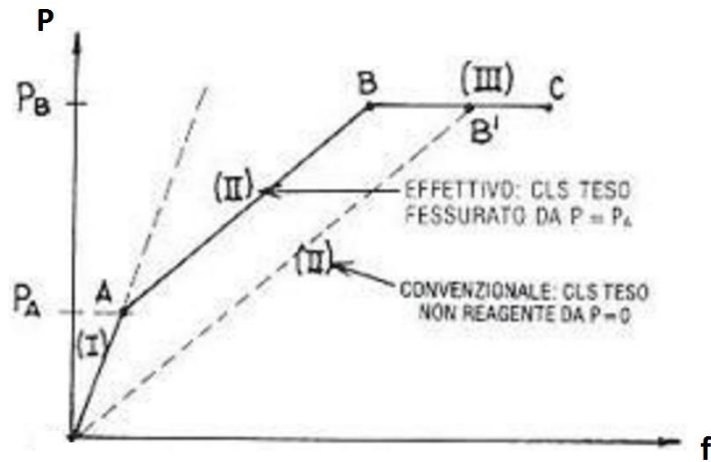


FIGURE 117 - CONCRETE SECTION'S ANALYSIS' CLASSICAL STAGES

Depending on the stage the section is undergoing, different mechanical models are required to define its strength and stiffness, based on different assumption. In order to extend the standard sectional model to externally reinforced applications, some addenda to the standard assumptions should be made (CNR, 2014):

- Ila. Perfect FRP – concrete bond up to failure
- IIIa. FRP behaves elastically up to failure

The perfect-bond-up-to-failure assumption does not mean the debonding failure mechanism should be disregarded, on the contrary debonding will generally control the element strength, determining its failure; but debonding can be very well modelled as a brittle mechanism, not preceded by any significant slipping between concrete and FRP.

The same assumptions are considered valid to proceed to sectional design of anchored FRP applications, as suggested by Lam & Teng (2001). It should anyway be considered that the authors only applied the method to laterally reinforced cantilevers and proved the effectiveness in case of sheet rupture; goal of this research is actually to validate the design method here proposed in standard flexural applications.

Along with the design-assumption-addenda discussed, the critical phases an externally reinforced anchored element would undergo and the different failures it can experience are here defined and summed up:

1. Cracking
2. Yielding
3. Intermediate Debonding
4. Anchors Failure
5. Sheet Rupture
6. Concrete Rupture
7. Steel Rupture

Each one of these stages is defined by a value of strain defining the cracking, yielding or failure of one of the material making the section. As already discussed, equivalent strains can be defined identifying the debonding occurrence, the same approach can be applied to anchors failure, as it will be proved and fully discussed.

The order can vary depending on the element's geometry and material properties, though the proposed one well define what experimentally experienced. End debonding and shear failure can be experienced as well and their occurrence should be checked.

5.4.2.1 Stage I – Uncracked Elastic Section

- I. Plane sections remain plane (Bernoulli-Navier's Assumption)
- II. Perfect steel – concrete bonding
- III. Elastic steel & concrete Behavior
- IV. Concrete working in tension

Under these assumptions, the structure rigorously behaves elastically, its inertia can be easily computed and is a geometric property, as long as the materials are homogenized. Rebars' contribution is clearly little when compared to concrete one and the differences between externally reinforced and unreinforced section are negligible as well, but nonetheless will be explicitly accounted for.

Since all the section is reacting, a neutral axis can be defined as the zero-strain line, but it won't divide the reacting portion from the non-reacting one; for this reason, it is preferred to refer to the neutral axis x simply as barycentric axis $y_{G,I}$. Also, the \bar{x} here referred is the distance from a generic axis, used as reference for centroid calculation.

$$x_I = y_{G,I}$$

$$y_{G,I} = \frac{S_{\bar{x},I}}{A_I}$$

$$A_I = b_c h_c + n_s A_s + n_f A_f$$

$$S_{\bar{x},I} = b_c h_c \left(\bar{x} - \frac{h_c}{2} \right) + n_s A_s (\bar{x} - d_s) + n_f A_f (\bar{x} - d_f)$$

$$I_{x,I} = \frac{b_c h_c^3}{12} \left(y_{G,I} - \frac{h_c}{2} \right)^2 + n_s A_s (y_{G,I} - d_s)^2 + n_f A_f (y_{G,I} - d_f)^2$$

$$n_s = \frac{E_s}{E_c} \quad n_f = \frac{E_f}{E_c}$$

Sectional Properties - Phase I

	US			SI		
	Virgin	FRP-Reinforced		Virgin	FRP-Reinforced	
x_I	-	-	[in]	-	-	[mm]
$y_{G,I}$	3.03	3.04	[in]	76.9	77.3	[mm]
A_I	85.09	85.55	[in ²]	54,898	55,191	[mm ²]
I_{xI}	257	261	[in ⁴]	1.068E+08	1.085E+08	[mm ⁴]

5.4.2.2 Stage II – Cracked Elastic Section

- I. Plane sections remain plane (Bernoulli-Navier's Assumption)
- II. Perfect steel – concrete bonding
- III. Elastic steel & concrete Behavior
- IV. Concrete not-working in tension

The section is divided in a concrete-reacting portion and a non-reacting one by the so-defined *neutral axis* (x). As long as a linear behavior is guaranteed, the neutral axis can be proved to be a geometrical property of the homogenized section and always coincide with the barycentric axis.

$$x_{II} = y_{G,II}$$

$$S_{II}(x_{II}) = 0 \quad \rightarrow \quad x_{II}$$

$$A_{II} = b_c x_{II} + n_s A_s + n_f A_f$$

$$S_{x,II} = \frac{b_c x^2}{2} + n_s A_s (x - d_s) + n_f A_f (x - d_f)$$

$$I_{x,II} = \frac{b_c x^3}{3} + n_s A_s (x - d_s)^2 + n_f A_f (x - d_f)^2$$

Sectional Properties - Phase II

	US			SI		
	Virgin	FRP-Reinforced	[in]	Virgin	FRP-Reinforced	[mm]
x_{II}	0.81	0.98	[in]	20.7	24.9	[mm]
$y_{G,II}$	0.81	0.98	[in]	20.7	24.9	[mm]
A_{II}	12.49	15.29	[in ²]	8,059	9,864	[mm ²]
$I_{x,II}$	22.24	34.13	[in ⁴]	9.255E+06	1.421E+07	[mm ⁴]

5.4.2.3 Stage III – Cracked Inelastic Section

- I. Plane sections remain plane (Bernoulli-Navier's Assumption)
- II. Perfect steel – concrete bonding
- III. Inelastic steel & concrete Behavior
- IV. Concrete not-working in tension

At increasing load, after yielding, steel rebars start flowing at constant stress, while the neutral axis moves upwards. The net load on rebars cannot grow beyond the yielding stress – according to a non-hardening model – hence the increasing load demand should be taken care of by an increasing couple's arm.

The neutral axis is no longer barycentric and should be computed thorough sectional translational equilibrium, as it will be fully discussed in the following. The geometrical properties of the reacting homogenized section can still be computed, now including a transport component for the concrete:

$$x_{III} \neq y_{G,III}$$

$$N(x_{III}) = 0 \quad \rightarrow \quad x_{III}$$

$$y_{G,III} = \frac{S_{\bar{x}}}{A_{II}}$$

$$A_{III} = b_c x_{III} + n_s A_s + n_f A_f$$

$$S_{x,III} = b_c x_{III} (x_{III} - y_{G,III}) + n_s A_s (x_{III} - d_s) + n_f A_f (x_{III} - d_f)$$

$$I_{x,III} = \frac{b_c x_{III}^3}{12} + b_c x_{III} (x_{III} - y_{G,III})^2 + n_s A_s (x_{III} - d_s)^2 + n_f A_f (x_{III} - d_f)^2$$

It should be noted that the homogenization theory relies on linearity assumptions; when elastic behavior is not guaranteed, such a theory ends up providing too conservative results when compared to the real behavior of a cracked, inelastic element. Further discussion will follow.

5.4.3 Sectional Analysis

5.4.3.1 Elastic Approach

The approach is applicable to stage I and stage II calculations, it relies on the standard Euler-Bernoulli theory, as well as on the Saint-Venant counterpart, applied referring to the homogenized section geometrical properties.

Dealing with a non-homogeneous section, the consistency assumptions of plane sections and perfect bonding are required in order to compute a continuous and linear strain distribution over the section, as function of the applied moment:

$$\varepsilon = \frac{M}{EI} (y_G - d_\varepsilon)$$

From the linear, continuous distribution of strains, the stress acting on each material at every height can be computed applying the standard Hook's Law, referring to the proper material properties. The resultant stress distribution will be discontinuous due to the varying stiffness, namely, at the II stage, all the tensioned concrete will react with zero stiffness.

$$\sigma_c = E_c \varepsilon$$

$$\sigma_s = E_s \varepsilon$$

The formula can very well be inverted and the sectional strength can be back-calculated, knowing the strain limit at any section's height.

5.4.3.2 Equilibrium Approach

The equilibrium approach is the natural solution for defining a section's bending strength and behavior; it can be widely applied to any kind of failure mode, material behavior and stage, as long as sound constitutive laws are provided for each material involved. It should be noted how a linear elastic approach is anyway easier to implement and generally preferred when applicable, particularly at the first stage.

Rigorously congruency should be accounted for, along with equilibrium, but the plane section and perfect bond assumptions easily take care of the kinetic consistency, making equilibrium the preferred approach for II and III stage applications, hence avoiding the need to differentiate between an elastic and inelastic cracked behavior.

Explicit solutions exist and cover almost every possible collapse mechanism, but limit the generality of the method; the most suitable solution is to implement an iterative approach in a spreadsheet or programming environment, using the neutral axis position as the parameter for the iteration.

Imposing a strain value at a certain section height and supposing known the neutral axis location, the strains at every section's location can be computed via simple linear formulas. Knowing the strains over the section it is possible to compute the stress distribution using the proper constitutive law for each material, knowing the stresses allows to compute the resultant coming from each material.

In order to do so, a stress-block approach is applied to concrete compressive stress integration, including parameters that allows to account for a non-completely developed parabola-rectangle. the usual elastic-perfectly plastic constitutive law is applied to steel rebars, while an elastic-up-to-failure law is assumed for external reinforcement.

Please refer to material characterization for parameters definition and consider that only EC2 (2008) will be referred to for ULS sectional analysis, considering that ACI (2014) doesn't allow for a detailed concrete modeling in all the failure modes not concrete-ruled. The minus sign in the steel resultant explicitly accounts for negative tensile stresses:

$$C(x) = \alpha_v \lambda \eta b x f_{cm}$$

$$S(x) = \begin{cases} A_s E_s \varepsilon_s(x) & \varepsilon_s < \varepsilon_y \\ A_s f_y & \varepsilon_s \geq \varepsilon_y \end{cases}$$

$$F(x) = A_f E_f \varepsilon_f(x)$$

Imposing the translational equilibrium and iteratively solving the equation allows to compute the neutral axis location:

$$N_i(x) = C(x) + S(x) + F(x) = 0$$

Knowing the neutral axis location, the actual resultants value can be computed and so the resisting internal bending moment:

$$M_i = C \left(1 - \frac{k_A \eta}{2} \right) x + S (x - d_s) + F (x - d_f)$$

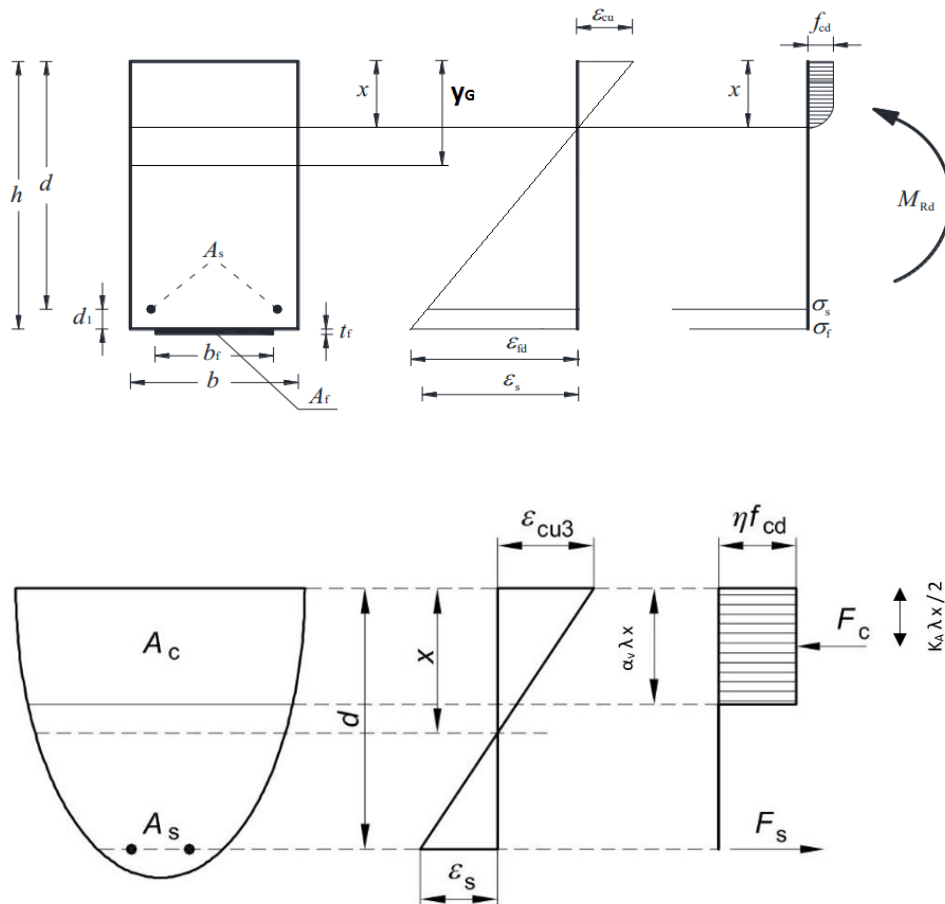


FIGURE 118 - SECTIONAL ANALYSIS GRAPHICAL REPRESENTATION, ADAPTED FROM CNR (2013) & EC2 (2008)

5.4.4 Structural Analysis

5.4.4.1 Equilibrium – Point Load

As discussed, the load is applied according to a standard 3-point-bending configuration, the related shear and bending moment diagrams are well known.

$$V(z) = \begin{cases} P/2 & z < L/2 \\ -P/2 & z > L/2 \end{cases}$$

$$M(z) = \begin{cases} P/2 z & z < L/2 \\ PL/4 - P/2(z - L) & z > L/2 \end{cases}$$

$$V_M = \frac{P}{2}$$

$$M_M = \frac{PL}{4}$$

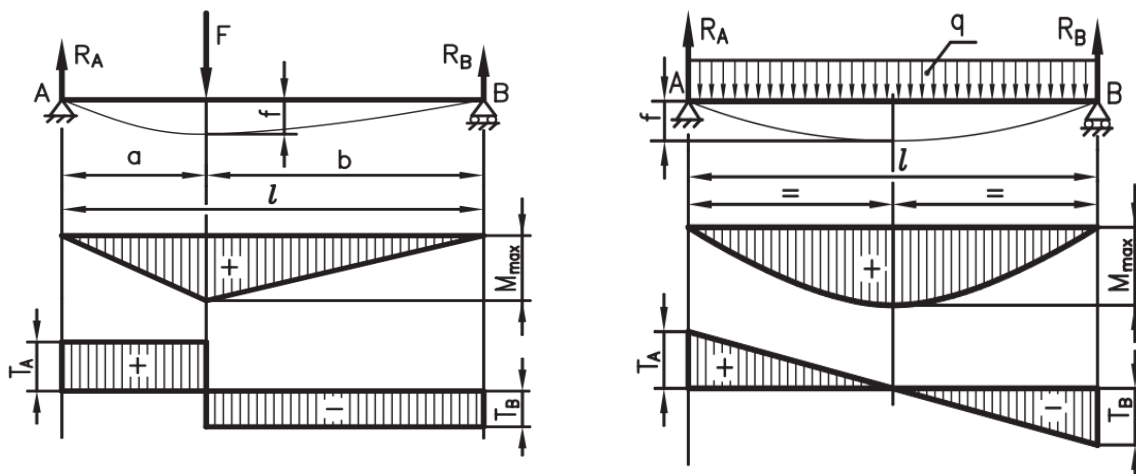


FIGURE 119 - CONCENTRATED & DISTRIBUTED LOAD STRUCTURAL ANALYSIS GRAPHICAL REPRESENTATION

5.4.4.2 Equilibrium – Self-Weight

Self-weight has a limited effect on the slabs behavior, but will be anyway accounted for; standard weight, according to ACI (2008) is assumed for the concrete; geometry and material parameters already characterized will generally not be recalled hereinafter.

$$w_c = \rho_c b h = 0.007 \text{ kip/in (0.00079 kN/m)}$$

$$V_w(z) = \frac{w_c L}{2} - w_c z$$

$$M_w(z) = \frac{w_c L}{2} z - \frac{w_c z^2}{2}$$

$$V_{Mw} = \frac{w_c L}{2} = 0.26 \text{ kip (1.16 kN)}$$

$$M_{Mw} = \frac{w_c L^2}{8} = 4.82 \text{ kip in (0.54 kNm)}$$

5.4.4.3 Deflection – Euler-Bernoulli Beam Theory

The standard Bernoulli theory is well-suited for deflection measurement in the elastic field and can be very well applied up to the II stage of R/C behavior, referring to the proper inertia definition in the formula:

$$\delta_{flex} = \frac{1}{48} \frac{PL^3}{EI} + \frac{5}{384} \frac{w_c L^4}{EI}$$

Further application of the theory in the III stage is possible, relying on the proposed III stage standard inertia definition, referred to the actual centroid and not to the neutral axis location. Such an elastic-based theory would provide a certain underestimation of the actual deflection.

5.4.4.4 Deflection – Timoshenko Beam Theory

For non-slender element, the shear-related deflection component might prove to be significant. Timoshenko beam theory is very well known to account for this component, easily computable applying the Principle of Virtual Works to the simply supported slab here considered. The resulting shear-related deflection is here reported; the flexural contribution is the same as per Bernoulli.

$$\delta_{shear} = \frac{1}{2} \frac{PL}{GA^*} + \frac{3}{16} \frac{w_c L^2}{GA^*}$$

$$A^* = \frac{5}{6} A$$

Timoshenko's theory should be applied to linear elastic materials, the extension to inelastic behavior requires more investigation into an effective shear-resisting-area definition.

5.4.4.5 Deflection – Strain-Based Approach

In order to go over elastic-based theories, a strain-based approach is proposed: considering the strain-based nature of ULS sectional analysis, the solution seems the most reasonable and guarantee consistency with the third stage sectional analysis assumptions.

Such an approach is derived from the standard elastic Bernoulli theory, but it has to be underlined how it is just the kinetic assumption of plane sections – hence linearly distributed strains – not necessarily elasticity, that will allow to directly compute the deflection, knowing the strain distribution over the section. The strain at any section's height is linked to the applied moment thorough the classical formula:

$$\varepsilon = \frac{M}{EI} (x - d_\varepsilon)$$

It will become clear how it is necessary to make the moment expression explicit:

$$\varepsilon = \left[\frac{P}{4} + \frac{w_c L}{8} \right] \frac{L}{EI} (x - d_\varepsilon)$$

Recalling the flexural deflection formula, also coming from Bernoulli's theory:

$$\delta_{flex} = \left[\frac{1}{48} P + \frac{5}{384} w_c L \right] \frac{L^3}{EI}$$

Extrapolating L/EI expression from the strain definition:

$$\frac{L}{EI} = \frac{1}{\left[\frac{P}{4} + \frac{w_c L}{8} \right]} \frac{\varepsilon}{x - d_\varepsilon}$$

And substituting in the deflection formula, the stiffness dependency elides:

$$\delta_{flex} = \left[\frac{\frac{P}{48} + \frac{5}{384} w_c L}{\frac{P}{4} + \frac{w_c L}{8}} \right] \frac{\varepsilon L^2}{x - d_\varepsilon}$$

The first term is adimensional and only depends on the applied loads, the second terms depends on the strain distribution over the section, computable according to any sectional theory, skipping a global stiffness definition and only relying on the plane-section kinetic assumption from Euler-Bernoulli; everything is multiplied by L^2 for dimensional consistency. Neglecting the distributed load, the formulation is way simpler:

$$\delta_{flex} = \frac{PL^2}{12} \frac{\varepsilon}{x - d_\varepsilon}$$

Any strain over the section's height can be used as reference, the easiest approach is to refer to the collapse-causing strain. The results provided by the proposed formula are

always consistent with the strain computed via sectional analysis, but not always higher than what computed with a standard Euler approach applied to III stage geometrical properties: this method proved to provide larger results under loads and deflections of a certain entity, a numerical comparison will follow later.

It should be noted how deflection prediction is beyond the focus of this dissertation and what discussed here should be intended as a suggestion for further studies toward a complete characterization of the ULS behavior of externally reinforced bended elements in presence of anchoring device. Interesting in this sense is the model proposed by Nardone et al. (2011), tough focused on mechanically fastened strips only.

Finally, notice that the proposed theory is flexural-based: the shear component, if deemed significant, should be separately added; Timoshenko's solution, in absence of different formulations, will be referred for the purpose.

5.4.4.6 Deflection – Results Discussion

It has already been spotted how a Euler-based approach provides an underestimated deflection prediction. A strain-based approach, though being consistent with the sectional equilibrium assumptions, tends to provide underestimated results as well.

The strain-based approach tends to be even less conservative than the Euler-based one at low level of load, while providing larger results at increasing load and strains; considering how both the proposed approaches are finally under-estimative, the larger value among the two, at each step, will be assumed as expected deflection.

δ_1	Euler + Timoshenko, III Stage
δ_2	Strain Based + Timoshenko, III Stage

Deflection [US]					
		P	δ_1	δ_2	δ_{max}
		[kip]	[in]	[in]	[in]
Cracking	EC2	2.74	0.02	0.02	0.02
	ACI	3.39	0.02	0.02	0.02
Yielding		6.55	0.51	0.29	0.51
Int. Debonding		9.68	0.75	0.62	0.75
Anchors' Failure	60x2	12.16	0.94	0.88	0.94
	90x2	13.67	1.05	1.04	1.05
	Sx2	16.21	1.24	1.31	1.31
Sheet Rupture		18.53	1.42	1.56	1.56
Concrete Collapse		21.94	1.67	1.95	1.95
Steel Rupture		96.28	1.59	19.1	19.1

Unreinforced - Deflection [US]					
		P	δ_1	δ_2	δ_{max}
		[kip]	[in]	[in]	[in]
Cracking	EC2	2.72	0.02	0.02	0.02
	ACI	3.32	0.02	0.02	0.02
Yielding		4.01	0.33	0.28	0.33
Concrete Collapse		4.14	0.42	8.80	0.42
Steel Rupture		4.14	0.42	9.46	9.46

FRP Reinforced - Deflection [SI]

		P	δ_1	δ_2	δ_{max}
		[kN]	[mm]	[mm]	[mm]
Cracking	EC2	12.19	0.5	0.5	0.5
	ACI	15.09	0.6	0.6	0.6
Yielding		29.13	13	7	13
Int. Debonding		43.05	19	16	19
Anchors' Failure	60x2	54.10	24	22	24
	90x2	60.81	27	26	27
	Sx2	72.10	32	33	33
Sheet Rupture		82.43	36	40	40
Concrete Collapse		97.61	42	49	49
Steel Rupture		428.3	40	485	485

Unreinforced - Deflection [US]

		P	δ_1	δ_2	δ_{max}
		[kN]	[mm]	[mm]	[mm]
Cracking	EC2	12.11	0.5	0.5	0.5
	ACI	14.75	0.55	0.54	0.55
Yielding		17.84	8.28	7.16	8.28
Concrete Collapse		18.43	10.66	223.58	10.66
Steel Rupture		18.44	10.73	240.26	240.26

5.4.5 Equivalent Ultimate Strain Approach

As widely discussed, external reinforcement's failure is rarely related to actual sheet's rupture, usually being debonding the controlling mechanism. The easiest way to account for debonding failure in a sectional analysis context is to define an equivalent debonding ultimate strain and to compute the sectional equilibrium, imposing that level of strain to the FRP sheet. The efficiency of such an approach and the easiness of implementation in a well-known design algorithm led to the idea of developing an Equivalent-Ultimate-Strain-based approach also for anchor-failure-governed ultimate limit states.

5.4.5.1 End Debonding

According to the discussed CNR formulation, the equivalent ultimate strain related to end debonding is a function of the material and geometrical properties of the lamina and of the concrete strength. It is a function of the *Specific Fracture Energy* that can either be experimentally defined, integrating the bond-slip law, eventually accepting the linearity assumption but referring to both experimental bond strength and slip measurements:

$$\Gamma_F^{exp} = \frac{1}{2} f_b s_u$$

or analytically defined, according to CNR definition, either referring to the average value or 5% percentile at varying k_G :

$$\Gamma_F^{an} = \frac{k_b k_G}{FC} \sqrt{f_{cm} f_{ctm}}$$

The strain value can be computed applying the same CNR formula in both cases, either keeping it implicit or explicating it:

$$\varepsilon_{fdd}^{exp} = \frac{1}{\gamma_{fd}} \sqrt{\frac{2 \Gamma_{Fd}^{exp}}{E_f t_f}}$$

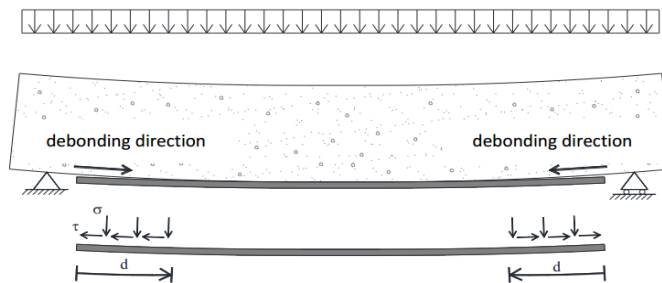
$$\varepsilon_{fdd}^{an} = \frac{1}{\gamma_{fd}} \sqrt{\frac{2}{E_f t_f} \frac{k_b k_G}{FC} \sqrt{f_{cm} f_{ctm}}}$$

$$k_G = \begin{cases} 0.077 \text{ mm} & \text{average} \\ 0.037 \text{ mm} & \text{5\% fractile} \end{cases}$$

The lack of an experimental measure for the slip at bond failure prevent from applying an experimental approach, hence the CNR values only will be reported. A sensible dependency on the calibration parameter k_G was noticed; the already discussed bond strength values suggest to refer to the 5% percentile for prediction purposes. The reason could be that the material and geometrical configuration tested lie in the 5%-percentile-surrounding of the experimental database used for CNR formulas calibration.

The choice will be confirmed a-posteriori while investigating results matching and may suggest the concrete strength dependency should be muffled for high strength concrete, expecting it to be more sound to refer to the average value for prediction purposes.

End Debonding Equivalent Strain ($\varepsilon_{idd,1}$)	
CNR (5%)	0.42%
CNR (Average)	0.61%



5.4.5.2 Intermediate Debonding

The exactly same approach, discussed for end debonding, can be applied to intermediate debonding equivalent strain calculation. The experimental expression for the modified fracture energy can be easily derived from the standard fracture energy definition; it seems reasonable to refer to average k_G and $k_{G,2}$ values when following the experimental approach:

$$\Gamma_{F,2}^{exp} = \frac{k_{G,2}}{k_G} \Gamma_F^{exp}$$

$$\Gamma_{F,2}^{an} = \frac{k_b k_{G,2}}{FC} \sqrt{f_{cm} f_{ctm}}$$

The experimental and analytical value can be computed applying the same formula, kept implicit in one case, explicated in the other.

$$\varepsilon_{fdd,2}^{exp} = \frac{k_q}{\gamma_{fd}} \sqrt{\frac{2 \Gamma_{Fd,2}^{exp}}{E_f t_f}}$$

$$\varepsilon_{fdd,2}^{an} = \frac{k_q}{\gamma_{fd}} \sqrt{\frac{2}{E_f t_f} \frac{k_b k_{G,2}}{FC} \sqrt{f_{cm} f_{ctm}}}$$

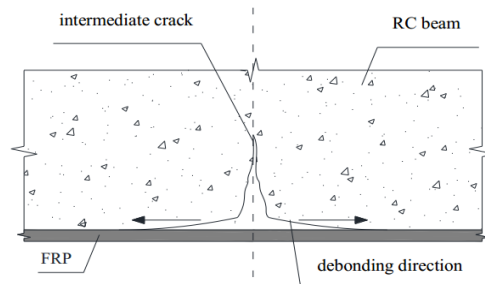
$$k_{G,2} = \begin{cases} 0.32 \text{ mm} & \text{average} \\ 0.10 \text{ mm} & 5\% \text{ fractile} \end{cases}$$

The ACI also proposes a different formulation for the intermediate debonding equivalent strain; here reported in US units:

$$\varepsilon_{fd} = 0.41 \sqrt{\frac{f'_c}{E_f t_f}}$$

The CNR average and 5% values are reported hereinafter, along with the ACI value. The average CNR and ACI value are very consistent one with the other, but the 5% CNR value will be preferred considering the better experimental matching in shear bond test already discussed.

Intermediate Debonding Equivalent Strain ($\epsilon_{fdd,2}$)	
CNR (5%)	0.70%
CNR (Average)	1.25%
ACI	1.27%



5.4.5.3 Anchors' Failure

In order to predict the failure load for an anchored slab, the system's response at increasing load needs to be predicted, namely focusing on how the applied load will engage the anchors.

Referring to the results from Eshwar et al. (2005) and Smith et al. (2011) (2013) it is clear how, at a certain level of load, intermediate debonding happens; at this point, all the tensile load engaging the sheet is suddenly transferred to the end anchors, providing the critical load transfer mechanism for system's equilibrium.

In order for the anchors to provide an effective strength increment for the overall system, the joint shear strength should be higher than the tensile resultant engaging the sheet at intermediate debonding; the system finally will fail, once the tensile load will reach either the joint's or the sheet's ultimate strength.

It is clear how, relying on a shear strength-based characterization for the anchors, a strength-oriented design approach seems the soundest, though not being particularly

suiting for a sectional analysis implementation. Luckily, the FRP sheet linear elasticity easily allows to step from a strength-oriented approach, to a strain-oriented approach, very well implementable in a standard sectional analysis algorithm.

An anchor-collapse-related equivalent ultimate strain can be simply defined, dividing the joint shear strength by the sheet area and elastic modulus; full-efficiency is assumed for the series solution:

$$S_{joint} = n_s S_{anchor}$$

$$\varepsilon_{fad,3} = \frac{S_{joint}}{A_f E_f}$$

The equivalent strain here computed is compared with the values measured on the shear specimens at failure; it seems clear that the uniform strain assumption over the width is a severe simplification of a more complex mechanism: results from Berneschi (2015) shows how uncovered sides won't basically be engaged, but also show that the measured strain is not a feasible design reference value, leading to too generous strength estimation.

The strain distribution over the width will be later fully discussed, and the fact that in the present applications all the FRP width will be covered makes the strain data from Berneschi (2015) hardly comparable; by now they are just referred in order to show the unfeasibility of the measured strain as design values, a-posteriori confirmed via experimental data-matching.

Also notice that a strength oriented approach easily allows to define a joint strength via simple multiplication, only later defining the equivalent failure strain; multiplying the actual strain by the number of anchors would make any sense and would force to directly test the actual n-anchors joint.

As a last notice, comparing the joint-collapse-related equivalent strains, with the debonding 0.7% value, it appears clear how a single anchor won't be able to guarantee a strength improvement for the bended system.

Anchor Failure Equivalent Strain ($\epsilon_{fd,3}$)			
	Average	Center	Side
	[%]	[%]	[%]
60	0.50%	0.89%	0.06%
90	0.59%	0.71%	0.05%
S	0.75%	-	-
60x2	1.00%	-	-
90x2	1.19%	-	-
Sx2	1.50%	-	-

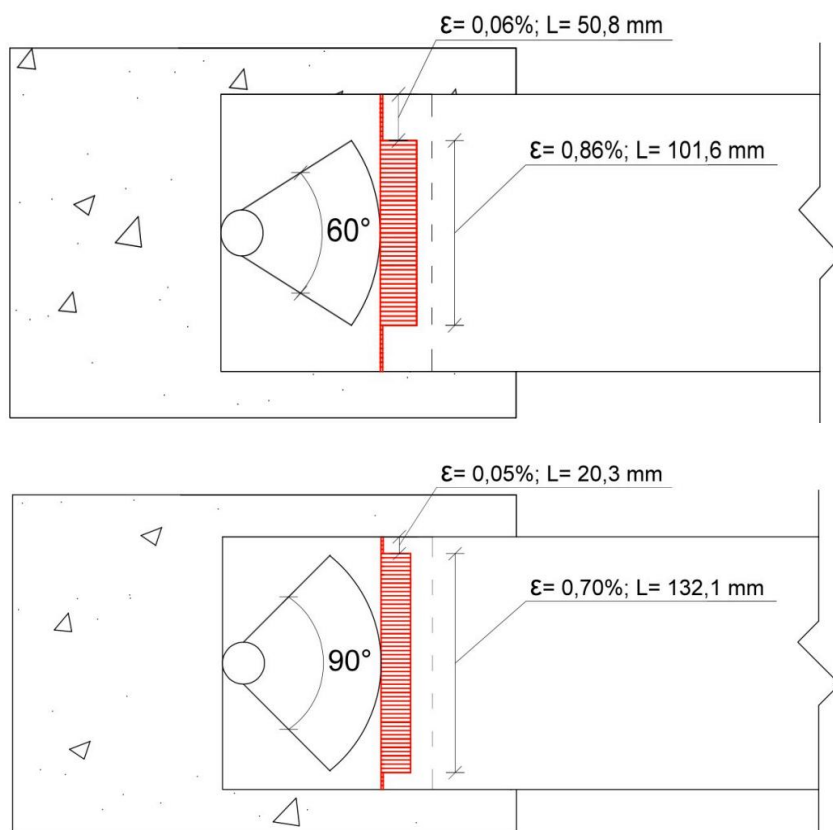


FIGURE 120 - STRAIN DISTRIBUTIONS FROM BERNESCHI (2015)

5.4.6 Balanced Section

The concept of sectional balance is a standard way to estimate the efficiency and ductility of a section: defining balanced, a section that undergoes concrete failure at the same instant steel yielding begins, it represents the most efficient solution. If the reinforcement area is lower than the balanced value, the section results under-reinforced, while, if the amount is higher, the section is called over-reinforced.

Adding rebars on an under-reinforced section would move down the neutral axis, increasing the amount of reacting concrete, without reducing the level of stress in the yielded rebars, hence efficiently increasing the sectional strength. On the contrary, adding rebars on an over-reinforced section, would still increase the amount of engaged concrete, while contemporary reducing the level of stress in the elastic rebars; the result is still a strength increment, but way less efficient.

Also, a balanced section represents the turning point from a brittle to a ductile sectional behavior. Wishing the section to undergo a ductile behavior, the provided reinforcement area should be smaller than the balanced one.

Either a limit on the reinforcement's area or on the strain level can be defined, the ACI, for example, requires at least a 0.5% strain level in the steel reinforcement. Imposing balance referring to a 0.5% strain level instead than the steel yielding strain, would provide the most efficient solution complying with the ductility requirements.

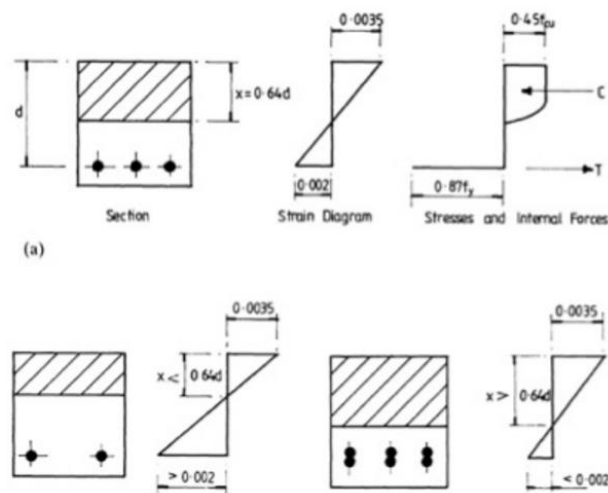


FIGURE 121 – EXAMPLES OF BALANCED (A), UNDER (B) & OVER-REINFORCED (C) SECTIONS

5.4.6.1 Internal Reinforcement Balance

Imposing compressed concrete collapse at top fiber and steel yielding at internal rebar level, it is possible to define the location of the neutral axis and eventually compute the strain at FRP sheet level:

$$\varepsilon_c = \varepsilon_{cu}$$

$$\varepsilon_s = \varepsilon_y$$

$$x = \frac{\varepsilon_c}{\varepsilon_c - \varepsilon_s} d_s$$

$$\varepsilon_f = \varepsilon_s \frac{x - d_f}{x - d_s}$$

Imposing the translational equilibrium, it is possible to explicitly compute the optimal amount of reinforcement required for a balanced section. Resisting moment can then be computed as usual. In computing C, remember the parabola-rectangle is always fully developed in a balanced section:

$$A_{s,opt} = \frac{C + F}{f_y}$$

Either in the unreinforced and externally reinforced samples, the design is showed to be largely under-reinforced, referring to the parameter:

$$\rho_{A_s} = \frac{A_s}{A_{s,opt}}$$

Internal reinforcement Ratio	
Unreinforced	6.02%
FRP-Reinforced	11.18%

5.4.6.2 External Reinforcement Balance

The same concept can be applied to external reinforcement design. In this case the, the optimal solution requires the compressed concrete to collapse at the same instant the external reinforcement fails, either because of debonding, anchor failure or sheet rupture.

$$\varepsilon_c = \varepsilon_{cu}$$

$$\varepsilon_f = \varepsilon_{fd}$$

$$x = \frac{\varepsilon_c}{\varepsilon_c - \varepsilon_f} d_f$$

$$\varepsilon_s = \varepsilon_f \frac{x - d_s}{x - d_f}$$

$$A_{f,opt} = -\frac{C + S}{E_f \varepsilon_f}$$

Clearly at increasing failure strain, the amount of reinforced required for an optimal solution reduces. At fixed external reinforcement area, its efficiency can be evaluated at varying failure strain as the provided area over optimal area ratio:

$$\rho_{A_f}(\varepsilon_{fd}) = \frac{A_f}{A_{f,opt}(\varepsilon_{fd})}$$

The effectiveness of such a parameter is shown referring to design data, it will be also referred as an evaluation parameter for experimental results evaluation. Clearly the efficiency increment provided by better anchors solutions is capped by the material's ultimate strain.

External Reinforcement Ratio	
	US / SI
Int. Debonding	11.18%
60x2	21.71%
90x2	30.04%
Sx2	47.72%
Sheet Rupture	68.46%

5.4.7 Load Phases

5.4.7.1 Cracking

Knowing the concrete cracking strain, it is easy to back-calculate the cracking moment for the section and the related cracking load, accounting for the self-weight as well. Concrete cracking is assumed as turning point from Phase I to Phase II, hence Phase I concrete properties are applied:

$$M_{cr} = \frac{EJ_I}{y_{G,I} - h_c} \varepsilon_{cr}$$

$$P_{cr} = 4 \frac{M_{cr} - M_w}{L}$$

Results vary whether the ACI or EC2 concrete characterization is referred and whether the external FRP reinforcement is accounted for or not (unreinforced sample). For the sake of simplicity, the overall maximum value will be accounted for, willing to provide an upper bound for cracking load, in order to be sure the element is cracked after the cracking cycle. The overall minimum will also be referred, not willing to crack the concrete during the first elastic load-cycle. Applying simple proportion, it is possible to compute the strains at any level in the section, for the sake of completeness:

$$\varepsilon_c = \varepsilon_{cr} \frac{y_{G,I}}{y_{G,I} - h_c}$$

$$\varepsilon_s = \varepsilon_{cr} \frac{y_{G,I} - d_s}{y_{G,I} - h_c}$$

$$\varepsilon_f = \varepsilon_{cr} \frac{y_{G,I} - d_f}{y_{G,I} - h_c}$$

5.4.7.2 Yielding

Yielding load can be simply computed applying sectional equilibrium analysis, imposing yielding strain on the rebars. Yielding can either happen in phase II or phase III, depending on the amount of rebar and on the concrete behavior; though in an under-reinforced system it usually marks the transit from phase I to phase II.

$$\varepsilon_s = \varepsilon_y$$

$$\varepsilon_c = \varepsilon_s \frac{x}{x - d_s}$$

$$\varepsilon_f = \varepsilon_s \frac{x - d_f}{x - d_s}$$

Once the internal yielding moment is defined, according to the already discussed sectional analysis formulas, the yielding load can be easily computed, accounting for the elements weight as well:

$$P_y = 4 \frac{M_y - M_w}{L}$$

5.4.7.3 Intermediate Debonding

Intermediate debonding is usually the ruling collapse mechanism for an externally reinforced, unanchored element. The formulas defining the equivalent debonding strain have already been discussed, the resulting strain should be applied at FRP level:

$$\varepsilon_f = \varepsilon_{fdd,2}$$

$$\varepsilon_c = \varepsilon_f \frac{x}{x - d_f}$$

$$\varepsilon_s = \varepsilon_f \frac{x - d_s}{x - d_f}$$

$$P_{fdd,2} = 4 \frac{M_{fdd,2} - M_w}{L}$$

5.4.7.4 Anchors' Failure

In the spirit of the equivalent ultimate strain approach, the anchors-related ultimate strain should be applied at FRP level:

$$\varepsilon_f = \varepsilon_{fdd,3}$$

$$\varepsilon_c = \varepsilon_f \frac{x}{x - d_f}$$

$$\varepsilon_s = \varepsilon_f \frac{x - d_s}{x - d_f}$$

$$P_{fdd,3} = 4 \frac{M_{fdd,3} - M_w}{L}$$

5.4.7.5 Sheet Rupture

The FRP rupture strain is imposed at FRP level:

$$\varepsilon_f = \varepsilon_{fu}$$

$$\varepsilon_c = \varepsilon_f \frac{x}{x - d_f}$$

$$\varepsilon_s = \varepsilon_f \frac{x - d_s}{x - d_f}$$

$$P_{fu} = 4 \frac{M_{fu} - M_w}{L}$$

5.4.7.6 Concrete Collapse

Compressed concrete reaches its ultimate strain triggering section's collapse. It is the only situation characterized by a fully developed parabola-rectangle.

$$\begin{aligned}\varepsilon_c &= \varepsilon_{cu} \\ \varepsilon_s &= \varepsilon_c \frac{x - d_s}{x} \\ \varepsilon_f &= \varepsilon_c \frac{x - d_f}{x} \\ P_{cu} &= 4 \frac{M_{cu} - M_w}{L}\end{aligned}$$

5.4.7.7 Steel Rupture

Even if possible, is an extremely rare condition in non-prestressed application. Steel rupture was never experienced in the tested specimen, not even after concrete collapse at very high deflection values.

$$\begin{aligned}\varepsilon_s &= \varepsilon_{su} \\ \varepsilon_c &= \varepsilon_s \frac{x}{x - d_s} \\ \varepsilon_f &= \varepsilon_s \frac{x - d_f}{x - d_s} \\ P_{su} &= 4 \frac{M_{su} - M_w}{L}\end{aligned}$$

5.4.7.8 Results

The load level related to each behavior are summed up, notice that the externally reinforced specimens cannot reach concrete collapse even if fully anchored, while unreinforced specimen is expected to fail because of concrete collapse, not reaching steel rupture.

Load Phases - FRP Reinforced [US]

		x	FRP Strain	Moment	Load	δ	F	C	S
		[in]	[%]	[kip in]	[kip]	[in]	check		
Cracking	EC2	3.04	0.011%	56	2.74	0.02	OK	OK	OK
	ACI	3.04	0.013%	68	3.39	0.02	OK	OK	OK
Yielding		0.78	0.32%	126	6.55	0.51	OK	OK	OK
Int. Debonding		0.66	0.70%	184	9.68	0.75	OK	OK	OK
Anchors' Failure	60x2	0.63	1.00%	230	12.16	0.94	OK	OK	OK
	90x2	0.622	1.19%	258	13.67	1.05	OK	OK	OK
	Sx2	0.625	1.50%	305	16.21	1.31	OK	OK	OK
Sheet Rupture		0.64	1.79%	348	18.53	1.56	OK	OK	OK
Concrete Collapse		0.68	2.22%	411	21.94	1.95	NO	OK	OK
Steel Rupture		2.66	14.99%	1786	96.28	19.1	NO	NO	OK

Load Phases - Unreinforced [US]

		x	Steel Strain	Moment	Load	δ	F	C	S
		[in]	[%]	[kip in]	[kip]	[in]	check		
Cracking	EC2	3.03	0.011%	55	2.72	0.02	-	OK	OK
	ACI	3.03	0.013%	66	3.32	0.02	-	OK	OK
Yielding		0.64	0.26%	79	4.01	0.33	-	OK	OK
Concrete Collapse		0.15	9.30%	81	4.14	0.42	-	OK	OK
Steel Rupture		0.15	10.00%	81	4.14	9.46	-	NO	OK

Load Phases - FRP Reinforced [SI]

		x	FRP Strain	Moment	Load	δ	F	C	S
		[mm]	[%]	[kN m]	[kN]	[mm]	check		
Cracking	EC2	77	0.011%	6	12	0.5	OK	OK	OK
	ACI	77	0.013%	8	15	0.6	OK	OK	OK
Yielding		20	0.32%	14	29	13	OK	OK	OK
Int. Debonding		17	0.70%	21	43	19	OK	OK	OK
Anchors' Failure	60x2	16	1.00%	26	54	24	OK	OK	OK
	90x2	16	1.19%	29	61	27	OK	OK	OK
	Sx2	16	1.50%	34	72	33	OK	OK	OK
Sheet Rupture		16	1.79%	39	82	40	OK	OK	OK
Concrete Collapse		17	2.22%	46	98	49	NO	OK	OK
Steel Rupture		68	13.99%	202	428	485	NO	NO	OK

Load Phases -Unreinforced [SI]

		x	Steel Strain	Moment	Load	δ	F	C	S
		[mm]	[%]	[kN m]	[kN]	[mm]	check		
Cracking	EC2	77	0.011%	6	12	0.5	-	OK	OK
	ACI	77	0.013%	7	15	0.6	-	OK	OK
Yielding		16	0.26%	8.93	17.84	8	-	OK	OK
Concrete Collapse		3.78	9.30%	9.21	18.43	11	-	OK	OK
Steel Rupture		3.72	10.00%	9.21	18.44	240	-	NO	OK

5.4.8 End Debonding Evaluation

End debonding is generally not critical with respect to intermediate debonding, as long as a proper development length is provided inside the slab's non-cracked portion. End debonding is also a non-desired failure mode in the present work, willing to focus on the most common situation and characterize the anchors behavior after intermediate debonding.

The design approach is generally a trial-and-error one: assuming end debonding non-critical, the element is designed in bending with respect to the already discussed failure modes; once the expected failure mode is defined, end debonding is checked not to be actually critical at that level of load.

In the present case, intermediate debonding is the ruling failure mode for the unanchored sample. Anchored solutions won't be checked, as the spikes are retained sufficient to counter the higher normal debonding stresses coming along with an increasing applied load.

5.4.8.1 Optimal Development Length

According to the ACI formulation the optimal bond length is rigorously a function of the sheet properties only, the CNR formulation corrects the value accounting for the concrete element geometry. Both CNR and ACI formulation will be computed, referring to 5% design values for CNR formulation, and choosing the biggest one as design parameter, willing to stay on the safe side against end debonding.

$$l_{ed}^{CNR} = \frac{\pi S_u}{2 \gamma_{Rd}} \sqrt{\frac{FC}{2 k_b k_G} \frac{E_f t_f}{\sqrt{f_{cm} f_{ctm}}}} \leq 200 \text{ mm}$$

$$l_{df}^{ACI,US} = 0.057 \sqrt{\frac{E_f t_f}{\sqrt{f'_c}}}$$

Optimal Development (l_{bd})		
	US	SI
	[in]	[mm]
CNR (Average)	2.02	51
CNR (5%)	2.92	74
ACI	3.74	95

5.4.8.2 Provided Development Length

It has been already discussed how to compute the provided bond length in a 3-point bending situation, applying the formula:

$$l_b = \frac{2 M_{crack}}{P_u} - d - a$$

Wishing to account for the presence of the self-weight, in order to identify the cracking section, it is required to solve the II grade equation:

$$z^2 - \left(\frac{P_u}{w_c} + L \right) z + \frac{2 M_{cr}}{w_c}$$

Then, also accounting for load diagram translation and the distance a between the sheet end and the beam's simply support:

$$l_b = \frac{1}{2} \left[\left(\frac{P_u}{w_c} + L \right) - \sqrt{\left(\frac{P_u}{w_c} + L \right)^2 - \frac{8M_{cr}}{w_c}} \right] - d - a$$

In order to compute l_b the minimum cracking moment, coming from EC2, will be accounted for; the provided bonded length will then be compared with the maximum

value, coming from ACI. A mixed approach is actually inconsistent, and is only performed in order to stay on the safe side, designing against a truly undesired failure mode. As discussed, the failure load is the one related to intermediate debonding, in this particular case. According to CNR, in case the provided bonded length is sub-optimal, a reduction factor should be applied to the end-debonding equivalent ultimate strain, defined as:

$$reduction\ factor = \frac{l_b(a)}{l_{ed}} \left(2 - \frac{l_b(a)}{l_{ed}} \right)$$

Once defined the sheet's properties, the only design parameter left is the end distance from the support, the influence of the parameter a on the reduction factor is plotted hereinafter.

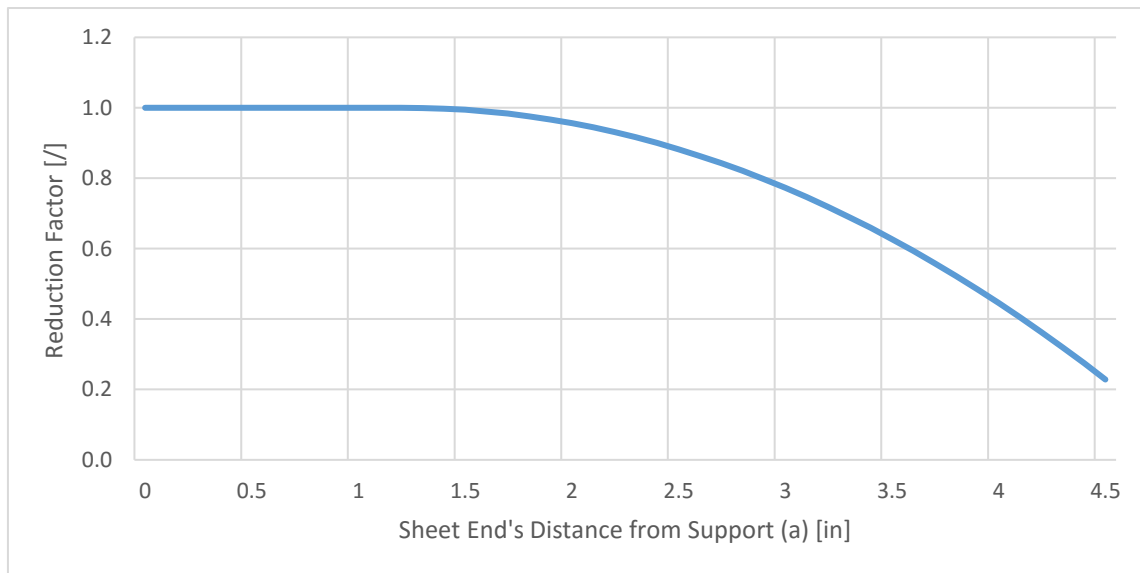


FIGURE 122 - REDUCTION FACTOR AT VARYING END DISTANCE FROM SUPPORT.
1 IN = 25.4 MM

It must be noticed how, under all the safe-side assumptions made, the bonded length related to the chosen distance from support leads to a suboptimal situation. The solution accounting for self-weight was considered, being the difference non negligible and on the unsafe side.

Development Length Design		
	US	SI
	[in]	[mm]
a	2.00	51
$l_{b, no\ sw}$	3.46	88
$l_{b, sw}$	2.95	75
l_{ed}	3.74	95
reduction	0.96	0.96

5.4.8.3 End Debonding Check

The strain acting on the sheet's end section at failure should be compared to the reduced end-debonding-equivalent-ultimate-strain. The moment on the end section can be easily computed, accounting for the required diagram translation:

$$M(a + d) = \left(\frac{P_u}{2} + \frac{w_c L}{L} \right) (a + d) - \frac{w_c}{2} (a + d)^2$$

assuming elastic-uncracked behavior, the strain acting on the FRP sheet can be computed applying Stage I geometrical properties:

$$\varepsilon_f(a + d) = \frac{M(a + d)}{E I_I} (y_{G,I} - d_f)$$

The strain ratio, as a function of the parameter a is plotted hereinafter, clearly the strain acting at the sheet's end are way lower than the critical one.

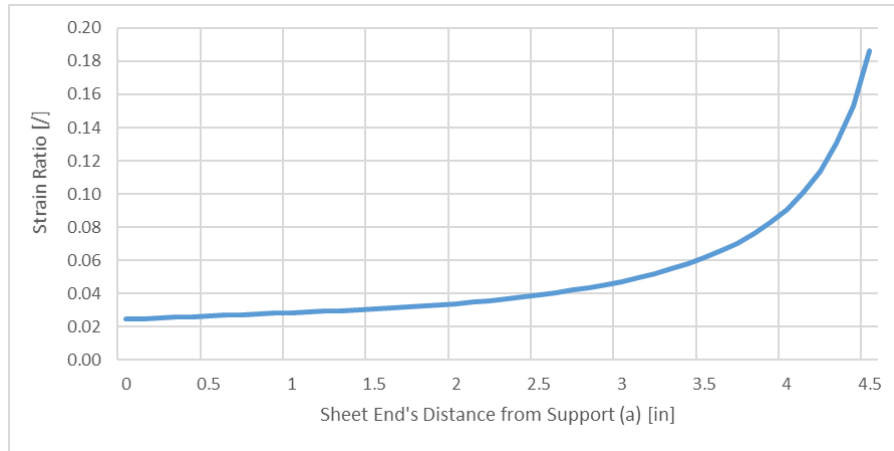


FIGURE 123 - STRAIN RATIO AT VARYING SHEET'S END FROM SUPPORT. 1 IN = 25.4 MM.

End Debonding Check		
	US	SI
	[kip in] [%]	[kN m] [%]
	[/]	[/]
M(a+d)	40.67	4.60
$\epsilon_{(a+d)}$	0.01%	0.01%
$\epsilon_{fdd,1}$	0.42%	0.42%
ratio	0.03	0.03

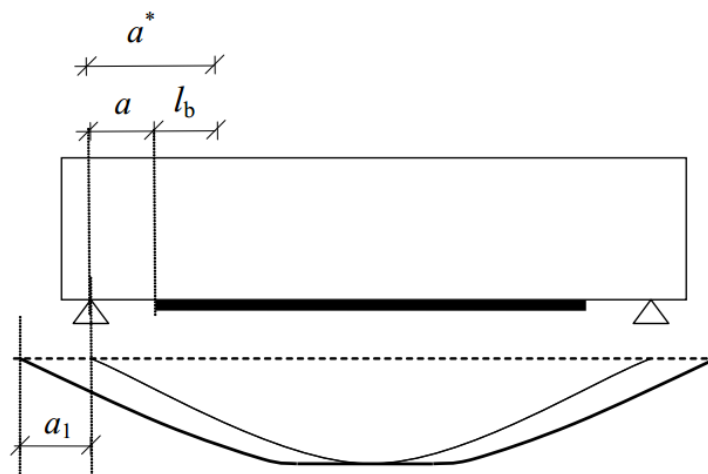


FIGURE 124 - BENDING MOMENT DIAGRAM SHIFTING

5.4.9 Shear Strength Evaluation

As for end debonding, shear failure is a highly undesirable failure mode, considering the purposes of the present work; in order to avoid such a mechanism, a particularly high strength concrete was chosen and it proved effective, has here discussed. Shear strength will be here computed according to both EC2 (2008) and ACI318 (2014) formulations.

5.4.9.1 Shear Strength – EC2

The EC2 provide a simple formula for shear strength computation, accounting for enmeshing, wedge effect and eventually the presence of normal stresses. The formula is meant for SI units:

$$V_{RC} = \max(V_{RC}, V_{min})$$

$$V_{RC} = \left[C_{Rd,c} k (100 \rho_l f_{ck})^{1/3} \right] A_c$$

$$V_{min} = \left[0.035 k^{3/2} f_{ck}^{1/2} \right] A_c$$

$$C_{Rd,c} = \frac{0.18}{\gamma_c}$$

No design coefficient is applied in present calculation [/]

$$k = 1 + \sqrt{\frac{200}{d}} \leq 2$$

d is in mm, k is adimensional [/]

$$\rho_l = \frac{A_{sl}}{A_c}$$

A_{sl} is the longitudinal rebars' area [/]

$$A_c = b d$$

Concrete Reacting Area [mm²]

$$d = d_s \vee d_f$$

Whether the unreinf. or reinf. sample is considered [mm]

5.4.9.2 Shear Strength – ACI318

The American counterpart provides two alternative formulations: a detailed approach and a rougher one; the least result coming from the two approaches will be considered:

$$V_C = \min(V_{C1}, V_{C2})$$

Being also:

$$V_{C2} = \min(V_{Ca}, V_{Cb}, V_{Cc})$$

V_{Ca} accounts for the chance of a contemporary shear-flexural failure and can be considered already accounted for via flexural design; V_{Cc} is always higher than V_{C1} by definition, hence the all calculation can be reduced to:

$$V_C = \min(V_{C1}, V_{Cb})$$

$$V_{C1} = [2 \lambda \sqrt{f'_c}] A_c$$

$$V_{Cb} = [1.9 \lambda \sqrt{f'_c} + 2,500 \rho_w] A_c$$

$$\lambda = 1$$

For standard concrete mix [/]

$$\rho_w = \frac{A_s}{A_c}$$

A_s is the longitudinal rebar area [/]

$$A_c = b d$$

Concrete Reacting Area [in²]

$$d = d_s \vee d_f$$

Whether the unreinf. or reinf. sample is considered [in]

Considering the results coming from ACI formulation are way higher than the EC2 counterparts, the 0.75 design safety factor will be applied:

$$V_{Cd} = 0.75 V_c$$

5.4.9.3 Shear Strength Check

Knowing the shear strength, the shear collapse load can be simply computed, accounting for the self-weight as well:

$$P_V = 2V_C - w_c L$$

It is required that the tested elements experience flexural failure before the shear strength is reached, the condition is largely verified for all the flexural failure modes, up to sheet tensile rupture, happening at 18.53 kip (82 kN).

Shear Check - Reinforced (P)		
	US	SI
	[kip]	[kN]
Flex. Limit	18.53	82.42
EC2	21.72	96.60
ACI318	24.75	110.09

For the Unreinforced sample the margin is even larger: the maximum load related to flexural collapse is 4.14 kip (18.43 kN), related to concrete collapse.

Shear Check - Unreinforced (P)		
	US	SI
	[kip]	[kN]
Flex. Limit	4.14	18.43
EC2	19.34	86.01
ACI318	20.98	93.33

5.5 Data Analysis

5.5.1 Experimental Sectional Properties

5.5.1.1 Neutral Axis Location

Knowing strains in two point over the section's height allows to estimate the experimental location of the neutral axis, simply applying the usual linear formulas.

If strains are measured either on steel and FRP, an average can be performed over the two different neutral axis values; the closer the two values are, the more the experimental shape is actually linear.

$$x_{exp} = \frac{\varepsilon_c d_f - \varepsilon_f d_c}{\varepsilon_c - \varepsilon_f}$$

d_c concrete strain gage distance from section's top (0.75 in) (19 mm)

d_f FRP sheet's distance from top, use d_s if steel strains are measured instead

5.5.1.2 Flexural Stiffness

Reversing the already referred standard Euler-Bernoulli formula, knowing experimental ultimate load and deflection, it is possible to compute the experimental flexural stiffness simply applying the formula:

$$EJ = \left[\frac{P_{exp}}{48} + \frac{5}{384} w_c L \right] \frac{L^3}{\delta_{exp}}$$

The formulation refers to the total experimental deflection, instead than the only flexural one, being impossible to separately measure the two contributions.

5.5.2 Experimental Equivalent Ultimate Strain

As it will be clear looking at the experimental results, while a reliable load measure is easy to achieve, the same cannot be said for a strain measure that could be considered representative of the uniform strain distribution assumed for design purposes. The reasons are intrinsic in the design assumptions, meant to properly describe the global system behavior, hence well matching a global strength measure, like the ultimate load; but lacking the level of detail required to predict the actual strain distribution at failure.

Discussing the shear-characterization results and implementation, it was already noticed how, referring to strain data is generally inconvenient and unprecise, not being consistent with a strength-oriented characterization. It should also be noticed that a detailed characterization for the strain distribution requires at least a three-point measurement over the sheet width, hard to achieve because of the limited number of acquisition channel at disposal.

These considerations lead to the choice of deriving an equivalent ultimate sheet strain, derived from the measured ultimate load. Such a value can be used to derive the tensile resultant acting on the FRP sheet, hence characterizing the effectiveness of the joint in a shear-test-comparable way. Such an equivalent strain can as well be applied to balanced area computation, allowing to evaluate the experimental efficiency of the anchor solution, as already done with reference to the theoretical values.

5.5.2.1 Backward Sectional Equilibrium

Knowing the ultimate strain of one of the constituent material allows to easily compute the section's strength at ULS. The solution can generally be analytically computed in an explicit way, requiring at worst one iteration over the neutral axis location.

To impose equilibrium under a known external load is a more complex problem, having to deal with an implicit non-linear system in two unknowns: the neutral axis location and the strain on the FRP sheet. Notice that the strain distribution over the section's height can be function of two generic unknowns in order to define slope and intersection with the zero-strain axis; these variables can be the neutral axis location itself and a generic strain, or the strain value in two different locations. Picking x and ε_f seems the most reasonable choice in this case.

$$\begin{cases} C(x, \varepsilon_c(x, \varepsilon_f)) + S(x, \varepsilon_s(x, \varepsilon_f)) + F(\varepsilon_f) = 0 \\ C(x, \varepsilon_c(x, \varepsilon_f)) b_c(x) + S(x, \varepsilon_s(x, \varepsilon_f)) b_s(x) + F(\varepsilon_f) b_f(x) = M_e \end{cases}$$

The internal resultants and the related arms have already been defined, the external moment can be easily computed, knowing the collapse load and the slabs weight:

$$M_e = \frac{PL}{4} + \frac{w_c L^2}{8}$$

5.5.2.2 Solving the Non-Linear Implicit System

In order to solve the system a two-level iterative approach seems the fittest: (1) An FRP strain value is firstly assumed, (2) this fixes the failure mode and allows to compute the neutral axis location, iteratively solving the translational equilibrium equation as usual; (3) knowing either x and ε_f , the internal moment can be simply computed and compared with the external one; (4) finally, a new FRP strain is assumed and the process is iterated until the moment equilibrium is guaranteed within the desired error range.

Knowing the theoretical equivalent strain makes the process way faster, as well as knowing whether the experimental result is lower or higher than the theoretical one, simply depending on whether the ultimate experimental load is higher or lower the expected one. This trend can be guaranteed as long as the collapse mechanism doesn't vary and is determined by the FRP linear behavior, but it should not be considered generally valid. Anyway, having at disposal a starting point and a direction, allows to write a simple two-phases iteration algorithm in the form:

```

Sub DoubleLoop()
'
' DoubleLoop Macro
'
' Scelta rapida da tastiera: CTRL+MAIUSC+D
'
Dim i As Integer

For i = 27 To 75 Step 8
Cells(17, i).Value = Cells(10, i)
Delta = -Cells(17, i).Value / 10000

Do While Abs(Cells(8, i).Value) > 0.01

    Cells(17, i).Value = Cells(17, i).Value + Delta
    Cells(7, i).GoalSeek Goal:=0, ChangingCell:=Cells(6, i)

Loop
Next i
End Sub

```

5.5.3 Effectiveness and Efficiency Parameters

The effects of an anchor joint on the system's performances can be evaluated in several different ways, usually the strength improvement over an unanchored joint is proposed as the characteristic parameter to pick up. Different, eventually more significant solutions, will be here proposed and later applied to results evaluation.

5.5.3.1 Shear Effectiveness

The most common way to evaluate the effectiveness of an anchoring solution in shear testing, is to compare the shear strength of the anchored joint to the shear strength of the unanchored, simply-bonded, joint.

$$\rho_{S_b} = \frac{S_{anchored}}{S_{bonded}}$$

This solution poses two main issues: first of all, the unanchored joint strength is a hard to define parameter, either from the theoretical and from the experimental point of view, considering its high variance; secondly, even if the bonded strength is properly defined and/or measured, such a parameter is only representative of a shear-test situation, hence the so-defined effectiveness ratio can be hardly applied to evaluate real-case scenarios. In order to overcome this issues a different adimensionalization is proposed, using the sheet's rupture strength as reference strength:

$$\rho_{S(fu)} = \frac{S_{anchored}}{A_f f_{fu}}$$

Such a parameter expresses the percentage of the actual sheet's strength that the anchoring solution allows to exploit; is capped at 1, considering that a debonding-preventing solution will never allow to overcome the sheet's own strength, allowing to easily understand the effectiveness of the solution.

Because of the composite's elastic behavior and the assumption of linear strains over the section, the parameter will always coincide with the later defined $\rho_{\varepsilon_s(fu)}$ ductility ratio, allowing for a complete system's strength and ductility characterization.

Also notice that the proposed parameter easily allows to compare results coming from different set-ups (Shear, Bending), not requiring a shear characterization of the unanchored joint and not relying on such a strictly set-up-dependent parameter.

5.5.3.2 Flexural Effectiveness

Now considering effectiveness definition in flexural set-ups, an easy solution would be to compare the anchored slab's strength to the unanchored one, or directly to the non-externally reinforced one:

$$\rho_{M_b} = \frac{M_{anchored}}{M_{bonded}}$$

$$\rho_{M_{(R/C)}} = \frac{M_{anchored}}{M_{R/C \text{ only}}}$$

An alternative solution would be to compare the anchored resisting moment to the ultimate moment provided by a fully exploitable sheet, either if caused by concrete or sheet rupture:

$$\rho_{M(fu)} = \frac{M_{anchored}}{\min(M_{cu}, M_{fu})}$$

Also in this case the parameter is capped at 1 and allows to easily estimate the actual effectiveness of the anchoring solution, it is however a less general parameter, considering the resisting moment – at numerator and denominator – to be largely dependent on the geometry, material properties and ruling collapse mechanism.

5.5.3.3 Flexural Efficiency

As discussed, the traditional concept of balanced section can be adapted to estimate the efficiency of an external reinforcement solution and so the efficiency of the provided anchoring system. At increasing (equivalent) ultimate strain, the amount of reinforcement area required to balance the section decreases, hence the efficiency of the reinforcing solution increases at constant provided-reinforcement-area:

$$\rho_{A_f} = \frac{A_f}{A_{f,opt}(\epsilon_{fd})}$$

Such a parameter is not collapse-mechanism dependent, the only experimental quantity required to compute it is the experimental sheet's equivalent ultimate strain, as already defined and discussed.

The efficiency ratio is not capped at one, even if providing an amount of reinforcement larger than the balanced one would not make sense, not providing any kind of strength increment. Notice the difference with the standard definition for steel: a super-optimal solution would still provide strength increment in that case, defining the balanced area as a function of the yield strain, not the ultimate one.

5.5.4 Ductility Parameters

The joint's effectiveness in enhancing the system's ductility can be either evaluated from the internal-reinforcement-yielding prospective or from the deflection-at-failure prospective.

5.5.4.1 Steel Strain Prospective

The most applied design norms (i.e. ACI 318-14) impose a minimum steel strain at failure, hence requiring the system to undergo visible deflection before peak is reached and failure happens, either because of concrete crushing or FRP failure. A simple ductility-improvement measure could be the ratio of the steel strain in an anchored solution versus a non-anchored or even non-externally-reinforced one:

$$\rho_{\varepsilon_s, b} = \frac{\varepsilon_s (anchored)}{\varepsilon (bonded)}$$
$$\rho_{\varepsilon_s, (R/C)} = \frac{\varepsilon_s (anchored)}{\varepsilon_s (R/C \text{ only})}$$

The same parameter can be defined as a ratio over the steel strain at slab's failure, assuming a fully exploitable sheet's strength. $\varepsilon_s (f_u)$ is defined as the steel strain related to $\min(M_{cu}, M_{fu})$, as already discussed regarding the ultimate moment ratio. Such a value is capped at 1 and, as a consequence of the linearity assumptions, coincide with the already defined shear effectiveness ratio $\rho_{S(f_u)}$.

$$\rho_{\varepsilon_s (f_u)} = \frac{\varepsilon_s (anchored)}{\varepsilon_s (f_u)}$$

As an alternative, willing to use as reference value a standard parameter, independent from the experimental set-up, the steel strain can be very well compared to the yielding strain. Such a yielding-ratio is not capped and the larger it is, the more ductile is the system at failure:

$$\rho_y = \frac{\varepsilon_s}{\varepsilon_y}$$

Notice that no steel stain measurements are available at failure, because of gages' early failure, steel strain will be computed via backward sectional equilibrium, knowing the measured ultimate load, as already discussed. The only difference is the unreinforced sample, for which an experimental steel strain measure is available up to failure.

5.5.4.2 Deflection at Failure Prospective

The goal in requiring a ductile ultimate behavior, is to allow failure detection before the actual collapse take place. From this prospective: the larger the deflections at failure, the more ductile the system. The unanchored or non-externally reinforced experimental deflections can be used as reference values, the parameter is uncapped and highly depending on set-up, geometry and material parameters.

$$\rho_{\delta_b} = \frac{\delta_{anchored}}{\delta_{bonded}}$$

$$\rho_{\delta_{(R/C)}} = \frac{\delta_{anchored}}{\delta_{R/C \text{ only}}}$$

The ratio can be as well referred to the deflection related to a fully exploitable FRP sheet. Such a parameter cannot be applied in the present dissertation, considering that a fully exploited sample has not been tested and reliable deflection formulas for externally reinforced concrete elements at ULS are not yet available.

$$\rho_{\delta_{(f_u)}} = \frac{\delta_{anchored}}{\delta_{f_u}}$$

6 Test Results

6.1 Specimen Response

6.1.1 Unreinforced Sample

The unreinforced sample shows a Standard R/C response in bending, the tri-linear behavior is clearly visible in the load-deflection diagram. Ultimate theoretical strength is reached right after yielding, then the experimental value still rises slowly because of steel hardening, neglected in theoretical calculations.

It is interesting to notice how the concrete strain at gages level turns from positive (compressive) to negative (tensile) at neutral axis raising; remember the gages are stuck on the slabs' sides.

After yielding, steel gages are lost soon and steel strains at peak are not available; strain linearity over the section's height, is directly confirmed up to yielding, via direct strain plotting and neutral axis location comparison. After yielding, the ultimate load, computed applying the linear strain assumption, is in good matching with the experimental one, neglecting the experimentally experienced hardening.

Regarding the experimental-analytical matching, a good agreement can be generally spotted. It should be noticed how some experimental load peak values do not have an analytical meaningful counterpart. The high level of error related to neutral axis location at failure is mainly due to the limited matched quantities' modulus: a 0.1'' (2 mm) difference can be very well considered acceptable.

	C-C [US]				
	Load	Deflection	Concrete	Steel	x
	[kip]	[in]	[%]	[%]	[in]
Elastic	1.57	0.09	-0.003%	0.03%	1.36
Cracked	3.30	0.33	-0.011%	0.22%	1.00
Yielding Start	4.41	0.48	-0.007%	0.31%	0.87
Zero	4.33	0.49	0.000%	0.31%	0.75
Failure	4.49	0.56	0.045%	0.39%	0.05

C-C [SI]					
	Load	Deflection	Concrete	Steel	x
	[kN]	[mm]	[%]	[%]	[in]
Elastic	6.99	2	-0.003%	0.03%	35
Cracked	14.70	8	-0.011%	0.22%	25
Yielding Start	19.60	12	-0.007%	0.31%	22
Zero	19.25	13	0.000%	0.31%	19
Failure	19.97	14	0.045%	0.39%	1

Experimental Matching [US]									
	Load [kip]			Deflection [in]			x [in]		
	Exp.	Th.	Δ	Exp.	Th.	Δ	Exp.	Th.	Δ
Elastic	1.57	-	-	0.09	-	-	1.36	3.04	-55.20%
Cracked	3.30	-	-	0.33	-	-	1.00	0.98	2.22%
Yielding Start	4.41	4.01	9.86%	0.48	0.33	48.45%	0.87	0.64	35.54%
Failure	4.49	4.14	8.32%	0.56	0.42	34.45%	0.05	0.15	-66.12%

Experimental Matching [SI]									
	Load [kN]			Deflection [mm]			x [mm]		
	Exp.	Th.	Δ	Exp.	Th.	Δ	Exp.	Th.	Δ
Elastic	6.99	-	-	2	-	-	35	77	-55.20%
Cracked	14.70	-	-	8	-	-	25	25	2.22%
Yielding Start	19.60	17.84	9.86%	12	8	48.45%	22	16	35.54%
Failure	19.97	18.43	8.32%	14	11	34.45%	1	4	-66.12%

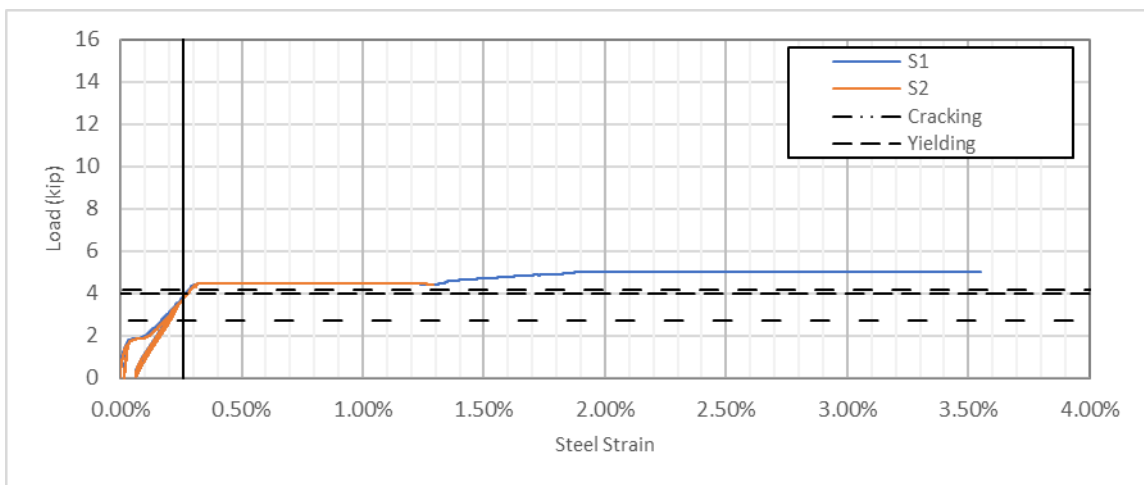
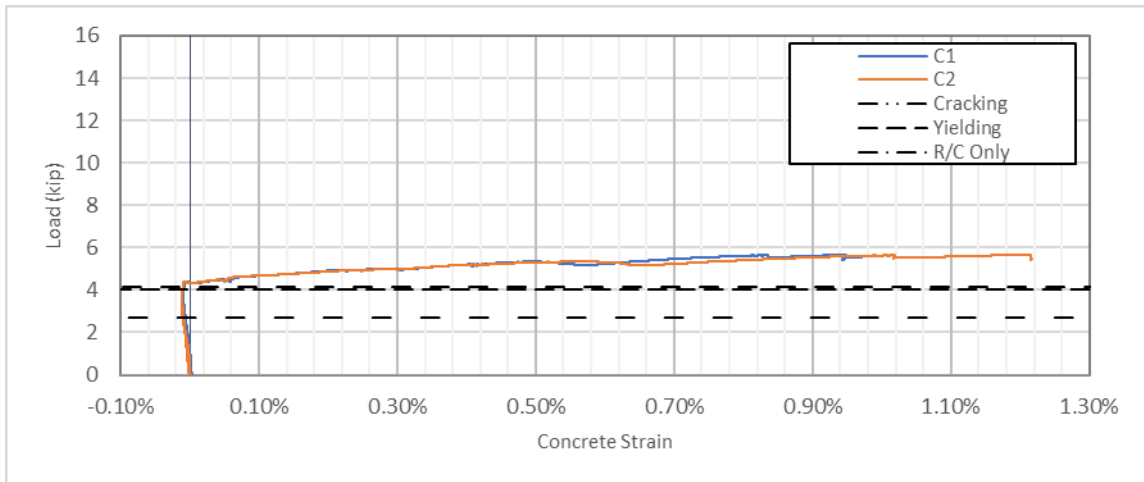
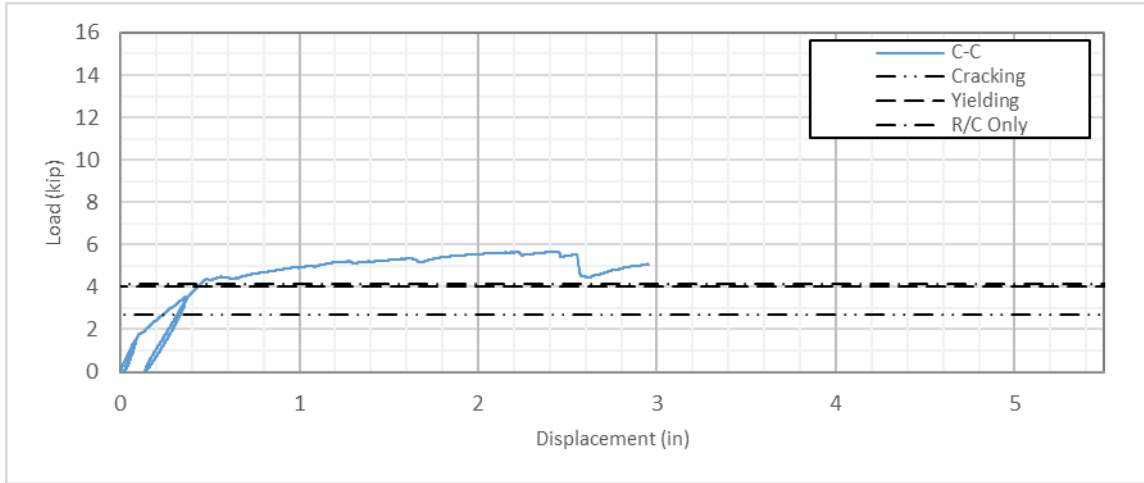


FIGURE 125 - (A) LOAD/DISPLACEMENT (B) CONCRETE STRAIN (C) STEEL STRAIN (C-C)
1 IN = 25.4 MM / 1 KIP = 4.448 kN

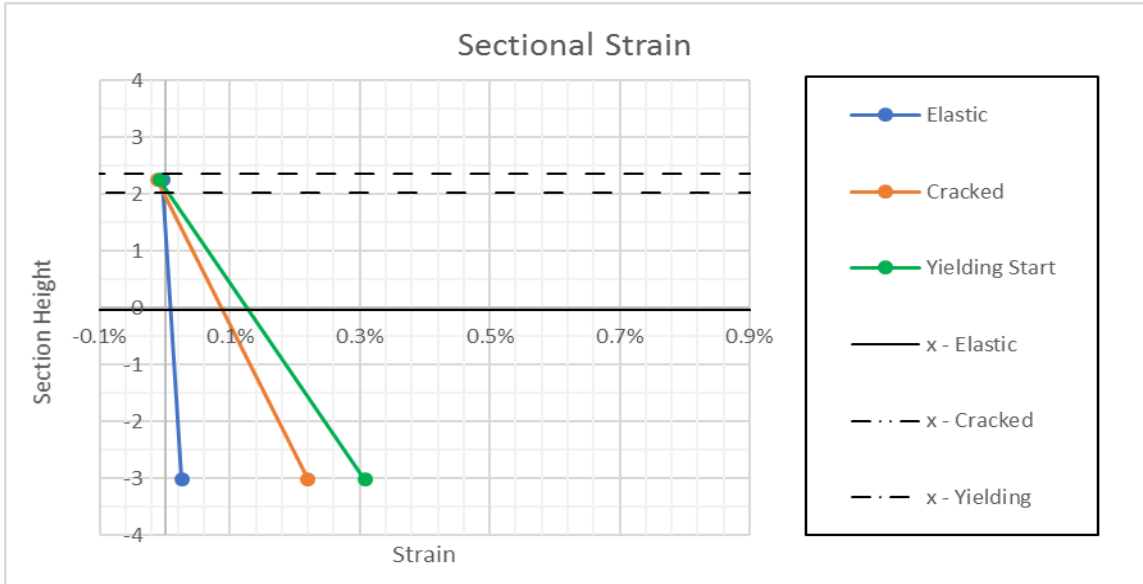


FIGURE 126 - SECTIONAL STRAINS (C-C). 1 IN = 25.4 MM / 1 KIP = 4.448 kN

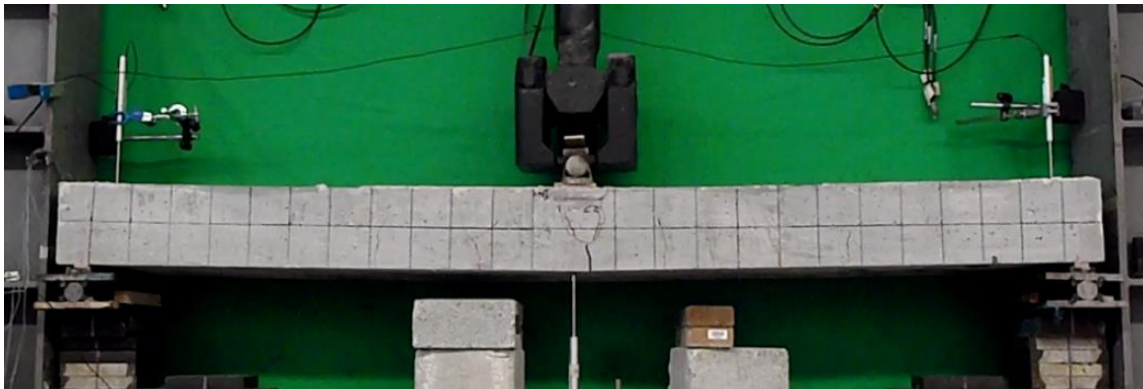


FIGURE 127 – FAILURE (C-C)



FIGURE 128 - POST-FAILURE (C-C)

6.1.2 Control Sample

The control Sample shows a bi-linear behavior up to intermediate debonding, when the slab's strength suddenly drops to standard R/C value. The strength then slowly linearly increases, because of rebars' hardening.

In this case the concrete strain stays positive up to failure, because of neutral axis lowering as a consequence of the external reinforcement added. Steel gages are lost even before yielding, but linearity – over three points – is fairly good verified, as long as measurements allows for an evaluation. The strength, computed from a linear strain assumption, is always in good matching with the measured one.

The measured strain value at FRP level is an average over three gages located at midspan: a concave strain distribution was spotted, with a peak on the side where debonding started. A very good average-strain matching can be noticed at failure. Notice also the very good matching on the deflection side.

Even more remarkable is how both theoretical load and strain show the same percentage error: this means the sectional theory perfectly applies to externally reinforced elements, while the small error is related to debonding prediction.

C-FRP [US]						
	Load	Deflection	Concrete	Steel	FRP	x
	[kip]	[in]	[%]	[%]	[%]	[in]
Elastic	1.50	0.06	-0.011%	0.006%	0.010%	3.80
Cracked	3.89	0.24	-0.047%	0.11%	0.22%	2.00
Loose S2	4.91	0.33	-0.055%	0.15%	0.25%	1.94
Yielded	6.75	0.55	-0.088%	-	0.40%	1.69
Debonding	9.33	0.82	-0.112%	-	0.66%	1.51

C-FRP [SI]						
	Load	Deflection	Concrete	Steel	FRP	x
	[kN]	[mm]	[%]	[%]	[%]	[mm]
Elastic	6.66	2	-0.011%	0.006%	0.010%	97
Cracked	17.31	6	-0.047%	0.11%	0.22%	51
Loose S2	21.84	8	-0.055%	0.15%	0.25%	49
Yielded	30.04	14	-0.088%	-	0.40%	43
Debonding	41.51	21	-0.112%	-	0.66%	38

C-FRP Experimental Matching [US]

	Load [kip]			Deflection [in]			ϵ_f [%]			x [in]		
	Exp.	Th.	Δ	Exp.	Th.	Δ	Exp.	Th.	Δ	Exp.	Th.	Δ
Elastic	1.50	-	-	0.06	-	-	0.01%	-	-	3.80	3.04	24.95%
Cracked	3.89	-	-	0.24	-	-	0.22%	-	-	2.00	0.98	103.85%
Loose S2	4.91	-	-	0.33	-	-	0.25%	-	-	1.94	0.98	97.74%
Yielding	6.75	6.55	3.12%	0.55	0.51	7.36%	0.40%	0.32%	26.37%	1.69	0.78	116.72%
Debonding	9.33	9.68	-3.58%	0.82	0.75	8.88%	0.66%	0.70%	-5.18%	1.51	0.66	130.74%

C-FRP Experimental Matching [SI]

	Load [kN]			Deflection [mm]			ϵ_f [%]			x [mm]		
	Exp.	Th.	Δ	Exp.	Th.	Δ	Exp.	Th.	Δ	Exp.	Th.	Δ
Elastic	6.66	-	-	2	-	-	0.01%	-	-	97	77	24.95%
Cracked	17.31	-	-	6	-	-	0.22%	-	-	51	25	103.85%
Loose S2	21.84	-	-	8	-	-	0.25%	-	-	49	25	97.74%
Yielding	30.04	29.13	3.12%	14	13	7.36%	0.40%	0.32%	26.37%	43	20	116.72%
Debonding	41.51	43.05	-3.58%	21	19	8.88%	0.66%	0.70%	-5.18%	38	17	130.74%

FRP Strains are a 3-point average measured at midspan

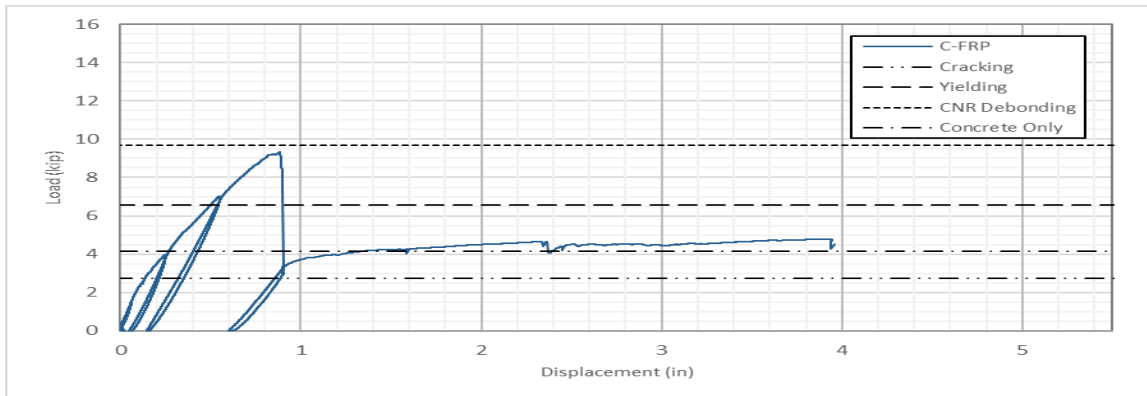


FIGURE 129 - LOAD / DISPLACEMENT (C-FRP). 1 IN = 25.4 MM / 1 KIP = 4.448 kN

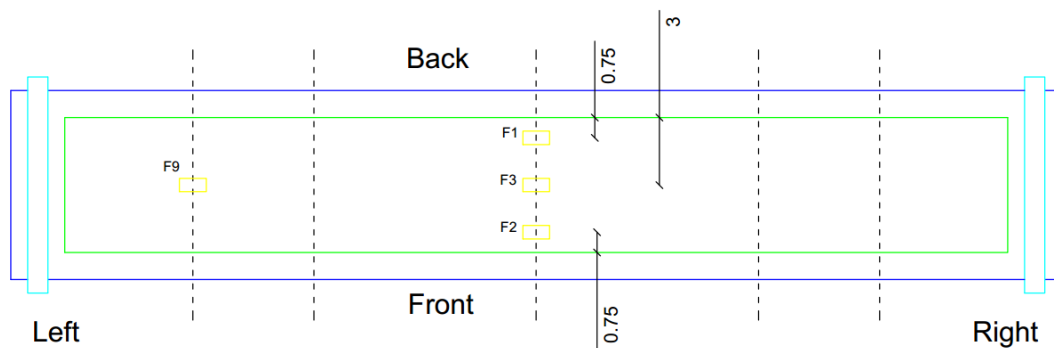


FIGURE 130 - STRAIN GAGES (C-FRP). DIMENSIONS IN INCHES. 1 IN = 25.4 MM

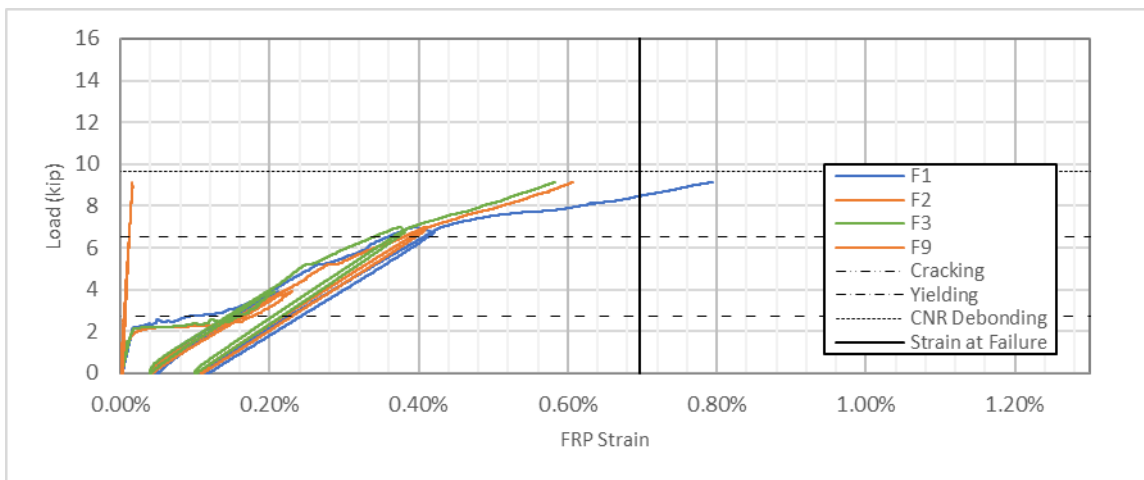
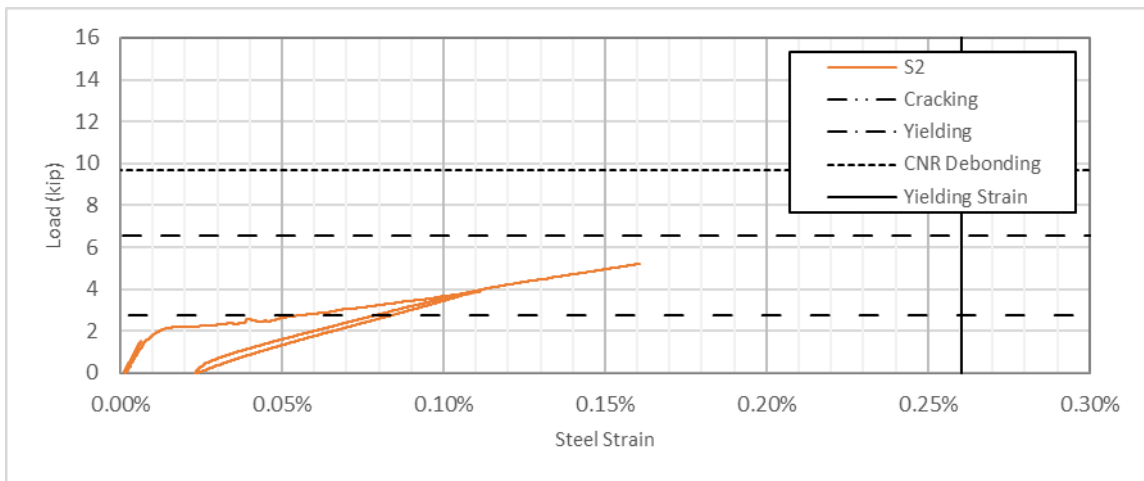
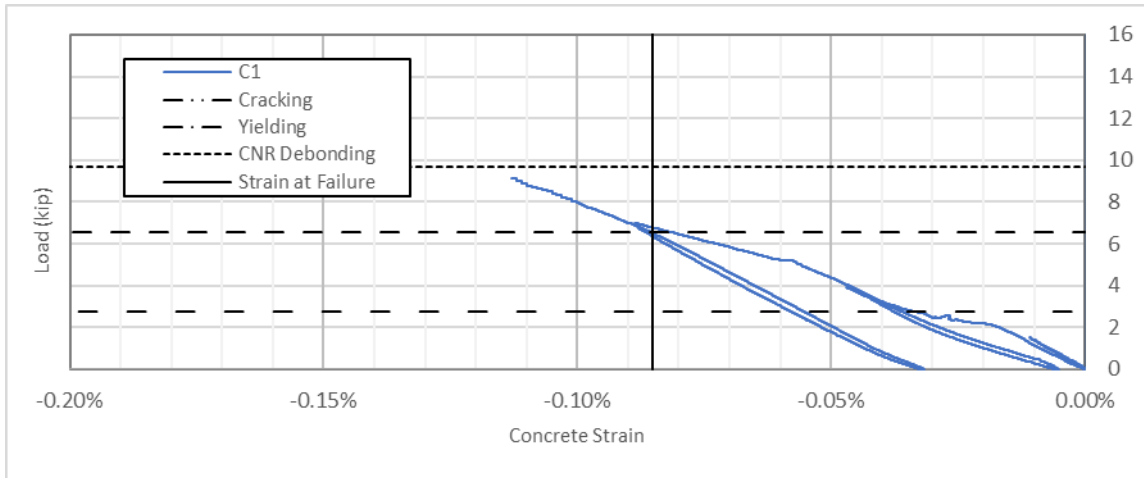


FIGURE 131 - (A) CONCRETE STRAIN (B) STEEL STRAIN (C) FRP STRAIN (C-FRP)
 1 IN = 25.4 MM / 1 KIP = 4.448 kN

Looking to the strains evolution in the FRP, the external reinforcement engagement as cracking starts can be clearly spotted, in good agreement with what theoretically computed. Also a larger engagement ratio can be spotted as yielding starts.

Notice the very low level of strain in location F9, at the very end of the sheet, in line with what computed checking on end debonding. Also notice the sudden strain increment in the concrete, as cracks appear. Regarding steel strain diagram, please notice the steel gage went lost before yielding.

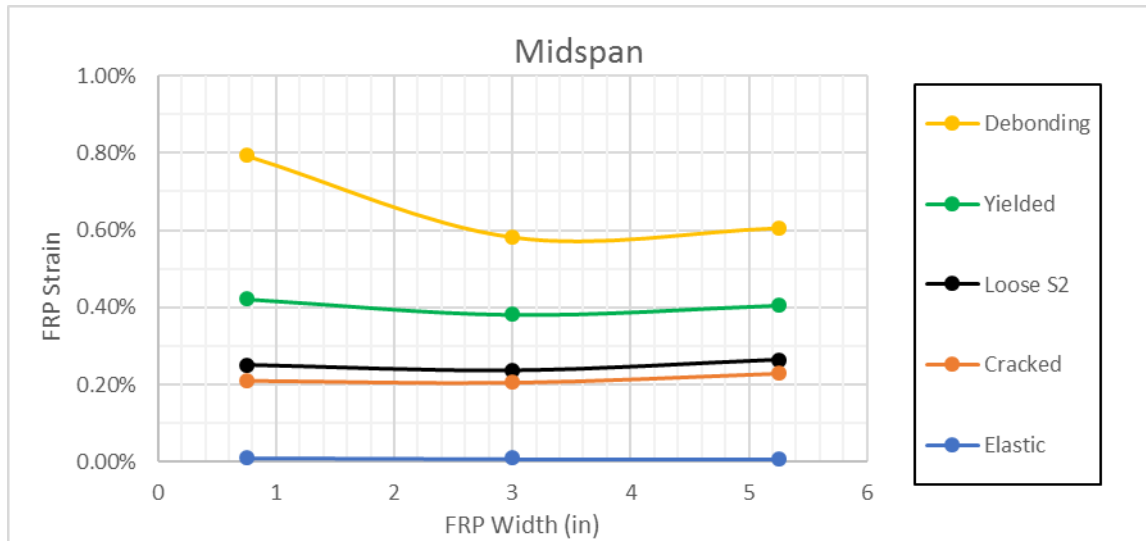
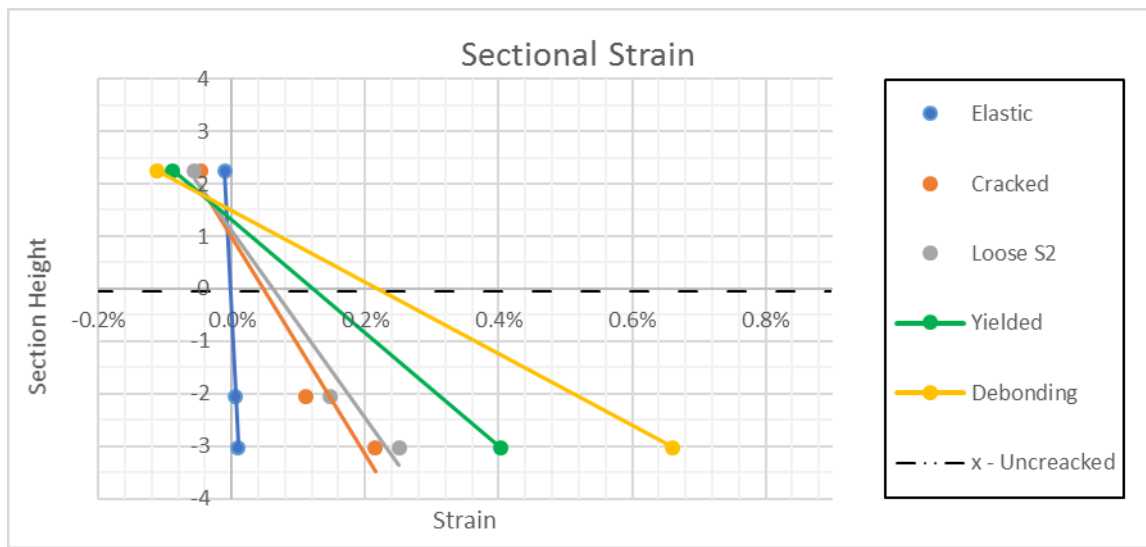


FIGURE 132 - (A) SECTIONAL STRAIN (B) FRP STRAIN OVER THE WIDTH (C-FRP)
 1 IN = 25.4 MM / 1 KIP = 4.448 kN

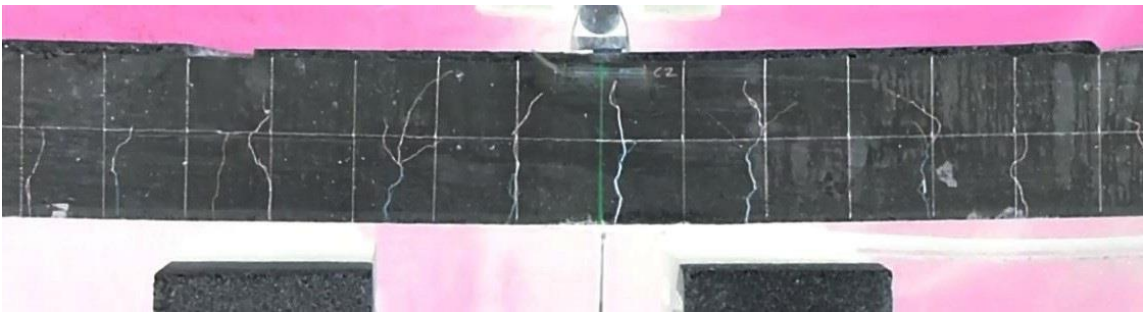
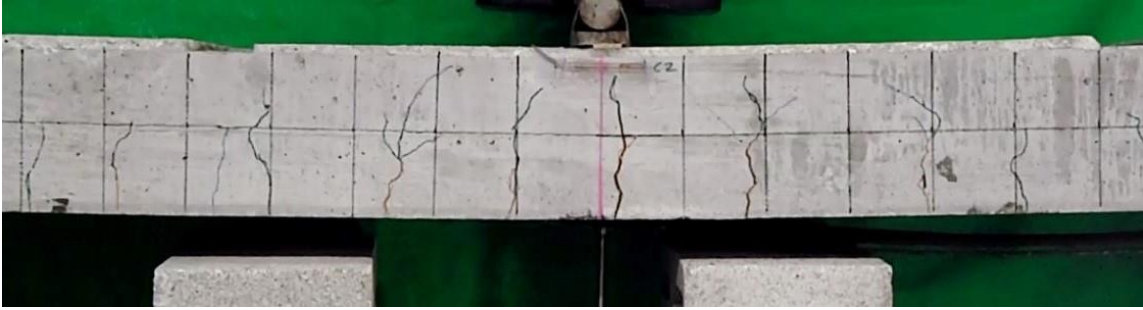


FIGURE 133 - C-FRP COLLAPSE PICTURES

6.1.3 Matching Series

6.1.3.1 60x2

As in the control sample, a bi-linear behavior up to debonding can be clearly spotted; as debonding happens, the end anchors are suddenly engaged, providing the critical mechanism for sheet-concrete load transfer. Over the debonded sheet, the strains are almost constant at varying abscissa and equal to the value registered in midspan.

As debonding proceeds behind the first anchor, the system experiences a series of load drops and increments; after this transition phase, the strength starts growing again, with a sensibly reduced stiffness, as bonding is no longer provided. The overall behavior can be properly modeled as a pseudo-tri-linear one.

It should be noticed how the anchors' presence has no influence on the value of intermediate debonding load, suggesting end anchors do not provide any intermediate bonding improvement (type I, II) at serviceability, while provide a relevant strength and ductility increment (type III, IV) at ultimate limit state.

In the end the anchors' failure is a slipping one, happening on the right side of the symmetrically anchored slab; it is peculiar to notice how the failure is triggered by the slipping of a central strip only, while the lateral strips, provided with a larger anchored area, still guarantee residual strength, until strength drops to R/C-only level.

Because of the limited number of acquisition channels, it was not possible to acquire the strains all over the sheet's width: only two points instead of the ideal three are available. The strain distribution over the width is built via symmetry assumption.

Such an approach cannot be assumed fully reliable, well knowing that complete symmetry is never achieved in a real-case scenario, and further discussion on the strain distribution is required. It should be noticed how, at least theoretically, the strain distribution should not vary significantly over the sheet's width or length, especially over a fully debonded sheet; hence the strain measure at the central strip's midspan can be assumed as roughly representative of the strain over the whole width, when an average approach is not feasible. The side value is referred after central strip's failure.

The additional strength guaranteed by the anchors allows a further raising of the neutral axis and the concrete strain's sign inversion; notice that concrete residual deformations in tension makes strain measurements, after sign reversion, unreliable for neutral axis calculation, even though the gage keeps working properly up to failure. No strain gages

are applied on steel rebars. Looking at the FRP strain evolution it can be noticed how strains at the sheet's end (F6, F12) suddenly jump to the midspan level as debonding happens (F3).

A very good load prediction can be spotted up to failure, the strain measured on the FRP are about 20-25% smaller than the expected ones either at debonding and failure. This can be very well related to the sub-optimal way strains are measured, considering highest values are generally registered on one side, rather than on the central strip. Anyway, the limited error rate still makes one-point measurement a decent solution to experimentally evaluate strains over the sheet's width when better solutions are not feasible.

60x2 [US]					
	Load	Deflection	Concrete	FRP	x
	[kip]	[in]	[%]	[%]	[in]
Elastic	1.52	0.10	-0.005%	0.011%	2.45
Cracked	4.28	0.36	-0.02%	0.19%	1.27
Yielding Start	7.01	0.62	-0.02%	0.34%	1.09
Concrete Zero	9.42	0.87	0.00%	0.57%	0.75
Debonding Left	9.55	0.89	0.01%	0.58%	-
Debonding Right	10.12	1.15	0.16%	0.61%	-
Ultimate Right - Central	12.09	1.90	0.25%	0.79%	-
Ultimate Right - Side	10.30	1.99	0.29%	0.76%	-

60x2 [SI]					
	Load	Deflection	Concrete	FRP	x
	[kN]	[mm]	[%]	[%]	[mm]
Elastic	6.77	3	-0.005%	0.011%	62
Cracked	19.02	9	-0.02%	0.19%	32
Yielding Start	31.20	16	-0.02%	0.34%	28
Concrete Zero	41.92	22	0.00%	0.57%	19
Debonding Left	42.48	23	0.01%	0.58%	-
Debonding Right	45.01	29	0.16%	0.61%	-
Ultimate Right - Central	53.77	48	0.25%	0.79%	-
Ultimate Right - Side	45.82	50	0.29%	0.76%	-

60x2 Experimental Matching [US]

	Load [kip]			Deflection [in]			ϵ_f [%]			x [in]		
	Exp.	Th.	Δ	Exp.	Th.	Δ	Exp.	Th.	Δ	Exp.	Th.	Δ
Elastic	1.52	-	-	0.10	-	-	0.01%	-	-	2.45	3.04	-19.31%
Cracked	4.28	-	-	0.36	-	-	0.19%	-	-	1.27	0.98	29.71%
Yielding Start	7.01	6.55	7.10%	0.62	0.51	21.20%	0.34%	0.32%	7.58%	1.09	0.78	39.64%
Concrete Zero	9.42	-	-	0.87	-	-	0.57%	-	-	0.75	-	-
Debonding L	9.55	9.68	-1.33%	0.89	0.75	17.86%	0.58%	0.70%	-17.52%	-	0.66	-
Debonding R	10.12	-	-	1.15	-	-	0.61%	-	-	-	-	-
Ultimate R - C	12.09	12.16	-0.62%	1.90	0.94	102.46%	0.79%	1.00%	-20.83%	-	0.63	-
Ultimate R - S	10.30	-	-	1.99	-	-	0.76%	-	-	-	-	-

60x2 Experimental Matching [SI]

	Load [kN]			Deflection [in]			ϵ_f [%]			x [mm]		
	Exp.	Th.	Δ	Exp.	Th.	Δ	Exp.	Th.	Δ	Exp.	Th.	Δ
Elastic	6.77	-	-	3	-	-	0.01%	-	-	62	77	-19.31%
Cracked	19.02	-	-	9	-	-	0.19%	-	-	32	25	29.71%
Yielding Start	31.20	29.13	7.10%	16	13	21.20%	0.34%	0.32%	7.58%	28	20	39.64%
Concrete Zero	41.92	-	-	22	-	-	0.57%	-	-	19	-	-
Debonding L	42.48	43.05	-1.33%	23	19	17.86%	0.58%	0.70%	-17.52%	-	17	-
Debonding R	45.01	-	-	29	-	-	0.61%	-	-	-	-	-
Ultimate R - C	53.77	54.10	-0.62%	48	24	102.46%	0.79%	1.00%	-20.83%	-	16	-
Ultimate R - S	45.82	-	-	50	-	-	0.76%	-	-	-	-	-

FRP Strains are measured on the central FRP strip at midspan

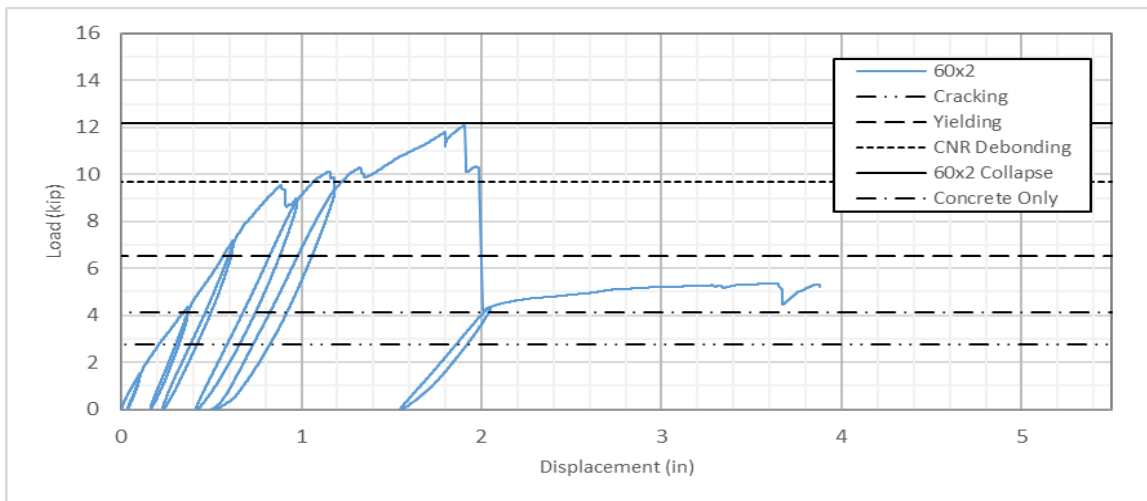


FIGURE 134 - LOAD/DISPLACEMENT (60x2)

1 IN = 25.4 MM / 1 KIP = 4.448 kN

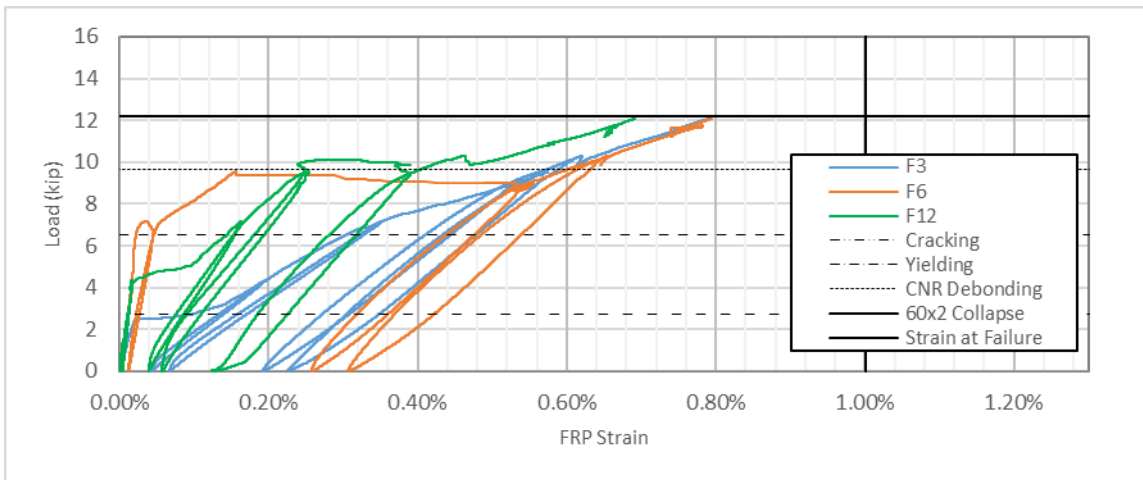
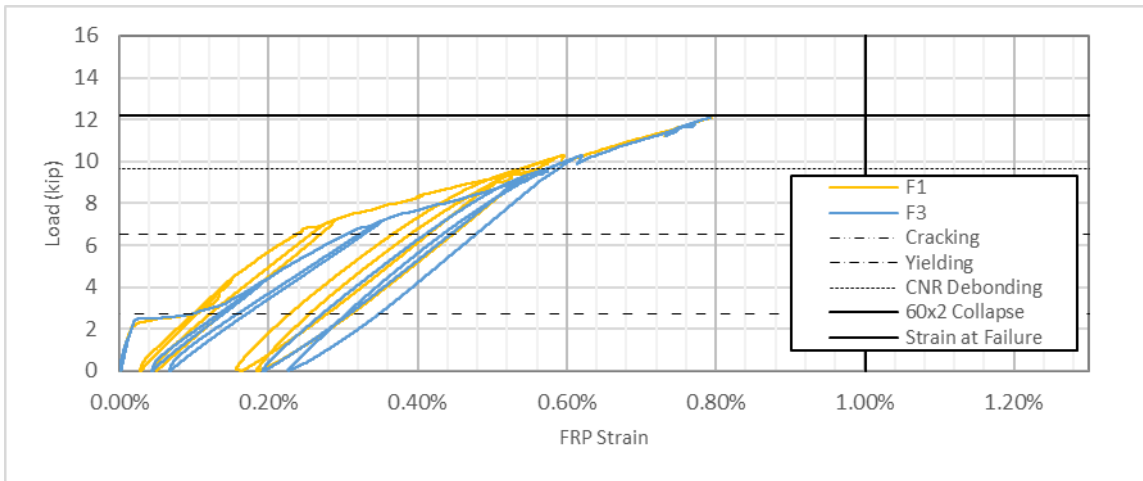
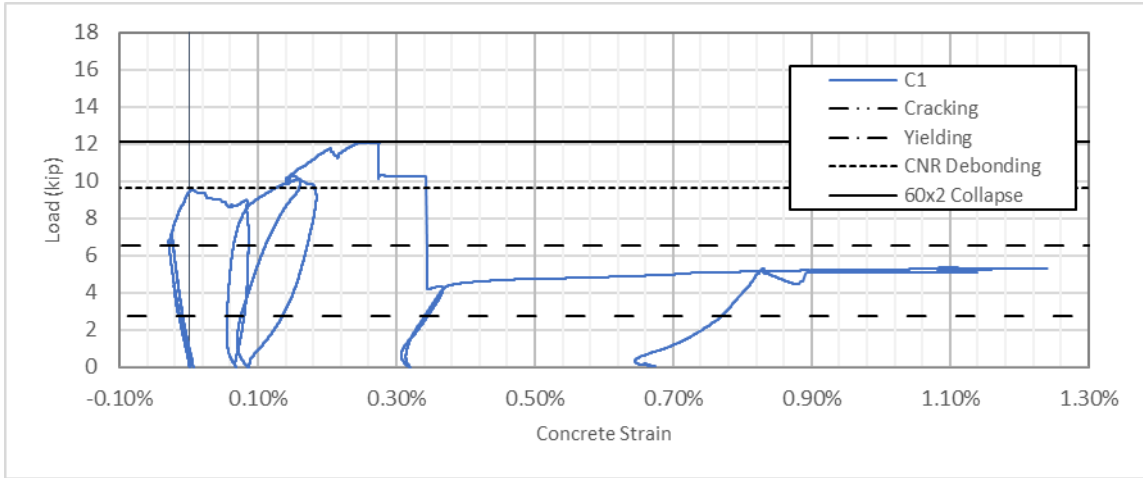


FIGURE 135 - (A) CONCRETE STRAIN (B, C) FRP STRAIN (60x2)
 1 IN = 25.4 MM / 1 KIP = 4.448 kN

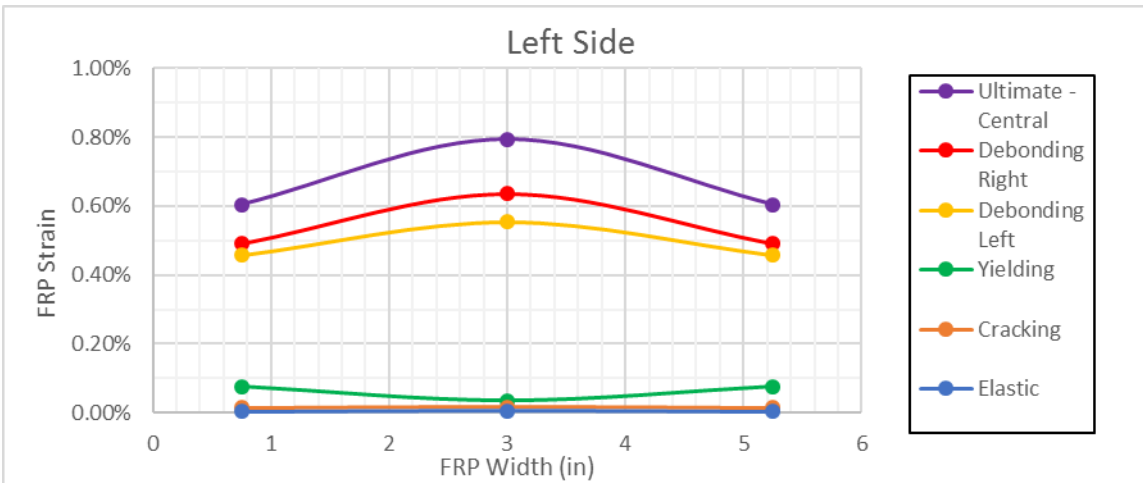
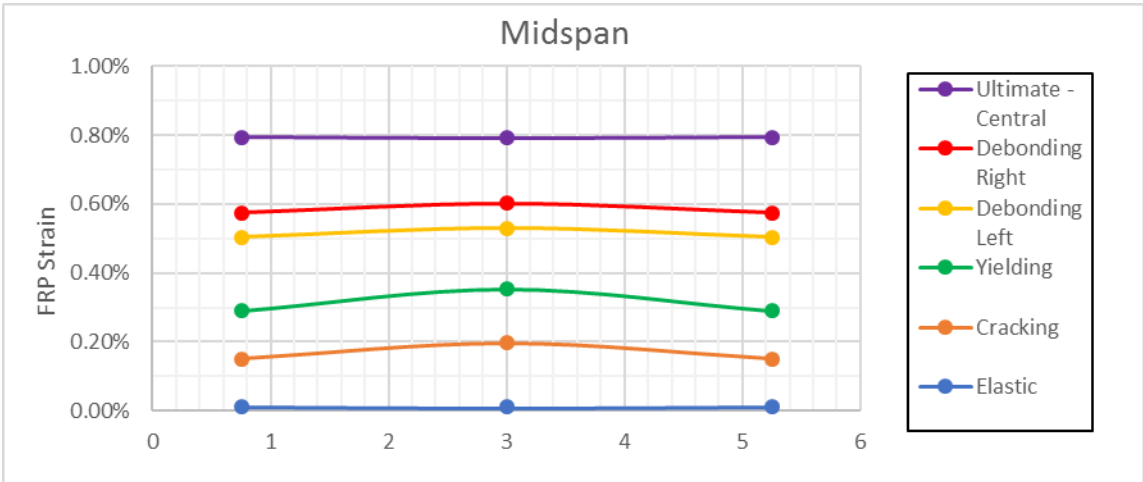


FIGURE 136 - FRP STRAINS OVER THE WIDTH (60x2). SYMMETRY IS ARTIFICIALLY IMPOSED FOR THE SAKE OF A BETTER READING. 1 IN = 25.4 MM / 1 KIP = 4.448 KN

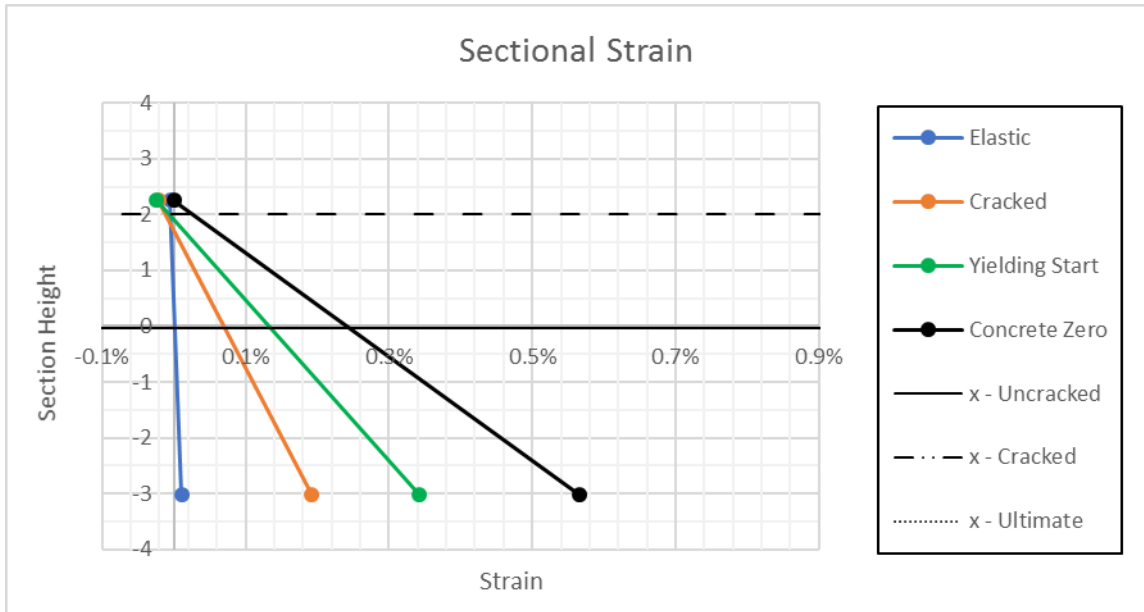


FIGURE 137 - SECTIONAL STRAIN (60x2). 1 IN = 25.4 MM / 1 KIP = 4.448 kN

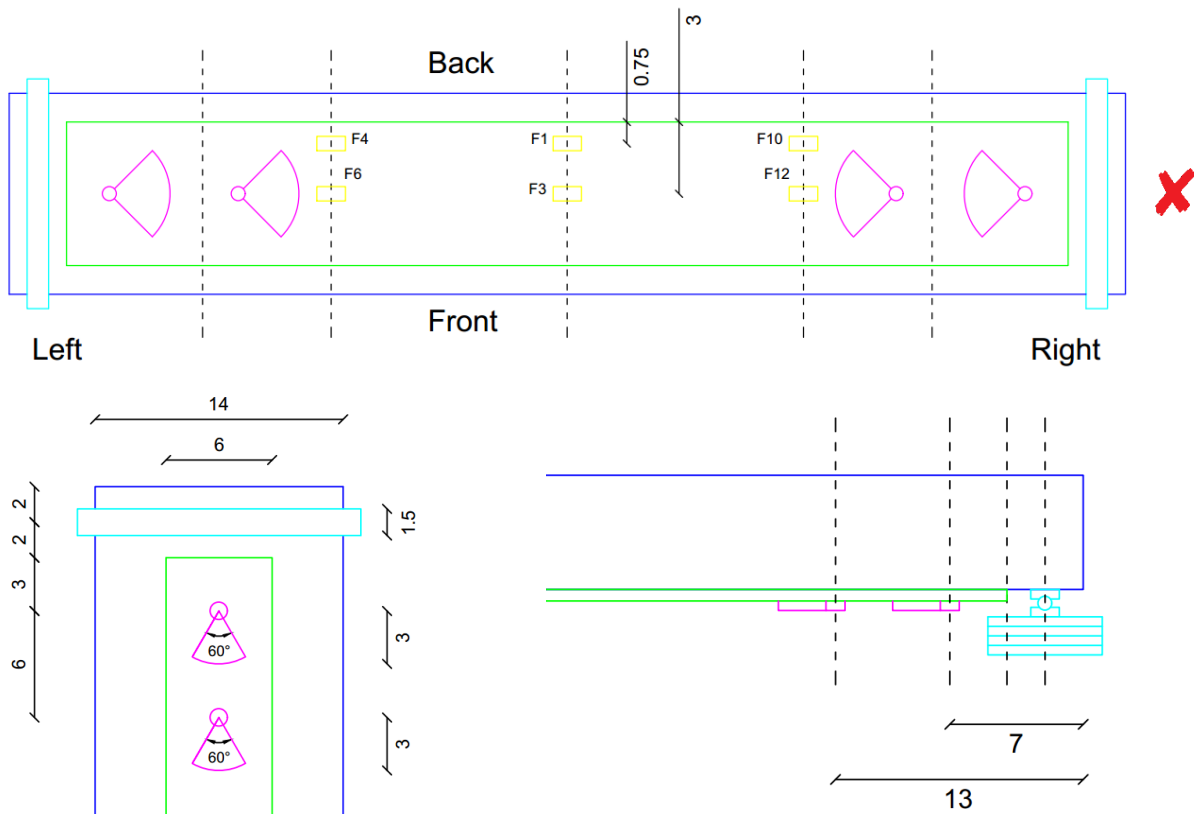


FIGURE 138 - STRAIN GAGES LOCATIONS & GEOMETRY (60x2), THE X MARKS THE FAILING SIDE. DIMENSIONS IN INCHES. 1 IN = 25.4 MM / 1 KIP = 4.448 kN



FIGURE 139 - 60x2 COLLAPSE PICTURES, THE X MARKS THE FAILING SIDE

6.1.3.2 90x2

The specimen showed pretty much the same behavior described for the 60° sample, as well as the same very good matching on the load side. The strain matching has got worse, still assuming the midspan value as representative of the strain all over the sheet at failure, not being possible to perform a 3-point average.

In this case it seems realistic to assume the strain distribution over the width would show a peak on the non-covered side, where visual observation showed debonding began. Also the strain distribution is far from uniform over the slab's length (F3, F6 F12), most probably because of non-negligible friction phenomena: the strain on the failing side (Left, F6) is sensibly higher than over the rest of the slab, but still midspan central strain will be used as a reference, for the sake of consistency.

Also in this case collapse was triggered by central strip's slipping, suddenly followed by side strips, the time lapse was so small that only one collapse load was spotted, before strength dropped to R/C only level.

Also interesting is how the stiffness reduction following debonding is way less evident rather than in the 60° sample. This might be explained considering that, in this case, the whole width is engaged by the anchor's fan, while in the 60° configuration only a central portion is covered and engaged after debonding.

90x2 [US]					
	Load	Displacement	Concrete	FRP	x
	[kip]	[in]	[%]	[%]	[in]
Elastic	1.54	0.10	-0.007%	0.009%	2.93
Cracked	3.53	0.32	-0.02%	0.11%	1.69
Yielding Start	6.92	0.83	-0.04%	0.31%	1.34
Concrete Zero	9.44	1.15	0.00%	0.53%	0.76
Debonding Right	9.47	1.16	0.00%	0.53%	-
Debonding Left	9.16	1.26	0.11%	0.48%	-
Collapse Left - Central	13.37	2.18	0.67%	0.77%	-
Collapse Left - Side	-	-	-	-	-

90x2 [SI]

	Load	Displacement	Concrete	FRP	x
	[kN]	[mm]	[%]	[%]	[mm]
Elastic	6.85	3	-0.007%	0.009%	75
Cracked	15.69	8	-0.02%	0.11%	43
Yielding Start	30.78	21	-0.04%	0.31%	34
Concrete Zero	42.00	29	0.00%	0.53%	19
Debonding Right	42.12	29	0.00%	0.53%	-
Debonding Left	40.73	32	0.11%	0.48%	-
Collapse Left - Central	59.46	55	0.67%	0.77%	-
Collapse Left - Side	-	-	-	-	-

90x2 - Experimental Matching [US]

	Load [kip]			Displacement [in]			ϵ_f [%]			x [in]		
	Exp.	Th.	Δ	Exp.	Th.	Δ	Exp.	Th.	Δ	Exp.	Th.	Δ
Elastic	1.54	-	-	0.10	-	-	0.01%	-	-	2.93	3.04	-3.56%
Cracked	3.53	-	-	0.32	-	-	0.11%	-	-	1.69	0.98	71.79%
Yielding Start	6.92	6.55	5.66%	0.83	0.51	62.96%	0.31%	0.32%	-3.27%	1.34	0.78	71.82%
Concrete Zero	9.44	-	-	1.15	-	-	0.53%	-	-	0.76	-	-
Debonding R	9.47	9.68	2.17%	1.16	0.75	54.10%	0.53%	0.70%	-23.87%	-	0.66	-
Debonding L	9.16	-	-	1.26	-	-	0.48%	-	-	-	-	-
Collapse L - C	13.37	13.67	2.22%	2.18	1.05	106.72%	0.77%	1.19%	-34.88%	-	0.62	-
Collapse L - S	-	-	-	-	-	-	-	-	-	-	-	-

90x2 - Experimental Matching [SI]

	Load [kN]			Displacement [mm]			ϵ_f [%]			x [mm]		
	Exp.	Th.	Δ	Exp.	Th.	Δ	Exp.	Th.	Δ	Exp.	Th.	Δ
Elastic	6.85	-	-	3	-	-	0.01%	-	-	75	77	-3.56%
Cracked	15.69	-	-	8	-	-	0.11%	-	-	43	25	71.79%
Yielding Start	30.78	29.13	5.66%	21	13	62.96%	0.31%	0.32%	-3.27%	34	20	71.82%
Concrete Zero	42.00	-	-	29	-	-	0.53%	-	-	19	-	-
Debonding R	42.12	43.05	-2.17%	29	19	54.10%	0.53%	0.70%	-23.87%	-	17	-
Debonding L	40.73	-	-	32	-	-	0.48%	-	-	-	-	-
Collapse L - C	59.46	60.81	-2.22%	55	27	106.72%	0.77%	1.19%	-34.88%	-	16	-
Collapse L - S	-	-	-	-	-	-	-	-	-	-	-	-

FRP Strains are measured on the central FRP strip at midspan

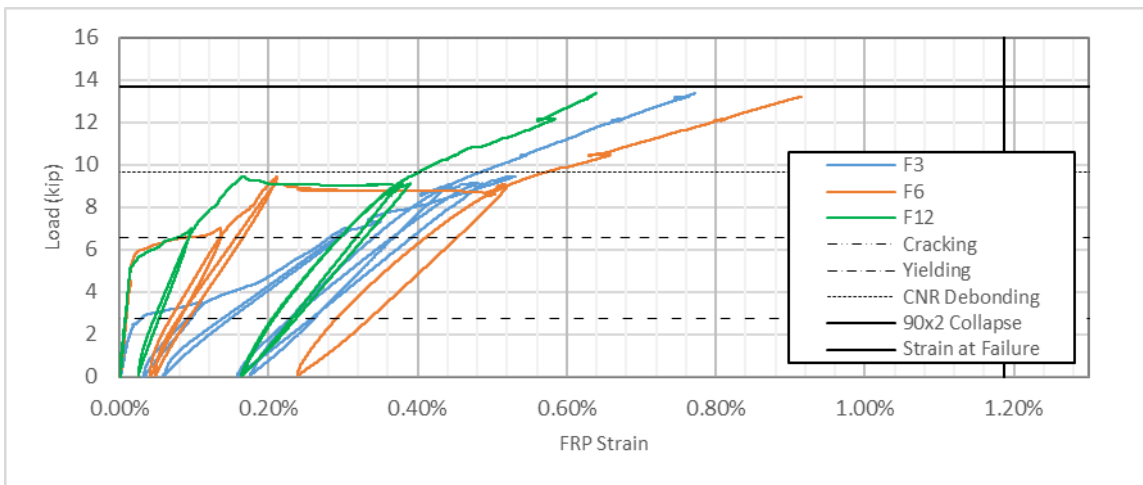
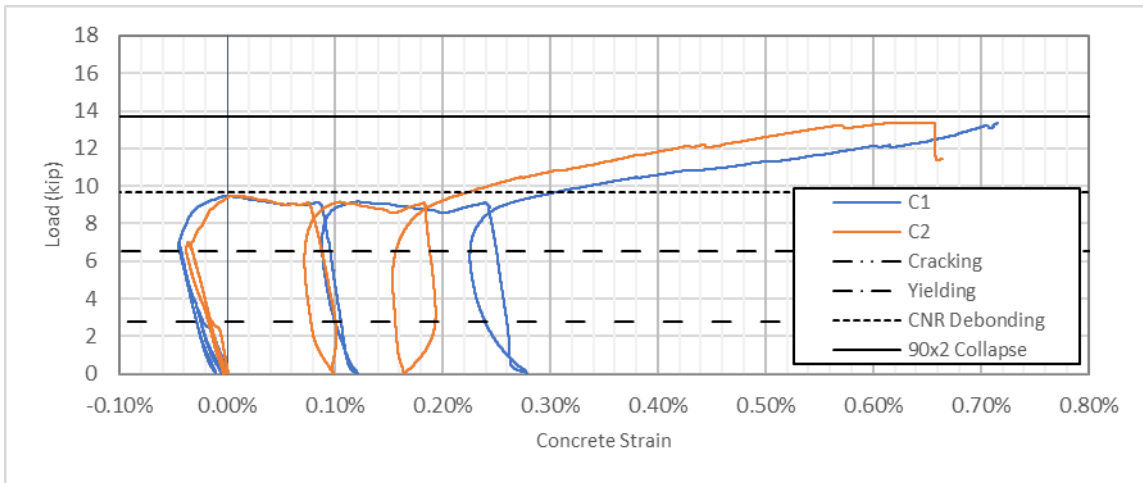
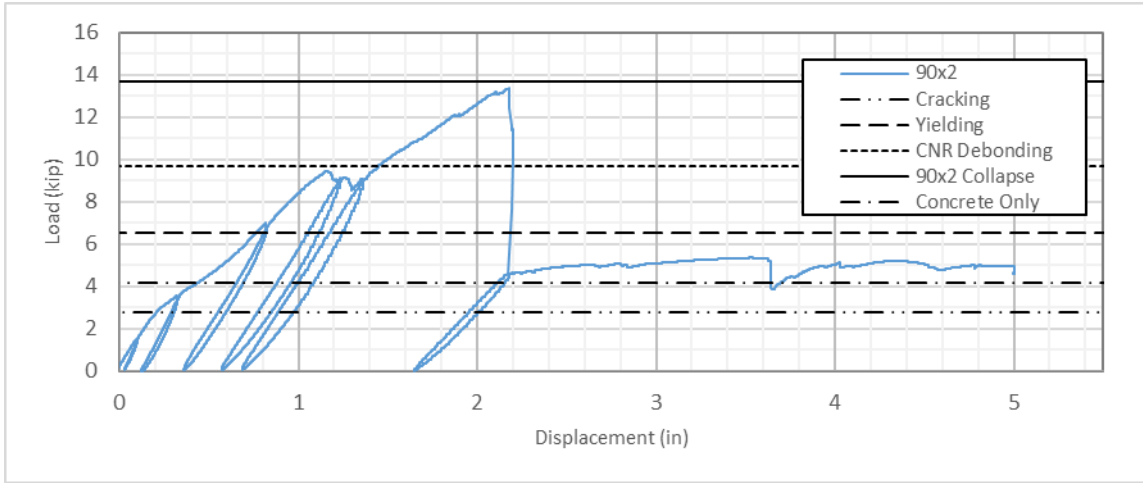


FIGURE 140 - (A) LOAD/DISPLACEMENT (B) CONCRETE STRAIN (C) FRP STRAIN (90x2)
 1 IN = 25.4 MM / 1 KIP = 4.448 kN

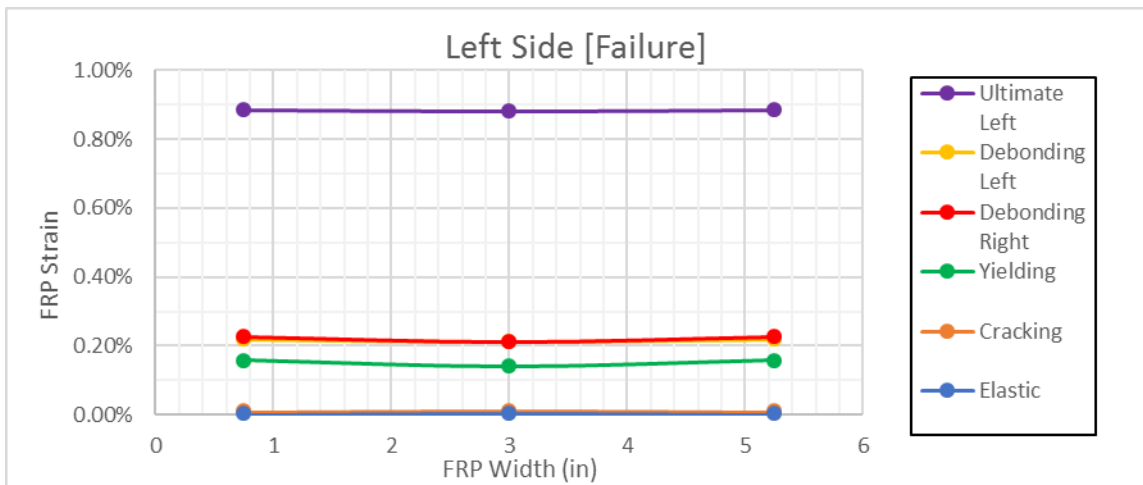
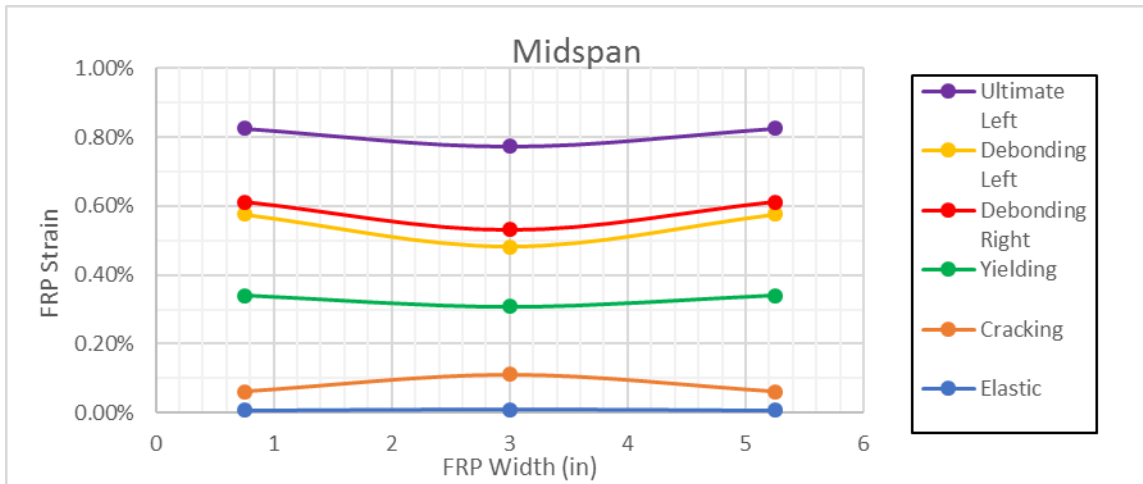
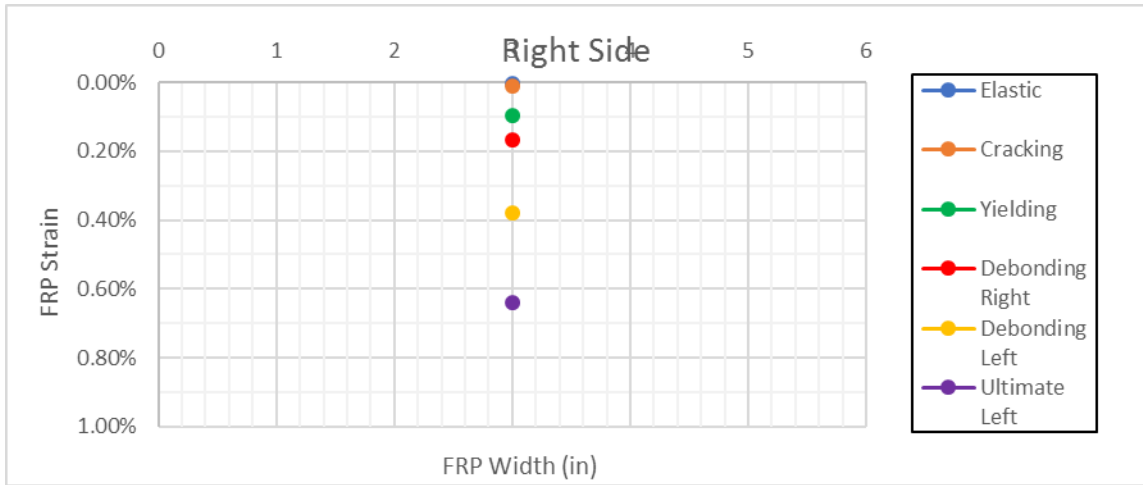


FIGURE 141 - FRP STRAINS OVER THE WIDTH (90x2). SYMMETRY IS ARTIFICIALLY IMPOSED FOR THE SAKE OF A BETTER READING. 1 IN = 25.4 MM / 1 KIP = 4.448 kN

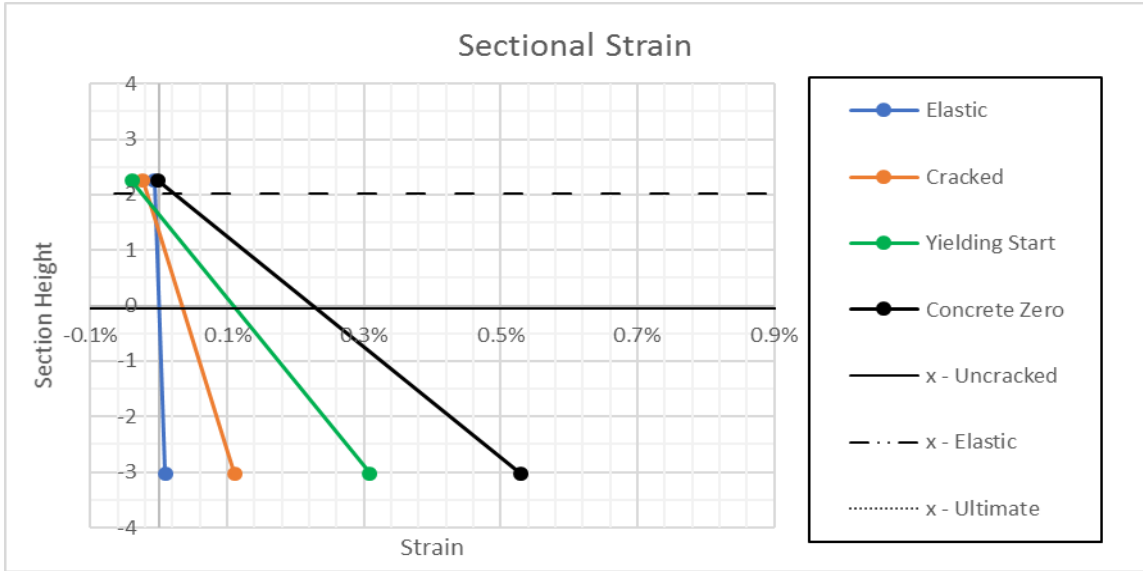


FIGURE 142 - SECTIONAL STRAINS (90x2). 1 IN = 25.4 MM / 1 KIP = 4.448 kN

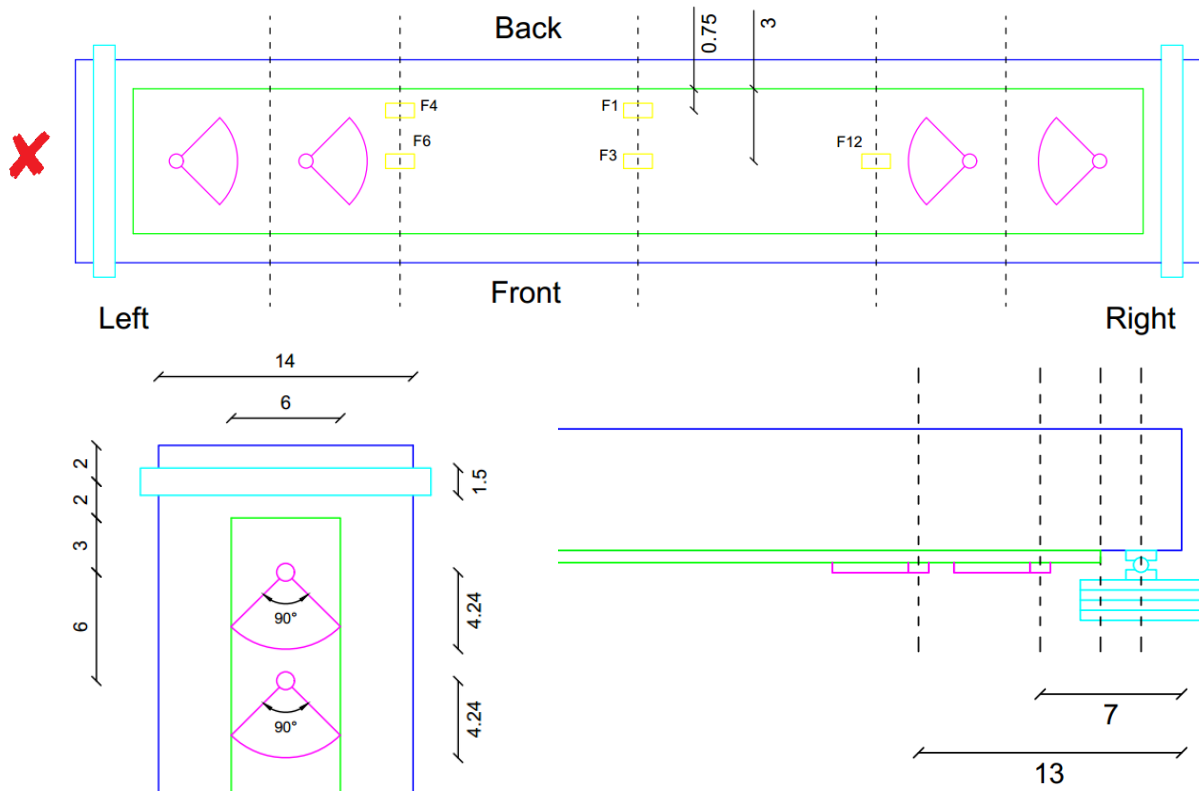


FIGURE 143 - STRAIN GAGES & GEOMETRY (90x2), THE X MARKS THE FAILING SIDE. DIMENSIONS IN INCHES. 1 IN = 25.4 MM / 1 KIP = 4.448 kN

X

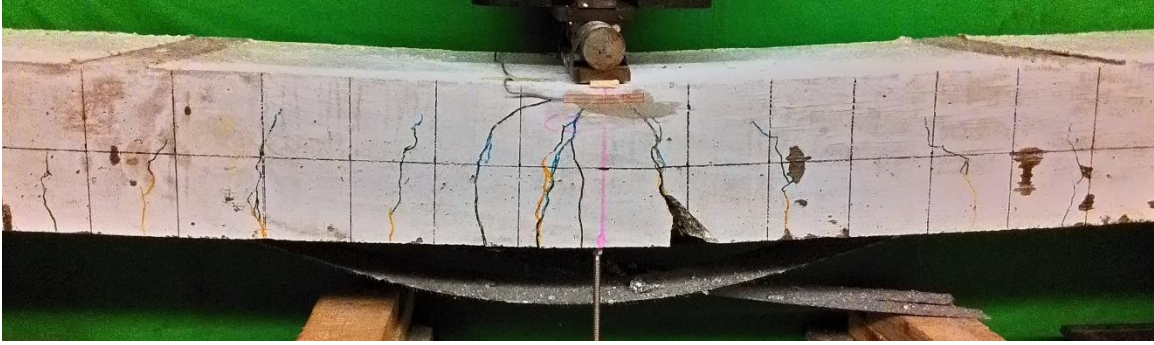


FIGURE 144 - 90x2 COLLAPSE PICTURES, THE X MARKS THE FAILING SIDE

6.1.4 Position Series

6.1.4.1 90x2 L/4

The collapse mechanism slightly varies with respect to the standard 90x2 sample. It seems that increasing the distance between anchors their behavior tends to be decoupled (13" vs 6" spacing) (330 vs 150 mm). It can be spotted how the two anchors don't fail together, but a partial slipping happens at the first anchor's location, before the ultimate load is reached and a complete slipping happens.

After the first anchor partial failure, during the re-loading cycle, a sudden, significant concrete displacement happens as well, as a consequence of concrete cracking up to the extrados. This could have been a concrete-failure-triggered collapse, but, after a sudden load drop, the slab is still able to sustain a new load cycle, bringing it to a sheet-induced failure at a level of load very well comparable to the concrete failure one.



FIGURE 145 - CONCRETE CRUSHING (90x2 L/4)

Whether the phenomena afflicted the slab's strength cannot be determined for sure, but it seems reasonable to assume not, being the ultimate load related to an anchor-triggered failure at a level of load very close to the 90x2 sample. Also, the well observed decoupled behavior, seems a sufficient explanation for the slightly reduced strength with respect to the standard 90x2 sample. For sure, the concrete loss of continuity, significantly affected the system's stiffness and increased the deflection at failure.

It seems very well plausible that, if the concrete-failure would have not happened, the slab would have just continued up to anchors' failure at the ultimate load later reached, but at a level of deflection very close to the concrete failure one. The concrete displacement made the slabs undergo a pseudo-ductile behavior, with a certain ultimate load reached and then *kept* at increasing deflection. In this case though, such a behavior seems a case-related phenomena and cannot be taken as a general trend.

To keep the discussion as general as possible, both the *failure* values will be presented and matched to the expected values in the table below, but later only the first ones will be referred as slab's failure load and deflection, willing to stay on the safe side. It should be noticed that, on the load side, this makes no difference at all while, on the deflection side, this means neglecting a significant ductile behavior that cannot be taken for guaranteed in a real case scenario.

Accepting the measured load as representative of the tested configuration, it can be notices that, with the already discussed slightly decoupled anchors' behavior, comes a slightly reduced ultimate strength, with respect to the standard 90x2 sample; the matching with the expected results, assuming perfect coupling, is anyway still good. Peculiar is the strain data matching: way better than in the standard 90x2 sample.

This matching paradox led to consider the chance the 90x2 strain data are somehow *corrupted*; most probably because of a non-perfect gage's alignment with the fibers' direction, or because of a thick epoxy layer interposition between gages and FRP sheet. It should be considered how the 90x2 sample was one of the first tested, and the quality of instruments' installation and testing performing had improved a lot up to 90x2 L/4. Also consider that, in this case, failure was induced on the right slab's side thanks to over-anchoring on the left side, this allowed to properly instrument the failing side, placing a 3-gages row in front of each anchor.

In order to properly understand the strain results on the central strip, it should be noticed that the strip is cut in three separate pieces because of the presence of the anchors themselves: one spanning over the central portion and two small portion between the anchors at each end. These short portions are not directly loaded and

obviously show a way smaller level of engagement rather than the side strips, hence the concave 2nd anchor shape, in spite of the convex 1st anchor shape. Whether the shape is concave or convex at midspan, cannot be spotted because of a lack of acquisition channels; for sure, the convex shape in front of the first anchor seems inconsistent with an expected concave shape at midspan, considering the control sample's results.



FIGURE 146 – CENTRAL STRIP, CENTRAL SPAN COLLABORATING, END PORTIONS NON-ENGAGED (90x2 L/4)

Looking at the strain evolution it can be clearly spotted the low level of engagement of the central strip behind the first anchor (F15) and the sudden engagement of the first anchor at intermediate debonding (F12, F10). Even more interesting is the sudden engagement of the second anchor (side strips) around 12 kips (F13) hence when the first anchor partially failed. No concrete or steel gages are provided, because of the already discussed lack of available channels.

On the deflection side, it is interesting to notice the very high level of deflection reached at failure, meaning an apparently very ductile behavior. The apparent ductility could be very well related only to the concrete displacement, not representing a systematic behavior. Considering the pseudo-elastic deflection as non-representative of the slab's real behavior, the specimen proved to be less ductile than the standard 90x2.

The referred strains are measured at midspan, on the central strip. After central strip's failure the maximum side value is referred, measured in front of the first anchor (F11).

90x2 L/4 - Experimental Matching [US]

	Load [kip]			Displacement [in]			ϵ_f [%]		
	Exp.	Th.	Δ	Exp.	Th.	Δ	Exp.	Th.	Δ
Elastic	1.54	-	-	0.12	-	-	0.01%	-	-
Cracked	4.04	-	-	0.33	-	-	0.18%	-	-
Yielding	7.05	6.92	1.93%	0.59	0.51	16.22%	0.30%	0.32%	-7.22%
Debonding R	9.81	9.47	3.64%	0.97	0.75	29.24%	0.65%	0.70%	-6.50%
First Anchor R	12.11	-	-	1.35	-	-	0.90%	-	-
Concrete Disp.	12.77	13.67	-6.59%	1.53	1.05	45.39%	0.97%	1.19%	-18.56%
Ultimate R - C	12.80	13.67	-6.38%	2.54	1.05	140.65%	1.08%	1.19%	-9.26%
Ultimate R - L	11.50	-	-	2.94	-	-	0.91%	-	-

90x2 L/4 - Experimental Matching [SI]

	Load [kN]			Displacement [mm]			ϵ_f [%]		
	Exp.	Th.	Δ	Exp.	Th.	Δ	Exp.	Th.	Δ
Elastic	6.83	-	-	0.53	-	-	0.01%	-	-
Cracked	17.97	-	-	1.48	-	-	0.18%	-	-
Yielding	31.37	30.78	1.93%	2.65	2.28	16.22%	0.30%	0.32%	-7.22%
Debonding R	43.65	42.12	3.64%	4.32	3.35	29.24%	0.65%	0.70%	-6.50%
First Anchor R	53.88	-	-	5.99	-	-	0.90%	-	-
Concrete Disp.	56.80	60.81	-6.59%	6.82	4.69	45.39%	0.97%	1.19%	-18.56%
Ultimate R - C	56.93	60.81	-6.38%	11.28	4.69	140.65%	1.08%	1.19%	-9.26%
Ultimate R - L	51.17	-	-	13.09	-	-	0.91%	-	-

FRP Strains are measured on the central FRP strip at midspan

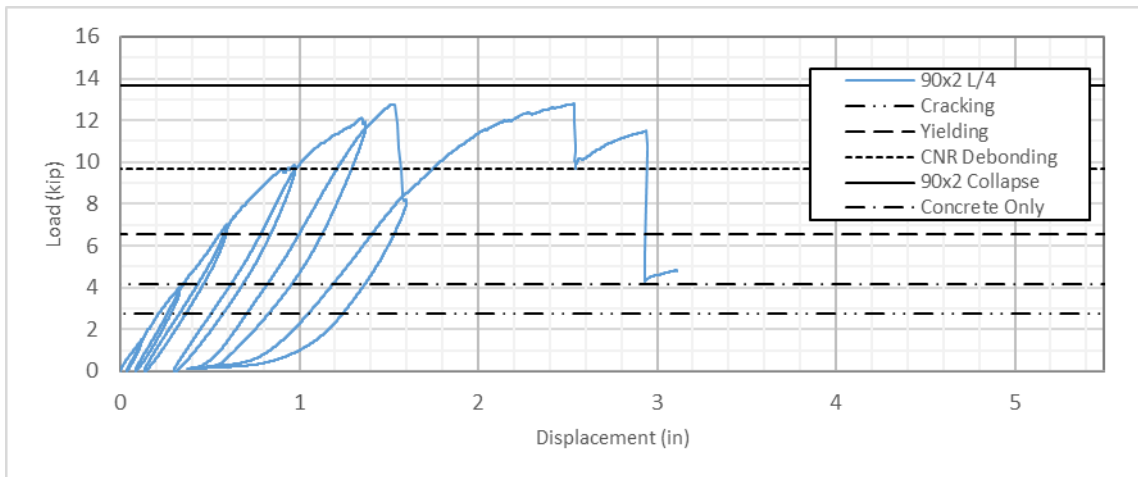


FIGURE 147 - LOAD/DISPLACEMENT (90x2 L/4)

1 IN = 25.4 MM / 1 KIP = 4.448 kN

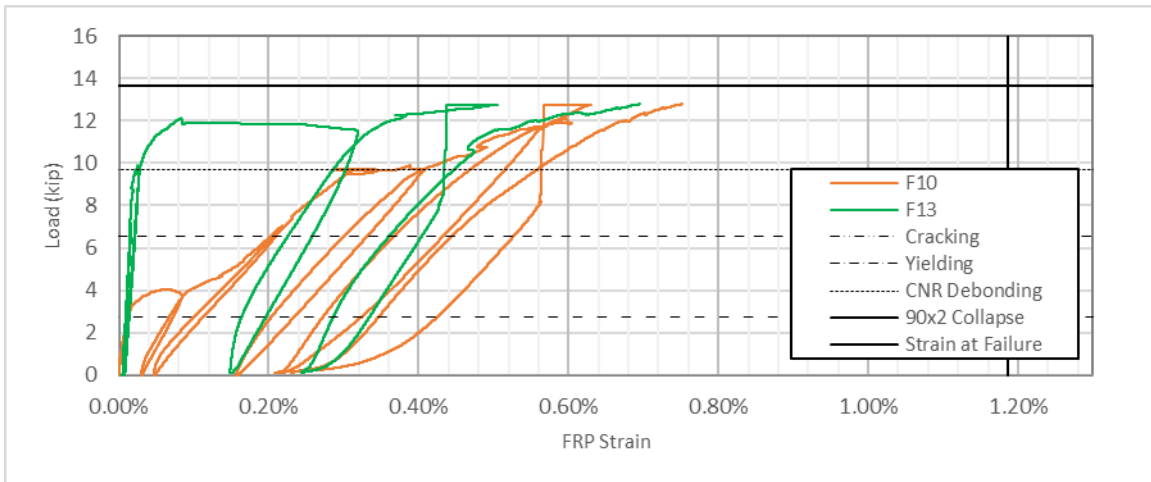
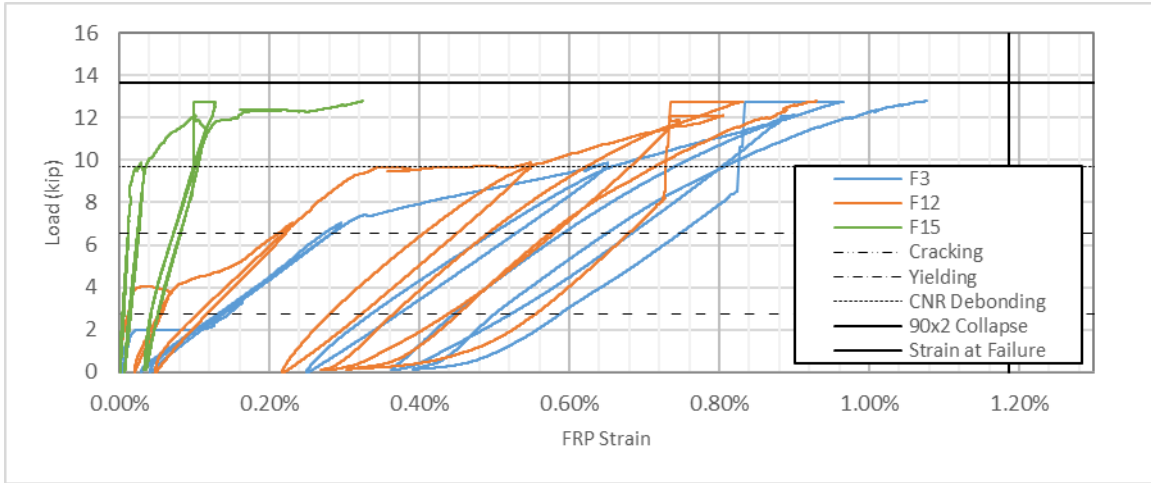
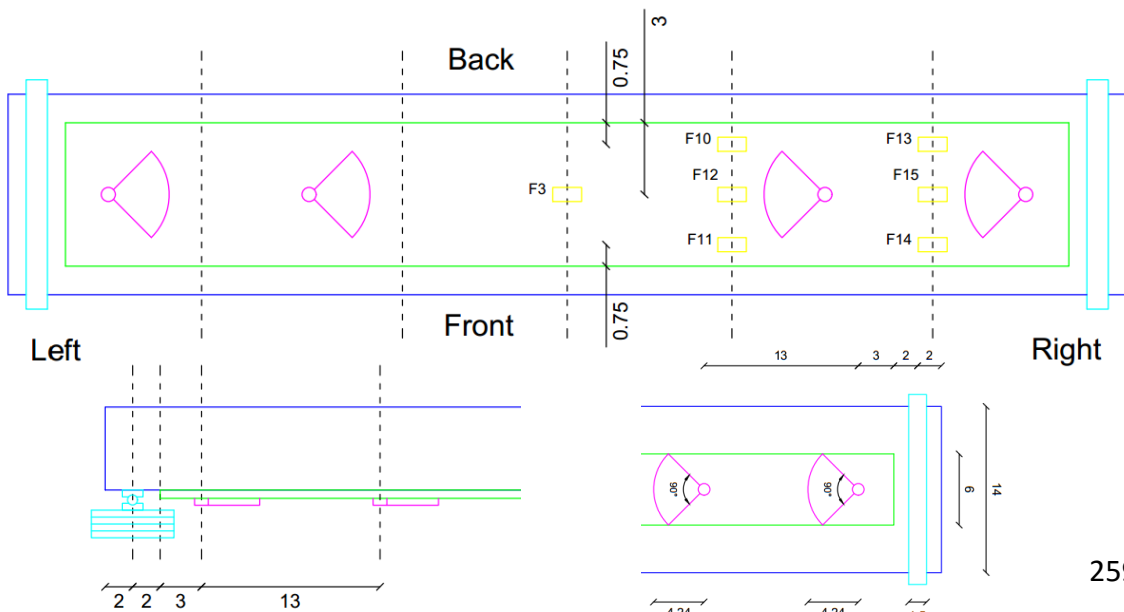


FIGURE 148 - (A, B) FRP STRAINS (C, D) STRAIN GAGES LOCATION & GEOMETRY (90x2 L/4). DIMENSIONS IN INCHES. 1 IN = 25.4 MM / 1 KIP = 4.448 KN



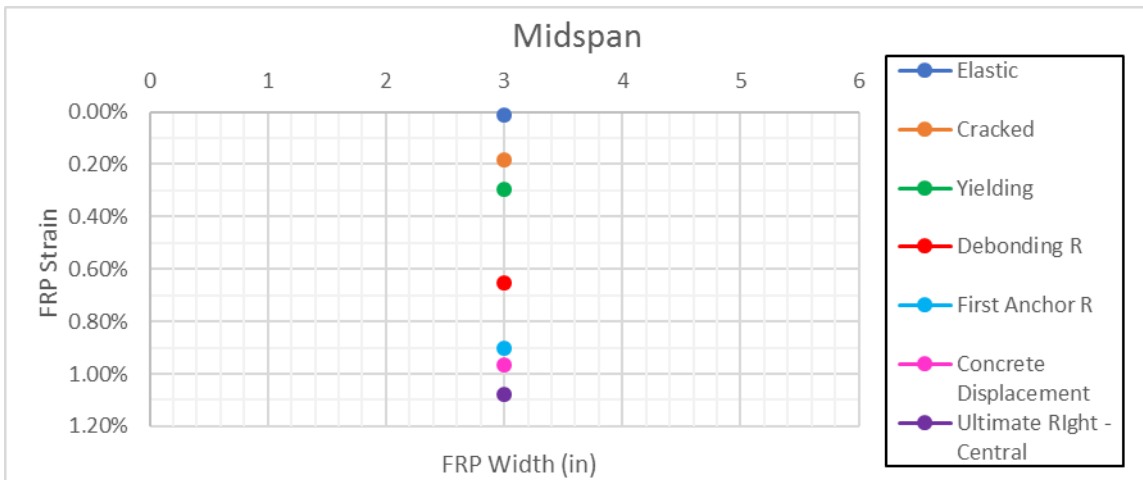
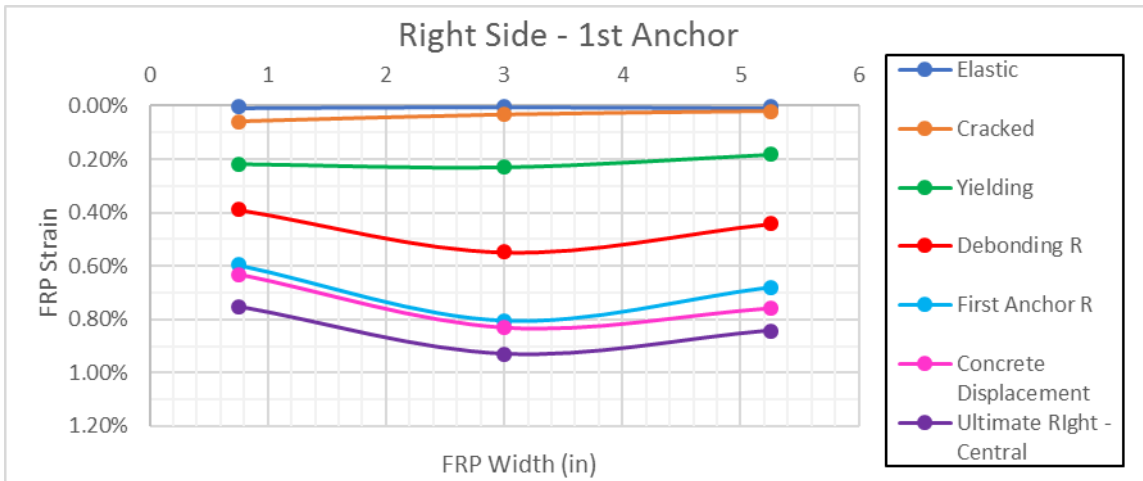
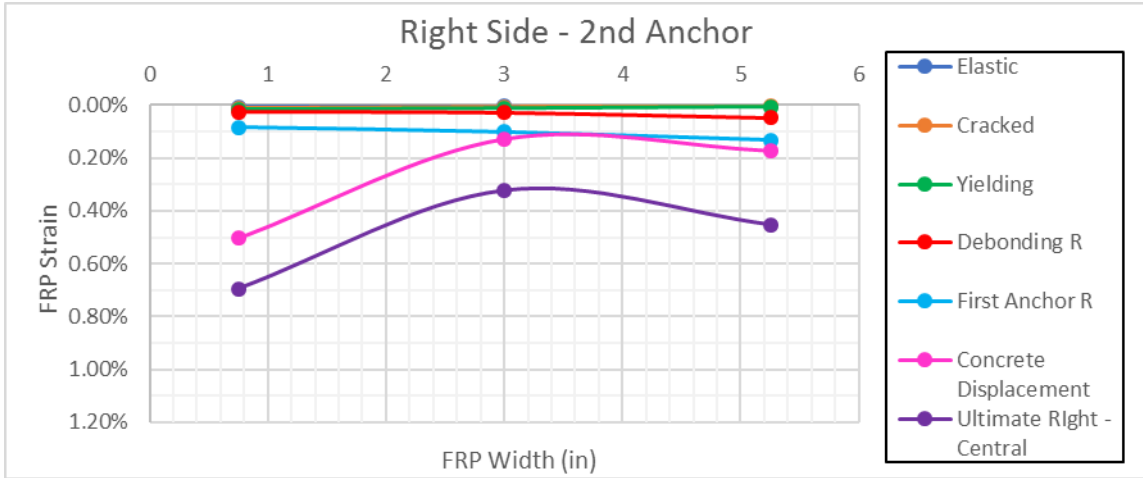


FIGURE 149 - FRP STRAINS OVER SHEET'S WIDTH (90x2 L/4)
 1 IN = 25.4 MM / 1 KIP = 4.448 kN



FIGURE 150 - 90x2 L/4 COLLAPSE PICTURES, THE X MARKS THE FAILING SIDE

6.1.4.2 90x2 L/3

Further increasing the anchors' distance, now 19'' (480 mm), further decouples their behavior and deeply modifies the overall collapse mechanism. The central anchors, located in a region of either high flexural and shear stresses, acts like a cracking trigger: at increasing load, a large cracks develops starting from the discontinuity represented by the dowel's hole; from this crack debonding starts, behind the first anchor and back to engaging the second one, at the slab's very end.

Because of this particular debonding pattern, the end anchors find himself engaged by a resultant way higher than the central anchor, that anyway contributes to the system's overall strength: at increasing load, the end anchor (on the left side) is the first to fail.

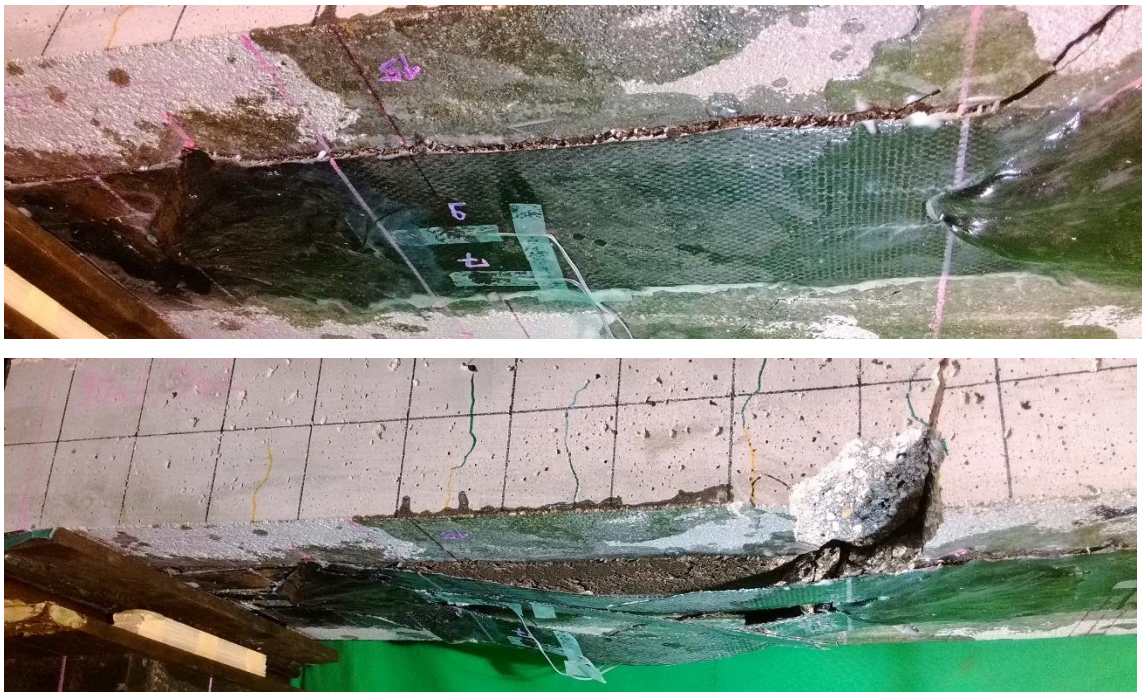


FIGURE 151 - DEBONDING & FAILURE BEHIND THE FIRST ANCHOR (90x2 L/3)

Collapse is triggered by the front side strip, in spite of the central one, as usually observed; that makes sense, considering the side strips absorb also a portion of the load coming from the central span, because of provided continuity, while the central strip only carries load directly transferred behind the central anchor, because of the anchor-induced discontinuity.

In this case the experimental load is significantly lower than the predicted one, while the strains at failure follows a completely different pattern than the simply, uniform assumed one, reflecting the actual level of engagement of each anchor and sheet strip. Also, the peak load is reached while all the anchors and sheet portions are still working, after peak is reached, a series of partial failures is triggered, progressively reducing the system's strength, hence providing some ductility at the cost of a reduced strength, but anyway not reaching the standard 90x2 deflection at failure.

Also notice that the pseudo-ductility is related to an actual load drop, hence can happen only in a displacement-controlled experimental scenario, even if, not being related to any concrete failure, can be taken as a systematic behavior and be interpreted, at least, as a residual strength after failure.

Interesting to point out, looking at the strains evolution at increasing load, is the sudden engagement of the end anchor, once debonding happens behind the central one. Particularly interesting is the high level of engagement on the central strip, usually way lower, when the end anchor works in pair with the front one.

In this case the whole length was instrumented, that allows to see how the non-failing side is practically non-engaged, at least behind the first anchor; this because engagement, due to the particular collapse mechanism, mainly comes directly from debonding behind the central anchor on the left side.

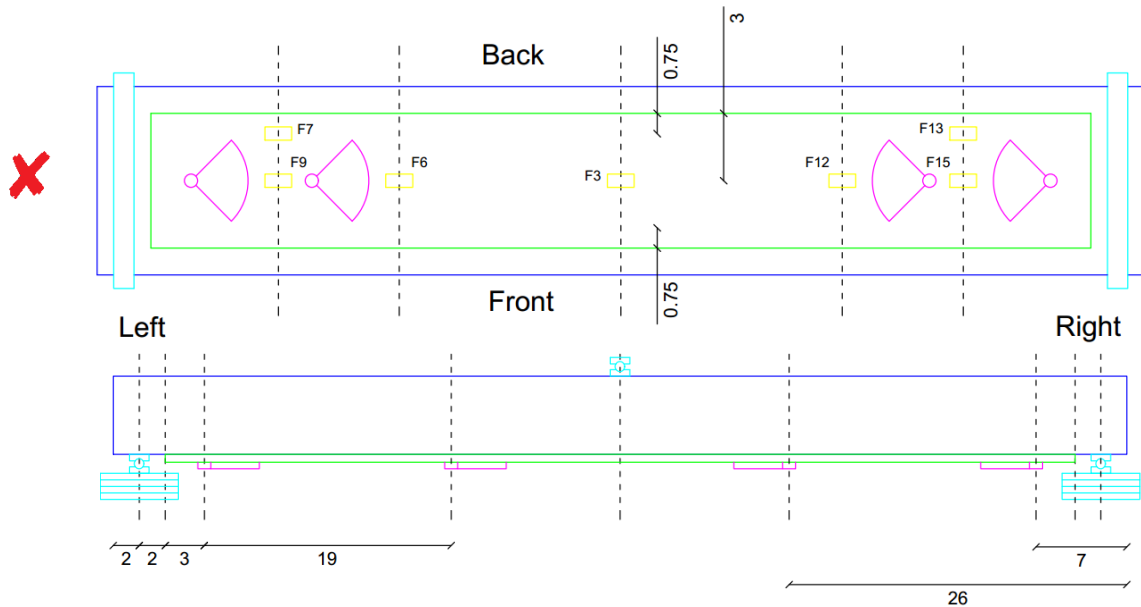


FIGURE 152 - STRAIN GAGES LOCATION & GEOMETRY (90x2 L/3), THE X MARKS THE FAILING SIDE. DIMENSIONS IN INCHES. 1 IN = 25.4 MM / 1 KIP = 4.448 kN

90x2 L/3 - Experimental Matching [US]									
	Load [kip]			Deflection [in]			ϵ_f [%]		
	Exp.	Th.	Δ	Exp.	Th.	Δ	Exp.	Th.	Δ
Elastic	1.56	-	-	0.08	-	-	0.01%	-	-
Cracked	3.15	-	-	0.20	-	-	0.12%	-	-
Yielded	7.17	6.55	9.42%	0.54	0.51	4.84%	0.36%	0.32%	12.41%
Debonding	9.72	9.68	0.48%	0.81	0.75	7.45%	0.70%	0.70%	0.17%
Peak	11.83	13.67	-13.43%	1.10	1.05	4.38%	0.77%	1.19%	-35.05%
Ultimate - L - End - F	11.40	-	-	1.11	-	-	0.71%	-	-
Ultimate - Left - End - Central	8.81	-	-	1.39	-	-	0.58%	-	-
Ultimate - Left - End - Back	9.47	-	-	1.55	-	-	0.61%	-	-
Ultimate - Left - Intermediate	10.54	13.67	-22.91%	1.78	1.05	69.04%	0.65%	1.19%	-44.88%

90x2 L/3 - C-FRP Experimental Matching [SI]									
	Load [kN]			Load [kN]			ϵ_f [%]		
	Exp.	Th.	Δ	Exp.	Th.	Δ	Exp.	Th.	Δ
Elastic	6.92	-	-	2	-	-	0.01%	-	-
Cracked	14.01	-	-	5	-	-	0.12%	-	-
Yielded	31.87	29.13	9.42%	14	13	4.84%	0.36%	0.32%	12.41%
Debonding	43.26	43.05	0.48%	21	19	7.45%	0.70%	0.70%	0.17%
Peak	52.64	60.81	-13.43%	28	27	4.38%	0.77%	1.19%	-35.05%
Ultimate - L - End - F	50.72	-	-	28	-	-	0.71%	-	-
Ultimate - Left - End - Central	39.19	-	-	35	-	-	0.58%	-	-
Ultimate - Left - End - Back	42.10	-	-	39	-	-	0.61%	-	-
Ultimate - Left - Intermediate	46.88	60.81	-22.91%	45	27	69.04%	0.65%	1.19%	-44.88%

FRP Strains are measured on the central FRP strip at midspan

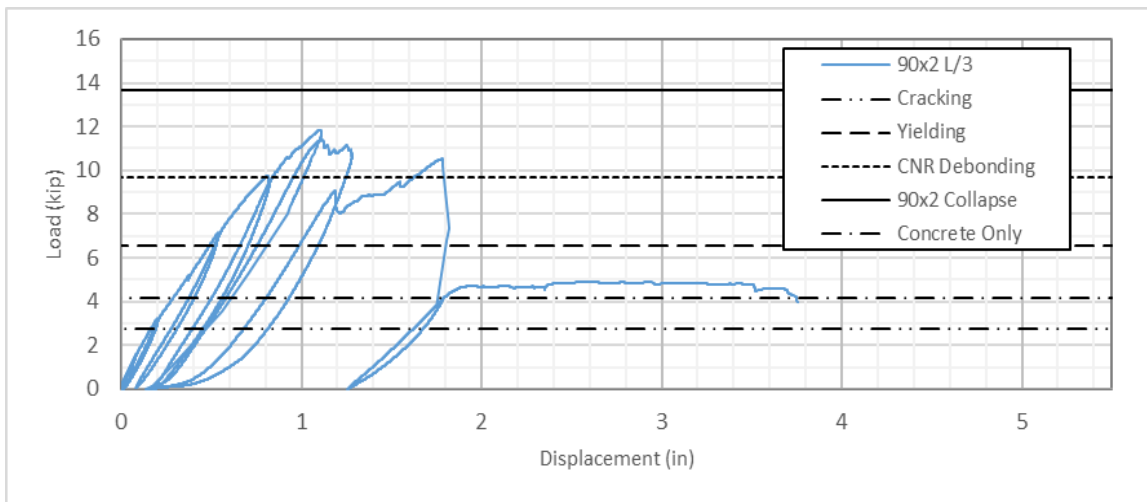


FIGURE 153 - LOAD/DISPLACEMENT (90x2 L/3)

1 IN = 25.4 MM / 1 KIP = 4.448 kN

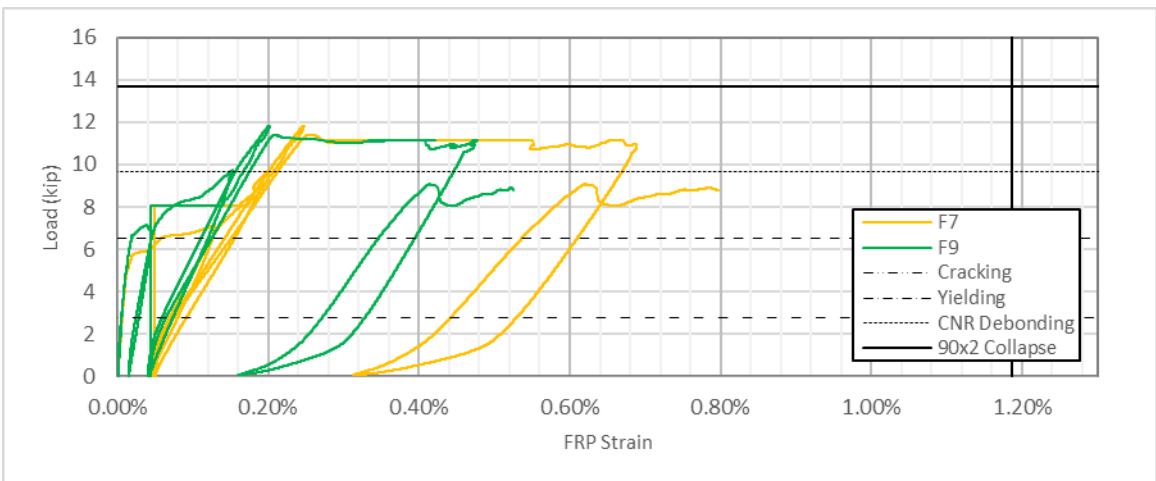
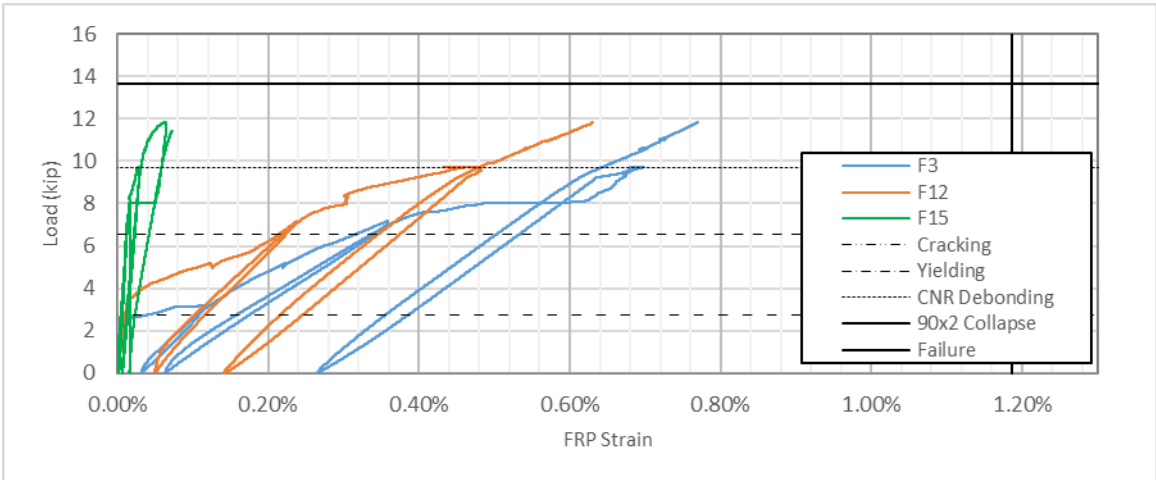
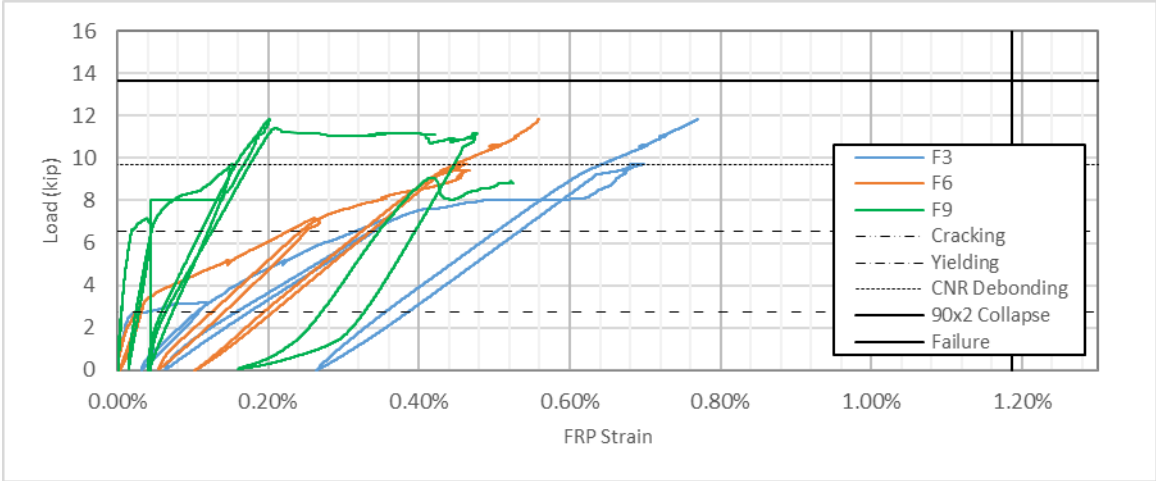


FIGURE 154 - FRP STRAINS (90x2 L/3)
 1 IN = 25.4 MM / 1 KIP = 4.448 kN

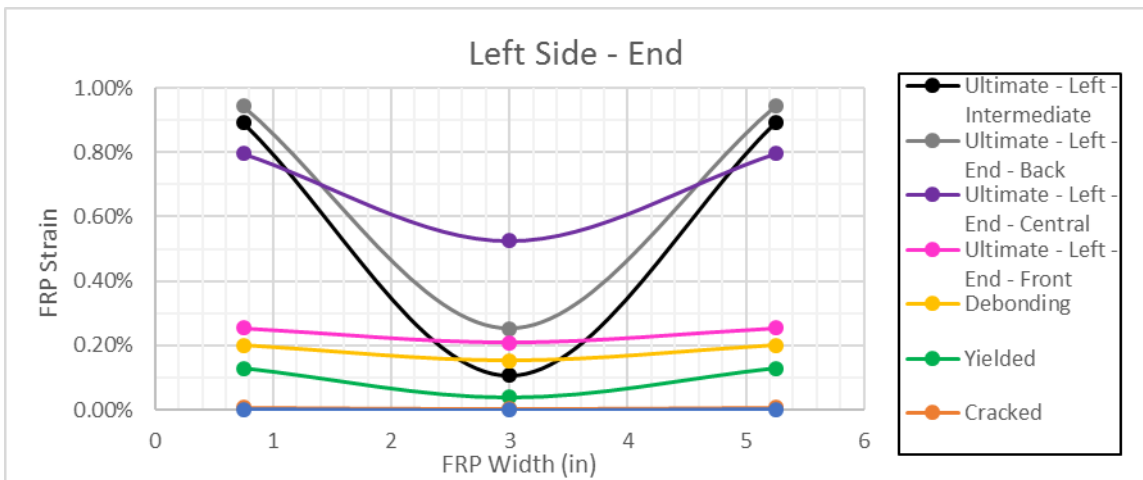
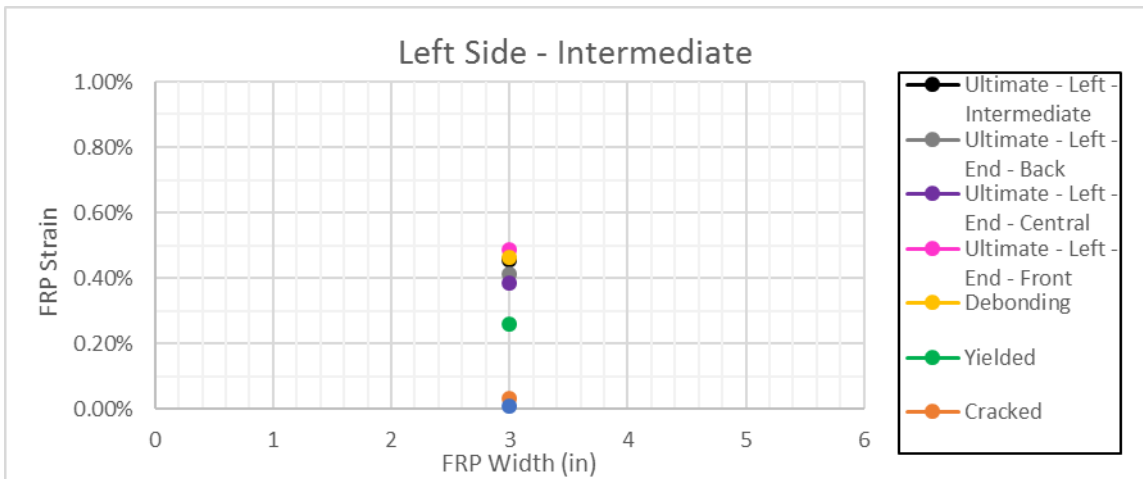
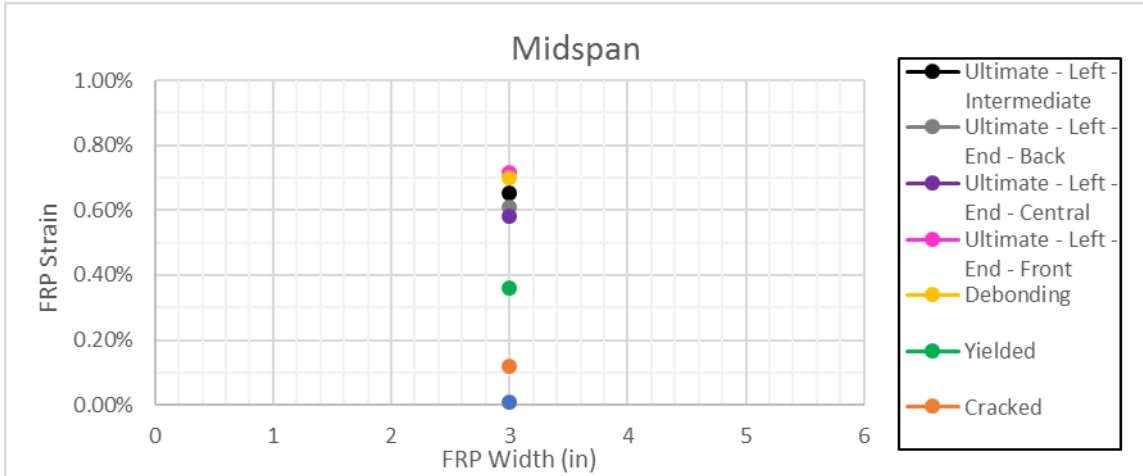


FIGURE 156 - FRP STRAINS OVER THE WIDTH, LEFT SIDE (90x2 L/3). SYMMETRY IS ARTIFICIALLY IMPOSED FOR THE SAKE OF A BETTER READING. 1 IN = 25.4 MM / 1 KIP = 4.448 kN

X



FIGURE 157 - 90x2 L/3 COLLAPSE PICTURES, THE X MARKS THE FAILING SIDE

6.1.5 Number of Anchors Series

6.1.5.1 90x3

Having noticed the completely decoupled behavior in sample 90x2 L/3, a third anchor was placed in between the two already discussed ones, hoping to prevent cracking and re-couple the joint behavior. The new anchor spaces 9'' (225 mm) from the end one and 10'' (254 mm) from the central one.

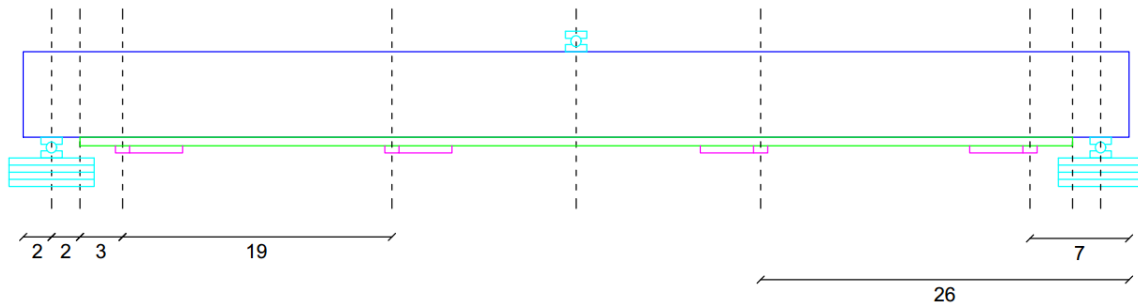


FIGURE 158 - 90x2 L/3. DIMENSIONS ARE IN INCHES, 1 IN = 25.4 MM / 1 KIP = 4.448 kN

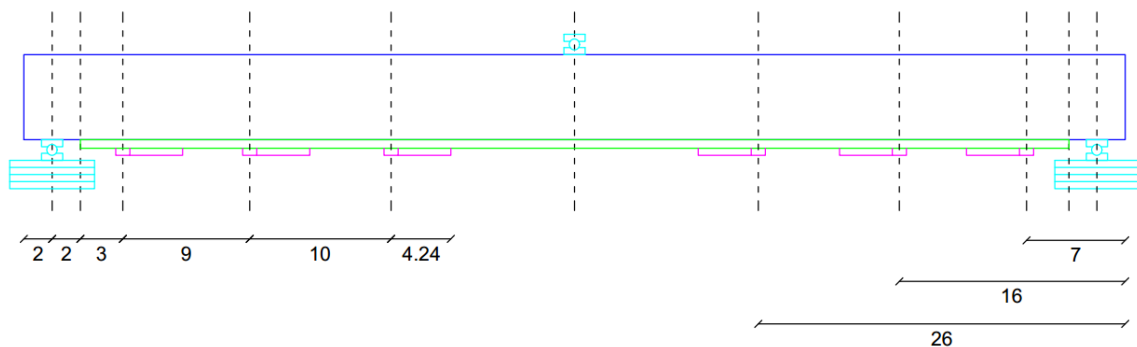


FIGURE 159 - 90x3. DIMENSIONS ARE IN INCHES, 1 IN = 25.4 MM / 1 KIP = 4.448 kN

The collapse mechanism, though, remained a decoupled one, very similar to what experienced in the 90x2 L/3 case: the first (central) anchor triggers debonding and the second one is the first to be engaged and independently collapse; after second anchor's collapse, the third (end) one is engaged and fails once the system reach is peak strength.

The central anchor slightly contributes to the overall strength and fails along with the end one, at a peak load in between the standard coupled 90x2 and the fully uncoupled

90x2 L/3 samples. The failure is triggered by the side strip on the slab's back, consistently with a lower central strip engagement, because of the already discussed, anchors-induced, discontinuity.



FIGURE 160 - DEBONDING BEHIND THE FIRST ANCHOR (90x3)

No load/strain matching is proposed: considering the particular strain and engagement pattern, and the peculiar failure mode, a matching with a theoretic 90x3 end joint seems meaningless. The load/deflection diagram shows an ultimate load capped at about 12 kips, while a series of partial failures allows the deflection to increase in a somehow pseudo-ductile behavior.

Considering the strain evolution, the first anchors' engagement appears to remain more or less constant after debonding and limited when compared to the back anchors. The second anchor shows a sudden engagement as soon as debonding happens, while the third one is suddenly engaged as the second fails. This behavior can be easily spotted looking at the number of cycles before and after sudden slipping in front of each anchor's (F13, F17). The central slip's engagement is kept low by the already discussed discontinuity: the portion in front of the second anchor particularly fails very soon, while the side strips are basically symmetrically engaged.

From the deflection prospective, a pseudo-ductile behavior at anchors' consequently collapses can be noticed, also in this case the ultimate deflection characterizing the 90x2 sample cannot be reached, but such a behavior, not related to any concrete slipping, can be considered systematic. Nevertheless, in order to stay on the safe side, not sure whether such a behavior can be guaranteed in a real load-controlled case scenario, the first peak will be assumed as the structure's ultimate load and deflection.

90x3 [US]			
	Load	Displacement	FRP
	[kip]	[in]	[%]
Elastic	1.55	0.13	0.01%
Cracked	4.05	0.44	0.08%
Yielding	7.12	0.74	0.22%
Debonding R - 2nd Anchor	12.32	1.37	0.60%
Ultimate - 2nd Anchor - Central	11.58	1.54	0.58%
Ultimate - 2nd Anchor - Front	12.48	1.74	0.64%
Ultimate - 2nd Anchor - Back	12.61	1.81	0.65%
Ultimate - 3rd Anchor - Back	12.67	1.99	0.66%
Ultimate - 3rd Anchor - Front	0.02	1.51	0.01%

90x3 [SI]			
	Load	Load	FRP
	[kip]	[kip]	[%]
Elastic	6.88	3	0.01%
Cracked	18.00	11	0.08%
Yielding	31.66	19	0.22%
Debonding R - 2nd Anchor	54.79	35	0.60%
Ultimate - 2nd Anchor - Central	51.50	39	0.58%
Ultimate - 2nd Anchor - Front	55.53	44	0.64%
Ultimate - 2nd Anchor - Back	56.07	46	0.65%
Ultimate - 3rd Anchor - Back	56.36	51	0.66%
Ultimate - 3rd Anchor - Front	0.09	38	0.01%

FRP Strains are measured on the central FRP strip in front of the first right side anchor (failing side)

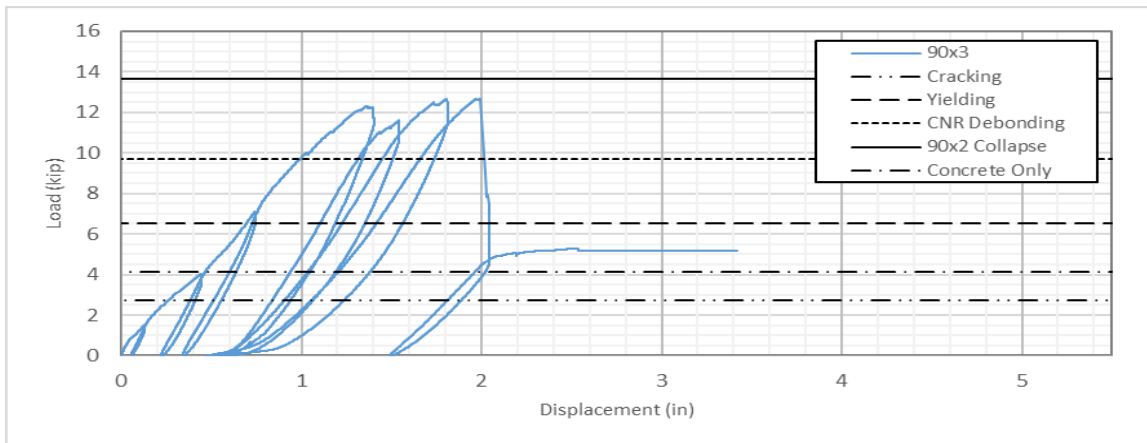


FIGURE 161 - LOAD/DISPLACEMENT (90X3). 1 IN = 25.4 MM / 1 KIP = 4.448 KN

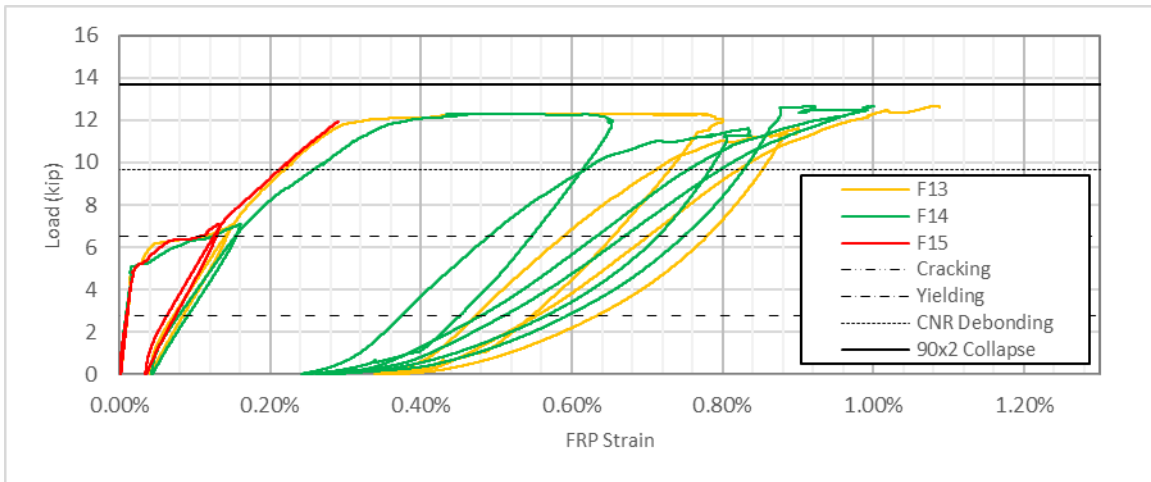
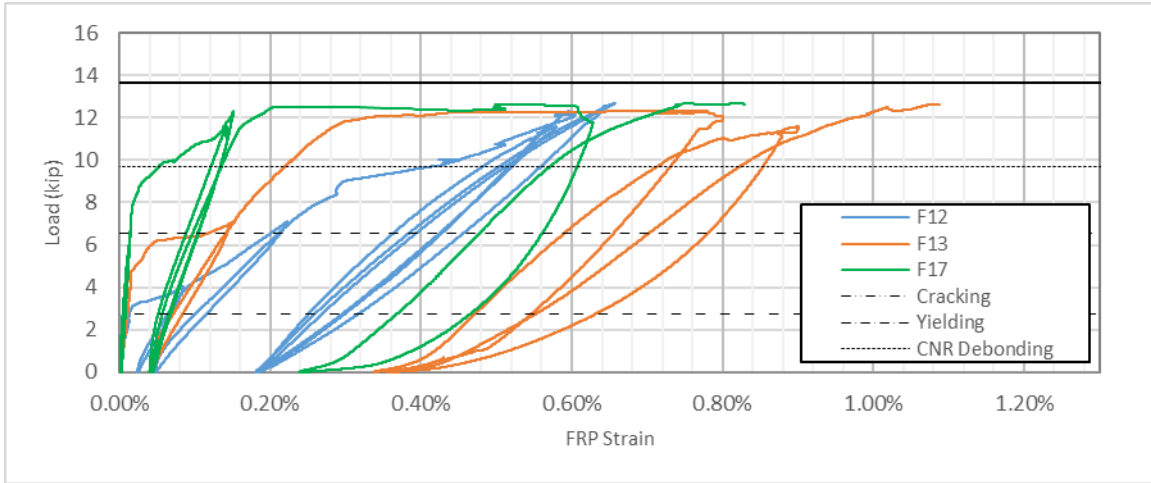


FIGURE 162 - FRP STRAINS (90x3). 1 IN = 25.4 MM / 1 KIP = 4.448 kN

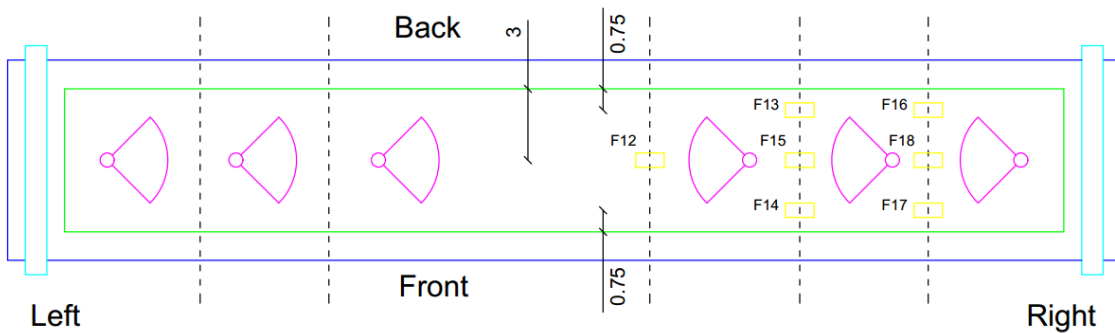


FIGURE 163 - STRAIN GAGES LOCATION (90x3), THE X MARKS THE FAILING SIDE
DIMENSIONS ARE IN INCHES. 1 IN = 25.4 MM / 1 KIP = 4.448 kN

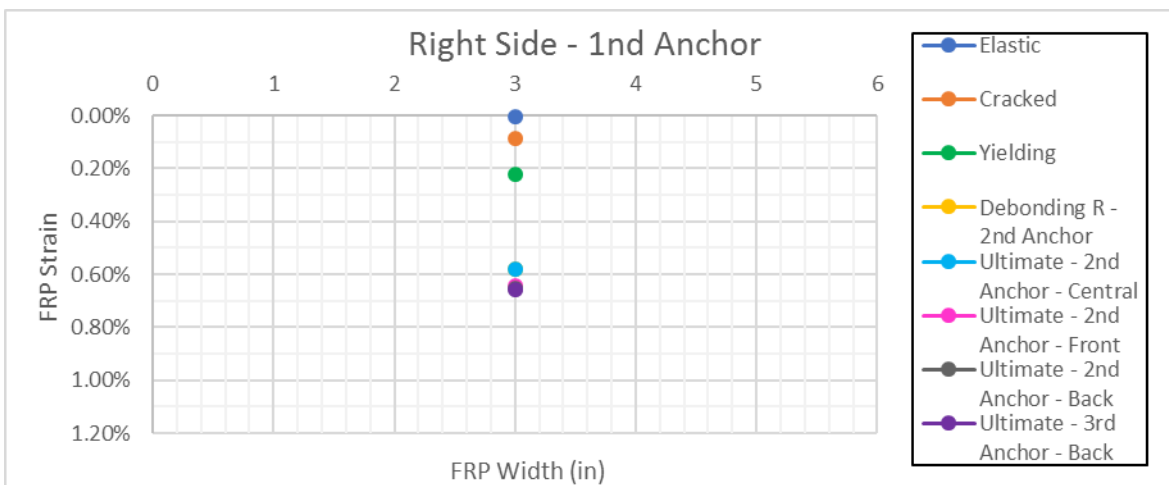
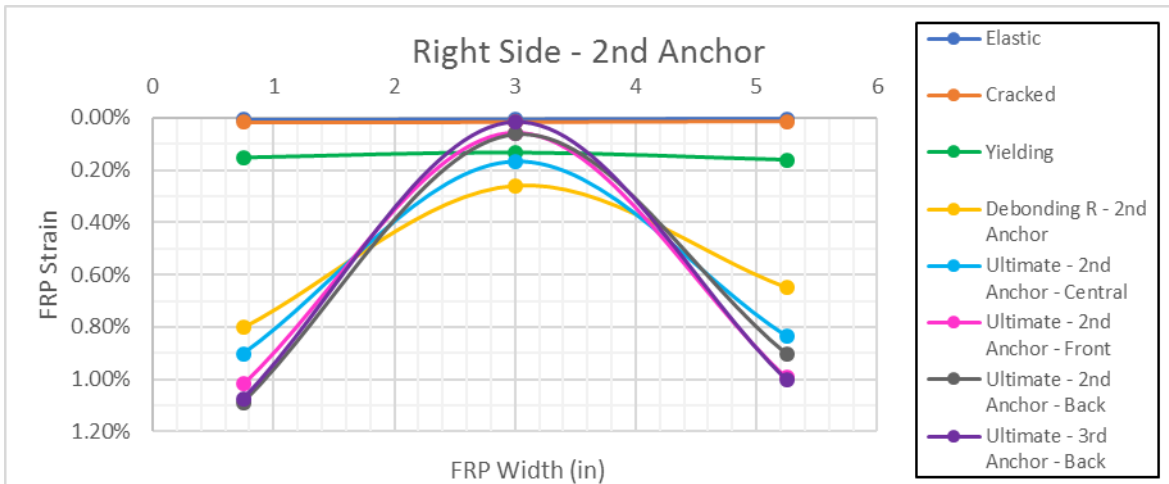


FIGURE 164 - FRP STRAINS OVER SHEET'S WIDTH (90x3). SYMMETRY IS ARTIFICIALLY IMPOSED FOR THE SAKE OF A BETTER READING. 1 IN = 25.4 MM / 1 KIP = 4.448 kN

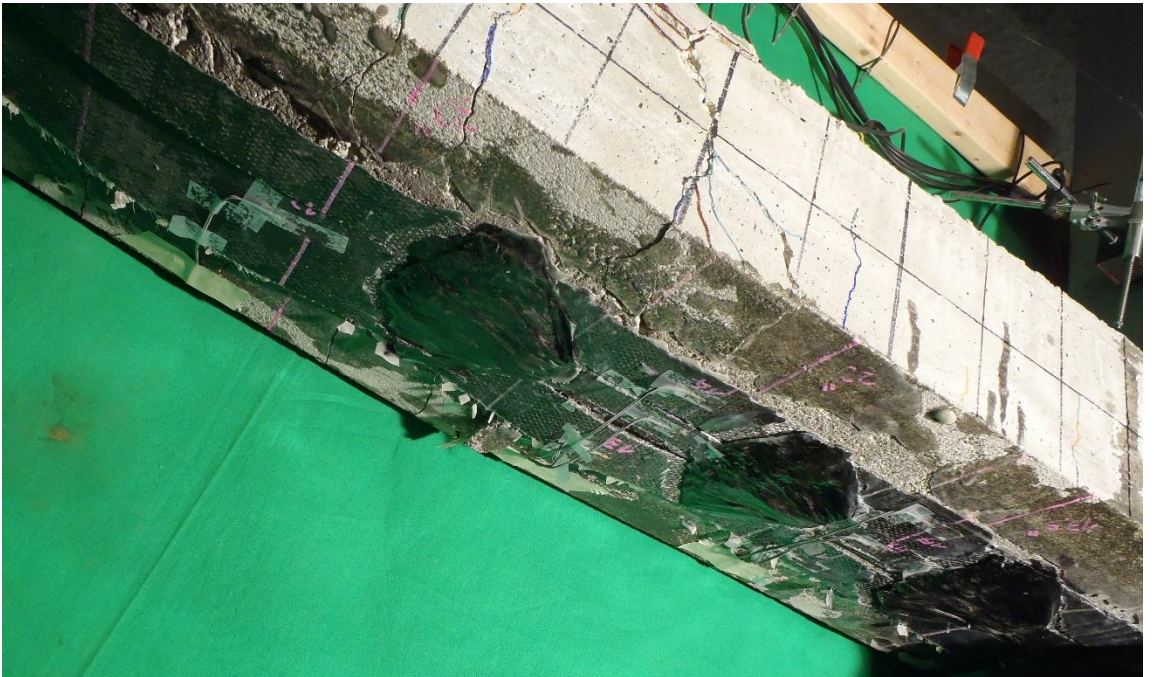


FIGURE 165 - 90X3 COLLAPSE PICTURES, THE X MARKS THE FAILING SIDE

6.1.6 Sandwich Effectiveness Series

As a general notice, the shear test's sandwich results seems not to be confirmed in flexural situations; the results will be matched also with 90x2 expected values, showing a way better matching and suggesting a standard 90x2 strength for sandwich configurations. Further discussion will follow.

6.1.6.1 Sx2-1

The slab shows a behavior very in line with the standard 90x2 sample, also with a failure triggered on the right side by central strip failure. The main difference, when compared to the 90x2 sample, is the sensibly higher deflection at failure, hence a sensibly higher system's ductility; this may be related to a better stress distribution over the slab, helped by the patch sandwich itself. The uniform stress distribution is very well confirmed by strain data over the width, even though, without a 3-point characterization, the conclusion cannot be taken for granted. A confirmation will actually come from the other sandwich specimen, later tested.

Such a behavior seems linked to another peculiarity: at a certain point it is possible to spot debonding going through the first anchor, without an actual failure of the anchor itself. A direct observation is made impossible by the sandwich patch, but it seems reasonable to assume the patch is helping the anchor's fan to stay attached to the FRP sheet, even after debonding from concrete under the fan itself.



FIGURE 166 - DEBONDING PAST A STILL COLLABORATING FIRST ANCHOR & FIRST ANCHOR FAILING ALONG WITH THE OVERALL JOINT (Sx2-1)

As seen in the standard 90x2 sample, debonding going through the first anchor actually means the anchor's failing and along with it the overall joint. The presence of the patch allows the first anchor to cooperate as long as the end anchor is still bonded; this means no strength increment are related to the patch itself, but a relevant pseudo-ductile behavior can be guaranteed. Such a behavior can be very well assumed as systematic, though it is unclear whether it can be exploited in real-case scenarios.

It should be noted that, not being able to take for guaranteed such a ductile behavior in a real load-controlled scenario, the first peak will be assumed as failure load and deflection, wishing to stay on the safe side. All the peak value will be anyway reported below and compared to the expected failure values; further discussion will follow.

The peak load reached is sensibly lower than what achieved with the standard 90x2 sample, the results seems paradoxical, not seeing any reason why an additional patch would reduce the system's strength. The reason actually lies in a sub-optimal FRP installation that was possible to spot in a second time, even if the anchor itself was already covered by the patch, thanks to visive records of the all installation process. Namely, the pictures show how, on the slab's failing side, on the sheet's failure-triggering strip, a significant gap existed in the anchor fan, providing a sensibly lower anchored area, hence the premature failure.



FIGURE 167 - ILL-INSTALLED RIGHT JOINT (Sx2-1)

Regarding the strain evolution at increasing load, a jump is clearly visible, the reasons are unclear, but most probably related to the acquisition equipment; the issue is not affecting any significant portion of the diagram, even though it makes the overall diagram quite messy. Good concrete readings are available allowing to confirm a linear behavior up to debonding. The strain errors are in line with the 90x2 sample ones.

SX2-1 [US]					
	Load	Displacement	Concrete	FRP	x
	[kip]	[in]	[%]	[%]	[in]
Elastic	1.73	0.16	-0.003%	0.012%	1.80
Cracked	3.99	0.38	-0.02%	0.17%	1.18
Yielding Start	7.57	0.72	-0.02%	0.37%	1.07
Concrete Zero	9.68	0.94	0.00%	0.56%	0.75
Debonding L&R	10.70	1.20	0.08%	0.62%	-
First Anchor Right	12.31	1.61	0.44%	0.76%	-
Collapse - Right - Central	12.40	2.74	-5.44%	0.88%	-
Collapse - Right - Back	12.25	3.27	-5.44%	0.74%	-

SX2-1 [SI]					
	Load	Displacement	Concrete	FRP	x
	[kN]	[mm]	[%]	[%]	[mm]
Elastic	7.71	4	-0.003%	0.012%	46
Cracked	17.73	10	-0.02%	0.17%	30
Yielding Start	33.69	18	-0.02%	0.37%	27
Concrete Zero	43.04	24	0.00%	0.56%	19
Debonding L&R	47.59	30	0.08%	0.62%	-
First Anchor Right	54.75	41	0.44%	0.76%	-
Collapse - Right - Central	55.18	70	-5.44%	0.88%	-
Collapse - Right - Back	54.48	83	-5.44%	0.74%	-

FRP Strains are measured on the central FRP strip at midspan

Sx2-1 - Experimental Matching [US]

	Load [kip]			Displacement [in]			ϵ_f [%]			x [in]		
	Exp.	Th.	Δ	Exp.	Th.	Δ	Exp.	Th.	Δ	Exp.	Th.	Δ
Elastic	1.73	-	-	0.16	-	-	0.01%	-	-	1.80	3.04	-40.96%
Cracked	3.99	-	-	0.38	-	-	0.17%	-	-	1.18	0.98	20.00%
Yielding Start	7.57	6.55	15.65%	0.72	0.51	41.08%	0.37%	0.32%	17.11%	1.07	0.78	37.09%
Concrete Zero	9.68	-	-	0.94	-	-	0.56%	-	-	0.75	-	-
Debonding L&R	10.70	9.68	10.55%	1.20	0.75	59.56%	0.62%	0.70%	-10.59%	-	0.66	-
First Anchor R	12.31	16.21	-24.06%	1.61	1.31	23.05%	0.76%	1.50%	-49.27%	-	0.62	-
Collapse R - C	12.40	16.21	-23.47%	2.74	1.31	109.41%	0.88%	1.50%	-41.28%	-	0.62	-
Collapse R - B	12.25	16.21	-24.44%	3.27	1.31	150.11%	0.74%	1.50%	-50.42%	-	0.62	-

Sx2-1 - Experimental Matching [SI]

	Load [kN]			Displacement [mm]			ϵ_f [%]			x [mm]		
	Exp.	Th.	Δ	Exp.	Th.	Δ	Exp.	Th.	Δ	Exp.	Th.	Δ
Elastic	7.71	-	-	4	-	-	0.01%	-	-	46	77	-40.96%
Cracked	17.73	-	-	10	-	-	0.17%	-	-	30	25	20.00%
Yielding Start	33.69	29.13	15.65%	18	13	41.08%	0.37%	0.32%	17.11%	27	20	37.09%
Concrete Zero	43.04	-	-	24	-	-	0.56%	-	-	19	-	-
Debonding L&R	47.59	43.05	10.55%	30	19	59.56%	0.62%	0.70%	-10.59%	-	17	-
First Anchor R	54.75	72.10	-24.06%	41	33	23.05%	0.76%	1.50%	-49.27%	-	16	-
Collapse R - C	55.18	72.10	-23.47%	70	33	109.41%	0.88%	1.50%	-41.28%	-	16	-
Collapse R - B	54.48	72.10	-24.44%	83	33	150.11%	0.74%	1.50%	-50.42%	-	16	-

Sx2-1 - Matching with 90x2 [US]

	Load [kip]			Displacement [in]			ϵ_f [%]		
	Exp.	Th.	Δ	Exp.	Th.	Δ	Exp.	Th.	Δ
First Anchor R	12.31	13.67	-9.97%	1.61	1.05	52.76%	0.76%	1.19%	-35.85%
Collapse R - C	12.40	13.67	-9.26%	2.74	1.05	159.98%	0.88%	1.19%	-25.75%
Collapse R - B	12.25	13.67	-10.41%	3.27	1.05	210.50%	0.74%	1.19%	-37.30%

Sx2-1 - Matching with 90x2 [SI]

	Load [kN]			Load [kN]			ϵ_f [%]		
	Exp.	Th.	Δ	Exp.	Th.	Δ	Exp.	Th.	Δ
First Anchor R	54.75	60.81	-9.97%	41	27	52.76%	0.76%	1.19%	-35.85%
Collapse R - C	55.18	60.81	-9.26%	70	27	159.98%	0.88%	1.19%	-25.75%
Collapse R - B	54.48	60.81	-10.41%	83	27	210.50%	0.74%	1.19%	-37.30%

FRP Strains are measured on the central FRP strip at midspan

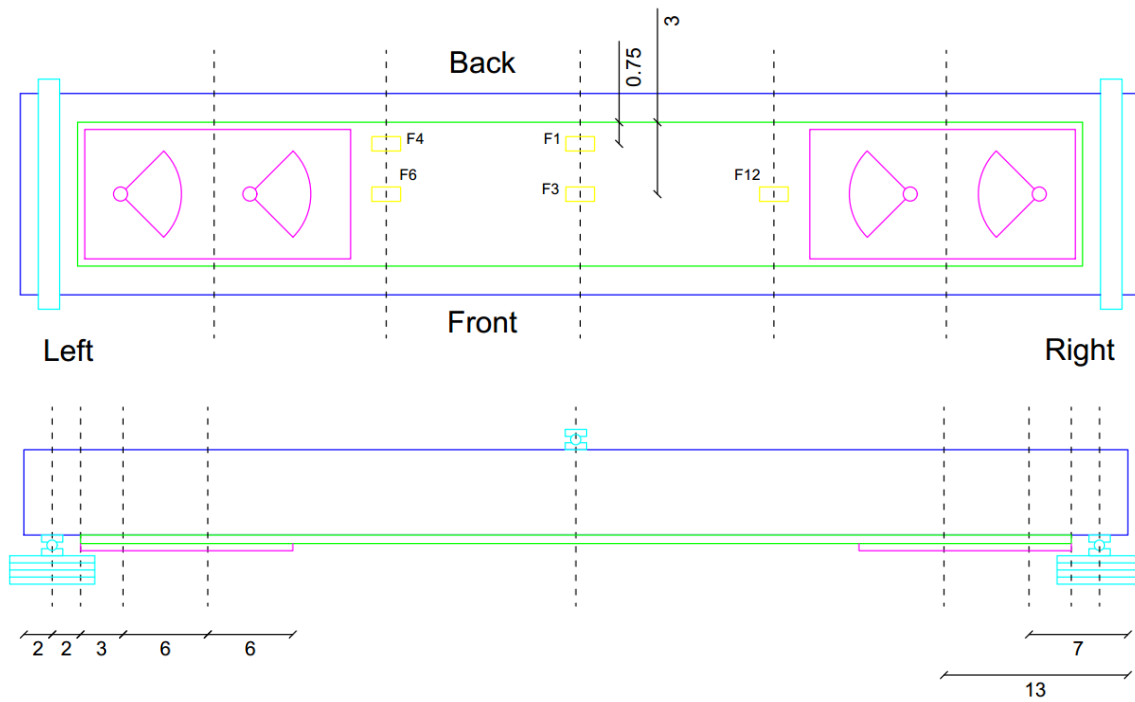


FIGURE 168 - STRAIN GAGES LOCATION & GEOMETRY (Sx2-1), THE X MARKS THE FAILING SIDE.
DIMENSIONS ARE IN INCHES. 1 IN = 25.4 MM / 1 KIP = 4.448 kN



FIGURE 169 - CRACKS SHAPE AT COLLAPSE (Sx2-1), THE X MARKS THE FAILING SIDE

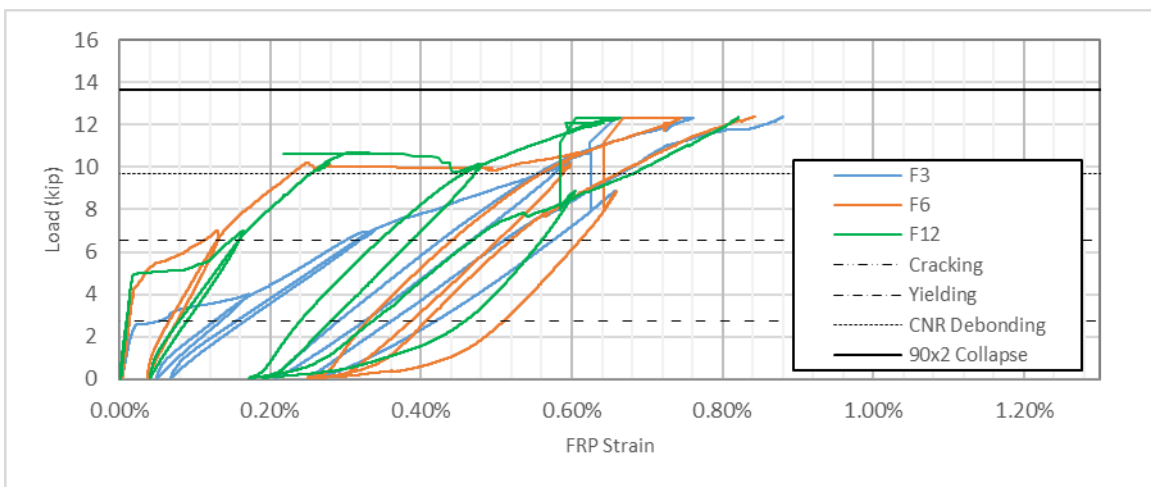
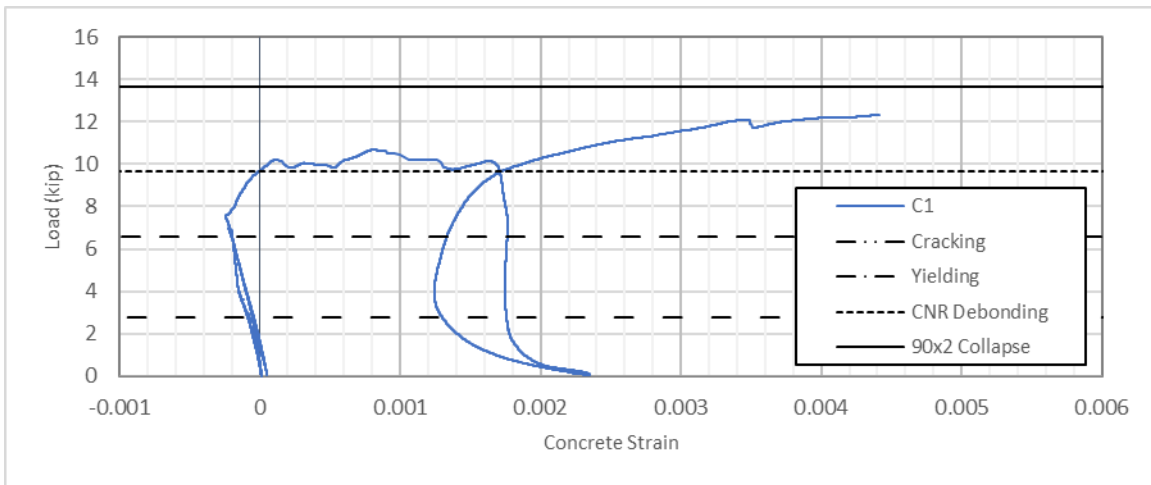
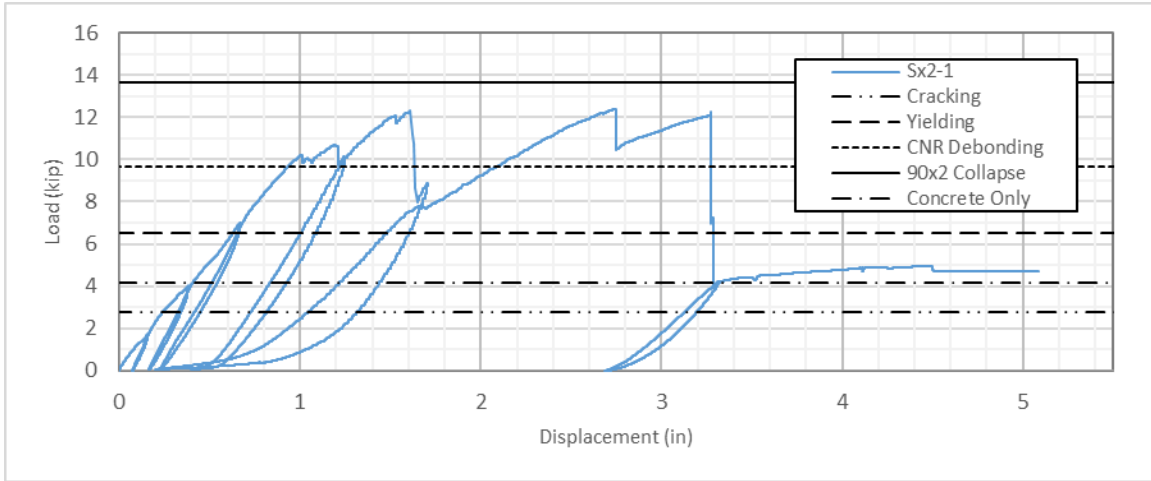


FIGURE 170 – (A) LOAD/DISPLACEMENT (B) CONCRETE STRAIN (C) FRP STRAIN (Sx2-1)
 1 IN = 25.4 MM / 1 KIP = 4.448 kN

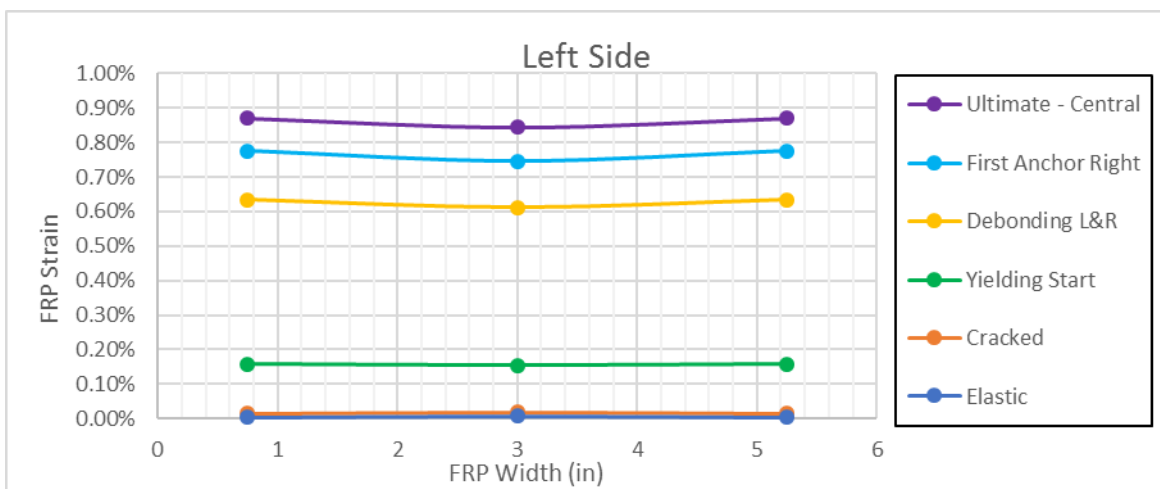
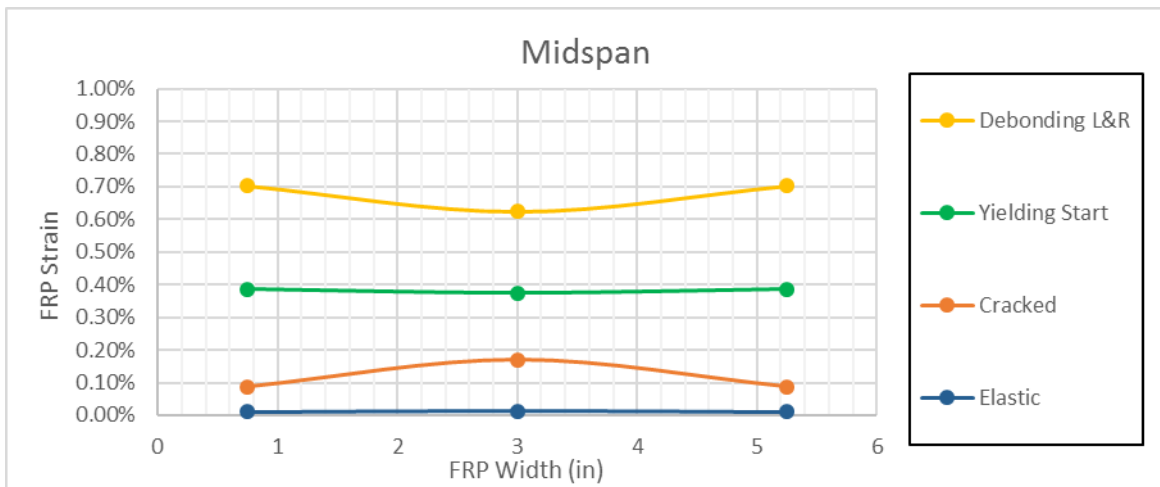


FIGURE 171 - FRP STRAINS OVER SHEET'S WIDTH (Sx2-1). SYMMETRY IS ARTIFICIALLY IMPOSED FOR THE SAKE OF A BETTER READING. 1 IN = 25.4 MM / 1 KIP = 4.448 kN

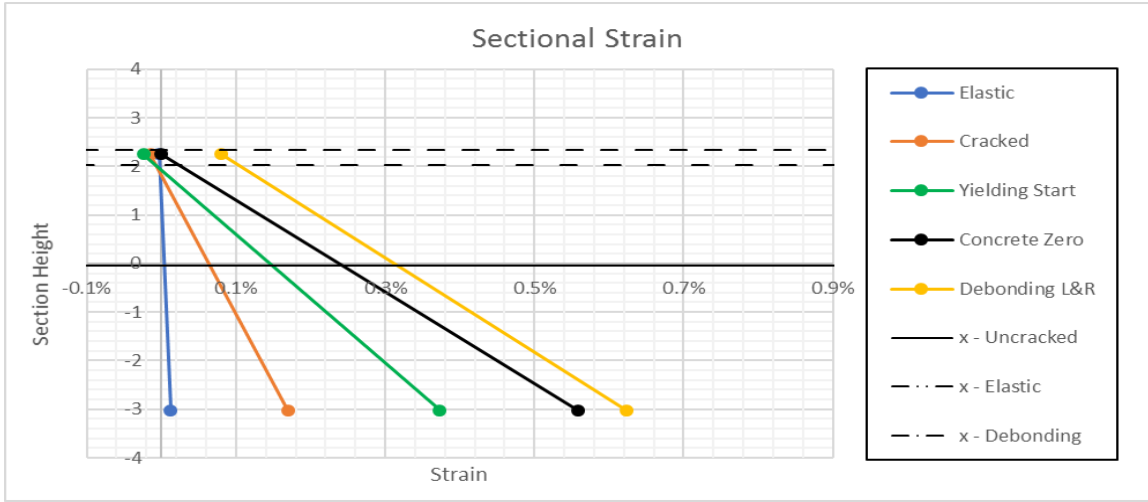


FIGURE 172 - SECTIONAL STRAINS (Sx2-1). 1 IN = 25.4 MM / 1 KIP = 4.448 KN

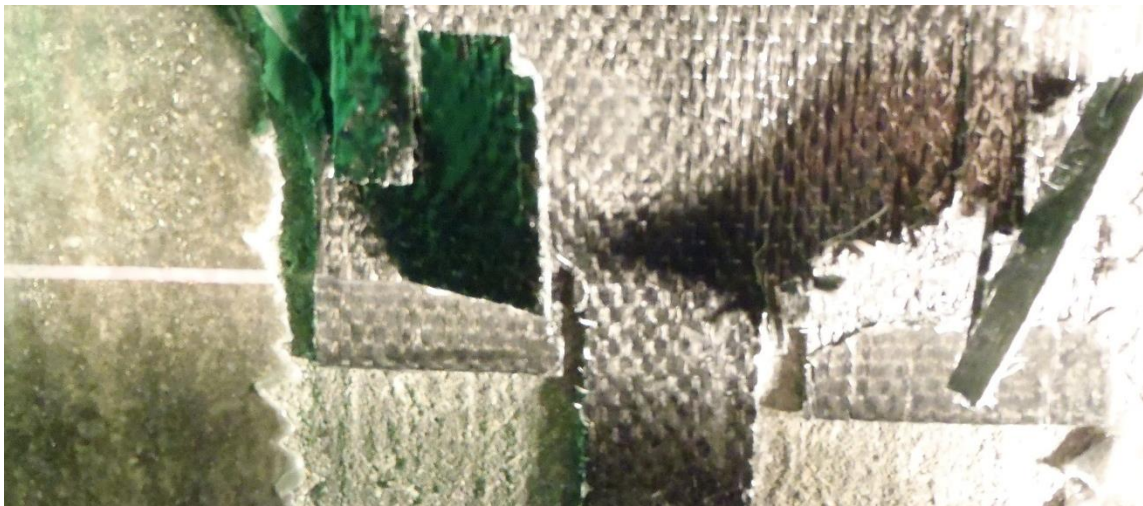
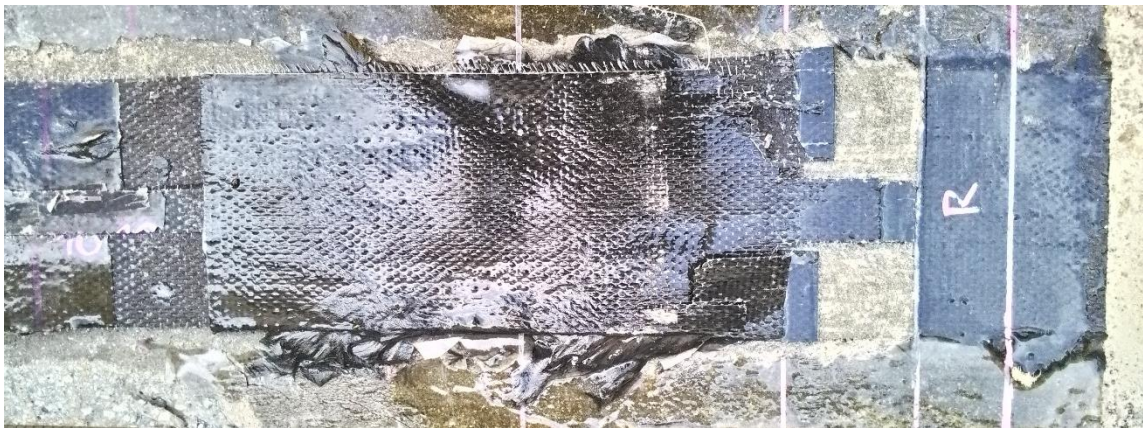


FIGURE 173 - Sx2-1 COLLAPSE PICTURES

6.1.6.2 Sx2-2

Considering the flexural/shear inconsistent behavior and the improper installation spotted in the previous specimen, a second one was properly prepared and tested, showing basically the same behavior, with a way better matching of the 90x2 predicted strength and the same pseudo-ductile behavior as spotted in Sx2-1.

It should be noticed the very good matching with the 90x2 expected results, also from the strain point of view, referring to the average strain measured on the left side. After central strip failure only lateral values are averaged. Notice also the almost-uniform, slightly concave, strain shape; consistent with both the control specimen and Sx2-1.

Peculiar is also the perfectly symmetric behavior of the element at failure, happened at the same instant on the left and right side in a perfectly specular way: The failure was triggered by the central strip slipping, happening at the same moment on the two sides. Then, the back strip underwent rupture on the left side, while slipping on the right. Finally, the front strip underwent rupture on the right side, while slipping on the left.

Also in this case a pseudo-ductile behavior can be spotted: the first peak will be assumed as the failure one, wishing to stay on the safe side, leaving further discussion for later.

	Load [kip]			Displacement [in]			ϵ_f [%]		
	Exp.	Th.	Δ	Exp.	Th.	Δ	Exp.	Th.	Δ
Elastic	1.55	-	-	0.08	-	-	0.01%	-	-
Cracked	4.02	-	-	0.40	-	-	0.02%	-	-
Yielding	7.04	6.55	7.48%	0.81	0.51	57.45%	0.17%	0.32%	-45.80%
Debonding L	9.64	-	-	1.21	-	-	0.53%	-	-
Debonding R	9.73	9.68	0.50%	1.25	0.75	65.54%	0.55%	0.70%	-21.54%
First Anchor L&R	13.24	16.21	-18.30%	1.86	1.31	41.99%	0.96%	1.50%	-36.22%
Ultimate - Central	13.28	16.21	-18.04%	2.50	1.31	91.33%	1.06%	1.50%	-29.18%
Ultimate - Lateral	12.68	16.21	-21.80%	3.49	1.31	167.06%	1.24%	1.50%	-17.23%

	Load [kip]			Displacement [in]			ϵ_f [%]		
	Exp.	Th.	Δ	Exp.	Th.	Δ	Exp.	Th.	Δ
First Anchor L&R	13.24	13.67	-3.14%	1.86	1.05	76.27%	0.96%	1.19%	-19.35%
Ultimate - Central	13.28	13.67	-2.83%	2.50	1.05	137.53%	1.06%	1.19%	-10.45%
Ultimate - Lateral	12.68	13.67	-7.28%	3.49	1.05	231.55%	1.24%	1.19%	4.66%

FRP Strains are measured as a 3-point average in front of the first anchor on the left side (failing side)

Sx2-2 - Experimental Matching [SI]									
	Load [kN]			Displacement [mm]			ϵ_f [%]		
	Exp.	Th.	Δ	Exp.	Th.	Δ	Exp.	Th.	Δ
Elastic	6.91	-	-	2	-	-	0.01%	-	-
Cracked	17.87	-	-	10	-	-	0.02%	-	-
Yielding	31.31	29.13	7.48%	20	13	57.45%	0.17%	0.32%	-45.80%
Debonding L	42.87	-	-	31	-	-	0.53%	-	-
Debonding R	43.27	43.05	0.50%	32	19	65.54%	0.55%	0.70%	-21.54%
First Anchor L&R	58.90	72.10	-18.30%	47	33	41.99%	0.96%	1.50%	-36.22%
Ultimate - Central	59.09	72.10	-18.04%	64	33	91.33%	1.06%	1.50%	-29.18%
Ultimate - Lateral	56.38	72.10	-21.80%	89	33	167.06%	1.24%	1.50%	-17.23%

Sx2-2 - Matching with 90x2 [SI]									
	Load [kN]			Load [kN]			ϵ_f [%]		
	Exp.	Th.	Δ	Exp.	Th.	Δ	Exp.	Th.	Δ
First Anchor L&R	58.90	60.81	-3.14%	47	27	76.27%	0.96%	1.19%	-19.35%
Ultimate - Central	59.09	60.81	-2.83%	64	27	137.53%	1.06%	1.19%	-10.45%
Ultimate - Lateral	56.38	60.81	-7.28%	89	27	231.55%	1.24%	1.19%	4.66%

FRP Strains are measured as a 3-point average in front of the first anchor on the left side (failing side)

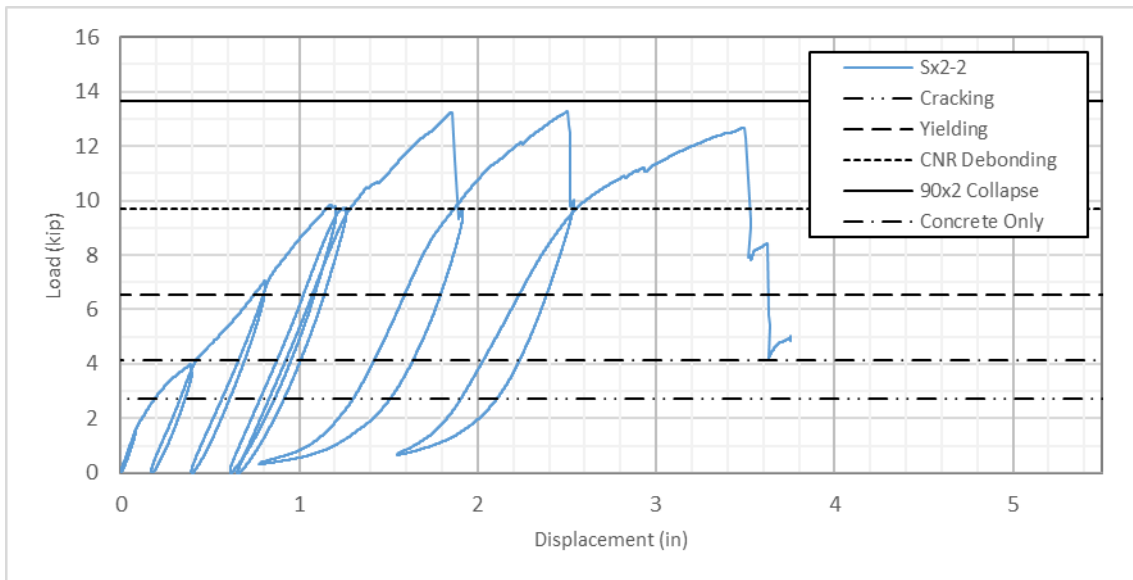


FIGURE 174 - LOAD/DISPLACEMENT (Sx2-2)
 1 IN = 25.4 MM / 1 KIP = 4.448 kN

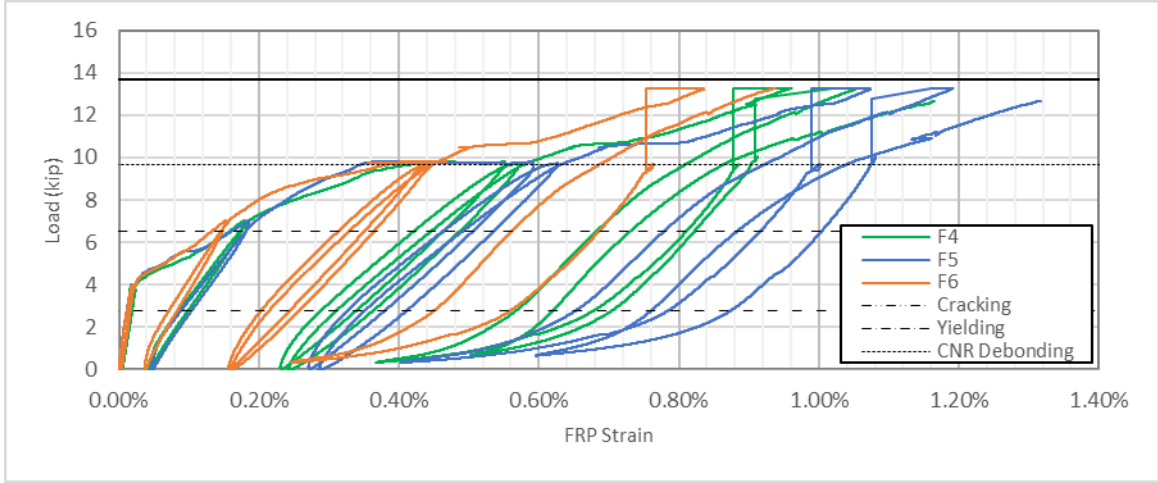
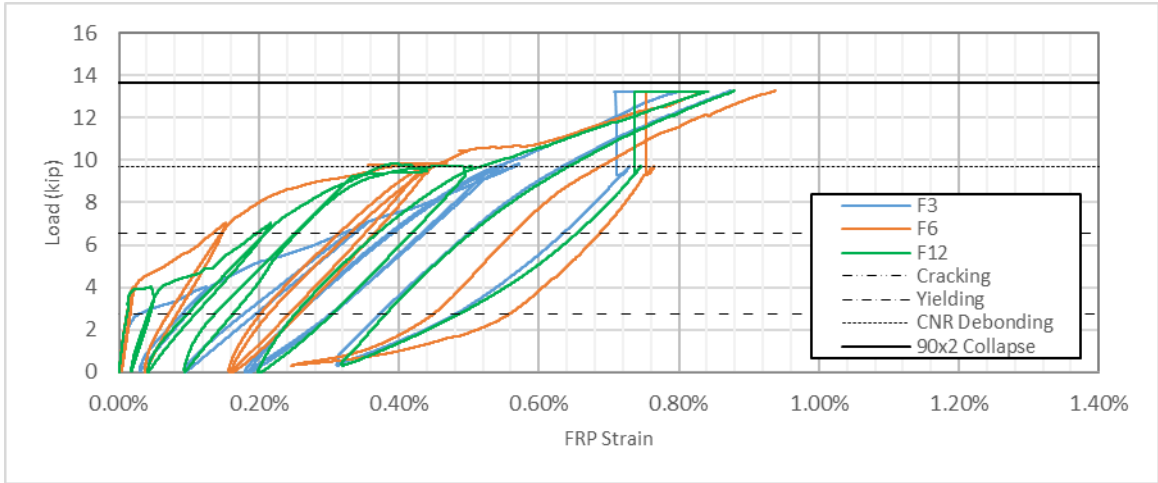


FIGURE 175 - FRP STRAIN (Sx2-2). 1 IN = 25.4 MM / 1 KIP = 4.448 KN

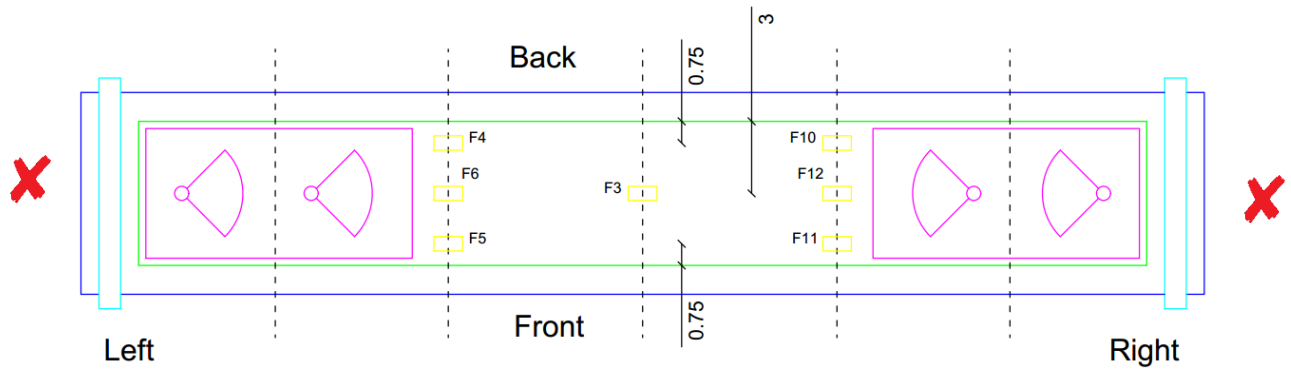


FIGURE 176 - STRAIN GAGES LOCATIONS (Sx2-2), THE X MARKS THE FAILING SIDES- DIMENSIONS ARE IN INCHES. 1 IN = 25.4 MM / 1 KIP = 4.448 KN

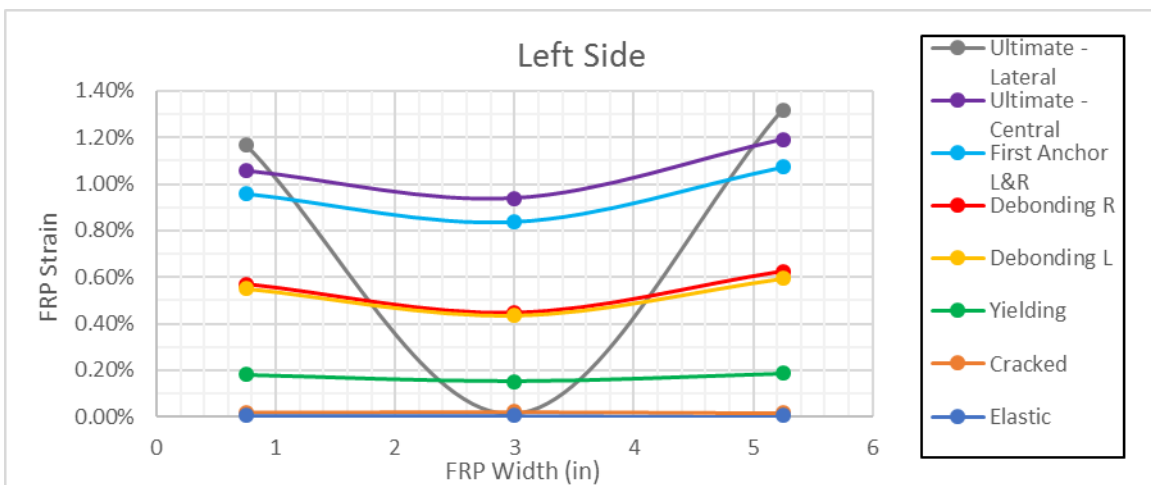
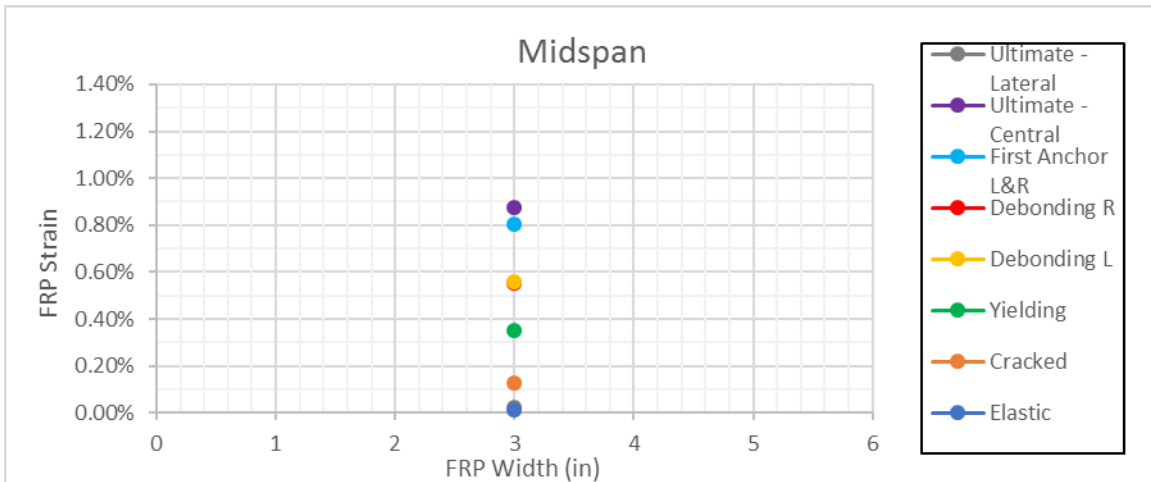
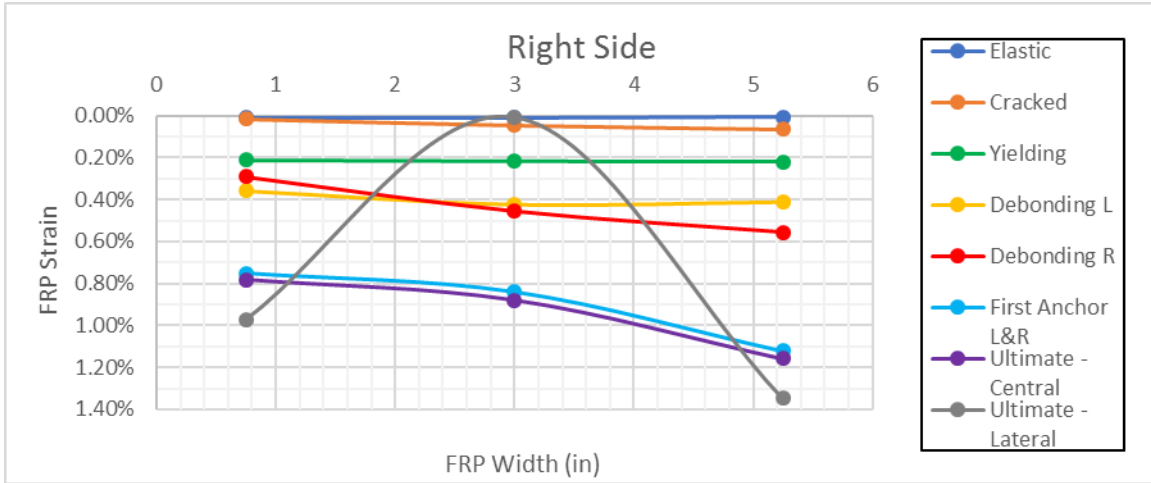


FIGURE 177 - FRP STRAINS OVER SHEET'S WIDTH. 1 IN = 25.4 MM / 1 KIP = 4.448 KN



**FIGURE 178 - Sx2-2 PERFECTLY SYMMETRIC COLLAPSE MECHANISM
THE X MARKS THE FAILING SIDES**

6.2 Longitudinal Strain Shapes

The strain shapes over the sheet's length are reported in the following, for all the tested specimens. Notice that in the following graphs a x marks the failing side, in some cases the failure was forced to happen on one side, over-anchoring the other.

It is interesting to notice how, after intermediate debonding, the strains at the sheets end jump at a level almost equal to the midspan value, hence the shape becomes almost uniform over the length; some differences remain because of FRP-concrete friction, typically the maximum strain is registered on the failing side.

6.2.1.1 C-CFRP

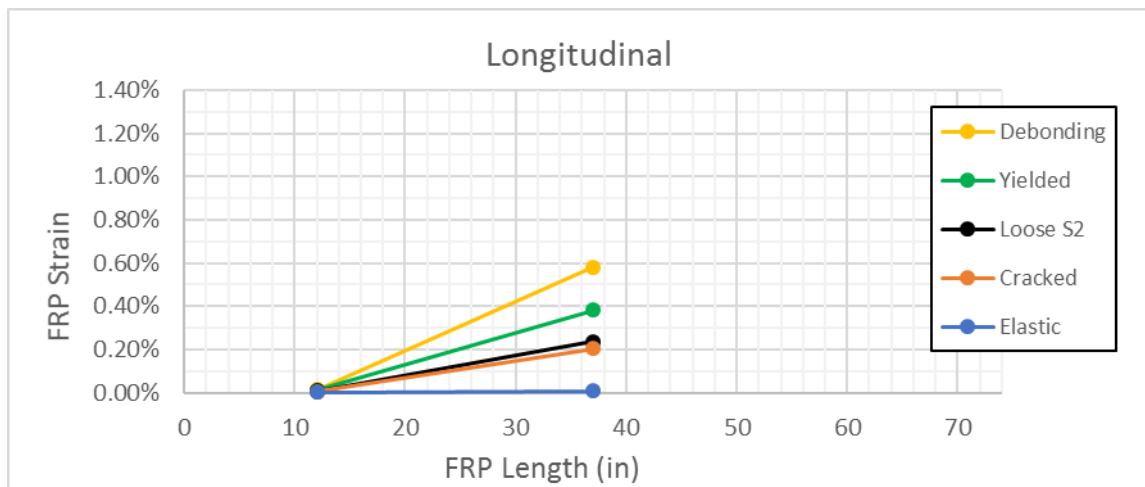
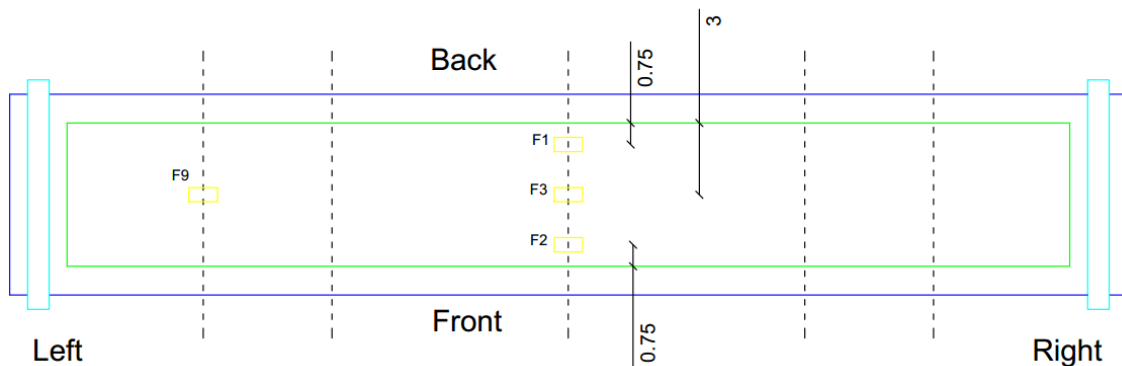


FIGURE 179 - F9, F3. DIMENSIONS ARE IN INCHES. 1 IN = 25.4 MM



6.2.1.2 60x2

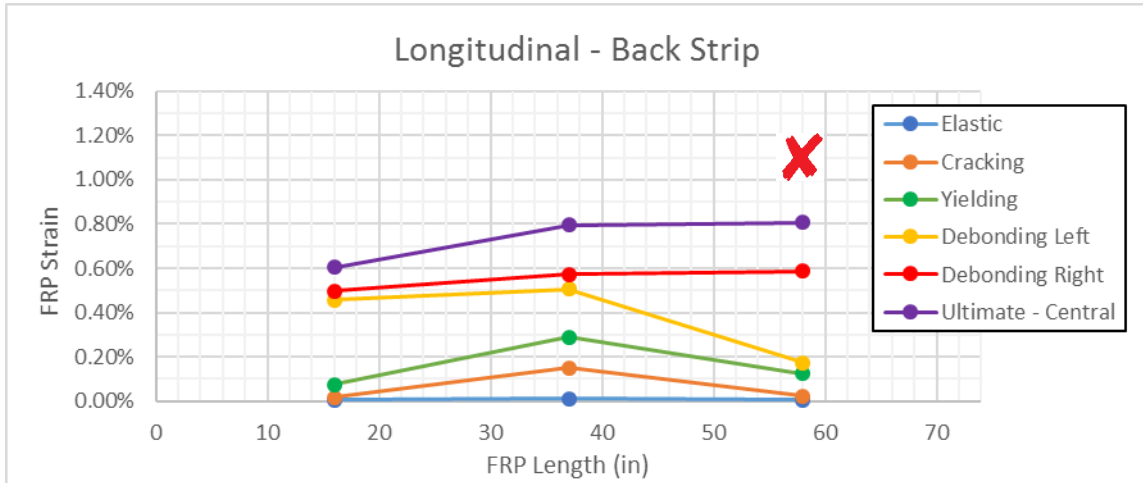


FIGURE 180 – F4, F1, F10

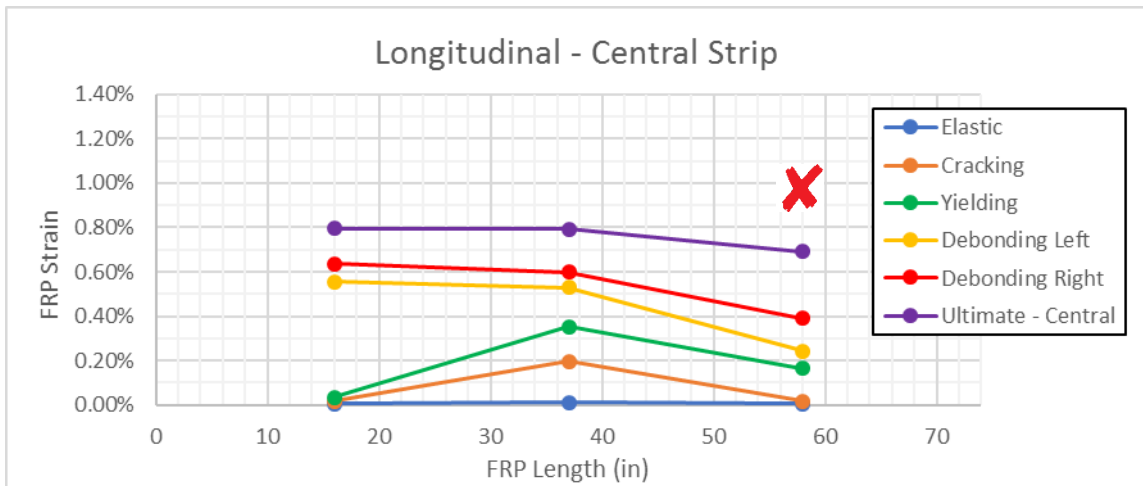


FIGURE 181 - F6, F6, F12

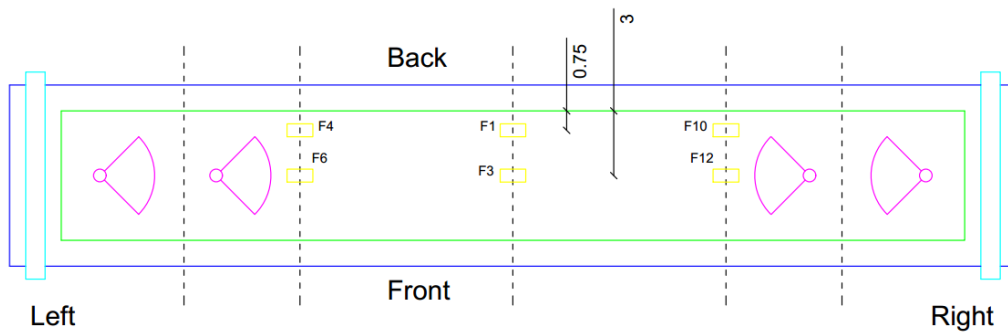


FIGURE 182 – DIMENSIONS ARE IN INCHES, 1 IN = 25.4 MM

6.2.1.3 90x2

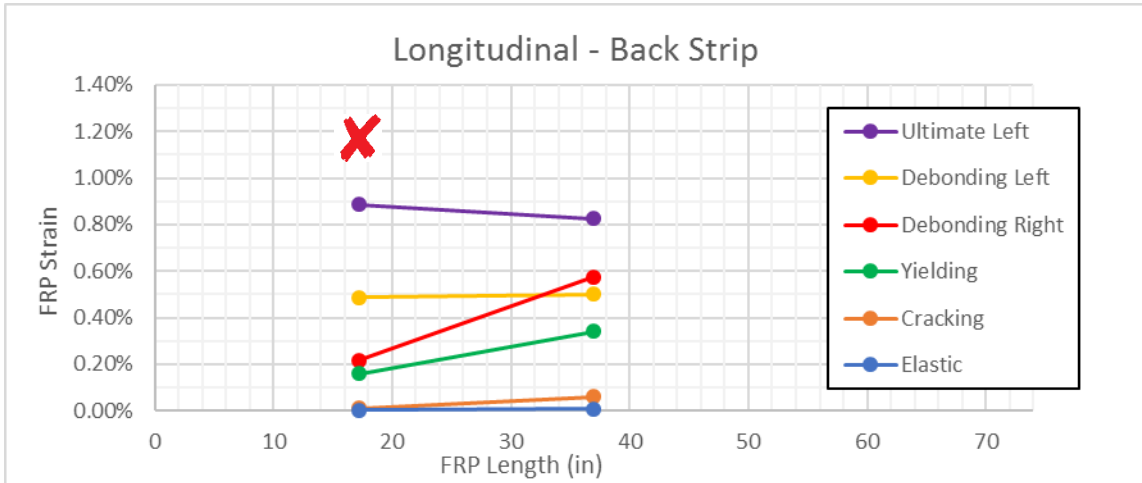


FIGURE 183 – F4, F1

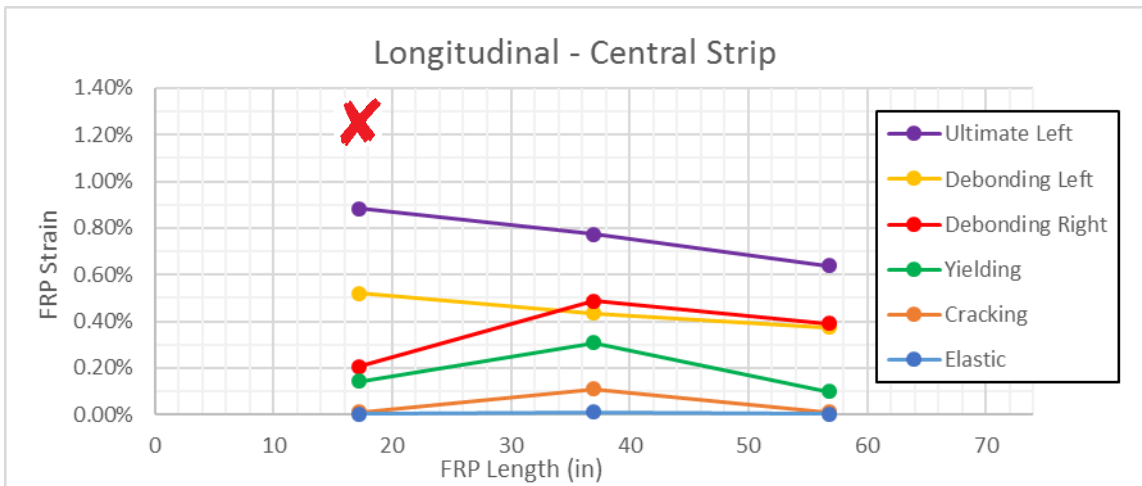


FIGURE 184 – F6, F3, F12

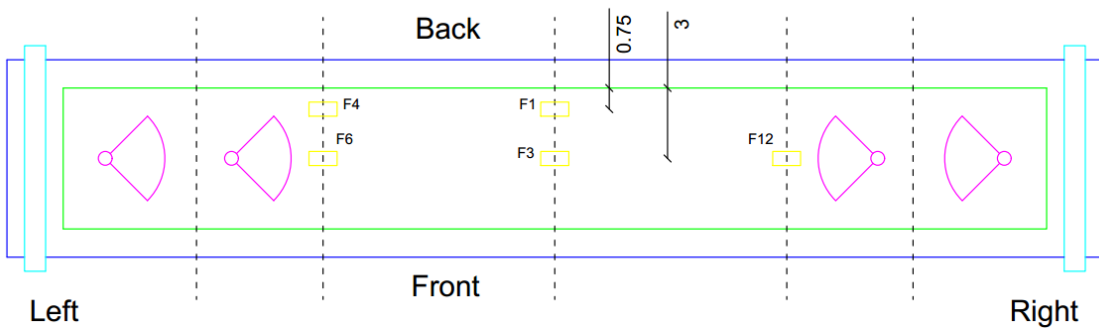


FIGURE 185 – DIMENSIONS ARE IN INCHES, 1 IN = 25.4 MM

6.2.1.4 90x2 L/4

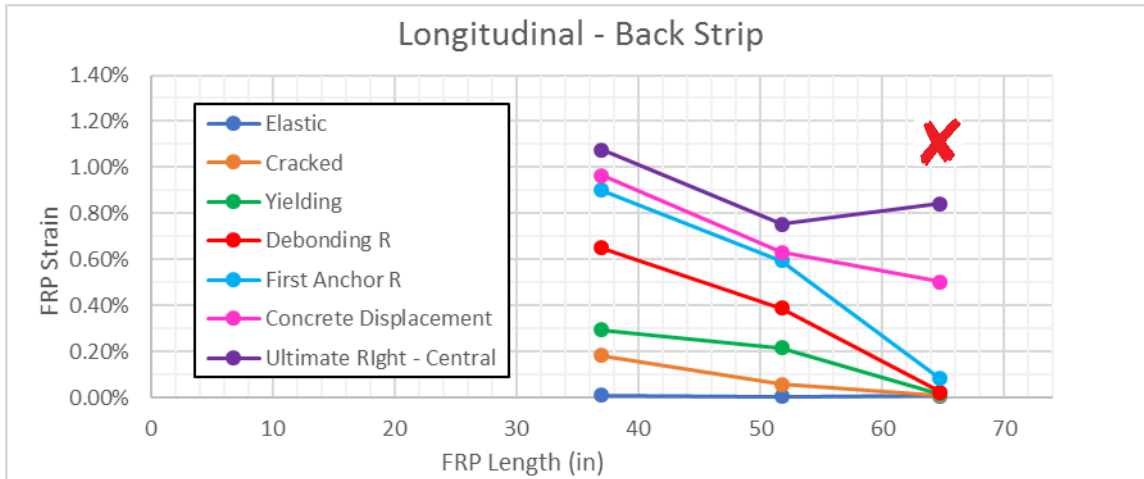


FIGURE 186 - F3, F10, F13

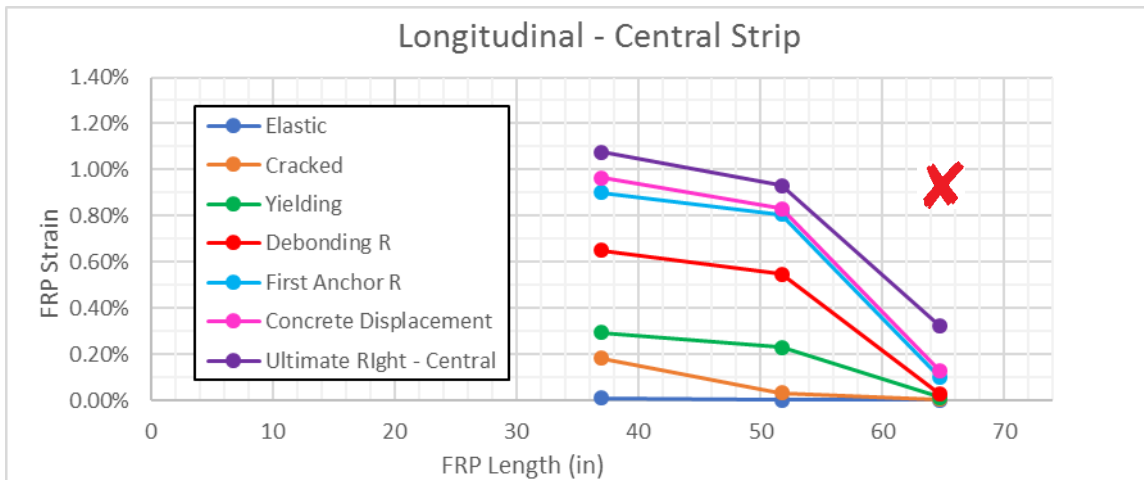


FIGURE 187 - F3, F12, F15

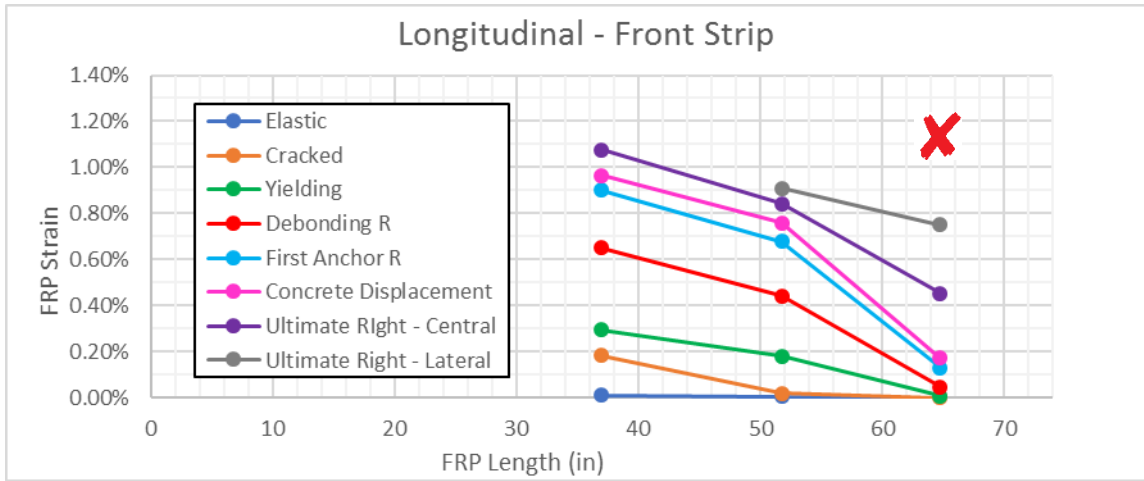


FIGURE 188 - F3, F11, F14

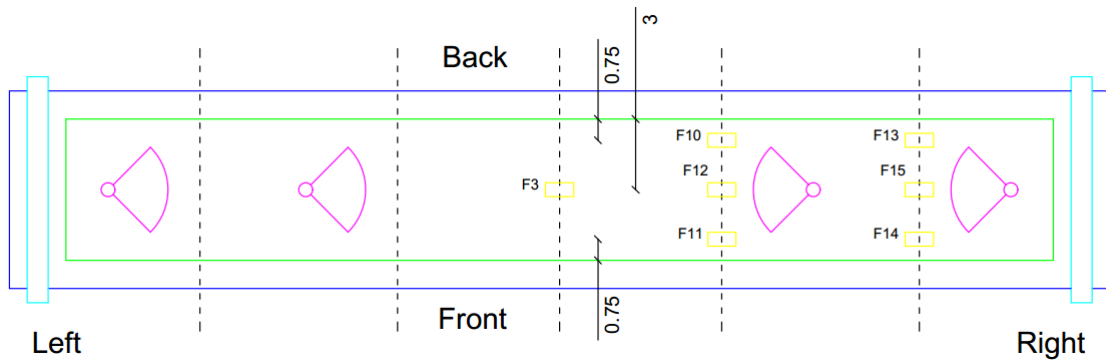


FIGURE 189 – DIMENSIONS ARE IN INCHES, 1 IN = 25.4 MM

6.2.1.5 90x2 L/3

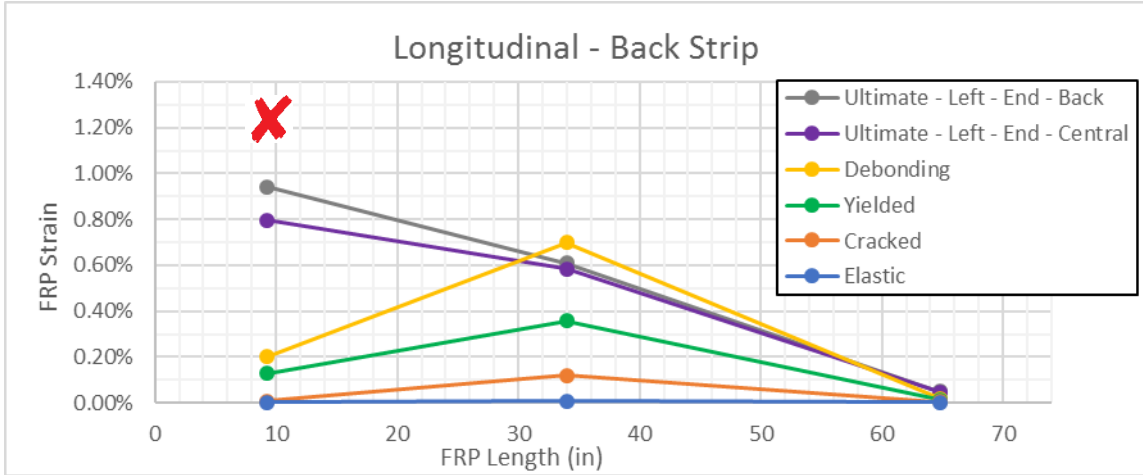


FIGURE 190 - F7, F3, F13

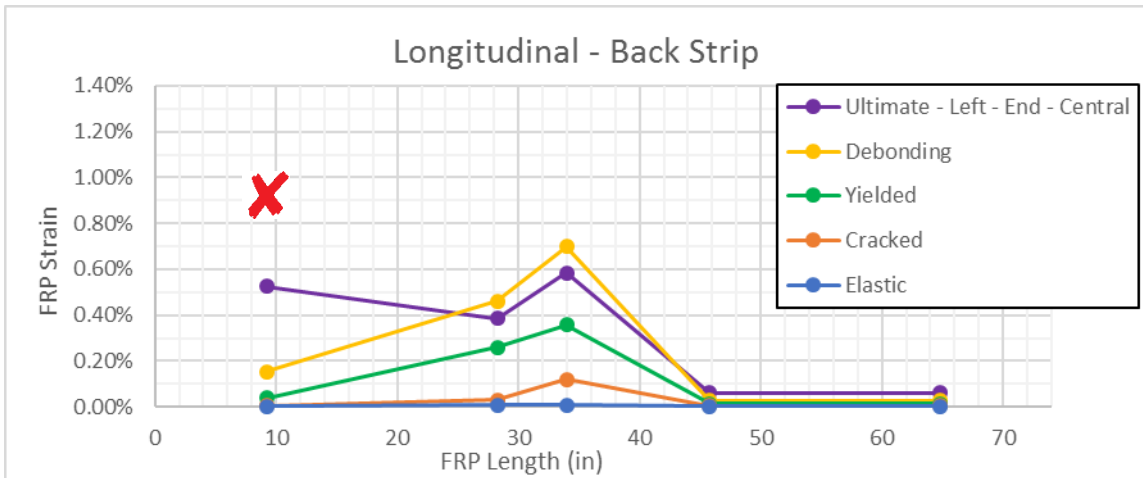


FIGURE 191 - F9, F6, F3, F12, F15

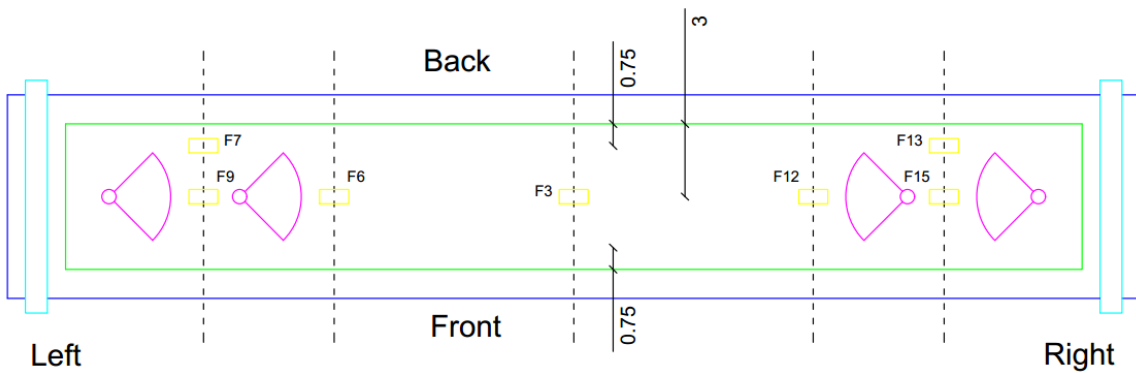


FIGURE 192 – DIMENSIONS ARE IN INCHES, 1 IN = 25.4 MM

6.2.1.6 90x3

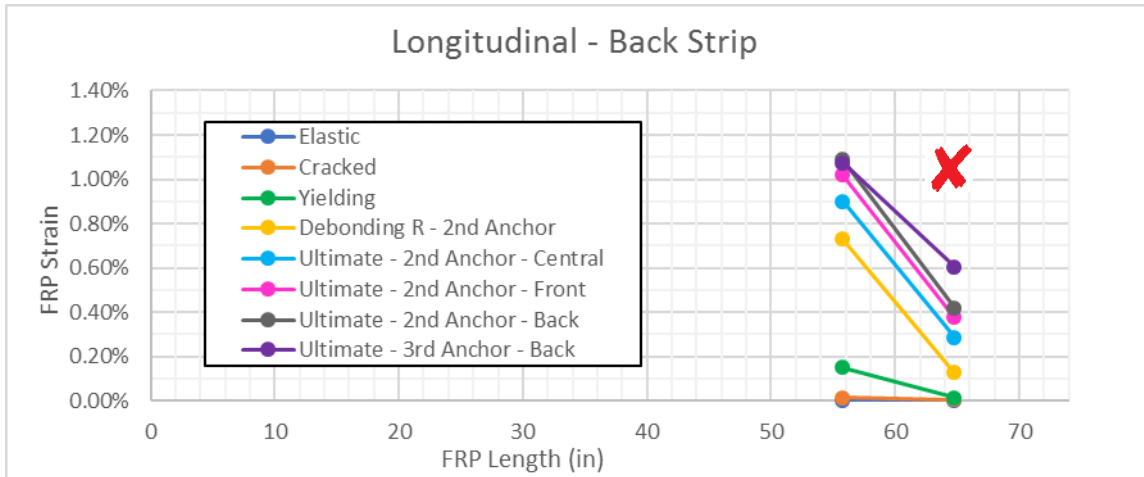


FIGURE 193 – F13, F16

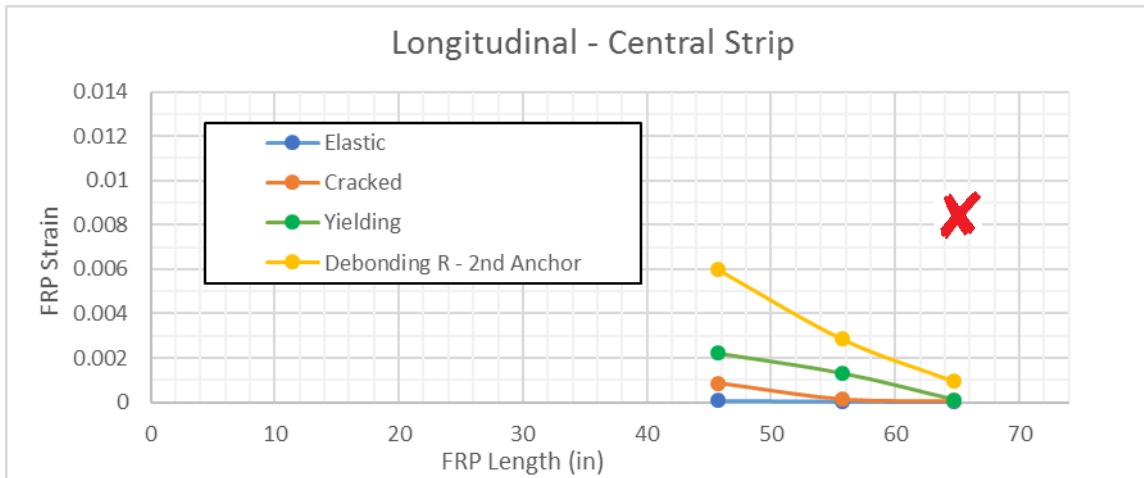


FIGURE 194 – F12, F15, F18

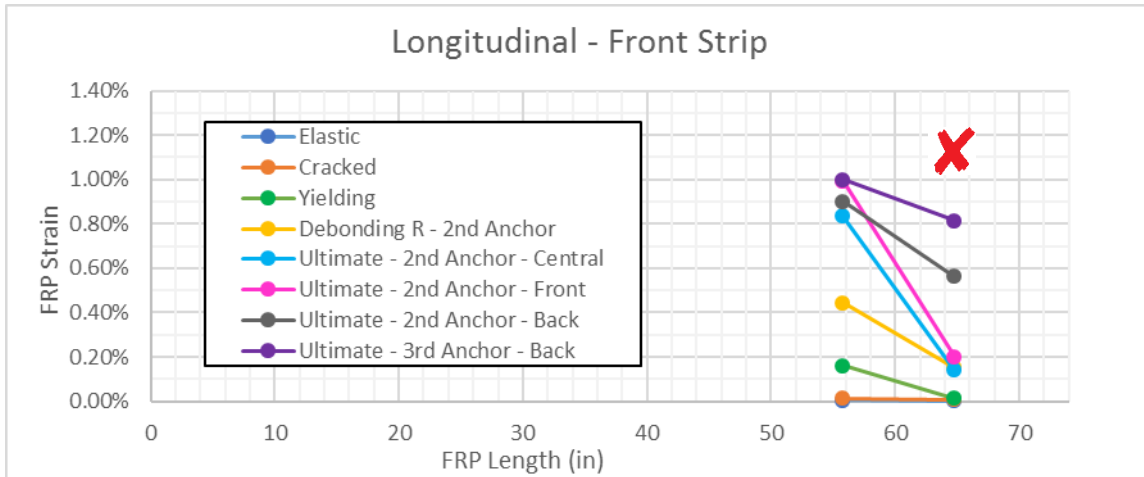


FIGURE 195 – F14, F17

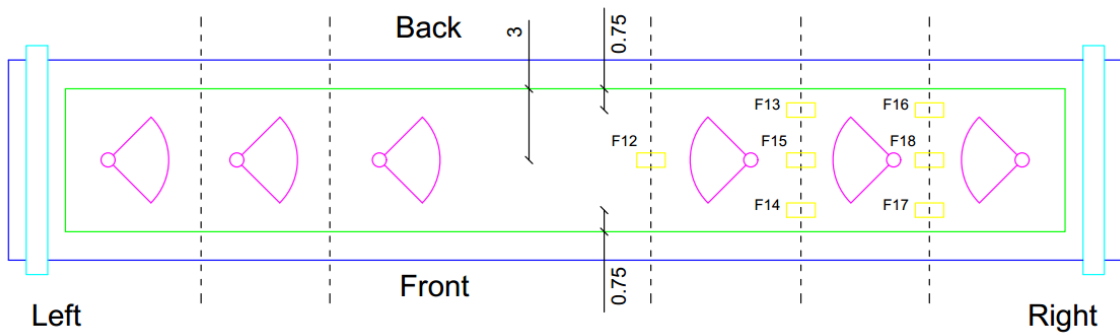


FIGURE 196 – DIMENSIONS ARE IN INCHES, 1 IN = 25.4 MM

6.2.1.7 Sx2 - 1

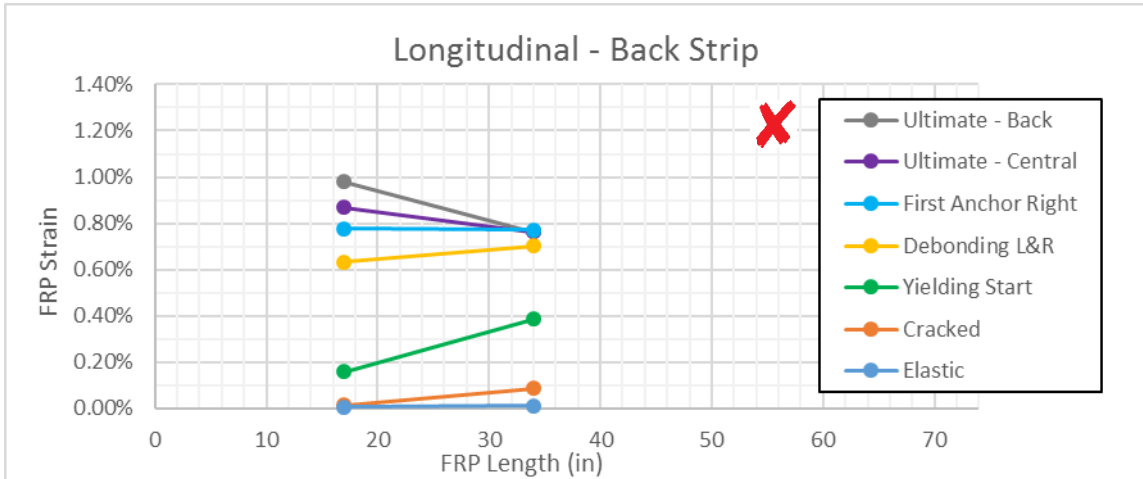


FIGURE 197 – F4, F1

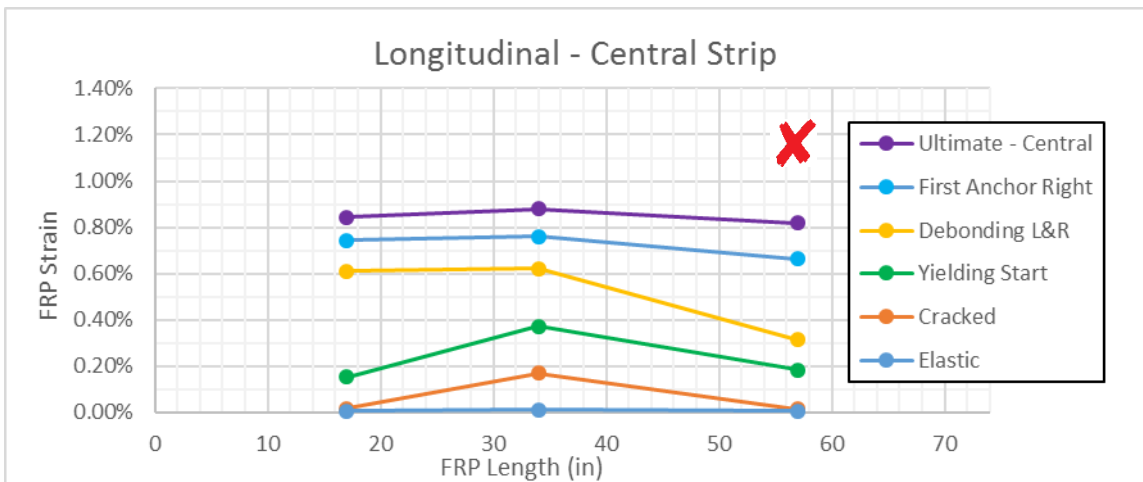


FIGURE 198 – F3, F6, F12

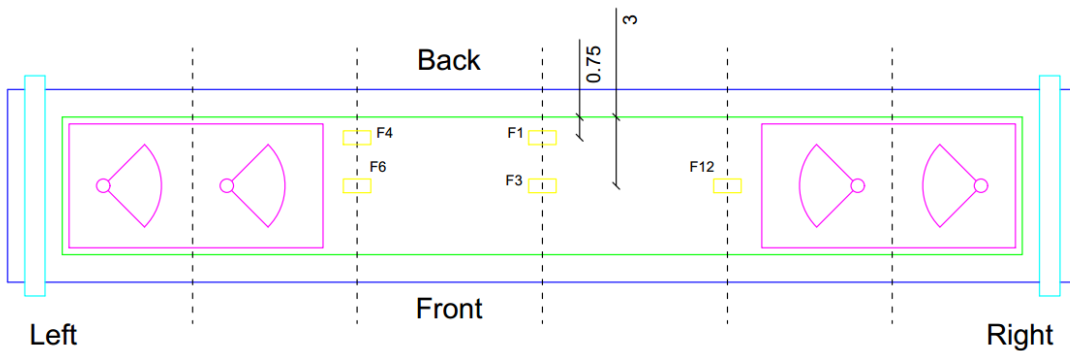


FIGURE 199 – DIMENSIONS ARE IN INCHES, 1 IN = 25.4 MM

6.2.1.8 Sx2-2

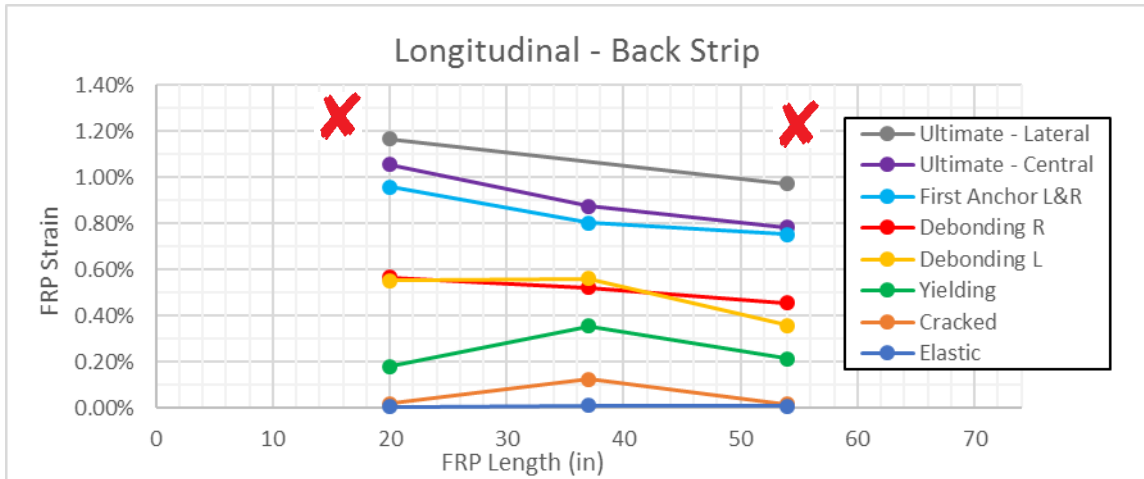


FIGURE 200 – F4, F3, F10

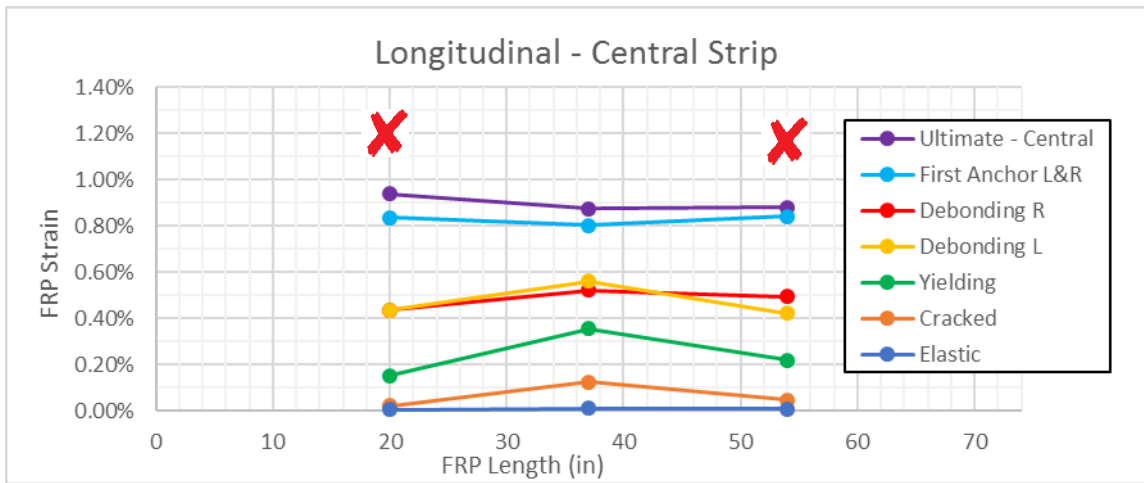


FIGURE 201 – F6, F3, F12

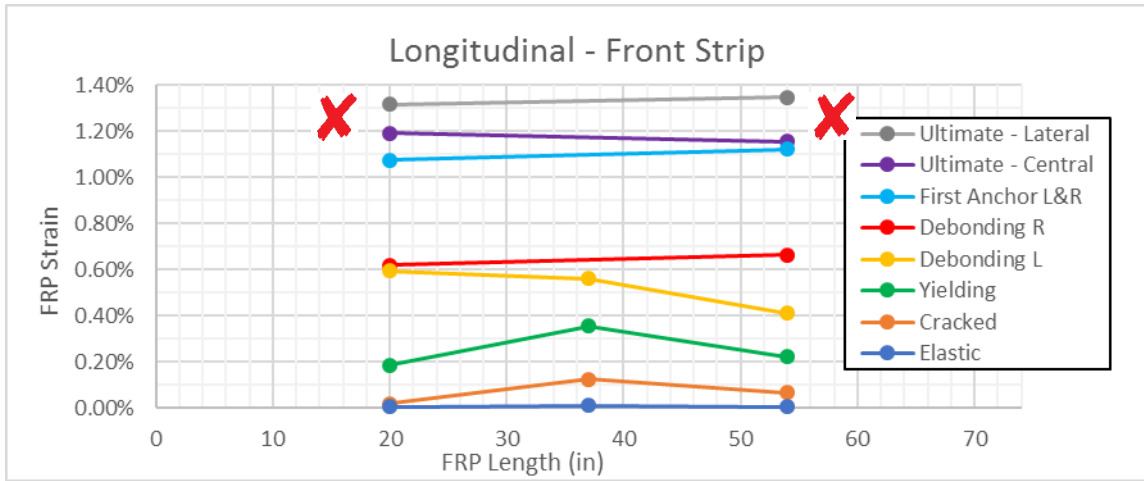


FIGURE 202 – F5, F3, F11

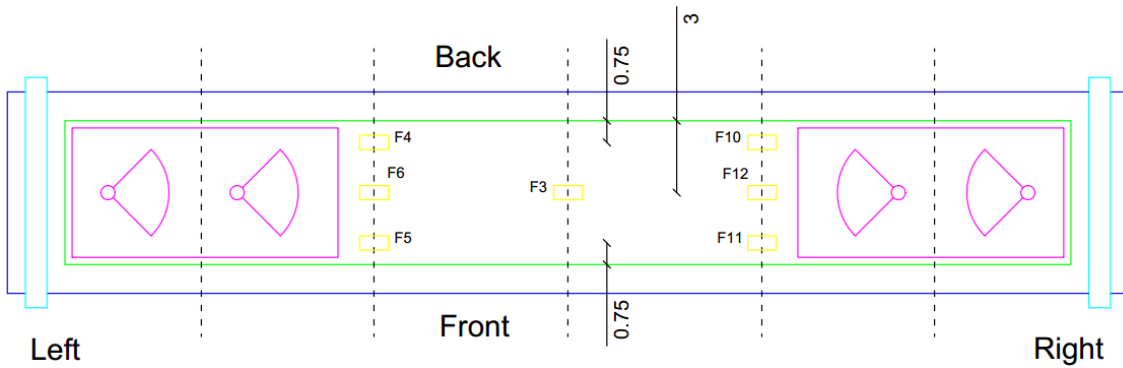


FIGURE 203 – DIMENSIONS ARE IN INCHES, 1 IN = 25.4 MM

6.3 Results Recap

Results related to all the tested samples are here summed up. The way the data are presented may seem redundant; the goal is actually to be as much exhaustive as possible – as done while characterizing the anchors' strength, geometry and material properties – in order for the results to be comparable with the variously presented results coming from other researches in this field. A more detailed and reasoned approach will be applied in the following chapter, while presenting the conclusions of this dissertation.

Regarding deflection measurements, where a pseudo-ductile behavior can be spotted, both the starting and ultimate pseudo-plateau values will be reported. Only the starting value will be referred for ductility parameter evaluation, though, wishing to stay on the safe side, not being sure such a ductile behavior can be guaranteed in real case scenarios. The ultimate load doesn't change much from peak to peak, but the first-peak value will be referred in any case; further discussion on ductility will follow.

6.3.1.1 Matching and Behavior

A very good matching can be noticed on the ultimate load side. Looking at the measured strains, the results are in line with the already discussed limits and quality of the measurements; the difference is generally way lower when a 3-point measurement is available. The errors are way lower when the equivalent experimental failure strain is referred, being function of the good matched experimental load. On the deflection side, the proposed analytical approach works very well up to debonding, while the stiffness loss after debonding is hard to model referring to standard R/C models.

Looking at the structure's behavior, all the specimens' shows a very similar tri-linear tendency up to the first peak, with the second and third branch not always easily differentiable. The post-failure behavior shows various tendencies, with relevant pseudo-ductility in some cases.

Looking at the data matching in the serviceability range, it seems clear how the presence of the anchors doesn't significantly affect the system's performances against intermediate debonding.

Matching - SLS [US]											
		C-C	C-FRP	60X2	90X2	SX2 - 1	SX2 - 2	90x2 0.25L	90x2 0.33L	90x3	Rupture
P_{db} [kip]	Exp.	-	9.33	9.55	9.46	10.19	9.84	9.88	9.75	10.00	-
	Th.	-	9.68	9.68	9.68	9.68	9.68	9.68	9.68	9.68	-
	Δ	-	-3.58%	-1.32%	-2.25%	5.30%	1.67%	2.06%	0.75%	3.37%	-
δ_{db} [in]	Exp.	-	0.82	0.89	1.17	1.01	1.18	0.97	0.81	1.03	-
	Th.	-	0.75	0.75	0.75	0.75	0.75	0.75	0.75	0.75	-
	Δ	-	8.88%	17.94%	55.57%	34.29%	57.01%	29.08%	8.21%	36.80%	-
EJ_{SLS} [kip in ²]	Exp.	-	99,566	93,993	70,615	87,906	72,675	88,724	104,531	84,765	-
	Th.	-	112,295	112,295	112,295	112,295	112,295	112,295	112,295	112,295	-
	Δ	-	-11.34%	-16.30%	-37.12%	-21.72%	-35.28%	-20.99%	-6.91%	-24.52%	-

Matching - ULS [US]											
		C-C	C-FRP	60X2	90X2	SX2 - 1	SX2 - 2	90x2 0.25L	90x2 0.33L	90x3	Rupture
P_u [kip]	Exp.	4.49	9.33	12.09	13.37	12.31	13.24	12.77	11.84	12.32	-
	Th.	4.14	9.68	12.16	13.67	13.67	13.67	13.67	13.67	-	1.42
	Δ	8.32%	-3.58%	-0.62%	-2.22%	-9.97%	-3.13%	-6.56%	-13.42%	-	-
δ_u [in]	Exp.	0.56	0.82	1.90	2.18	1.61	1.86	1.53	1.10	1.37	-
	Th.	0.42	0.75	0.94	1.05	1.05	1.05	1.05	1.05	-	1.56
	Δ	34.45%	8.88%	102.47%	106.84%	52.76%	76.18%	45.16%	4.43%	-	-
EJ_u [kip in ²]	Exp.	72,005	99,566	55,057	53,026	66,250	61,692	72,286	93,285	78,143	-
	Th.	89,883	112,295	112,147	112,117	112,117	112,117	112,117	112,117	-	9,430
	Δ	-19.89%	-11.34%	-50.91%	-52.70%	-40.91%	-44.98%	-35.53%	-16.80%	-	-
ϵ_{ru} [%]	Exp.	-	0.66%	0.79%	0.77%	0.76%	0.96%	0.97%	0.77%	0.64%	-
	Th.	-	0.70%	1.00%	1.19%	1.19%	1.19%	1.19%	1.19%	-	0.00%
	Δ	-	-5.18%	-20.83%	-34.88%	-35.85%	-19.35%	-18.56%	-35.05%	-	-
$\epsilon_{f,eq}$ [%]	Exp.	-	0.65%	0.99%	1.15%	1.03%	1.14%	1.08%	0.96%	1.06%	-
	Th.	-	0.70%	1.00%	1.19%	1.19%	1.19%	1.19%	1.19%	-	0.00%
	Δ	-	-6.05%	-0.92%	-3.30%	-13.09%	-4.01%	-9.04%	-19.00%	-	-
		a	b	b	b	c	e	b	d		

- a 3-point average, midspan
- b 1-point, central strip, midspan
- c 3-point average, left, failing side
- d central strip - right, failing side
- e 1-point, central strip, midspan / preferred to 3-point average right, failing side

Matching - SLS [SI]

		C-C	C-FRP	60X2	90X2	SX2 - 1	SX2 - 2	90x2 0.25L	90x2 0.33L	90x3	Rupture
P_{db} [kN]	Exp.	-	41.51	42.48	42.08	45.33	43.77	43.93	43.37	44.50	-
	Th.	-	43.05	43.05	43.05	43.05	43.05	43.05	43.05	43.05	-
	Δ	-	-3.58%	-1.32%	-2.25%	5.30%	1.67%	2.06%	0.75%	3.37%	-
δ_{db} [mm]	Exp.	-	21	23	30	26	30	25	21	26	-
	Th.	-	19	19	19	19	19	19	19	19	-
	Δ	-	8.88%	17.94%	55.57%	34.29%	57.01%	29.08%	8.21%	36.80%	-
EJ_{SLS} [kN m ²]	Exp.	-	2,857	2,697	2,027	2,523	2,086	2,546	3,000	2,433	-
	Th.	-	3,223	3,223	3,223	3,223	3,223	3,223	3,223	3,223	-
	Δ	-	-11.34%	-16.30%	-37.12%	-21.72%	-35.28%	-20.99%	-6.91%	-24.52%	-

Matching - ULS [SI]

		C-C	C-FRP	60X2	90X2	SX2 - 1	SX2 - 2	90x2 0.25L	90x2 0.33L	90x3	Rupture
P_u [kN]	Exp.	19.97	41.51	53.77	59.46	54.75	58.91	56.82	52.65	54.79	-
	Th.	18.43	43.05	54.10	60.81	60.81	60.81	60.81	60.81	-	6.31
	Δ	8.32%	-3.58%	-0.62%	-2.22%	-9.97%	-3.13%	-6.56%	-13.42%	-	-
δ_u [mm]	Exp.	14	21	48	55	41	47	39	28	35	-
	Th.	11	19	24	27	27	27	27	27	-	40
	Δ	34.45%	8.88%	102.47%	106.84%	52.76%	76.18%	45.16%	4.43%	-	-
EJ_u [kN m ²]	Exp.	2,066	2,857	1,580	1,522	1,901	1,770	2,074	2,677	2,243	-
	Th.	2,579	3,223	3,218	3,218	3,218	3,218	3,218	3,218	-	1,412
	Δ	-19.89%	-11.34%	-50.91%	-52.70%	-40.91%	-44.98%	-35.53%	-16.80%	-	-
ϵ_{fu} [%]	Exp.	-	0.66%	0.79%	0.77%	0.76%	0.96%	0.97%	0.77%	0.64%	-
	Th.	-	0.70%	1.00%	1.19%	1.19%	1.19%	1.19%	1.19%	-	1.79%
	Δ	-	-5.18%	-20.83%	-34.88%	-35.85%	-19.35%	-18.56%	-35.05%	-	-
$\epsilon_{f,eq}$ [%]	Exp.	-	0.65%	0.99%	1.15%	1.03%	1.14%	1.08%	0.96%	1.06%	-
	Th.	-	0.70%	1.00%	1.19%	1.19%	1.19%	1.19%	1.19%	-	1.79%
	Δ	-	-6.05%	-0.92%	-3.30%	-13.09%	-4.01%	-9.04%	-19.00%	-	-

a b b b c e b d

- a 3-point average, midspan
- b 1-point, central strip, midspan
- c 3-point average, left, failing side
- d central strip - right, failing side
- e 1-point, central strip, midspan / preferred to 3-point average right, failing side

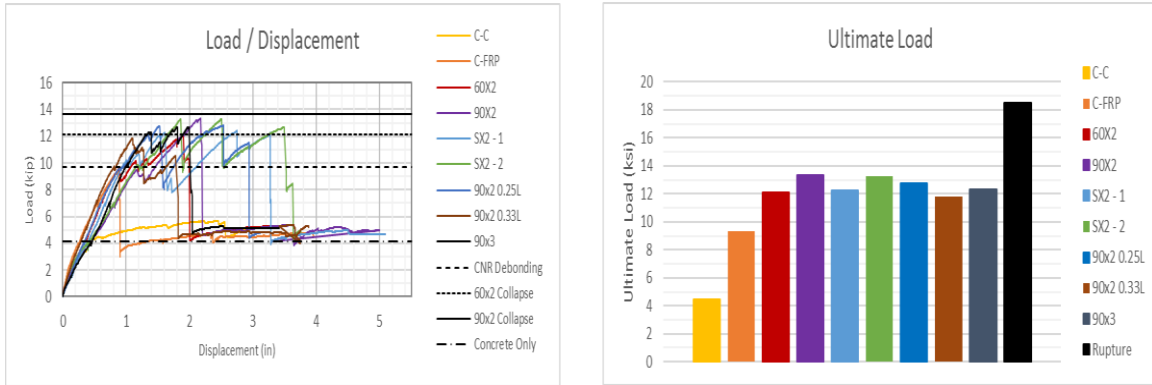


FIGURE 204 - ULTIMATE LOAD RECAP

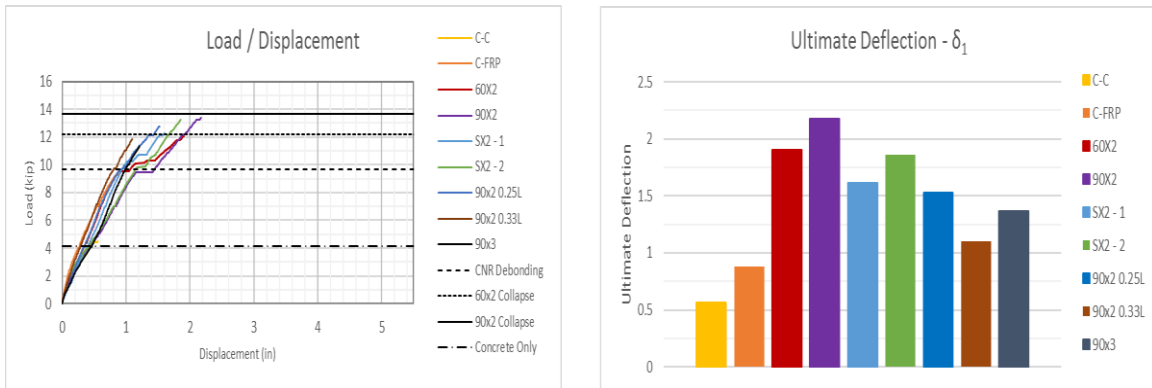


FIGURE 205 - ULTIMATE DEFLECTION RECAP, NO PSEUDO-DUCTILITY

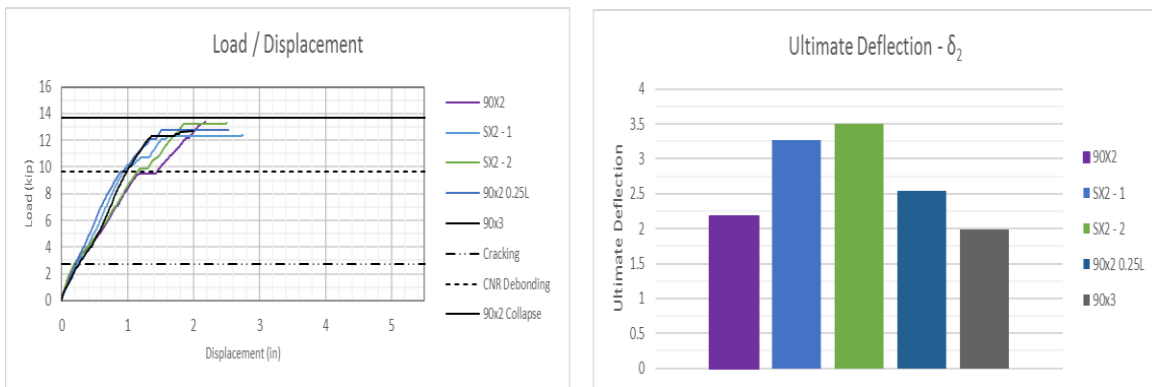


FIGURE 206 - ULTIMATE DEFLECTION RECAP, WITH PSEUDO-DUCTILITY

1 IN = 25,4 MM / 1 KIP = 4.448 KN

6.3.1.2 Effectiveness, Efficiency & Ductility Ratios

The comprehensive approach here applied, allows to evaluate the efficacy of the different ratios proposed for effectiveness and efficiency improvement evaluation.

Plotting those ratios at varying equivalent-failure-strain, a linear strength and ductility effectiveness increment can be spotted, regardless of the chosen parameter; consistently with the linear strain distribution over the section and the elastic behavior of the composite material. Considering the efficiency, an almost exponential increment can be spotted, further promoting the implementation of anchoring solutions, focused on enhancing the equivalent-ultimate-strain that a composite can withstand.

Assessed how almost every ratio shows the same linear behavior, in the further discussions the ratios capped to one will be preferred, being easier to read. Namely these ratios will be referred, while discussing conclusions in the next chapter:

$\rho_{S(f_u)}$	Effectiveness Ratio (joint's shear w/ respect to sheet's rupture resultant)
$\rho_{\varepsilon_s(f_u)}$	Ductility Ratio (with respect to steel strain at fiber rupture)
ρ_{A_f}	Efficiency Ratio (with respect to balanced area)

Notice that the picked effectiveness and ductility ratios always coincide, hence only two parameters need to be referred to for a global evaluation:

$$\rho_{S\&\varepsilon_s} = \frac{S(anchored)}{A_f f_{fu}} = \frac{\varepsilon_s(anchored)}{\varepsilon_s(f_u)} \quad \text{Strength \& Ductility Ratio}$$

$$\rho_{A_f} = \frac{A_f}{A_{f,opt}(\varepsilon_{fd})} \quad \text{Efficiency Ratio}$$

Having already widely presented the strain-gages measured strain data and having discussed their limited reliability, the only measured quantities here referred are the ultimate load and ultimate midspan deflection; every other quantity is derived according to the formulas already discussed, strains are defined as equivalent-ultimate-strains via sectional equilibrium under the known external ultimate load.

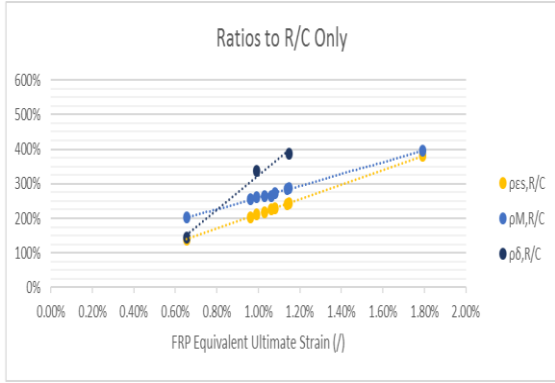
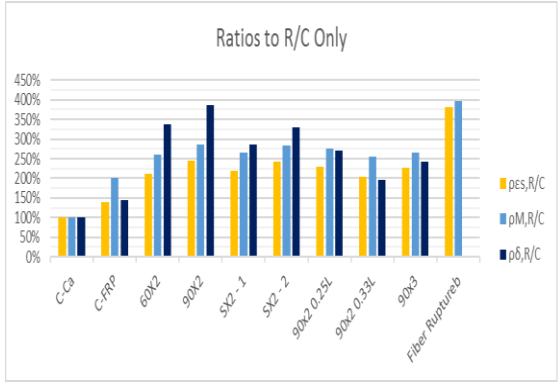


FIGURE 207 - RATIOS TO UNREINFORCED SAMPLE, R/C ONLY

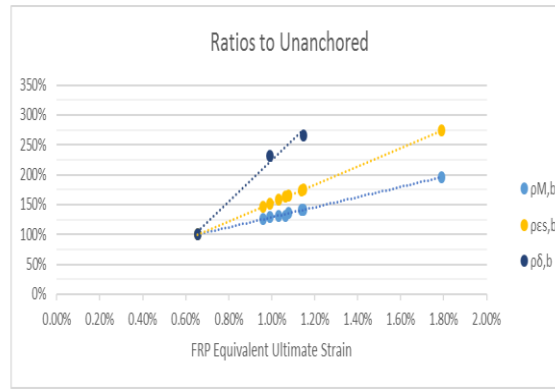
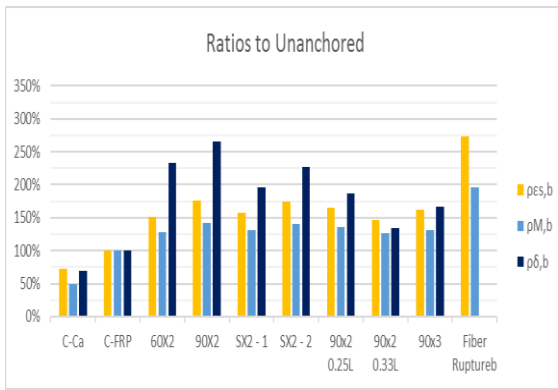


FIGURE 208 - RATIOS TO CONTROL SAMPLE, C-FRP ONLY

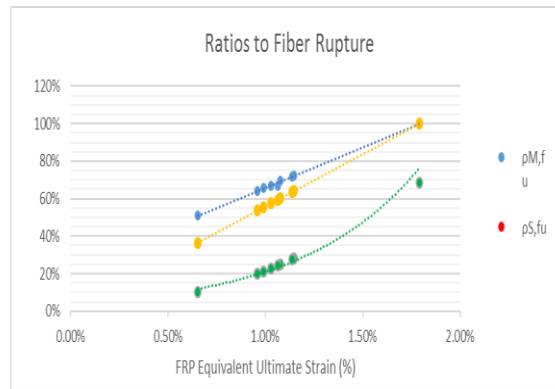
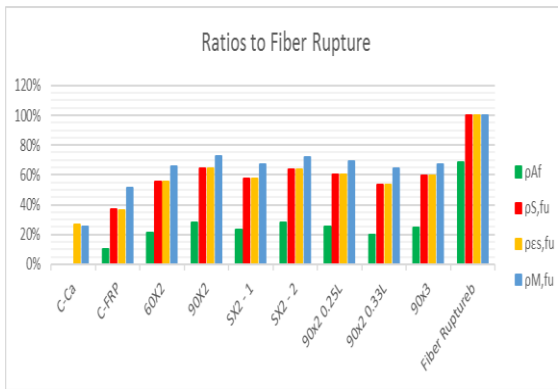


FIGURE 209 - RATIOS TO FIBER RUPTURE

Results Recap [US]

	C-C	C-FRP	60X2	90X2	SX2 - 1	SX2 - 2	90x2 0.25L	90x2 0.33L	90X3	Fiber Rupture	
P_{db} [kip]	-	9.33	9.55	9.46	10.19	9.84	9.88	9.75	10.00	-	Experimental - Serviceability
δ_{db} [in]	-	0.82	0.89	1.17	1.01	1.18	0.97	0.81	1.03	-	
P_u [kip]	4.49	9.33	12.09	13.37	12.31	13.24	12.77	11.84	12.32	18.53	Experimental - Ultimate
δ_u [in]	0.56	0.82	1.90	2.18	1.61	1.86	1.53	1.10	1.37	-	
δ_{u2} [in]	-	-	-	-	3.27	3.49	2.54	-	1.99	-	
$\epsilon_{s,eq}$ [%]	0.39%	0.54%	0.82%	0.94%	0.85%	0.94%	0.89%	0.79%	0.87%	1.47%	
$\epsilon_{f,eq}$ [%]	-	0.65%	0.99%	1.15%	1.03%	1.14%	1.08%	0.96%	1.06%	1.79%	Analytically Derived
M_u [kip in]	88	177	228	252	233	250	241	224	233	348	
F_{eq} [kip]	-	17.01	25.75	29.78	26.77	29.56	28.01	24.95	27.61	46.48	
$\rho_{s, fu}$ [%]	-	37%	55%	64%	58%	64%	60%	54%	59%	100%	Shear Effectiveness
$\rho_{M,R/C}$ [%]	100%	202%	260%	287%	265%	284%	274%	255%	265%	396%	
$\rho_{M,b}$ [%]	50%	100%	129%	142%	131%	141%	136%	126%	131%	196%	Flexural Effectiveness
$\rho_{M, fu}$ [%]	25%	51%	66%	73%	67%	72%	69%	64%	67%	100%	
ρ_{Af} [%]	-	10%	21%	28%	23%	28%	25%	20%	24%	68%	Flexural Efficiency
$\rho_{es,R/C}$ [%]	100%	139%	210%	244%	219%	242%	229%	204%	226%	380%	
$\rho_{es,b}$ [%]	72%	100%	152%	175%	158%	174%	165%	147%	163%	274%	Ductility - Steel Strain POV
$\rho_{es, fu}$ [%]	26%	37%	55%	64%	58%	64%	60%	54%	59%	100%	
ρ_y [%]	149%	206%	313%	362%	325%	359%	341%	303%	336%	565%	Yielding Ratio
$\rho_{\delta,R/C}$ [%]	100%	145%	337%	386%	285%	329%	271%	195%	242%	-	
$\rho_{\delta,b}$ [%]	69%	100%	232%	266%	197%	227%	187%	134%	167%	-	Ductility - Deflection POV
$\rho_{\delta, fu}$ [%]	-	-	-	-	-	-	-	-	-	-	

a

b



Ratio to Fiber Rupture

Ratio to Reinforced Concrete Only

Ratio to Debonding Failure

a steel strain is gage-measured

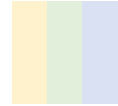
b all values are analytically estimated

Results Recap [SI]

	C-C	C-FRP	60X2	90X2	SX2 - 1	SX2 - 2	90X2 0.25L	90X2 0.33L	90x3	Fiber Rupture	Experimental - Serviceability
P_{db} [kN]	-	42	42	42	45	44	44	43	45	-	-
δ_{db} [mm]	-	21	23	30	26	30	25	21	26	-	-
P_u [kN]	20	42	54	59	55	59	57	53	55	82	Experimental - Ultimate
δ_u [mm]	14	21	48	55	41	47	39	28	35	-	-
δ_{u2} [mm]	-	-	-	-	83	89	64	-	51	-	-
$\epsilon_{s,eq}$ [%]	0.39%	0.54%	0.82%	0.94%	0.85%	0.94%	0.89%	0.79%	0.87%	1.47%	1.47%
$\epsilon_{f,eq}$ [%]	-	0.65%	0.99%	1.15%	1.03%	1.14%	1.08%	0.96%	1.06%	1.79%	1.79%
M_u [kN mm]	9.93	20.05	25.81	28.48	26.27	28.23	27.25	25.28	26.29	39.28	Analytically Derived
F_{eq} [kN]	-	17.01	25.75	29.78	26.77	29.56	28.01	24.95	27.61	46.48	46.48
$\rho_{s,fu}$ [%]	-	37%	55%	64%	58%	64%	60%	54%	59%	100%	100%
$\rho_{M,R/C}$ [%]	100%	202%	260%	287%	265%	284%	274%	255%	265%	396%	396%
$\rho_{M,b}$ [%]	50%	100%	129%	142%	131%	141%	136%	126%	131%	196%	196%
$\rho_{M,fu}$ [%]	25%	51%	66%	73%	67%	72%	69%	64%	67%	100%	100%
ρ_{Af} [%]	-	10%	21%	28%	23%	28%	25%	20%	24%	68%	68%
$\rho_{Es,R/C}$ [%]	100%	139%	210%	244%	219%	242%	229%	204%	226%	380%	380%
$\rho_{Es,b}$ [%]	72%	100%	152%	175%	158%	174%	165%	147%	163%	274%	274%
$\rho_{Es,fu}$ [%]	26%	37%	55%	64%	58%	64%	60%	54%	59%	100%	100%
ρ_y [%]	149%	206%	313%	362%	325%	359%	341%	303%	336%	565%	565%
$\rho_{\delta,R/C}$ [%]	100%	145%	337%	386%	285%	329%	271%	195%	242%	-	-
$\rho_{\delta,b}$ [%]	69%	100%	232%	266%	197%	227%	187%	134%	167%	-	-
$\rho_{\delta,fu}$ [%]	-	-	-	-	-	-	-	-	-	-	-

a

b



Ratio to Fiber Rupture

Ratio to Reinforced Concrete Only

Ratio to Debonding Failure

a steel strain is gage-measured

b all values are analytically estimated

6.4 Results Discussion

6.4.1 Behavior

6.4.1.1 Slabs' behavior

When anchors are located at the very end of the fiber sheet, the observed behavior is in line with what reported by other authors (Piyong et al. 2003) (Smith et al. 2011, 2013).

As in the control sample, a bi-linear behavior up to debonding can be clearly spotted, looking at the load-deflection diagram on the following page. When debonding occurs, the end anchors are suddenly engaged, providing the critical load-transfer mechanism for system's equilibrium. Over the debonded sheet, the strains are almost constant at varying abscissa and equal to the value registered in midspan.

As debonding proceeds behind the first anchor, the system experiences a series of load drops and increments; after this transition phase, the strength start growing again, with a sensibly reduced stiffness, as bonding is no longer provided. The overall behavior can be properly modeled as a pseudo-tri-linear one.

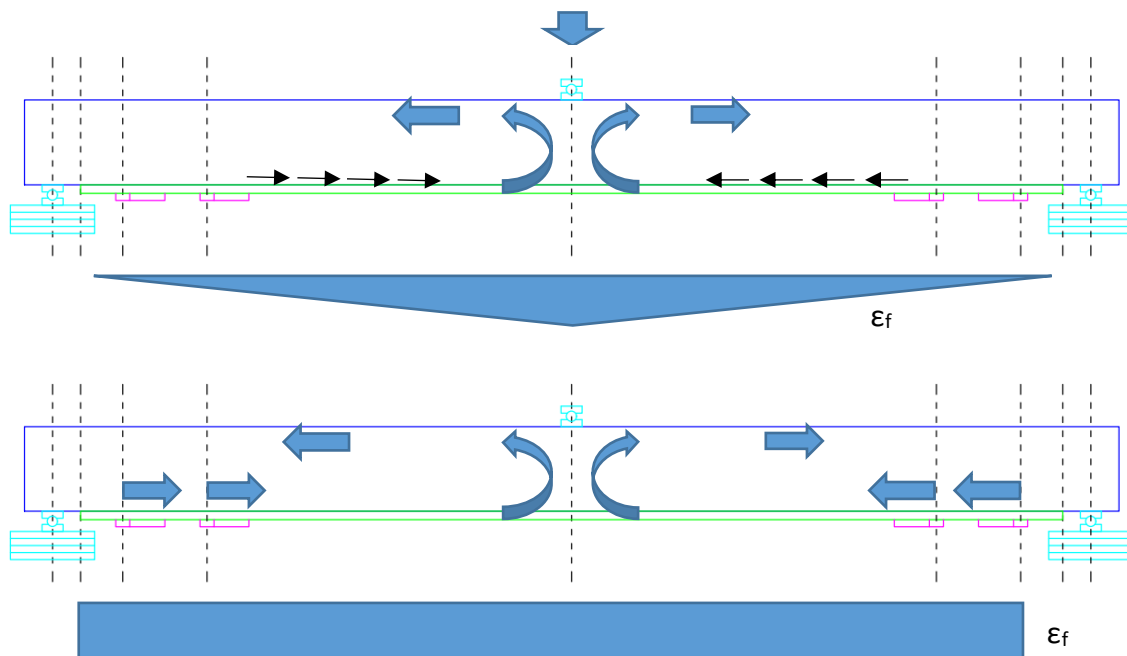


FIGURE 210 - STRUCTURAL EQUILIBRIUM BEFORE & AFTER INTERMEDIATE DEBONDING

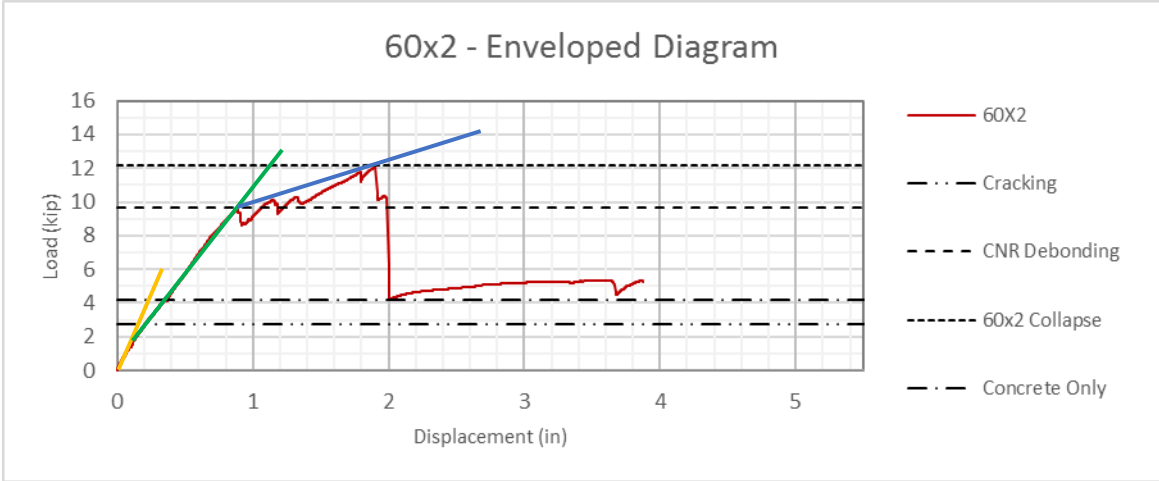


FIGURE 211 - TRI-LINEAR BEHAVIOR. 1 IN = 25,4 MM / 1 KIP = 4.448 kN

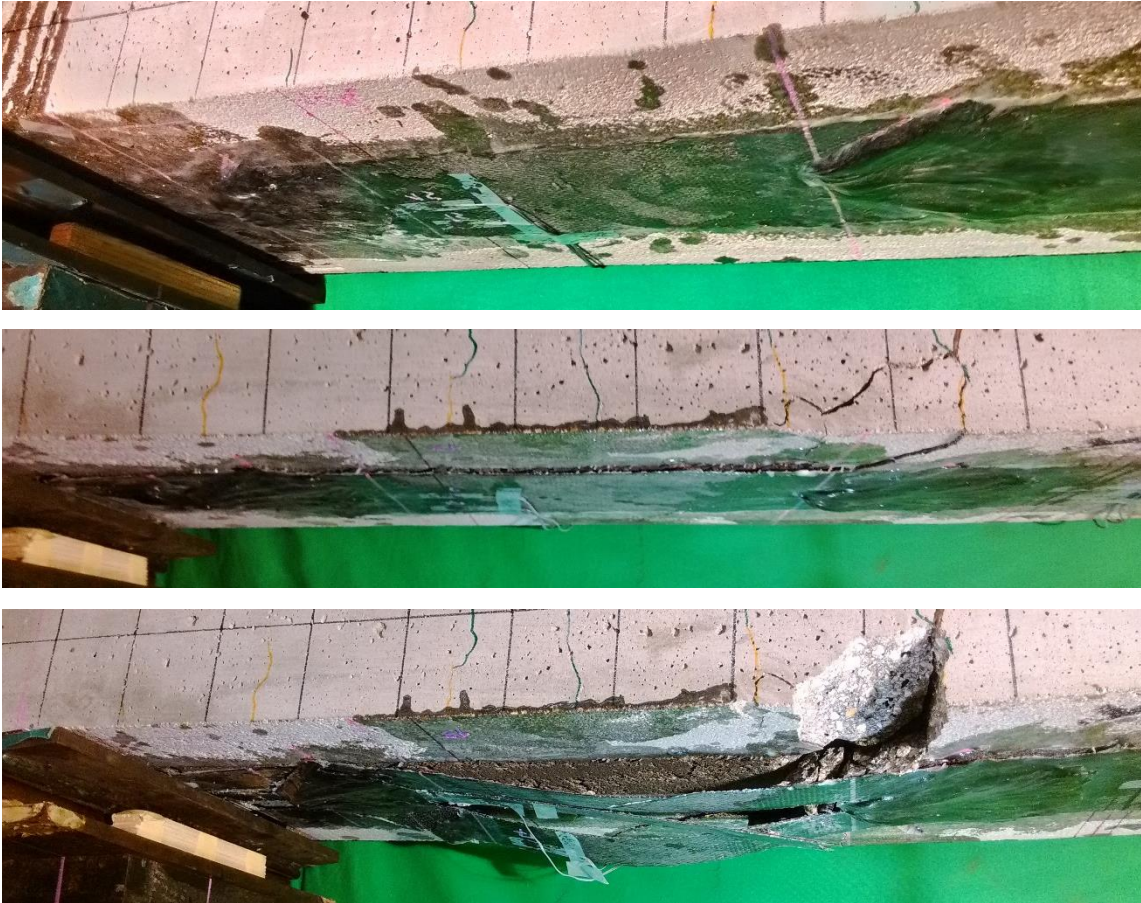


FIGURE 212 - THE SAME SHEET: BONDED, DEBONDED & FAILED (90x2 L/3)

6.4.1.2 Serviceability & Ultimate Limit States

It should be noticed how the anchors' presence has no influence on the value of intermediate debonding load, suggesting end anchors do not provide any intermediate bonding improvement (type I, II) at serviceability, while provide a relevant strength and ductility increment (type III, IV) at ultimate limit state.

		SLS & ULS [US]									
		C-C	C-FRP	60X2	90X2	SX2 - 1	SX2 - 2	90x2 0.25L	90x2 0.33L	90x3	Rupture
P _{db} [kip]	Exp.	-	9.33	9.55	9.46	10.19	9.84	9.88	9.75	10.00	-
	Th.	-	9.68	9.68	9.68	9.68	9.68	9.68	9.68	9.68	-
	Δ	-	-3.58%	-1.32%	-2.25%	5.30%	1.67%	2.06%	0.75%	3.37%	-
P _u [kip]	Exp.	4.49	9.33	12.09	13.37	12.31	13.24	12.77	11.84	12.32	-
	Th.	4.14	9.68	12.16	13.67	13.67	13.67	13.67	13.67	-	1.42
	Δ	8.32%	-3.58%	-0.62%	-2.22%	-9.97%	-3.13%	-6.56%	-13.42%	-	-

		SLS & ULS [SI]									
		C-C	C-FRP	60X2	90X2	SX2 - 1	SX2 - 2	90x2 0.25L	90x2 0.33L	90x3	Rupture
P _{db} [kN]	Exp.	-	42	42	42	45	44	44	43	45	-
	Th.	-	43	43	43	43	43	43	43	10	-
	Δ	-	-3.58%	-1.32%	-2.25%	5.30%	1.67%	2.06%	0.75%	3.37%	-
P _u [kN]	Exp.	20	42	54	59	55	59	57	53	55	-
	Th.	18	43	54	61	61	61	61	61	-	6
	Δ	8.32%	-3.58%	-0.62%	-2.22%	-9.97%	-3.13%	-6.56%	-13.42%	-	-

6.4.1.3 Anchors' Failure

In all the tested configurations, the shear-engaged anchors failed because of FRP sheet slipping under the anchors' fan. The failure is triggered by the slipping of a central strip only, while the lateral strips – provided with a larger anchored area – still guarantee residual strength, until strength drops to R/C-only level.

None of the application is pull-out or shear critical, in net contrast with results from Smith et al. (2011) (2013). The configurations tested here have a larger and deeper dowel, leading to the conclusion that it is enough to provide a certain minimum shear area and embedded length in order to switch the failure mode to a slipping one. The definition of such minimum values requires a wider samples database.



FIGURE 213 - 60x2 ANCHORS COLLAPSE, GENERALLY REPRESENTATIVE

6.4.1.4 Strain Shapes over the Sheet's Width

Looking at the strain measurements taken, a non-uniform strain distribution over the width can be spotted. It is interesting to notice how different strain shapes can be spotted on different specimens; two main tendencies can be observed: a concave and a convex one. In both cases the variation is not significant from a design point of view, but, from a measurement point of view, missing one critical point over the width would lead to a severe under or overestimation of the actual strain the lamina is subjected to.

Both concave and convex shapes were already documented by other authors (Niemits et al. 2010) (Brena & McGuirk, 2013) even if the lack of measurements in front of each one of the anchors in parallel makes their results hardly interpretable.

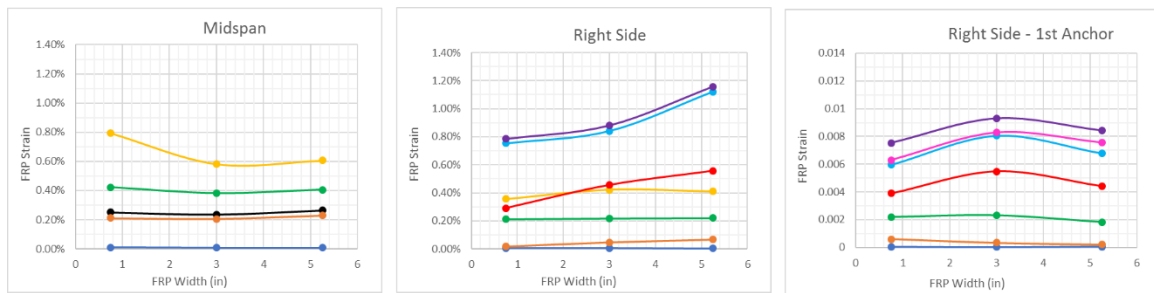


FIGURE 214 - (A) C-FRP (B) Sx2-2 (C) 90x2

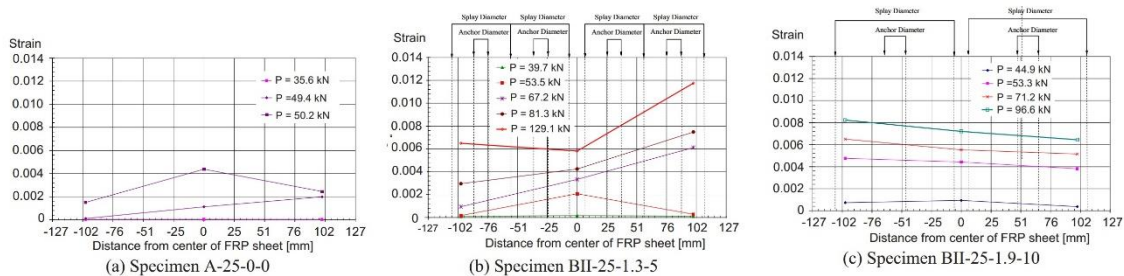


FIGURE 215 - NIEMITS ET AL. (2010)

A concave shape seems more common in flexural applications, also taking into account the two-point measures available on the other slabs. The shape is not symmetric and present a maximum on the side where debonding is triggered. It seems reasonable to assume the FRP sheet to act against crack opening, hence the confinement is higher at sheet's center, while, moving towards the sides, the cracks are not as efficiently countered and the strains increase.

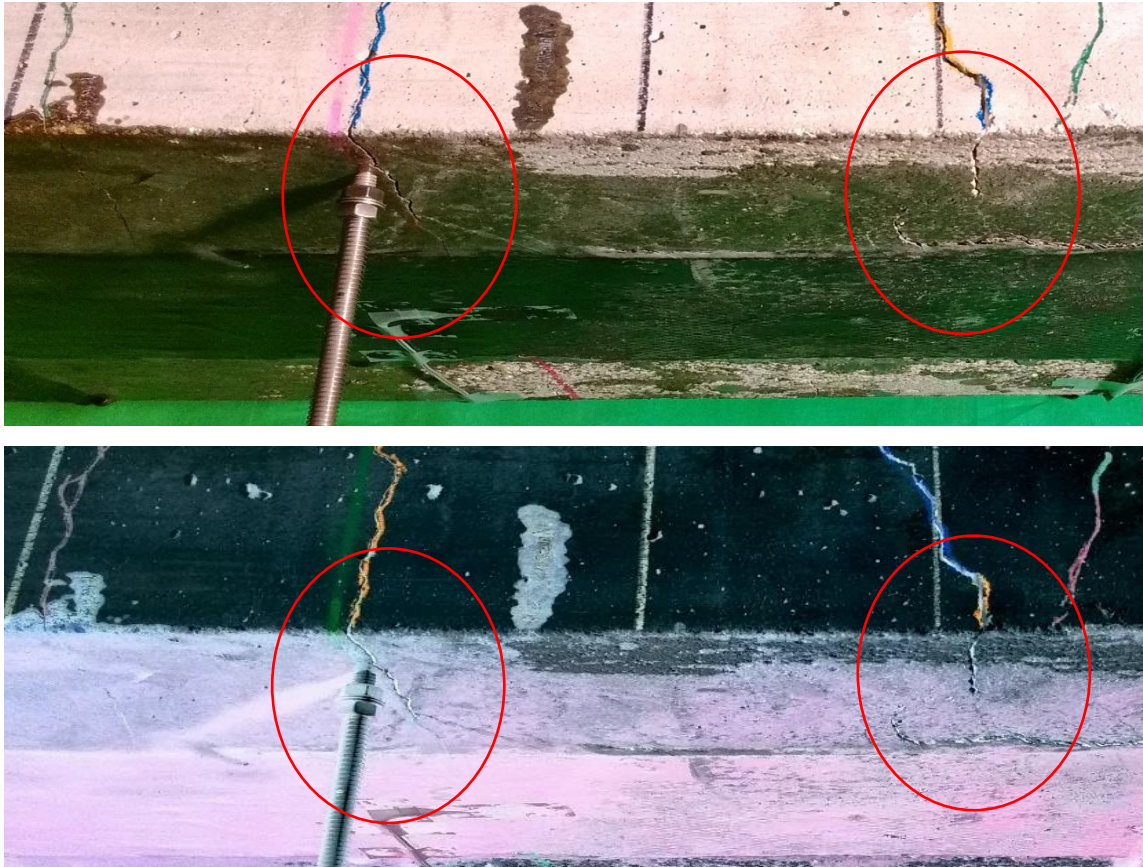


FIGURE 216 - CRACKS CLOSING MOVING TOWARDS THE FRP SHEET

A convex shape is documented as well; in this case a closer symmetry can be spotted. In this case the higher strains on sheet's central fiber are probably related to a perfectly symmetrically applied external load, that engages with a higher ratio the central portion of the slab, hence the central portion of the FRP sheet.

Assuming the central portion of the strip to be better bonded to the concrete underneath it also shows a higher stiffness, further justifying the higher level of engagement, resulting in higher strains. Assuming the anchor fan's fiber direction to affect the anchoring ratio of the fiber sheet, fiber aligned as the sheet's fiber will guarantee a higher ratio, hence a higher stiffness and a higher load engagement ratio.

The actual strain shape is a balance of the two tendencies, considering symmetry to be hard to achieve in real case scenarios, a concave, asymmetric shape seems generally most common.

6.4.1.5 Strain Shapes Over the Sheet's Length

Looking at the strains over the sheet's length, it is evident how the shape turns from a triangular to a uniform one as intermediate debonding occurs: as already discussed, over the debonded sheet, the strains are almost constant at varying abscissa and equal to the value registered at midspan. Some variations are still observable because of FRP-concrete friction; the collapse usually happens on the side showing the higher strains.

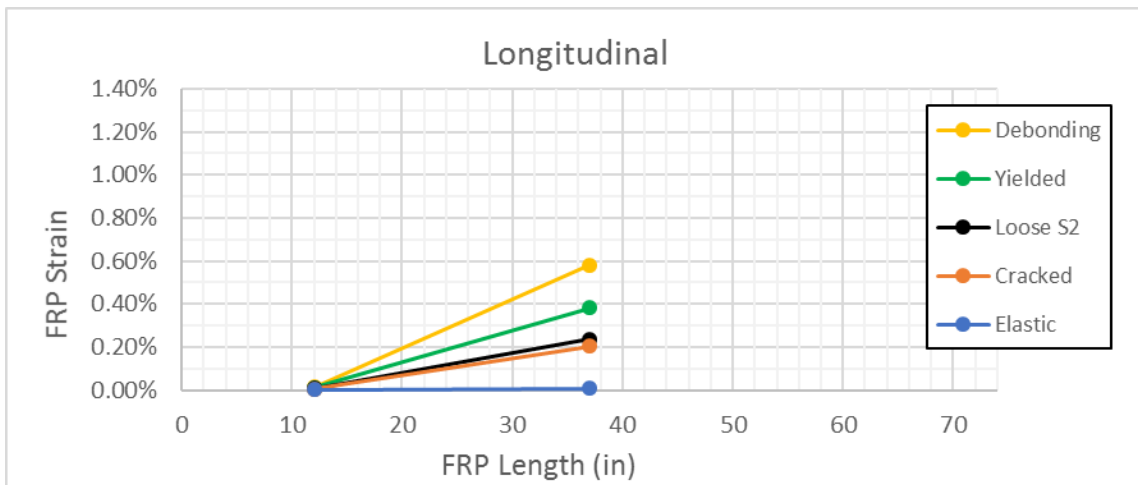


FIGURE 217 - CONTROL SAMPLE (C-FRP).

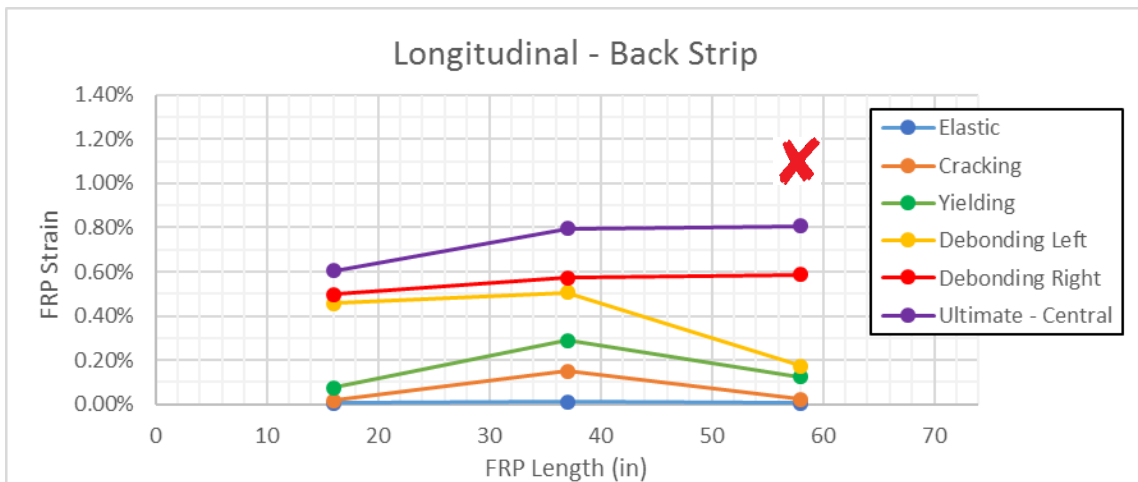


FIGURE 218 - 60x2 SAMPLE, THE X MARKS THE FAILING SIDE.

1 IN = 25,4 MM / 1 KIP = 4.448 kN

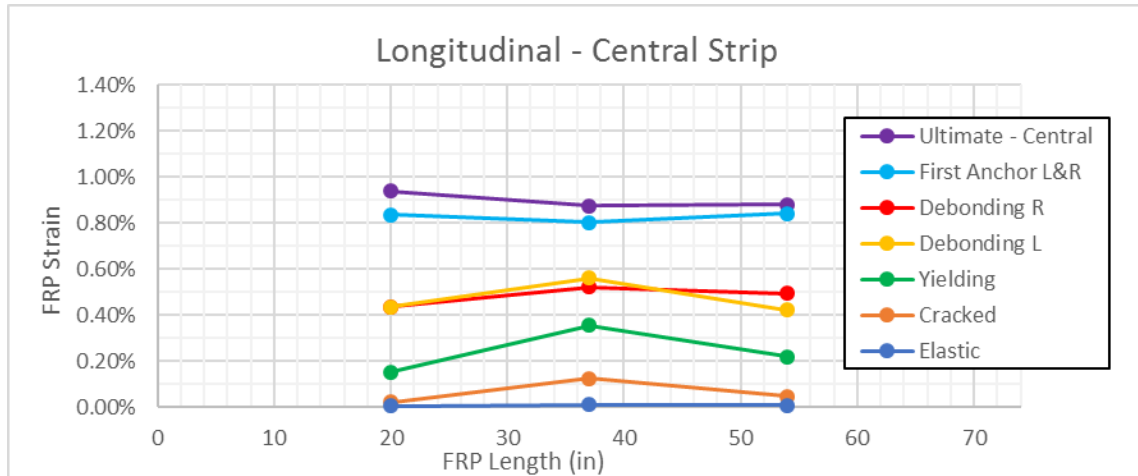


FIGURE 219 - SX2-2 SAMPLE SHOWS A PERFECTLY SYMMETRIC FAILURE, FURTHER DISCUSSION WILL FOLLOW

6.4.2 Design

6.4.2.1 ULS Design

Accounting for the expected behavior, very in line with the experienced one, the end anchor joints were designed in order to be engaged after intermediate debonding, providing the critical shear transfer mechanism required to further enhance the system strength at Ultimate Limit State, postponing collapse.

The main goal was to develop an algorithm easily acceptable and implementable into everyday design practice, in order to do so, the well accepted CNR-DT200 sectional analysis approach to external flexural strengthening design was taken as a reference.

The standard III stage sectional analysis assumptions are imposed, along with a couple of addenda required to model the external reinforcement behavior:

- I. Plane sections remain plane (Bernoulli-Navier's Assumption)
- II. Perfect steel – concrete bonding
- III. Inelastic steel & concrete Behavior
- IV. Concrete not-working in tension

- IIa. Perfect FRP – concrete bond up to failure
- IIIa. FRP behaves elastically up to failure

The bended element collapse can be triggered by any of the involved materials, even though a steel failure is highly improbable and it is generally enough to check concrete and external reinforcement. Regarding FRP, the ultimate sheet's strength cannot be guaranteed a-priori and the minimum value between the sheet's and anchor joint's strength will eventually govern the collapse.

$$\varepsilon_{fd,ULS} = \min(\varepsilon_{fdd,3}, \varepsilon_{fu})$$

Clearly the joint-related equivalent strain $\varepsilon_{fdd,3}$ has to be larger than the intermediate debonding strain $\varepsilon_{fdd,2}$, otherwise the anchors would fail in the same instant at which end debonding occurs and the anchoring solution would prove totally useless, not providing any improvement in terms of serviceability performances.

$$\varepsilon_{fdd,3} > \varepsilon_{fdd,2}$$

No safety factors are accounted here, but the standard CNR safety and exposure factors can be applied to sheet's strength, while a wider statistic database is required to define proper safety factors for anchor's strength.

The FRP triggered flexural collapse can rule the system's failure as well as a concrete triggered flexural one. The element shear strength should be checked as well, while end debonding can generally be assumed non critical in anchored, slip-critical applications.

6.4.2.2 SLS Design

The tested anchor spikes do not provide any significant performance improvement in terms of retarding intermediate debonding that keeps occurring at a load level very close to what predicted via CNR formulation. The FRP serviceability limit is still defined by:

$$\varepsilon_{fd,SLS} = \min(\varepsilon_{fdd,2}, \varepsilon_{fu})$$

6.4.3 Joint Characterization

The first part of this dissertation has clearly pointed out the lack of a reliable characterization model for anchor spikes, forcing to rely on an experimental solution. The standard characterization method for FRP anchors is a direct shear test, providing a very reliable strength measurement and, eventually, less reliable strain readings.

6.4.3.1 Strength Based Characterization

Among the advantages coming with a strength based characterization, are an always available strength measurement and the reliability of such a measurement. Conceptually speaking, a strength measurement globally describes the joint's contribution: is less dependent on the testing set-up and well consistent with a globally-oriented design approach, such a ULS sectional analysis, very suited to flexural strength evaluation, but less precise in detailing the section's actual behavior.

On the other side, the need to switch from a strength-based anchor characterization, to a strain based sectional analysis seems evident. Luckily, the FRP sheet linear elasticity makes the task extremely easy:

$$\varepsilon_{fdd,3} = \frac{S_{anchor}}{A_f E_f}$$

A strength based characterization proved to be versatile, allowing to switch from a single anchor to a whole joint characterization. In the present case, a full-coupling assumption proved to be effective in characterizing the behavior of 3'' (75 mm) spaced anchors, in line with conclusions from Brena & McGuirk (2013) for closely spaced anchors.

$$S_{joint} = n_s S_{anchor} \qquad \varepsilon_{fdd,3} = \frac{S_{joint}}{A_f E_f}$$

A more complex model, defined at varying anchors' distance from sheet's end was proposed by Zhang & Smith (2013) and further discussed later for comparison purposes.



FIGURE 220 - SHEAR CHARACTERIZATION SET-UP, LOAD CELL VISIBLE IN THE LEFT PICTURE

6.4.3.2 Strain Based Characterization

A strain based characterization comes with a certain number of details to take into consideration. First of all, a strain measurement is local, hence a certain number of measurements over the width is required, in order to properly define an equivalent (averaged) sectional strain. Secondly, strain measurement comes with a higher number of uncertainties, in the gages application and data interpretation, and even one single gage failing can undermine the measurement reliability. Thirdly, strain measurements are not always available in published papers, or properly performed, because of errors or limits in the equipment (e.g. a limited number of acquisition channel).

In order to have a reliable measure of the FRP strain over the width, at least a three-point measure is required, in order to be sure to catch either the extreme maximum and minimum values. It can be noticed how, when a three-point average was performed, the observed error was way lower, with respect to the expected equivalent failure. In presence of various anchors in parallel, it is recommended to measure strains in front of each dowel and on the sides of each fan.

Such an averaged measure can be assumed as the equivalent failure strain $\epsilon_{fd,3}$ in alternative to a strength based approach, being however more case-related and less prone to multiple-anchor joint characterization, if not via multiple anchors direct testing.



FIGURE 221 - THREE & EIGHT STRAIN GAGES CONFIGURATIONS & A STRAIN GAGE REPRESENTATION

6.4.4 Matching

Goal of the so-called matching series is to prove the good matching between the design and experimental ultimate strength, computing the analytical value in accordance to the method already discussed. A good matching validates the proposed sectional model as a reliable design method and the double shear test as a reliable strength-oriented experimental characterization method. The full-coupled behavior of close-spaced anchors is well proved as well.

The sandwich configuration is compared to the standard 90x2 design value, once assessed the inefficacy of the sandwich itself, and allows to notice the better strain matching when a 3-point average can be performed.

6.4.4.1 Load

A very good matching is guaranteed on the ultimate load side, validating the proposed sectional model as a design tool to describe the global system's behavior. Approaching the problem from a global prospective, a global shear strength characterization for the implemented anchors seems the soundest and is certified as well.

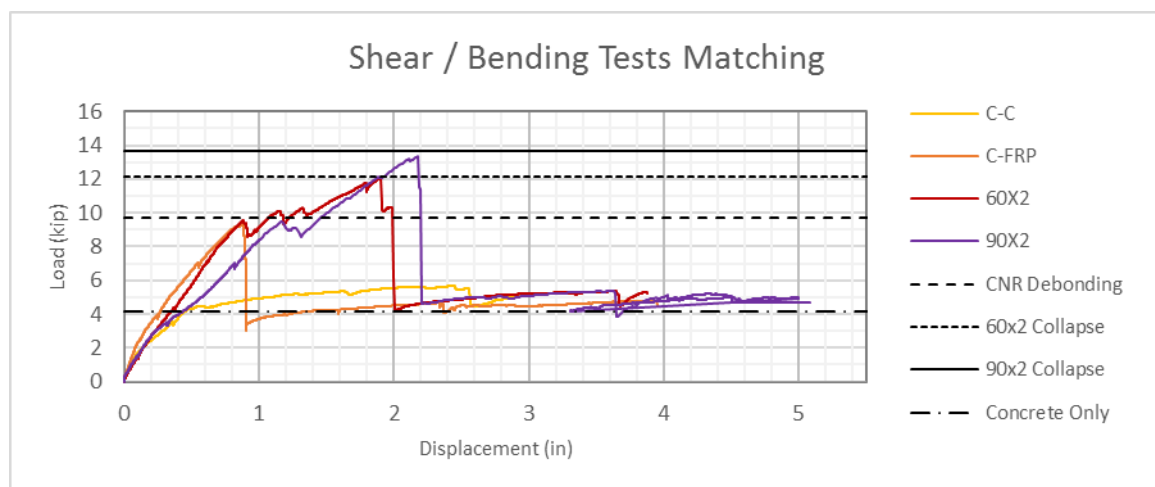


FIGURE 222 - ULTIMATE LOAD MATCHING.

1 IN = 25,4 MM / 1 KIP = 4.448 kN

6.4.4.2 Deflection

On the deflection side, the proposed approach presents a good experimental matching up to laminate debonding; after debonding occurs the third linear branch present a stiffness way lower than the predicted one and the theoretical deflection proved to be largely underestimated.

The results point out the need to develop an ad-hoc model for deflection prediction at ultimate limit state, in presence of debonded external FRP reinforcement. However, this is beyond the purposes of this dissertation.

6.4.4.3 Stiffness

The stiffness matching is naturally a balance between the load and deflection ones, proving to be quite accurate up to debonding, but clearly failing at ultimate limit state.

The stiffness here considered is the equivalent-third stage stiffness, namely the slope of a straight line going from the origin to the failure point. The actual system's stiffness at failure, going from the debonding peak to the failure peak, is way lower.

As for the deflection, the stiffness matching points out the need for an ad-hoc modeling approach, behind the purposes of this dissertation.

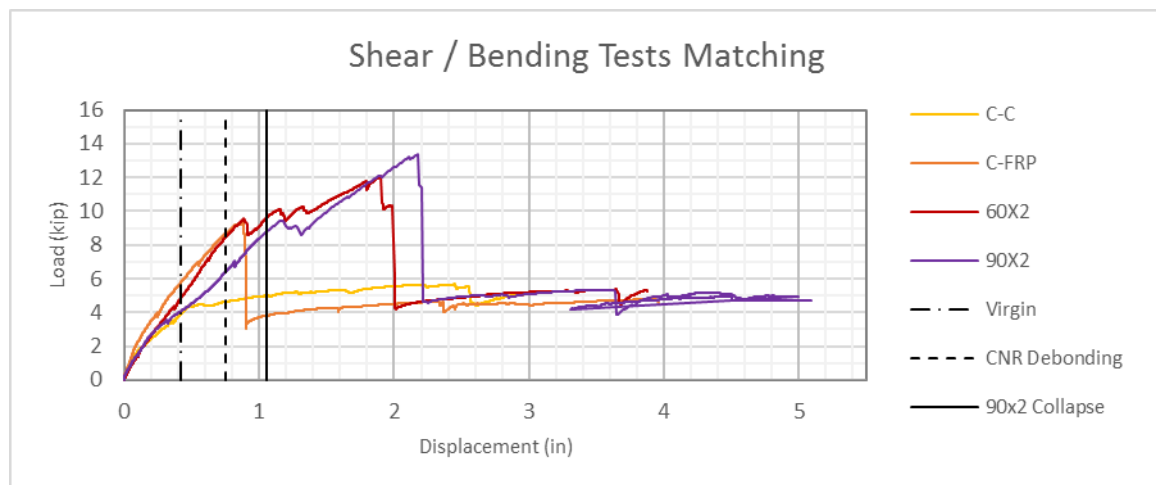


FIGURE 223 - DEFLECTION MATCHING.

$$1 \text{ IN} = 25,4 \text{ MM} / 1 \text{ KIP} = 4.448 \text{ kN}$$

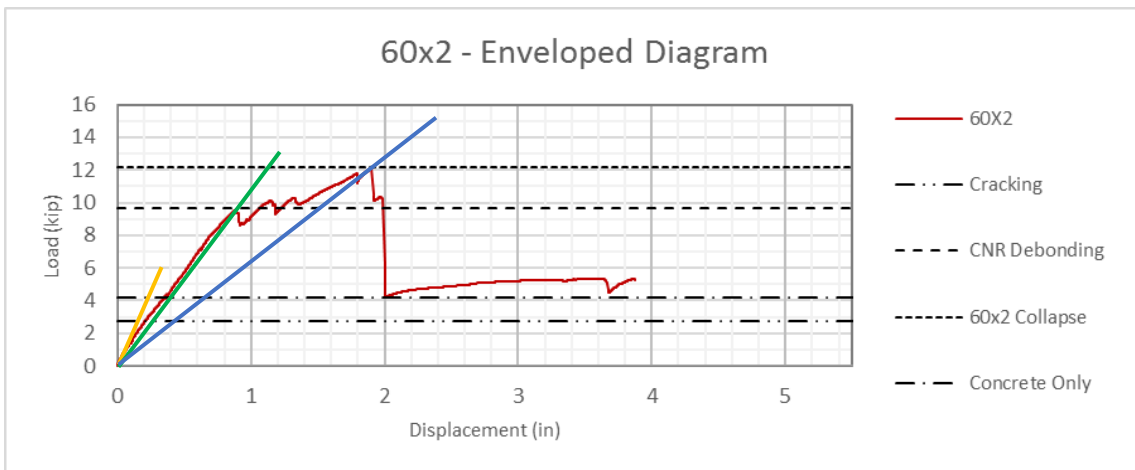
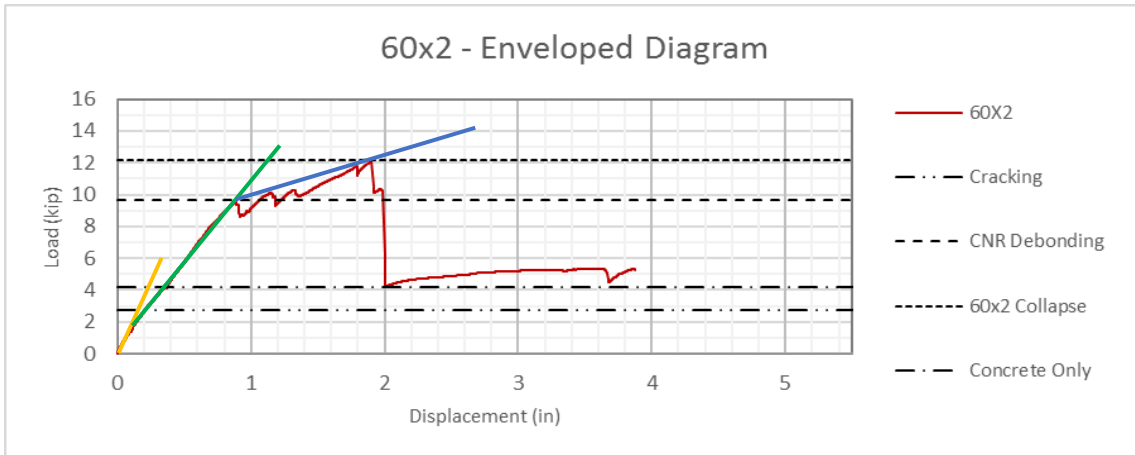


FIGURE 224 – EFFECTIVE VS EQUIVALENT STIFFNESS (YELLOW) I STAGE, UNCRACKED (GREEN) II STAGE, CRACKED ELASTIC [SLS] (BLUE) III STAGE, CRACKED INELASTIC [ULS]. 1 IN = 25,4 MM / 1 KIP = 4.448 kN

6.4.4.4 Strains

As already discussed, matching a local strain measure with a theoretical value, coming from a global model, intrinsically presents a higher degree of uncertainty. Expecting the theoretical value to be registered all over the sheet's width is unrealistic, while an average approach seems the soundest option and a significantly lower error can be noticed when a three-point measurement is available.

Matching the design value to the equivalent ultimate experimental strain, computed imposing sectional equilibrium under the ultimate experimental load, a way lower level of error can be spotted, very in line with the error measured on the ultimate load, as it was obvious to expect.

Matching - SLS [US]

		C-C	C-FRP	60X2	90X2	SX2 - 2
P_{db} [kip]	Exp.	-	9.33	9.55	9.46	9.84
	Th.	-	9.68	9.68	9.68	9.68
	Δ	-	-3.58%	-1.32%	-2.25%	1.67%
δ_{db} [in]	Exp.	-	0.82	0.89	1.17	1.18
	Th.	-	0.75	0.75	0.75	0.75
	Δ	-	8.88%	17.94%	55.57%	57.01%
EJ_{SLS} [kip in ²]	Exp.	-	99,566	93,993	70,615	72,675
	Th.	-	112,295	112,295	112,295	112,295
	Δ	-	-11.34%	-16.30%	-37.12%	-35.28%

Matching - ULS [US]

		C-C	C-FRP	60X2	90X2	SX2 - 2
P_u [kip]	Exp.	4.49	9.33	12.09	13.37	13.24
	Th.	4.14	9.68	12.16	13.67	13.67
	Δ	8.32%	-3.58%	-0.62%	-2.22%	-3.13%
δ_u [in]	Exp.	0.56	0.82	1.90	2.18	1.86
	Th.	0.42	0.75	0.94	1.05	1.05
	Δ	34.45%	8.88%	102.47%	106.84%	76.18%
EJ_u [kip in ²]	Exp.	72,005	99,566	55,057	53,026	61,692
	Th.	89,883	112,295	112,147	112,117	112,117
	Δ	-19.89%	-11.34%	-50.91%	-52.70%	-44.98%
ϵ_{fu} [%]	Exp.	-	0.66%	0.79%	0.77%	0.96%
	Th.	-	0.70%	1.00%	1.19%	1.19%
	Δ	-	-5.18%	-20.83%	-34.88%	-19.35%
$\epsilon_{f,eq}$ [%]	Exp.	-	0.65%	0.99%	1.15%	1.14%
	Th.	-	0.70%	1.00%	1.19%	1.19%
	Δ	-	-6.05%	-0.92%	-3.30%	-4.01%

a

b

b

c

- a 3-point average, midspan
- b 1-point, central strip, midspan
- c 3-point average, left, failing side

		Matching - SLS [SI]				
		C-C	C-FRP	60X2	90X2	SX2 - 2
P_{db} [kN]	Exp.	-	41.51	42.48	42.08	43.77
	Th.	-	43.05	43.05	43.05	43.05
	Δ	-	-3.58%	-1.32%	-2.25%	1.67%
δ_{db} [mm]	Exp.	-	21	23	30	30
	Th.	-	19	19	19	19
	Δ	-	8.88%	17.94%	55.57%	57.01%
EJ_{SLS} [kN m ²]	Exp.	-	2,857	2,697	2,027	2,086
	Th.	-	3,223	3,223	3,223	3,223
	Δ	-	-11.34%	-16.30%	-37.12%	-35.28%

		Matching - ULS [SI]				
		C-C	C-FRP	60X2	90X2	SX2 - 2
P_u [kN]	Exp.	19.97	41.51	53.77	59.46	58.91
	Th.	18.43	43.05	54.10	60.81	60.81
	Δ	8.32%	-3.58%	-0.62%	-2.22%	-3.13%
δ_u [mm]	Exp.	14	21	48	55	47
	Th.	11	19	24	27	27
	Δ	34.45%	8.88%	102.47%	106.84%	76.18%
EJ_u [kN m ²]	Exp.	2,066	2,857	1,580	1,522	1,770
	Th.	2,579	3,223	3,218	3,218	3,218
	Δ	-19.89%	-11.34%	-50.91%	-52.70%	-44.98%
ε_{fu} [%]	Exp.	-	0.66%	0.79%	0.77%	0.96%
	Th.	-	0.70%	1.00%	1.19%	1.19%
	Δ	-	-5.18%	-20.83%	-34.88%	-19.35%
$\varepsilon_{f,eq}$ [%]	Exp.	-	0.65%	0.99%	1.15%	1.14%
	Th.	-	0.70%	1.00%	1.19%	1.19%
	Δ	-	-6.05%	-0.92%	-3.30%	-4.01%
		a	b	b	c	

- a 3-point average, midspan
- b 1-point, central strip, midspan
- c 3-point average, left, failing side

6.4.5 Effectiveness

6.4.5.1 *At Increasing Joint's Strength*

At increasing joints strength, the slab's strength increases consistently, as well as the efficiency of the reinforcing solution and the ductility of the system. Assuming the plain R/C slab as a reference, strength and ductility increments, ranging from 150 to 300 % can be spotted, at varying anchoring solutions. Referring to the unanchored control sample, increments ranges from 150 to 200%.

Assessed the effectiveness of external reinforcement solutions, most interesting is to refer the ratios to the most effective solution at constant amount of reinforcement, i.e. the case in which failure is triggered by fiber sheet's rupture. Such a failure mode was not experimentally reached; hence reference will be made to theoretical values.

Notice that the efficiency of the external reinforcement solution is computed referring to the balanced section concept; in case of theoretical fiber-rupture, the provided reinforcement is not enough to guarantee a balanced section, hence such a parameter is capped at 68% in this case and not 100%.

Ratios are plotted over the equivalent ultimate strain in the FRP, computed imposing sectional equilibrium under ultimate experimental load. The linearity of the strain and load ratios are implicit in the way they are computed, while the linearity of the deflection ratio is purely experimental.

As already discussed, the efficiency ratio is defined in an autonomous way and shows an almost exponential shape at increasing equivalent ultimate strain. This result points out the true advantage related to anchoring solutions: not only increasing the external reinforcement effectiveness, that is possible also thorough multi-layer solutions, but mainly increasing its efficiency, with a more-than-linear tendency.

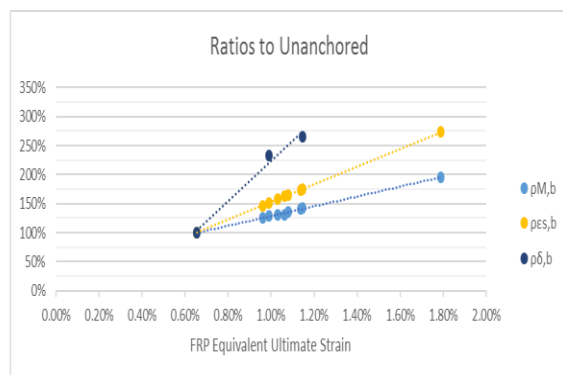
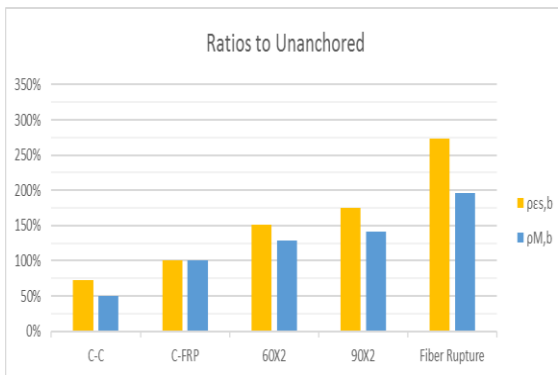
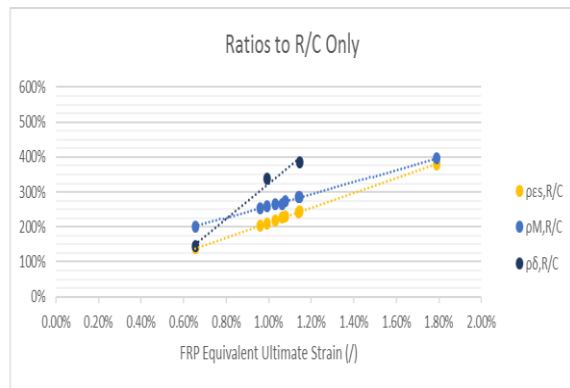
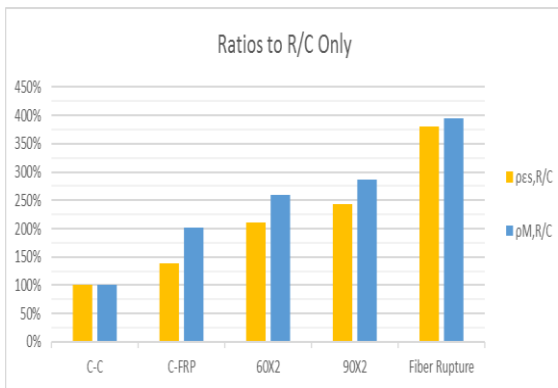
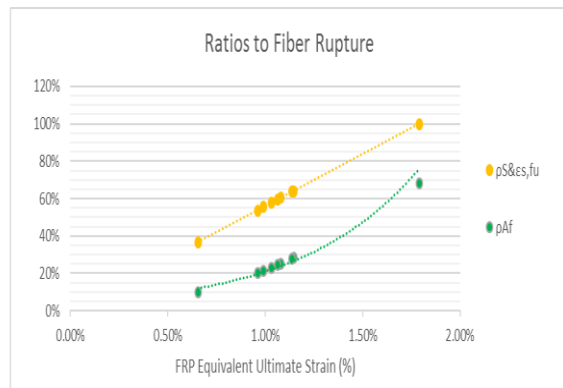
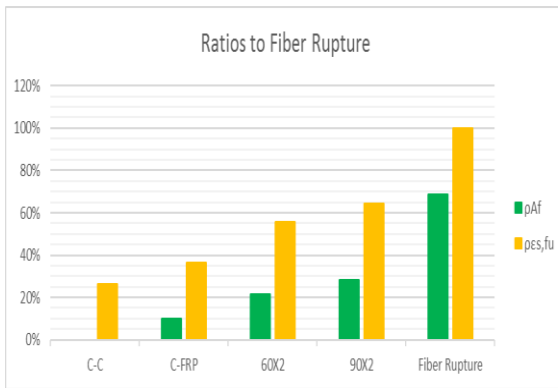
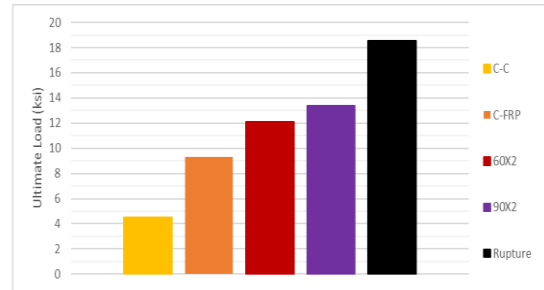
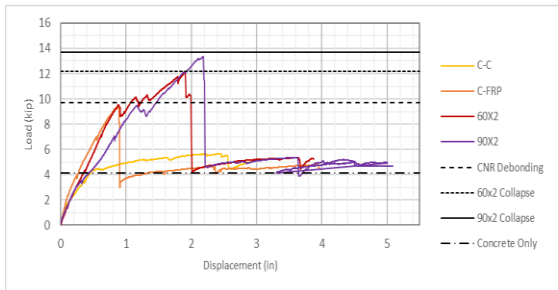


FIGURE 225 - (A) ULTIMATE LOAD (B) RATIOS TO FIBER RUPTURE (B) RATIOS TO UNREINFORCED, R/C ONLY (c) RATIOS TO CONTROL, UNANCHORED C-FRP. INCREASING JOINT STRENGTH. 1 IN = 25,4 MM / 1 KIP = 4.448 kN

6.4.5.2 *At Varying Anchors' Location*

Purpose of the location series is to investigate how anchors' distance and location affects the strength of the joint, three different configurations are tested, along with a three-anchors one, showing a reduced strength at increasing anchors' distance, as a consequence of a progressively decoupled behavior. The decoupling becomes critical when moving the central anchor too close to midspan.

Such a solution turns the standard pure-bending collapse mechanism into a somehow shear-related one: the central anchor dowel's hole acts like a point of discontinuity, causing the formation of a wide bending-shear crack, that triggers debonding behind the first anchor; in such a situation the most of the load is carried by the end anchor, while the central one only carries a limited portion of load, coming from the central span.

The reduced strength reflects in a reduced ductility and efficiency, clearly visible in all the diagrams. A Linear regression model seems reasonable at a first look, further investigation though points out the need of a quadratic model or eventually a bi-linear one: drilling the dowel holes in the Sx2-2 configuration, an obstacle was encountered forcing to drill the hole at a distance of 9" instead of the standard 6", assessed the ineffectiveness of the sandwich configuration, at least from the ultimate load and equivalent strain side, this specimen can be added to the location series.

The Sx2-2 specimen shows a strength very close to the 90x2 sample, even if slightly lower, adding it into the regression series and trying a quadratic approach points out how a bi-linear model seems most suited to describe the specimens' behavior at varying anchors' distance: the joint shows a perfectly coupled behavior as long as the anchors are close enough, up to 9" (225 mm) at least, after a certain limit distance the strength start decreasing with an almost linear shape.

Whether this behavior is directly caused by the increasing anchor spacing or by the central anchor approaching the midspan is yet to be determined. For sure, the two effects concur to the result, with a significant role played by moving the central anchor very close to midspan, in a high shear-bending stress zone.

Further testing on real scale models, where the two effects can be easily decoupled, is critical in order to understand the behavior. It is interesting to point out how a reduced effectiveness of anchors too close to the slab's midspan are very well in line with findings from Smith et al.. (2010) (2013), on the other side, a reduced effectiveness at increasing anchors' distance is in direct opposition with the discussed shear test model from Zhang & Smith (2013) though being backed up by Brena & McGuirk (2013).

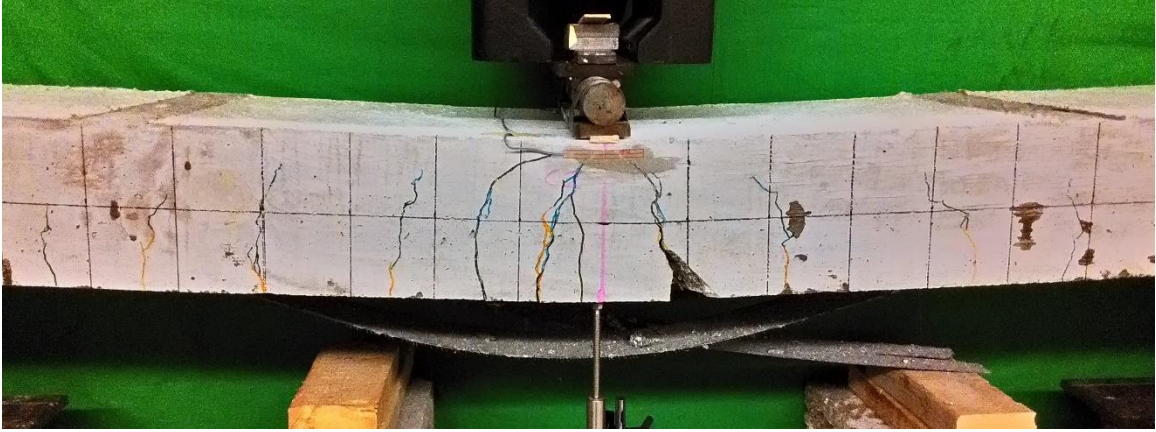


FIGURE 226 - 90x2



FIGURE 227 - 90x2 L/4



FIGURE 228 - 90x2 L/3

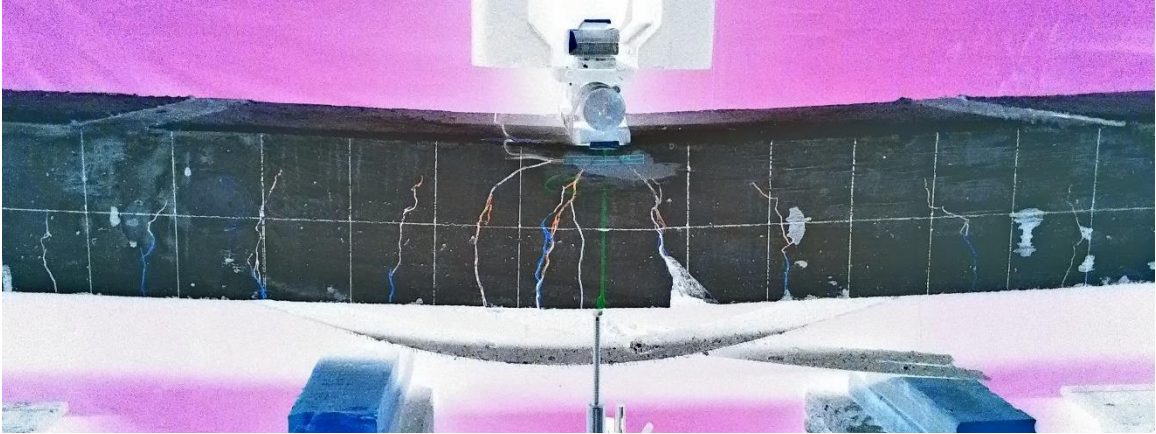


FIGURE 229 - 90x2



FIGURE 230 - 90x2 L/4



FIGURE 231 - 90x2 L/3



FIGURE 232 - 90x2



FIGURE 233 - 90x2 L/4



FIGURE 234 - 90x2 L/3

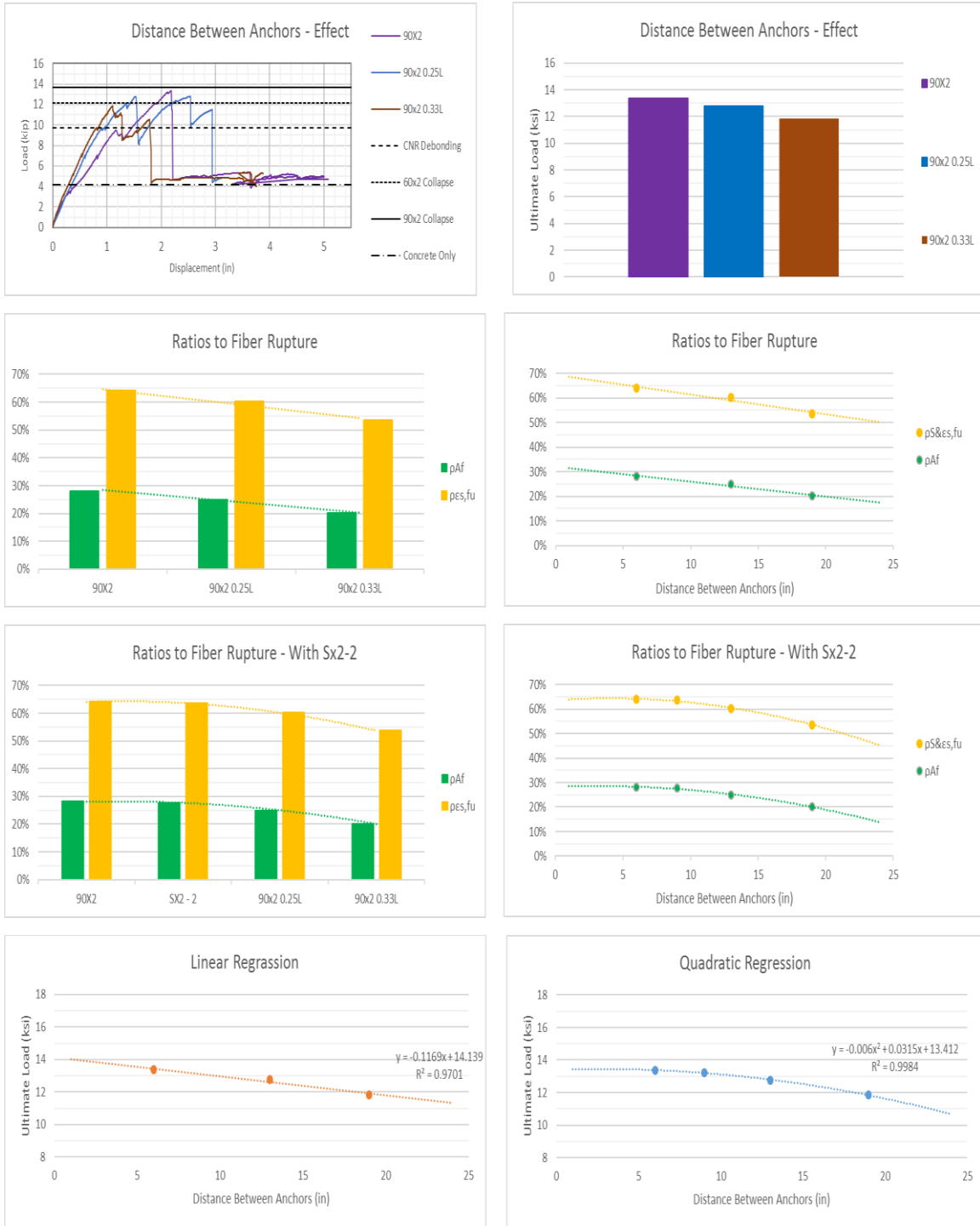


FIGURE 235 - (A) ULTIMATE LOAD (B) RATIOS TO FIBER RUPTURE, NO Sx2-2 (C) RATIOS TO FIBER RUPTURE, WITH Sx2-2 (D) LINEAR & QUADRATIC REGRESSIONS, WITHOUT & WITH Sx2-2.

1 IN = 25,4 MM / 1 KIP = 4.448 kN

The proposed bi-linear model is strictly case-related, but it seems reasonable to assume the same tendency to be present also in full-size specimens, probably with a larger plateau or eventually a tri-linear tendency: a fully-coupled plateau, a progressively decoupled behavior at increasing anchor's spacing, a steeper strength reduction as the central anchor get closer to midspan and the collapse mechanism turns into a shear-related one. In the following formulation s_a is the anchors' spacing, the 9'' limit is strictly case-related, further investigation is required to develop general results.

$$P_u(s_a) = \begin{cases} 13.30 & s_a \leq 9'' \\ 14.56 - 0.14 s_a & s_a > 9'' \end{cases} \quad [\text{kip}]$$

$$P_u(s_a) = \begin{cases} 59.18 & s_a \leq 228 \text{ mm} \\ 64.75 - 0.025 s_a & s_a > 228 \text{ mm} \end{cases} \quad [\text{kN}]$$

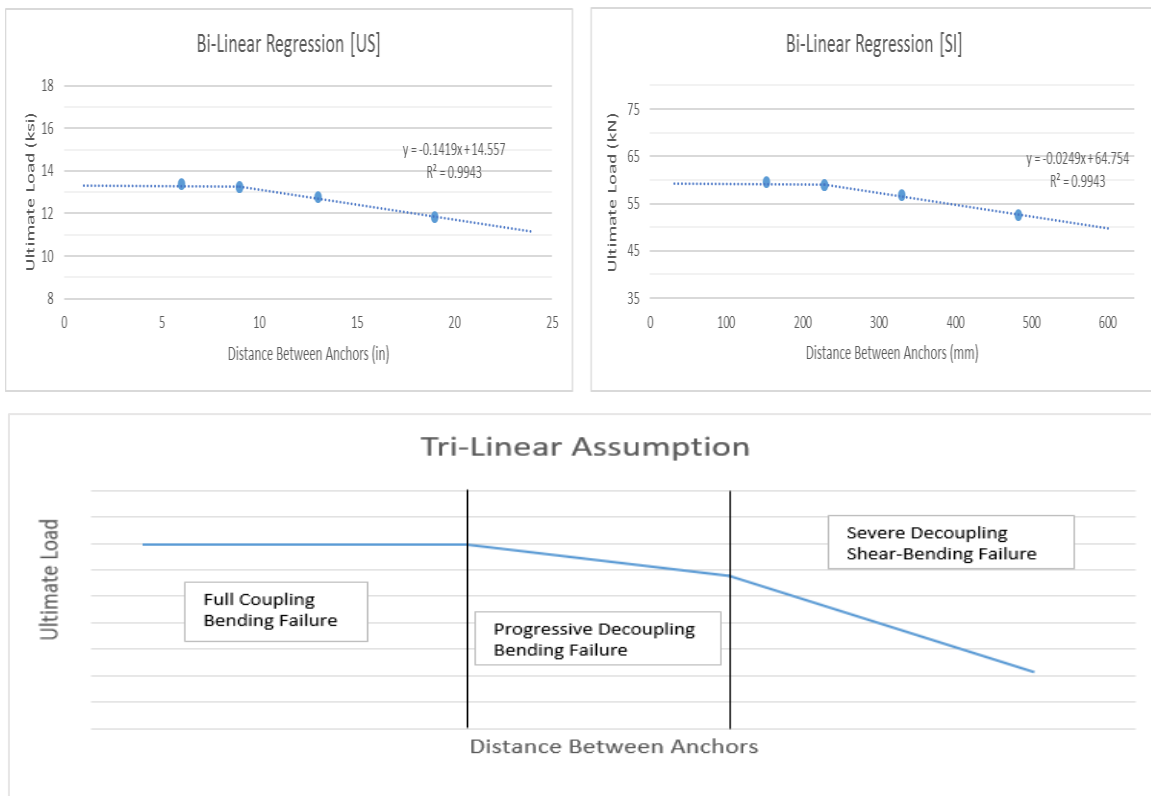


FIGURE 236 - BILINEAR REGRESSIONS OVER THE EXPERIMENTAL DATA & TRI-LINEAR ASSUMED BEHAVIOR FOR FULL-SIZE SAMPLES. 1 IN = 25,4 MM / 1 KIP = 4.448 kN

6.4.5.3 At Varying Anchor's Number

Wishing to re-couple the fully decoupled behavior of the 90x2 L/3 specimen, an additional anchor was located in-between the decoupled two and a 90x3 specimen was tested. The results were not promising: the collapse mechanism remained a fully decoupled one, with the central anchor almost non-engaged, and the ultimate load did not even reach the standard 90x2 value.

The continuity of the central sheet's strip is interrupted by the central anchor dowel's hole, hence the reduced strength of the system. In general, the particular anchors' placement varies the strain shape over sheet's width and length and the engagement ratio of each anchor. The result is very case-related and in general it seems reasonable to assume a 90x3 closely spaced configuration to guarantee a full coupling and a consistent strength increment. Further investigation is clearly required, either into anchors' coupling and the effect of different positioning over the slab's length.

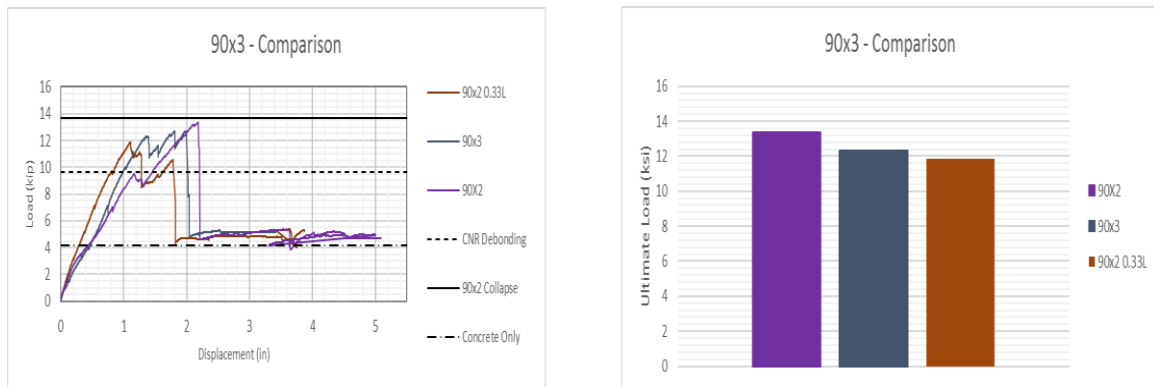


FIGURE 237 - ULTIMATE LOAD COMPARISON (90x2, 90x3, 90x2 L/3). 1 IN = 25,4 MM / 1 KIP = 4.448 KN



FIGURE 238 - CONTINUITY INTERRUPTION IN THE CENTRAL FRP STRIP

6.4.5.4 Sandwich Effectiveness

As discussed, what is defined a sandwich in the present dissertation is simply a mono-directional fiber patch to be put on top of the anchors' fan. Such a solution was proved to greatly enhance the joint's strength in shear characterization by Berneschi (2015); such a result was however not recognized in the performed flexural tests.

The Sx2-1 specimen showed a particularly low strength because of a suboptimal installation, but also the optimally installed Sx2-2 showed a level of strength simply comparable to the standard 90x2 configuration. As a proof of the optimal installation consider the perfectly symmetrical failure experienced by the specimen itself.

The ineffectiveness of sandwich configurations from the strength side can be taken as a reliable conclusion; the reason behind the severe improvement registered by Berneschi cannot be exactly defined, but it is worth noticing how such a result came from only one repetition that can hardly be considered representative of the configuration's behavior in absence of further testing.

A repetition of three shear test on sandwich configurations was performed in order to confirm the flexural results, however the test set-up proved to be more complex than expected and highly eccentricity-sensitive. All the tested specimens failed by dry fiber rupture in presence of intact anchors, making the results not failure-representative, various alternatives were discussed in order to improve the test set-up and a very effective solution will be presented in a thesis currently in preparation (Cadenazzi, 2016)

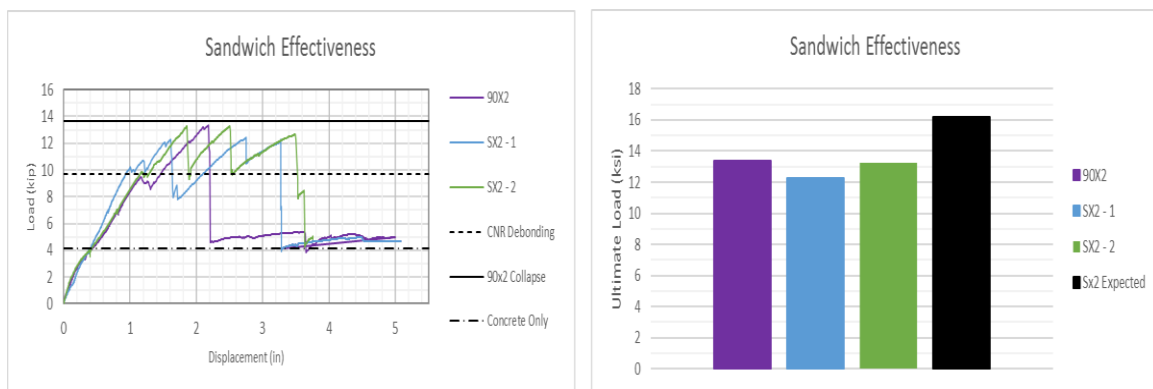


FIGURE 239 - SANDWICH NON-EFFECTIVENESS ON THE LOAD SIDE.
1 IN = 25,4 MM / 1 KIP = 4.448 kN

The sandwich ineffectiveness on the strength side doesn't mean that patches themselves doesn't provide any advantage: a systematic pseudo-ductile behavior can be noticed; the ultimate load can be sustained at increasing deflection, whether this behavior can be experienced in real case scenarios is to be determined, though it proves the ability of the upper patch of allowing a more uniform stress distribution over the width, limiting the risk of localized failures. Such a redistribution capacity is proved as well by the perfectly symmetric collapse mechanism, over the length and over the width, showed by Sx2-2.

Neglecting the pseudo-ductility, the sandwich configurations fails at a lower deflection than the standard 90x2; taking into account the pseudo-plateau, the sandwich variant proved to be way more ductile.

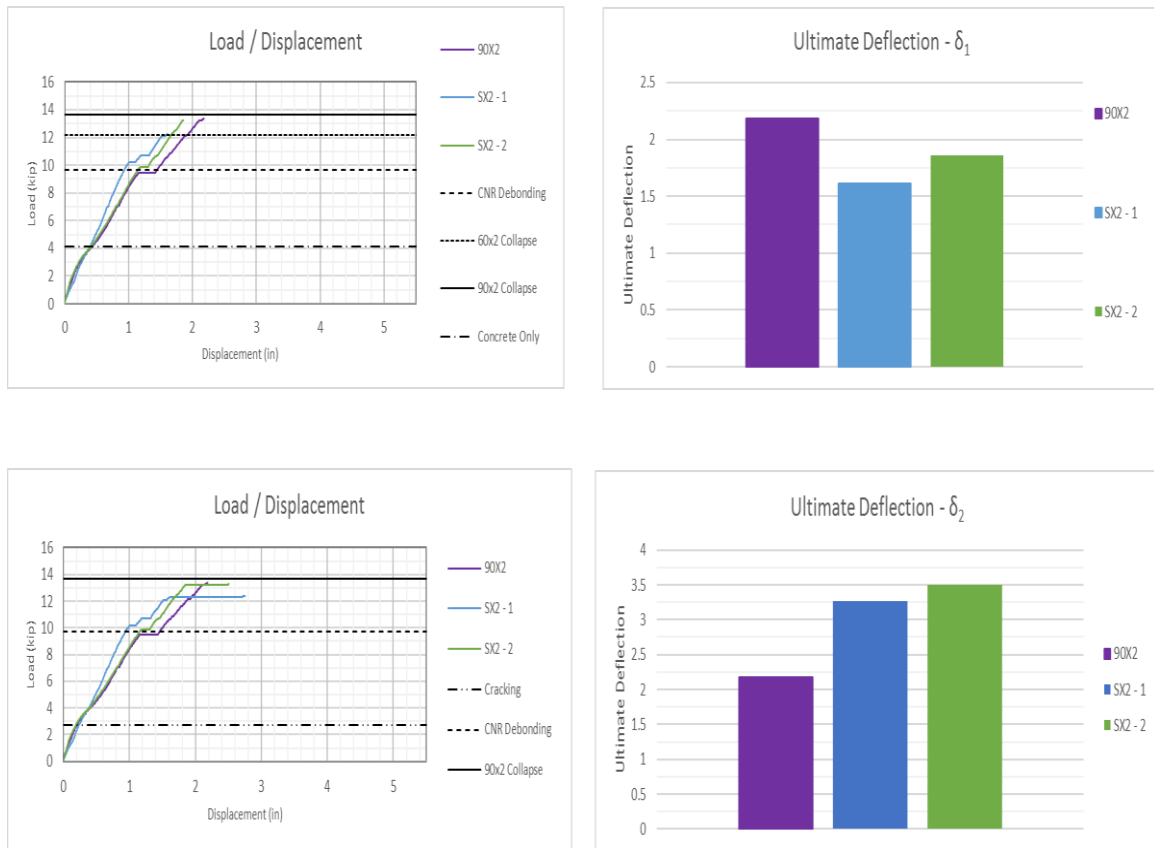
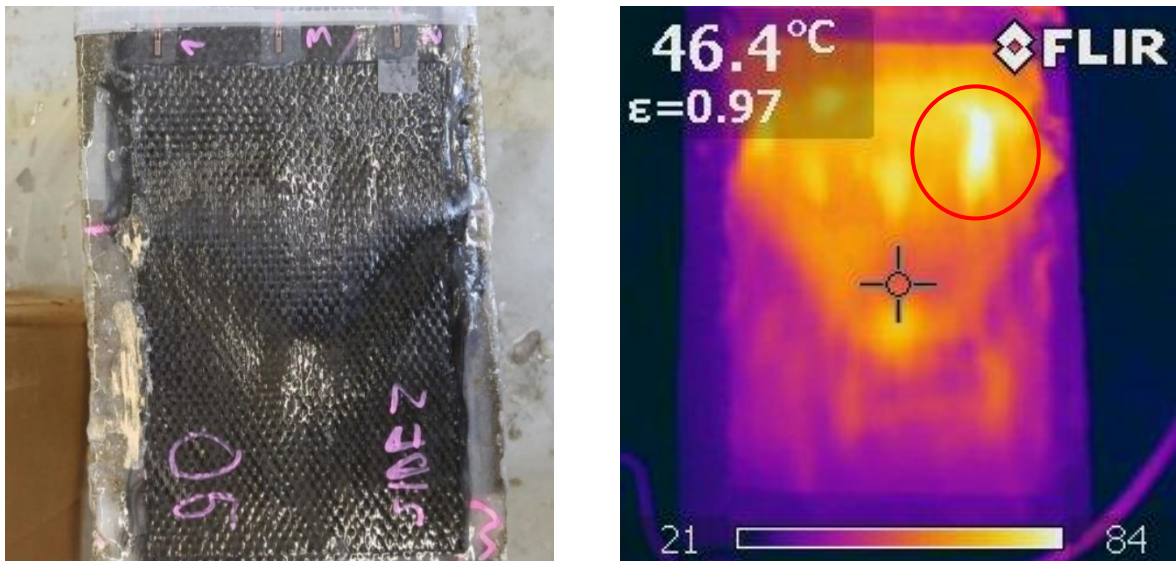


FIGURE 240 - SANDWICH-RELATED PSEUDO-DUCTILITY ON THE DEFLECTION SIDE.
1 IN = 25,4 MM / 1 KIP = 4.448 kN

As a final notice, it seems important to underline that, positioning an FRP patch on top of a not-perfectly-flat anchor fan, comes with the risk of voids forming in the interspace. Such voids may not have a severe effect on the patch mechanical behavior, though they expose the system to durability hazards, related to water infiltrations.

Even if carbon is a very environment-resistant material, the organic matrix presents a certain sensibility to humidity and aggressive environments; the critical point though is ice: a trapped small amount of water, freezing at low temperatures, basically results in an explosion closely followed by FRP detachment.



Considering the ineffectiveness of the sandwich patch in enhancing the system's strength, the uncertain advantages on the strain redistribution and pseudo-ductility side, all coming with the risk of undermining the durability of the intervention, at the present level of knowledge on the matter, sandwich patch are not recommended to be applied on the field.

6.4.5.5 Defective installation

Ozbakkaloglu & Saatcioglu (2009) pointed out the need to properly prepare the dowel's hole and carefully attend to the anchors' installation, in order to guarantee a fully exploited pull-out strength. On the other hand, Orton et al. (2008) concluded that the concrete surface preparation is not a critical parameter in presence of anchoring devices,

while Zhang & Smith (2011) pointed out how anchors' manufacturing does not critically influence the spikes' performances in shear.

In the present work much attention was devoted to anchors installation, even though, because of the author's inexperience, the quality of the installations improved proceeding from specimen to specimens. No significant installation-quality effects can be noticed, particularly considering the baseline 90x2 specimen, one of the firsts to be prepared and tested, compared to the Sx2-2, one of the lasts: both of them show very similar strength, even if the Sx2-2 collapse mechanism is beautifully symmetric, as a consequence of the state-of-the-art installation performed.



FIGURE 241 - 90x2 ASYMMETRIC FAILURE

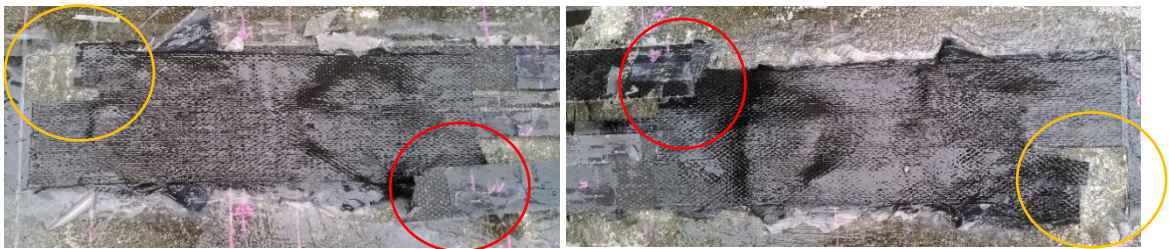


FIGURE 242 - Sx2-2 PERFECTLY SYMMETRIC FAILURE

In slipping-critical applications, the fan-covered area is believed to be the most influential parameter in defining the joint's strength. While other parameters are of secondary importance, much care should be taken in properly covering all the prescribed area while performing the installation.

If the fan is ill-positioned, a reduced strength should be expected, as it happened in specimen Sx2-1: checking the pictures documenting the installation, a wide non-covered area was spotted, undermining the system's strength. The pictures compare the ill-installed Sx2-1 to the properly installed Sx2-2, before patch application.

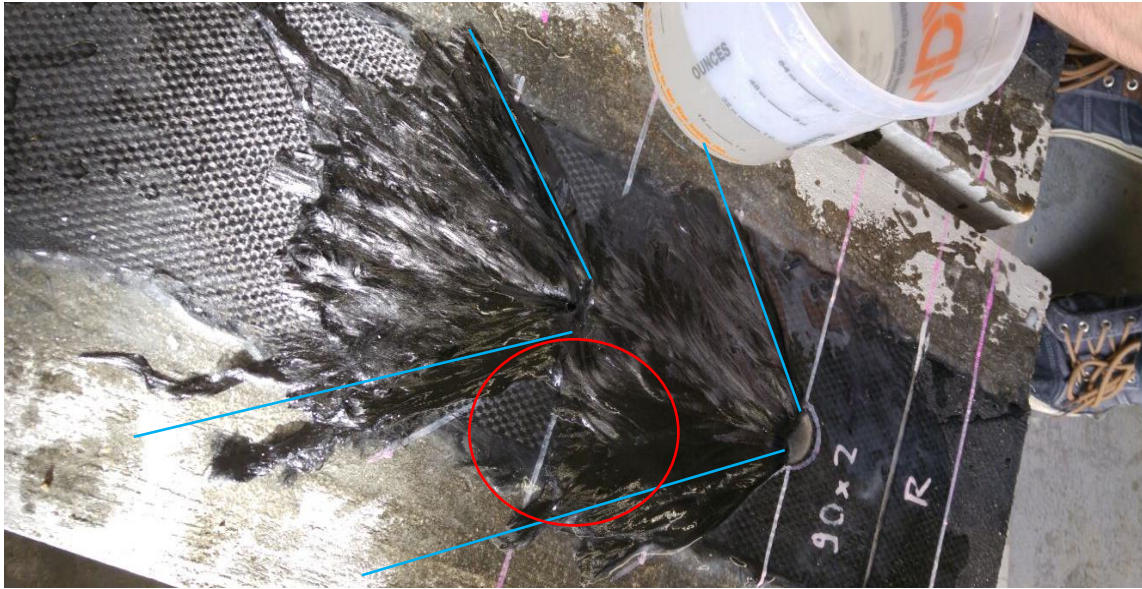


FIGURE 243 - Sx2-1 ILL-INSTALLED ANCHOR



FIGURE 244 - Sx2-2 PERFECTLY INSTALLED ANCHORS

6.4.5.6 *An Efficient Inspection Method*

Even if Orton et al. (2008) proved the secondary importance of concrete surface preparation in presence of anchoring systems, guaranteeing a good concrete-sheet adherence seems anyway a good prescription in order to fully develop the system's strength. The same applies to sandwich patch: even if the advantages eventually coming from such a solution seems not enough to justify its employment, if such a solution is applied, a proper installation should be performed. Regarding the fan-sheet adherence, on the other side, it was clearly proved its importance in guaranteeing a proper anchoring performances. Besides the mechanical behavior of the system, as pointed out already, the durability issues coming along an improper installation are the most critical aspect, making inspection an essential step in real-case applications.

Among the standard inspection method, knocking on the sheet's surface with a hammer, in order to spot eventual voids, is the most commonly employed on the field. Clearly is a non-systematic solution, with the advantages of being inexpensive and easily performable. A slightly more expensive and onerous solution is proposed, coming with the advantage of guaranteeing a systematic inspection of the installation and allowing an easy detection and documentation of the eventual voids.

The only required instruments are a thermal camera and a heat-gun: after the fiber sheet is uniformly heated, an inspection is performed using the camera, the voids will appear sensibly warmer than the surrounding properly-bonded zones.

The solution well-suits research purposes as well, allowing to properly define the defect-pattern and look for a direct relation with the experienced failure mode. Such an approach was tentatively performed on a set of three shear-tested sandwich configurations, but the experienced dry-fiber failure made the results at failure unrepresentative of a real case scenario. The same solution is being exploited in the context of a thesis currently under preparation (Cadenazzi, 2016).

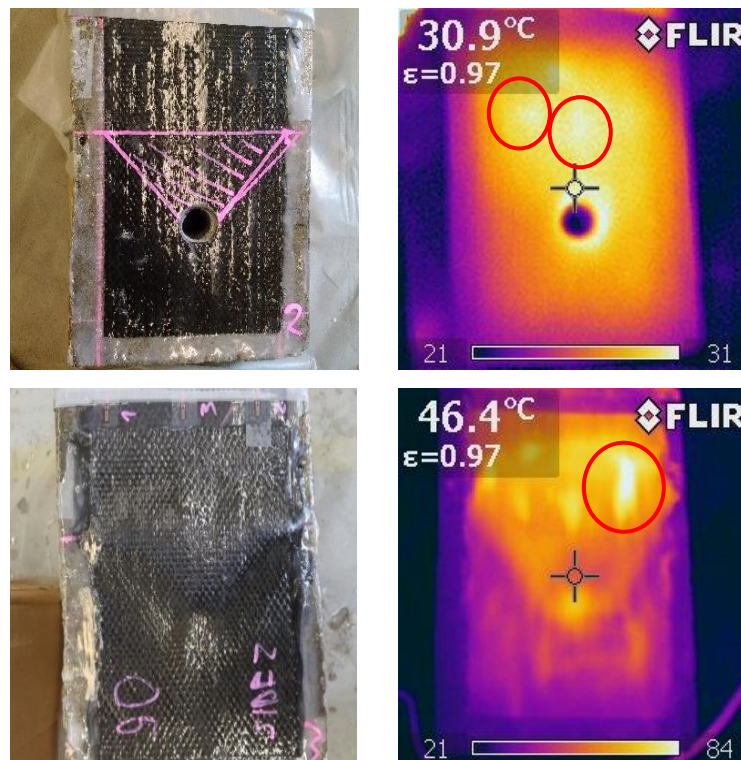


FIGURE 245 - THERMAL CAMERA INSPECTED SHEAR SAMPLES

7 Conclusions

The main purpose of this dissertation is to develop an effective and reliable design algorithm for anchor spikes flexural applications. In order to achieve the goal, a standard sectional analysis approach was proposed, wishing to keep the design procedures as close as possible to currently employed ones. Defining a globally representative parameter for the anchor's strength, to be easily implemented in a strain-based ULS sectional analysis, proved to be the critical point in developing an algorithm to step from a single anchor's shear characterization, to a flexural application design.

Instead of relying on direct strain measurements, coming with a certain level of uncertainty, a strength-based *equivalent ultimate strain* was proposed and imposed as collapse threshold for the external reinforcing lamina. Such a solution proved to be much effective in predicting the system's failure load, giving errors below 5% for the pure-matching samples (60x2, 90x2, Sx2-2). The proposed approach proved to be quite efficient as well, not requiring to modify the standard sectional analysis algorithm.

A strength-oriented anchor's characterization, proved to be efficiently extendible to a multiple-joint characterization: multiplying the single anchor's strength for the number of anchors and then defining the related equivalent strain via elastic constitutive law. In the present case, 6"-spaced anchors in series showed a fully coupled behavior, the coupling was maintained up to 9" while for larger distances a progressively decoupling can be spotted. A matching formula was derived and a more general modeling concept for anchors in series in flexural applications was proposed, as a hint for further studies.

The behavior of an anchored bended element was deeply discussed and only its fully understanding allowed to propose an effective design procedure. None of the tested joint configurations were engaged at serviceability or managed to retard intermediate debonding: in all the tested specimens, the joints were fully engaged by the FRP tensile resultant once intermediate debonding happened.

All the tested configurations proved to effectively enhance the system's strength, ductility and efficiency at ULS. A reinforcement ratio, based on the concept of balanced section, was proposed in order to characterize the efficiency of the tested external reinforcement configuration, at increasing equivalent failure strain.

None of the tested configurations proved to be pull-out critical, even if the anchors surely improved the system's performances against end debonding. All the joint's failed in

shear, because of FRP sheet's slipping under the anchors' fan. Such a failure mode is believed to be non-significantly affected by choices in terms of dowel geometry and hole preparation, while being highly affected by the amount of fan-covered area and by the fan geometry itself.

The critical parameters influencing a single anchor's strength were widely discussed, as well as the different failures the joint can undergo: a collapse-mechanism-oriented analytical characterization is believed to be the main goal future researches in this field should focus on, though being beyond the purposes of this work.

Sandwich – or patch – solutions proved to be ineffective in enhancing the system's strength. They guaranteed a certain amount of pseudo-ductility to the bended element as a consequence of better distributed stress and strains and improved fan-sheet adherence, but whether such a behavior can be exploited in real-case scenarios seems doubtful. These considerations, along with the durability hazard presented by voids in the interspace between sheet, fan and patch, lead to the conclusion that, at the current level of knowledge, patch configurations are better not being employed on the field.

The quality of the installation was noticed not to play a critical role in defining the system's strength, if not affecting the fan-covered area. This should not be intended as a suggestion to relax the quality check on field installations, on the contrary, a cheap, effective and efficient inspection method via thermal camera was proposed and briefly discussed, proving to be accurate enough for research purposes as well.

As a final notice, reviewing the already significant amount of researches published on the subject, a general lack of directions has been noticed. While all the results agree to confirm the effectiveness of spikes as anchoring solutions, the lack of unified testing methods, the employment of questionable data analysis techniques, the tendency to focus on less-significant variables, to test ill-designed specimens or extremely complex configurations, results in a hardly interpretable, unorganized, results database, as partly pointed out by others (Kalfat et al. 2011) (Grelle & Sneed, 2013). Further research is surely needed, mainly in the field of shear characterization, but it will be critical for such researches to be focused on clear goals, staying off over-complex configurations and switching the focus from raw-data production to model development.

Finally, the author wants to point out how all the conclusions of this dissertation are only referred to the particular anchors' type here discussed, and needs to be verified through a full scale testing campaign before proceeding to any field application. The results may very well be generalized to different anchoring devices through further testing.

8 Appendices

8.1 Appendix A: Units Conversion Table

Unit	Divisions	SI Equivalent
UNIT FOR LENGTH		
1 inch (in)		25,4 mm
1 foot (ft)	12 in	0.305 m
1 yard (yd)	3 ft (36 in)	0.914 m
1 mile (mi)	1760 yd (5280 ft)	1.609 Km
UNIT FOR AREA		
1 square inch (in ²)		645.16 mm ²
1 square foot (in ²)	144 in ²	0.093 m ²
1 acre (ac)	43560 ft ²	4046.873 m ²
UNIT FOR VOLUME		
1 cubin inch (in ³)		16.387 mm ³
1 cubic foot (ft ³)	1728 in ³	0.028 m ³
1 gallon (gal US)		0.004 m ³
UNIT FOR MASS		
1 ounce (oz)		28.350 g
1 pound (lb)	16 oz	453.592 g
UNIT FOR FORCE		
1 pound force (lbf)		4.448 N
1 kip force (kipf)	1000 lbf	4448.222 N
UNIT FOR DENSITY		
1 pounds per cubic foot (b/ft ³)		16.018 Kg/m ³
UNIT FOR SPEED		
1mile per hour (mph)		1.609 Km/h
UNIT FOR MOMENT		
1 inch-pound force (in lbf)		0.113 Nm
1 foot-pound force (ft lbf)		1.356 Nm
UNIT FOR PRESSURE		
1 pound per square inch (psi)		6894.757 Pa
UNIT FOR TEMPERATURE		
1 degree Fahrenheit (°F)		*F = 9/5°C + 32

8.2 Appendix B: Shear Tests on Sandwich Configurations

The discussed discrepancy in sandwich behavior between Berneschi's shear characterization (Berneschi, 2015) and performed flexural tests, along with the single repetition Berneschi performed on sandwich configurations, led to the decision of enlarging the samples database performing three more shear characterization tests.

All the tested samples unfortunately failed because of dry fibers rupture in a non-representative way, the recorder results from the strain side proved anyway to be interesting and will be reported hereinafter.

The specimens' preparation was performed as per concrete slabs and the test set-up was the double wrapped shear set-up already discussed for Berneschi's characterization tests. The dry-fiber failure was triggered by an intrinsic eccentricity in the loading mechanism, considered non-critical as non-pointed out in the available literature. The issue was later addressed providing a solution to impregnate the loose fiber sheet wrapped around the steel contrast, such a solution will be widely discussed in a dissertation in fulfillment of the requirements for a Master's degree from Polimi and currently in preparation (Cadenazzi, 2016).

8.2.1.1 60x2 S – 1

A 60-degree sandwich configuration, completely equivalent to what tested by Berneschi (2015) was prepared and instrumented with 3 strain gages in front of the sandwich patch, on the FRP tensioned sheet. The sample failed because of dry fibers rupture at a load of 7.94 kip (35,3 kN) way lower than the standard 60° slipping failure load of 12.99 kip (57.8 kN) and clearly non-representative of a real-case scenario.

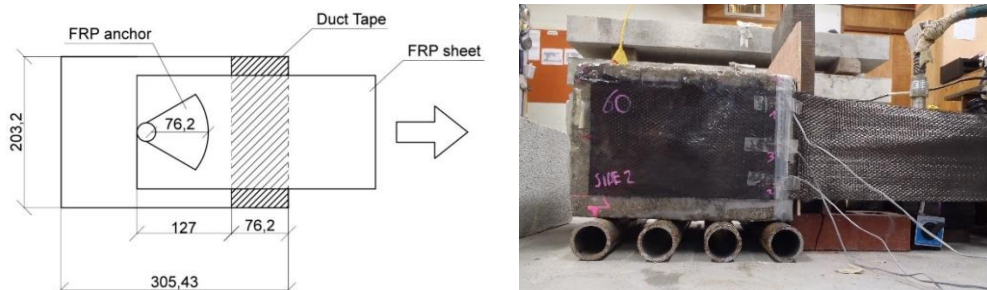


FIGURE 246 - TESTED CONFIGURATION & SET-UP

It is interesting to notice the concave strain shape over the sheet's width:

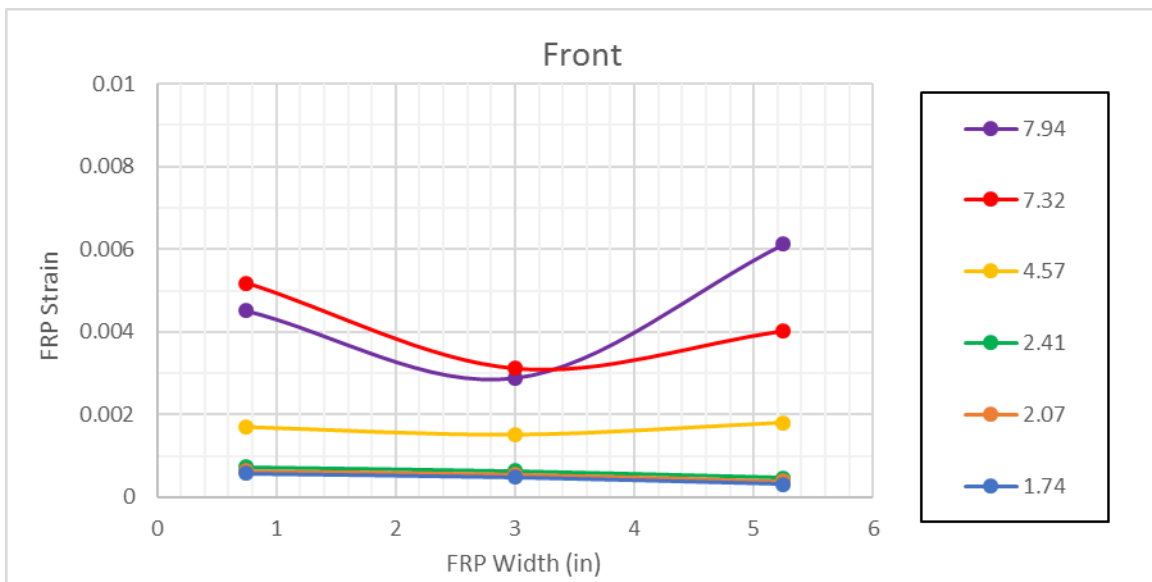
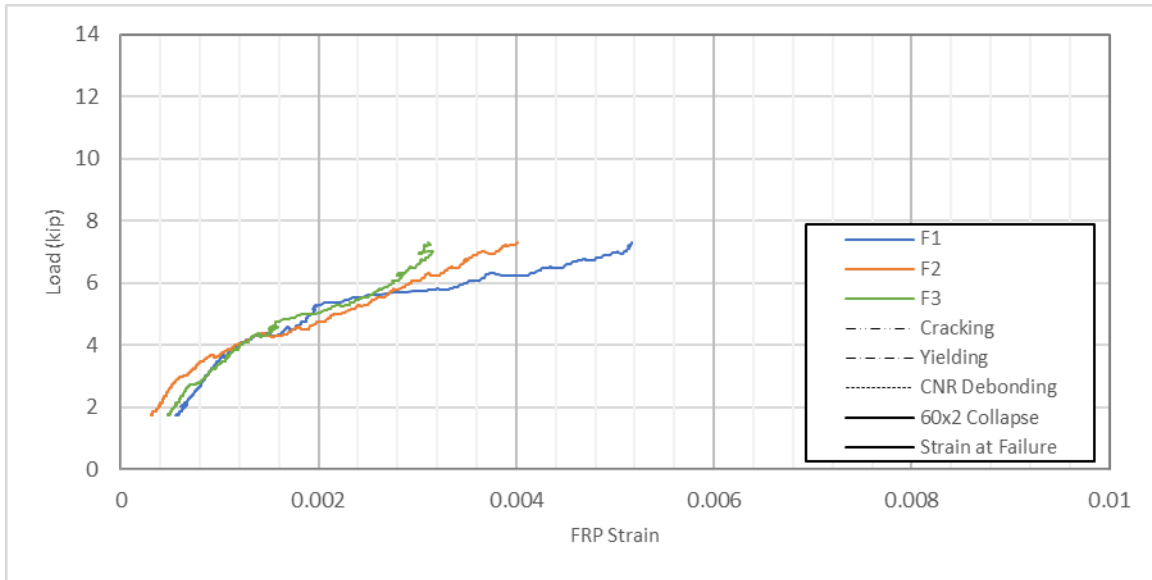


FIGURE 247 - STRAINS SHAPE OVER THE SHEET'S WIDTH AT INCREASING LOAD

8.2.1.2 90x2 S - 1

A 90-degree sandwich configuration was prepared and instrumented with eight strain gages in order to define the strain level on the sandwich patch itself, eventually characterizing its level of engagement. Only seven readings were taken because of an acquisition channel non properly working.

The sample failed because of dry fibers rupture at a load of 8.83 kip (39 kN) way lower than the standard 90° slipping failure load of 15.40 kip (68,5 kN) and clearly non-representative of a real-case scenario.

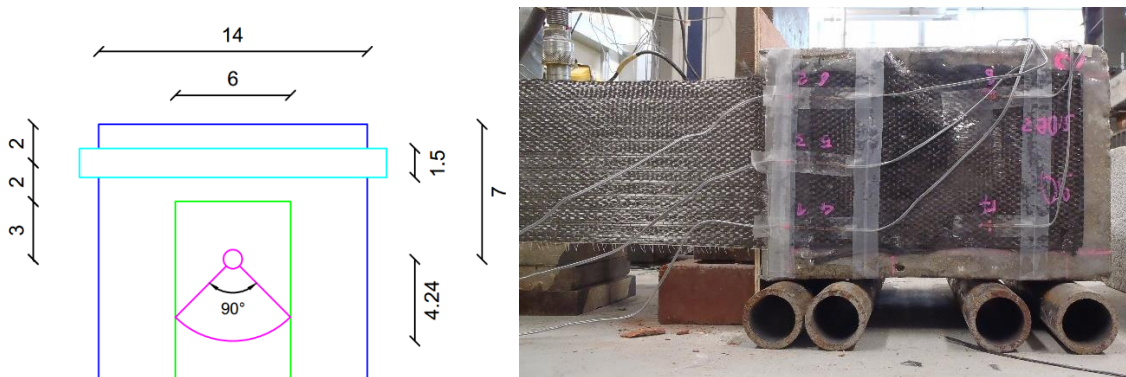


FIGURE 248 - TESTED CONFIGURATION & SET-UP

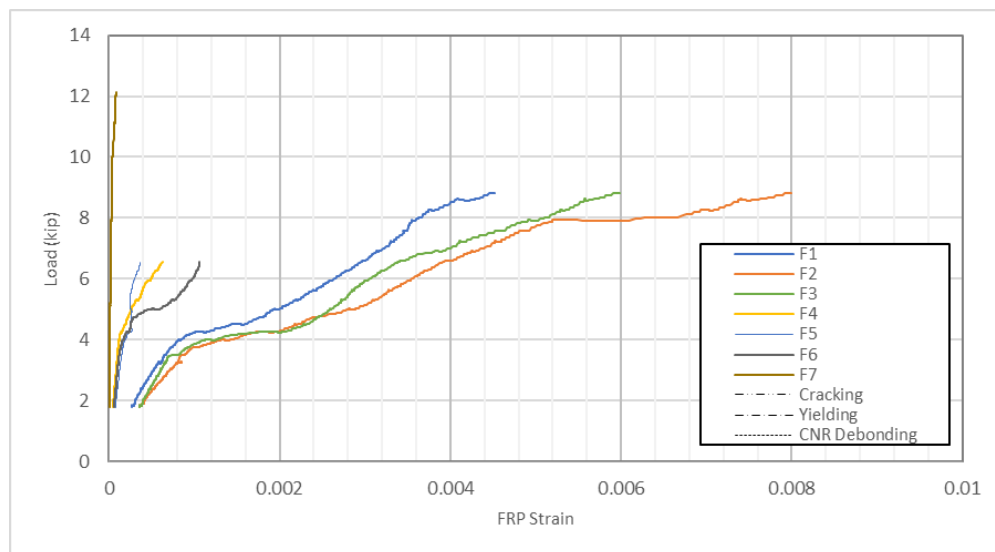


FIGURE 249 - LOAD/STRAIN DIAGRAM

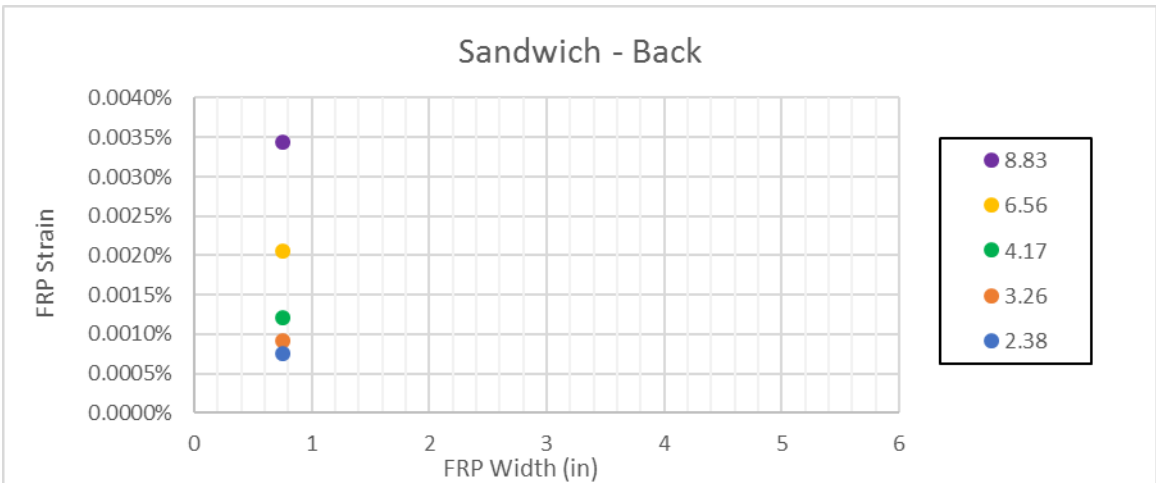
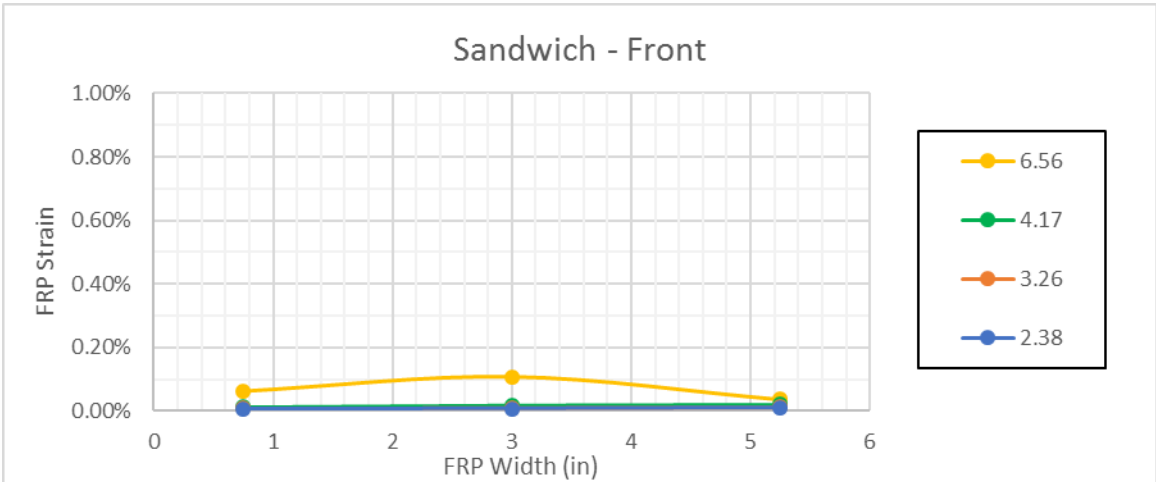
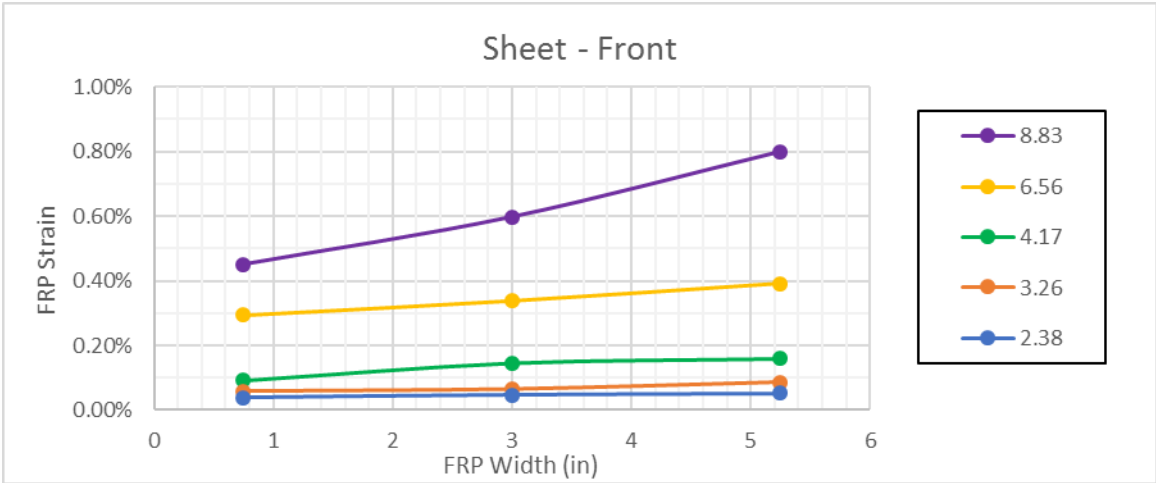


FIGURE 250 - STRAIN SHAPE OVER THE SHEET'S WIDTH, NOTICE THE DIFFERENT SCALE FOR THE LAST GRAPH

Looking at the strains, a concave shape can be noticed in the tensioned sheet, in front of the anchored region. Notice that behind the anchor, on the sandwich, the strains coherently increase at increasing load level, but the modulus points out how the portion is basically unengaged (the graph is plotted with a different scale).

A very low level of strain can be noticed on the sandwich patch, even in front of the anchoring spike. The patch results basically unloaded, confirming that it doesn't contribute to the joint's strength.

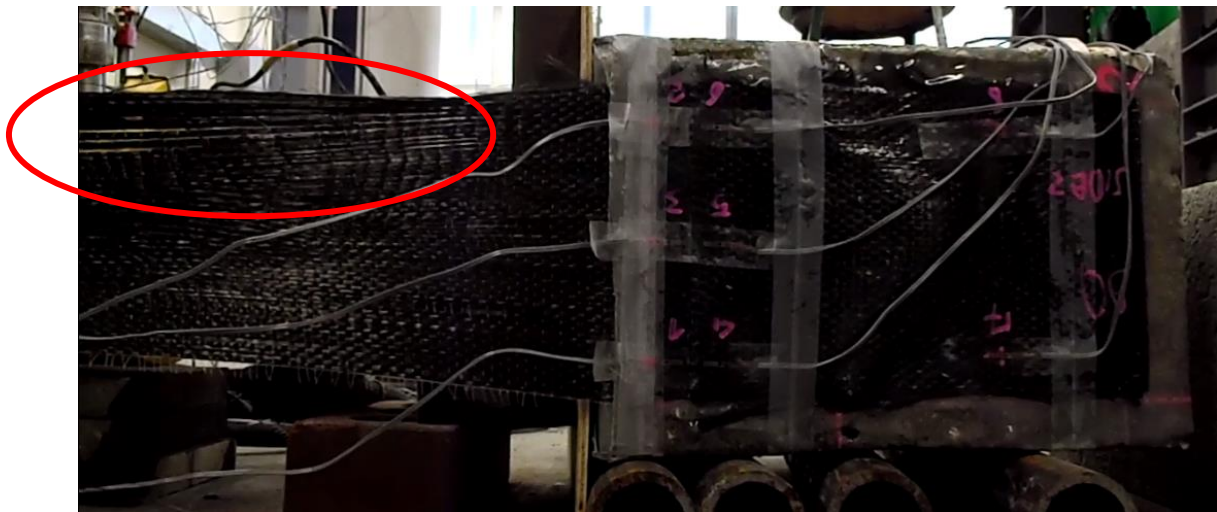


FIGURE 251 - FAILED SAMPLE, NOTICE THE DRY FIBER COLLAPSE ON THE LEFT, WHERE STRAINS ARE HIGHER

8.2.1.3 90x2 S – 2

A second 90-degree configuration was tested, in this case failing because of dry fibers rupture at a higher load: 12.54 kip (55,8 kN) anyway lower than the standard 90° slipping failure load of 15.40 kip (68,5 kN) and non-representative of a real-case scenario.

The strain shape also is different, being almost constant and slightly convex, probably because of a better centered applied load, this consideration confirms that the symmetry of the system and the eccentricity of the applied load play a relevant role in defining the actual FRP strain shape over the sheet's width.

Only the sheet, in front of the anchored portion is instrumented in this case.

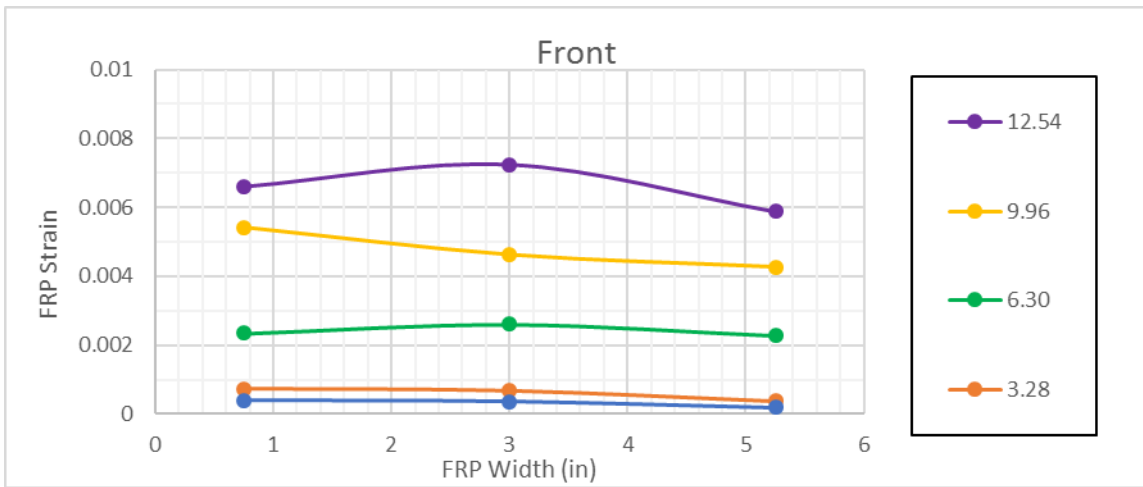
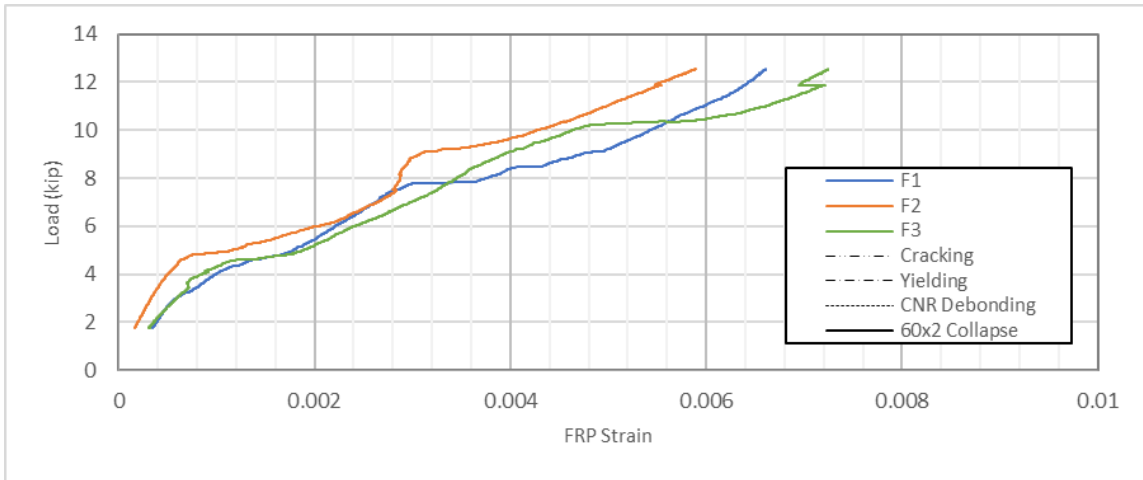


FIGURE 252 - (A) LOAD/STRAIN (B) FRP STRAINS OVER SHEET'S WIDTH (C) SAMPLE RIGHT BEFORE COLLAPSE

8.3 Appendix C: PhD Project Proposal

The work presented in this dissertation is the basis for the PhD project proposed by the student to the Polimi department of Architecture Build Environment and Construction Engineering (ABC). The proposal is reported hereinafter as a natural continuation of the discussion; the text is in Italian.

<u>Project title</u>	Developing a Comprehensive Characterization Model for FRP Anchors and Efficient Design Algorithms for Flexural and Shear Strengthening Applications.
----------------------	--

<u>Area</u>	Advanced Construction Materials and Innovative Building Technologies
-------------	--

<u>Summary of project</u>	<p>appieno le proprietà del materiale e migliorando la sicurezza dell'intervento, con ritorni in termini di economicità.</p> <p>La mancanza di adeguati algoritmi di progettazione limita in modo critico l'efficienza dei sistemi di ancoraggio: la mancanza di comprovati modelli per il calcolo della resistenza dell'intervento rende impossibile una stima esatta del numero di ancoraggi necessari e della disposizione ottimale.</p>
---------------------------	---

<u>Project description</u>	<p>Numerose sono le pubblicazioni nell'ambito dei sistemi di ancoraggio per FRP e l'efficacia della soluzione, dal punto di vista qualitativo, può ritenersi validata.</p> <p>L'ostacolo principale verso una piena implementazione del sistema nell'industria del restauro e della riabilitazione edilizia, è rappresentato dall'assenza di modelli di calcolo o algoritmi di progettazione che permettano al progettista di valutare, in termini quantitativi, l'efficacia dell'intervento.</p> <p>Se una modellazione del comportamento dei suddetti ancoraggi a pull-out è già stata proposta e sostanzialmente accettata dalla comunità scientifica (Ozbakkaloglu & Saatcioglu, 2009) (Kim & Smith, 2010) poiché facente riferimento a modelli precedenti – ampiamente convalidati nella loro applicazione ad ancoraggi in</p>
----------------------------	---

	<p>acciaio (Cook, 1993) - Lo stesso non può dirsi della caratterizzazione a taglio.</p> <p>In questo caso il comportamento dell'ancoraggio vede il sistema resistere alla combinazione di taglio-trazione agente alle estremità di una lamina di FRP, come ampiamente documentato dal documento CNR (2014). La complessa geometria dell'ancoraggio richiede una specifica indagine sperimentale volta a definire l'influenza di ciascun parametro nel determinare la resistenza del sistema, nell'ottica della definizione, tanto di un semplice modello di caratterizzazione ad orientamento progettuale, quanto di un modello numerico/analitico descrittivo della complessità del comportamento del sistema.</p> <p>Considerando che proprio la risultante di taglio è generalmente la sollecitante principale per l'ancoraggio stesso, la necessità di suddetta caratterizzazione appare critica.</p> <p>La modellazione del comportamento a Pull-Out adotta un approccio razionale, basato sull'individuazione dei possibili meccanismi di collasso e dei parametri che influenzano la resistenza dell'ancoraggio in ciascun caso.</p> <p>Una tale impostazione è a tutt'oggi assente in sede di caratterizzazione a taglio. La necessità di una impostazione di questo tipo viene suggerita nel lavoro di tesi dello studente e qui proposta. I possibili meccanismi di collasso individuabili in letteratura e direttamente sperimentati possono essere catalogati come segue:</p> <ol style="list-style-type: none">I. Lamine Tensile RuptureII. Fan-Lamine SlippingIII. Dowel Shear RuptureIV. Dowel Pull OutV. Lamine SplittingVI. Concrete Crushing <p>A seconda del meccanismo di collasso sembra ragionevole proporre una diversa modellazione per il calcolo della resistenza dell'ancoraggio.</p> <p>Nel caso di rottura della lamina di FRP sembra ragionevole un calcolo basato sulla resistenza a pura trazione della lamina stessa, corretta mediante l'introduzione di coefficienti sperimentali che tengano conto degli effetti di alcuni parametri significativi:</p>
--	---

$$S_I = \left(\prod \alpha_{I,i} \right) * A_f f_{fu}$$

Tra i parametri influenti in questo caso si possono individuare tutti i fattori che vanno a influenzare la distribuzione di sforzi trasversali determinando eventuali concentrazioni:

- Numero di Ancoraggi in serie e parallelo
- Spaziatura trasversale tra gli ancoraggi
- Larghezza di ciascun ancoraggio
- Rapporto tra area ancorata e area libera

Per quanto riguarda il **collasso per slipping**, una formulazione basata sull'integrale degli sforzi di taglio trasmessi tra lamina e ventaglio sembra la più adatta:

$$S_{II} = \left(\prod \alpha_{II,i} \right) * \int_{A_{fan}} \tau_{b,u}(x,y) dA$$

$$S_{II} = \left(\prod \alpha_{II,i} \right) * A_{fan} \tau_{bm,u}$$

sono particolarmente influenti:

- l'area coperta dall'ancoraggio e la larghezza coperta, dipendenti dalla geometria del ventaglio.
- L'influenza dell'angolo di apertura delle fibre è ancora ampiamente oggetto di indagine.
- Numero e spaziatura degli ancoraggi, in serie e in parallelo, giocano un ruolo fondamentale.

La **rottura a taglio** del cosiddetto *dowel*, la parte immersa nel calcestruzzo, può essere evitata provvedendo a un semplice dimensionamento a taglio dell'elemento, influenzato principalmente dalla curvatura imposta al bordo del foro.

$$S_{III} = \left(\prod \alpha_{III,i} \right) * A_{dowel} f_{fu}$$

I **meccanismi IV e V** richiedono specifica sperimentazione e modellazione prima che sia possibile procedere a proporre un modello, data la limitata disponibilità di risultati in letteratura.

Onde procedere alla costruzione del modello, una vasta campagna sperimentale è richiesta, eventualmente coinvolgendo i laboratori delle università di Miami – dove l’embrione della ricerca qui proposta ha messo radici – e della Federico II di Napoli, già molto attivo nella sperimentazione di sistemi di rinforzo esterno e attiva collaboratrice della University of Miami.

Le modalità di sperimentazione a taglio sono in via di affinamento, in seno a una serie di progetti di tesi in co-tutela Miami-Milano, incluso il già citato lavoro del sottoscritto. La modalità di double-shear-test proposta vuole essere facilmente attuabile, veloce da implementare e ragionevolmente economica: requisiti imprescindibili nell’ottica di una vasta campagna inter-laboratorio.

Una volta definite le modalità di caratterizzazione per il singolo ancoraggio si pone il problema di definire l’efficacia dell’intervento di rinforzo in termini quantitativi e predittivi.

Focus della tesi magistrale del sottoscritto è, fra gli altri, la validazione di un consueto approccio sezionale al dimensionamento di un intervento di rinforzo esterno, con ancoraggi, per un elemento soggetto a flessione. I risultati sono promettenti, ma una più ampia sperimentazione è richiesta per la validazione del metodo, auspicabilmente su elementi in scala reale.

Lo stesso approccio andrà poi applicato all’investigazione di interventi di rinforzo a taglio, con ancoraggi, dal punto di vista progettuale e quantitativo.



FIGURE 253 - ESEMPIO DI ANCORAGGIO IN FRP (ZHANG & SMITH, 2013)



FIGURE 254- SHEAR TEST SET-UP (BERNESCHI, 2015)



FIGURE 255- ESEMPIO DI SLIPPING FAILURE (BERNESCHI, 2015)

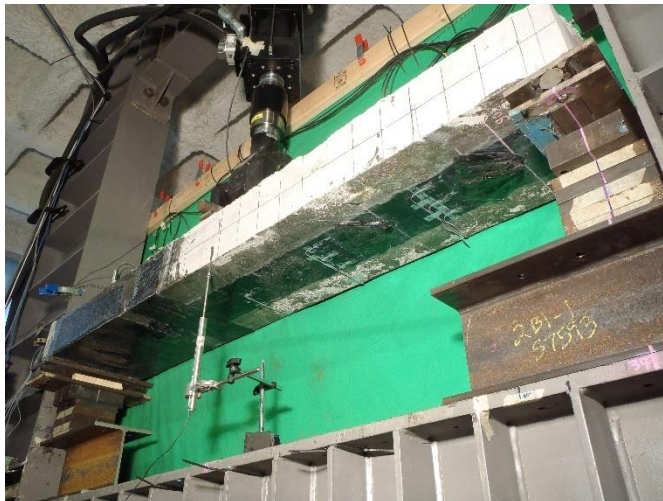


FIGURE 256- ESEMPIO DI RINFORZO FLESSIONALE (ROSSINI, 2016, IN PREPARAZIONE)

8.4 Appendix D: Flexural Test Procedure

The experience matured performing the discussed flexural tests, has allowed the author to review and redefine the UM Structures & Materials Lab Flexural Test Procedure, reported in the following.



Notation

55kip	Frame's load capacity, identifies the frame as well
DAQ	Data Acquisition System
NI	The computer coupled with the DAQ
LabVIEW	the software used to calibrate and record
MTS	The computer used to interface with the pump and actuator

Preliminary Beam Setup (1 person)

- 1) Measure beam/slab length and height.
- 2) Decide distance between supports as per design.
- 3) $\frac{\text{beam/slab length} - \text{distance between supports}}{2} = \text{Support distance from beam/slab end}$
- 4) Mark (required) support distances from each end on beam/slab.
- 5) Mark midspan of beam.
- 6) Flip Beam and repeat 4 & 5 on either side & on top and bottom.
- 7) Place strain gages according to following provisions.

Strain Gage Positioning (on Concrete) (1 person)

- 8) Strain gage position may vary depending on each individual test, verify before placement. Strain gages are usually placed at mid-span, approximately 1.5" from mid-span to allow space for the load application.
- 9) Choose a location which is on a smooth and level concrete surface, use a grinder if necessary. If the upper surface is too warped, then place the strain gages on the side face of the beam.
- 10) Remove dust using a brush and clean with acetone or compressor.

- 11) Create a 60mm long x 10mm wide **thin** layer of epoxy, to act as a level base for the strain gage to be glued to. Note: A 1/2 packet of epoxy should be used per strain gage used.
- 12) Allow the epoxy **5-10 minutes** to harden before placing strain gages.
- 13) Remove the strain gage from the plastic protective cover. **Take note of which side of the strain gage is to be facing outwards: once strain gage is stacked, text must be readable.**
- 14) Using scotch tape as a guide, stick the outward face of the strain gage to the tape. Fold ends of the tape for easy removal. **Make sure the copper wires entering the strain gage are not touching.** This prevents a short circuit. Make sure **NOT TO DIRECTLY TOUCH** the strain gage.
- 15) Stick the strain gage on top of the hardened epoxy. Make sure the strain gage is square and flush with the surface of the beam.
- 16) Peel the tape away from the beam to expose the **underside** of the strain gage. In the meantime, squeeze a light layer of super glue to the underside of the strain gage. Take care not to use too much! **Less is more.**
- 17) Press the strain gage back onto the epoxy surface and hold firm for **60 seconds**. Use the plastic protective cover to distribute pressure evenly if necessary. Make sure the whole surface of the strain gage is touching the epoxy with no air bubbles.
- 18) Label the end of each strain gage with painter's tape. C1, C2, C3 denotes concrete strain gage. F1, F2, F3 denotes an internal or force strain gage (typically for gages attached to rebar or FRP)
- 19) Take note of which strain gage is used in each position and keep the box reporting the information required to set up the acquisition software (point 55)

MTS Setup – Pump Turn On (1 person)

- 20) Open Station Manager/Project/55_kip_Frame.cfg;
- 21) Before pressing Open double check:
 - Parameter Sets: 55-kip_25k_cell
 - Interlock chain: Interlock 1
- 22) Open the valve;
- 23) Click on “Exclusive Control” and turn on the HSM 1T6-J28A pump.

MTS Setup – Pump Warm Up Procedure

(1 person)

24) Go to Function Generator;

- Channel: Axial
- Control Mode: Displacement
- Command Type: Cyclic
- Target Setpoint: 0"
- Amplitude: 1"
- Frequency: 0.50Hz
- Wave Shape: Sine
- Compensator: None

25) Run for 5-10 min.

Support Setup (55kip)

(1 person)

26) Move the base plates in order to achieve the correct distance between supports. Make sure the plates are square with the testing frame.

27) A clear distance of about **23"** from the top of the frame's base steel I-beam to the bottom of the actuator (once in position, touching the beam/slab upper surface) is needed. Place a proper number of steel spacers on each of the base plates in order to achieve the needed distance.

$$\text{Base Plate} + \text{Spacers} + \text{Pin Support} + \text{Beam Height} + \text{Actuator Plate} = 23"$$

28) Place cylindrical hinges supports.

29) Add thin wood spacer on top of pin support to protect concrete from damage and provide equal concrete/support pressure distribution.

30) Check the middle line of the supporting system to be in position, according to design (point 2) and everything to be square with the testing frame.

Move Beam in Place

(2-3 people) (forklift training)

31) Move actuator in top position in order to have enough space to put the beam/slab in position. Use manual command on the MTS.

32) Using a forklift lift the beam/slab and put it in place. Make sure the supports are in line with the correspondent marks on the beam (point 4) and that the beam is centered with respect to the testing frame, in order to do so measure beam ends distance from frame columns on each side. Make sure the beam is square with the testing frame and the supports. Proper training is required to use the forklift, ask for help if not

33) Place the "knife" on the structure, namely composed by (from bottom to top): rubber pad, steel plate, steel cylinder, steel plate)

- 34) On the MTS, **offset the force** and **engage** the actuator until the force applied is about -200-300lb. Once engaged, **offset the displacement**. (IMPORTANT: Meters Displacement MUST be equal to 0).

Draw Grid (1 person)

- 35) Remove all dust on beam/slab with a brush
36) Choose a grid spacing which will line up with the support and mid-span markings (usually 2", 3")
37) Use a level to draw straight lines starting from the centroid for horizontal and from midspan for vertical lines.

LVDT Positioning (1 person)

- 38) Determine the LVDT position, may depend on the particular test performed. Usually LVDT are placed at midspan and at side supports.
39) In order to measure only the **vertical displacement**, best practice is to take the measure at **beam's centroid line**. In order to do that, L bracket can be used. In order to fix the bracket at centroid axis best practice is sticking to concrete using epoxy. when feasible, using a C-clamp to keep brackets in position, while epoxy is hardening, is recommended. When displacement measurement is not the main test's target, also measure taken at the upper face at beam's end and at bottom face at beam's midspan are acceptable, thou this practice is strongly discouraged. both options will be discussed in the following:

L Bracket Sticking

- I. Place a thin layer of epoxy on the bracket surface. A half-packet or less should be used per bracket.
- II. Stick the bracket to the surface of the concrete, making sure the bracket is straight and level.
- III. Hold the bracket in position for 5-10' in order to make the epoxy harden. If feasible, using a C-clamp to keep the bracket in position is best practice.
- IV. Remove the C-clamp after hardening.

Direct Measure on Concrete

- I. Place a **thin** layer of epoxy on the beam/slab surface to avoid direct concrete-LVDT contact. A half-packet or less should be used for each LVDT.
- 40) Once epoxy is hardened, LVDT's may be placed using the magnetic holders. Make sure the LVDT is straight and vertical.
- 41) Take note of which LVDT is being used in each location (.15mm, .25mm, .50mm).

Acoustic Emission Sensor Attachment (1 person)

- 42) Retrieve the six acoustic sensors and place upside down (white sensor pad facing upwards) at 5", 15", and 25" from beam/slab mid-span. Note: These distances should be coordinated beforehand.
- 43) Place a thin layer of epoxy onto each sensor pad. One packet should be good for all six sensors!
- 44) Now turn each sensor over and stick to the top of the beam. The cable ports should face to the back face of the beam.

Cables Wiring (1 person)

- 45) It is good practice to make sure all cables and wires are running down the back of the beam. This keeps the front face clear for photographs and analysis.
- 46) All the wires should be neatly tied and **labeled**. Cables and other objects **should not be in contact with the beam as they could interfere with acoustic emission sensors**.
- 47) All cables should have **slack** in the event the beam fails and drops suddenly.

Cables to DAQ Module (1 person)

- 48) Connect cables as reported below, take notes in case of changes and beware of non-working channel labeled on DAQ.
- C1 to Ch0, C2 to Ch 2, C3 to Ch4**
- F1 to Ch1, F2 to Ch 3, F3 to Ch5**

LabVIEW – Software Setup (1 person)

- 49) Open **LabVIEW** on the NI system.
- 50) Click on:
Browse/Desktop/RUREDIL_003_BEAMS/4Strain3Load3LVDTs_20120622
- 51) Check LVDTs and Load Cell, no need for calibration.

Strain Gage Calibration (1 person)

- 52) Click on Step Setup
- 53) Click on Strain
- 54) Select all the strain gages
- 55) Modify the gage factor and resistance, check them on relative strain gage box.
- 56) Click on Device/Strain Calibration;
- 57) Set initial voltage to 0 for all strain gages.
- 58) Click on Next;
- 59) Click first Measure and then Calibrate. Err% MUST be very close to the 0%.

Create a New Specimen on the MTS (1 person)

- 60) Create a new specimen category. Go to:
Specimen editor/Specimen Directory Path:
Desktop/RUREDIL_003_BEAMS/RXX_
- 61) Create a new specimen.
- 62) File the technical Report. R-4.13

Test Performing (1 person)

- 63) **Run acquisition on the NI before starting the procedure.** Click “record”. Select the channel of interest (Load, Mean, Mean1). Name: RUREDIL_RXX.
- 64) Open the Procedure on the MTS: Go to MTP/Open procedure/Look in: RUREDIL_003_BEAMS and select the procedure.
- 65) Start the test with the MTS.
- 66) During the test: Take pictures. Mark cracks propagation.
- 67) **Stay away from the beam when ultimate load is to be reached.**
- 68) End of the test. Save data using the following format

RXX_YMMMDD_RAW DATA

From NI:

From MTS:

69) Backup the recorded data and the used procedure on a safe computer outside the lab, a cloud backup is even better.

Clean up (2-3 people) (forklift training)

70) Remove the beam from the testing frame using the forklift.

71) Remove strain gages from the beam.

72) Clean the area.

<p>Step 4 – Mark Support distance from each end</p> <p>Blue Arrow indicates the distance from the beam end. Red arrow indicates the marks.</p>	
<p>Step 4,5,6 – Complete beam markings. Lines show where support and mid-span should be marked.</p>	

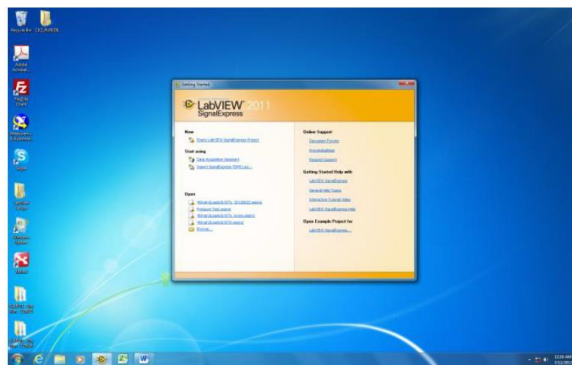
<p>Step 8-19) Strain Gages installation kit</p> <ul style="list-style-type: none"> A. Surface grinder B. Acetone C. Epoxy Conditioner D. Super Glue 	
<p>Step 9-11) Dispense half-packet of epoxy per 60mm strip.</p> <p>Notice epoxy strip is 1.5" from mid-span marking and roughly 1.5" from beam edge</p> <p>If concrete has indentation (see blue arrow), strain gage placement can be moved slightly to a flatter surface.</p>	
<p>Step 13-15) Note the strain gage text is backwards – This will be the side to be glued to the beam.</p>	
<p>Step 16-17) Note the plastic protective cover is used to apply pressure to the strain gage.</p>	
<p>Step 26) Move supports to correct distance. Make sure supports are measured from mid-span on the test frame.</p> <p>Clear Distance 23"</p>	

<p>Step 26-30) Make sure supports are square with testing frame.</p> <p>Roller Support</p> <p>Spacer Plates</p> <p>Base Plate</p>	
<p>Step 27)</p> <p>Actuator</p>	
<p>Step 30) Beam & test frame markings are lined up with support markings</p>	
<p>Step 39) Pictures display the bracket on both faces of the beam using the same c-clamp</p>	
<p>Step 40) Note the LVDT's are placed vertically and the magnetic supports are not touching the beam or in an area where they could be damaged from beam failure.</p>	
<p>Step 42-44) Notice the white sensor pad</p> <p>Note the equal spacing of the acoustic sensors</p>	

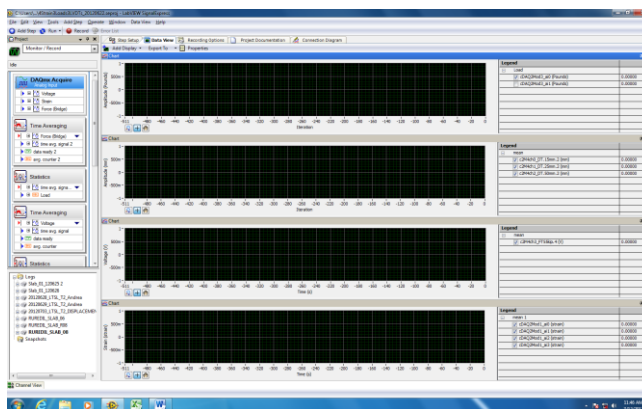
Step 44) Note the cable ports are facing to the back of the beam and cables are plugged in numerical order.



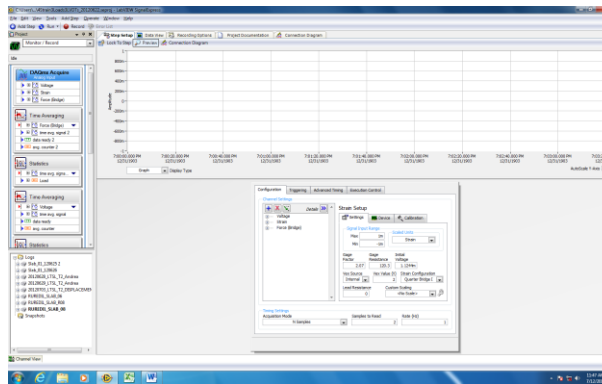
Step 49) Open LabVIEW on the NI system.



Step 50) Click on: Browse/Desktop/RUREDIL_003_BEAMS/4Strain3Load3LVDTs_20120622



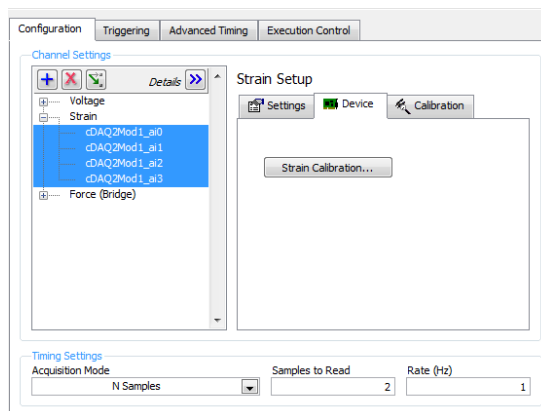
Step 52) Strain Gage Calibration: click on Step Setup;



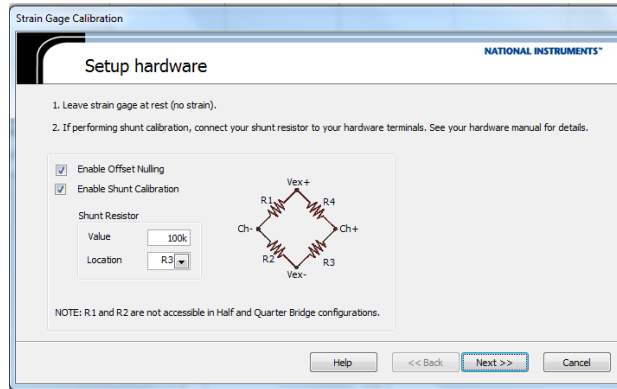
Step 53-55) Configuration and setting. Click on Strain. Select all the strain gages. Modify the Gauge Factor and Resistance (both of them are on relative strain gage box);

TYPE	FLA-5-11-3L		
LOT NO.	A515611	GAUGE LENGTH	5 mm
GAUGE FACTOR	2.11 ±1 %		
GAUGE RESISTANCE	120.4 ±0.5 Ω	QUANTITY	10
TEMP COMPENSATION FOR	11 × 10 ⁻⁶ /°C	TEST CONDITION	23°C 50%RH
TRANSVERSE SENSITIVITY	0.0 %	BATCH NO.	KK15g

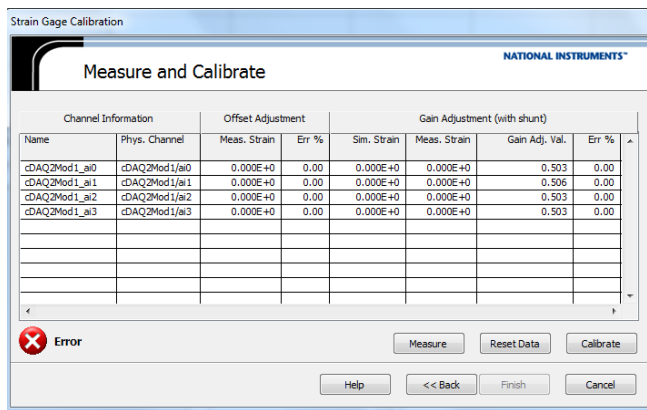
Step 56) Click on Device/Strain Calibration;



Step 57) Set initial voltage to 0 for all strain gages



Step 58) Click on Next;



Step 59) Click first Measure and then Calibrate. Err% MUST be very close to the 0%.

8.5 Appendix E: Hecht Bridge

The work presented in this dissertation was not the only research activity the author was involved into during the period spent at the University of Miami. The student contributed to a parallel project, namely the design, construction and testing of a full size FRP prestressed bridge, recently completed and now serving the University of Miami.

Three are the main peculiarities of the 70-foot long structure: pre-compression is provided thorough carbon fiber tendons, the bridge does not contain any piece of black steel, not even the supporting plates or the hanging hooks, made of stainless steel, finally it is one of the first examples of basalt internal reinforcement field implementation.

The student significantly contributed to the construction supervision, behavior prediction and load-testing phases: matching calculations were developed in order to predict the behavior of the structure over the short and long term, accounting for creep and load losses; in order to match the predicted and experimental behavior, a monitoring procedure was developed and two load tests were performed, including a crane-loaded 27 kip (12 ton) test performed at the pre-casting facility.

In the following, a short slide-show is reported, in order to give an idea of the overall project. Bachelor students were involved in the monitoring phase under the student's supervision, in an attempt to merge didactics and research activities; the presentation was meant for them to understand the activity, hence the elementary approach.

The overall project, and the promising results toward an FRP implementation in the pre-stressing field, are fully presented in two papers currently under preparation.

Marco Rossini
MS, Politecnico di Milano
MS, University of Miami



Hecht

A Bridge Towards Innovation



Enhancing

1. Concrete
2. Reinforced
3. Prestressed
4. FRP Reinforced
5. Everlasting

Keeping the Score

- How to 1.
A Good Matching 2.

An Old Idea

1. Concrete (150 B.C)



A Well Settled Technology

2. Reinforced Concrete (1853)



Made More Efficient

3. Prestressed Concrete (1925)



The Challenge of Time

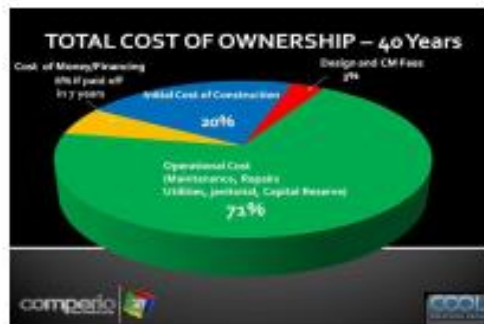
4. Fiber Reinforced Polymers, FRP (1970)



- No Rust
- Long Lasting
- Labor Saving
- Material Saving
- Energy Efficient
- Low Impact
- Economical

The Challenge of Time

4. Fiber Reinforced Polymers, FRP (1970)



- No Rust
- Long Lasting
- Labor Saving
- Material Saving
- Energy Efficient
- Low Impact
- Economical

The Challenge of Time

4. Fiber Reinforced Polymers, FRP (1970)



Building An Everlasting Bridge



75 years service life
Carbon Fiber Tendons
75% Level of pre-stress
Light thin walled section
Not a pound of black steel

Building An Everlasting Bridge

1. The pre-tensioning facility



Building An Everlasting Bridge

2. Wiring the Tendons



Building An Everlasting Bridge

3. Tensioning



Building An Everlasting Bridge

4. Pouring



Building An Everlasting Bridge

5. Cutting



Building An Everlasting Bridge

6. Final Product



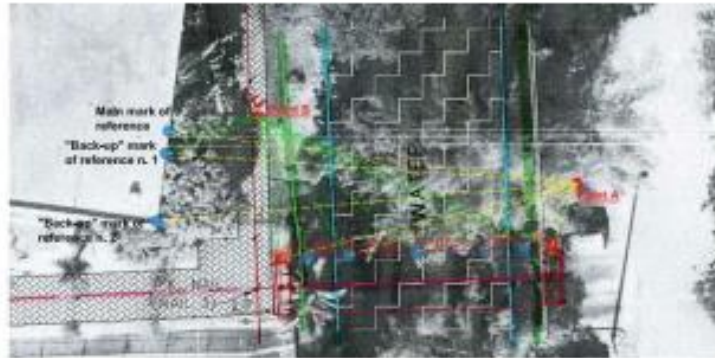
Building An Everlasting Bridge

7. On Site Positioning



Keeping the Score

1. How To: Deflection Measurements



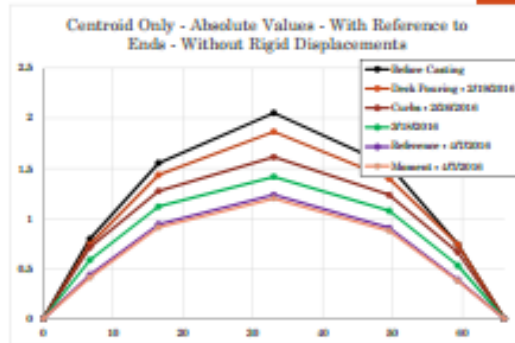
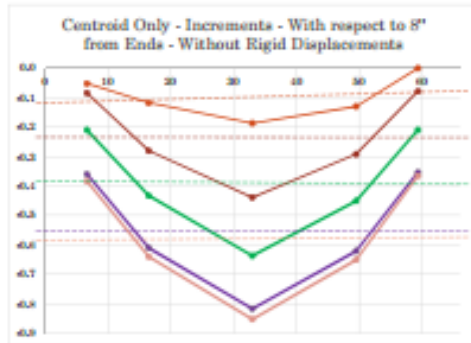
Keeping the Score

1. How to: Deflection Measurements



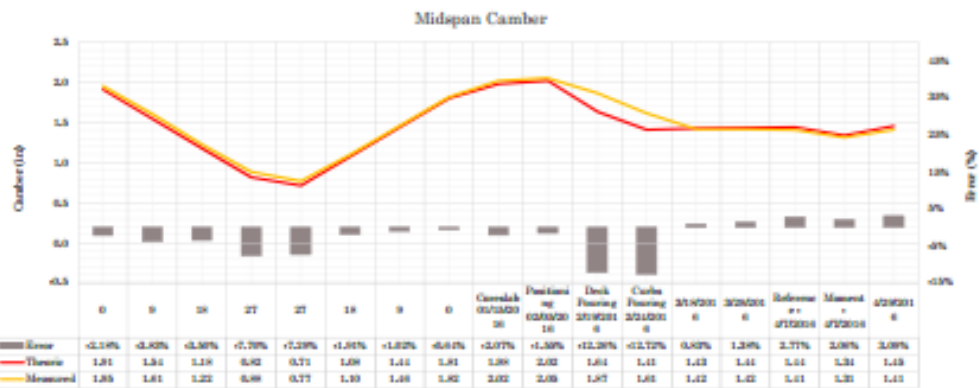
Keeping the Score

2. A Good Matching



Keeping the Score

2. A Good Matching



Keeping the Score

" The analytical exact solution is one and only one,
The numerical *exact* solution lies within an error range of E-6, E-9
The engineering *exact* solution lies within an error range of 2%
The civil engineering *exact* solution lies within an error range of 20% "

Thank you

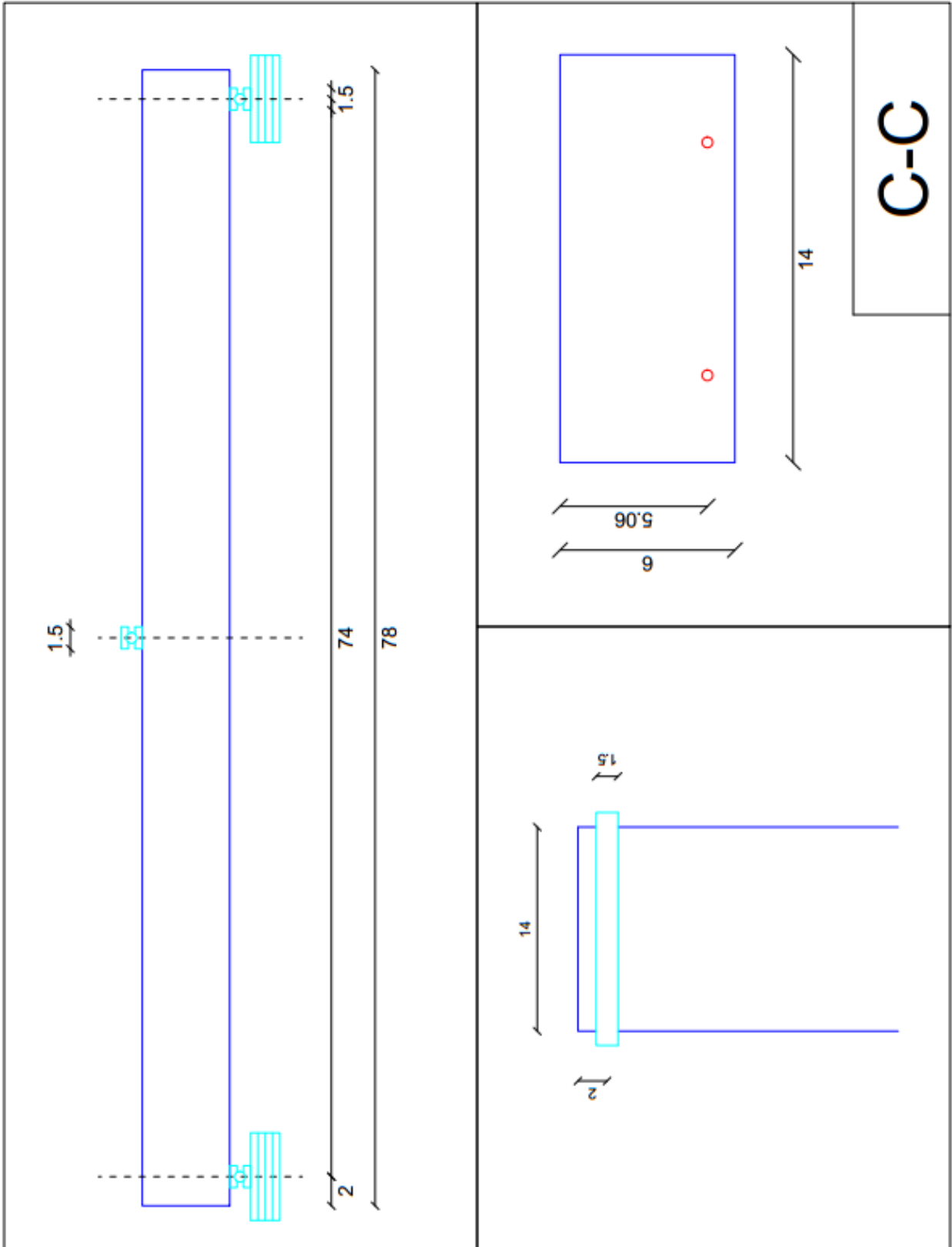
UM Hecht Research Team

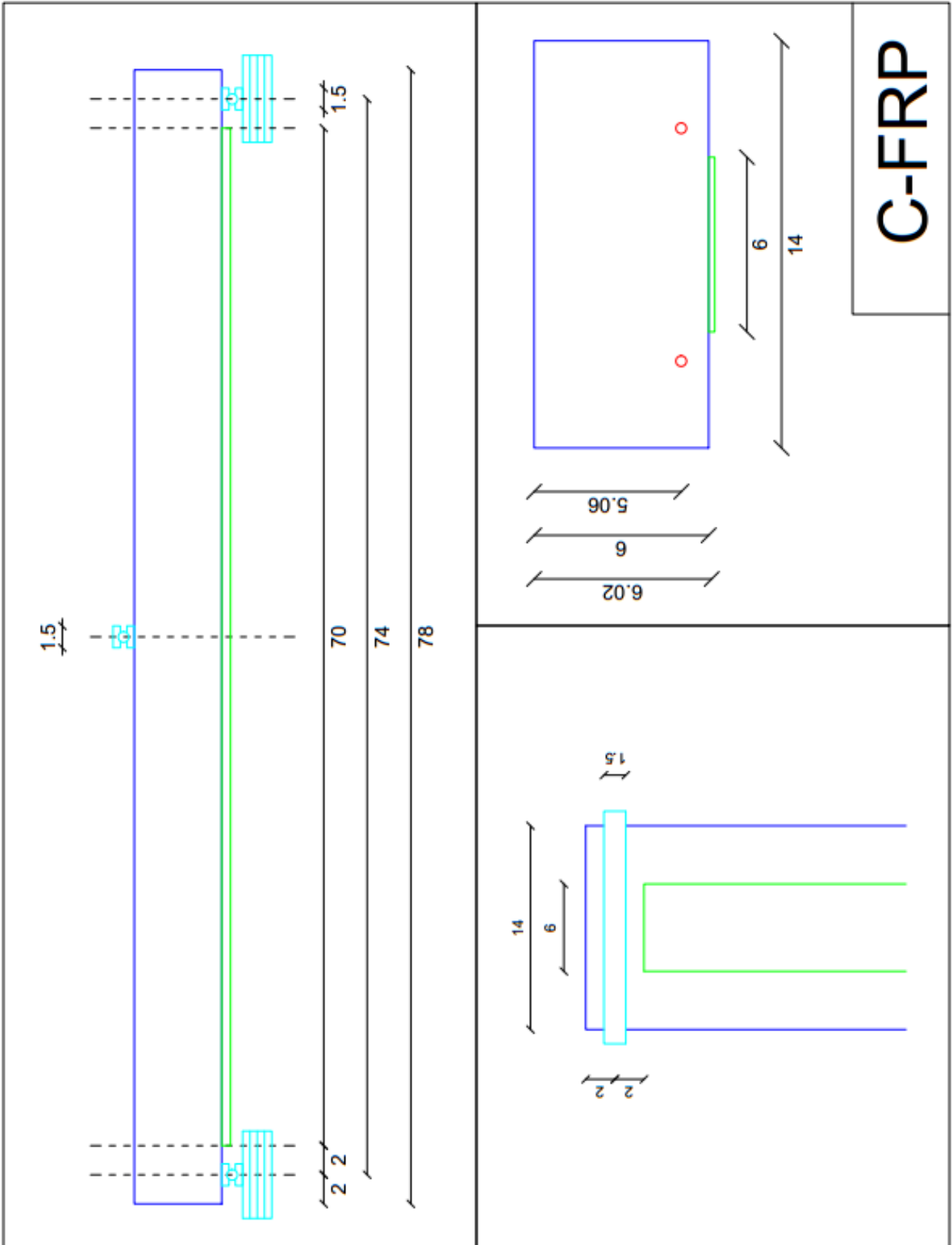


Antonio Nanni
Francisco de Caso
Guillermo Claure
Saverio Spadea
Omid Goorani
Marco Rossini
Thomas Cadenazzi
Vanessa Pino
Carlos Noel

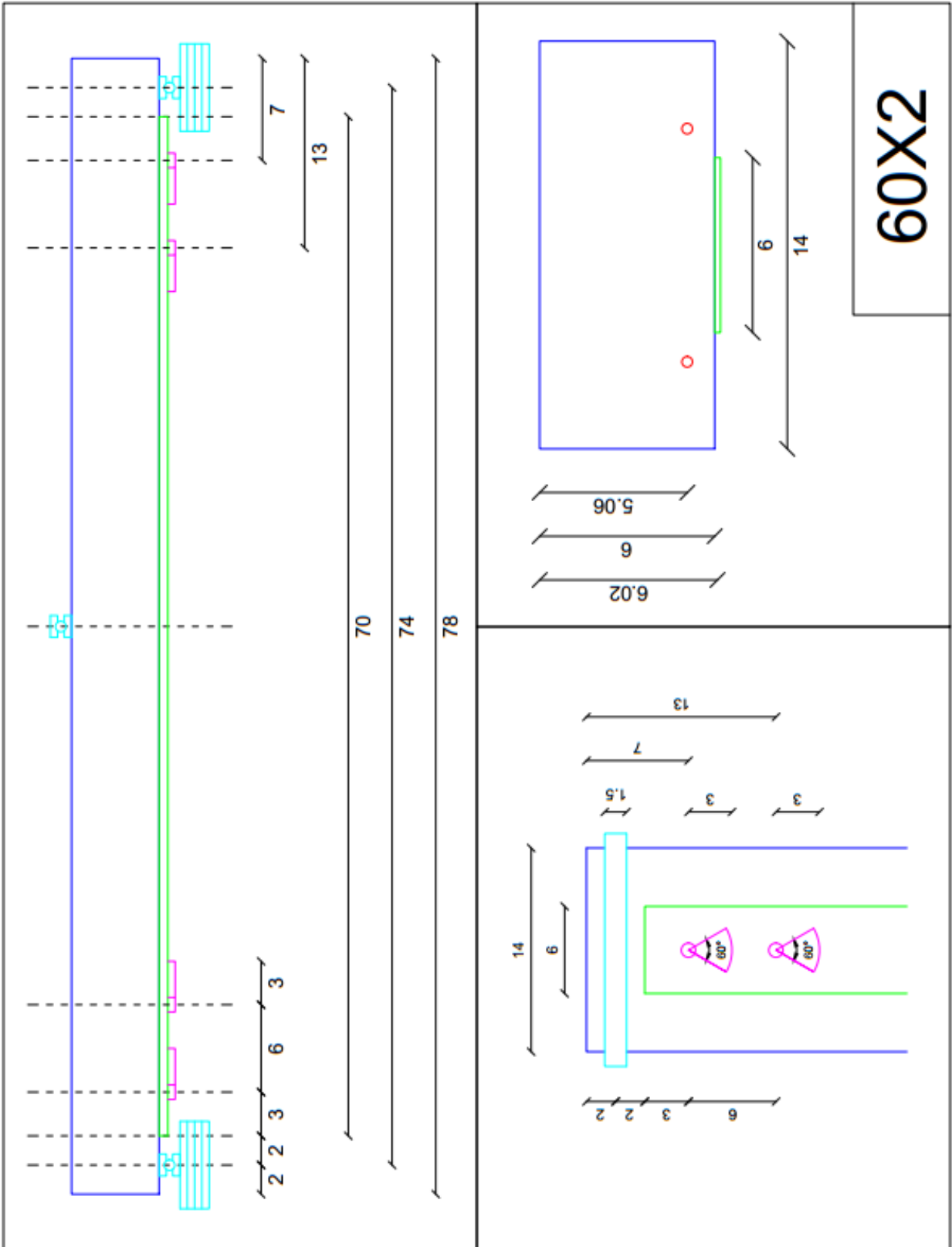
8.6 Appendix F: Slabs' Geometry

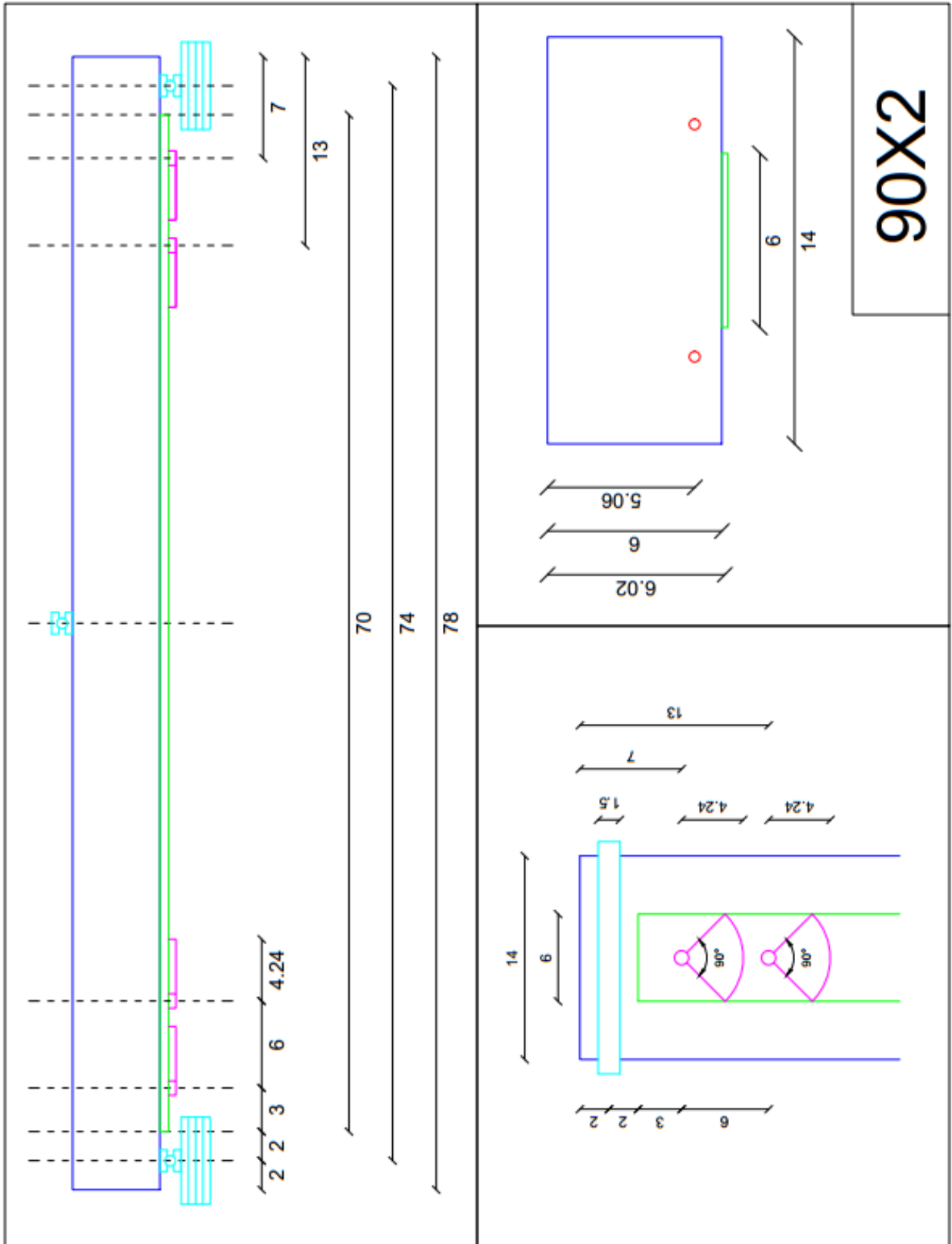
The side, plain and sectional view for each tested sample is reported hereinafter as a recap. The significant dimensions are reported as well. All the dimensions are in inches (1 in = 25.4 mm).

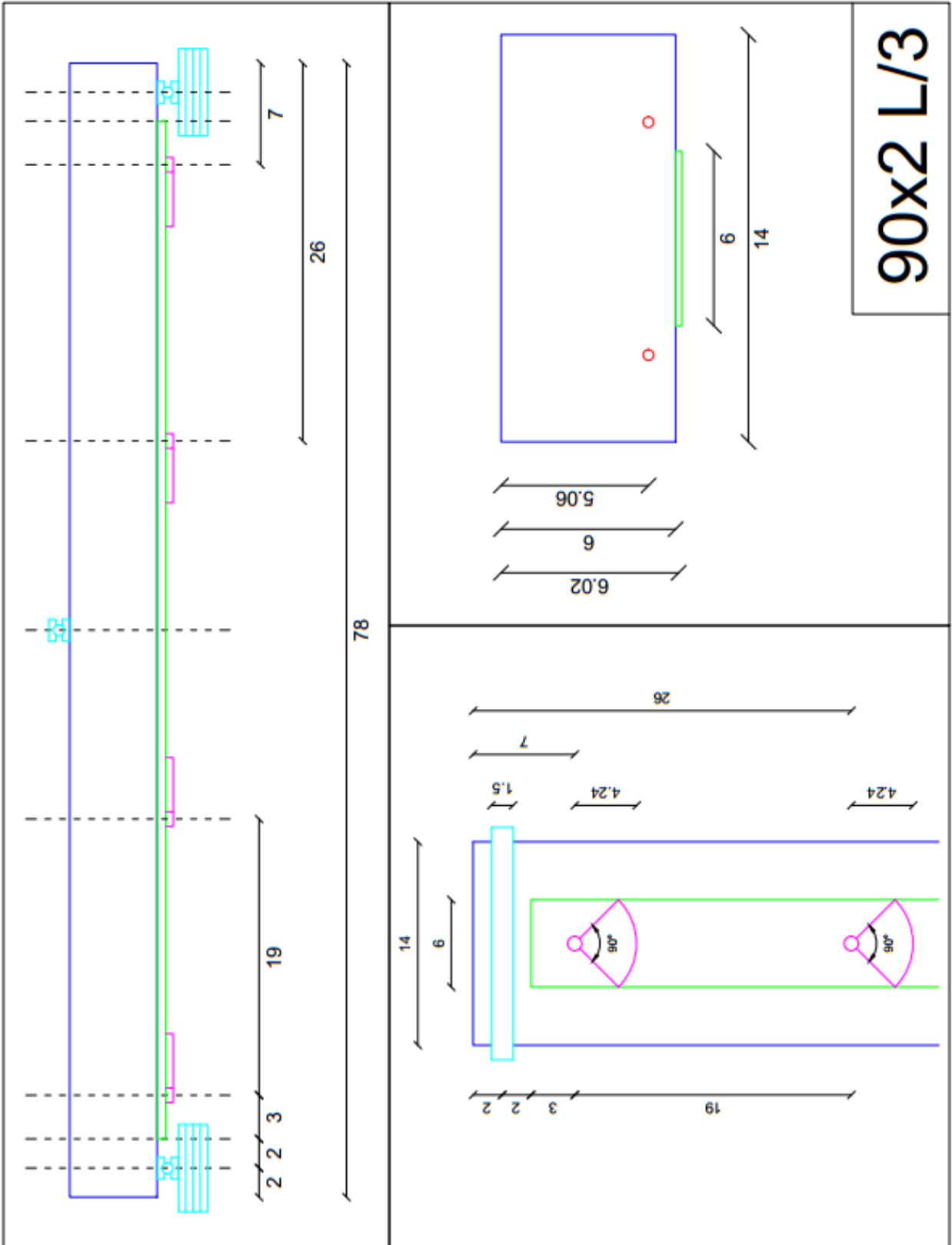




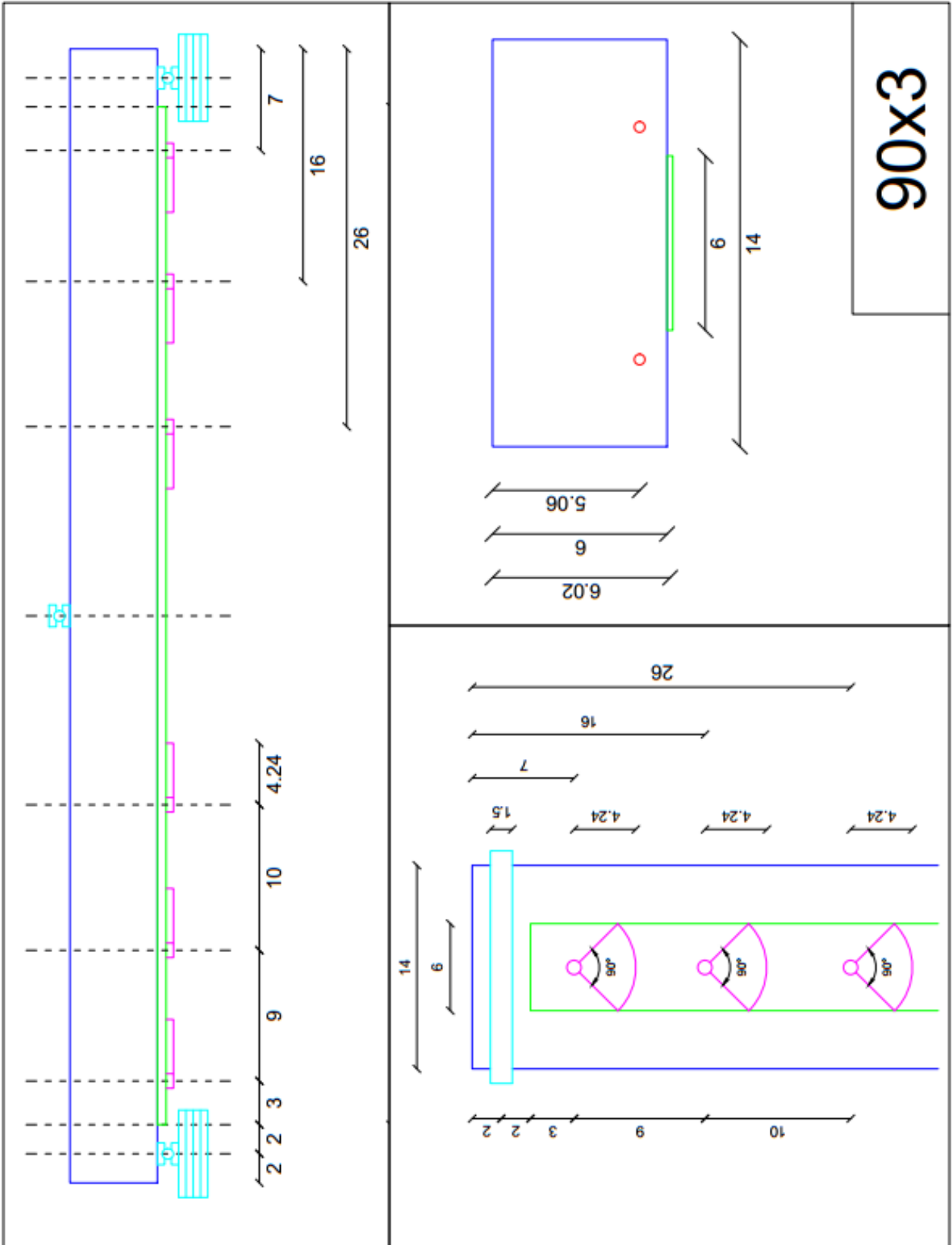
C-FRP



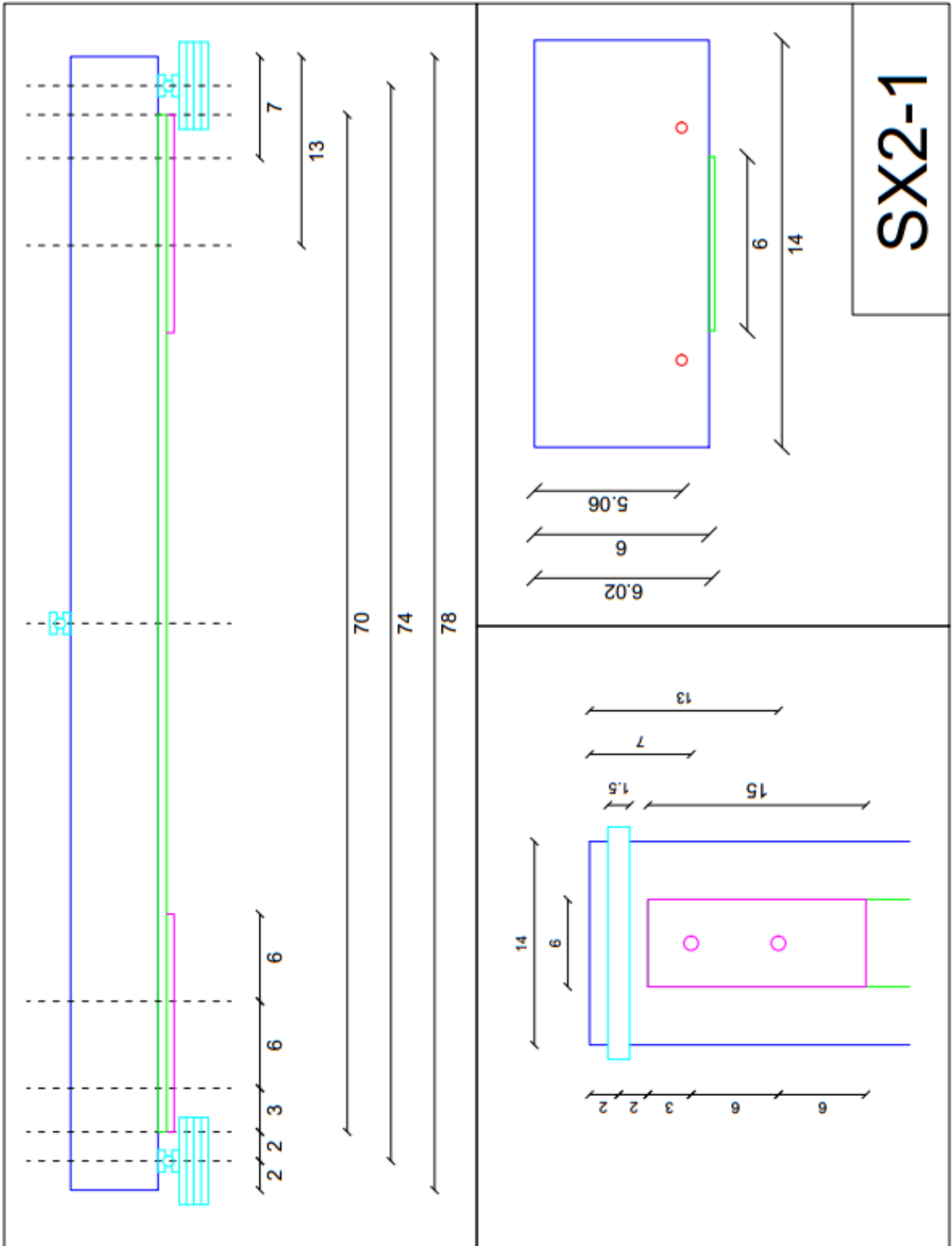




90x2 L/3



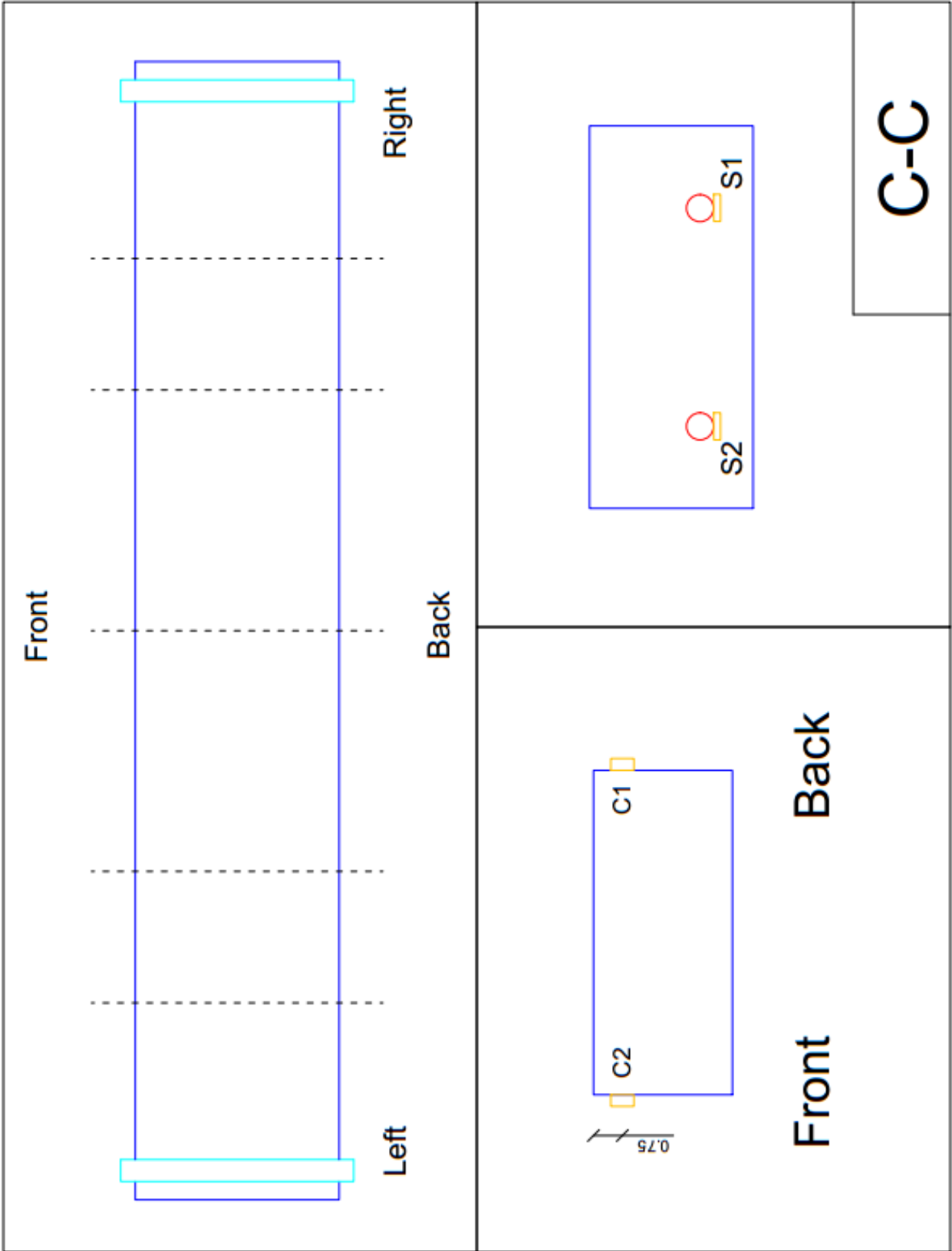
90x3

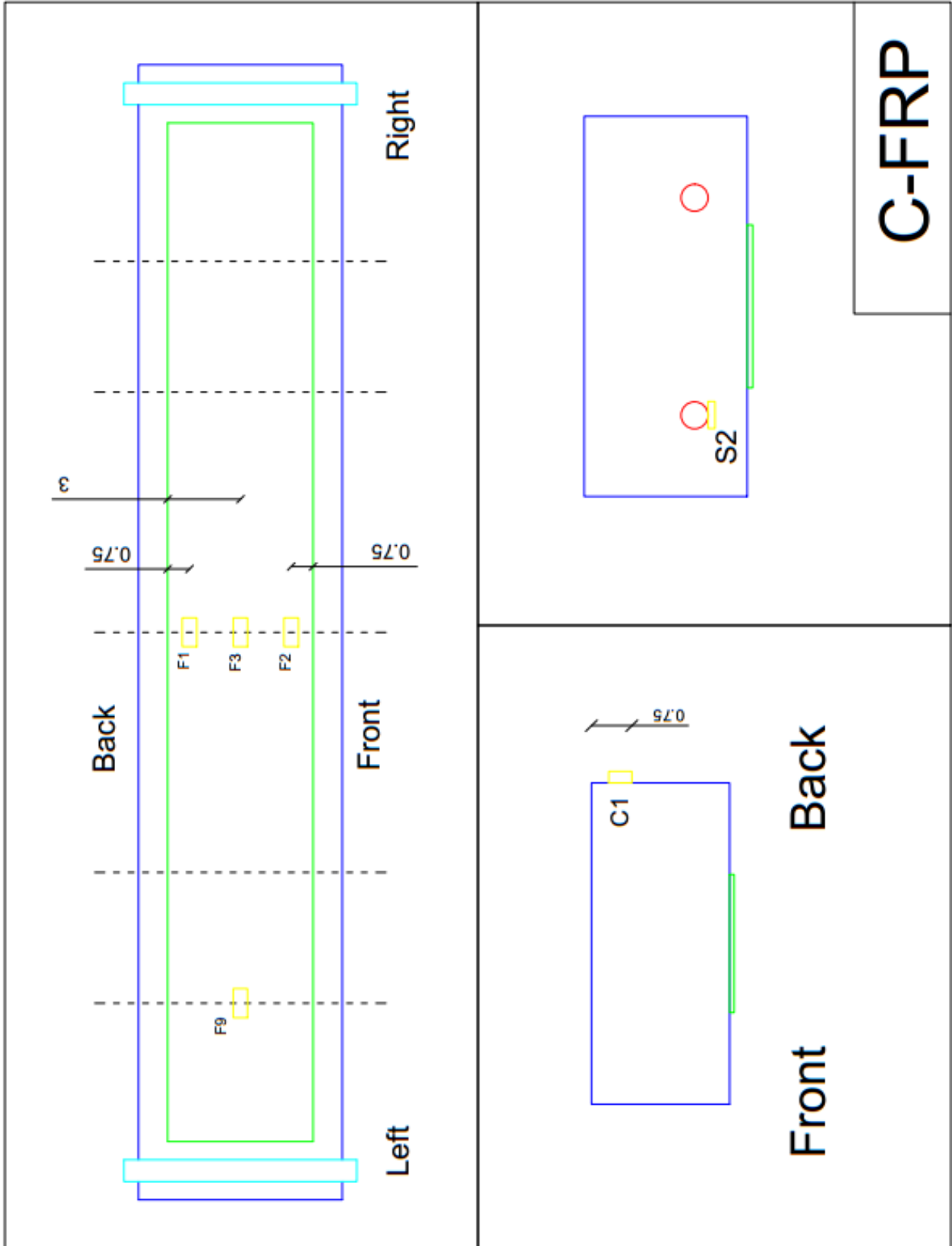


SX2-1

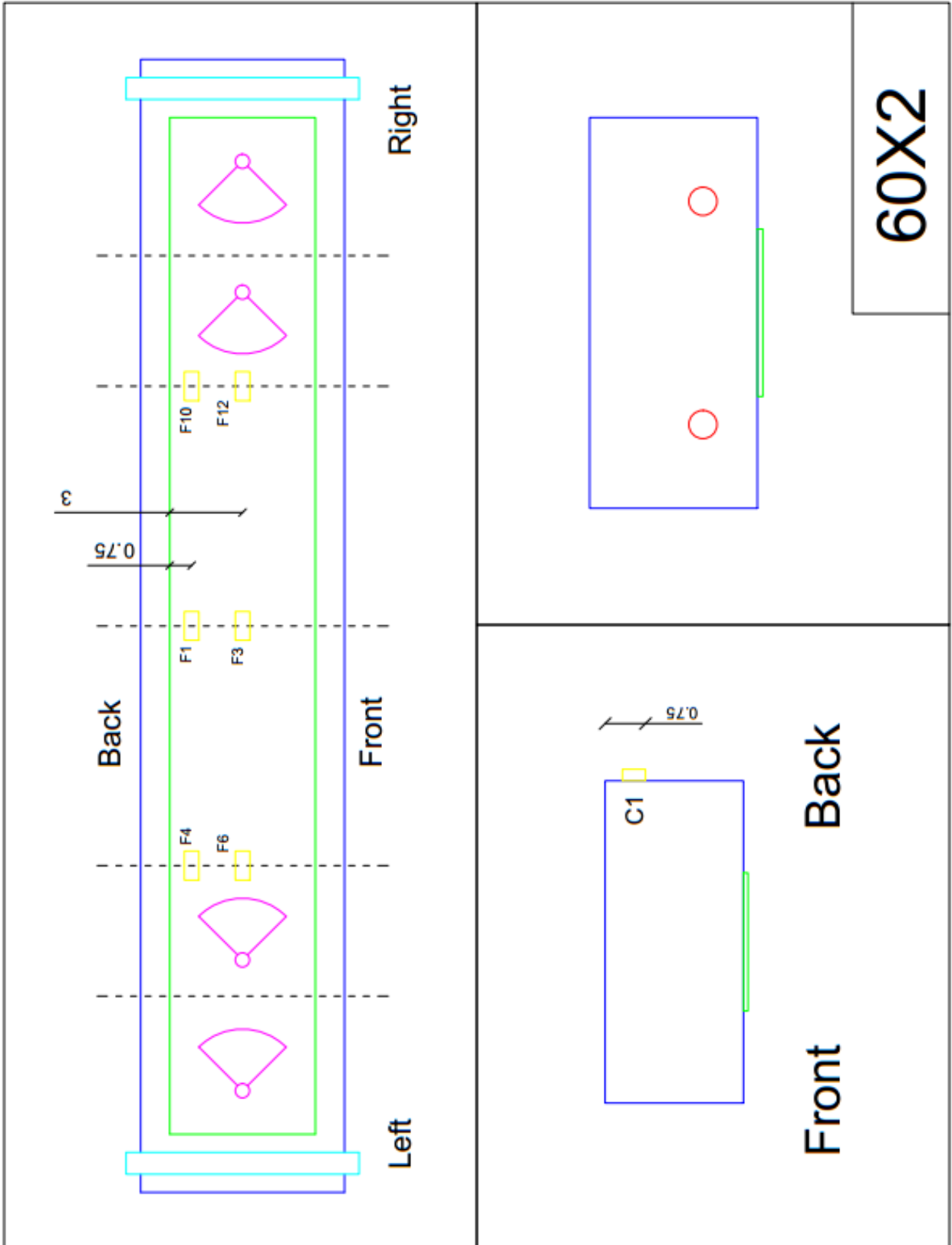
8.7 Appendix G: Strain Gages Locations

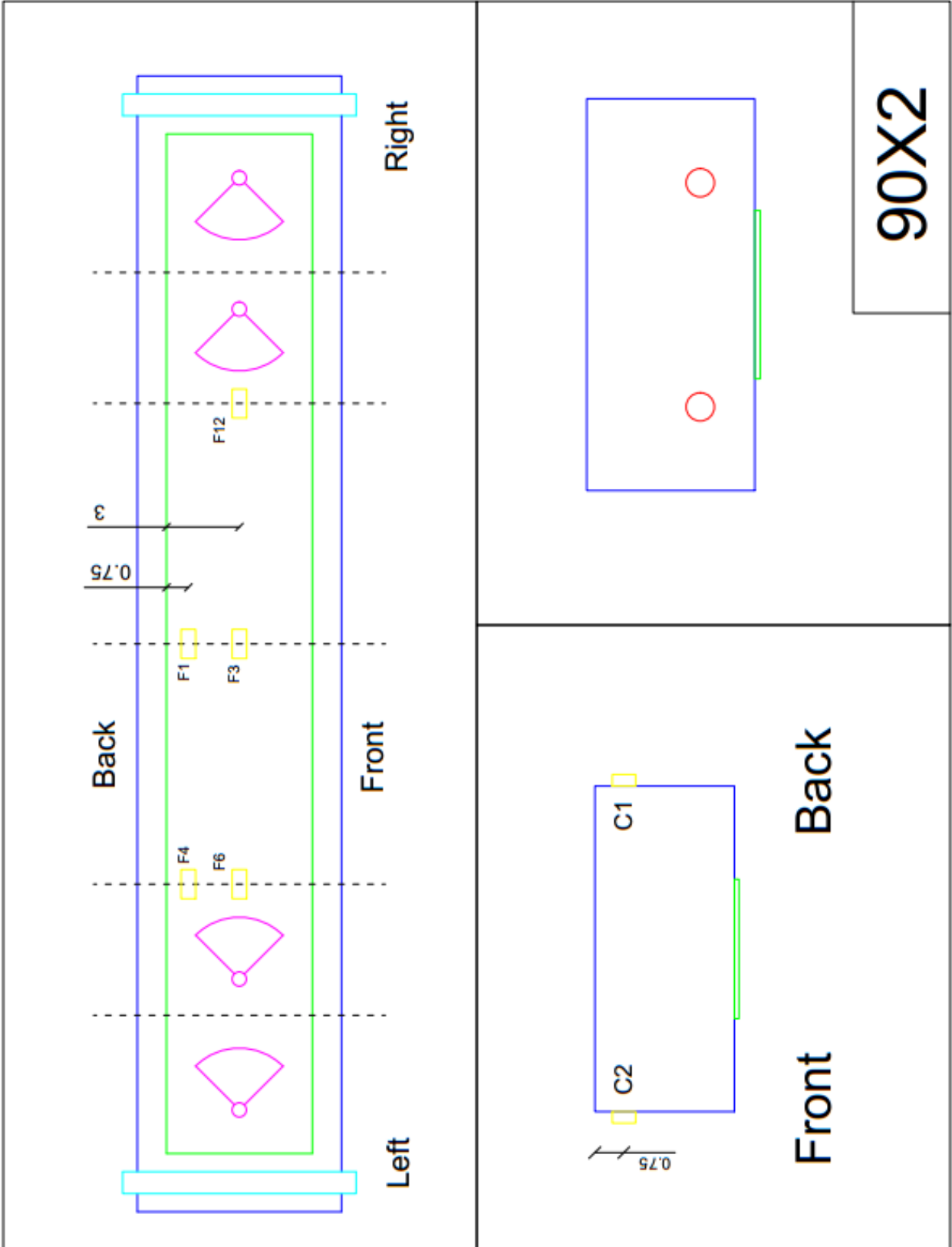
The strain gages locations for all the tested configurations are here recapped. All the dimensions are in inches (1 in = 25.4 mm).



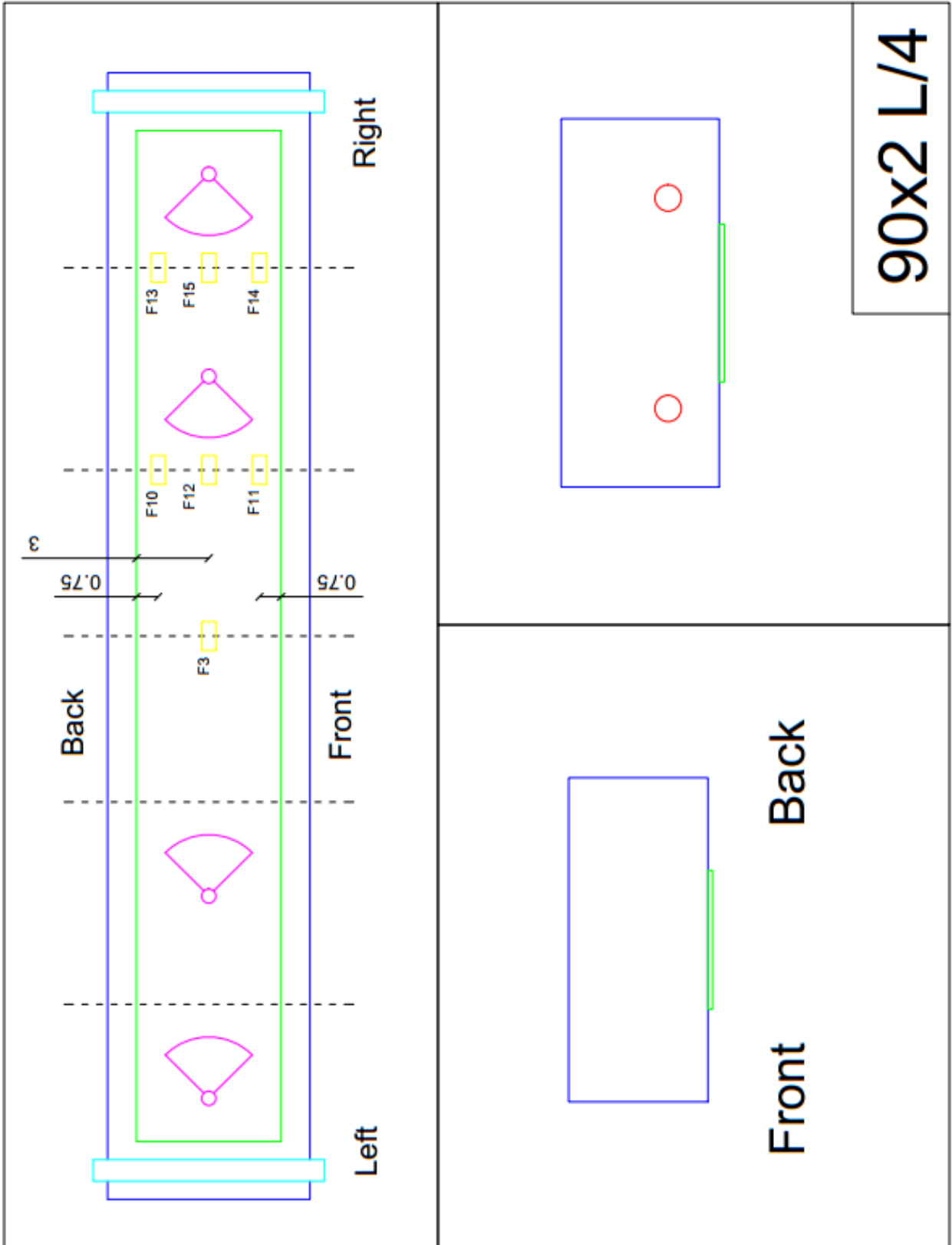


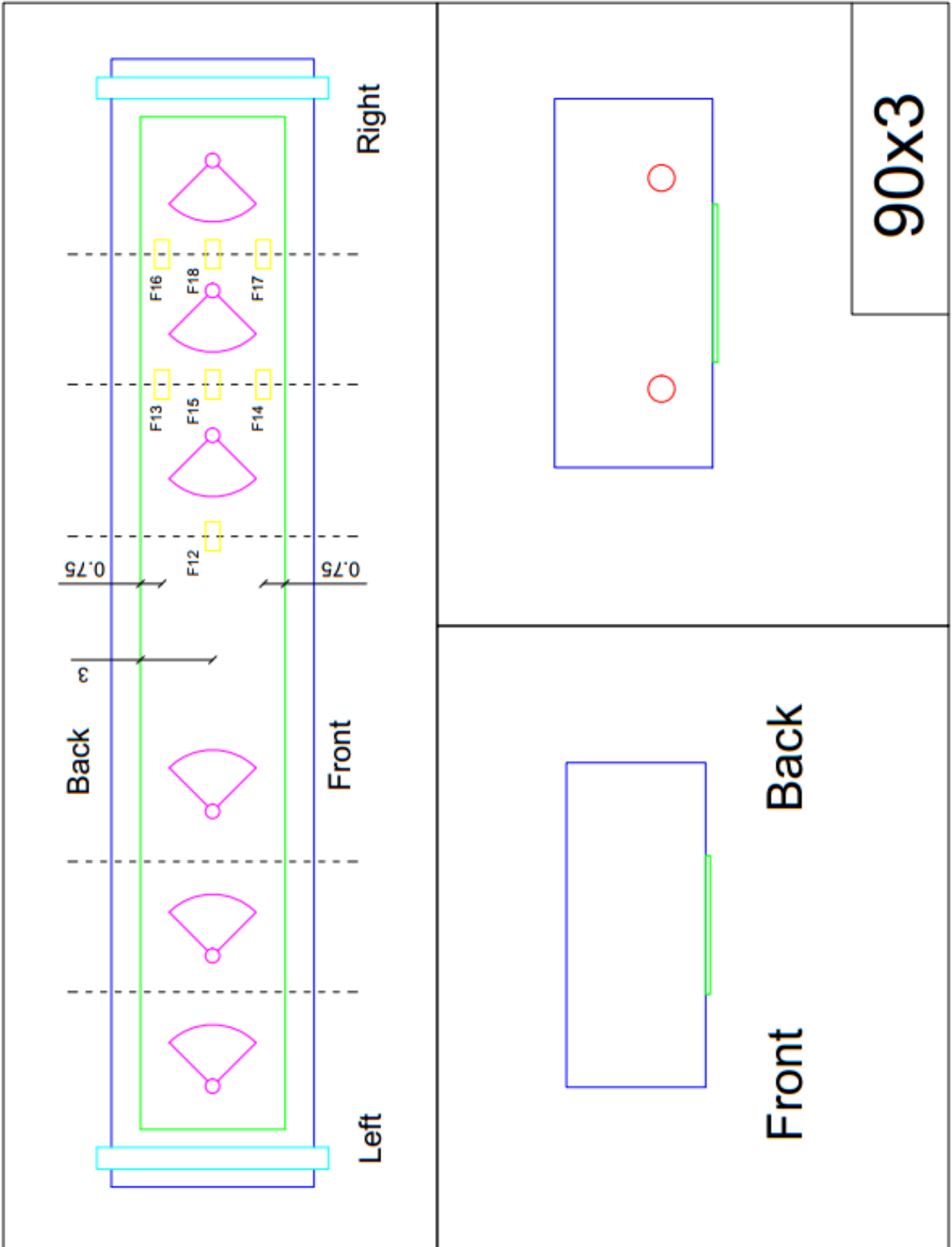
C-FRP

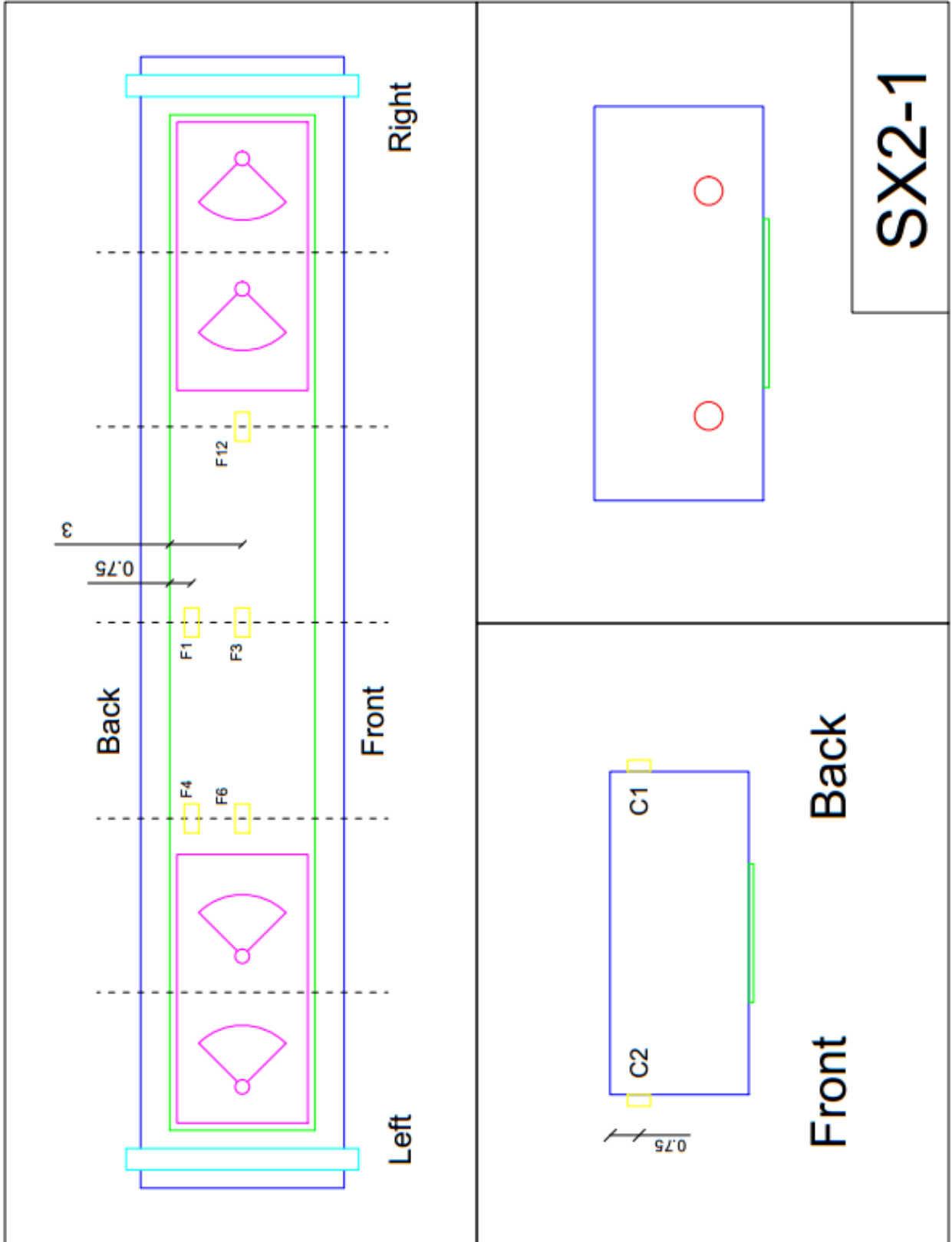




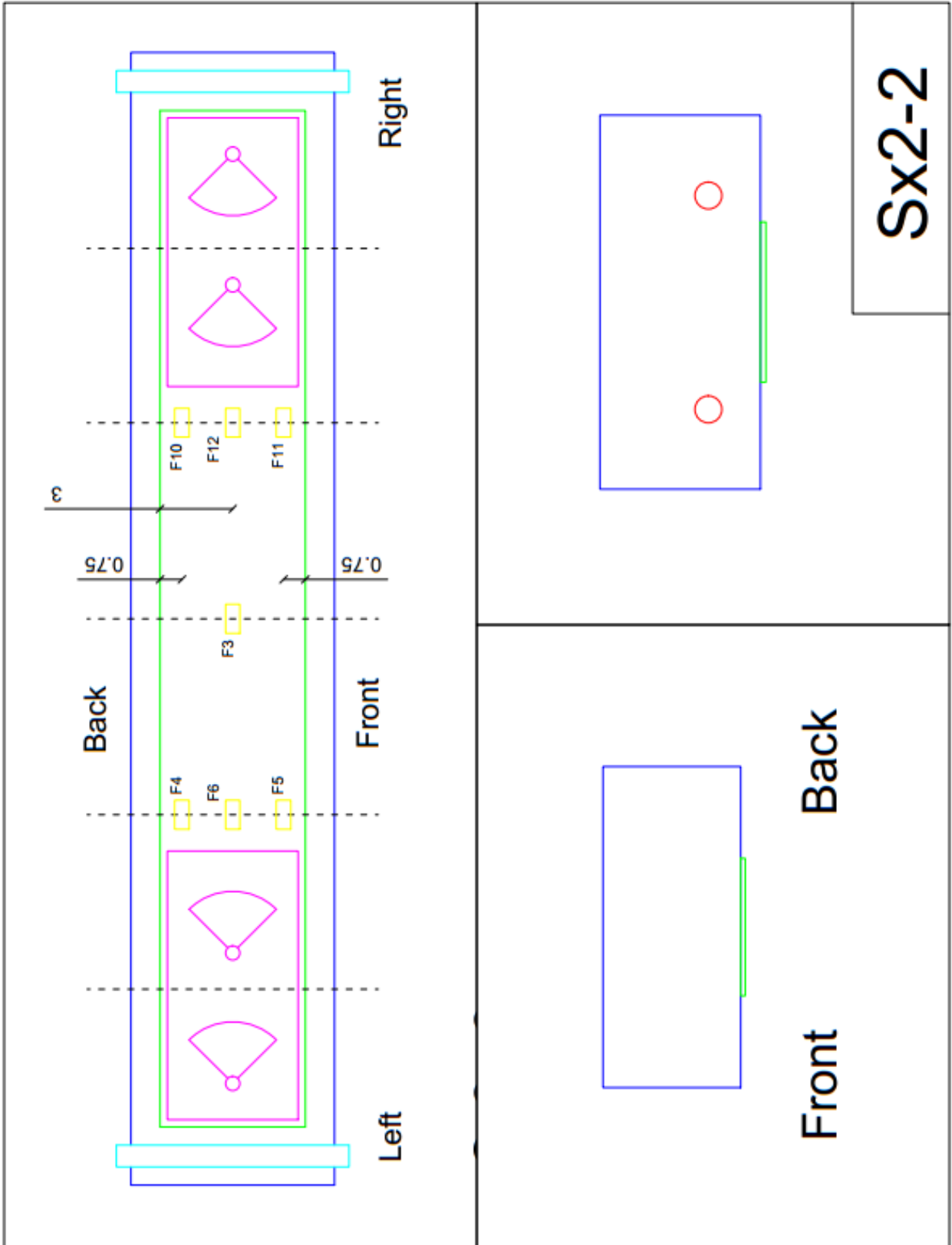
90X2







SX2-1



Sx2-2

9 List of Figures

Figure 1 – Carbon Fibers Production Process (Berneschi, 2015).....	33
Figure 2 – Epoxy’s Molecular Structure (Berneschi, 2015).....	35
Figure 3 – Fibers, Epoxy & Composite’s properties comparison (CNR, 2013)	37
Figure 4 – Stresses’ Convention (CNR, 2013)	39
Figure 5 - Maximum Strength (a) & Strain (B) Criteria at varying lamina orientation (Jones, 1998)	42
Figure 6 - Tsai-Hill Criterion at Varying Lamina Orientation (Jones, 1998)	44
Figure 7 - Tsai-Wu Criterion at Varying Lamina Orientation (Jones, 1998).....	45
Figure 8 - Conventions for Lamina Orientation	46
Figure 9 - mechanical properties at varying lamina orientation (CNR, 2013).....	48
Figure 10 - Failure modes for a lamina tensile test (ASTM, 2014)	50
Figure 11 – Exposure & Long Term Coefficients from ACI (a) & CNR (b)	51
Figure 12 - FRP flexural applications (Nanni, 2000).....	54
Figure 13 - Shear strengthening configurations (CNR, 2013).....	54
Figure 14 - Confinement applications (Nanni, 1999).....	55
Figure 15 - Chimney & wall reinforcement with FRP (Nanni, 2000)	56
Figure 16 - Debonding definitions according to CNR (a, c) & ASTM (b)	58
Figure 17 - Debonding & stresses at sheet's ends (CNR, 2013).....	59
Figure 18 - Intermediate debonding (CNR, 2013)	60
Figure 19 - Shear-cracks debonding (CNR, 2013)	61
Figure 20 - Shear-bond-test scheme (CNR, 2013)	61
Figure 21 - Slip laws (CNR, 2013)	62
Figure 22 – external VS internal bonding (savoia, 2015).....	65
Figure 23 - Experimental calibration & matching (a) wet lay-up (b) pre-cured FRP (CNR,2013).....	67
Figure 24 - Bending Moment Diagram Shifting (CNR, 2013).....	69
Figure 25 - Graphical representation of the provisions on bonding length (ACI, 2008) .	70
Figure 26 - Intermediate debonding formulations matching (Savoia, 2015)	73
Figure 27 - Anchoring Solutions for flexural strengthening (Grelle & Sneed, 2013).....	76
Figure 28 - Anchoring solutions for shear strengthening (Kalfat et al. 2011)	76
Figure 29 - Anchoring solutions for columes confinement & walls strengthening (Kobayashi, 2001) (Prota, 2015)	77
Figure 30 - Example of type I anchorage device (Grelle & Sneed, 2013)	78

Figure 31 - Example of type II anchoring devices	79
Figure 32 - Example of type III anchoring devices (Grelle & Sneed, 2013)	80
Figure 33 - Transverse wrapping (Grelle & Sneed, 2013).....	82
Figure 34 - Anchoring spike's typical slip law (Kalfat et al. 2011).....	83
Figure 35 - Examples of anchoring spikes (Smith, 2009).....	83
Figure 36 - Anchoring spikes in a pull-out critical application (kalfat et al. 2011)	84
Figure 37 - Metallic anchors examples (Grelle & Sneed, 2013)	86
Figure 38 - Metallic anchors examples (Grelle & Sneed, 2013)	87
Figure 39 – Concrete Embedment (Grelle & Sneed, 2013) (Kalfat et al. 2011).....	88
Figure 40 - Surface preparation with embedded rebar (kalfat et al. 2011)	89
Figure 41 - Near Surface Mounted Rods (NSM) (Nanni, 2000)	89
Figure 42 - Anchoring System Design & Validation (Grelle & Sneed, 2013).....	90
Figure 43 - Pull-out setup (Ozbakkaloglu & Saatcioglu, 2009)	91
Figure 44 – Single shear test (Kalfat et al.-Mahaidi, 2010), Double shear tests (Ceroni et al. 2007), Double blocks shear test (Eshwar et al. 2008), Double wrapped shear test (Berneschi, 2015)	93
Figure 45 - Bendin Test (adapted from Grelle & Sneed, 2013)	94
Figure 46 - Anchoring Spikes Manufacturing & Installation (Smith, 2009) (Zhang et al. 2011)	99
Figure 47 - Dowel geometry	102
Figure 48 - Fan Geometry	103
Figure 49 - Fan larger than the FRP sheet	104
Figure 50 - CSR Graphic representation (Sun, 2014)	106
Figure 51 - Pull-out failure modes (Ozbakkaloglu & Saatcioglu, 2009).....	109
Figure 52 - Results from Ozbakkaloglu & Saatcioglu (2009).....	111
Figure 53 – Results from Kim & Smith (2010).....	113
Figure 54 - Laminate Tensile Rupture & Fan-Laminate Slipping (Niemitz et al. 2010)..	115
Figure 55 - Dowel shear rupture & dowel pull-out (Brena & McGuirk, 2013) (Smith et al. 2011)	115
Figure 56 - Laminate splitting & concrete crushing (Zhang & Smith, 2011b) (Berneschi, 2015)	115
Figure 57 - Graphic representation for Kobayashi's law (adapted from Kobayashi et al. 2001)	117
Figure 58 - Kobayashi's configurations (kobayashi et al. 2001)	117
Figure 59 - Set-up from Eshwar et al. (2008).....	118
Figure 60 - Set-up from Norton et al. (2008).....	119
Figure 61 – Shear strength distance from end dependency (Zhang & Smith, 2013) ...	121

Figure 62 - Shear Strength dowel angle dependency (Zhang & Smith, 2013).....	122
Figure 63 - Shear strength sheet width dependency (Zhang & Smith, 2013)	122
Figure 64 - Multiple anchors matching.....	124
Figure 65 - Tested configurations from Brena & McGuirk (2013).....	125
Figure 66 - Results from Berneschi (2015).....	126
Figure 67 - Results from Sun et al. (2016)	128
Figure 68 - Set-up from Lam & Teng (2001)	129
Figure 69 - Tested Configuration & failure mode from Piyong et al. (2003).....	130
Figure 70 - Tested Configuration & failure mode from Eshwar et al. (2005).....	131
Figure 71 - Load/deflection response of tested slabs (B) anchored slabs with increasing strength & deflection (c) anchoring slab with predominantly increasing deflection (Smith et al. 2011)	132
Figure 72 - Tested configurations from Smith et al. (2011).....	133
Figure 73- Failure modes from Smith et al. (2011).....	133
Figure 74 - Load/Deflection response of tested slabs (b) anchored slabs with similar stiffness (c) anchored slabs with reduced stiffness (Smith et al. 2013)	134
Figure 75 - Tested configurations from Smith et al. (2013).....	135
Figure 76 - Failure modes from Smith et al. (2013).....	136
Figure 77 - Matching Examples (Nardone et al. 2011)	137
Figure 78 - Examples of tested concrete cylinders.....	139
Figure 79 - Concrete Constitutive Law (EC2, 2008)	143
Figure 80 - Steel Stress [MPa]/Strain [%] diagrams from material characterization.....	144
Figure 81 - Steel & FRP laminate tensile characterization	146
Figure 82 - Laminate samples preparation.....	147
Figure 83 - Failure modes from ASTM D3039 (2008)	149
Figure 84 - Load/Slip diagram from pull-out characterization (Berneschi, 2015).....	153
Figure 85 - Pull-out specimens (Berneschi, 2015)	153
Figure 86 - Shear Characterization set-up (Berneschi, 2015).....	154
Figure 87 - Slipping Failure Modes (Berneschi, 2015)	155
Figure 88 - Applied configurations (a) 60° (b) 90°-R, the sandwich one is simply a 90° configuration with a patch applied on top, refer to slab's geometry for details. All the dimensions are in inches (1 in = 25.4 mm).....	159
Figure 89 - Rebar instrumentation	160
Figure 90 - Molds set-up.....	161
Figure 91 - Casting & Demolding	162
Figure 92 - Sandblasting performed by a professional.....	163
Figure 93 - Carbon fibers impregnation.....	164

Figure 94 - FRP Application	165
Figure 95 - Hole drilling & Chamfer Radius.....	166
Figure 96 - Anchors cutting & impregnation	167
Figure 97 - Anchors installation	168
Figure 98 - Cured anchor extracted from a collapsed slab.....	169
Figure 99 - Strain Gages Application on FRP sheets	170
Figure 100 - Unreinforced Sample (C-C). All the dimensions are in inches (1 in = 25.4 mm).	172
Figure 101 - FRP Control Sample (C-FRP). All the dimensions are in inches (1 in = 25.4 mm).....	173
Figure 102 - 60x2 & 90x2 configurations. All the dimensions are in inches (1 in = 25.4 mm).....	174
Figure 103 - 90x2	175
Figure 104 - 90x2 L/4	175
Figure 105 - 90x2 L/3. All the dimensions are in inches (1 in = 25.4 mm).	175
Figure 106 - 90x2	176
Figure 107 - 90x2 L/3	176
Figure 108 - 90x3. All the dimensions are in inches (1 in = 25.4 mm).....	176
Figure 109 - Sx2-1 & Sx2-2 configurations. All the dimensions are in inches (1 in = 25.4 mm).....	177
Figure 110 – From right to left: Testing Frame, DAQ & Control System	178
Figure 111 - LVDTs & cylindrical hinge detail	179
Figure 112 - Concrete, Steel & FRP strain Gages	180
Figure 113 - Strain Gages General Positions. All the dimensions are in inches (1 in = 25.4 mm).....	181
Figure 114 – Configuration's Geometry	182
Figure 115 - 90x2 sample's load cycles from MTS. 1 lbf = 4.448 N	185
Figure 116 - Sectional Analysis' conventions (Adapted from CNR, 2013).....	186
Figure 117 - Concrete section's analysis' classical stages.....	187
Figure 118 - Sectional Analysis graphical representation, adapted from CNR (2013) & EC2 (2008).....	194
Figure 119 - Concentrated & distributed load structural analysis graphical representation	195
Figure 120 - Strain Distributions from Berneschi (2015).....	207
Figure 121 – Examples of balanced (a), under (b) & over-reinforced (c) sections.....	208
Figure 122 - Reduction Factor at Varying End Distance from Support. 1 in = 25.4 mm	219
Figure 123 - Strain Ratio at varying sheet's end from support. 1 in = 25.4 mm.....	221

Figure 124 - Bending moment diagram shifting	221
Figure 125 - (a) Load/Displacement (B) Concrete Strain (c) Steel Strain (C-C) 1 in = 25.4 mm / 1 kip = 4.448 kN.....	235
Figure 126 - Sectional strains (C-C). 1 in = 25.4 mm / 1 kip = 4.448 kN	236
Figure 127 – Failure (C-C).....	236
Figure 128 - Post-failure (C-C).....	236
Figure 129 - Load / Displacement (C-FRP). 1 in = 25.4 mm / 1 kip = 4.448 kN.....	238
Figure 130 - Strain gages (C-FRP). Dimensions in inches. 1 in = 25.4 mm.....	238
Figure 131 - (a) Concrete strain (b) Steel strain (c) FRP strain (C-FRP) 1 in = 25.4 mm / 1 kip = 4.448 kN	239
Figure 132 - (a) Sectional strain (b) FRP strain over the width (C-FRP) 1 in = 25.4 mm / 1 kip = 4.448 kN	240
Figure 133 - C-FRP collapse pictures.....	241
Figure 134 - Load/Displacement (60x2) 1 in = 25.4 mm / 1 kip = 4.448 kN	244
Figure 135 - (a) Concrete strain (b, c) FRP strain (60x2) 1 in = 25.4 mm / 1 kip = 4.448 kN	245
Figure 136 - FRP strains over the width (60x2). symmetry is artificially imposed for the sake of a better reading. 1 in = 25.4 mm / 1 kip = 4.448 kN	246
Figure 137 - Sectional strain (60x2). 1 in = 25.4 mm / 1 kip = 4.448 kN.....	247
Figure 138 - Strain gages locations & geometry (60x2), the x marks the failing side. Dimensions in Inches. 1 in = 25.4 mm / 1 kip = 4.448 kN.....	247
FIGURE 139 - 60x2 COLLAPSE PICTURES, THE X MARKS THE FAILING SIDE	248
Figure 140 - (a) Load/Displacement (b) Concrete Strain (c) FRP strain (90x2) 1 in = 25.4 mm / 1 kip = 4.448 kN.....	251
Figure 141 - FRP Strains over the width (90x2). symmetry is artificially imposed for the sake of a better reading. 1 in = 25.4 mm / 1 kip = 4.448 kN	252
Figure 142 - Sectional strains (90x2). 1 in = 25.4 mm / 1 kip = 4.448 kN	253
Figure 143 - Strain gages & geometry (90x2), the x marks the failing side. Dimensions in inches. 1 in = 25.4 mm / 1 kip = 4.448 kN.....	253
Figure 144 - 90x2 Collapse pictures, the x marks the failing side.....	254
Figure 145 - Concrete crushing (90x2 L/4).....	255
Figure 146 – Central strip, central span collaborating, end portions non-engaged (90x2 L/4).....	257
Figure 147 - Load/Displacement (90x2 L/4) 1 in = 25.4 mm / 1 kip = 4.448 kN	258
Figure 148 - (a, b) FRP strains (c, d) Strain gages location & geometry (90x2 L/4). Dimensions in Inches. 1 in = 25.4 mm / 1 kip = 4.448 kN.....	259

Figure 149 - FRP strains over sheet's width (90x2 L/4) 1 in = 25.4 mm / 1 kip = 4.448 kN	260
Figure 150 - 90x2 L/4 Collapse Pictures, the x marks the failing side	261
Figure 151 - Debonding & Failure behind the first anchor (90x2 L/3)	262
Figure 152 - Strain gages location & geometry (90x2 L/3), the x marks the failing side. Dimensions in Inches. 1 in = 25.4 mm / 1 kip = 4.448 kN	263
Figure 153 - Load/Displacement (90x2 L/3) 1 in = 25.4 mm / 1 kip = 4.448 kN	264
Figure 154 - FRP strains (90x2 L/3) 1 in = 25.4 mm / 1 kip = 4.448 kN	265
Figure 155 - FRP strains over the width, right side (90x2 L/3) 1 in = 25.4 mm / 1 kip = 4.448 kN	266
Figure 156 - FRP strains over the width, left side (90x2 L/3). symmetry is artificially imposed for the sake of a better reading. 1 in = 25.4 mm / 1 kip = 4.448 kN	267
Figure 157 - 90x2 L/3 Collapse pictures, the x marks the failing side	268
Figure 158 - 90x2 L/3. Dimensions are in inches, 1 in = 25.4 mm / 1 kip = 4.448 kN....	269
Figure 159 - 90x3. Dimensions are in inches, 1 in = 25.4 mm / 1 kip = 4.448 kN	269
Figure 160 - Debonding behind the first anchor (90x3)	270
Figure 161 - Load/Displacement (90x3). 1 in = 25.4 mm / 1 kip = 4.448 kN	271
Figure 162 - FRP strains (90x3). 1 in = 25.4 mm / 1 kip = 4.448 kN	272
Figure 163 - Strain gages location (90x3), the x marks the failing side Dimensions are in inches. 1 in = 25.4 mm / 1 kip = 4.448 kN	272
Figure 164 - FRP strains over sheet's width (90x3). symmetry is artificially imposed for the sake of a better reading. 1 in = 25.4 mm / 1 kip = 4.448 kN	273
Figure 165 - 90x3 Collapse pictures, the x marks the failing side.....	274
Figure 166 - Debonding past a still collaborating first anchor & first anchor failing along with the overall joint (Sx2-1)	275
Figure 167 - Ill-installed right joint (Sx2-1)	276
Figure 168 - Strain gages location & geometry (Sx2-1), the x marks the failing side. Dimensions are in inches. 1 in = 25.4 mm / 1 kip = 4.448 kN	279
Figure 169 - Cracks shape at collapse (Sx2-1), the x marks the failing side	279
Figure 170 – (a) Load/Displacement (b) Concrete strain (c) FRP strain (Sx2-1) 1 in = 25.4 mm / 1 kip = 4.448 kN	280
Figure 171 - FRP strains over sheet's width (Sx2-1). symmetry is artificially imposed for the sake of a better reading. 1 in = 25.4 mm / 1 kip = 4.448 kN	281
Figure 172 - Sectional Strains (Sx2-1). 1 in = 25.4 mm / 1 kip = 4.448 kN	282
Figure 173 - Sx2-1 Collapse pictures.....	282
Figure 174 - Load/Displacement (Sx2-2) 1 in = 25.4 mm / 1 kip = 4.448 kN	284
Figure 175 - FRP Strain (Sx2-2). 1 in = 25.4 mm / 1 kip = 4.448 kN	285

Figure 176 - Strain Gages Locations (Sx2-2), the x marks the failing sides- Dimensions are in inches. 1 in = 25.4 mm / 1 kip = 4.448 kN.....	285
Figure 177 - FRP strains over sheet's width. 1 in = 25.4 mm / 1 kip = 4.448 kN	286
Figure 178 - Sx2-2 Perfectly Symmetric Collapse Mechanism the x marks the failing sides	287
Figure 179 - F9, F3. dimensions are in inches. 1 in = 25.4 mm.....	288
Figure 180 – F4, F1, F10	289
Figure 181 - F6, F6, F12	289
Figure 182 – Dimensions are in inches, 1 in = 25.4 mm	289
Figure 183 – F4, F1.....	290
Figure 184 – F6, F3, F12	290
Figure 185 – Dimensions are in inches, 1 in = 25.4 mm	290
Figure 186 - F3, F10, F13.....	291
Figure 187 - F3, F12, F15.....	291
Figure 188 - F3, F11, F14.....	292
Figure 189 – Dimensions are in inches, 1 in = 25.4 mm	292
Figure 190 - F7, F3, F13.....	293
Figure 191 - F9, F6, F3, F12, F15	293
Figure 192 – Dimensions are in inches, 1 in = 25.4 mm	293
Figure 193 – F13, F16.....	294
Figure 194 – F12, F15, F18	294
Figure 195 – F14, F17.....	295
Figure 196 – Dimensions are in inches, 1 in = 25.4 mm	295
Figure 197 – F4, F1.....	296
Figure 198 – F3, F6, F12	296
Figure 199 – Dimensions are in inches, 1 in = 25.4 mm	296
Figure 200 – F4, F3, F10.....	297
Figure 201 – F6, F3, F12	297
Figure 202 – F5, F3, F11.....	298
Figure 203 – Dimensions are in inches, 1 in = 25.4 mm	298
Figure 204 - Ultimate Load Recap.....	302
Figure 205 - Ultimate Deflection Recap, no pseudo-ductility	302
Figure 206 - Ultimate deflection recap, with pseudo-ductility	302
Figure 207 - Ratios to unreinforced sample, R/C only.....	304
Figure 208 - Ratios to control sample, C-FRP Only	304
Figure 209 - ratios to fiber rupture.....	304
Figure 210 - Structural equilibrium before & after intermediate debonding	307

Figure 211 - Tri-linear behavior. 1 in = 25,4 mm / 1 kip = 4.448 kN	308
Figure 212 - The same sheet: bonded, debonded & failed (90x2 L/3)	308
Figure 213 - 60x2 anchors collapse, generally representative	310
Figure 214 - (a) C-FRP (b) Sx2-2 (c) 90x2.....	311
Figure 215 - Niemits et al. (2010)	311
Figure 216 - Cracks closing moving towards the FRP sheet	312
Figure 217 - Control Sample (C-FRP).	313
Figure 218 - 60x2 Sample, the x marks the failing side. 1 in = 25,4 mm / 1 kip = 4.448 kN	313
Figure 219 - Sx2-2 Sample shows a perfectly symmetric failure, further discussion will follow	314
Figure 220 - Shear Characterization set-up, load cell visible in the left picture.....	317
Figure 221 - three & eight strain gages configurations & a strain gage representation	317
Figure 222 - Ultimate Load Matching.	318
Figure 223 - Deflection Matching.	319
Figure 224 – Effective vs equivalent stiffness (yellow) I stage, uncracked (green) II stage, cracked elastic [SLS] (blue) III stage, cracked inelastic [ULS]. 1 in = 25,4 mm / 1 kip = 4.448 kN	320
Figure 225 - (a) ultimate load (b) ratios to fiber rupture (b) ratios to unreinforced, R/C only (c) ratios to control, unanchored C-FRP. Increasing joint strength. 1 in = 25,4 mm / 1 kip = 4.448 kN	324
Figure 226 - 90x2	326
Figure 227 - 90x2 L/4	326
Figure 228 - 90x2 L/3	326
Figure 229 - 90x2	327
Figure 230 - 90x2 L/4	327
Figure 231 - 90x2 L/3	327
Figure 232 - 90x2	328
Figure 233 - 90x2 L/4	328
Figure 234 - 90x2 L/3	328
Figure 235 - (a) Ultimate Load (b) ratios to fiber rupture, no Sx2-2 (c) Ratios to fiber rupture, with Sx2-2 (d) Linear & Quadratic regressions, without & with Sx2-2. 1 in = 25,4 mm / 1 kip = 4.448 kN.....	329
Figure 236 - Bilinear regressions over the experimental data & tri-linear assumed behavior for full-size samples. 1 in = 25,4 mm / 1 kip = 4.448 kN.....	330

Figure 237 - Ultimate load comparison (90x2, 90x3, 90x2 L/3). 1 in = 25,4 mm / 1 kip = 4.448 kN	331
Figure 238 - Continuity interruption in the central FRP strip	331
Figure 239 - Sandwich non-effectiveness on the load side. 1 in = 25,4 mm / 1 kip = 4.448 kN	332
Figure 240 - Sandwich-related pseudo-ductility on the deflection side. 1 in = 25,4 mm / 1 kip = 4.448 kN	333
Figure 241 - 90x2 Asymmetric Failure	335
Figure 242 - Sx2-2 Perfectly Symmetric Failure	335
Figure 243 - Sx2-1 ill-installed anchor.....	336
Figure 244 - Sx2-2 Perfectly Installed anchors.....	336
Figure 245 - Thermal camera inspected shear samples	337
Figure 246 - Tested configuration & set-up.....	345
Figure 247 - Strains shape over the sheet's width at increasing load	346
Figure 248 - Tested Configuration & set-up	347
Figure 249 - Load/Strain Diagram.....	347
Figure 250 - Strain shape over the sheet's width, notice the different scale for the last graph	348
Figure 251 - Failed sample, notice the dry fiber collapse on the left, were strains are higher	349
Figure 252 - (a) Load/Strain (b) FRP strains over sheet's width (c) Sample right before collapse	350
Figure 253 - Esempio di Ancoraggio in FRP (Zhang & Smith, 2013)	355
Figure 254- Shear test Set-Up (Berneschi, 2015).....	355
Figure 255- Esempio di Slipping Failure (Berneschi, 2015)	356
Figure 256- Esempio di Rinforzo Flessionale (Rossini, 2016, in preparazione)	356

10 References

- AASHTO. (2012). *Guide Specification for Design of Bonded FRP Systems for Repair and Strengthening of Concrete Bridge Elements*. Washington, DC: American Association of State Highway and Transportation Officials (AASHTO).
- AC125. (2012). *Acceptance criteria for concrete and reinforced and unreinforced masonry strengthening using externally bonded fiber reinforced polymer (FRP) composite systems*. International Code Council Evaluation Service.
- ACI 318-14. (2014). *Building Code Requirements for Structural Concrete and Commentary*. American Concrete Institute (ACI).
- ACI 355.4-11. (2011). *Qualification of Post-Installed Adhesive Anchors in Concrete and Commentary*. American Concrete Institute (ACI).
- ACI 440.2R-08. (2008). *Guide for the Design and Construction of Externally Bonded FRP Systems for Strengthening Concrete Structures*. American Concrete Institute (ACI).
- ACI 440.3R-12. (2012). *Guide Test Methods for Fiber-Reinforced Polymer (FRP) Composites for Reinforcing or Strengthening Concrete and Masonry Structures*. American Concrete Institute (ACI).
- ACI 440.8-13. (2013). *Specification for Carbon and Glass Fiber-Reinforced Polymer (FRP) Materials Made by Wet Layup for External Strengthening of Concrete and Masonry Structures*. American Concrete Institute (ACI).
- Al-Amery, R., & Al. Mahaidi, R. (2006). Coupled flexural-shear retrofitting of RC beams using CFRP straps. *Composite Structures*, 457-464.
- Al-Mahaidi, R., & Kalfat, R. (2011). Investigation into CFRP plate end anchorage utilising uni-directional fabric wrap. *Composite Structures*, 821-830.
- Al-Mahaidi, R., & SENTRY, M. W. (2009). *Testing the efficiency of anchorage systems applied to CFRP laminate strips bonded to concrete-Westgate bridge strengthening project*. Melbourne, Australia: Dept. of Civil Engineering, Monash University.
- Aridome, Y., Kanakubo, T., Furuta, T., & Matsui, M. (1998). Ductility of T-shape RC beams strengthened by CFRP sheet U-anchor. *Trans. Japan Concrete Institute*, 117-124.

- Ashraf, A., Tavakol, B., Das, R., Joven, R., Roozbehjavan, P., & Minaie, B. (2012). Study of Thermal Expansion in Carbon Fiber Reinforced Polymer Composites. *SAMPE International Symposium*. Charleston, SC.
- ASTM C143/143M-12. (2012). *Standard Test Method for Slump of Hydraulic-Cement Concrete*. American Society for Testing and Materials (ASTM) .
- ASTM C31/C31M-12. (2012). *Standard Practice for Making and Curing Concrete Test Specimens in the Field*. American Society for Testing and Materials (ASTM).
- ASTM C39/C39M-14. (2014). *Standard Test Method for Compressive Strength of Cylindrical Concrete Specimens*. American Society for Testing and Materials (ASTM).
- ASTM D3039/D3039M-08. (2008). *Standard Tests Method for Tensile Properties of Polymer Matrix Composite Materials*. American Society for Testing and Materials (ASTM).
- ASTM E178-08. (2008). *Standard Practice for Dealing With Outlying Observations*. American Society for Testing and Materials (ASTM) .
- ASTM E4-13 . (2013). *Standard Practice for Force Verification of Testing Machines*. American Society for Testing and Materials (ASTM).
- ASTM E488/E488M-10. (2010). *Standard Test Methods for Strength of Anchor in Concrete Elements*. American Society for Testing and Materials (ASTM).
- ASTM E83-10. (2010). *Standard Practice for Verification and Classification of Extensometer Systems*. American Society for Testing and Materials (ASTM).
- Baggio, D. F. (2013). *Effect of FRP Anchors on the FRP Rehabilitation of Shear Critical RC Beams and Flexure Critical RC Slabs, Master's Thesis*. Waterloo, Ontario: The University of Waterloo.
- Barros, J. A., Dias, S. J., & Lima, J. L. (2007). Efficacy of CFRP-based techniques for the flexural and shear strengthening of concrete beams. *Elsevier, Cement & Concrete Composites*.
- Belarbi, A., & Acun, B. (2013). FRP Systems in Shear Strengthening of Reinforced Concrete Structures. *Elsevier, Procedia Engineering*.
- Berneschi, A. (2015). *Enhancing the use of externally bonded FRP laminates with FRP anchor spikes, Master's Thesis*. Milano, Italy: Politecnico di Milano.

- Bilotta, A., Ceroni, F., Di Ludovico, M., Nigro, E., Pecce, M., & Manfredi, G. (2011). Bond efficiency of EBR and NSM FRP systems for strengthening concrete members. *Journal of Composites for Construction* 15 (5), 757-772.
- Bonacci, J. F., & Maalej, M. (2000). Externally bonded fiber-reinforced polymer for rehabilitation of corrosion damaged concrete beams. *Structural Journal*, 703-711.
- Bousias, S., Triantafillou, T., Fardis, M., Spathis, L., & O'Regan, B. (2004). Fiber-Reinforced Polymer Retrofitting of Rectangular Reinforced Concrete Columns with or without Corrosion. *ACI Structural Journal*, V. 101, No. 4, 512-520.
- Brena, S. F., & McGuirk, G. N. (2013). Advances on the Behavior Characterization of FRP-Anchored Carbon Fiber-Reinforced Polymer (CFRP) Sheets Used to Strengthen Concrete Elements. *International Journal of Concrete Structures and Materials*, 3-16.
- Brosens, K., & Van Gemert, D. (1999). Anchorage Design for Externally Bonded Carbon Fiber-Reinforcement Polymer Laminates. *Proceedings of the FRP RCS-4 SP-188* (pp. 635-645). Farmington Hills, Michigan: ACI.
- Buyle-Bodin, F., & David, E. (2004). Use of carbon fibre textile to control premature failure of reinforced concrete beams strengthened with bonded CFRP plates. *Journal of Industrial Textiles*, 145-157.
- Cadenazzi, T. (2016). *Study of an experimental anchor system ("staple" anchors) for externally bonded FRP laminates used for the consolidation and retrofitting of reinforced concrete structures, through an innovative double shear test method, Master's Thesis, in Preparation*. Milano, Italy: Politecnico di Milano.
- Caggeggi, C., Pensee, V., Fagone, M., Cuomo, M., & Chevalier, L. (2014). Experimental global analysis of the efficiency of carbon fiber anchors applied over CFRP strengthened bricks. *Elsevier Construction and Building Materials*.
- Cardenas, G. D. (2009). *Quality Control Test For Carbon Fiber Reinforced Polymer (CFRP) Anchors For Rehabilitation, Master's Thesis*. Austin, Texas: The University of Texas.
- Carey, S. A., & Harries, K. A. (2005). Axial Behavior and Modeling of Small, Medium, and Large-Scale Circular Sections Confined with CFRP Jackets. *ACI Structural Journal*, V. 102, No. 4, 596-604.
- Casadei, P., Galati, N., Parretti, R., & Nanni, A. (2003). Strengthening of a Bridge Using Two FRP Technologies. *Field Application of FRP Reinforcement: Case Studies, ACI Convention* (pp. 219-237). Boston: ACI Special Publication No. 15.

- Ceroni, F., Pecce, M., Matthys, S., & Taerwe, L. (2008). Debonding strength and anchorage devices for reinforced concrete elements strengthened with FRP sheets. *Elsevier, Composites Part B*.
- Chaallal, O., & Shahawy, M. (2000). Performance of Fiber-Reinforced Polymer-Wrapped Reinforced Concrete Column under Combined Axial-Flexural Loading. *ACI Structural Journal, V. 97, No. 4*, 659-668.
- Chen, G. M., Teng, J. G., Chen, J. F., & Rosenboom, O. A. (2010). Interaction between Steel Stirrups and Shear-Strengthening FRP Strips in RC Beams. *ASCE Journal of Composites for Construction*, 498-509.
- Chen, J. F., & Teng, J. G. (2001). Anchorage strength models for FRP and steel plates bonded to concrete. *ASCE Journal of Structural Engineering*, 784-791.
- Chen, J. F., & Teng, J. G. (2003). Shear capacity of FRP-strengthened RC beams: FRP debonding. *Elsevier, Construction and Building Materials*.
- CNR DT-200 R1/2013. (2014). *Guide for the Design and Construction of Externally Bonded FRP Systems for Strengthening Existing Structures*. Roma, Italy: National Research Council, Advisory Committee on Technical Recommendations for Construction (CNR).
- Cook, R. A. (1993). Behavior of Chemically Bonded Anchors. *ASCE Journal of Structural Engineering*, 2744-2762.
- De Lorenzis, L., & Tepfers, R. (2003). Comparative Study of Models on Confinement of Concrete Cylinders with Fiber-Reinforced Polymer Composites. *ASCE Journal of Composites for Construction, V. 7, No. 3*, 219-237.
- De Lorenzis, L., Lundgren, K., & Rizzo, A. (2004). Anchorage Length of Near-Surface-Mounted FRP Bars for Concrete Strengthening—Experimental Investigation and Numerical Modeling. *ACI Structural Journal, V. 101, No. 2*, 269-278.
- De Lorenzis, L., Miller, B., & Nanni, A. (2001). Bond of Fiber-Reinforced Polymer Laminates to Concrete. *ACI Materials Journal*.
- Deifalla, A., & Ghobarah, A. (2010). Strengthening RC T-beams subjected to combined torsion and shear using FRP fabrics: Experimental study. *ASCE Journal of Composites in Construction*, 301-311.
- Demers, M., & Neale, K. (1999). Confinement of Reinforced Concrete Columns with Fibre Reinforced Composites Sheets—An Experimental Study. *Canadian Journal of Civil Engineering, V. 26*, 226-241.

- Dong, J., Wang, Q., & Guan, Z. (2012). Structural behaviour of RC beams with external flexural and flexural–shear strengthening by FRP sheets. *Elsevier, Composites: Part B*.
- Duthin, D., & Starnes, M. (2001). Strengthening of reinforced concrete beams with carbon FRP. *Composites in construction*, 493–498.
- Elnabesity, G., & Saatcioglu, M. (2004). Seismic Retrofit of Circular and Square Bridge Columns with CFRP Jackets. *Advanced Composite Materials in Bridges and Structures*, (pp. CD-ROM Version). Calgary, AB, Canada.
- EN 1992-1-1. (2008). *Eurocode 2: Design of concrete structures - Part 1-1: General rules and rules for buildings*. Brussels: European Committee for Standardization (CEN).
- Eshwar, N., Ibell, T. J., & Nanni, A. (2005). Effectiveness of CFRP Strengthening on Curved Soffit RC Beams. *Advances in Structural Engineering*, Vol. 8, No. 1, 55-68.
- Eshwar, N., Nanni, A., & Ibell, T. J. (2008). Performance of Two Anchor Systems of Externally Bonded Fiber-Reinforced Polymer Laminates. *ACI Materials Journal*, 72-80.
- Fagone, M., Ranocchiai, G., Caggegi, C., Briccoli Bati, S., & Cuomo, M. (2014). The efficiency of mechanical anchors in CFRP strengthening of masonry: An experimental analysis. *Elsevier, Composites Part B*.
- Fardis, M. N., & Khalili, H. (1981). Concrete Encased in Fiberglass Reinforced Plastic. *ACI Journal, Proceedings*, Vol. 78, No. 6, 440-446.
- Ferreira, D., Oller, E., Mari, A., & Bairàn, J. (2016). Analysis of FRP Shear Strengthening Solutions for Reinforced Concrete Beams Considering Debonding Failure. *ASCE Journal of Composites for Construction*.
- FIB. (2001). *Externally bonded FRP reinforcement for RC structures, Technical report prepared by Task Group 9.3, Bulletin 14*. Lausanne, Switzerland: Fédération International du Béton (FIB).
- Fiore, V., Scalici, T., Di Bella, G., & Valenza, A. (2015). A Review on Basalt Fibers and its Composites. *Elsevier, Composites Part B*.
- Galal, K., & Mofidi, A. (2009). Strengthening RC Beams in Flexure Using New Hybrid FRP Sheet/Ductile Anchor System. *ASCE Journal of Composites for Construction*, 217-225.

- Galal, K., & Mofidi, A. (2010). Shear strengthening of RC T-beams using mechanically anchored unbonded dry carbon fiber sheets. *ASCE Journal of Performance of Constructed Facilities*, 31-39.
- Garcia, J., Sun, W., Kim, C., Ghannoum, W. M., & Jirsa, J. O. (2012). *Procedures for the Installation and Quality Control of Anchored CFRP Sheets for Shear Strengthening of Concrete Bridge Girders*. Austin, Texas: The University of Texas at Austin, Center for Transportation Research.
- Garden, H. N., & Hollaway, L. C. (1998). An experimental study of the influence of plate end anchorage of carbon fibre composite plates used to strengthen reinforced concrete beams. *Composite Structures*, 175-188.
- Gibson, D. (2002). *The Nabataeans, Builders of Petra*. Amman, Jordan: CanBooks.
- Godat, A., Chaallal, O., & Neale, K. W. (2013). Nonlinear finite element models for the embedded through-section FRP shear-strengthening method. *Elsevier, Computers and Structures*.
- Grelle, S. V. (2011). *Categorization and Experimental Evaluation of Anchorage Systems for Fiber Reinforced Polymer Laminates Bonded to Reinforced Concrete Structures, Master's Thesis*. Rolla, Missouri: Missouri University of Science and Technology.
- Grelle, S. V., & Sneed, L. H. (2013). Review of Anchorage Systems for Externally Bonded FRP Laminates. *International Journal of Concrete Structures and Materials*, Vol.7, No.1, 17-33.
- Halpin, J. C., & Halpin, H. C. (1992). *Primer on Composite Materials Analysis*. CRC Press.
- Harajli, M., & Rteil, A. (2004). Effect of Confinement Using Fiber-Reinforced Polymer or Fiber-Reinforced Concrete on Seismic Performance of Gravity Load-Designed Columns. *ACI Structural Journal*, V. 101, No. 1, 47-56.
- Harries, K. A., & Carey, S. A. (2003). Shape and 'Gap' Effects on the Behavior of Variably Confined Concrete. *Cement and Concrete Research*, V. 33, No. 6, 881-890.
- Hollaway, L. (2009). Polymer composites in construction: a brief history. *Proceedings of the Institution of Civil Engineers, Engineering and Computational Mechanics*, 107-118.
- Hoult, N. A., & Lees, J. M. (2009). Efficient CFRP strap configurations for the shear strengthening of reinforced concrete T-beams. *ASCE Journal of Composites in Construction*, 45-52.

- ICRI Committee 160. (2015). *Sustainability for Repairing And Maintaining Concrete and Masonry Buildings*. Rosemont, IL: International Concrete Repair Institute.
- Insulander, R. (2002). The Two-Wood Bow. *Acta Borealia*, 49-73.
- IstructE. (1999). *Interim guidance on the design of reinforced concrete structures using fibre composite reinforcement*. London, UK: Institute of Structural Engineers.
- Iyer, S. L., & Sen, R. (1991). Advanced Composite Materials in Civil Engineering Structures. *ASCE Proceedings*, 443.
- Iyver, S. L., & Sen, R. (1991). Advanced Composite Materials in Civil Engineering Structures. *ASCE Proceedings*, 443.
- Jensen, A. P., Petersen, C. G., Poulsen, E., Ottosen, C., & Thorsen, T. (1999). On the anchorage to concrete of sika carbodur CFRP strips. *Proc., Int. Congress on Creating with Concrete*. London: Thomas Telford Publishing.
- Jones, R. M. (1998). *Mechanics of Composite Materials*. Philadelphia, PA: Taylor & Francis.
- JSCE. (1986 (English Translation 1996)). *Standard specification for concrete structures*. Tokyo, Japan: Japanese Society of Civil Engineers.
- JSCE. (2001). *Recommendation for the upgrading of concrete structures with use of continuous fiber sheet, Concrete engineering series nr 41*. Tokyo, Japan: Japanese Society of Civil Engineers.
- Jung, K., Hong, K., Han, S., Park, J., & Kim, J. (2015). Shear Strengthening Performance of Hybrid FRP-FRCM. *Advances in Materials Science and Engineering*.
- Kalfat, R. (2008). The strengthening of post-tensioned slabs using CFRP composites at White City, London. *Proc., Structural Faults and Repair, 12th Int. Congress and Exhibition* (pp. CD-ROM Version). Edinburgh, U.K.: Engineering Technics Press.
- Kalfat, R., & Al-Mahaidi, R. (2015). The Influence of FRP Spike and Patch Anchors on the Bond Performance of FRP-to-Concrete Joints. *SMAR 2015, Third Convention on Smart Monitoring, Assessment and Rehabilitation of Civil Structures*. Antalya.
- Kalfat, R., Al-Mahaidi, R., & Smith, S. T. (2011). Anchorage Devices Used to Improve the Performance of Reinforced Concrete Beams Retrofitted with FRP Composites: State-of-the-Art Review. *ASCE Journal of Composites for Construction*, 14-33.

- Karantzikis, M., Papanicolaou, C. G., Antonopoulos, C. P., & Triantafillou, T. C. (2005). Experimental Investigation of Nonconventional Confinement for Concrete Using FRP. *ASCE Journal of Composites for Construction*, 480-487.
- Karpowicz, A. (2015). *Ottoman Turkish Bows, Manufacture & design*.
- Katsumata, H., Kobatake, Y., & Takeda, T. (1987). A Study on the Strengthening with Carbon Fiber for Earthquake-Resistant Capacity of Existing Concrete Columns. *Proceedings from the Workshop on Repair and Retrofit of Existing Structures, U.S.-Japan Panel on Wind and Seismic Effects* (pp. 1816-1823). Tsukuba, Japan: U.S.-Japan Cooperative Program in Natural Resources.
- Kaw, A. K. (2005). *Mechanics of Composite Materials, II Edition*. Boca Raton, FL: Taylor & Francis.
- Khalifa, A., & Nanni, A. (2000). Improving shear capacity of existing RC T-section beams using CFRP composites. *Elsevier, Cement & Concrete Composites*.
- Khalifa, A., Alkhrdaji, T., Nanni, A., & Lansburg, S. (1999). Anchorage of Surface-Mounted FRP Reinforcement. *Concrete International, V. 21, No. 10*, 49-54.
- Kim, I., Jirsa, J. O., & Bayrak, O. (2011). Use of Carbon Fiber-Reinforced Polymer Anchors to Repair and Strengthen Lap Splices of Reinforced Concrete Columns. *EBSCO Host Connection*.
- Kim, S. J., & Smith, S. T. (2009a). Behaviour of Handmade FRP Anchors under Tensile Load in Uncracked Concrete. *Advances in Structural Engineering, Vol. 12, No. 6*, 845-865.
- Kim, Y., Ghannoum, W. M., & Jirsa, J. O. (2015). Shear behavior of full-scale reinforced concrete T-beams strengthened with CFRP strips and anchors. *Elsevier, Costruction and Building Materials*.
- Kim, Y., Quinn, K., Ghannoum, W. M., & Jirsa, J. O. (2014). Strengthening of Reinforced Concrete T-Beams Using Anchored CFRP Materials. *ACI Structural Journal*, 1027-1035.
- Kim, Y., Quinn, K., Sotrom, N., Garcia, J., Sun, W., Ghannoum, W. M., & Jirsa, J. O. (2012). *Shear Strengthening of Reinforced and Prestressed Concrete Beams Using Carbon Fiber Reinforced Polymer (CFRP) Sheets and Anchors*. Austin, TX: Texas Department of Transportation Research and Technology Implementation Office.
- Kobayashi, K., Fujii, S., Yabe, Y., Tsukagoshi, H., & Sugiyama, T. (2001). Advanced Wrapping System with CF-anchor - Stress Transfer Mechanism of CF-anchor -.

- FRPRCS-5, Fibre Reinforced Plastics for Reinforced Concrete Structures* (pp. 379-388). University of Cambridge, UK: Thomas Telford.
- Lam, L., & Teng, J. (2003). Design-Oriented Stress-Strain Model for FRP-Confined Concrete. *Construction and Building Materials*, V. 17, 471-489.
- Lam, L., & teng, J. G. (2001). Strength of RC Cantilever Slabs Bonded with GFRP Strips. *ASCE Journal of Composites for Construction*, 221-227.
- Lee, T. K., & Al-Mahaidi, R. (2008). An experimental investigation on shear behaviour of RC T-beams strengthened with CFRP using photogrammetry. *Composite Structures*, 185-193.
- Li, B., & Chua, G. H. (2008). Rapid Repair of Earthquake Damaged RC Interior Beam-Wide Column Joints and Beam-Wall Joints Using FRP Composites. *Scientific.net bu Trans Tech Publications Ltd*.
- Louis, M. A., Jarallah, H. K., & Hameed, B. M. (2013). Load-Deflection Behavior of Reinforced Concrete Beams Strengthened with CFRP sheets. *Journal of Engineering and Development*, Vol. 17, No.4, 1813-1822.
- Lu, X. Z., Chen, J. F., Ye, L. P., Teng, J. G., & Rotter, J. M. (2008). RC beams shear-strengthened with FRP: Stress distributions in the FRP reinforcement. *Elsevier, Construction and Building Materials*.
- Martinelli, E., Bilotta, A., Faella, C., & Nigro, E. (2011). On the Behavior of FRP-to-concrete Adhesive Interface: Theoretical Models and Experimental Results. *Advances in Composite Materials - Ecodesign and Analysis*, 517-546.
- Matthys, S., Toutanji, H., Audenaert, K., & Taerwe, L. (2005). Axial Load Behavior of Large-Scale Columns Confined with Fiber-Reinforced Polymer Composites. *ACI Structural Journal*, V. 102, No. 2, 258-267.
- McGuirk, G. N. (2011). *Development of Anchorage System for FRP Strengthening Applications Using Integrated FRP Composites Anchors*. Amherst, Massachusetts: University of Massachusetts.
- McGuirk, G. N., & Brena, S. F. (2012). *Development of Anchorage System for FRP Strengthening Applications Using Integrated FRP Composite Anchors*. ACI Foundation, Concrete Research Council.
- Meier, U. (1987). Bridge repair with high performance composite materials (In German). *Mater Tech*, 125-128.

- Meier, U., Deuring, M., Meier, H., & Schwegler. (1992). Strengthening of structures with CFRP Laminates: Research and applications in Switzerland. *Advanced composite materials in bridges and structures*, 243-251.
- Mela, D. (2013). *Shear Bond Strength of Carbon FRP Laminates to Concrete*. Milano, Italy: Politecnico di Milano.
- Memon, M., & Sheikh, S. (2005). Seismic Resistance of Square Concrete Columns Retrofitted with Glass Fiber-Reinforced Polymer. *ACI Structural Journal*, V. 102, No. 5, 774-783.
- Micelli, F., Annaiah, R. H., & Nanni, A. (2002). Strengthening of short shear span reinforced concrete T joists with fiber-reinforced plastic composites. *ASCE Journal for Composites in Construction*, 264-271.
- Micelli, F., Rizzo, A., & Galati, D. (2010). Anchorage of composite laminates in RC flexural beams. *ICE Structural Concrete*, 117-126.
- Mohammadi, T. (2009). *Failure Mechanisms and Key Parameters of FRP Debonding from Cracked Concrete Beams*, MS Thesis. Milwaukee, Wisconsin: Marquette University.
- Monti, G., & Liotta, M. (2006). Tests and design equations for FRP-strengthening in shear. *Elsevier, Construction and Building Materials*.
- Mostofinejad, D., & Mahmoudabad, E. (2010). Grooving as Alternative Method of Surface Preparation to Postpone Debonding of FRP Laminates in Concrete Beams. *ASCE Journal of Composites for Construction*, 804-811.
- Nanni, A. (1995). Concrete repair with externally bonded FRP reinforcement. *Concrete International*, 22-26.
- Nanni, A. (1997). Carbon FRP Strengthening: New Technology Becomes Mainstream. *Concrete International: Design and Construction*, Vol. 19, No. 6, pp. 19-23.
- Nanni, A. (1999). Composites: Coming on Strong. *Concrete Construction*, vol. 44, 120.
- Nanni, A. (2000). Carbon Fibers in Civil Structures: Rehabilitation and New Construction. *The Global Outlook for Carbon Fiber*, Intertech. San Antonio, Texas.
- Nanni, A. (2004). Fiber Reinforced Polymer Composites for Infrastructure Strengthening - From Research to Practice.
- Nanni, A., & Bradford, N. (1995). FRP Jacketed Concrete Under Uniaxial Compression. *Construction and Building Materials*, V. 9, No. 2, 115-124.

- Nanni, A., & Lopez, A. (2004). Validation of FRP technology Through Field Testing. *16th World Conference on Nondestructive Testing*. Montreal, Canada.
- Nanni, A., Huang, P. C., & Tumialan, G. (2001). Strengthening of Impact-Damaged Bridge Girder Using FRP Laminates. *9th International Conference, Structural Faults and Repair* (pp. CD-ROM Version). London, UK: Engineering Technics Press.
- Narayanaswami, R., & Howard, A. M. (1977). Evaluation of the Tensor Polynomial and Hoffman Strength Theories for Composite Materials. *Journal of Composite Materials*, 366-377.
- Nardone, F., Lignola, G. P., Prota, A., Manfredi, G., & Nanni, A. (2011). Modeling of flexural behavior of RC beams strengthened with mechanically fastened FRP strips. *Elsevier, Composite Structures*, 1973-1985.
- Nicolais, L., & Borzacchiello, A. (2012). *Wiley encyclopedia of composites*. NJ: Wiley & Sons.
- Niemitz, C. W. (2014). *Anchorage of Carbon Fiber Reinforced Polymers to Reinforced Concrete in Shear Applications, Master's Thesis*. Amherst, Massachusetts: University of Massachusetts.
- Niemitz, C. W., Ryan, J., & Brena, S. F. (2010). Experimental Behavior of Carbon Fiber-Reinforced Polymer (CFRP) Sheets Attached to Concrete Surfaces Using CFRP Anchors. *ASCE Journal of Composites for Construction*, 185-194.
- Nosho, K. J. (1996). *Retrofit of Rectangular Reinforced Concrete Columns using Carbon Fiber, MS Thesis*. Seattle, WA: University of Washington.
- Obaidat, Y. T. (2011). *Structural Retrofitting of Concrete Beams Using FRP - Debonding Issues*. Lund, Sweden: Lund University.
- Orton, S. L. (2007). *Development of a CFRP System to Provide Continuity in Existing Reinforced Concrete Buildings Vulnerable to Progressive Collapse, PhD Thesis*. Austin, Texas: The University of Texas.
- Orton, S. L., Jirsa, J. O., & Bayrak, O. (2008). Design Considerations of Carbon Fiber Anchors. *ASCE Journal of Composites for Construction*, 608-616.
- Ozbakkaloglu, T., & Saatcioglu, M. (2009). Tensile Behavior of FRP Anchors in Concrete. *ASCE Journal of Composites in Construction*, 82-92.
- Ozdemir, G. (2005). *Mechanical Properties of CFRP Anchorages, Master's Thesis*. Ankara, Turkey: Middle East Technical University.

- Parretti, R., Nanni, A., Cox, J., Jones, C., & Mayo, R. (2003). Flexural Strengthening of Impacted PC Girder with FRP Composites. *Field Application of FRP Reinforcement: Case Studies, ACI Convention* (pp. 249-261). Boston: ACI Special Publication No. 15.
- Pellegrino, C., & Vasic, M. (2012). Assessment of design procedures for the use of externally bonded FRP composites in shear strengthening of reinforced concrete beams. *Elsevier, Composites: Part B*.
- Pessiki, S., Harries, K. A., Kestner, J., Sause, R., & Ricles, J. M. (2001). The Axial Behavior of Concrete Confined with Fiber Reinforced Composite Jackets V. 5, No. 4. *ASCE Journal of Composites in Construction*, 237-245.
- Pham, H. B., & Al-Mahaidi, R. (2004). Assessment of available prediction models for the strength of FRP retrofitted RC beams. *Composites Structure*, 601-610.
- Pham, H. B., & Al-Mahaidi, R. (2006). Prediction models for debonding failure loads of carbon fiber reinforced polymer retrofitted reinforced concrete beams. *Journal of Composite Structures*, 48-59.
- Pham, L. T. (2009). *Development of a Quality Control Test for Carbon Fiber Reinforced Polymer Anchors*. Austin, Texas: The University of Texas at Austin.
- Piyong, Y., Silva, P. F., & Nanni, A. (2003). Flexural Strengthening of Concrete Slabs by a Three-stage Prestressing FRP System Enhanced with the Presence of GFRP Anchor Spikes.
- Reed, C. E., Peterman, R. J., & Rasheed, H. A. (2005). *Evaluating FRP Repair Method for Cracked Prestressed Concrete Bridge Members Subjected to Repeated Loadings, KTRAN Report No. K-TRAN: KSU-01-2*. Topeka, KS: Kansas Department of Transportation.
- Reuter, J., & Robert, C. (1971). Concise Property Transformation Relations for an Anisotropic Lamina. *Journal of Composite Materials*, 270-272.
- Rocca, S., Galati, N., & Nanni, A. (2006). *Experimental Evaluation of FRP Strengthening of Large-Size Reinforced Concrete Columns, Report No. UTC-142*. Rolla, MO: University of Missouri.
- Rostasy, F. S. (1987). *Bonding of Steel and GFRP Plates in the Area of Coupling Joints, Research Report No. 3126/1429 (in German)*. Braunschweig, Germany: Federal Institute for Materials Testing.

- Saadatmanes, H., Ehsani, M. R., & Jin, L. (1996). Seismic Strengthening of Circular Bridge Pier Models with Fiber Composites. *ACI Structural Journal*, V. 93, No. 6, 639-647.
- Sami, Q., Ferrier, E., Michel, L., Si-Larbi, A., & Hamelin, P. (2011). Experimental Investigation of CF Anchorage System Used for Seismic Retrofitting of RC Columns. *Springer, Advances in FRP Composites in Civil Engineering*, 541-544.
- Sause, R., Harries, K. A., Walkup, S. L., Pessiki, S., & Ricles, J. M. (2004). Flexural Behavior of Concrete Columns with Carbon Fiber Composite Jackets. *ACI Structural Journal*, V. 101, No. 5, 708-716.
- Schiebel, S. R., Parretti, R., Nanni, A., & Huck, M. (2002). Strengthening and Load Testing of Three Bridges in Boone County, Missouri. *ASCE Practice Periodical on Structural Design and Construction*, 156-163.
- Schiebel, S., Parretti, R., & Nanni, A. (2001). *Repair and Strengthening of Impacted PC Girders on Bridge A4845, Final Report RDT01-017/RI01-016*. Jefferson City, Missouri: Missouri DOT.
- Smith, S. T. (2009). FRP Anchors: Recent Advantages in Research and Understanding. *APFIS 2009, The Second Official International Conference of International Institute for FRP in Construction for Asia Pacific Region*. Seoul, Korea.
- Smith, S. T. (2010). Strengthening of Concrete, Metallic and Timber Construction Materials with FRP Composites. *CICE 2010, The 5th International Conference on FRP Composites in Civil Engineering*. Beijing, China.
- Smith, S. T., & Kim, S. J. (2007). Pull-Out Tests on FRP Anchors. *APFIS 2007, Asia-Pacific Conference on FRP in Structures* (pp. 775-782). Hong Kong, China: International Institute for FRP in Construction.
- Smith, S. T., & Kim, S. J. (2010). Pullout Strength Models for FRP Anchors in Uncracked Concrete. *ASCE Journal of Composites for Construction*, 406-414.
- Smith, S. T., & Teng, J. G. (2002). FRP-strengthened RC beams: review of debonding strength. *ASCE Journal of Structural Engineering*, 385-395.
- Smith, S. T., & Teng, J. G. (2003). Shear-bending interaction in debonding failures of FRP-plated RC beams. *Advances in Structural Engineering*, 183-199.
- Smith, S. T., Hu, S., Kim, S. J., & Seracino, R. (2011). FRP-strengthened RC slabs anchored with FRP anchors. *Elsevier, Engineering Structures*, 1075-1087.

- Smith, S. T., Zhang, H., & Wang, Z. (2013). Influence of FRP anchors on the strength and ductility of FRP-strengthened RC slabs. *Elsevier, Construction and Building Materials*, 998-1012.
- Spadea, G., Bencardino, F., & Swamy, R. N. (1998). Structural behavior of composite RC beams with externally bonded CFRP. *ASCE Journal of Composites in Construction*, 132-137.
- Sun, W. (2014). *Behavior of Carbon Fiber Reinforced Polymer (CFRP) Anchors Strengthening Reinforced Concrete Structures, PhD Thesis*. Austin, Texas: The University of Texas.
- Sun, W., & Ghannoum, W. M. (2015). Modeling of anchored CFRP strips bonded to concrete. *Elsevier, Construction and Building Materials*.
- Sun, W., Jirsa, J. O., & Ghannoum, W. M. (2016). Behavior of Anchored Carbon Fiber-Reinforced Polymer Strips Used for Strengthening Concrete Structures. *ACI Materials Journal*, 163-172.
- Taljsten, B. (1997). Strengthening of beams by plate bonding. *ASCE Journal*, 206-212.
- Tanarslan, H., Murat, Y. E., & Sinan, A. (2008). The effects of CFRP strips for improving shear capacity of RC beams. *Journal of Reinforced Plastic Composites*, 1287-1308.
- Teng, J. G., & Yao, J. (2005). Plate End Debonding Failures of FRP - or Steel - Plated RC Beams: a New Strength Model. *Proceedings of the International Symposium on Bond Behaviour of FRP in Structures (BBFS 2005)*. Hong Kong, China.
- Teng, J. G., Chen, J. F., Smith, S. T., & Lam, L. (2002). *FRP Strengthened RC Structures*. West Sussex, UK: John Wiley & Sons.
- Tetta, Z. C., Koutas, L. N., & Bournas, D. A. (2015). Textile-reinforced mortar (TRM) versus fiber-reinforced polymers (FRP) in shear strengthening of concrete beams. *Elsevier, Composites: Part B*.
- Toutanji, H. (1999). Stress-Strain Characteristics of Concrete Columns Externally Confined with Advanced Fiber Composite Sheets. *ACI Materials Journal*, V. 96, No. 3, 397-404.
- Triantafillou, T. C. (1998). Shear Strengthening of Reinforced Concrete Beams Using Epoxy-Bonded FRP Composites. *ACI Structural Journal*, V. 95, No. 2, 107-115.

- Turco, A. (2014). *Influence of Geometry of Composite Laminate in Flexural Behavior of Reinforced Concrete Beams and Slabs, MS Thesis*. Milano. Italy: Politecnico di Milano.
- University of Miami, College of Engineering, Structures and Materials Laboratory. (2016). *Report Number IR-5.10_NRR_AC454/932, Evaluation of RockRebar TM per ICC-ES Acceptance Criteria and FDOT Section 932-3, Fiber Reinforced Polymer (FRP) Reinforcing Bars*. Coral Gables, FL: University of Miami, College of Engineering, Structures and Materials Laboratory.
- Wang, H. H. (2013). *Test of Glass Fiber Reinforced Polymer (GFRP) Anchors*. Austin, Texas: The University of Texas.
- Wu, Y. F., & Huang, Y. (2008). Hybrid bonding of FRP to reinforced concrete structures. *ASCE Journal of Composites in Structures*, 266-273.
- Yalim, B., Kalayci, A. S., & Mirmiran, A. (2008). Performance of FRP-Strengthened RC beams with different concrete surface profiles. *ASCE Journal of Composites in Construction*, 626-634.
- Zhang, H. (2013). *Influence of FRP anchors on FRP-to-concrete bond interfaces, PhD Thesis*. Hong Kong, China: The University of Hong Kong.
- Zhang, H. W., & Smith, S. T. (2011a). Influence of FRP anchor fan configuration and dowel angle on anchoring FRP plates. *Elsevier, Composites Part B*.
- Zhang, H. W., & Smith, S. T. (2011b). FRP-to-concrete joint assemblages anchored with multiple FRP anchors. *Elsevier, Composite Structures*.
- Zhang, H. W., Smith, S. T., & Kim, S. J. (2011). Optimisation of carbon and glass FRP anchor design. *Elsevier, Construction and Building Materials*.
- Zhang, H., & Smith, S. T. (2013). Fibre-Reinforced Polymer (FRP)-to-Concrete Joints Anchored with FRP Anchors: Tests and Experimental Trends. *NRC Research Press*, 1103-1116.
- Zheng, J.-J., & Dai, J.-G. (2014). Analytical solution for the full-range pull-out behavior of FRP ground anchors. *Elsevier, Construction and Building Materials*.

*“Ma propre vie ne me préoccupait plus:
je pouvais de nouveau penser au reste des hommes.”*

*Marguerite Yourcenar
MÉMOIRES D'HADRIEN*

